MANOEUVRING SIMULATION AND CONTROL STUDIES FOR APPLICATION TO DRY AND WET TOWING OF JACK UP UNITS.

Owen Skae Williams B.Eng.

Submitted as a Thesis for the Degree of Doctor of Philosophy.
The Department of Naval Architecture and Ocean Engineering.
University of Glasgow, Scotland. May 1995.

ProQuest LLC.
789 East Eisenhower Parkway
P.O. Box 1346
Ann Arbor, MI 48106 – 1346

DECLARATION.

Except where reference is made to the work of others this thesis is believed to be original.

This work is dedicated to my
parents and sister.

Acknowledgements.

I would like to take this opportunity to thank the following individuals either for their direct contributions or for their support and encouragement which has inspired me in the process of the completion of this work.

Firstly I will thank Professor Douglas Faulkner, John Elder Professor and Head of the Department. I also thank Dr. Atilla Incecik for his encouragement and Dr. Kamlesh S. Varyani for his assistance in the very early stages of the simulation work. I also thank Prof. Michael M. Bernitsas of the University of Michigan for his generosity in obtaining much of the literature on towing.

Mr David J. Percival the computer manager, with out whose help none of the simulation models would have been developed. Mr Robert B. Christison, the chief technician at the hydrodynamics laboratory and to Mr John Gillan for the model construction and all the technicians of the hydrodynamics laboratory who helped in the experimental program.

I thank Dr. Hoi Sang Chan, Mr Chih Chung Fang, Mr Stuart Hannah, Mr Zhi Xiang Tao, Mr Constantinos Tolikas and Dr. Tong Ming Wu for their illuminating discussions. I also thank the lectures, Mrs. Thelma Will and the secretaries and students of the Department.

I would also like to thank the Engineering and Physical Sciences Research Council, formally known as the Science and Engineering Research Council for their Research Studentship. I acknowledge the help of Wijsmuller and Noble Denton Associates.

Finally, I thank my parents, family and friends who have encouraged and supported my studies in the Department since October 1987.

Thesis Abstract.

The work contained in this Thesis presents manoeuvring simulation models which can be applied to the dry and wet towing of jack up units. The first chapter is a general introduction on the applications and methods of transportation of jack up units. In Chapter Two, a single vessel modular manoeuvring simulation model is presented and the modelling of wind and current loading is then discussed in Chapter Three. The wind loading on jack up legs is studied in Chapter Four using three models proposed by Det Norske Veritas, the British Standards Institution and Marathon Marine Engineering Company. The most appropriate leg loading model from this study is then incorporated into the simulation studies of the dry towing of a jack up on a heavy lift vessel in Chapter Five. The modelling of a skeg is also presented for these simulations. In Chapter Six, an experimental program is presented to obtain the linear drift manoeuvring derivatives and the current loading coefficients for a jack up geometry. In Chapter Seven, the Classical linear theoretical model and the extended analysis is presented for the prediction of directional stability of three single tow line systems. The system conditions for these theoretical studies are then simulated in two tow simulation models and the results are compared. The two tow simulation models employ a rigid and elastic tow rope assumption. These tow models are further compared under wind loading and for the location of the towed vessel superstructure. The elastic tow rope model is then extended to model the towing simulation with a bridle. The main conclusions to Chapter Two through to Seven are presented in Chapter Eight with some recommendations for towing operations and future work.

List of Symbols.

a_H	Ratio of Additional Lateral Force
a	Rudder Yaw Rate Constant
a_i	Location of Aft Tow Point from LCG on i^{th} Vessel
A_L	Lateral Projected Wind Area
A_T	Transverse Projected Wind Area
A_R	Rudder Area
AR	Aspect Ratio of Skeg
A_S	Area of Skeg
B	Beam of Vessel
b′	Rudder Yaw Gain Rate Constant
C	Coefficient of Port and Starboard Turn
C_B	Block Coefficient
C_D	Drag Coefficient
C_F	Basic Skin Friction Coefficient
C_L	Lift Coefficient
C_M	Mean Chord of Skeg
C_m	Coefficient of Added Mass
C_r	Residual Resistance Coefficient
C_T	Total Resistance Coefficient
C_X	Wind Force Coefficient in Surge
C_Y	Wind Force Coefficient in Sway
C_{XY}	Wind Moment Coefficient in Yaw
C_{CX}	Current Force Coefficient in Surge
C_{CY}	Current Force Coefficient in Sway
C_{CN}	Current Moment Coefficient in Yaw
$C_{1,2,3}$	Coefficients of Propeller Thrust
D	Draft of Vessel
D_P	Propeller Diameter
d_F	Draft Forward
d_A	Draft Aft
F'_N	Normal Force on Rudder. (Non dimensionalised)
f_i	Location of Forward Tow Point from LCG on i^{th} Vessel
G	Longitudinal Center of Gravity of Vessel (=LCG)
g	Acceleration due to gravity
h_R	Rudder Span

i_Z	Added Inertia
I_Z	Inertia and Added Inertia
I'_Z	Non Dimensionalised Total Inertia
J	Vessel Inertia
J_P	Advance Coefficient
$k_{X,Y,Z}$	Lambs Coefficients of Accession to Inertia
K_R	Rudder Aspect Ratio
L	Length of Vessel
L'_β	Lift Derivative
l_T	Length of Tow Rope
m	Mass of Vessel
$m_{X,Y}$	Added Mass in x and y respectively
$M_{X,Y}$	Mass and Added Mass in x and y respectively
$M'_{x,y}$	Non Dimensionalised Total Mass
N	Yaw Moment
N'	Non Dimensionalised Yaw Moment
$N'_{\beta r}$	Yaw Manoeuvring Derivative (non dim.) as a function of β and r
n	Propeller Revolutions
P_N	Propeller Number
P	Propeller Pitch
r	Angular Velocity of Vessel
r'	Non Dimensional Angular Velocity
$\dot{r}$	Angular Acceleration of Vessel
$\dot{r}'$	Non Dimensional Angular Acceleration
R_e	Reynolds Number
R_{SPAN}	Rudder Span
R_{ROOT}	Rudder Root
R_{TIP}	Rudder Tip
S	Wetted Surface Area
s	Slip Ratio
S_b	Breaking Strength of Elastic Tow Rope
T_1	Tow Rope Tension
t_P	Thrust Deduction Coefficient
t_R	Coefficient of Additional Drag.
u	Surge Component Velocity in Local Coordinate System
u_R	Relative Wind Velocity in Surge
U_R	Resultant Relative Wind Velocity

U_W	Wind Velocity
U_C	Current Velocity
U_{CC}	Corrected Current Velocity
$\overline{U}$	Resultant Velocity of Vessel in Local Coordinate System
$\dot{\overline{U}}$	Resultant Acceleration of Vessel in Local Coordinate System
U_R	Effective Rudder Inflow Velocity
v	Sway Component Velocity in Local Coordinate System
v_R	Relative Wind Velocity in Sway
∇	Volume
Δ	Mass Displacement
X	Forces Acting on Vessel in Surge Direction
X	Positional Vector of Vessel in Global Coordinate System
X_i	Longitudinal Position of i^{th} vessel in the Global Coordinate System
x'_R	Distance from cog to Center of Lateral Force. (Non dimensionalised)
x'_H	Distance from cog to Center of Additional Lateral Force.(Non dim.)
x_p	Location of Towpoint on Towed Vessel from LCG
Y	Forces Acting on Vessel in Sway Direction
Y	Positional Vector of Vessel in Global Coordinate System
Y_i	Transverse Position of i^{th} vessel in the Global Coordinate System
$Y'_{\beta r}$	Drift Manoeuvring Derivative (Non dim.) as function of β and r
α_0	Apparent Rudder Inflow Angle
$\alpha_{1,2}$	Bridle Angle
α_R	Effective Rudder Inflow Angle
β	Drift Angle
$\dot{\beta}$	Drift Angular Velocity
β'_R	Effective Drift Angle at Rudder
δ_R	Rudder Angle
$\dot{\delta}_R$	Rudder Deflection Rate
ε	Wake Fraction Ratio
ε_W	Working Strain of Towrope
ε_1	Angle of Tow rope with centreline of Towed Vessel
ϕ	Course Angle

ϕ_T Tow Rope Diameter
ϕ_B Bridle Rope Diameter
φ Roll Angle
θ Heading Angle
θ_e Required Heading Angle
θ_1 Heading Angle of Towed Vessel
$\dot{\theta}$ Angular Velocity
ρ Mass Density of Water
ρ_A Mass Density of Air
τ Trim
τ Specific Tension of Towrope
υ Kinematic Viscosity of Water
ω_P Effective Wake Fraction at Propeller
ω_R Effective Wake Fraction at Rudder
ω_{RO} Effective Wake Fraction at Rudder going Straight ahead
ω_{PO} Effective Wake Fraction at Propeller going Straight ahead
γ Flow Straightening Coefficient
ψ_W Angle of Wind in Global Coordinate System
ψ_R Relative Wind Angle
ψ_C Angle of Current in Global Coordinate System
ψ_{RC} Relative Current Angle
Λ Rudder Aspect Ratio

Coordinate Systems
x,y Local Coordinate System
X,Y Global or Earth Fixed Coordinate System

Subscripts.
B Bridle
C Current
H Hull
P Propeller
R Denotes Relative Quantity used in Wind Force Formulation
R Rudder
S Skeg
W Wind

List of Tables

List of Figures

Chapter Two.

Chapter Three.

Chapter One.

1.1 Introduction.

The number of jack up units used in present offshore operations is a reflection on the economic advantages of employing such rigs. In the offshore industry the jack up has been used primarily as a drilling and production unit as well as an accommodations platform. It has also found military applications such as a mobile missile launcher. The varied applications of the jack up is clearly a result of its many qualities. These include that it is self installing and once installed provides a stable platform. It is also reusable with low removal and reinstallation costs. The primary advantage is its high mobility.

Traditionally jack up units were used predominantly in the exploratory drilling sector of the offshore industry for which it is ideally suited. The production of oil and gas was usually undertaken by fixed jackets and gravity type platforms. The jack up has however been used in production where there has been an uncertainty of field life, as well as other economic considerations such as regulations which require the removal of jacket structures. The use of jack ups in production appears as an attractive solution and may increase in the future as the oil industry needs solutions to reduce production costs and develop marginal fields. The operational design concepts for a drilling rig as opposed to a production rig are very much different. The drilling platforms are used in exploration and are relocated usually 5-6 times a year with a short installation procedure. The production platforms move between 2-5 times in their lifetime.

The present trends for jack up units are also leading the industry into greater water depths and longer lasting commitments. The newest generation of jack ups are capable of operation in water depths up to 130 meters. The need for high mobility of the drilling jack ups coupled with increasing leg lengths will inevitably result in higher risks in transportation. Towing historically is a hazardous operation for these

mobile rigs. The method of transportation of a jack up depends upon the distance the rig must be towed. In the case of a transocean transportation, the jack up is placed upon a heavy lift vessel. This is known as a dry tow. This method is preferred for several reasons. The transportation speeds of 14 knots means that the rig can be located and functional in a shorter time frame as opposed to wet towing Ref. 5.1, 5.7. Due to the unpredictability of the weather, there is also greater control and bad weather can be avoided. In addition, with the reduction in the motion responses, the fatigue life of the legs can be prolonged.

In the case of a local move, the most common undertaken by drilling rigs, the jack up is towed by tugs to its new location. The speed of such a tow is usually 5-6 knots. A larger weather window is required and good forecasting is essential for such moves. In the case of the larger rigs it may become necessary for the legs to be cut when undertaking a location move. This action should be avoided not only because of the cost in cutting the legs and reattaching them, but there are also problems with stresses induced by the welding and the misalignment of corner posts with jacking equipment. The loading due to wind is important in the transit mode of the jack up. These loads will produce large overturning moments. The legs can contribute typically 85% of this wind heel which results in the reduction of the static stability of the tow. The wind heel is more significant in dry towing due too the raised vcg and the loss in metacentric height due to the narrower beam of the heavy lift vessel. The static wind heel is not a problem in wet towing of jack up units.

The loss of several jack up platforms through capsize while under tow has caused great concern from all those involved in the jack up community. In the past, most research and discussion have focused on the jack up in its elevated condition Refs. 1.1-1.4. These articles typically include soil and spud can fixity, wave loading and fatigue associated with the legs. This focus is absolutely necessary as jack ups are designed primarily for operational uses, but there is a clear deficit in the research on safe towing of jack ups. It has only been recently, that a greater emphasis

has been placed upon addressing the problems associated with towing which can easily lead to capsize. These include watertight integrity of the platform, better weather forecasting, damage stability, leg dynamics and the motion responses. It can be argued that this increased emphasis is due primarily to papers which highlighted the risks involved in towing as well as reports on the losses themselves, Refs. 1.5-1.9.

One such review paper Ref. 1.8, concerning the losses of jack ups has spotlighted the lack of published experimental studies on wet towing and capsizing of jack up rigs. This can be due to the confidentiality and sensitivity of the findings of such studies. The review paper also recommends that more research should focus on the prediction of the motion responses both theoretically and experimentally such as studies conducted in Refs. 1.10-1.13.

Another approach which has been neglected, for improving the safety and control of jack ups under tow is through the study of directional stability and use of manoeuvring simulation.

It is felt that capsizing can occur as a direct result of the jack up breaking its tow line connection. A factor which results in the loss of the tow connection could be attributed to the loss of directional stability of the tow under environmental loading. It is not known whether the geometric hull design and arrangements of the top side structures have consciously evolved with a view to optimum directional stability but one suspects not. In the future, design studies of the type conducted in the USA and Japan on barges Refs. 7.16- 7.18, for the addition of bilge keels and skegs to improve directional stability could be applied to jack up geometries.

At present it is believed there has not been any published work related to the field of towing simulation of jack up units and that this Thesis is first attempt in addressing the subject.

1.2 Objectives of the Research Work.

The objectives of the research work were to increase the understanding and knowledge of the mechanisms occurring when undertaking the dry and wet transportation of jack up rigs. The route to

achieve these objectives was through the use of computer simulation modelling. These methods would therefore concentrate on the control aspects of jack up transportation rather than motion response studies. Due to this fact, the major part of the work has been in the development of the necessary simulation models. As the work has evolved it was realised that the research program was ambitious and far beyond the resources available to any single researcher. The ultimate aims and hopes for this work unfortunately have not been realised. The main stumbling block was due to the limitations of the hydrodynamics laboratory which were insufficient to provide a complete set of linear manoeuvring derivatives for a jack up geometry. It had been an intention to undertake a further series of unconstrained towing experiments in an attempt to obtain these manoeuvring derivatives. This would be achieved by the method proposed by Burcher Ref. 1.14, but various factors have made this impossible. The work however has been successful in introducing new ideas and raising an awareness in the study of jack up towing. It is hoped that this Thesis will stimulate further research in the future.

1.3 Composition of the Thesis.

The work contained in this Thesis has covered many areas and fields of related research. The work has included manoeuvring and towing simulation with environmental loading for conventional vessels and studies on the modelling of wind loading on lattice legs. Additionally directional stability studies in towing and physical modelling through experiments were also conducted.

Literature reviews will be detailed at the beginning of each chapter where appropriate. In Chapter Two, the mathematical manoeuvring model for the single vessel simulation of a tanker model is presented. The effects of varying forward velocity, rudder area, rudder deflection, interaction coefficients and load condition on the turning circle trajectory are shown. The work in Chapter Three simulates the effects of wind loading on the model tanker and introduces the formulation of an

automatic pilot for rudder control. The modelling of current is also discussed. In Chapter Four, various lattice leg wind loading models are investigated using methods proposed in Refs. 4.1-4.4. The effects of cornerpost design, leg geometry, Reynolds number, orientation, marine growth are all discussed. The selected lattice leg loading model is then incorporated in the single vessel manoeuvring model for the simulation studies of Chapter Five. These simulations are conducted to investigate the behaviour of a heavy lift vessel with a jack up under wind loading. The simulation model is limited by the maximum allowable wind heeling moment for which the manoeuvring derivatives are valid. The effect of the wind speed, leg length, positioning of jack up relative to the system l.c.g. are shown and quantified using the auto pilot. Chapter Six introduces the jack up model design based on the most advanced deep water jack up 'Galaxy 1'. Also included in this chapter are the experiments undertaken to obtain the drift manoeuvring derivatives along with the determination of the current loading coefficients. In Chapter Seven, theoretical studies on the directional stability of single point towing systems are conducted. The conditions which predict stable and unstable tow configurations are then simulated using two tow rope models. These tow rope models employ a rigid tow rope and elastic tow rope assumptions. The elastic tow rope model is then extended further to simulate towing with a bridle. Recommendations for towing operations are then detailed in Chapter Eight along with the main conclusions of Chapters Two through Seven.

1.4 Development of Computer Programs.

The manoeuvring simulation results presented in this Thesis were obtained from simulation programs developed by the author. The basic single vessel manoeuvring simulation program was developed from an old version of a single vessel modular manoeuvring simulation model, Ref. 1.15. Extensive modifications were performed by the author on all the hull force modelling and the rudder model. The results from the program, now referred to as SSC are given in Chapter Two. This program was further developed to include an automatic pilot control, skeg

and environmental loading for the studies conducted in Chapters Three and Five and Seven. The wind loading subroutine was developed to model wind acting on a vessel turning for all angles of wind incidence. The leg loading program MMEC of Chapter Four was included in the wind loading program and named COMBWIND. This wind loading subroutine is used in conjunction with the program SSC HLV.The rigid and elastic towing simulation programs, RIGIDTOW and ELASTOW contain many of subroutines used in SSC HLV. The wind loading subroutine COMBTOWIND was extended to include a second vessel. The single point tow simulation programs have additional subroutines for directional stability analysis using linear theory. The elastic tow rope model was further developed for BRIDLETOW. All these programs mentioned with associated subroutines are the property of the author and are protected under copy right.

Chapter Two.

2.1 Introduction.

The prediction of the manoeuvring characteristics of any vessel is a complex matter. The manoeuvring behaviour of a ship is important when one considers the vessel's safety. There are numerous factors which affect manoeuvring performance and some of the predominant factors include the vessel's control devices such as rudder, skeg, bow thrusters, the water depth, load and trim condition, environmental loading from wave, current and wind and the vessel's inherent manoeuvring characteristics.

Perturbation theory exists to predict the degree of dynamic stability of vessels Ref. 2.1, and the results take the form of stability indices. These indices are obtained from a knowledge of the vessel manoeuvring derivatives which are determined from constrained model experiments. The perturbation model is limited however as it will predict the manoeuvrability of a specific vessel for a defined condition. It is not possible to model the variations in draft or rudder dimensions for example, without first performing a series of experiments at differing drafts or for various rudder geometries to obtain new derivatives and this makes the approach very rigid. The perturbation model is also a linear model. One method to examine the effects of varying load condition or rudder geometry is to use a modular manoeuvring computer simulation model. The simulation model will allow us to visualise the vessel's performance in the time domain. This will generate a clearer understanding of the vessel's manoeuvring behaviour than by merely comparing the stability indices obtained from perturbation theory.

The number of computer time domain simulation models have increased over the years each with varying degrees of sophistication and accuracy. These computer simulation models could be used in future at the initial design stage as a tool to check that vessels meet any future IMO minimum manoeuvring performance standards which are currently

under discussion. The accuracy of the simulation model should however be confirmed. A comparison study of various simulation models was undertaken Ref. 2.2, but this study failed to give any insight as to which of the simulation models was most accurate. The comparison of the components of the simulation models such as rudder, propeller and hull is inappropriate. The rudder and propeller models will have different interaction variables. Any comparison of the manoeuvring derivatives is also incorrect as each model uses different combinations of derivatives to sum the total forces and moments. Isolating one derivative and comparing it with a similarly named derivative from another model is inconclusive.

One of the best methods to determine the accuracy of the individual simulation models concerned, is to compare the prediction of the trajectory of the turning circle with trials data or if possible with free running model experiments. A turning manoeuvre can generate sufficient information for a comparison using the time of the manoeuvre, the advance, transfer and the tactical diameter to determine if the simulation matches the trials data or model tests. Additionally one can examine other manoeuvring tests like the Kempf overshoot manoeuvre, commonly called the Z manoeuvre, Ref. 2.3 but such a comparison is more difficult to perform than the more simpler turning manoeuvre.

The equations presented in this chapter to predict the manoeuvring of a vessel were formulated by the Manoeuvring Model Group (MMG) Refs. 2.6 and 2.7, which was specially organised by the manoeuvring sub committee of Japanese Towing Tank Conference. The first manoeuvring reports on the form of the modular simulation model were published in 1976, Ref.2.7. The manoeuvring model is complex as it describes the forces on the hull, rudder and propeller in open water and also includes the interactions between them. The manoeuvring derivatives and the interactions coefficients were determined through an extensive manoeuvring experimental program. The form of the equations of motion can however be traced back to work carried out by Davidson and

Schiff in 1946 Ref. 2.8. The model presented contains the deep water nonlinear hydrodynamic derivatives derived by Kijima et al., Refs. 2.3, 2.4, 2.5. These derivatives include the loading conditions from full to ballast and for even and trimmed conditions. The empirical formula describing the hull forces derived by Kijima et al. are specifically for relatively high block coefficient forms such as tankers and container vessels and are usually single screw and applicability should be considered.

In order to determine the accuracy of this specific modular manoeuvring simulation model, several experimental investigations were undertaken by the MMG with free running remote controlled models for various vessel types and loading conditions Refs. 2.5, 2.9. The results reported from these investigations present the real and predicted turning circle manoeuvres for the models in a controlled environment. There is in general, very good agreement for the model simulation and the model experiments. Scale effects will not affect the comparison as the derivatives and interaction coefficients were obtained by model experiments. We can therefore conclude that there is strong confidence of the accuracy of the simulation prediction method but there is a dependence upon the accurate calculation of manoeuvring derivatives and the interaction coefficients. There are problems however, associated with free running model tests and a discussion of these may be found in Ref. 2.10.

In this chapter, the formulation of the non dimensionalised equations of motion and the non dimensionalised hull, propeller and rudder forces and moments acting on a vessel is given. The procedure to obtain the time domain trajectories for the simulations is detailed in Appendix A. Simulations of the turning performance of a model tanker will be investigated for the varying parameters of vessel velocity, load condition, rudder area, rudder deflection, flow straightening coefficient and wake ratio. The tanker model chosen for this study is the Esso Osaka as this vessel was the subject of full scale manoeuvring trials in deep and shallow waters Ref. 2.11. Sufficient information was generated from these trials that the Osaka has become almost the standard vessel used to

determine the accuracy of many manoeuvring simulation models. The main dimensions of the Osaka tanker and model and the propulsion characteristics are given in Table 2.1. The trim and shallow water derivative corrections determined by Kijima et. al., Refs. 2.4, 2.5 are included in the Appendix B for completeness, but no investigations were carried out as there is insufficient information concerning certain coefficients. A discussion on the modelling of a full scale vessel will be presented and is related to the simulations conducted in Chapter Five.

2.2 Equations of Motion.

The formulation of the equations of motion are based on the coordinate system shown in figure 2.1. The x axis is defined along the centerline of the vessel, the y axis is positive in the starboard direction and angular velocity and moments are positive in a clockwise sense. The origin of the body fixed coordinate system is located at the center of gravity of the vessel. In addition to this, the axes are assumed to be the principle axes of inertia through the origin at G. We assume the mass distribution of the vessel does not change with time and the motions are in the horizontal plane only i.e. pitch, roll and heave are neglected. The equations of motion are derived in Ref. 2.1 and can be described as,

$$M\left(\frac{du}{dt} - \frac{d\theta}{dt}v\right) = X, \qquad 2.1.a.$$

$$M\left(\frac{dv}{dt} + \frac{d\theta}{dt}u\right) = Y, \qquad 2.1.b$$

$$I\frac{d^2\theta}{dt^2} = N \qquad 2.1.c$$

We can rewrite these in terms of mass and added mass in the local x and y directions as,

$$\frac{du}{dt}(m+m_x)-v\frac{d\theta}{dt}(m+m_y)=X, \qquad 2.2.a$$

$$\frac{dv}{dt}(m+m_y)+u\frac{d\theta}{dt}(m+m_x)=Y, \qquad 2.2.b$$

$$\frac{d\dot{\theta}}{dt}(J+i_z)=N, \qquad 2.2.c$$

We let,

$$M_X=(m+m_x)$$
$$M_Y=(m+m_y)$$
$$I_z=(J+i_z)$$

The added mass and added inertia may be determined from Lambs dimensionless coefficients of accession to inertia for spheroid bodies. These coefficients are shown in fig. 2.2. as indicated in Ref. 2.8. The above equations can therefore be rewritten as,

$$M_X=m\ (1+k_X) \qquad 2.3a$$
$$M_Y=m\ (1+k_Y) \qquad 2.3b$$
$$I_Z=(0.24L)^2m(1+k_Z) \qquad 2.3c$$

The inertia term, equation 2.3c is an empirical approximation common in Japanese manoeuvring literature. A similar empirical form may be obtained from Ref. 2.12. By the definition of drift angle figure 2.1, the component surge and sway velocities and accelerations are defined as,

$$u=\overline{U}\cos\beta, \qquad 2.4.a$$
$$v=-\overline{U}\sin\beta, \qquad 2.4.b$$
$$\dot{u}=\dot{\overline{U}}\cos\beta-\overline{U}\sin\beta\dot{\beta}, \qquad 2.4.c$$
$$\dot{v}=-\dot{\overline{U}}\sin\beta-\overline{U}\cos\beta\dot{\beta} \qquad 2.4.d$$

and we can write,

$$r = \frac{d\theta}{dt} \qquad 2.4e$$

$$\dot{r} = \frac{d\dot{\theta}}{dt} \qquad 2.4.f$$

Placing 2.4 a-f in the equations of motion 2.2 we get,

$$X = M_X\left\{\dot{\overline{U}}\cos\beta - \overline{U}\sin\beta\,\dot{\beta}\right\} + M_Y\overline{U}r\sin\beta \qquad 2.5.a$$

$$Y = -M_Y\left\{\dot{\overline{U}}\sin\beta + \overline{U}\cos\beta\,\dot{\beta}\right\} + M_X\overline{U}r\cos\beta \qquad 2.5.b$$

$$N = I_Z\dot{r} \qquad 2.5.c$$

Non dimensionalising the forces, moments, mass and inertia terms in the following manner, equations 2.6 and placing them in the above equations of motion 2.5, we obtain equations 2.7,

$$M_X' = \frac{2M_X}{\rho DL^2},\ M_Y' = \frac{2M_Y}{\rho DL^2},\ I_Z' = \frac{2I_z}{\rho DL^4},$$

$$X' = \frac{2X}{\rho DL\overline{U}^2},\ Y' = \frac{2Y}{\rho DL\overline{U}^2},\ N' = \frac{2N}{\rho DL^2\overline{U}^2}, \qquad 2.6$$

$$r = \frac{r'\overline{U}}{L},\ r' = \frac{rL}{\overline{U}},\ \dot{r}' = \frac{\dot{r}L}{\overline{U}} - \frac{\dot{\overline{U}}}{\overline{U}^2}Lr,\ \dot{r} = \left\{\frac{\dot{\overline{U}}r'}{L} + \frac{\dot{r}'\overline{U}}{L}\right\}$$

$$\frac{\rho DL\overline{U}^2}{2}X' = \frac{\rho DL^2}{2}M_X'\left\{\dot{\overline{U}}\cos\beta - \overline{U}\sin\beta\,\dot{\beta}\right\} + \frac{\rho DL^2}{2}M_Y'\overline{U}r'\frac{\overline{U}}{L}\sin\beta \qquad 2.7.a$$

$$\frac{\rho DL\overline{U}^2}{2}Y' = -\frac{\rho DL^2}{2}M_Y'\left\{\dot{\overline{U}}\sin\beta + \overline{U}\cos\beta\,\dot{\beta}\right\} + \frac{\rho DL^2}{2}M_X'\overline{U}r'\frac{\overline{U}}{L}\cos\beta \qquad 2.7.b$$

$$\frac{\rho DL^2\overline{U}^2}{2}N' = \frac{\rho DL^4}{2}I'_Z\left\{\frac{\dot{\overline{U}}r'}{L} + \frac{\dot{r}'\overline{U}}{L}\right\} \qquad 2.7.c$$

These equations then reduce to,

$$X' = \frac{L}{\overline{U}}M'_X\left\{\frac{\dot{\overline{U}}}{\overline{U}}\cos\beta - \sin\beta\,\dot{\beta}\right\} + M'_Y r'\sin\beta \qquad 2.8.a$$

$$Y' = -\frac{L}{\overline{U}}M'_Y\left\{\frac{\dot{\overline{U}}}{\overline{U}}\sin\beta + \cos\beta\,\dot{\beta}\right\} + M'_X r'\cos\beta \qquad 2.8.b$$

$$N' = I'_Z\frac{L}{\overline{U}}\left\{\frac{\dot{\overline{U}}r'}{\overline{U}} + \dot{r}'\right\} \qquad 2.8.c$$

The above are the form of the non dimensionalised equations of motion used in the simulation model with reference to the coordinate system of fig. 2.1.

2.3 Forces acting on the Vessel.

The total forces and moments acting on the vessel include contributions from the hull, rudder, propeller and external forces due to wind and current. The environmental forces are shown in the formulation and wind and current will be investigated in Chapter Three. These forces are shown with subscripts H, R, P and E.

$$X = X_P + X_H + X_R + X_E$$
$$Y = Y_H + Y_R + Y_E$$
$$N = N_H + N_R + N_E.$$

2.3.1 Hull Resistance Forces.

The forces acting on the hull can be described essentially in components along the x and y axes and a moment about the vessel origin

at LCG. There are however cross coupling terms and the force along the x axis can be written as,

$$X_H = -m_x\dot{u} + (m_y + X_{vr})vr + X(u) \qquad 2.9$$

The above equation may be found in Ref. 2.14. The resistance of the vessel advancing along a straight course is described as,

$$X(u) = -\frac{1}{2}\rho S\bar{U}^2 C_t, \qquad 2.10$$

The wetted surface area S, is given by Denny's approximate formula

$$S = 1.7LD + \frac{\nabla}{D}. \qquad 2.11$$

The total resistance coefficient C_t is determined from the addition of the basic skin friction coefficient derived from the 1957 ITTC model ship correlation equation 2.13 and a residual resistance coefficient.

$$R_N = \frac{\bar{U}L}{\upsilon} \qquad 2.12$$

$$C_F = \frac{0.075}{(\log_{10} R_N - 2)^2} \qquad 2.13$$

The residual resistance coefficient can be estimated from figures 2.3 which were taken from Ref. 2.13. We rewrite the cross coupling term of equation 2.9 as,

$$m_y + X_{vr} = C_m m_y, \qquad 2.14$$

where C_m is a coefficient of added mass and varies from 0.5-0.75 and this can be written as a function of block coefficient as,

$$C_m = 1.7C_B - 0.52. \qquad 2.15$$

If we consider the first two terms of equation 2.9 appear in the equation of motion, rearrange equation 2.14 and then place this and equations 2.10 and 2.11, in equation 2.9 we then arrive at,

$$X_H = -m_y(1-C_m)vr - \frac{1}{2}\rho\overline{U}^2C_t\left(1.7LD + \frac{\nabla}{D}\right) \qquad 2.16$$

If we rewrite the terms of the above equation in their non dimensionalised form with equation 2.4b and remove the common terms,

$$\frac{\rho DL\overline{U}^2}{2}X'_H = \frac{\rho DL^2}{2}m'_y(1-C_m)\frac{\overline{U}^2}{L}r'\sin\beta - \frac{1}{2}\rho\overline{U}^2C_t\left(1.7LD + \frac{\nabla}{D}\right) \qquad 2.17$$

$$X'_H = m'_y(1-C_m)r'\sin\beta - C_t\left(1.7 + \frac{BC_B}{D}\right) \qquad 2.18$$

2.3.2 Non Linear Deep Water Manoeuvring Derivatives.

The sway force and yaw moment acting on the vessel can be determined from the vessel's manoeuvring derivatives in sway and yaw. These forces are represented by the Kijima nonlinear deep water derivatives Ref. 2.3, which are based on the earlier work of Inoue Ref. 2.14. These derivatives take the form of non dimensional empirical formulae which are functions of the vessel's main dimensions and load condition but for trim by stern only. It is also noted that these equations apply to type vessels and applicability of the equations should be considered. The shallow water derivatives are determined using a correction factor applied to the deep water derivative equations for fully loaded condition only Ref. 2.5. These equations are given in Appendix B. These manoeuvring derivatives were obtained experimentally for a series of high block coefficient vessels for varying load conditions and geometries. These vessels are typically crude oil tankers, cargo and container vessels. The sway and yaw drift derivatives can be determined from oblique towing

experiments as detailed in Chapter Six. The derivatives dependent upon the angular velocity can be determined from PMM tests or from rotating arm experiments as explained in Refs. 2.1, 2.10.

The equations of lateral force and yaw moment are written in the non dimensionalised form as functions of drift angle and angular velocity and can be described as,

$$Y'_H = Y'_\beta\,\beta + Y'_r\,r' + Y'_{\beta\beta}\,\beta|\beta| + Y'_{rr}\,r'|r'| + Y'_{\beta rr}\,\beta r'|r'| + Y'_{\beta\beta r}\,\beta\beta|r'| \qquad 2.19a$$

$$N'_H = N'_\beta\,\beta + N'_r\,r' + N'_{\beta\beta}\,\beta|\beta| + N'_{rr}\,r'|r'| + N'_{\beta rr}\,\beta r'|r'| + N'_{\beta\beta r}\,\beta\beta|r'| \qquad 2.19b$$

where the linear and nonlinear derivatives are written as functions of the vessel's main dimensions.

$$Y'_\beta = \frac{1}{2}\pi k + 1.4C_B\frac{B}{L}$$

$$Y'_r - (m' + m'_x) = -1.5C_B\frac{B}{L}$$

$$Y'_{\beta\beta} = 2.5d\frac{(1-C_B)}{B} + 0.5$$

$$Y'_{rr} = 0.343d\frac{C_B}{B} - 0.07$$

$$Y'_{\beta rr} = 5.95d\frac{(1-C_B)}{B}$$

$$Y'_{\beta\beta r} = 1.5d\frac{C_B}{B} - 0.65$$

$$N'_\beta = k$$

$$N'_r = -0.54k + k^2$$

$$N'_{\beta\beta} = -0.96d\frac{(1-C_B)}{B} + 0.066$$

$$N'_{rr} = 0.5\frac{C_B B}{L} - 0.09$$

$$N'_{\beta rr} = -(0.5d\frac{C_B}{B} - 0.05)$$

$$N'_{\beta\beta r} = -(57.5(\frac{C_B B}{L})^2 - 18.4\frac{C_B B}{L} + 1.6)$$

$$k = \frac{2D}{L}$$

2.3.3 Propeller Forces.

The propeller forces can be described in terms of the propeller open water characteristics by the following equation,

$$X_P = (1-t_p)\rho n^2 D_p{}^4 K_T(J_P) \qquad 2.20$$

We then non dimensionalise the propeller force to obtain,

$$X'_P = (1-t_p)n^2 D_p{}^4 K_T(J_P) / (LD\overline{U}^2 / 2) \qquad 2.21$$

where,

$$K_T(J_P) = C_1 + C_2 J_P + C_3 J_P^2 \qquad 2.22$$

$$J_P = \overline{U}\cos\beta(1-\omega_P) / nD_P \qquad 2.23$$

$$\omega_{PO} = 0.5C_B - 0.05$$

t_P	Thrust deduction coefficient
n	No. of propeller revolutions
D_P	Propeller diameter
ω_P	Effective wake fraction at the propeller
J_P	Advance coefficient.

The thrust is dependent upon the propeller diameter, the speed of advance and the number of revolutions of the propeller. The thrust coefficient $K_T(J_P)$ can be determined as a quadratic function of the advance coefficient as indicated in Ref. 2.13 and equation 2.22 where C_1,C_2,C_3 are constants. The values of these constants for the simulations are given in Table 2.1. The propeller is assumed constant pitch and the propeller revolutions are constant.

2.3.4 Rudder Forces.

An outline of the form of the rudder force and moment equations can be found in Appendix C. The equations presented below are commonly found in Japanese manoeuvring literature, Ref. 2.3-2.5. The rudder force and moment equations are shown in terms of the rudder and hull interaction coefficients, the normal non dimensionalised rudder force F'_N and rudder angle as,

$$X'_R = -(1-t_R)F'_N \sin\delta \qquad 2.24.a$$

$$Y'_R = -(1+a_H)F'_N \cos\delta \qquad 2.24.b$$

$$N'_R = -(x'_R + a_H x'_H)F'_N \cos\delta \qquad 2.24.c$$

The other terms are described below,

F'_N Normal Force on rudder. (Non dimensionalised.)

t_R Coefficient of additional drag.

x'_R Distance from cog to center of lateral force. (Non dimensionalised.)

a_H Ratio of additional lateral force.

x'_H Distance from cog to center of additional lateral force. (Non dimensionalised.)

δ Rudder angle.

a_H and x'_H are the interaction coefficients of hull and rudder and are obtained from experiment but can be estimated from figures 2.4. t_R is determined from the empirical formula.

$$t_R = 1-(0.28C_B + 0.55)$$

The non dimensionalised normal force can be written as,

$$F'_N = \left(\frac{A_R}{LD}\right) C_N U_R^2 \sin\alpha_R \qquad 2.25$$

The terms in the above equation are described as,

$$C_N = 6.13\frac{K_R}{K_R + 2.25}$$

$$U_R^2 = (1-\omega_R)^2(1 + C\cdot g(s))$$

$$g(s) = \eta K\{2-(2-K)s\}\frac{s}{(1-s)^2}$$

$$\beta'_R = \beta - 2x'_R \cdot r'$$

$$x'_R \approx -0.5$$

$$\omega_P = \omega_{PO}\exp(-4\,\beta_R^2)$$

$$K = 0.6\frac{(1-\omega_P)}{(1-\omega_R)}$$

$$\omega_R = \omega_{RO}\frac{\omega_P}{\omega_{PO}}$$

$$\alpha_R = \delta - \gamma\cdot\beta'_R$$

$$\eta = \frac{D_P}{h_R}$$

$$s = 1-(1-\omega_P)\frac{U\cos\beta}{nP}$$

A_R	Rudder area
U_R	Effective rudder inflow velocity
K_R	Rudder aspect ratio
α_R	Effective rudder inflow angle
n	Propeller revolutions
P	Propeller pitch
ω_P	Effective wake fraction at propeller
s	Slip ratio
ω_{RO}	Effective wake fraction at rudder going straight ahead
β'_R	Effective drift angle at rudder
h_R	Rudder span
ω_{PO}	Effective wake fraction at propeller going straight ahead

γ Flow straightening coefficient

C Coefficient of Port and Starboard turn

ε Wake fraction ratio

The following approximations can be used if experimental data is not available,

$$\omega_{PO} = 0.5C_B - 0.05 \qquad 2.26$$

$$\gamma = -22.2\left(\frac{C_B B}{L}\right)^2 + 0.02\left(\frac{C_B B}{L}\right) + 0.68 \qquad 2.27$$

$$\varepsilon = \frac{1-\omega_{RO}}{1-\omega_{PO}} = -156.2\left(\frac{C_B B}{L}\right)^2 + 41.6\left(\frac{C_B B}{L}\right) - 1.76 \qquad 2.28$$

It is stated by Kijima Refs. 2.3, 2.4, that the flow straightening coefficient γ and wake fraction ratio ε, have the greatest effect on the simulation of the turning ability of a vessel. These effects will be studied and the results will be included in the discussions. The determination of the interaction coefficients, a_H, x'_H, γ, ω_{PO}, ω_{RO} and ε for the model simulation are obtained through model tests under controlled environment. In the case of a full scale vessel, these interaction coefficients will be affected by the vessel scale. It is very difficult to obtain these full scale interaction coefficients as there will be the additional problems of external environmental factors such as wind and current as well as the control of the full scale ship. It is recommended that the model interaction coefficients are used in the simulations with full scale ship dimensions until such time as the full scale interactions are able to be modelled accurately. If the path of the full scale trajectory is known from sea trials, then the interaction coefficients of flow straightening γ and wake fraction ratio ε, may be varied to match the predicted trajectory by simulation to the full scale trials. There are obvious dangers in adjusting the simulations results to suit and as stated above, further work on the

accurate prediction of the full scale interactions is necessary. The matching technique will be employed in Chapter Five for the manoeuvring simulation of a heavy lift vessel.

2.4. Determination of Rudder Area.

The area of the rudder is determined using the DNV minimum rudder area equation Ref. 2.10.

$$A_R = LD\frac{\left(1+25\left(B/L\right)^2\right)}{100} \qquad 2.29$$

In the simulation program the geometry of the rudder assumes an aspect ratio of 1.4 and a taper ratio of 0.8. The rudder span, root, and tip can be obtained from the following simple equations,

$$R_{SPAN} = \sqrt{\frac{1.4A_R}{P_N}}$$

$$R_{ROOT} = \frac{2A_R}{1.8P_N R_{SPAN}}$$

$$R_{TIP} = 0.8R_{ROOT}$$

A_R Rudder Area
P_N Propeller Number
R_{SPAN} Rudder Span
R_{ROOT} Rudder Root
R_{TIP} Rudder Tip

2.5 Discussion of Results.

The discussions presented here are for the manoeuvring simulation of a model tanker. The simulations carried out in this chapter were purely to demonstrate the behaviour of the simulation model to variations of the parameters of forward velocity, load condition, rudder area and rudder deflection. In addition to this, attention is also drawn to the effects of varying the interaction coefficients namely the flow straightening coefficient and the wake ratio.

2.5.1 Variation in Vessel Velocity.

The effect of increased velocity of the vessel are shown in figs. 2.6. The model velocities chosen were 0.36, 0.54, 0.72, 0.81, 0.9 m/s which correspond to full scale 8, 12, 16, 18, 20 knots, Table 2.1. The rudder deflection is 20 degrees to starboard. This trajectory figure clearly shows that increased speed has little effect on the turning circle dimensions. This fact is stated in Ref. 2.10 and can be seen in Ref. 2.17. The velocity ratio of the five different velocities are the same, as are the final drift and angular velocities. It is clear however that the time taken to reach these steady turning conditions decreases with increased velocity. The effect of increased speed would however increase the vessel heel in the turn. This simulation model does not however include roll in the equations of motion and therefore the results of the turning circle may be different from those simulated here for the larger velocities.

2.5.2 Variation in Rudder Area.

For the increased rudder area, the turning circle advance, tactical diameter and transfer are reduced as one would naturally expect. The time of the turn is not affected greatly by the increased rudder area however. This behaviour is clearly shown in fig. 2.7a and is due to the increased speed loss for the increase in rudder area. The rudder area varies as 0.5, 0.75, 1.0, 1.5, 2.0 of the minimum rudder area equation 2.29.

2.5.3 Variation in Rudder Deflection.

The increased rudder deflection reduces the turning circle dimensions dramatically. The speed loss, drift angle and angular velocity are significantly increased as shown in figs. 2.8. The rudder deflection angles are 5, 10, 15, 25, 35 degrees.

2.5.4 Variation in Wake Fraction at the Rudder.

The interaction coefficients of wake fraction at the rudder and the flow straightening coefficient γ, are investigated figs. 2.9-2.10. It was concluded by Kijima et al., Refs. 2.3, 2.4, that an accurate determination of these coefficients was essential for the prediction of the full scale turning simulations. The effects of varying the interaction coefficients are included to emphasise these conclusions drawn by the above authors. As can be seen in the trajectory plot figure 2.9a, the increased wake fraction at the rudder increases the advance but has little effect on the transfer and the tactical diameter. The time of the manoeuvre is unaffected by this parameter. The speed loss ratio, drift, and angular velocity are very similar for the values of wake fraction at the rudder. The values of wake fraction were 0.3, 0.4, 0.5, 0.6, 0.7.

2.5.5 Variation in Flow Straightening Coefficient.

The flow straightening coefficient values were 0.2, 0.25, 0.3, 0.35, 0.4. It is clear from the rudder model that these interaction coefficient values have a greater effect on the turning trajectory. It is essential that accurate values should be obtained for model and full scale vessels to obtain an accurate turning simulation. This increased flow straightening coefficient γ increases the turning circle dimensions. There is also a marked difference between speed loss ratio, drift angle and angular velocity.

2.5.6 Variation in Load Condition.

The three load conditions simulated are given in Table 2.1 for an

approach speed of 0.36m/s and a 20 degrees starboard rudder. The fully loaded vessel has a slightly increased advance than in the ballast condition, figure 2.11a. The tactical diameter and transfer seem to be unaffected by the load condition. The velocity loss ratio is approximately the same for each of the load conditions. There is however, an increased drift for reduction in loading, figure 2.11b. This is something we would expect as the vessel will be easier to manoeuvre in the lighter condition. The angular velocity appears to be unaffected by loading condition as does the heading angle.

Esso Osaka Full Dimensions

		Propeller	
Length B.P. (m)	325	Diameter (m)	9.1
Breadth (m)	53	Pitch (m)	6.507
Draft (m)	22.05	Number of	1
Block Coefficient	0.831		
Transverse Windage Area (m^2)		3160	
Longitudinal Windage Area (m^2)		1130	

Esso Osaka Model Dimensions

Scale 1:130	Full	Half	Ballast
Length (m)	2.5	2.5	2.5
Breadth (m)	0.408	0.408	0.408
Draft (m)	0.17	0.1367	0.104
Block Coefficient	0.831	0.8185	0.797

Propeller		Interaction	
Diameter (m)	0.07	ah	0.369
Pitch (m)	0.05	tr	0.2
C1	0.22	gamma	0.3
C2	-0.131	wpo	0.54
C3	-0.158	wro	0.35

Table 2.1

Coordinate System.

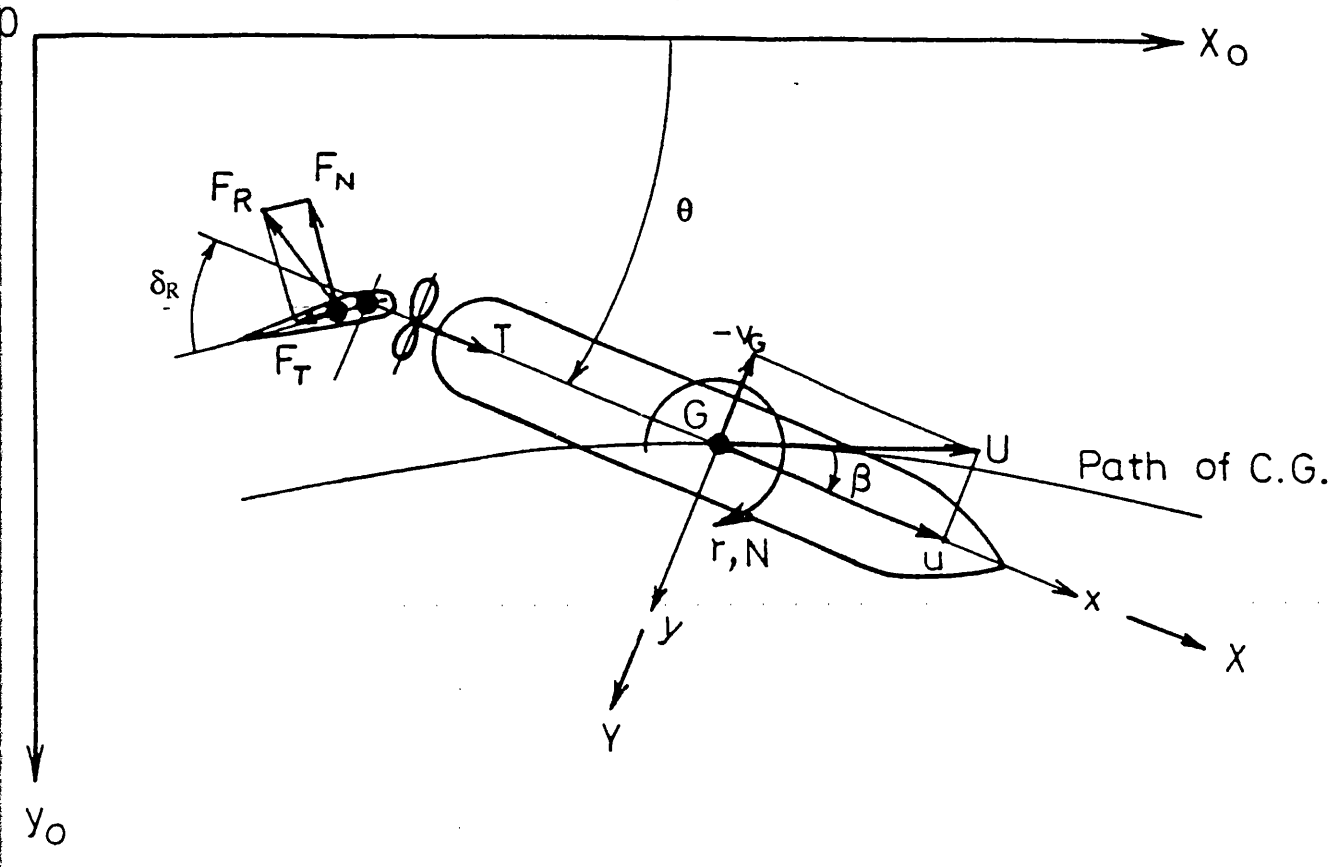

Figure 2.1

Lambs Coefficients of Accession to Inertia.

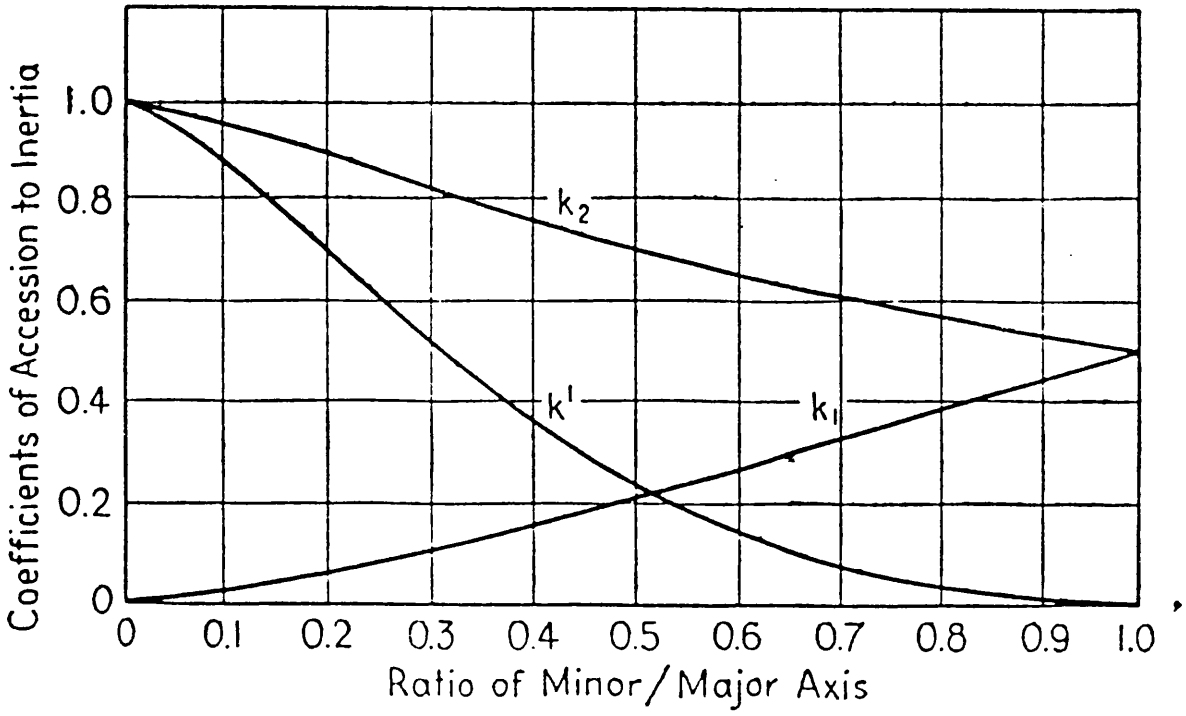

Figure from Ref. 2.8

Figure 2.2

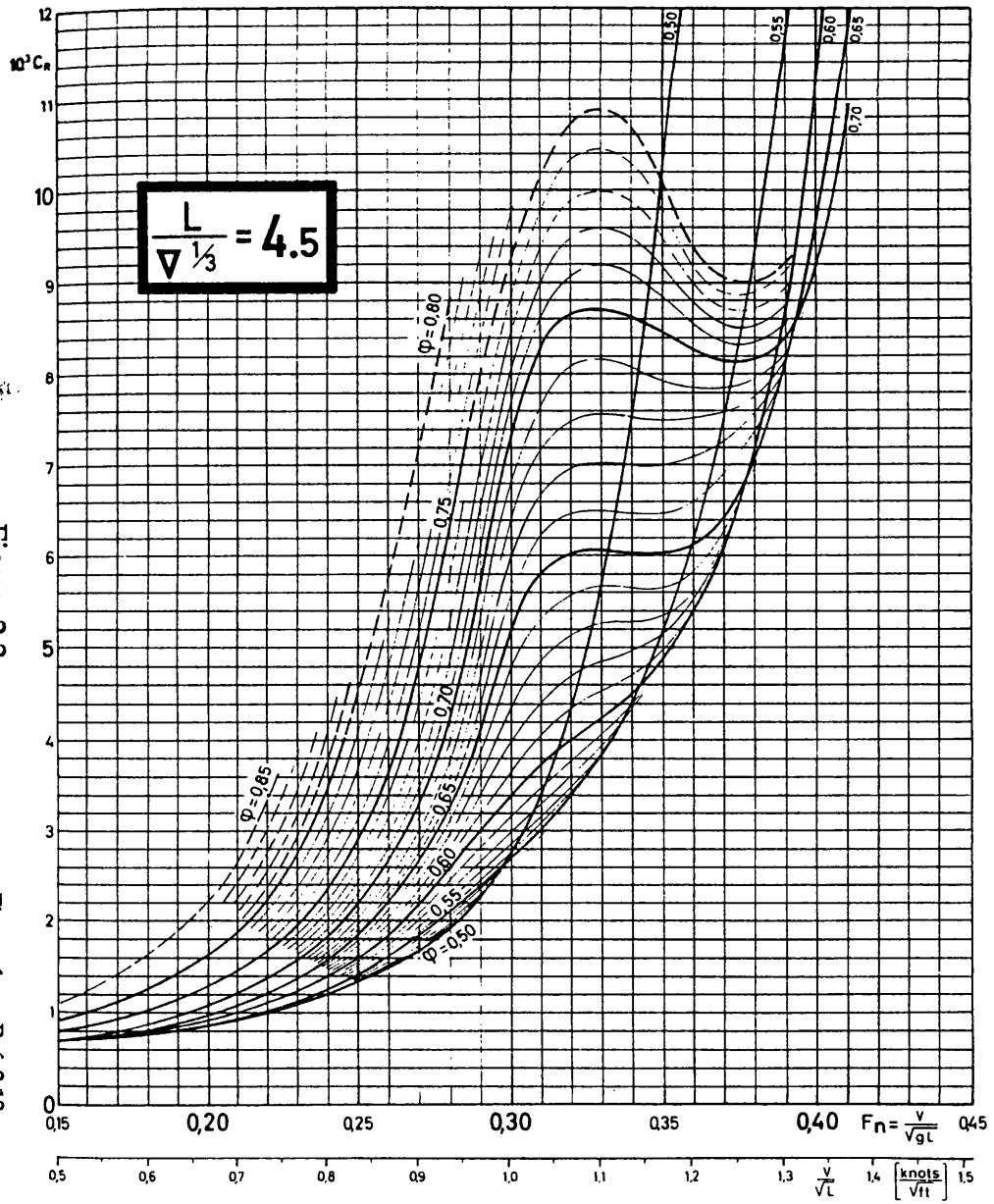

Figure 2.3a Residuary resistance coefficient versus speed–length ratio for different values of longitudinal prismatic coefficient.

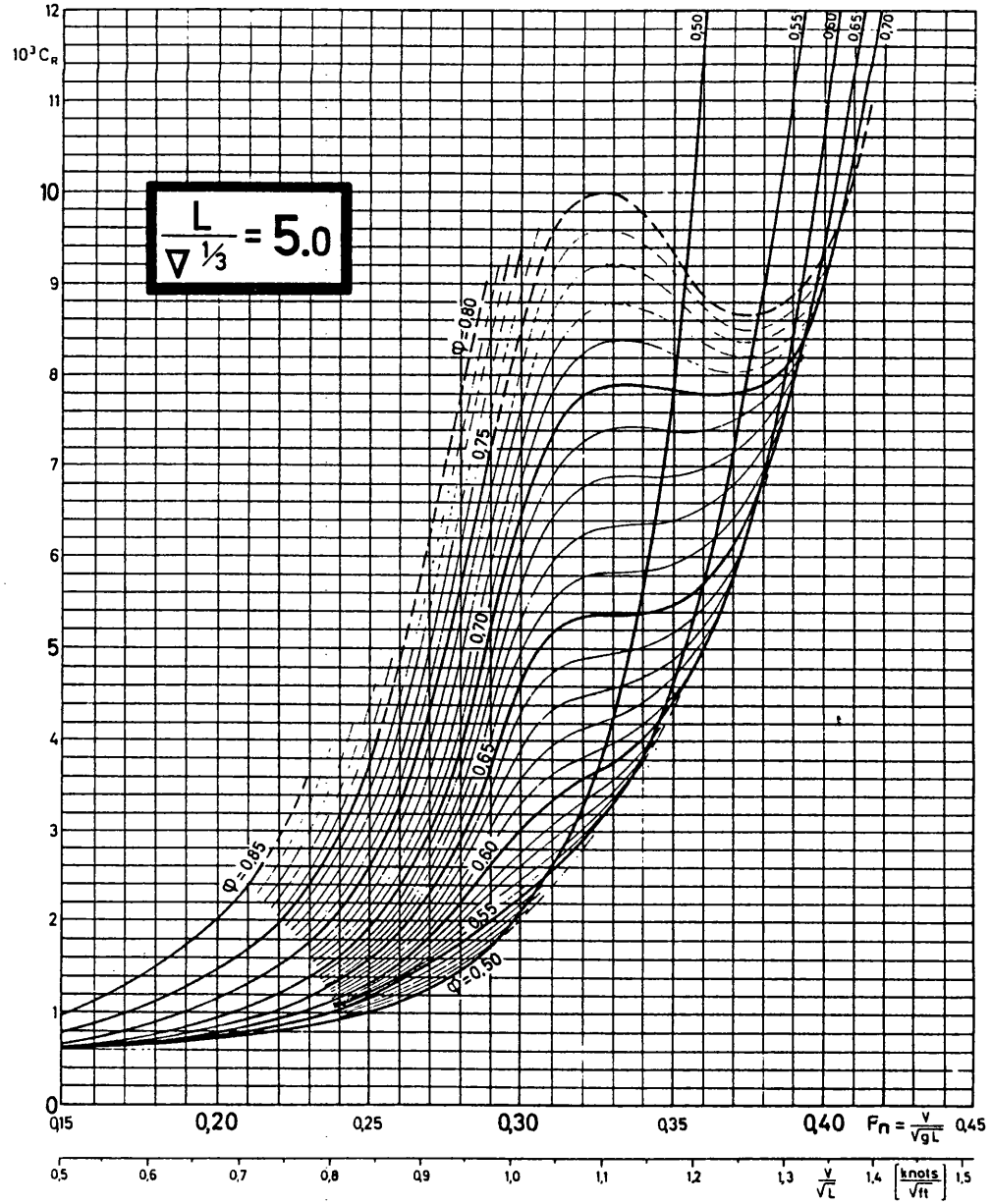

Figure from Ref. 2.13 Residuary resistance coefficient versus speed–length ratio for different values of longitudinal prismatic coefficient.

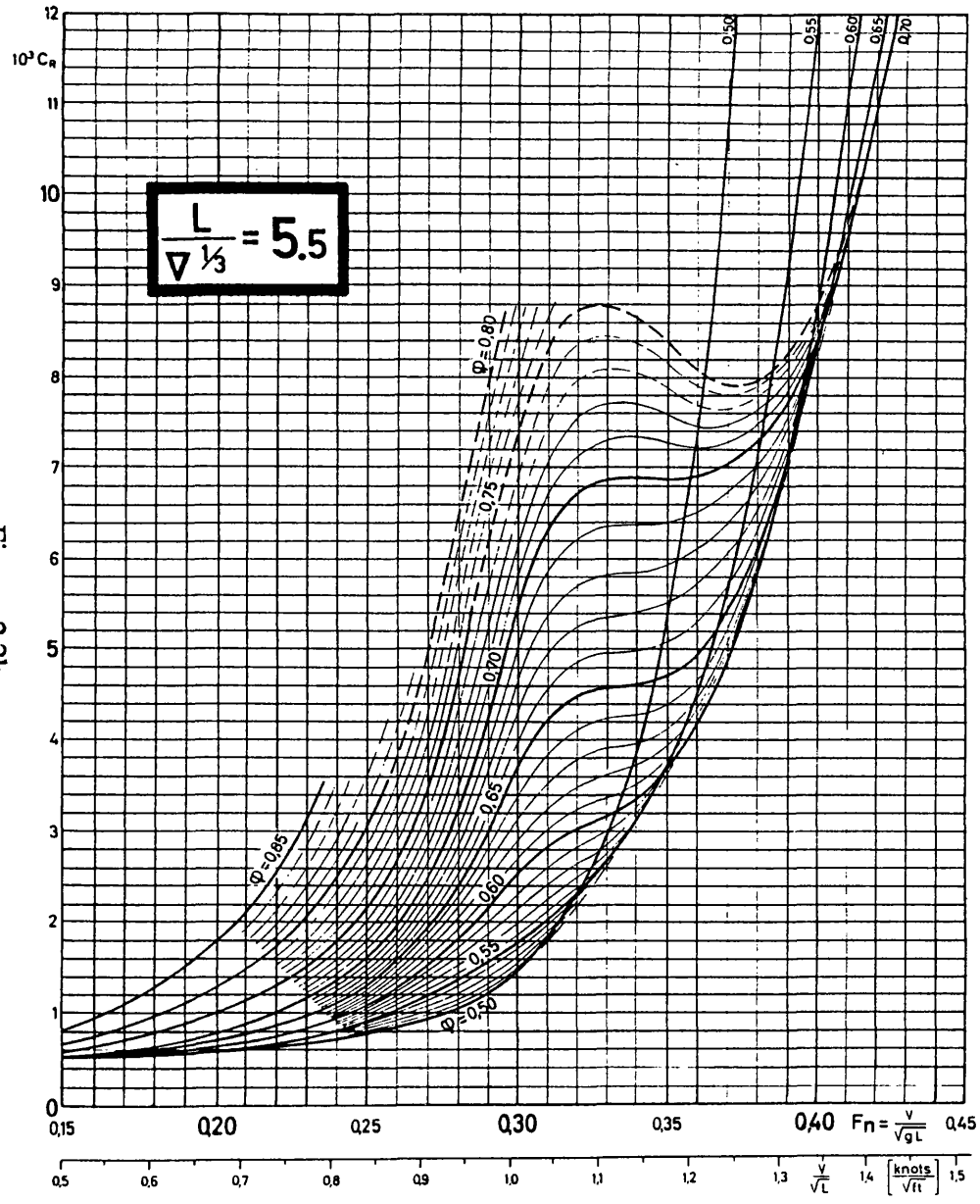

Residuary resistance coefficient versus speed–length ratio for different values of longitudinal prismatic coefficient.

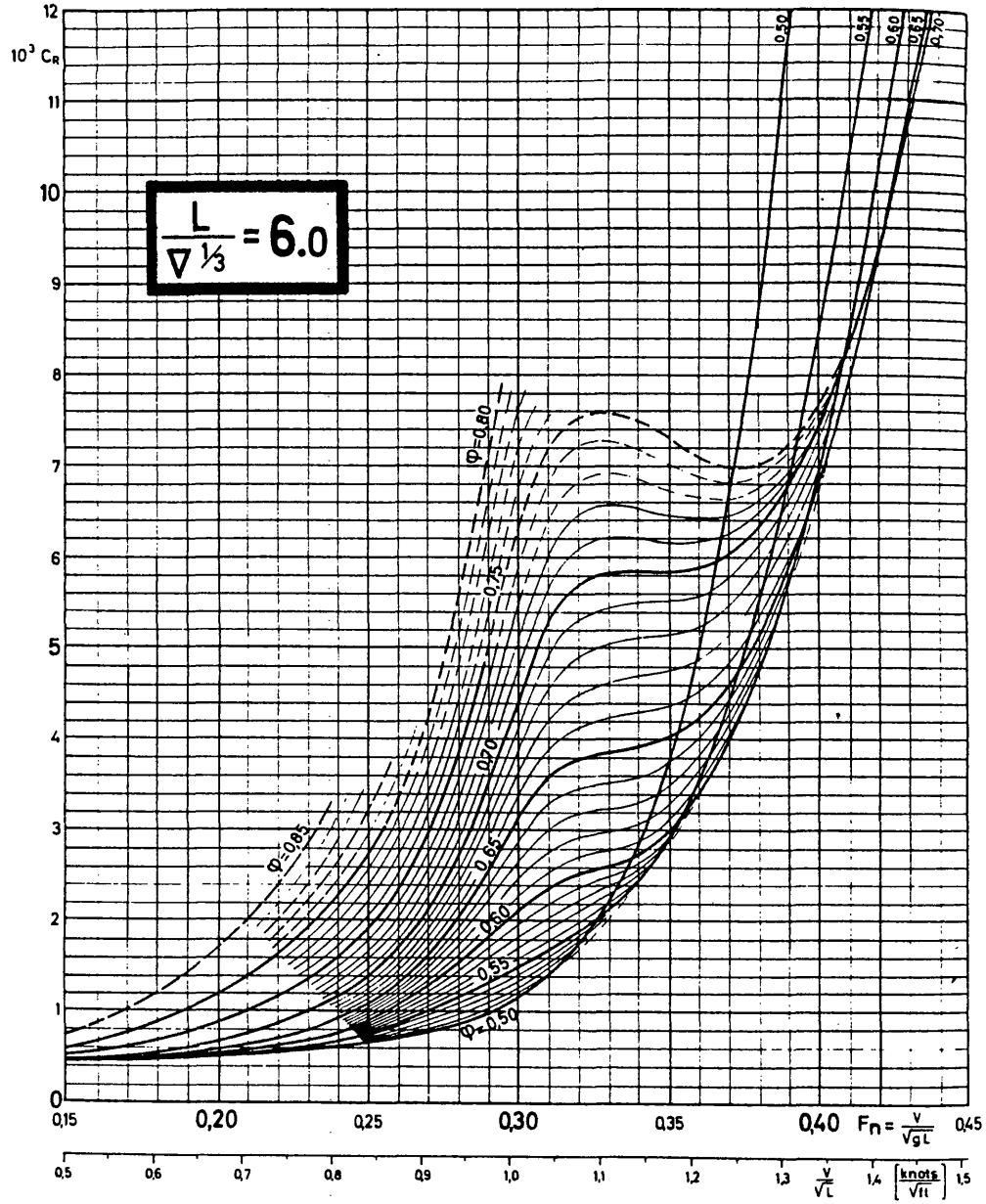

Residuary resistance coefficient versus speed–length ratio for different values of longitudinal prismatic coefficient.

Figure 2.3b

Figure from Ref. 2.13

Rudder and Hull Interaction

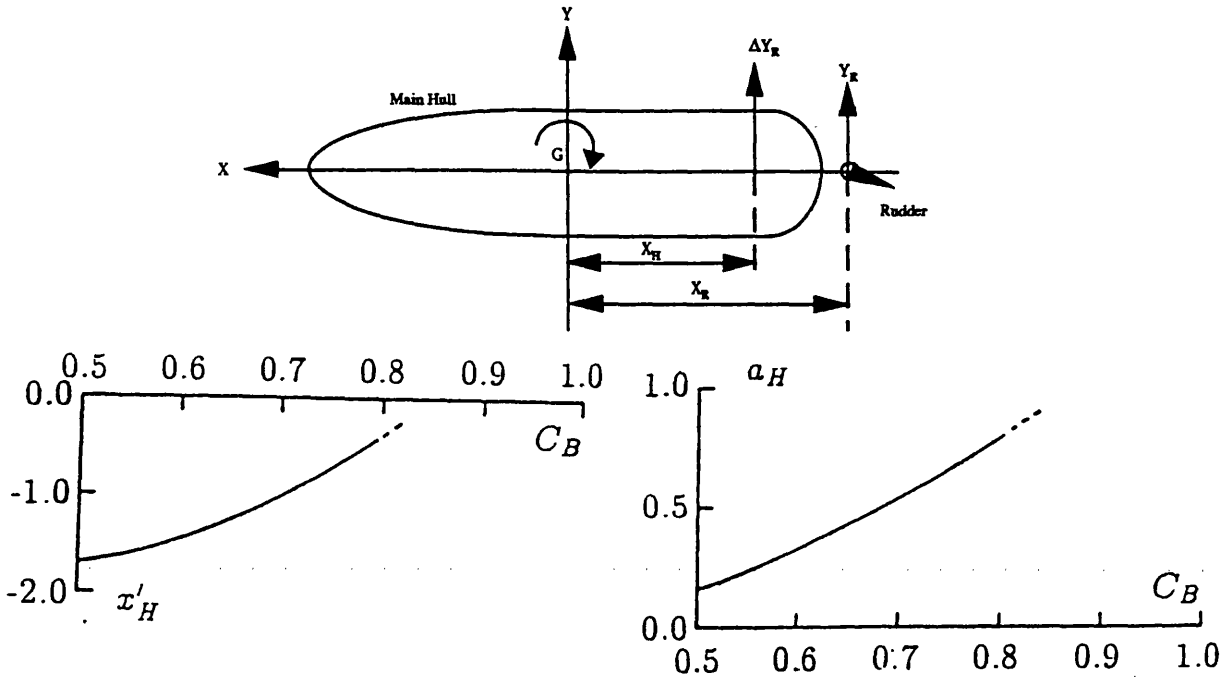

The interaction force coefficients a_H and x_H.

Figures 2.4

Trajectory and Course Angle

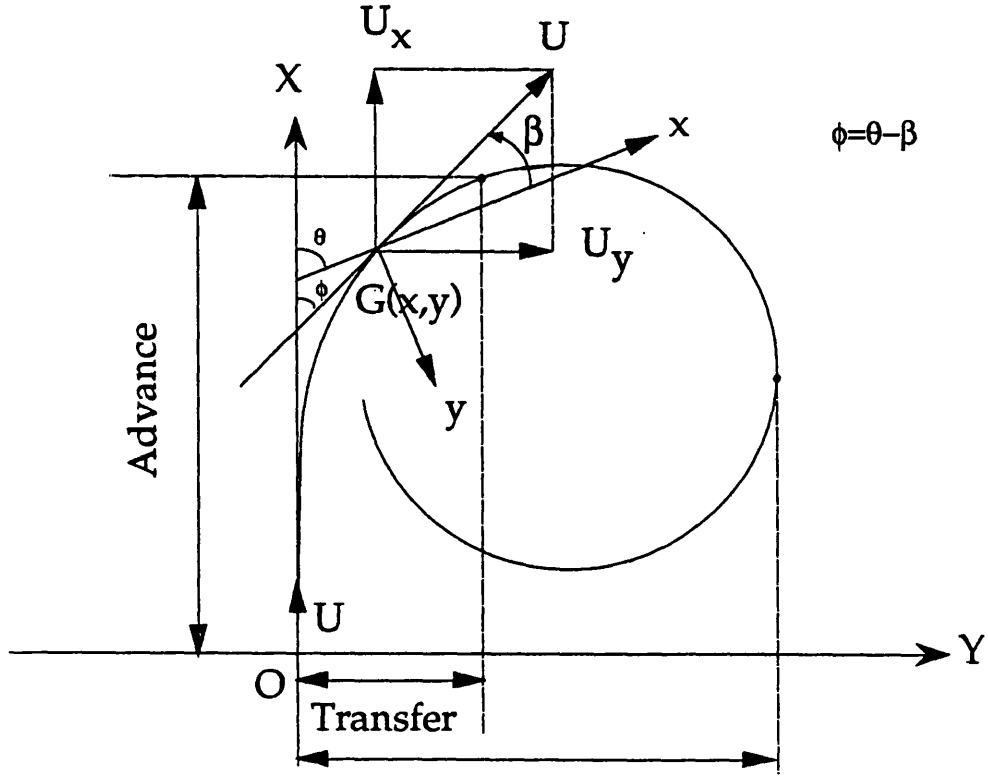

Figure 2.5

ESSO OSAKA MODEL TRAJECTORY

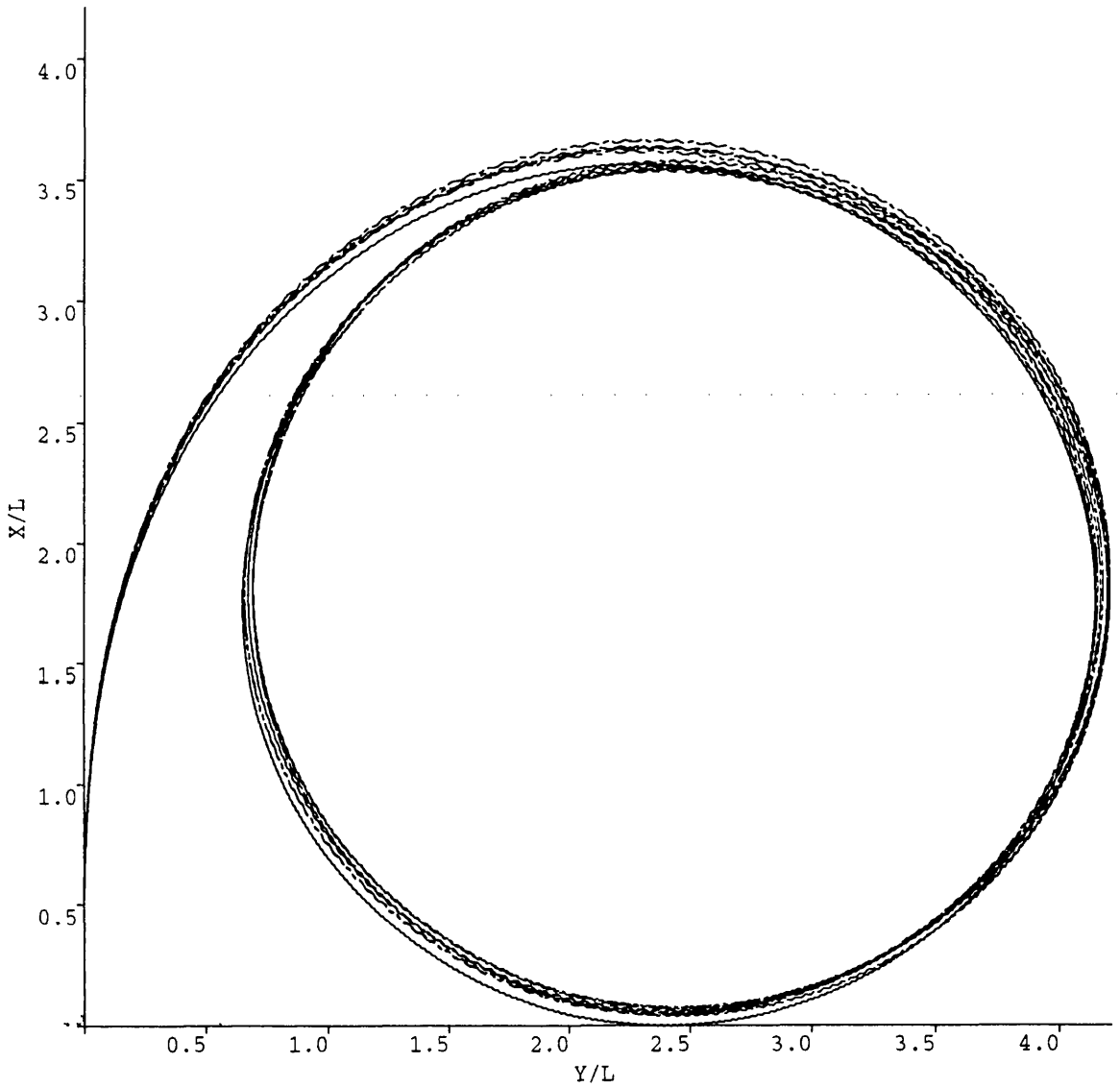

Model Velocities. 0.36, 0.54, 0.72, 0.81, 0.9 m/s
Rudder Angle. 20 Degrees Starboard
Condition. Full

Figure 2.6a

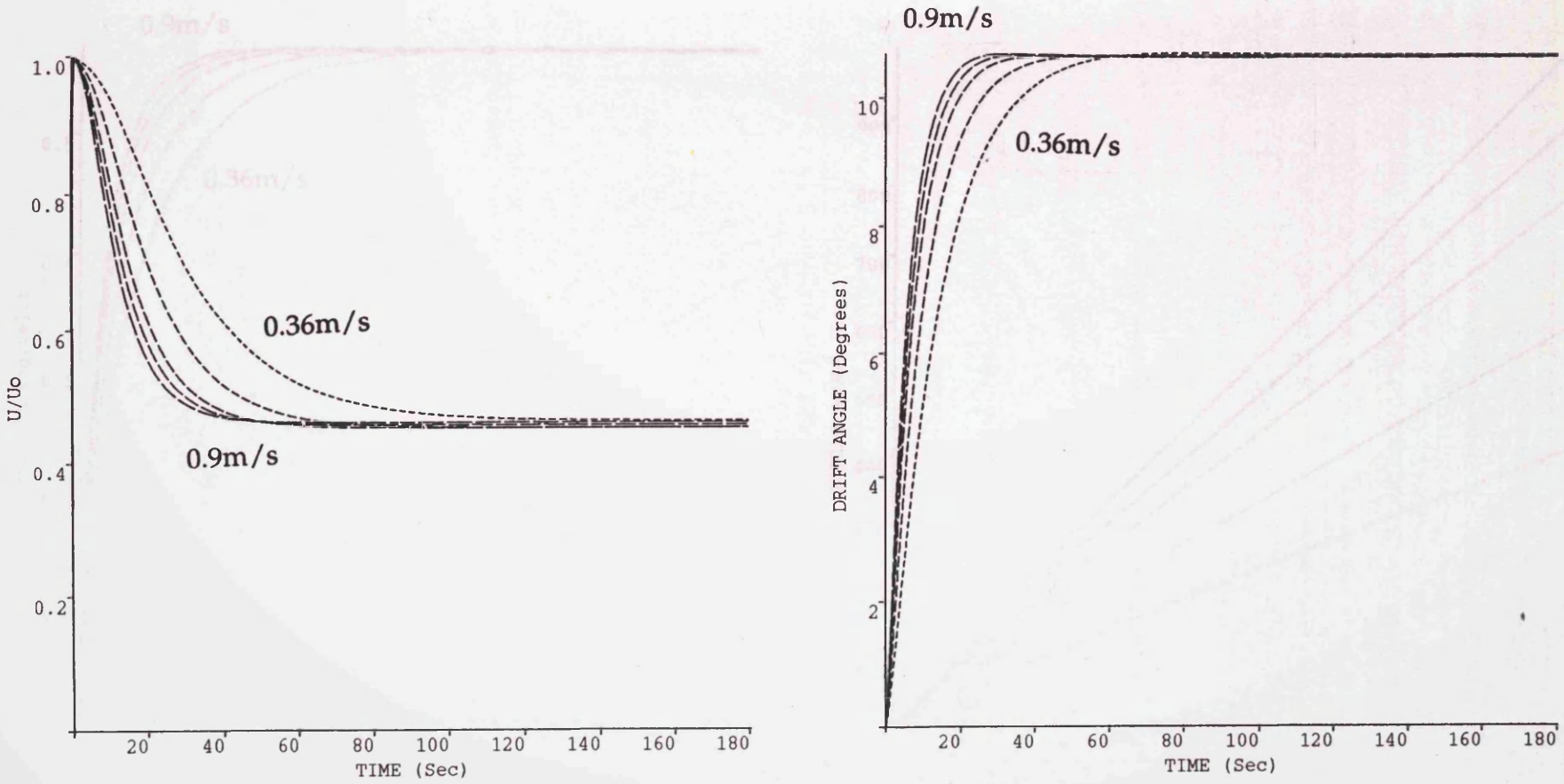

Model Velocities. 0.36, 0.54, 0.72, 0.81, 0.9 m/s
Rudder Angle. 20 Degrees Starboard
Condition. Full

Figure 2.6b

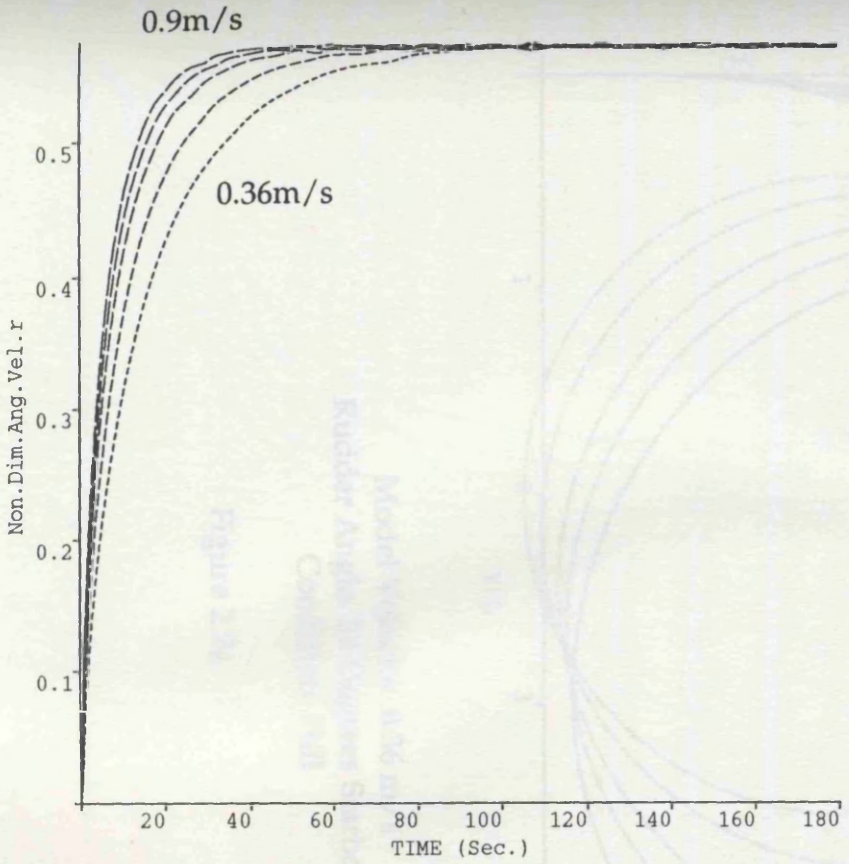

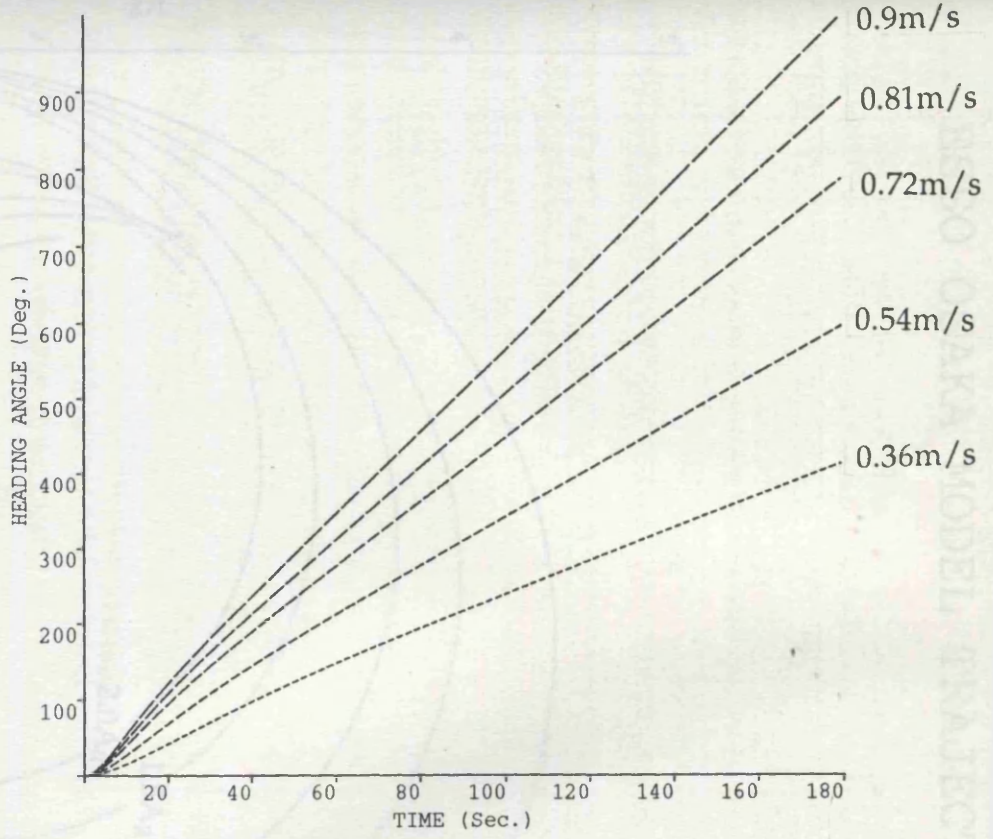

Model Velocities. 0.36, 0.54, 0.72, 0.81, 0.9 m/s
Rudder Angle. 20 Degrees Starboard
Condition. Full

Figure 2.6c

ESSO OSAKA MODEL TRAJECTORY

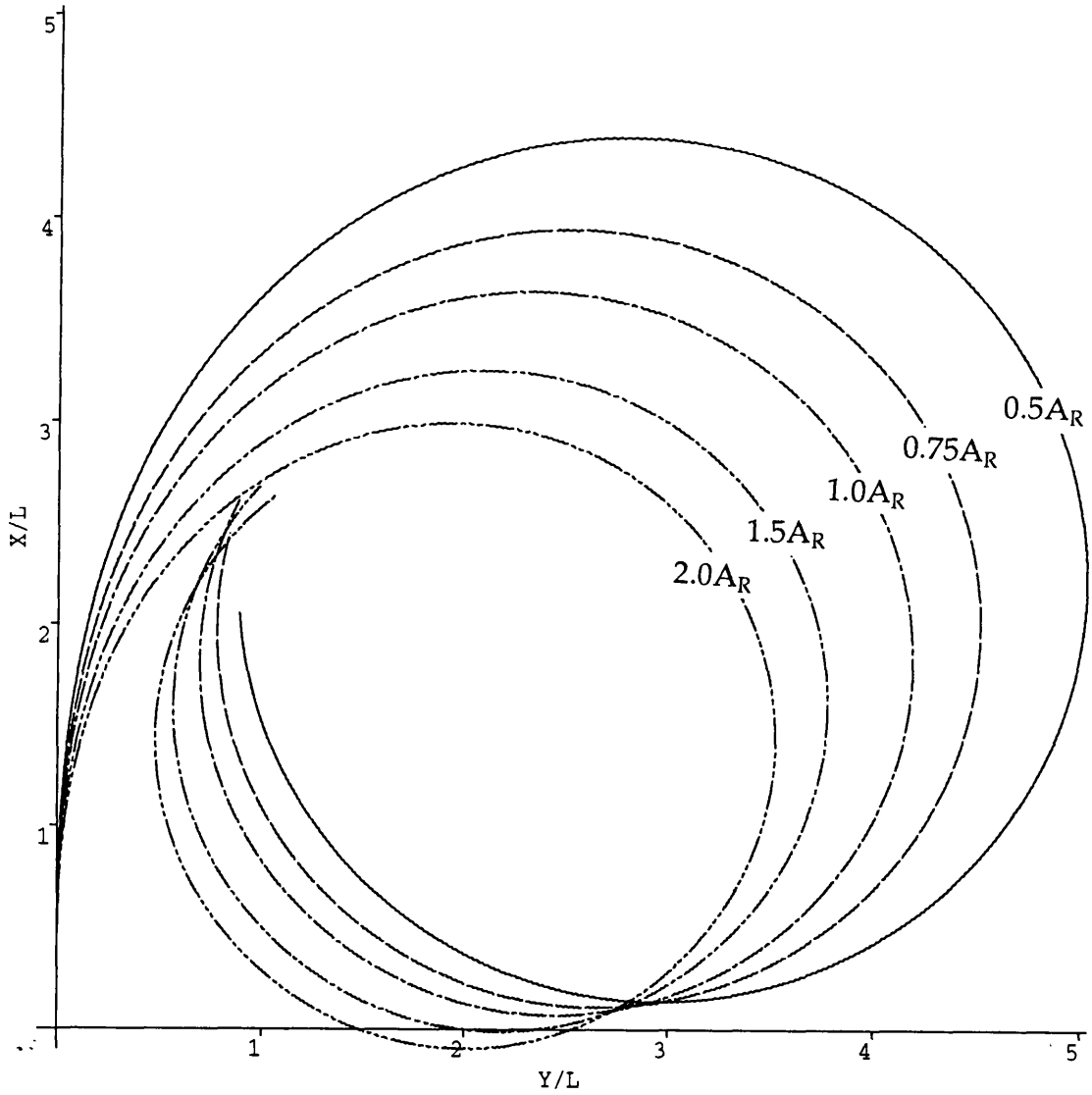

Model Velocity. 0.36 m/s
Rudder Angle. 20 Degrees Starboard
Condition. Full

Figure 2.7a

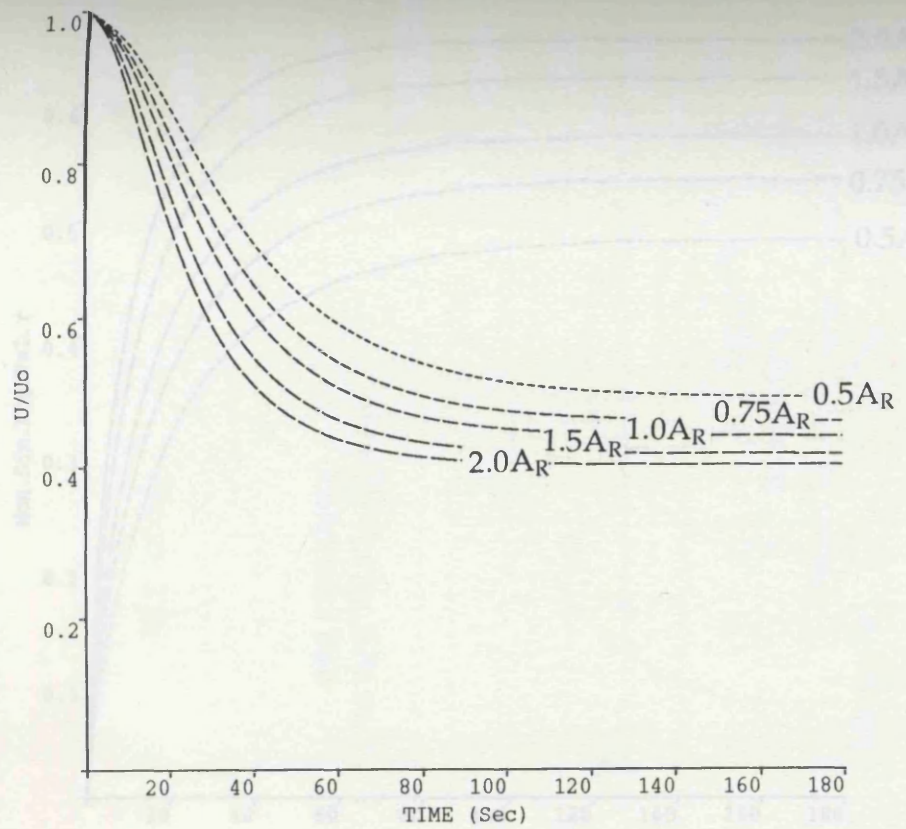

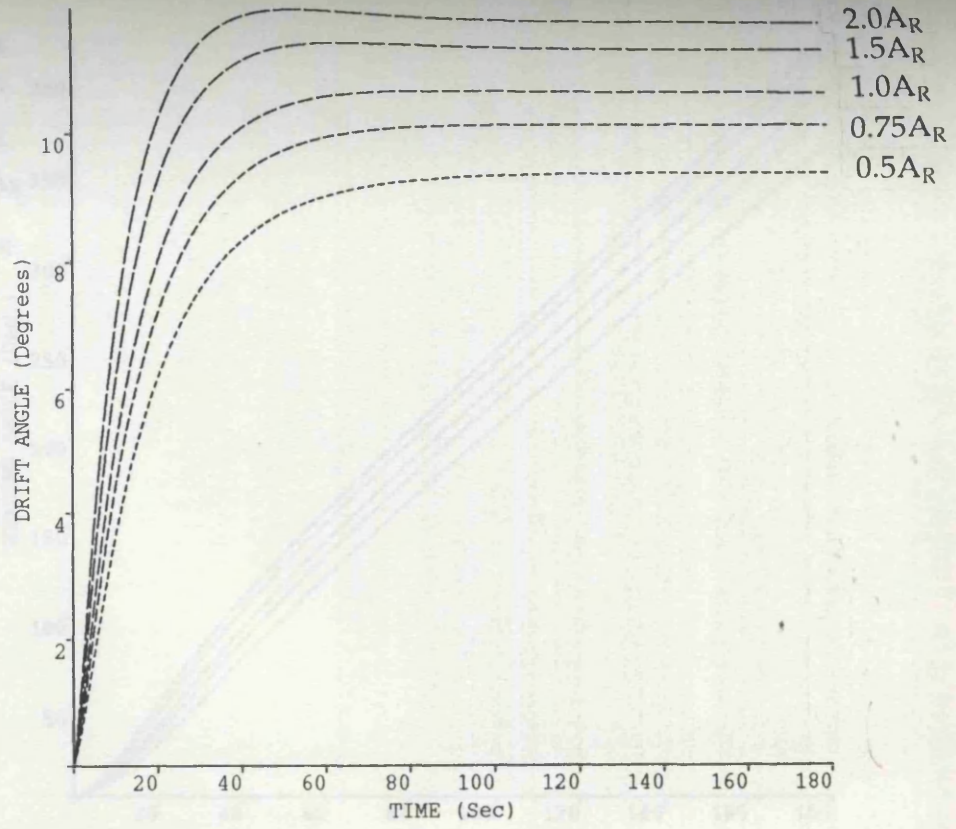

Model Velocity. 0.36 m/s
Rudder Angle. 20 Degrees Starboard
Condition. Full

Figure 2.7b

ANGULAR VELOCITY AND HEADING ANGLE

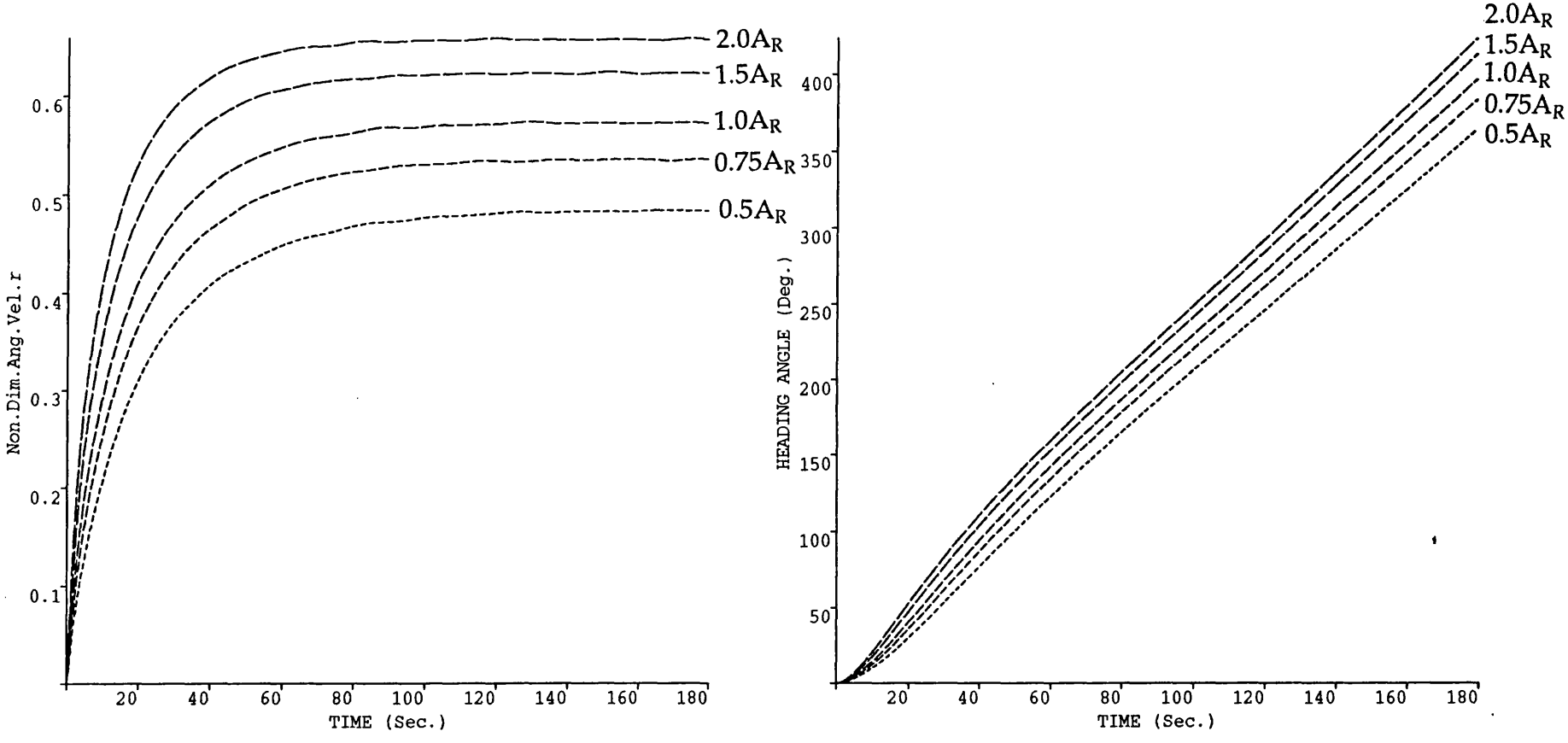

Model Velocity. 0.36 m/s
Rudder Angle. 20 Degrees Starboard
Condition. Full

Figure 2.7c

ESSO OSAKA MODEL TRAJECTORY

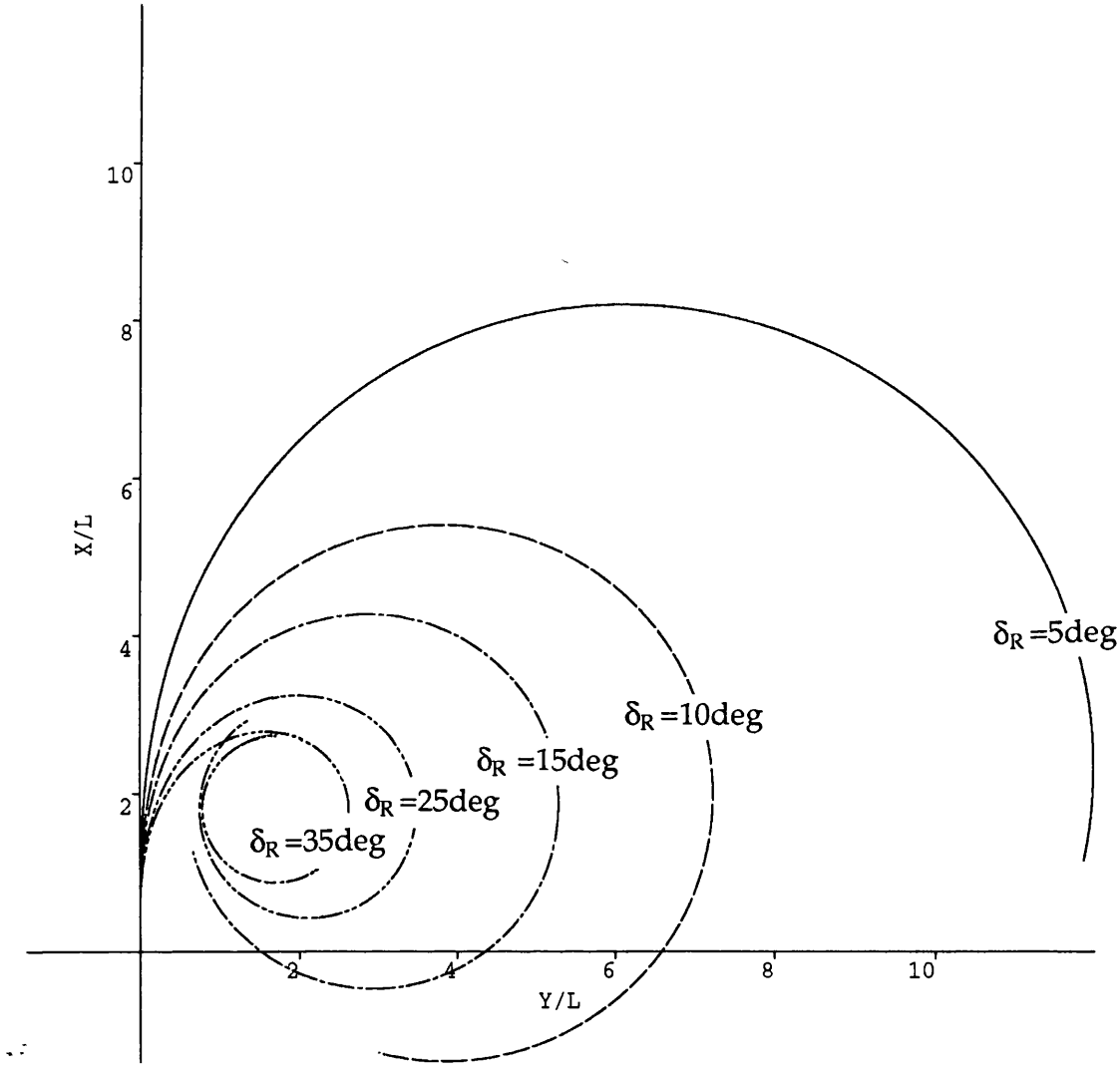

Model Velocity. 0.36 m/s
Condition. Full

Figure 2.8a

VELOCITY RATIO & DRIFT ANGLE

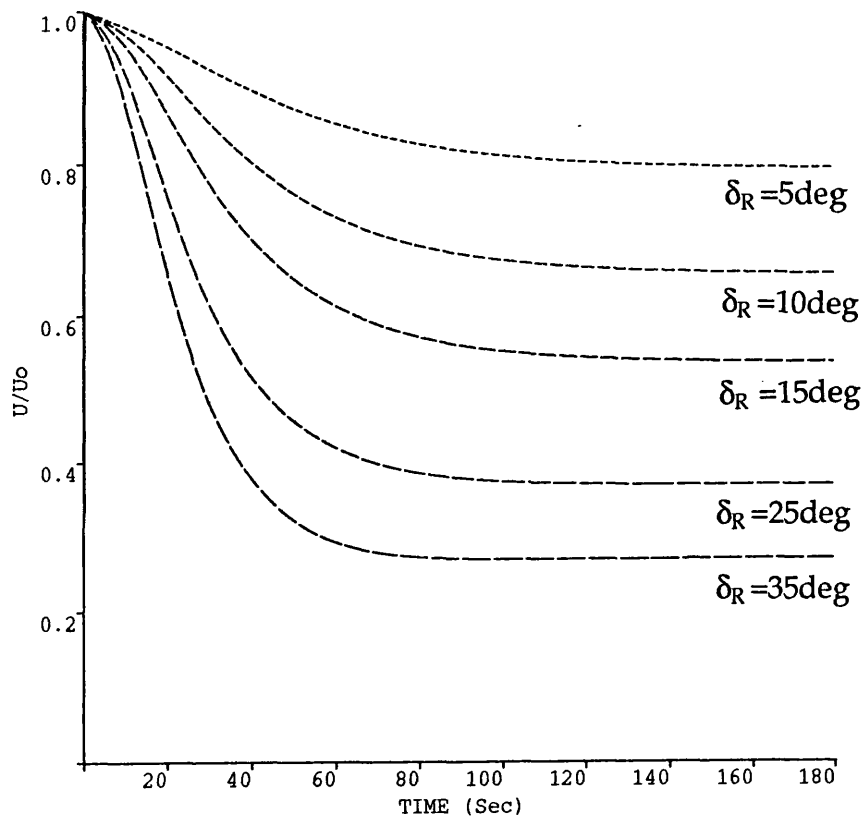

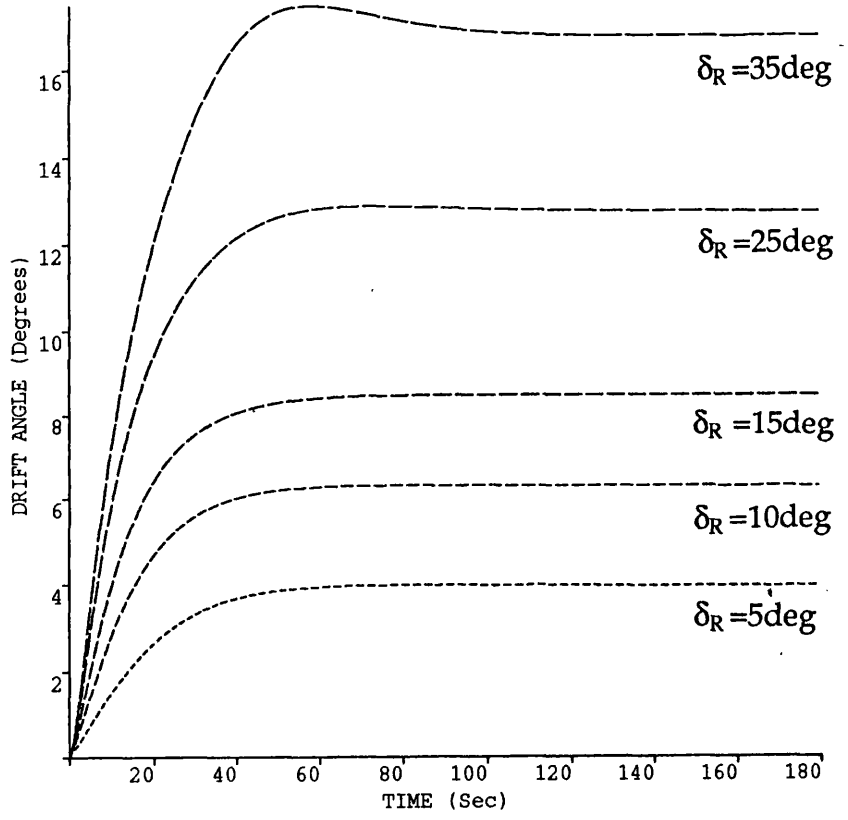

Model Velocity. 0.36 m/s
Condition. Full

Figure 2.8b

ANGULAR VELOCITY AND HEADING ANGLE

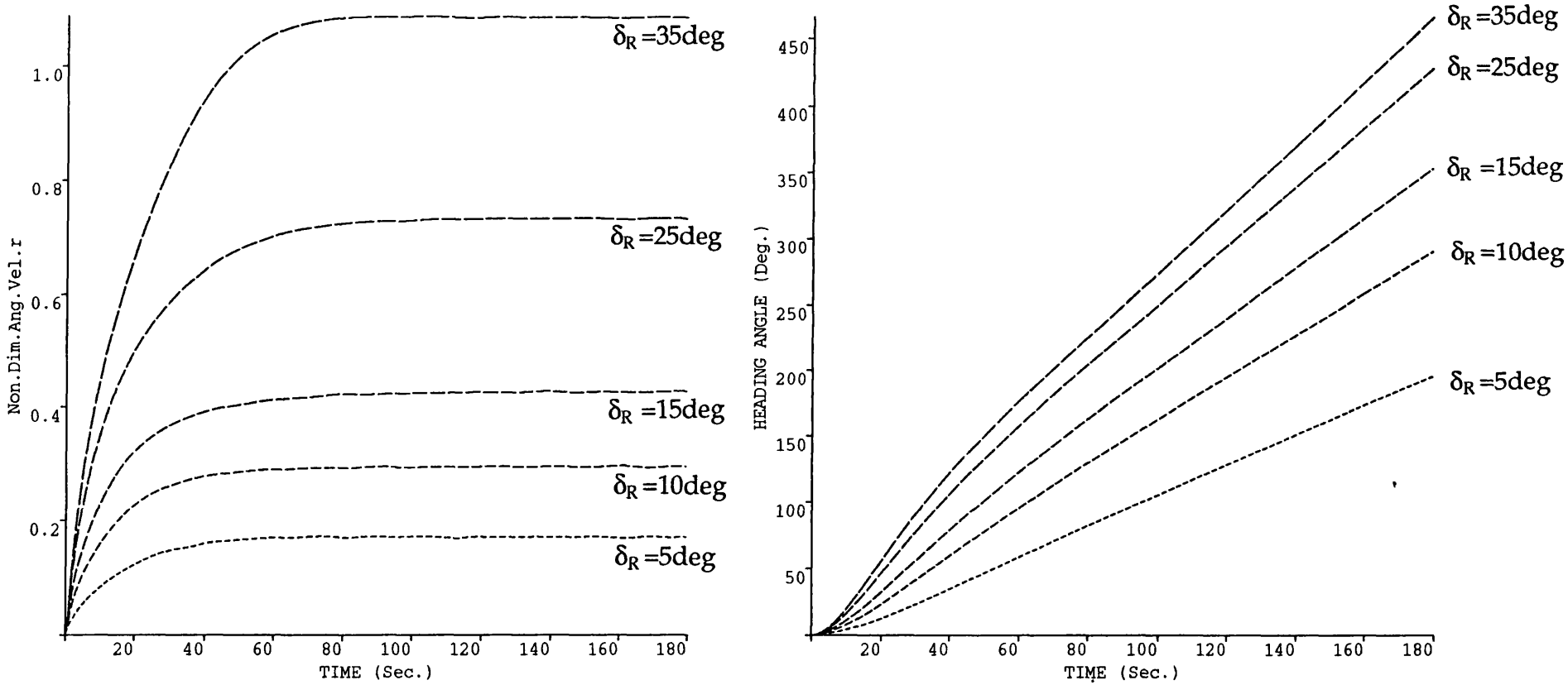

Model Velocity. 0.36 m/s
Condition. Full

Figure 2.8c

ESSO OSAKA MODEL TRAJECTORY

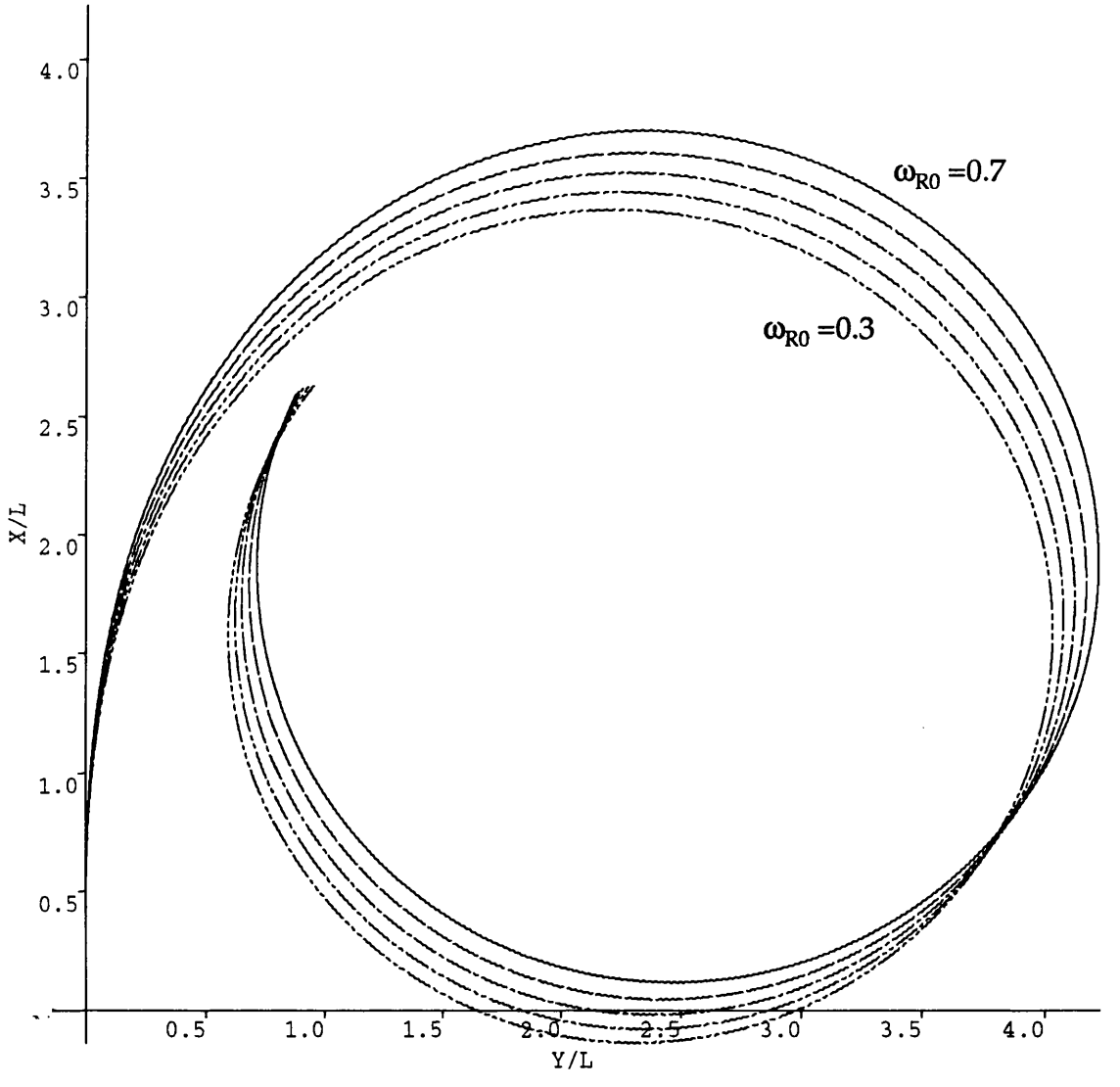

Figure 2.9a

Model Velocity. 0.36 m/s
Rudder Angle. 20 Degrees Starboard
Condition. Full
ω_{R0} . 0.3, 0.4, 0.5, 0.6, 0.7

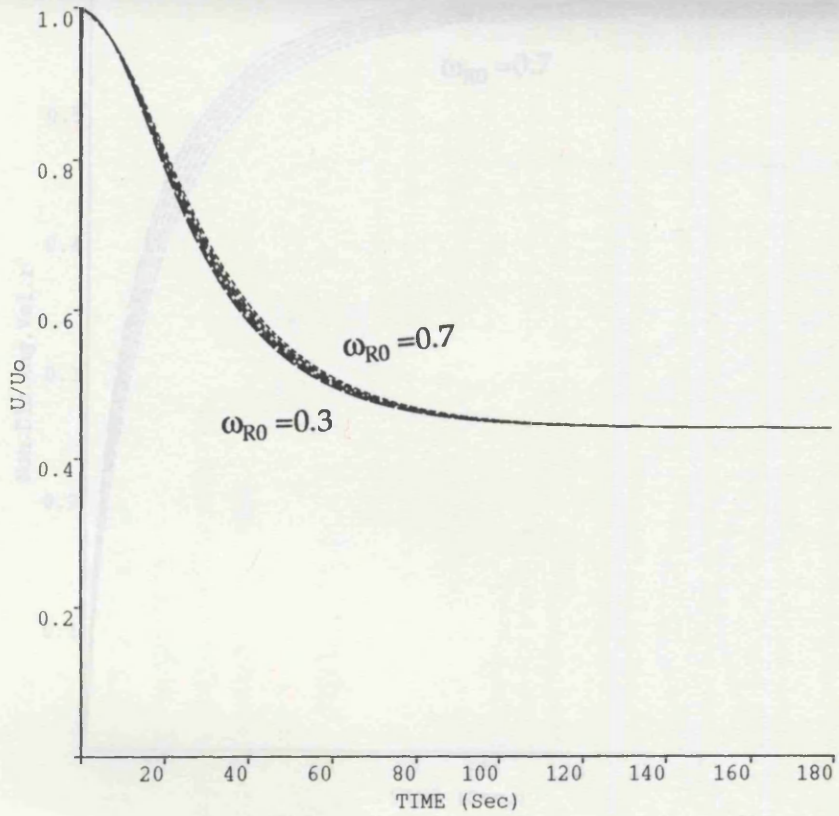

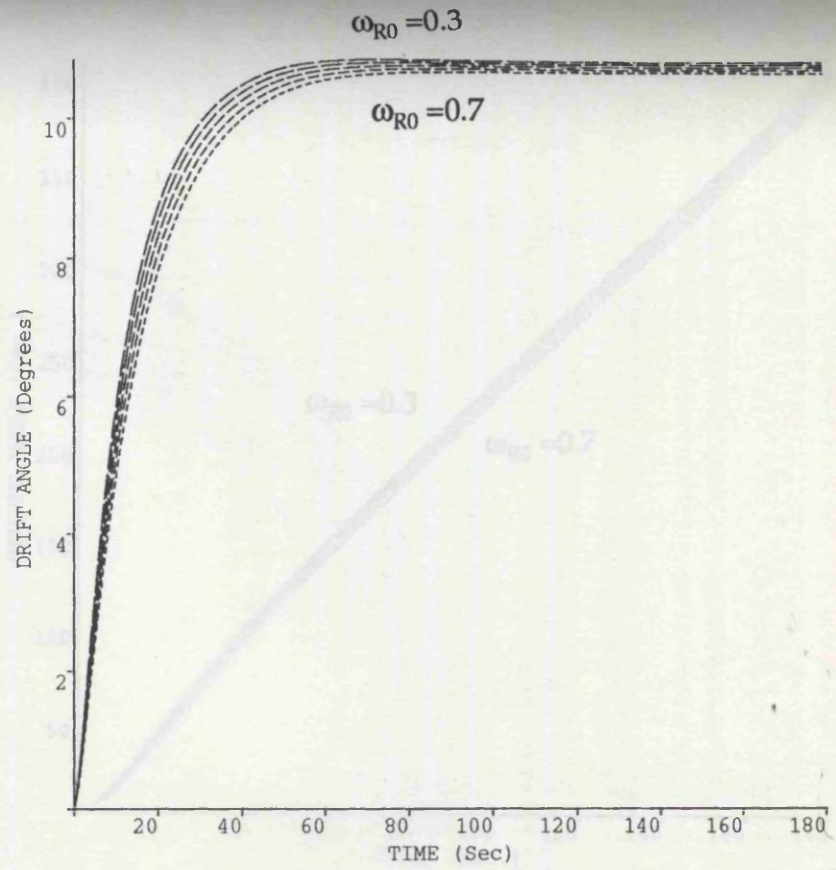

Figure 2.9b

Model Velocity. 0.36 m/s
Rudder Angle. 20 Degrees Starboard
Condition. Full
ω_{R0} . 0.3, 0.4, 0.5, 0.6, 0.7

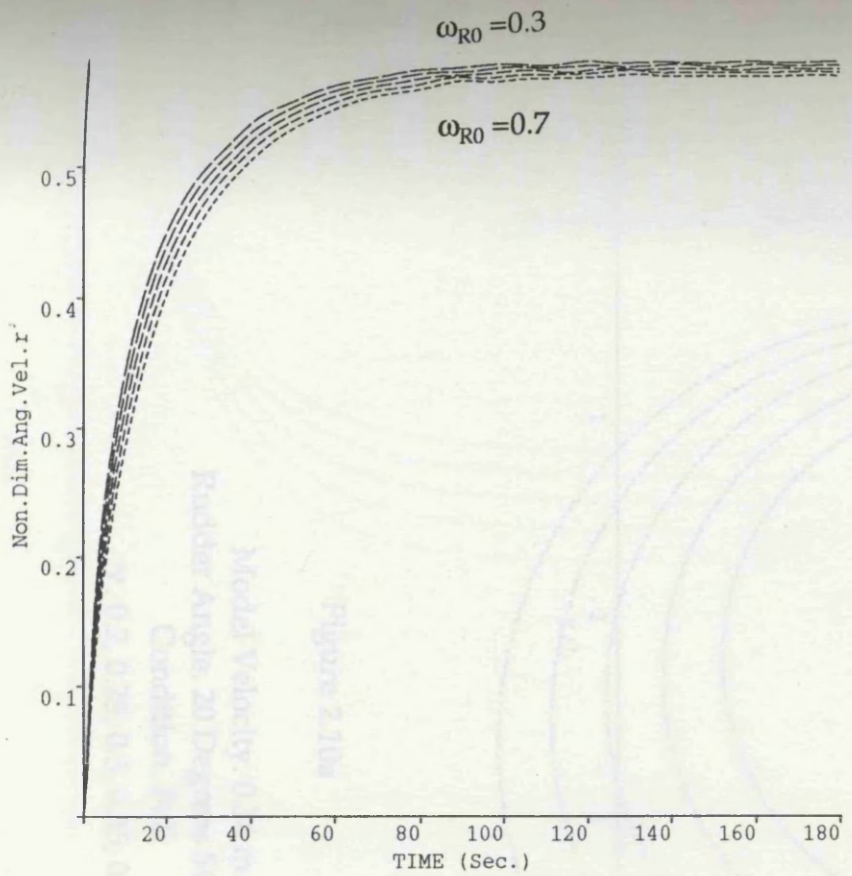

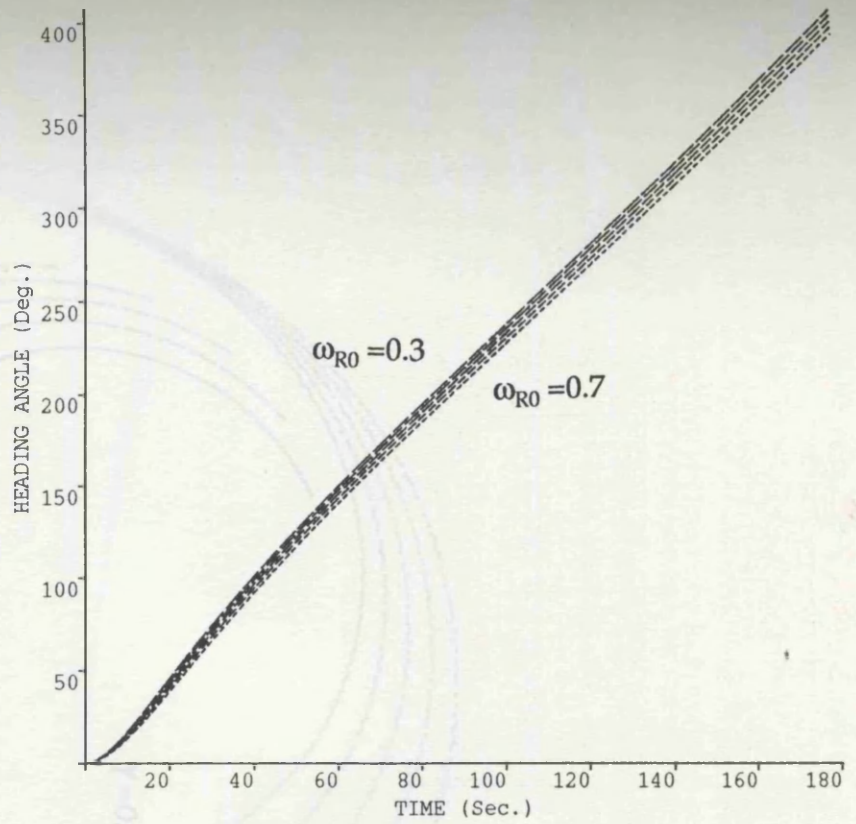

Figure 2.9c

Model Velocity. 0.36 m/s
Rudder Angle. 20 Degrees Starboard
Condition. Full
ω_{R0} . 0.3, 0.4, 0.5, 0.6, 0.7

ESSO OSAKA MODEL TRAJECTORY

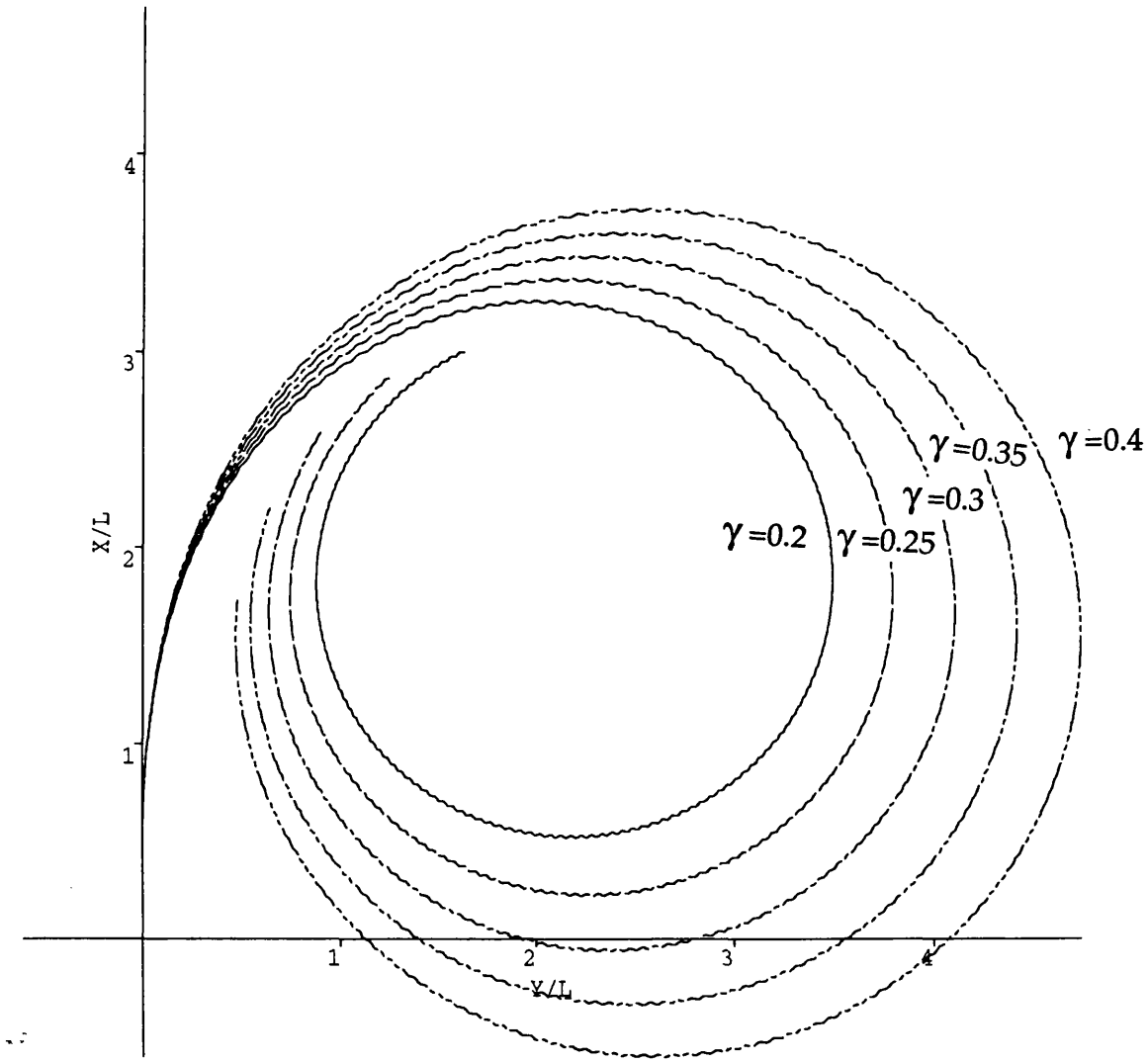

Figure 2.10a

Model Velocity. 0.36 m/s
Rudder Angle. 20 Degrees Starboard
Condition. Full
γ. 0.2, 0.25, 0.3, 0.35, 0.4

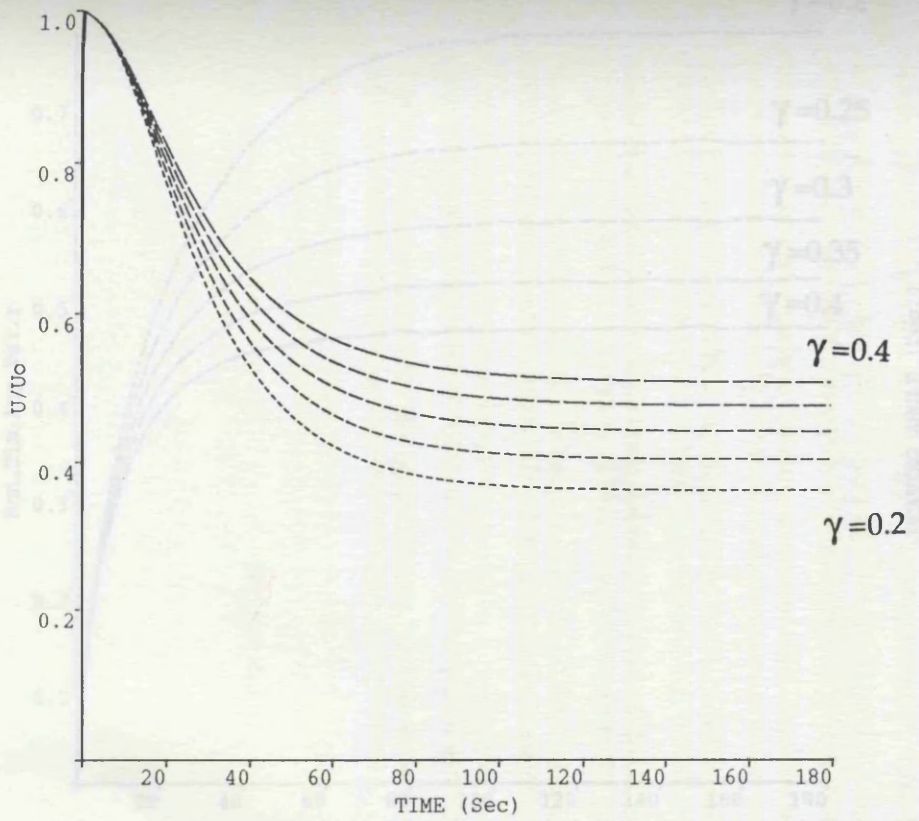

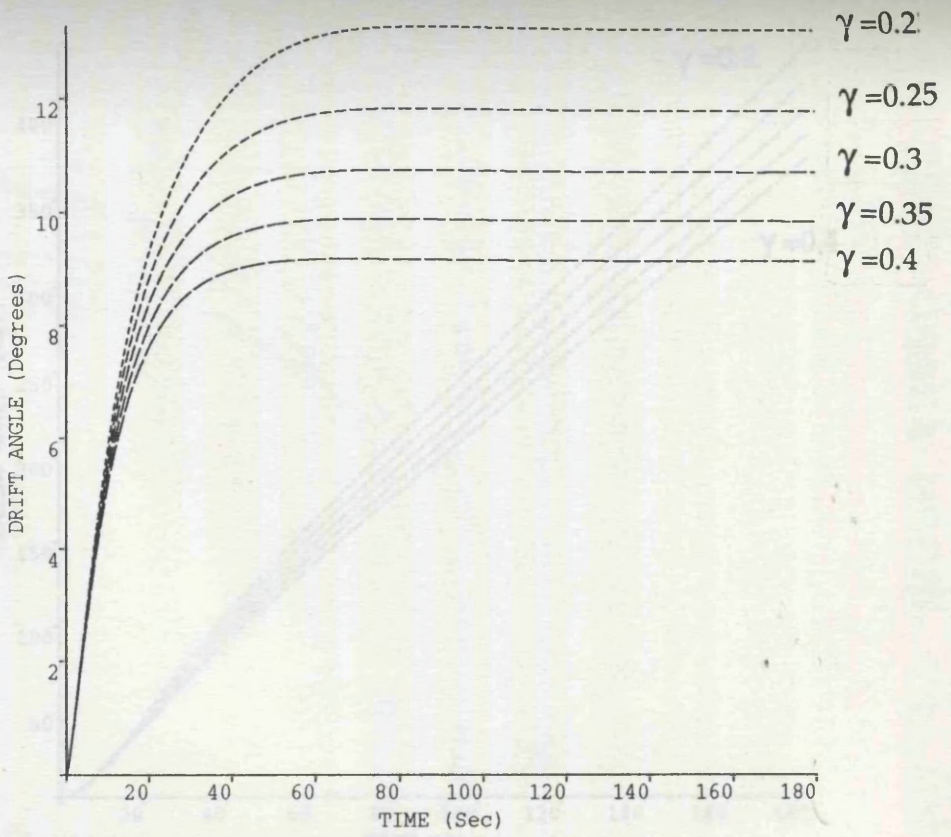

Model Velocity. 0.36 m/s
Rudder Angle. 20 Degrees Starboard
Condition. Full
γ. 0.2, 0.25, 0.3, 0.35, 0.4

Figure 2.10b

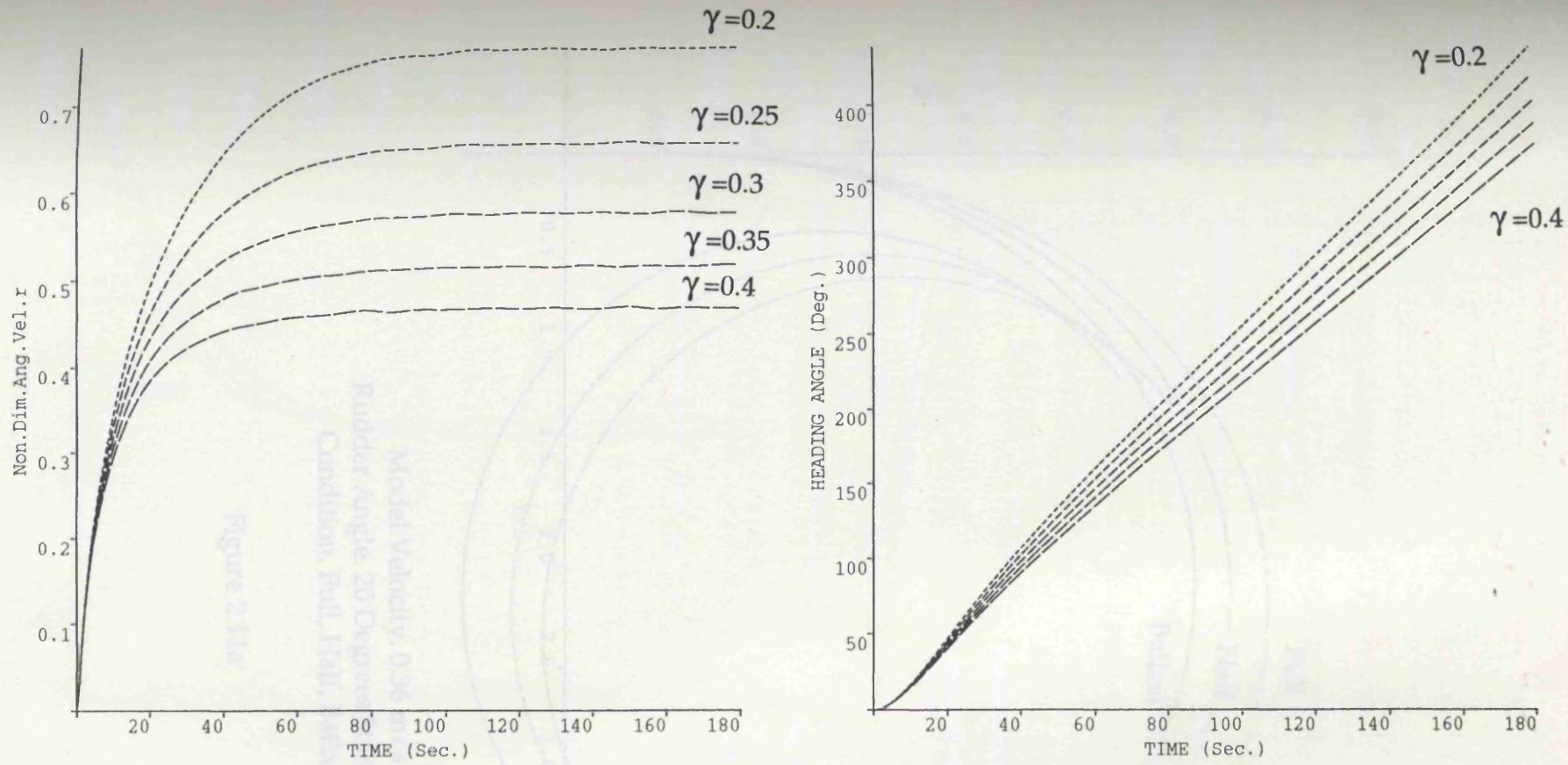

Model Velocity. 0.36 m/s
Rudder Angle. 20 Degrees Starboard
Condition. Full
γ. 0.2, 0.25, 0.3, 0.35, 0.4

Figure 2.10c

ESSO OSAKA MODEL TRAJECTORY

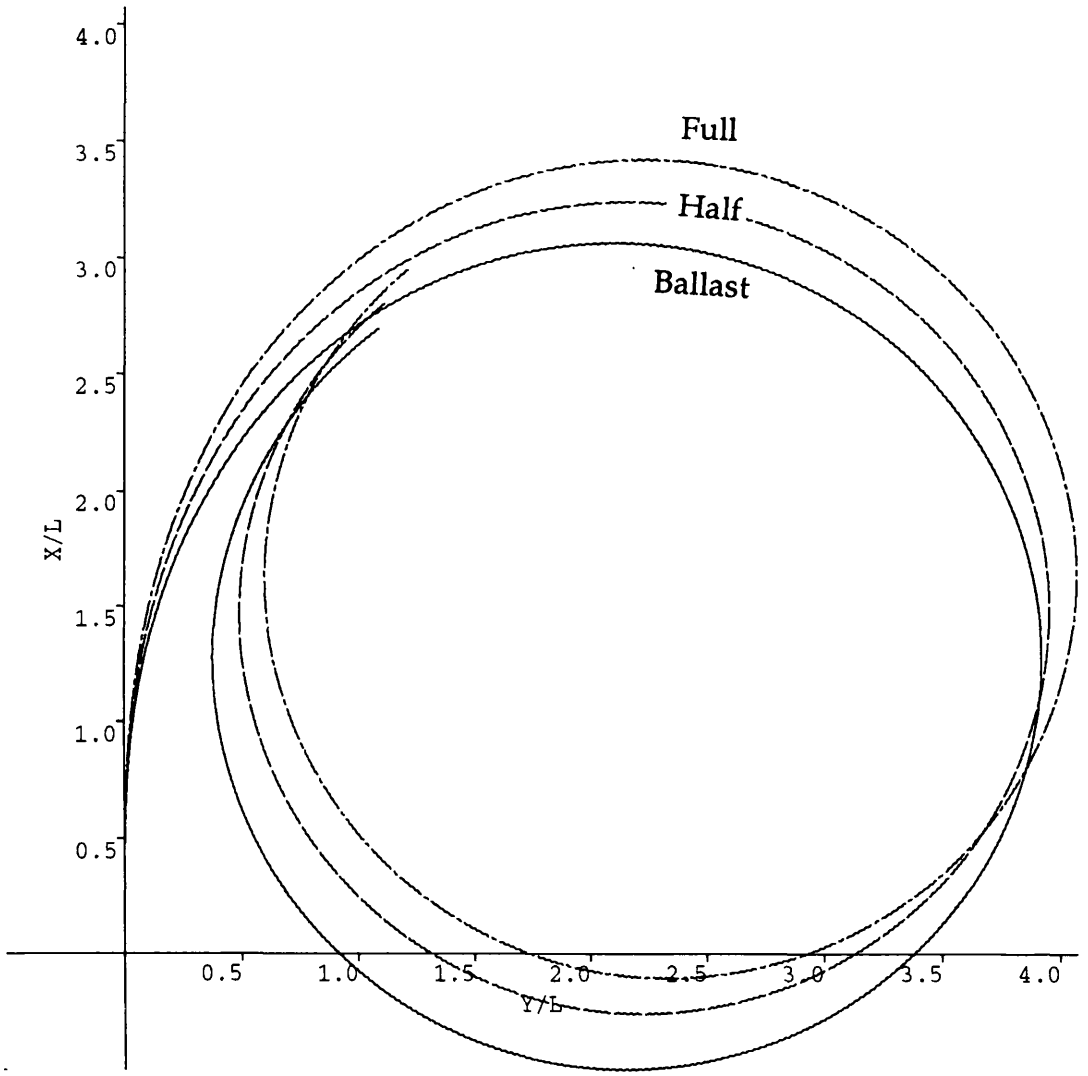

Model Velocity. 0.36 m/s
Rudder Angle. 20 Degrees Starboard
Condition. Full, Half, Ballast.

Figure 2.11a

VELOCITY RATIO & DRIFT ANGLE

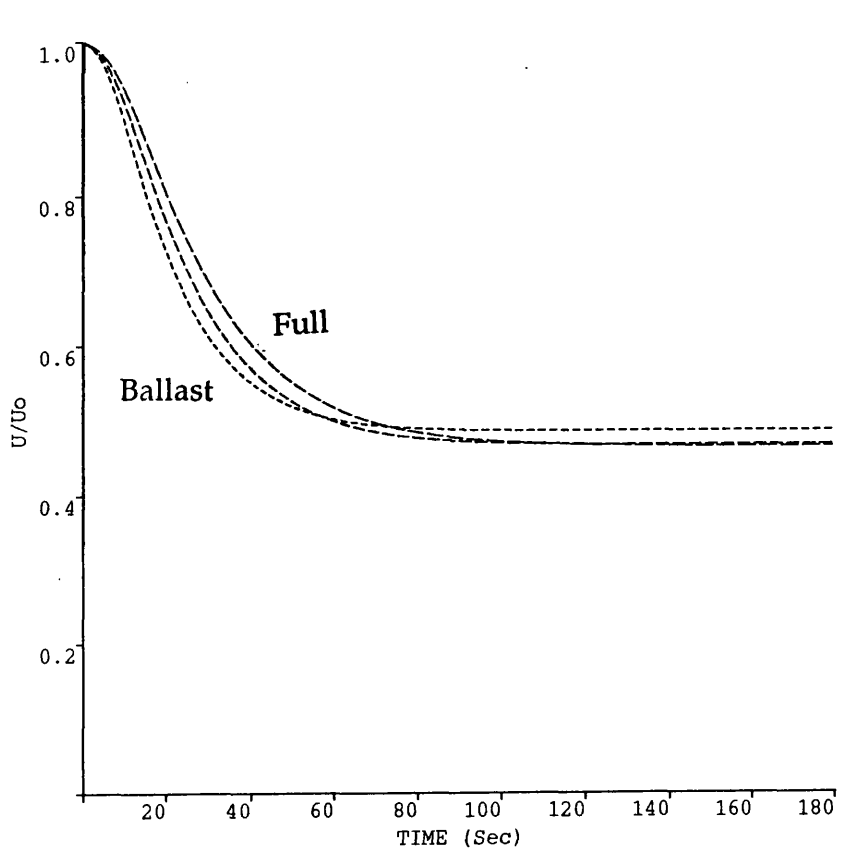

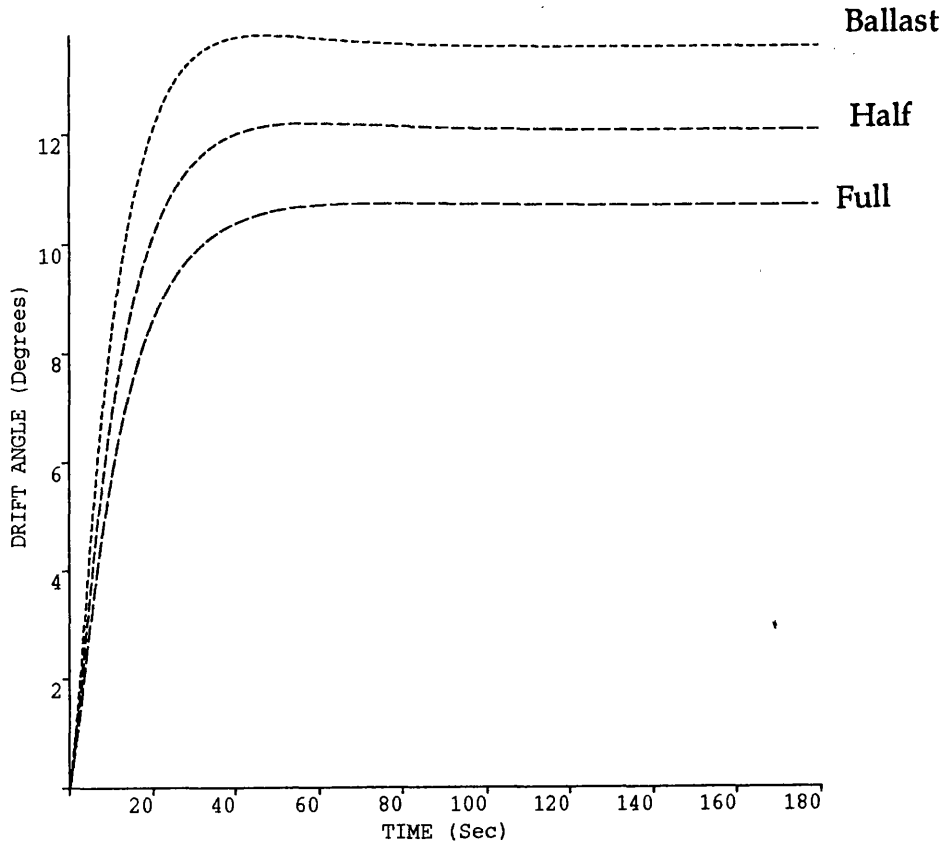

Model Velocity. 0.36 m/s
Rudder Angle. 20 Degrees Starboard
Condition. Full, Half, Ballast.

Figure 2.11b

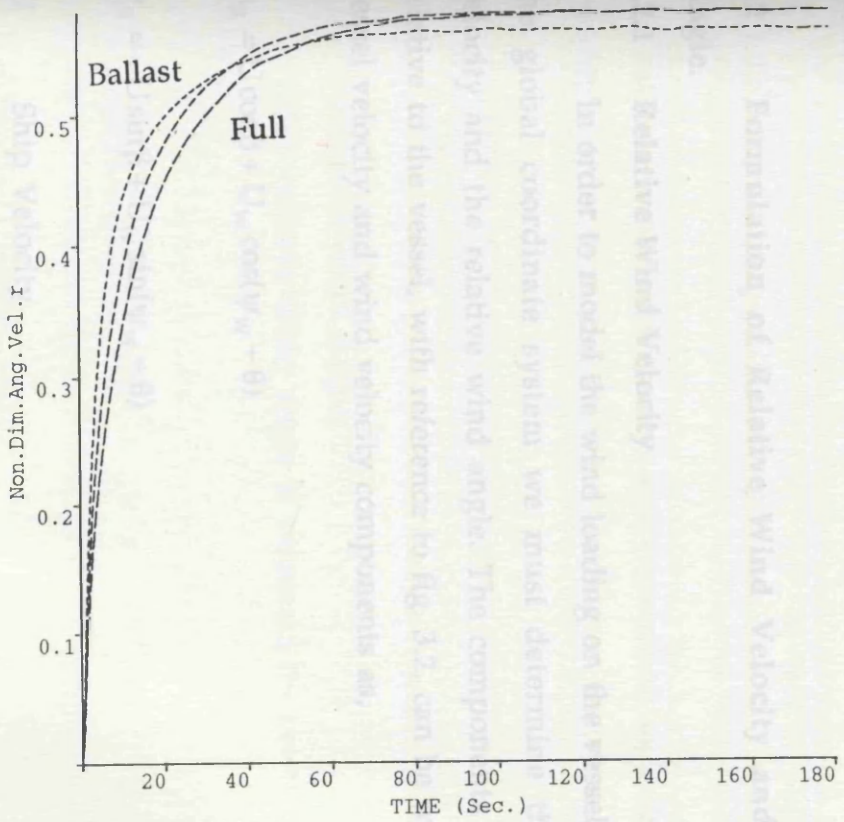

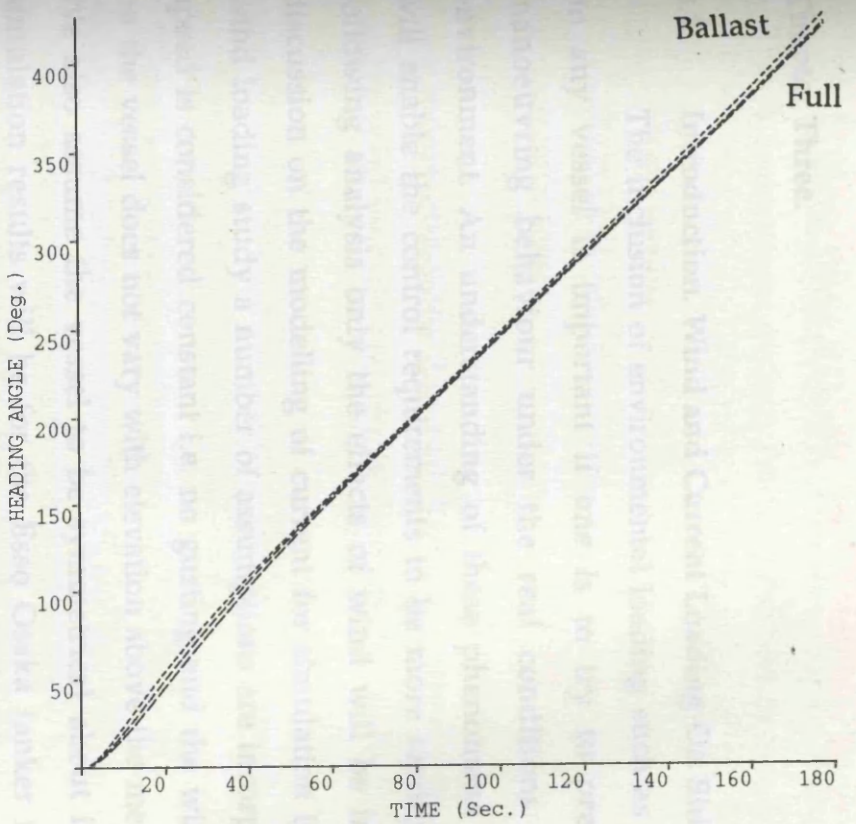

Figure 2.11c

Model Velocity. 0.36 m/s
Rudder Angle. 20 Degrees Starboard
Condition. Full, Half, Ballast.

Chapter Three.

3.1 Introduction. Wind and Current Loading On Ships.

The inclusion of environmental loading such as wind and current on any vessel is important if one is to try to predict the vessel's manoeuvring behaviour under the real conditions imposed by the environment. An understanding of these phenomena and their effects will enable the control requirements to be more readily assessed. In the following analysis only the effects of wind will be investigated but a discussion on the modelling of current for simulation is included. In the wind loading study a number of assumptions are incorporated. The wind speed is considered constant i.e. no gusting and the wind velocity acting on the vessel does not vary with elevation above the mean still water line. We also assume the vessel to be symmetrical about its centerline. The simulation results will be for the Esso Osaka tanker model of Chapter Two.

3.2 Formulation of Relative Wind Velocity and Relative Wind Angle.

3.2.1 Relative Wind Velocity

In order to model the wind loading on the vessel as it advances in the global coordinate system we must determine the relative wind velocity and the relative wind angle. The components of wind velocity relative to the vessel, with reference to fig. 3.2, can be written in terms of vessel velocity and wind velocity components as,

$$u_R = U\cos\beta + U_W\cos(\psi_W - \theta) \qquad 3.1.a$$

$$v_R = -U\sin\beta + U_W\sin(\psi_W - \theta) \qquad 3.1.b$$

U Ship Velocity

U_W Wind Velocity

U_R Relative Wind Velocity

u_R x Component of Ship Velocity Relative to the Wind

v_R y Component of Ship Velocity Relative to the Wind

θ Ship Heading Angle

β Ship Drift Angle

ψ_W Wind Angle

If we square equations 3.1a and 3.1b and then add them, we obtain the relative wind velocity and rearranging results in the following,

$$U_R^2 = u_R^2 + v_R^2 = (U\cos\beta + U_W\cos(\psi_W - \theta))^2 + (-U\sin\beta + U_W\sin(\psi_W - \theta))^2 \quad 3.2$$

$$= U^2\cos^2\beta + 2U\cos\beta U_W\cos(\psi_W - \theta) + U_W^2\cos^2(\psi_W - \theta)$$
$$+U^2\sin^2\beta - 2U\sin\beta U_W\sin(\psi_W - \theta) + U_W^2\sin^2(\psi_W - \theta)$$

$$= U^2(\cos^2\beta + \sin^2\beta) + U_W^2(\cos^2(\psi_W - \theta) + \sin^2(\psi_W - \theta))$$
$$+2UU_W(\cos(\psi_W - \theta)\cos\beta - \sin(\psi_W - \theta)\sin\beta)$$

$$U_R^2 = U^2 + U_W^2 + 2UU_W\cos(\psi_W - \theta + \beta) \quad 3.3$$

The relative wind velocity can also be written as a ratio of the vessel velocity as,

$$\frac{U_R^2}{U^2} = 1 + \frac{U_W^2}{U^2} + 2\frac{U_W}{U}\cos(\psi_W - \theta + \beta) \quad 3.4$$

3.2.2 Relative Wind Angle.

The relative wind angle is obtained by rewriting equations 3.1a and b as,

$$u_R = U\cos\beta + U_W\cos(\psi_W - \theta)$$

$$v_R = -U\sin\beta + U_W\sin(\psi_W - \theta)$$

and dividing these results in the expression for the relative wind angle.

$$\tan\psi_R = \frac{-U\sin\beta + U_W \sin(\psi_W - \theta)}{U\cos\beta + U_W \cos(\psi_W - \theta)}$$

$$\psi_R = \tan^{-1}\left(\frac{-U\sin\beta + U_W \sin(\psi_W - \theta)}{U\cos\beta + U_W \cos(\psi_W - \theta)}\right) \qquad 3.5$$

The wind forces and moments are included in the equations of motion as environmental loading and are written as,

$$F_{WX} = \frac{\rho_A A_T C_X U_R^2}{2}\ ,\ F_{WY} = \frac{\rho_A A_L C_Y U_R^2}{2}\ ,\ F_{WN} = \frac{\rho_A A_L L C_N U_R^2}{2} \qquad 3.6$$

ρ_A mass density of air $1.222\,kg/m^3$

$A_{T,L}$ Transverse and Longitudinal Wind Projected Areas

$C_{X,Y,N}$ Wind Loading Coefficients

Non dimensionalising equations 3.6 in the same manner as the hydrodynamic, rudder and propeller forces and moments we obtain,

$$F'_{WX} = \frac{\rho_A A_T C_X}{\rho L D}\frac{U_R^2}{U^2}\ ,\ F'_{WY} = \frac{\rho_A A_L C_Y}{\rho L D}\frac{U_R^2}{U^2}\ ,\ F'_{WN} = \frac{\rho_A A_L L C_N}{\rho L^2 D}\frac{U_R^2}{U^2} \qquad 3.7$$

We have calculated the velocity ratio previously in equation 3.4. The only unknowns remaining are the wind loading coefficients C_X, C_Y, C_N. These coefficients are functions of the vessels form above the water and can be determined from experiments in a wind tunnel with a scale model, Ref. 3.1. This is an expensive procedure and takes a great deal of time for analysis. The second method is to use previous experimental data of type vessels or further, to employ empirical formulae derived from regression analysis of previous wind tunnel test on type vessels as described in Isherwood, Ref. 3.2. In the Isherwood method, the wind coefficients are determined around the vessel from bow to stern at 10 degree intervals and

are then plotted to obtain the loading coefficients as a function of relative wind angle. Additional references for wind loading coefficients and wind loading studies can be found in Refs. 3.3.-3.7.

In the present analysis, the wind loading coefficients were obtained from an experimental study carried out in 1977, Ref. 3.1. The study also produced results for current loading coefficients. These loading coefficients apply to VLCC's for a deadweight range of 150,000-500,000 tonnes with deckhouse located aft. This includes fully loaded and ballast conditions with tankers of conventional and cylindrical bow types. The condition investigated in this chapter will be for a fully loaded tanker with a conventional bow. The wind loading coefficients from Ref. 3.1 are reproduced in figs. 3.1. In order to use these wind loading coefficients in the simulation program it was necessary to curve fit these coefficients with 5th order polynomial equations which ensures accurate results. This curve fitting was accomplished using an Apple Macintosh Computer and Cricket Graph curve fitting software. The typical wind loading coefficients are shown in the program output for the turning simulations. The output shows different loading coefficients for port and starboard turns as expected. It is noted from these figures, that the output is not continuous at certain points in the simulation. This is due to the formulation of the wind loading in the subroutine to model the wind from any direction for a port and starboard turn. The size and duration of these discontinuities are small when compared with the magnitude of the loading coefficients and can easily be regarded wind changing direction or gusting. The full scale transverse and longitudinal windage areas for the fully loaded 280,000 tonnes dwt tanker are 1130m^2 and 3160m^2 respectively were obtained from Ref. 3.1 and these have been scaled to the model simulation.

3.3 Current Loading on Ships.

In the simulations the forces imposed by currents need to be modelled in a different manner to the procedure adopted for the wind

loading. In the form comparable with the wind, the current force would be dependent upon the relative current velocity. The relative current velocity will therefore include the contributions of the vessel velocity as well as the actual current velocity. The problem arises as the derivative forces acting on the hull from the vessel velocity are also included in the simulation force summation. We would therefore include the effect of the vessel velocity twice which is obviously incorrect. The present formulation is reasonable for the wind loading as the hydrodynamic hull forces and wind hull forces are acting in different fluids i.e. water and air. Summing the forces imposed by the individual velocity contributions separately is also incorrect as we are dealing with a force summation due to the relative velocity squared. This is more easily explained in the case of a head current as,

$$U_{RC}^2 = (U + U_C)^2 \neq U^2 + U_C^2$$

It is necessary to modify the formulation of the relative velocity for input to the current loading. A method of including the effect of the relative velocity squared is to formulate the contribution of the current velocity as follows.

The relative current may be written in the form as that of the relative wind velocity,

$$U_{RC}^2 = U^2 + U_C^2 + 2UU_C\cos(\psi_C - \theta + \beta)$$

U_{RC} Relative Current Velocity
U_C Current Velocity
U Vessel Velocity

The contribution of the current alone can be modelled as a corrected current velocity which takes account of the square of the relative current

velocity.

$$U_{RC}^2 - U^2 = U_C^2 + 2UU_C\cos(\psi_C - \theta + \beta) \qquad 3.8$$

$$U_{CC}^2 = U_{RC}^2 - U^2$$

$$U_{CC} = \sqrt{U_{RC}^2 - U^2} \qquad 3.9$$

U_{CC} Corrected Current Velocity

Using this formulation, the total hydrodynamic forces acting on the vessel are determined as the contribution of the vessel forward speed in association with the manoeuvring derivatives and the corrected current velocity in association with the current loading coefficients. The above summation is an approximation as the contributions to the hull forces of both the forward speed and current velocity are in reality inseparable.

The relative current angle can be determined in a similar manner to the relative wind as,

$$\psi_{RC} = \tan^{-1}\left(\frac{-U\sin\beta + U_{CC}\sin(\psi_C - \theta)}{U\cos\beta + U_{CC}\cos(\psi_C - \theta)}\right) \qquad 3.10$$

Once we have obtained this angle it is possible to find the values of corresponding current loading coefficients. The contribution of the current forces and moments when non dimensionalised are written as,

$$F'_{CX} = \frac{\rho\, LDC_{XC}}{\rho LD}\frac{U_{CC}^2}{U^2},\ F'_{CY} = \frac{\rho\, LDC_{YC}}{\rho LD}\frac{U_{CC}^2}{U^2},\ F'_{CN} = \frac{\rho\, L^2DC_{NC}}{\rho L^2D}\frac{U_{CC}^2}{U^2} \qquad 3.11$$

The velocity used in the formulation is the corrected current velocity and not the actual current velocity.

It is assumed the current velocity profile does not to vary with depth and the vessel is symmetrical about its centerline. Using the appropriate current loading coefficients, the current loads can be determined. Extreme care must be taken when considering the loading coefficients for currents from model tests especially if blockage and shallow water effects are apparent. It is also difficult to predict current because of its dependency on phenomena like wind, waves and tidal effects. The current load coefficients are given in figs. 3.3.

3.4 Automatic Pilot Control.

We will now introduce an automatic pilot control to the simulation model which will keep the vessel on a straight course under external loadings. The automatic pilot model used is that found in Eda, Refs. 3.8, 3.9. The rudder constants a and b′ can be varied to obtain an optimum stable course trajectory. The values of these constants will depend upon the conditions. The required rudder angle is obtained from the following relationship.

$$\delta_R = a(\theta - \theta_e) + b'r' = \delta_R + \dot{\delta}_R t \qquad 3.12$$

δ_R Rudder Angle (maximum value of 35 degrees)

a Yaw Rate Constant (Rudder Constant 1)

b′ Yaw Rate Gain Constant (Rudder Constant 2)

$\dot{\delta}_R$ Rudder Deflection Rate (recommended as 2.33 degrees/second)

θ_e Required Heading (=0 degrees)

θ Heading Angle

t Time Step.

3.5 Discussion of Results.

3.5.1 Manoeuvrability with Wind Velocity and Wind Incidence Angle.

In figure 3.4 we see an example from the model tanker simulations. The results show the variation of three wind velocity ratios with the angle of wind incidence angle around the hull (0-180 degrees) and the effect on the maximum rudder deflection required to hold a steady straight course when employing the automatic pilot control model. The results show that greater rudder angles are required for beam winds. If the rudder angle is greater than 35 degrees then the vessel may lose its ability to manoeuvre. The wind velocity ratio of 12.5 for head winds produces a condition where the vessel is unable to manoeuvre. This condition may be due to limits associated with the NAG integration, Ref. 2.16. Typical trajectory output for beam winds can be seen in figs. 3.7-3.8 for the variation in automatic pilot rudder constants.

3.5.2 Turning Circle Simulations.

The results of the tanker model simulations for port and starboard turns in wind with a variation in wind incidence angles of 0, 90, 180, 270 degrees for the wind velocity ratio of 7.5 (60 knots full scale), can be seen in figures 3.5-3.6. If the wind velocity were reduced then the amplitude of the vessel velocity, drift angle and angular velocity will reduce. The wind loading coefficients are also presented for the 0 degrees wind angle for starboard and port. These can be compared with the wind loading coefficients, figures 3.2 obtained from the experimental study of Ref 3.1. It can be seen that turning into the wind greatly reduces the required turning area. This is important in busy seaways.

3.5.3 Variation in Rudder Constants for Automatic Pilot.

In figures 3.7 we see the variation of the yaw rate rudder constant (Rudder Constant 1), for the condition of beam wind with a wind velocity ratio of 7.5. The increase in Rudder Constant 1 has a significant effect on the trajectory but has little effect on the actual vessel velocity and drift

angle. This difference in trajectory is due to the definition of the course angle.

$$\phi = \theta - \beta$$

with the increased Rudder Constant 1 from 1.25 - 5, the heading angle reduces from 7- 2 degrees. The drift is relatively constant. The transverse displacement will therefore reduce. This will not always be the case as seen in Chapter Five. The choice of rudder constant depends on the behaviour of the particular system. The auto pilot model does not account for the vessel position in the global coordinate system or course angle.

The variation in yaw rate gain constant b′, (Rudder Constant 2), for the same condition can be seen in figures 3.8. The scalar increase in b′ is seen to have less effect on the trajectory as Rudder Constant 1. The vessel course heads into the wind as the superstructure is located aft.

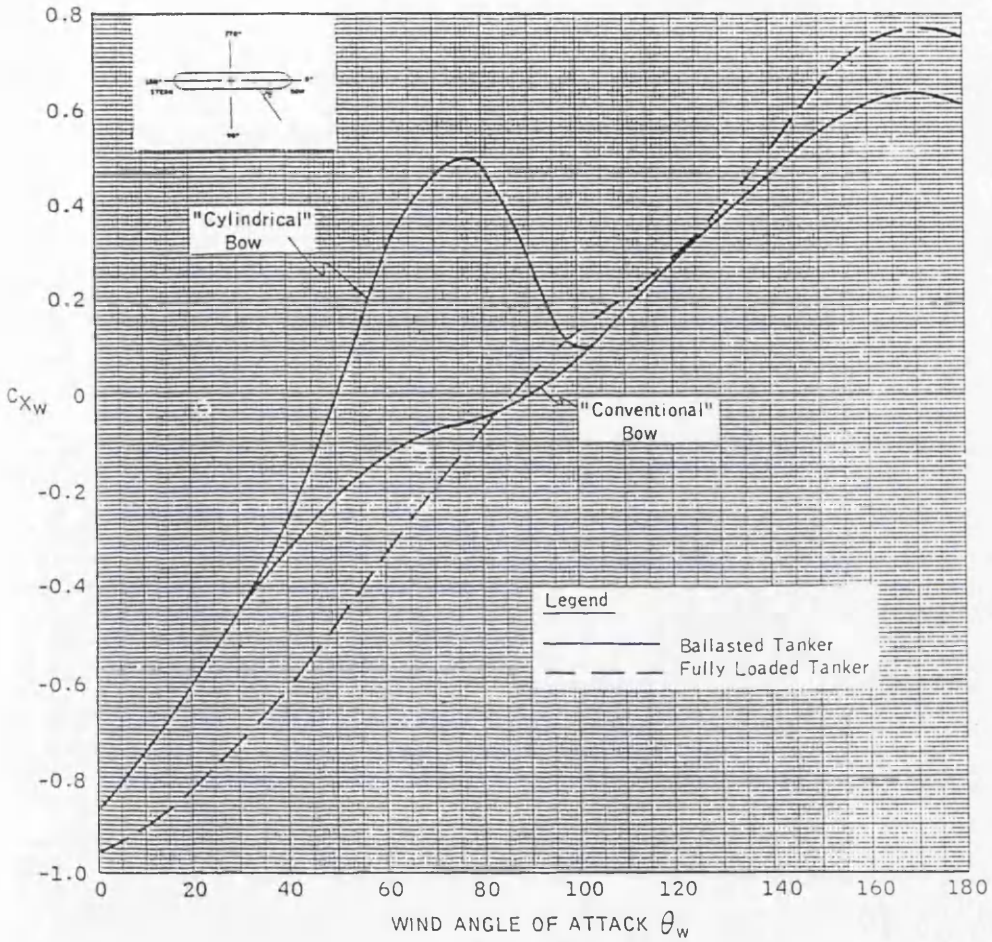

Figure 3.1a

Figures from Ref. 3.1

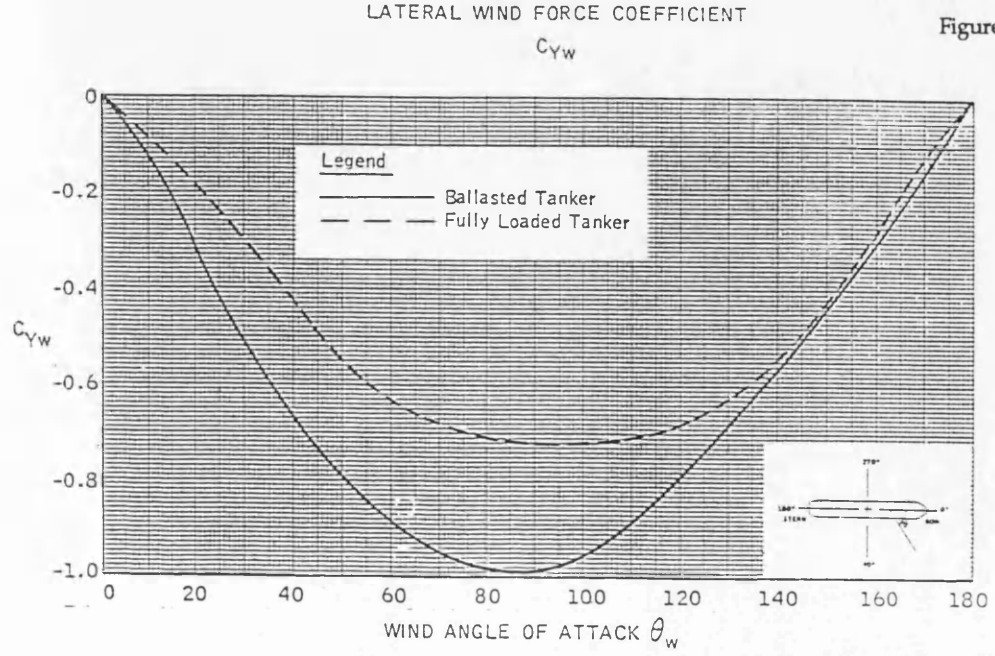

Figure 3.1b

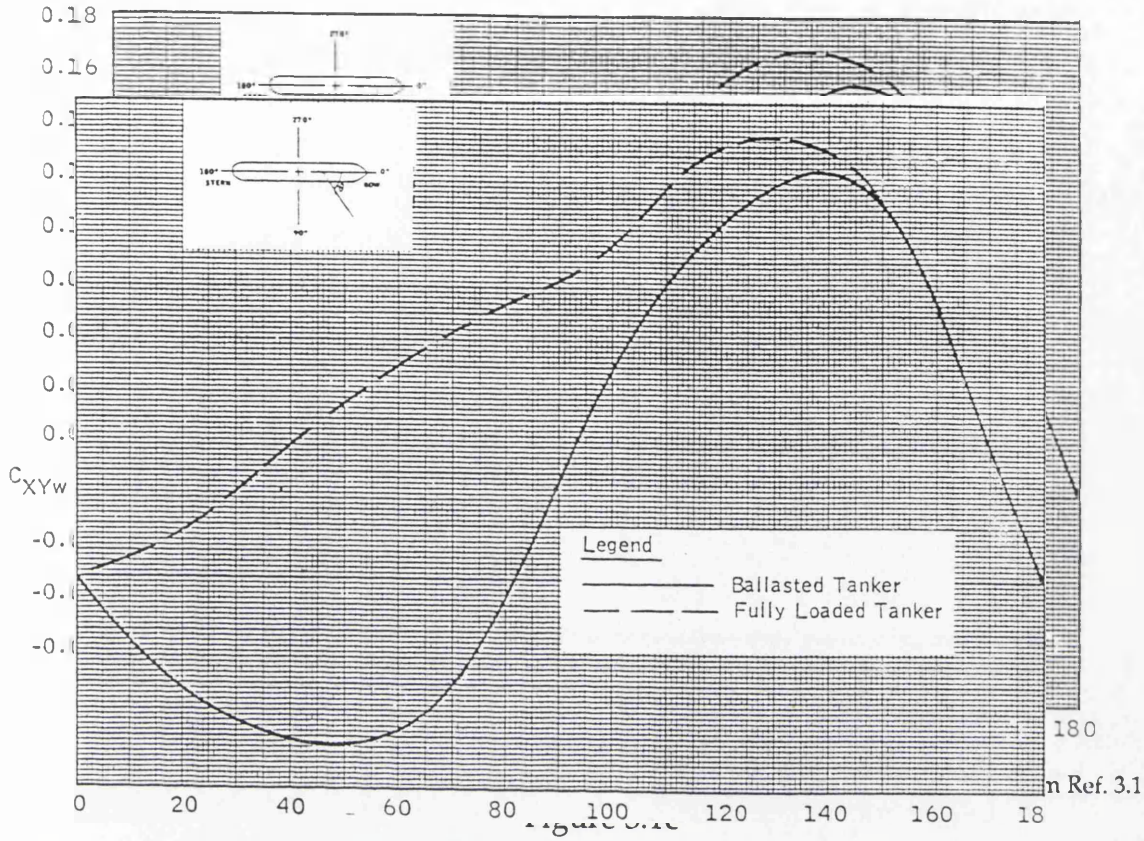

n Ref. 3.1

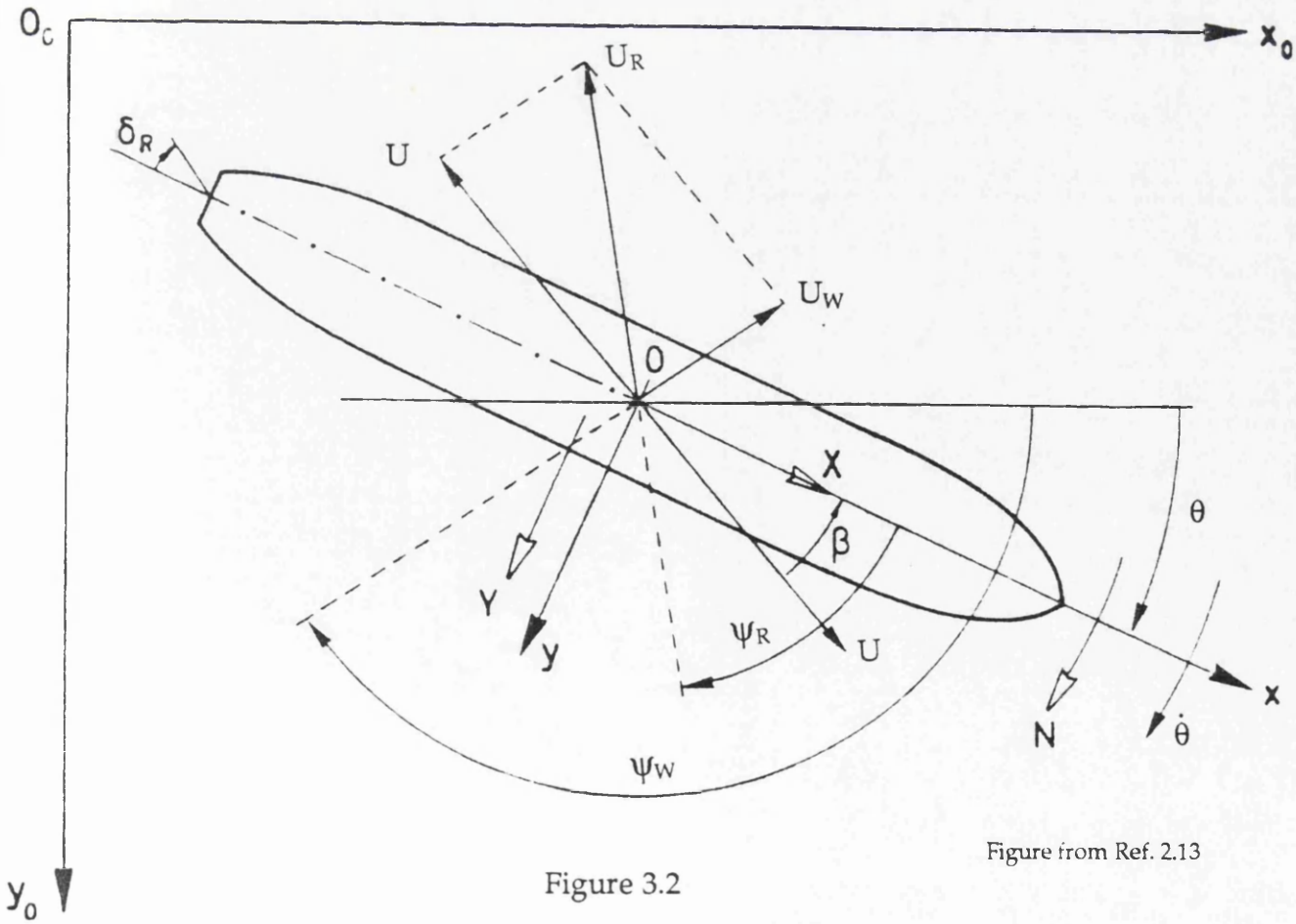

Figure from Ref. 2.13

Figure 3.2

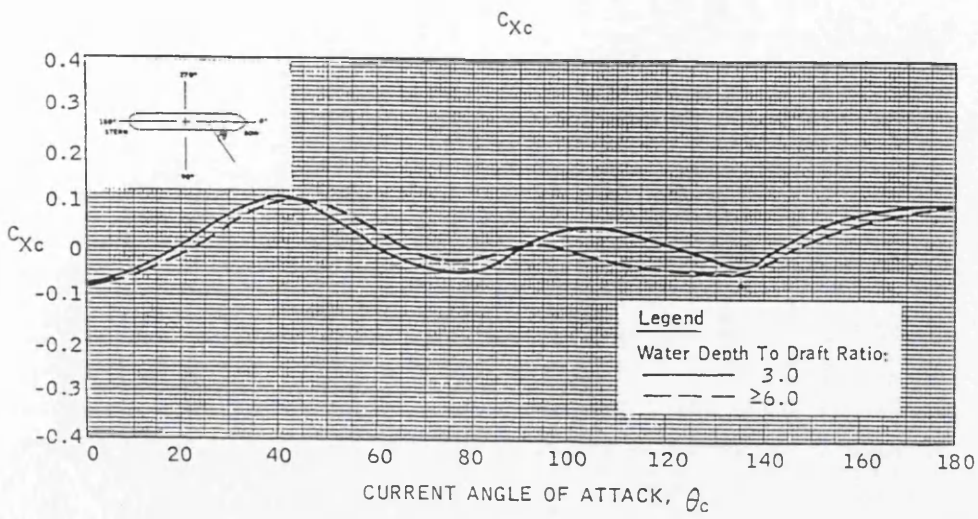

Figure 3.3a

Figures from Ref. 3.1

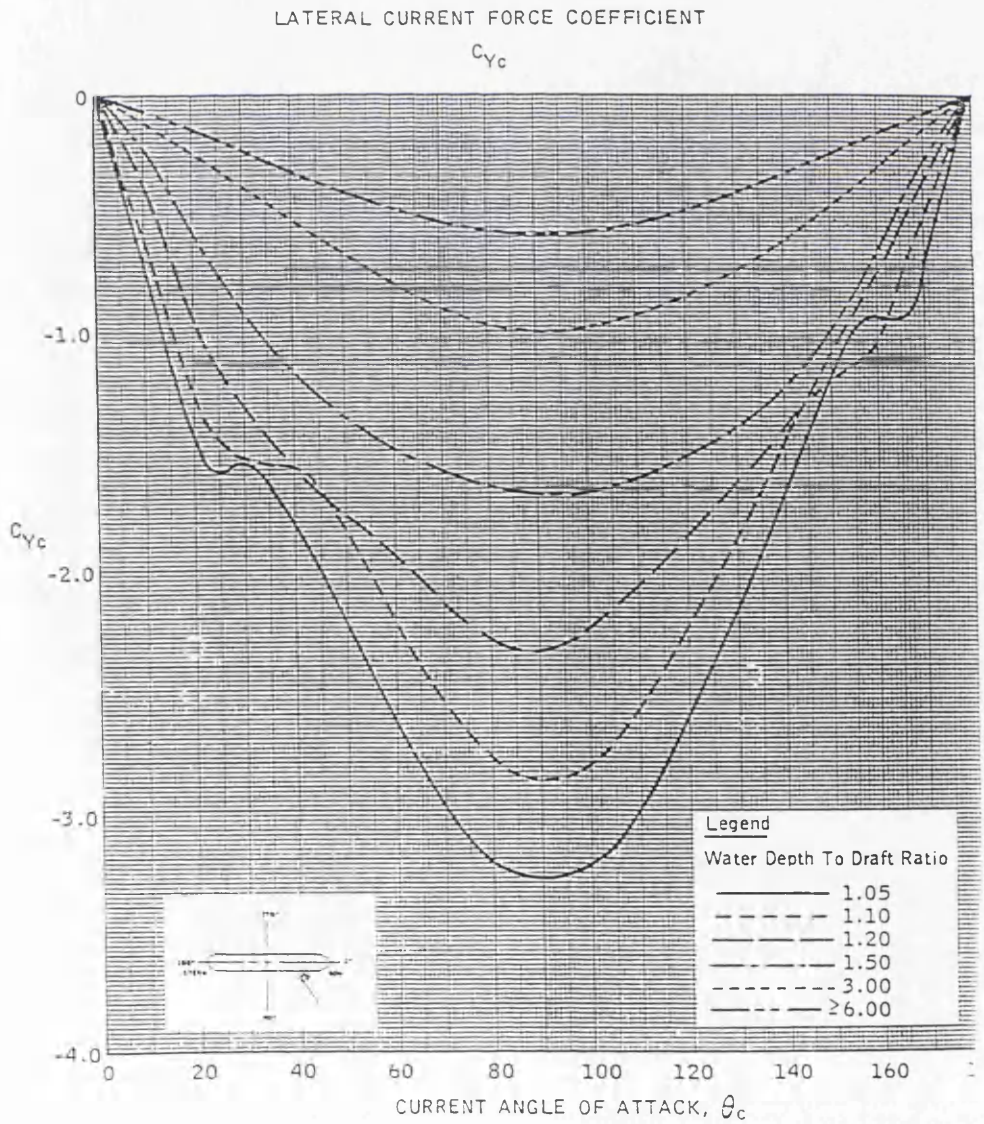

Figure 3.3b

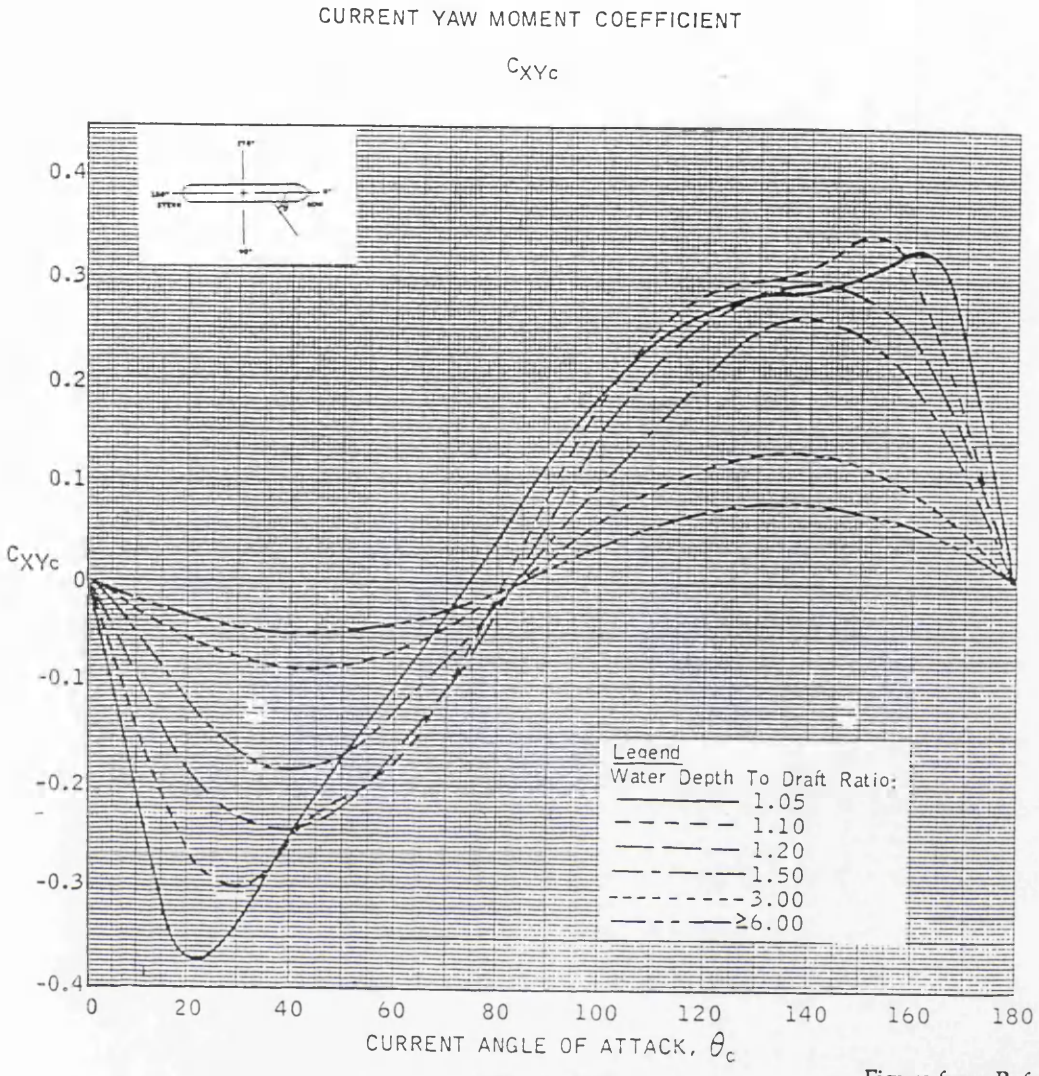

Figure 3.3c

Figure from Ref. 3.1

Relationship of Rudder Deflection and Wind Velocity Ratio Required to keep a Straight Path.

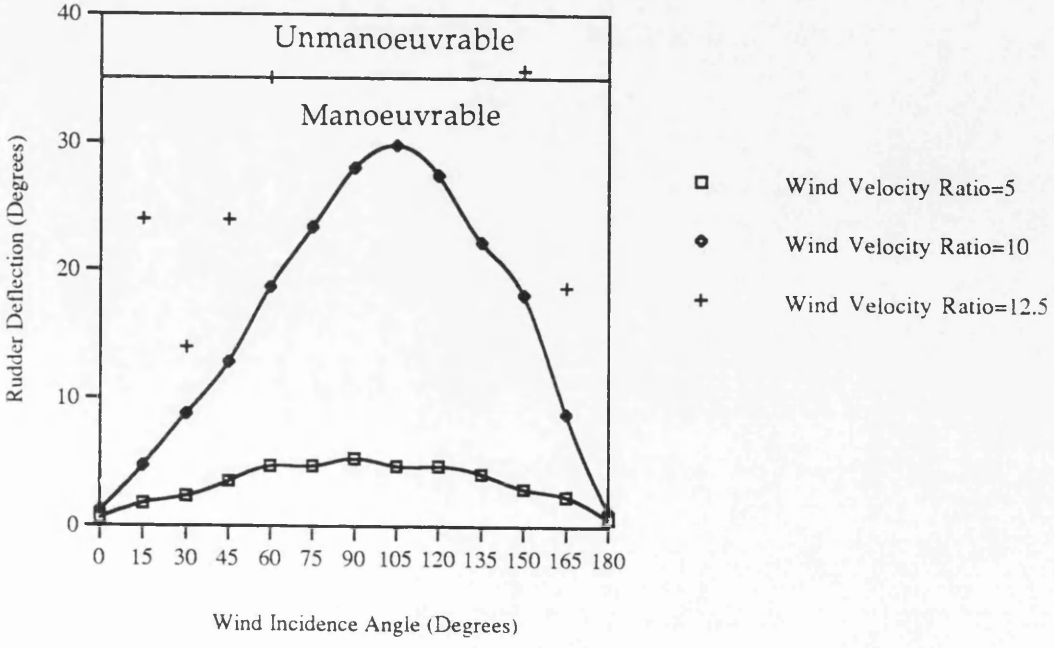

Figure 3.4

ESSO OSAKA MODEL TRAJECTORY

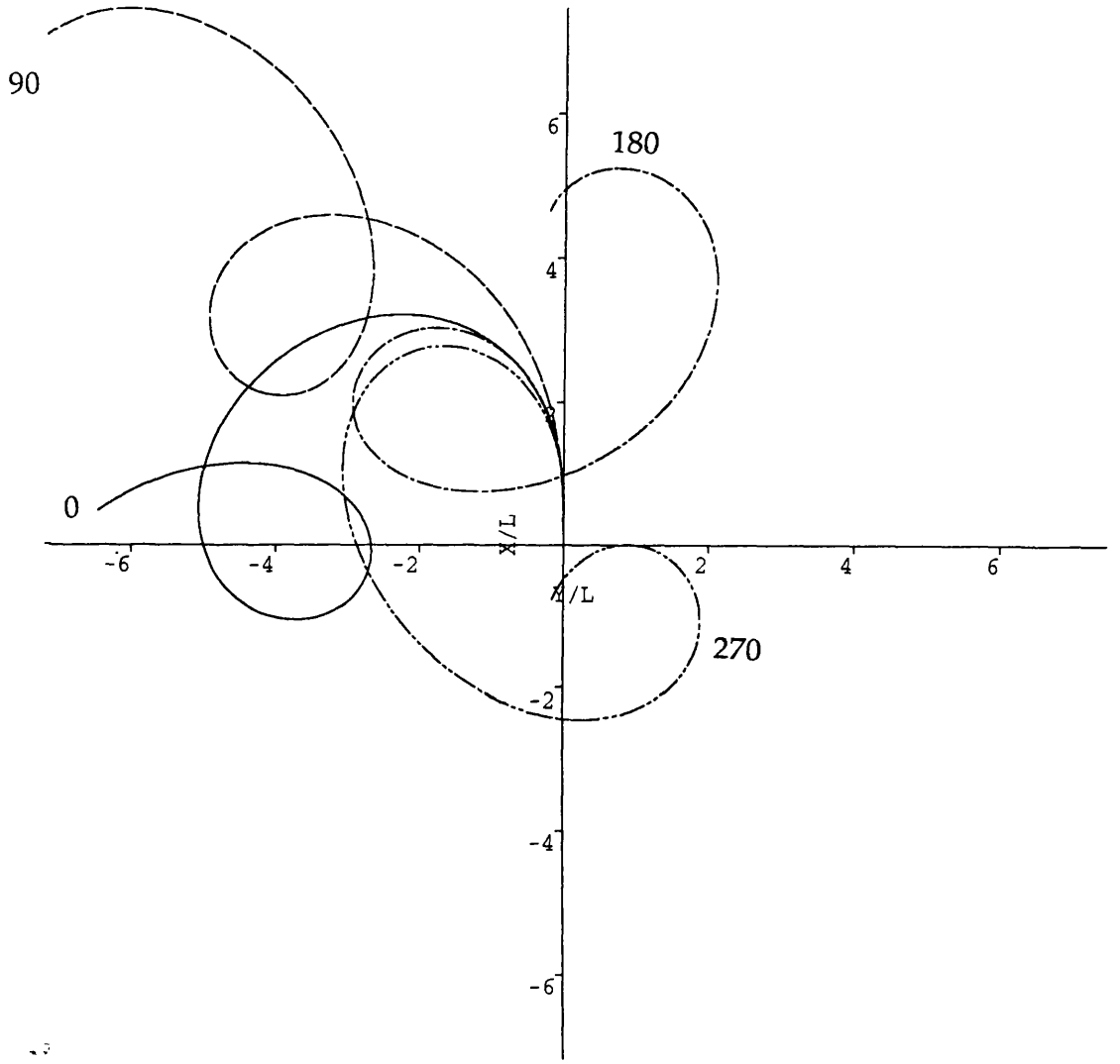

Model Ship Velocity : 0.36m/s
Rudder Angle : 25 degrees Port
Wind Velocity Ratio U_W/U : 7.5
Wind Direction : 0, 90, 180, 270 degrees

Figure 3.5a

VELOCITY RATIO & DRIFT ANGLE

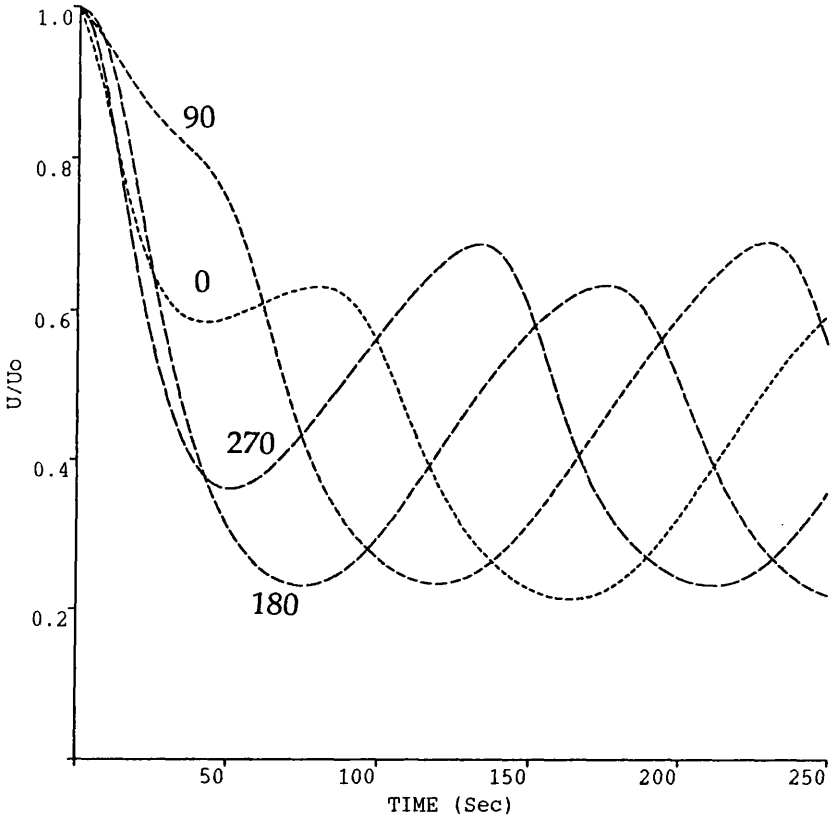

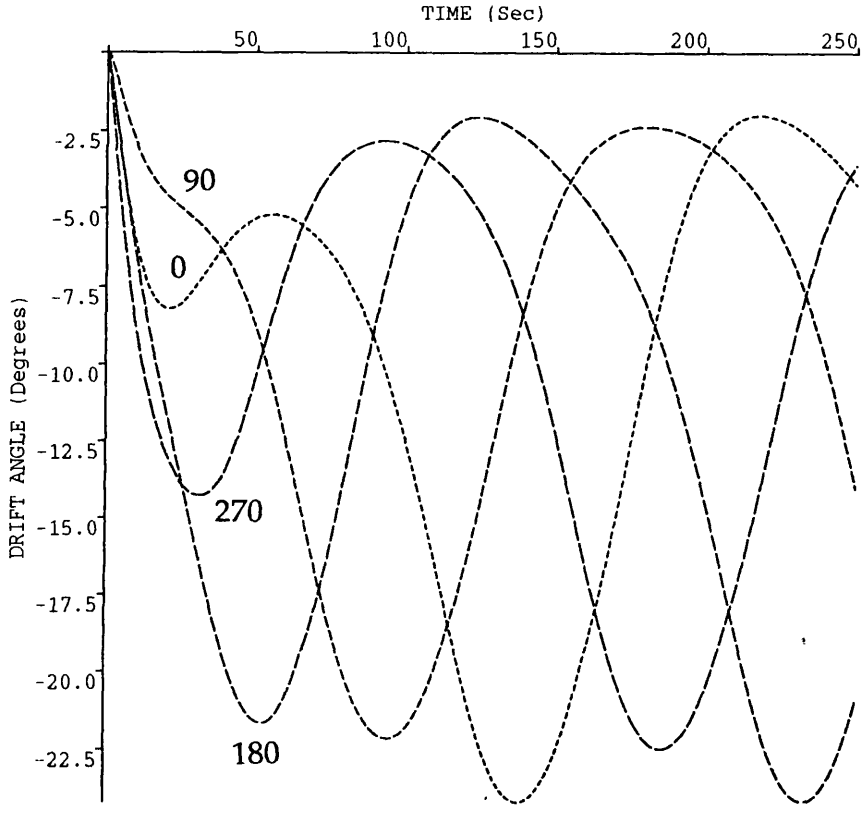

Model Ship Velocity : 0.36m/s
Rudder Angle : 25 degrees Port
Wind Velocity Ratio U_W/U : 7.5
Wind Direction : 0, 90, 180, 270 degrees

Figure 3.5b

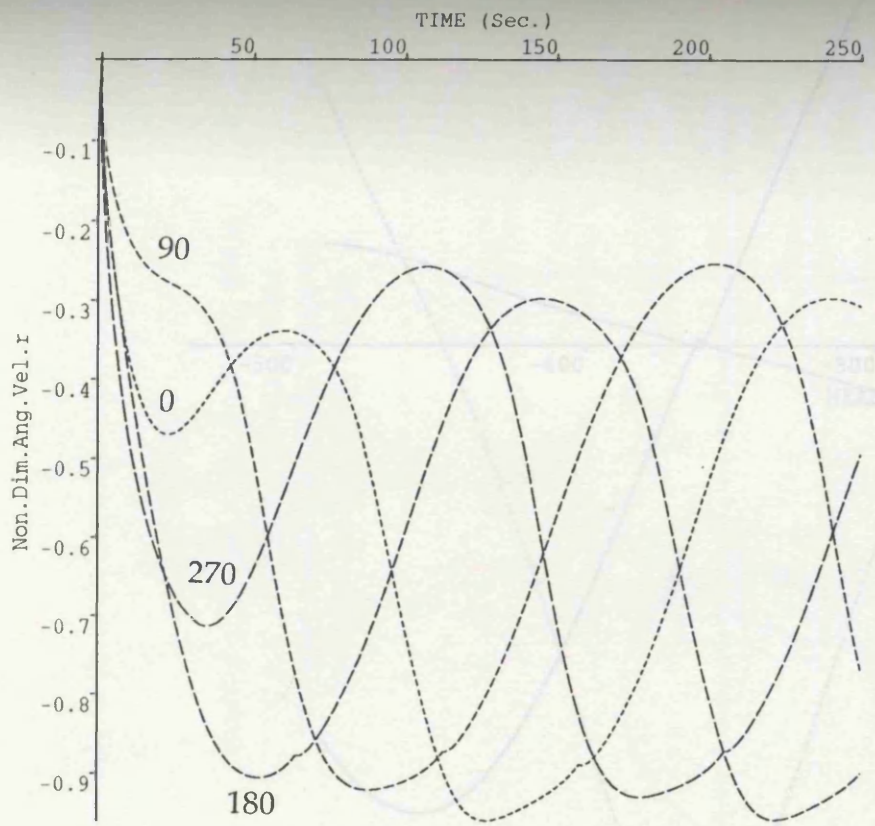

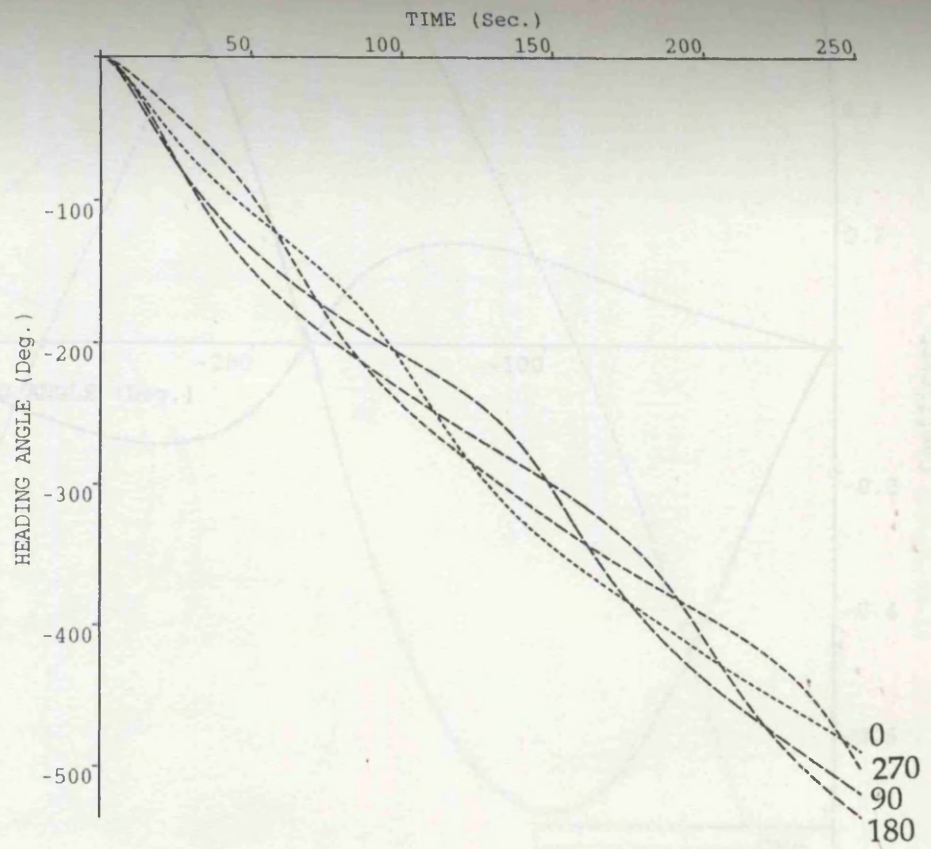

Model Ship Velocity : 0.36m/s
Rudder Angle : 25 degrees Port
Wind Velocity Ratio U_W/U : 7.5
Wind Direction : 0, 90, 180, 270 degrees

Figure 3.5c

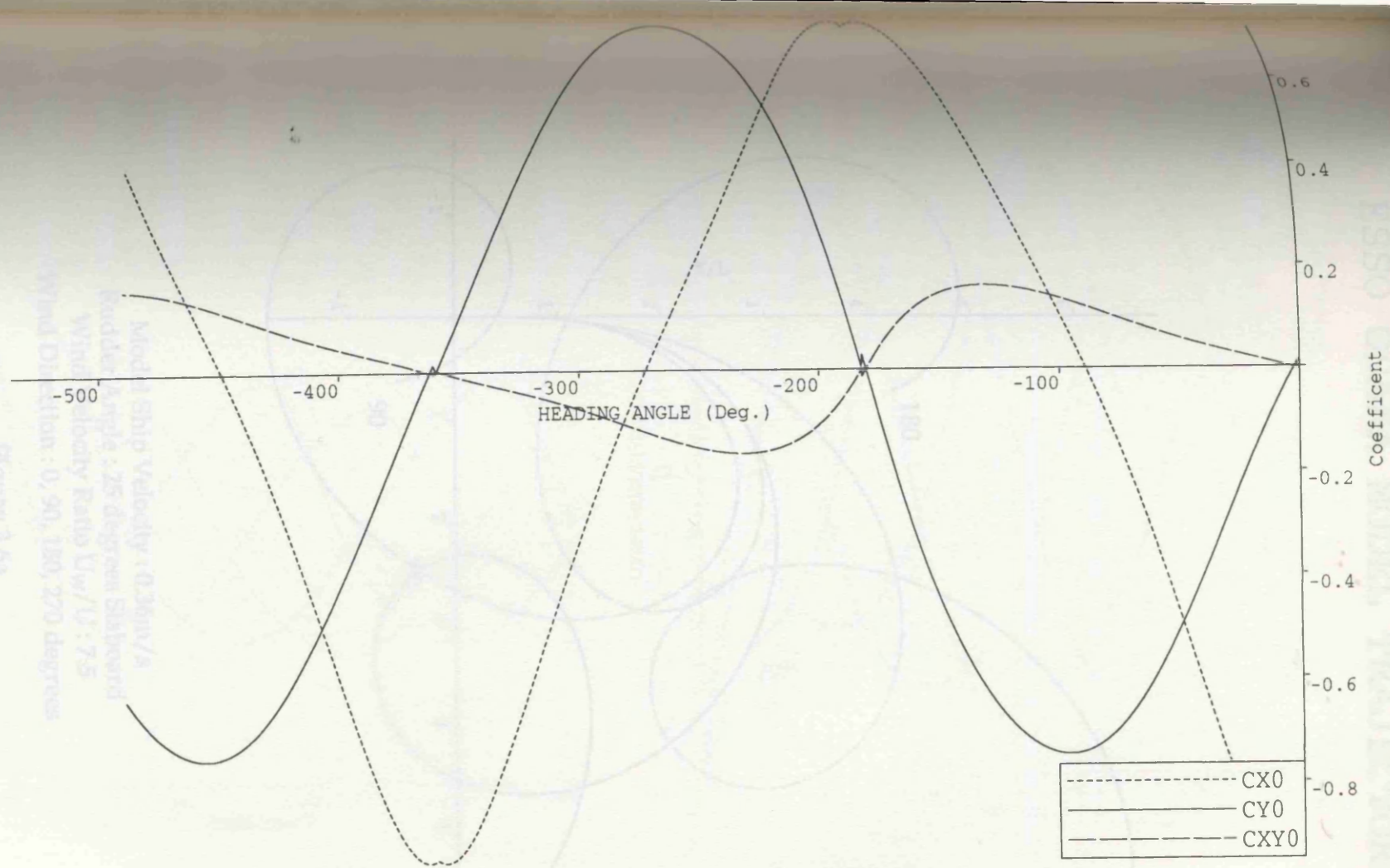

Wind Loading Coefficients for Port Turn.

Figure 3.5d

ESSO OSAKA MODEL TRAJECTORY

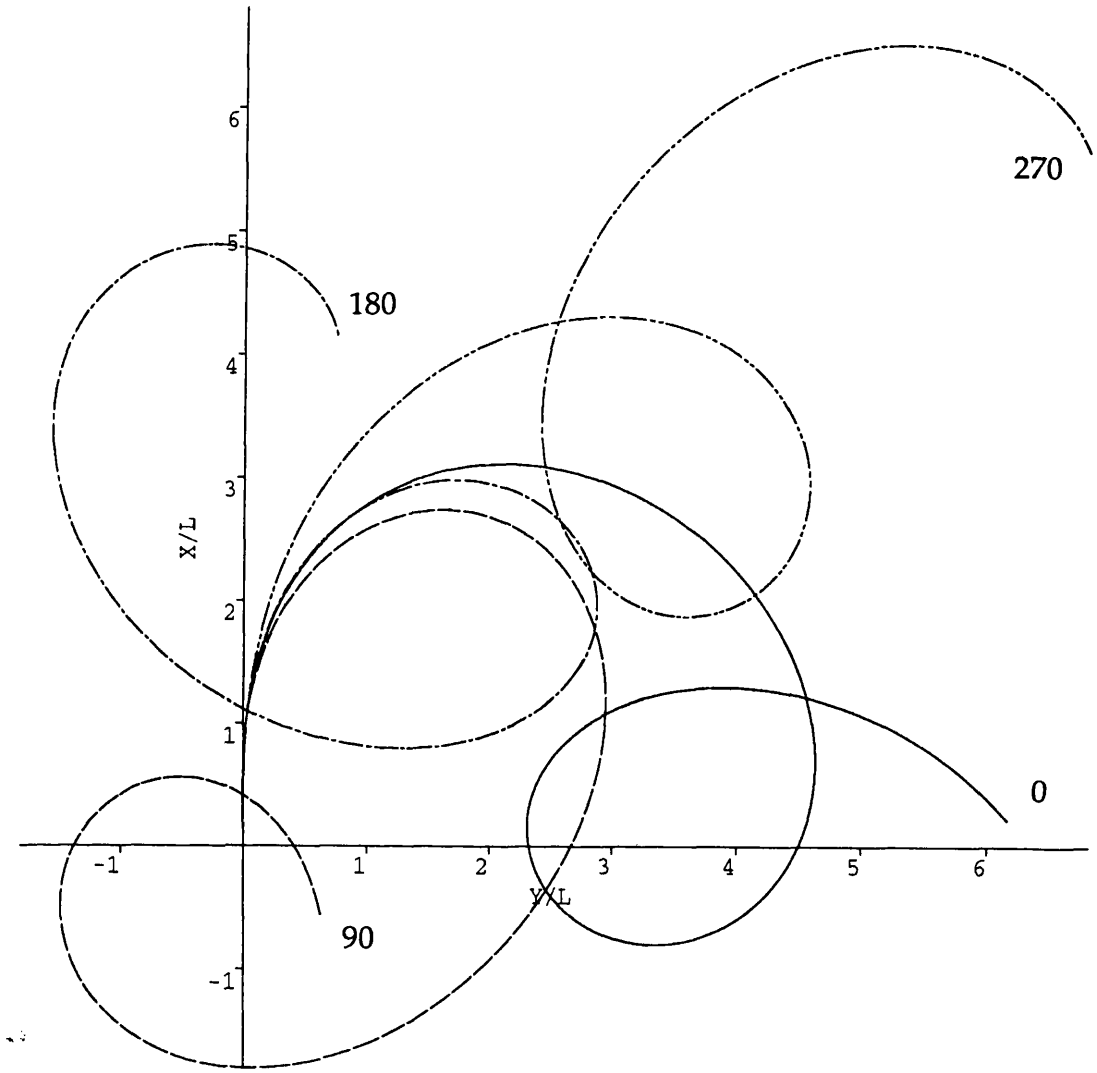

Model Ship Velocity : 0.36m/s
Rudder Angle : 25 degrees Staboard
Wind Velocity Ratio U_W/U : 7.5
Wind Direction : 0, 90, 180, 270 degrees

Figure 3.6a

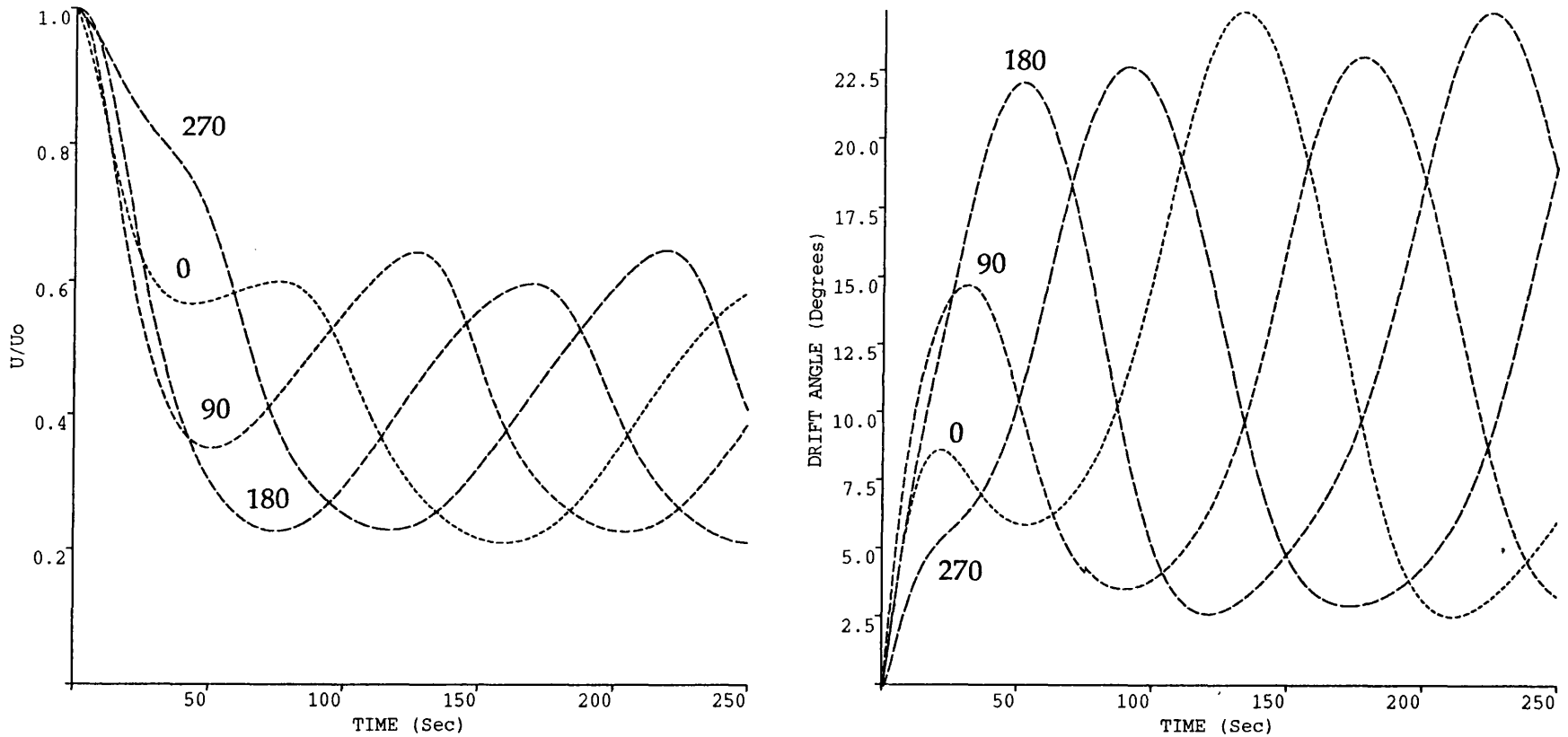

Model Ship Velocity : 0.36m/s
Rudder Angle : 25 degrees Staboard
Wind Velocity Ratio U_W/U : 7.5
Wind Direction : 0, 90, 180, 270 degrees

Figure 3.6b

ANGULAR VELOCITY AND HEADING ANGLE

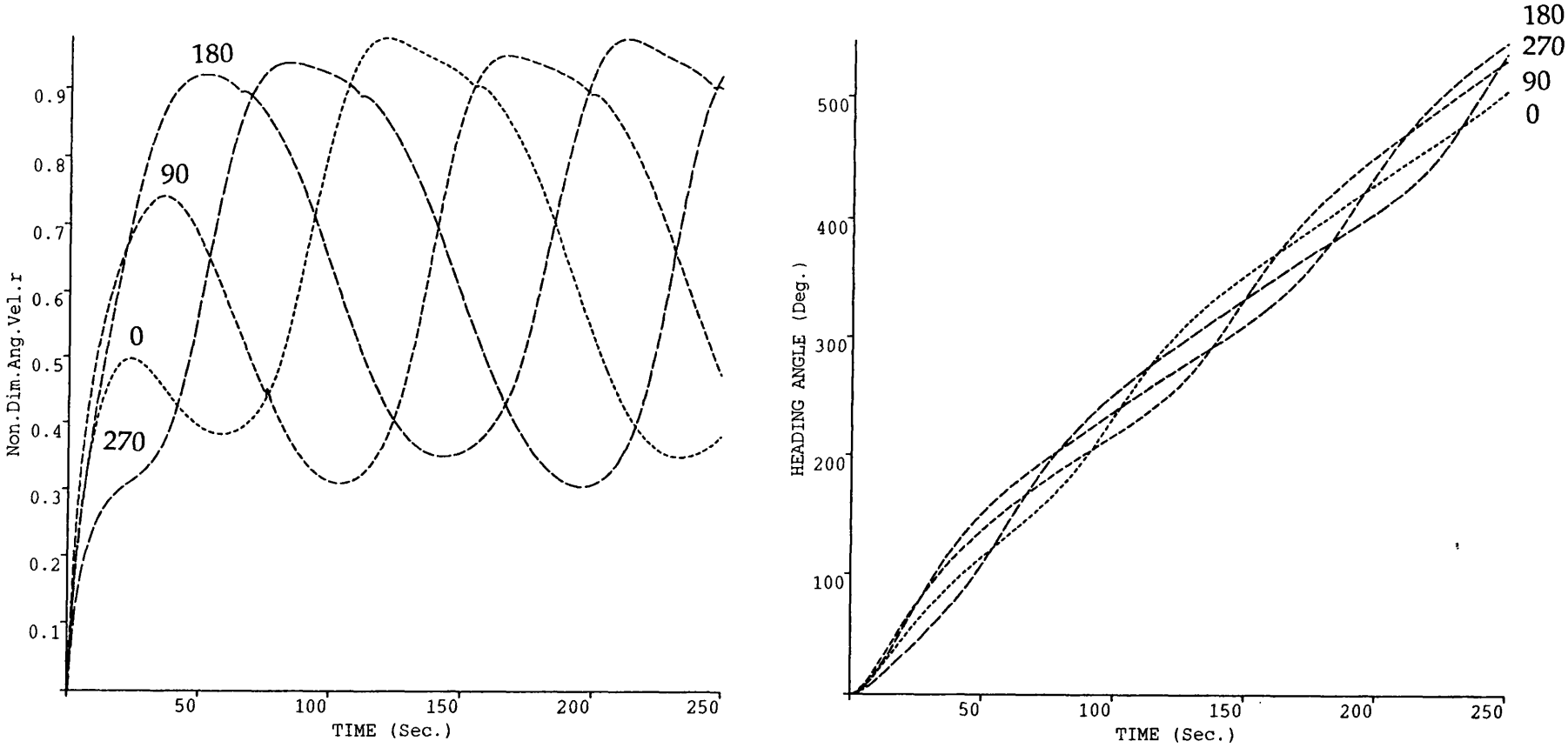

Model Ship Velocity : 0.36m/s
Rudder Angle : 25 degrees Staboard
Wind Velocity Ratio U_W/U : 7.5
Wind Direction : 0, 90, 180, 270 degrees

Figure 3.6c

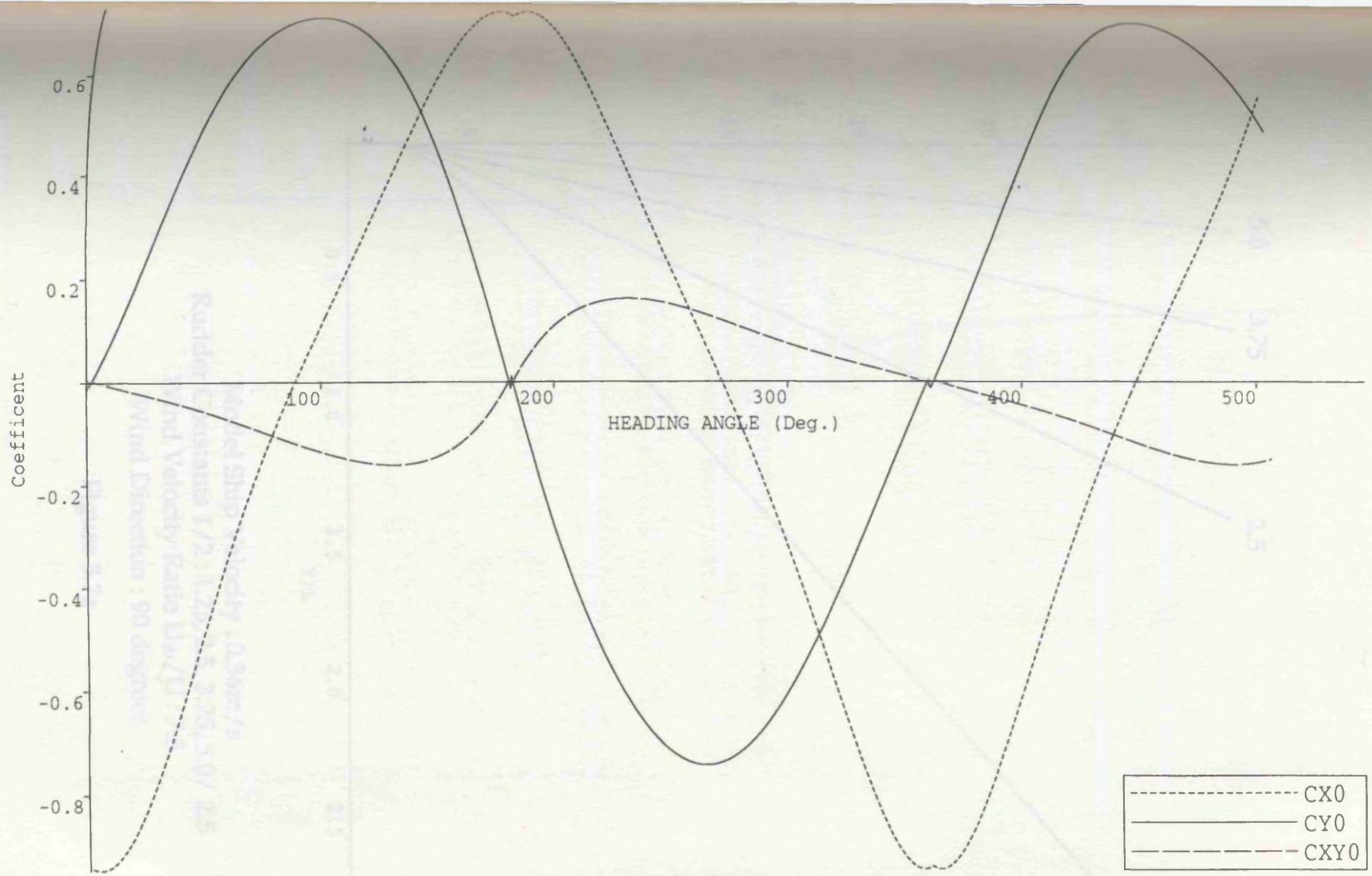

Wind Loading Coefficients for Starboard Turn.

Figure 3.6d

ESSO OSAKA MODEL TRAJECTORY

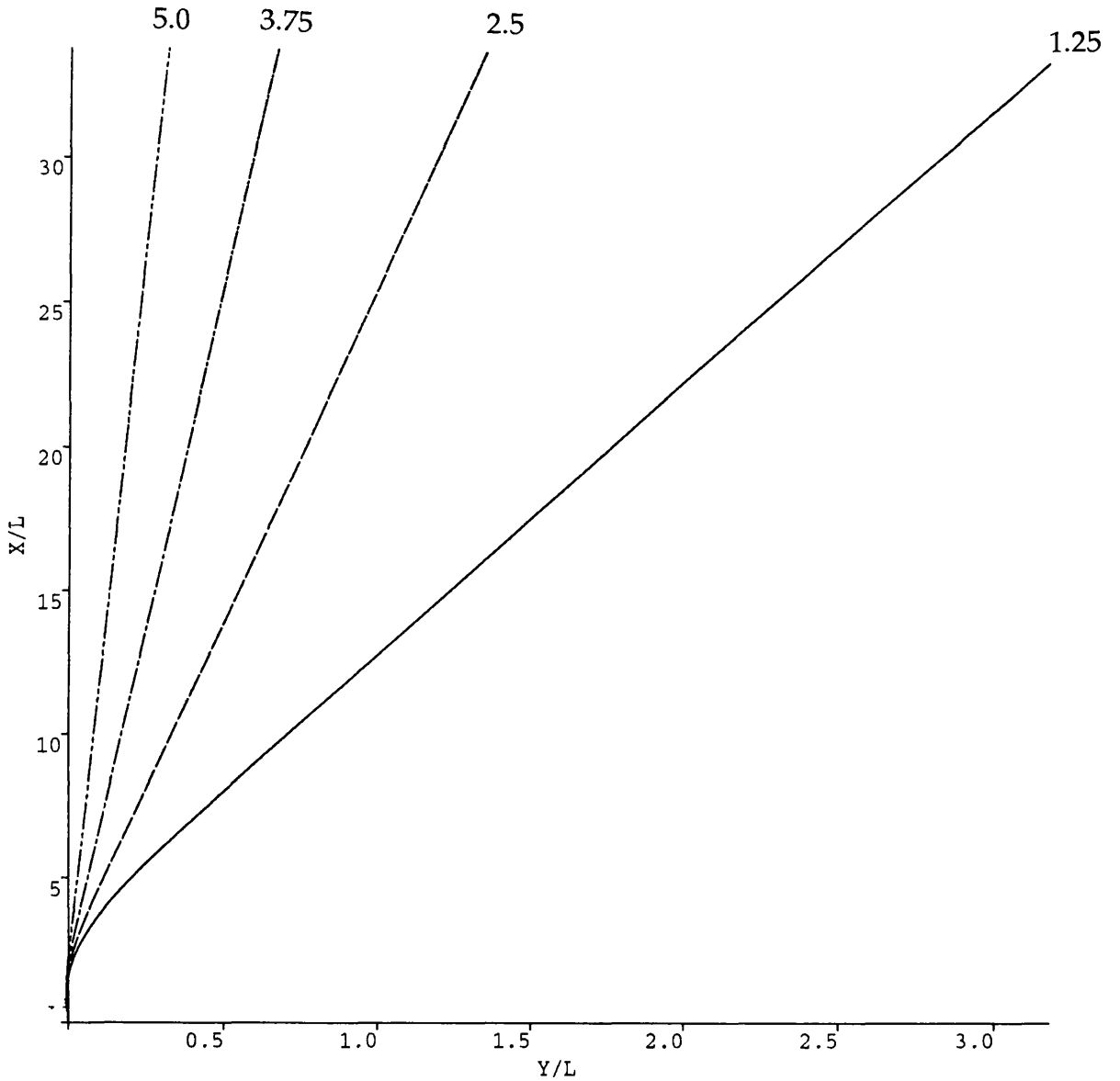

Model Ship Velocity : 0.36m/s
Rudder Constants 1/2 : 1.25, 2.5, 3.75, 5.0/ 2.5
Wind Velocity Ratio U_W/U : 7.5
Wind Direction : 90 degrees

Figure 3.7a

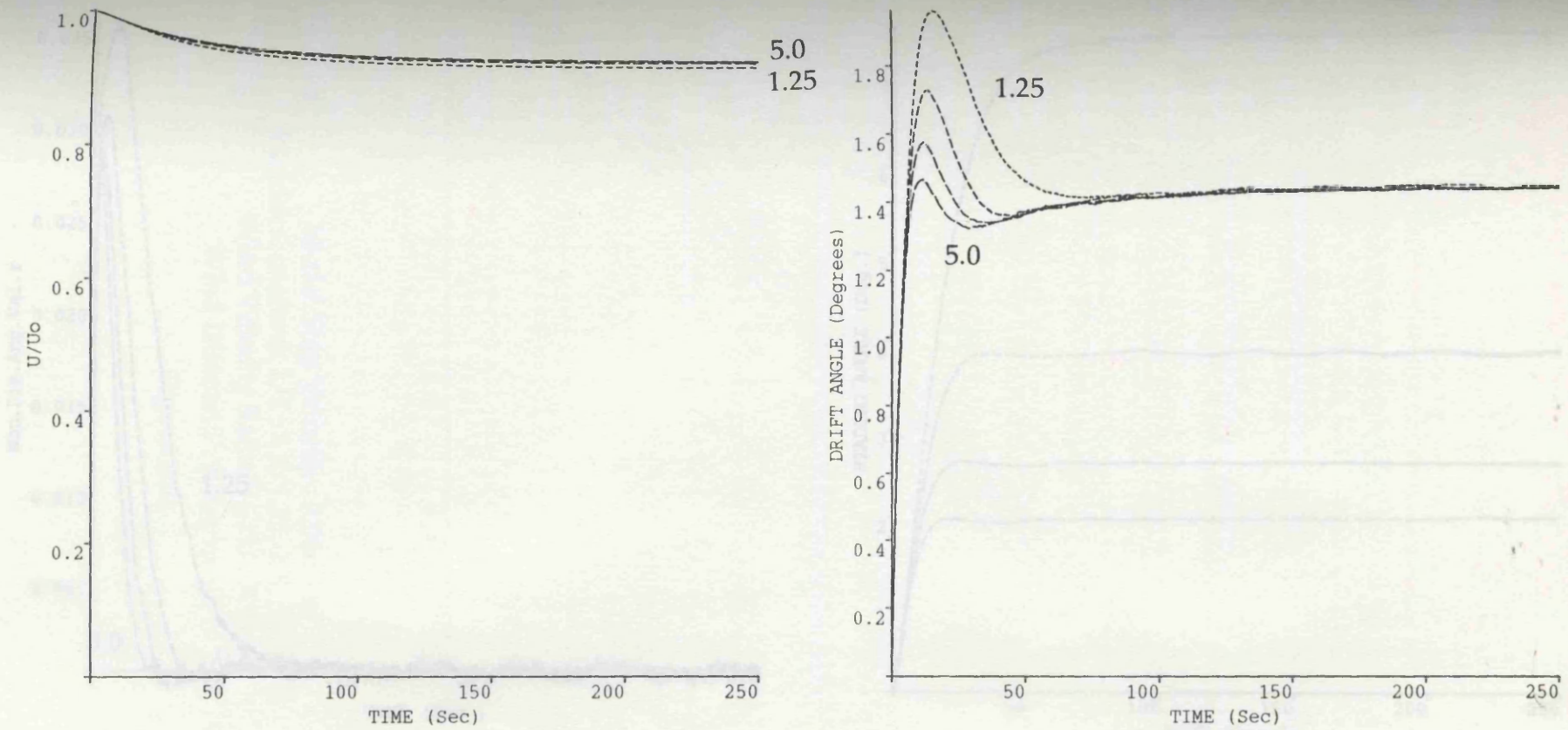

Model Ship Velocity : 0.36m/s
Rudder Constants 1/2 : 1.25, 2.5, 3.75, 5.0/ 2.5
Wind Velocity Ratio U_W/U : 7.5
Wind Direction : 90 degrees

Figure 3.7b

ANGULAR VELOCITY AND HEADING ANGLE

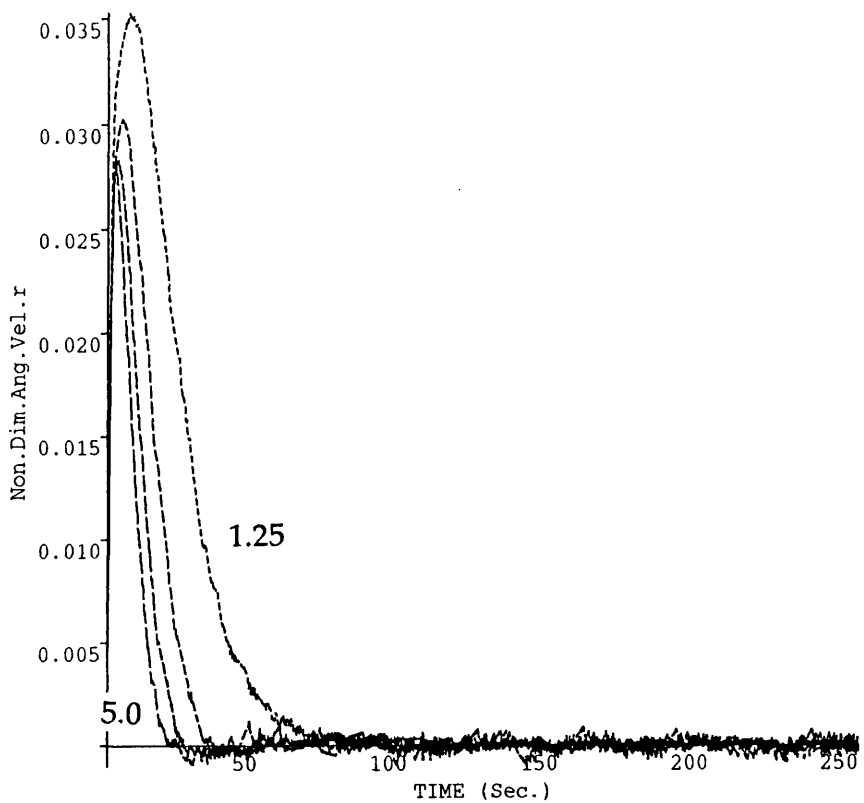

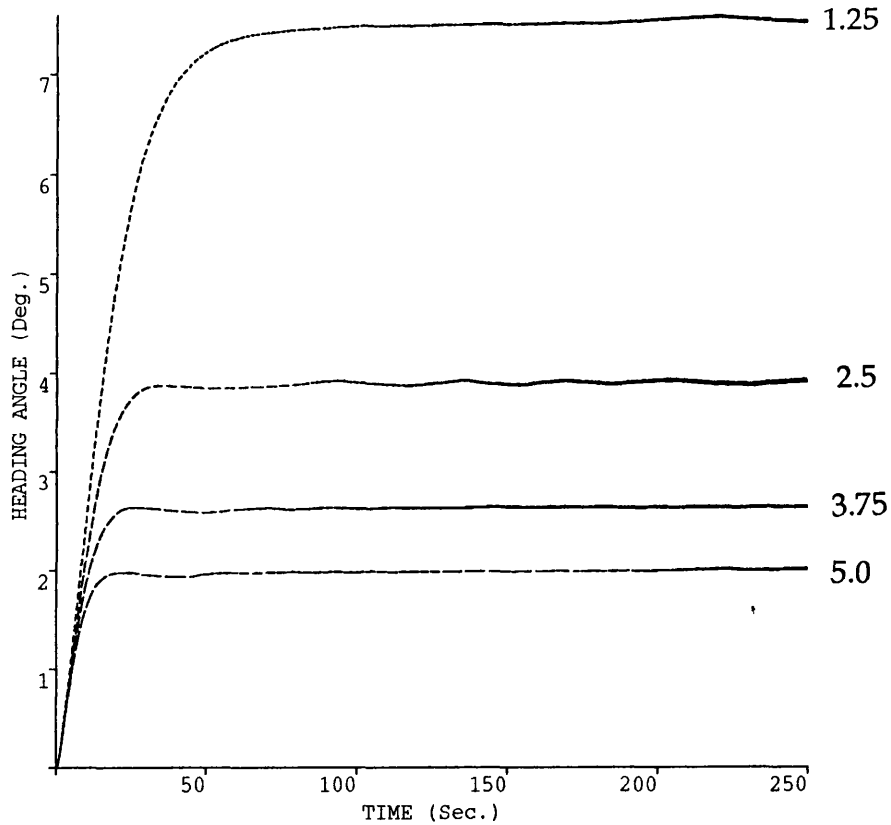

Model Ship Velocity : 0.36m/s
Rudder Constants 1/2 : 1.25, 2.5, 3.75, 5.0/ 2.5
Wind Velocity Ratio U_W/U : 7.5
Wind Direction : 90 degrees

Figure 3.7c

ESSO OSAKA MODEL TRAJECTORY

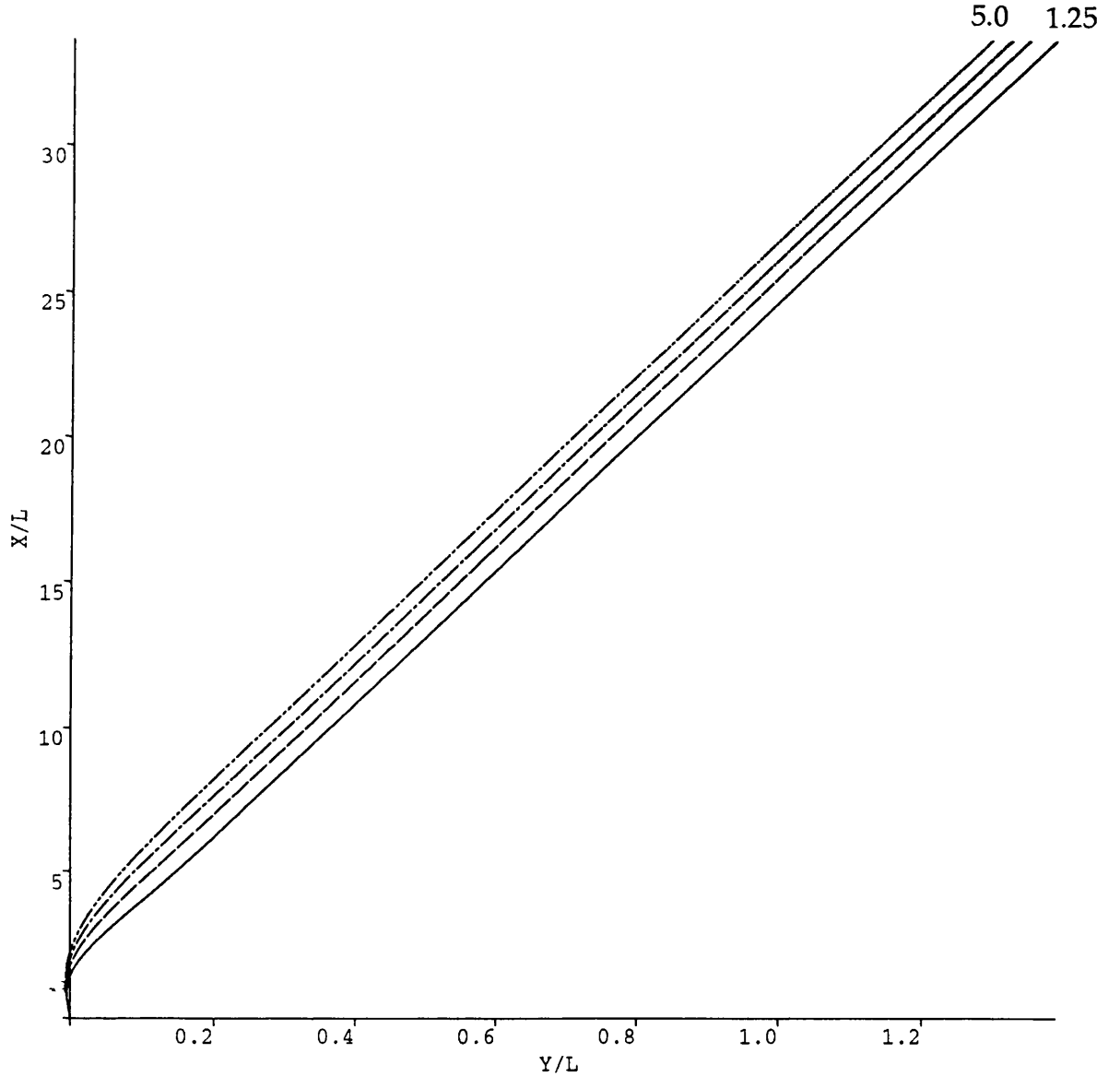

Model Ship Velocity : 0.36m/s
Rudder Constants 1/2 : 2.5/1.25, 2.5, 3.75, 5.0
Wind Velocity Ratio U_W/U : 7.5
Wind Direction : 90degrees

Figure 3.8a

VELOCITY RATIO & DRIFT ANGLE

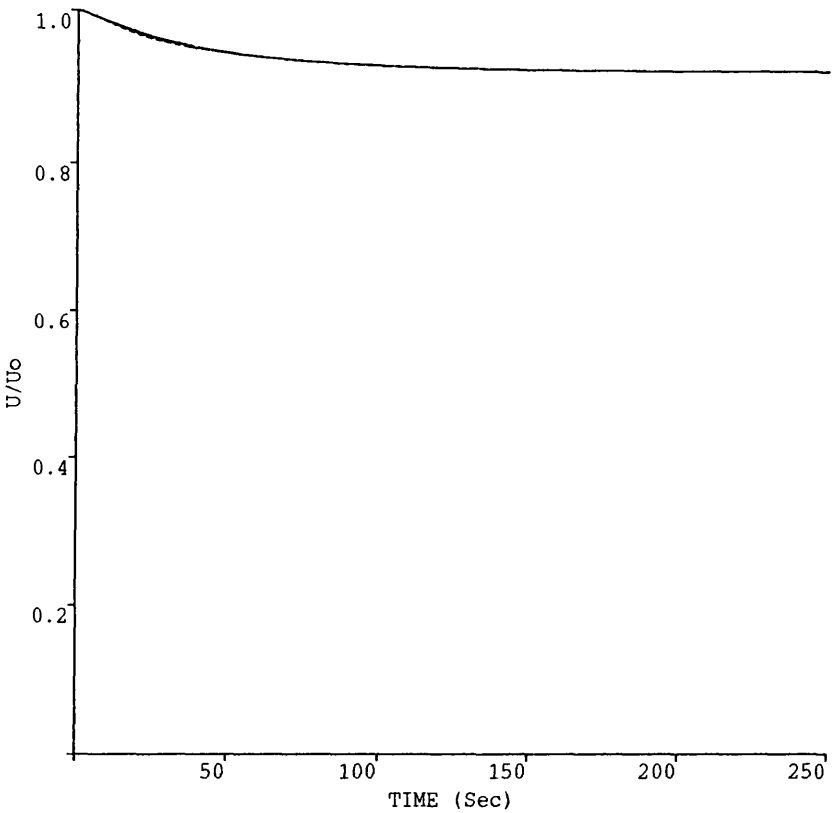

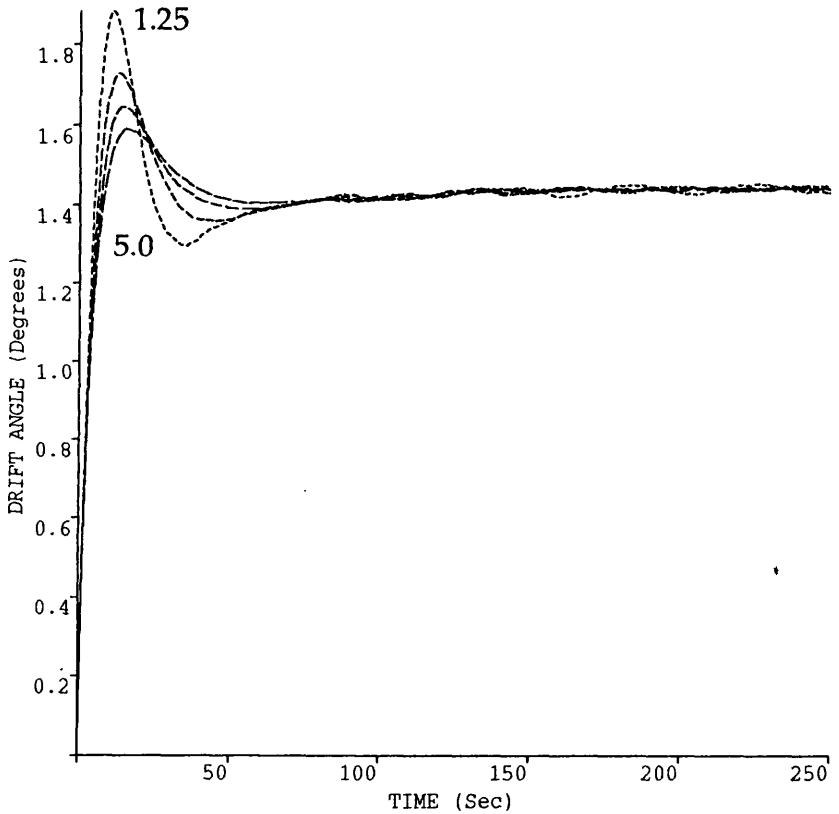

Model Ship Velocity : 0.36m/s
Rudder Constants 1/2 : 2.5/1.25, 2.5, 3.75, 5.0
Wind Velocity Ratio U_W/U : 7.5
Wind Direction : 90 degrees
Figure 3.8b

ANGULAR VELOCITY AND HEADING ANGLE

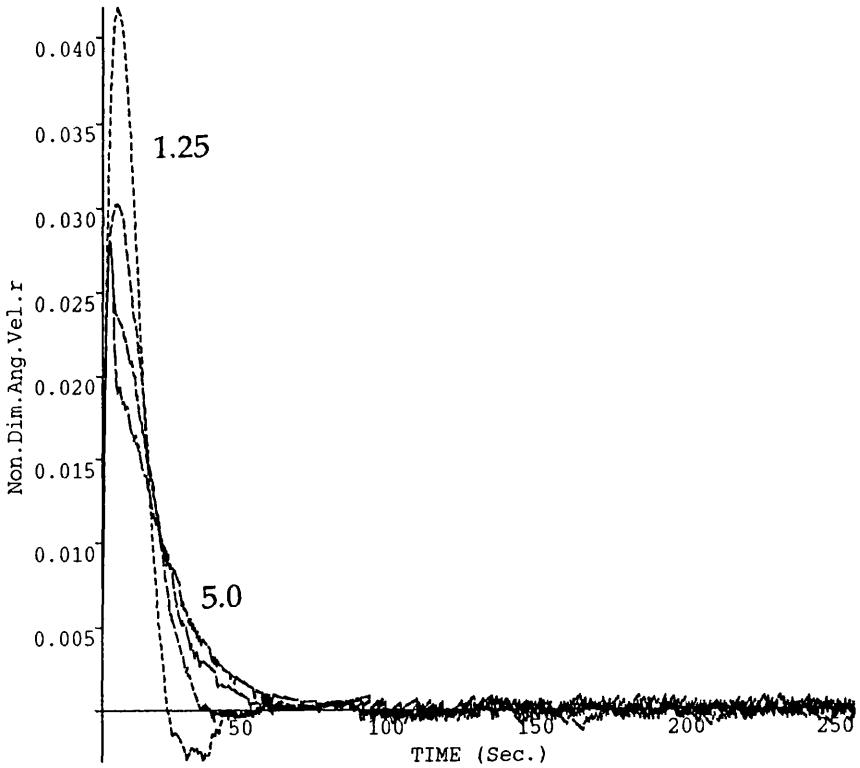

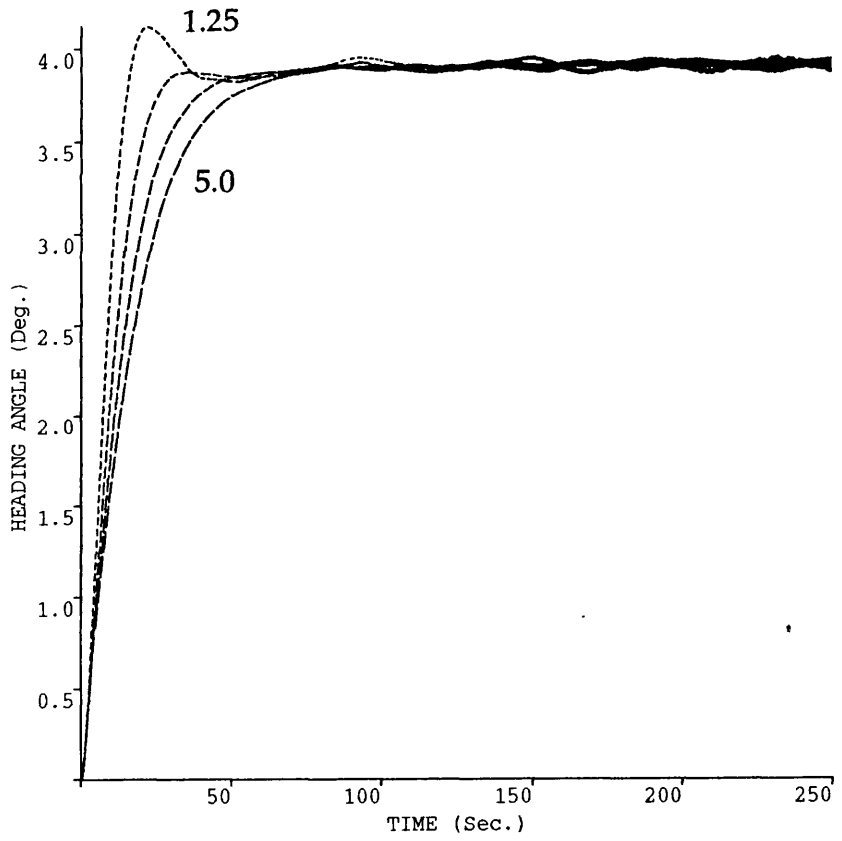

Model Ship Velocity : 0.36m/s
Rudder Constants 1/2 : 2.5/1.25, 2.5, 3.75, 5.0
Wind Velocity Ratio U_W/U : 7.5
Wind Direction : 90 degrees

Figure 3.8c

Chapter Four.

4.1 Modelling Wind Loads on Jack Up Legs and Lattice Type Structures.

The accurate prediction and modelling of hydrodynamic and aerodynamic loads imposed on jack up legs is extremely important when we consider aspects of jack up design, strength, stability and cost. As explained in Ref. 4.1, the drag characteristics of the leg design dictate the strength requirements. If the modelled leg drag is conservative, this will increase the strength requirements and this may in turn increase the leg geometry. This 'design spiral' may also affect the jacking capabilities and the hull arrangements of the jack up. In the case of simulations for the transportation of the jack up under wind loading detailed in Chapter Five, the need to have an accurate prediction of leg drag is also important. If we consider the dry transportation of jack ups commonly by heavy lift vessel the leg geometry and drag will affect the overturning moments and hence this will dictate the limit of the leg length exposed to the wind. The steering requirements of the heavy lift vessel as well as the fixing requirements will also be affected. Under a wet tow, the leg length again affects the wind heel. In addition, wind loading will also cause the jack up to yaw, pitch and roll, and as a result the tow stability will reduce.

The modelling of loads on jack up legs is a very complex problem. Many factors affect the flow of fluid through the leg structure such as solidity, shielding, corner post geometry, teeth size, root, flow regime and roughness to mention a few, Ref. 4.2. There have been numerous experimental studies on the loadings of isolated cylinders, Ref. 4.3 and these studies have reinforced much of what has already been established and also extended our knowledge of flow regimes and the effects of surface roughness such as marine growth. Experimental studies on lattice frames and lattice towers have also been undertaken but to a lesser extent, Refs. 4.4, 4.5. It was only recently 1986 that the British Standards Institution, BSI, Ref. 4.6 produced its design codes for loadings on lattice towers. These

guidelines were specifically formulated for lattice towers such as those used in the telecommunications and electricity industries. Methods for the calculation of wind loads have also been produced by the Engineering Science Data Units, ESDU, Ref. 4.7. Both the BSI and ESDU calculation procedures were obtained from the results of experimental studies employing data in a building block approach with factors for orientation, solidity and shielding. The building block method determines the overall drag by a summation of the drag contributions on each leg component. These methods can be used for the determination of wind loads on jack up legs and have been applied in comparison studies along with other wind load codes and classification rules. They however fail to take account of the numerous legs chord configurations and designs as studied by Pharr-Smith of Marathon Marine Engineering Company, MMEC, Refs. 4.1, 4.2. The experimental work by Pharr-Smith et al., has been very important for the accurate determination of loads on legs at near full scale Reynolds number. They showed not only the influence of the leg chord design but also the tooth size and root.

In this Chapter the calculation methods proposed by Det Norske Veritas, DnV, Ref. 4.8, BSI, Ref. 4.6 and Pharr-Smith of MMEC are compared for square and triangular leg geometries. The calculation methods are shown in the Appendices D-F. The assumptions common to all three methods is that the wind velocity is steady i.e. no gusting. The variation in wind velocity with elevation above the still water level may be described by the DnV power rule as,

$$V = V_o\left(\frac{z}{z_o}\right)^{0.09} \qquad 4.1$$

V_o wind velocity at reference height

z height of load point above the mean still water level

z_o reference height (z_o=10.0 m)

Fig. 4.1 shows the relationship of wind velocity with elevation for

equation 4.1.

We also assume the leg geometry dimensions do not vary with elevation and that the leg is symmetrical. No ancillaries such as ladders or stringers are considered.

4.2 Leg Geometries.

There will be six leg geometries studied and these will include 3 square and 3 triangular lattice structures. In figures 4.3 through to 4.6 we see typical examples of leg geometries and corner post design. The initial analysis will study loading of a square and triangular leg design with idealised cylindrical cornerposts. The leg member dimensions for this investigation were obtained from Ref. 4.9. The study will then be extended to more realistic cornerpost geometries shown in figures 4.4. The leg bracing member dimensions for these geometries were estimated from information given in Refs. 4.1 and 4.2. The dimensions of the bracings were chosen to give the required leg solidity ratios and member areas. A calculation showing the method of obtaining the estimates of leg member dimensions for square and triangular geometries is given in Table 4.1. The leg member dimensions for this study are given in Table 4.2 for all the square and triangular geometries considered. The effects of Reynolds Number will be investigated where appropriate as will the effects of orientation and surface roughness. The results of the comparison of DnV, BSI, and MMEC methods can be seen in figs. 4.14-4.42. Each of the calculation methods are detailed in Appendices D-F. All the leg lengths studied are 100m long and the base of the legs are located 15 meters above the mean still waterline.

4.3.1 DnV Method

The DnV Classification Rules method for the calculation of wind loading is different from the MMEC and BSI methods because it uses a concept of effective diameter. It should therefore be limited to cylindrical cornerposts and members. The method determines the forces acting on

each member in the entire volume of the structure as opposed to the projected area of the face over one bay in the case of BSI and MMEC methods. It gives no account for shielding factors. The method can easily be adapted to study surface roughness by increasing the area and drag coefficient on each cylindrical member. The DnV method is complicated because knowledge of the angles of the bracings are required both vertically and horizontally, fig. 4.6. The DnV method was not used in the comparison study for the real leg geometries 3-6.

4.3.2 BSI Method.

The BSI method is applicable to free standing tower structures of lattice construction and these include guyed masts. This method is not ideally suited to jack up lattice legs as the formulation of forces does not treat the drag on the corner posts of different geometries individually. The forces on the structure are obtained from the projected areas of the members over one bay height. The method determines the overall drag from contributions of sub/supercritical cylindrical members drag and flat plate drag which are functions of solidity and leg geometry. It therefore treats the drag on the lattice face as a whole as opposed to a summation of individual members drag in the MMEC method. The effects of orientation on the square geometry is calculated as a function of solidity, cylindrical area and flat plate area. In the case of the triangular geometry, drag varies with orientation for flat plates only. The BSI method does not include any means of including surface roughness, such as marine growth. The BSI method treats all cornerpost geometries which are not cylindrical as flat plate. The flat plate drag is independent of Reynolds number. The variation of wind velocity is determined from the DnV power rule. The drag coefficients on the cylindrical members is dependent upon which region of sub and supercritical Reynolds numbers the member lie. The transition Reynolds number is chosen as 4×10^5 and is multiplied by a factor of 1.5 as outlined in Appendix E. No transcritical behaviour is modelled.

The BSI method is more involved than MMEC method. It can be extended to model ladders, stringers, ice loading, gusting factors, etc as indicated in the BSI guidelines. MMEC does not include any means of including such items.

4.3.3 MMEC Method.

The MMEC method was developed from extensive experiments carried out on jack up leg geometries at near full scale Reynolds numbers. The drag coefficients and areas for each corner post design and cylindrical members are input for the windward and leeward faces. It is noted that only the projected members in the windward and leeward faces make contributions to the overall drag. Members which are inside the volume and hidden are not taken into account. The leeward areas are multiplied by a shielding factor which is a function of solidity. The transition Reynolds number is chosen as 4×10^5. The member drag for sub/supercritical behaviour is 1.2 and 0.7 respectively. The Reynolds number effect is clearly shown in fig. 4.2 for 15m/s base wind velocity. No transcritical behaviour is modelled as recommended in Ref. 4.1.

The MMEC calculations were extended further to study the effects of surface roughness. The leg drag coefficients were determined using an increased area and increased drag coefficients as recommended by Ref. 4.2 on all cylindrical members. The values chosen for increased drag are 1.25/1.1 for the sub/supercritical behaviour and the definition of increased area is given in Ref. 4.10 and figs. 4.8 and 4.9. The transition Reynolds number is chosen as 1×10^5.

The MMEC method is easy to use but accurate cornerpost drag coefficients must be known. Orientation is taken into account for square legs only. The drag on the triangular legs is assumed constant with orientation.

4.4 Discussion of Results.

4.4.1 DnV Method.

On inspection of the all cylindrical square leg geometry 1, figs. 4.14 -4.18 we see that the DnV results converge with the results of MMEC and BSI for increasing angle of incidence. If we examine further the orientation of the three methods, fig. 4.15 we see that DnV method decreases to a minimum value at 45 degrees. This behaviour seems to be incorrect because of the increased area of exposed members to the wind at 45 degrees. In addition, figure 4.5 taken from Ref. 4.1 clearly shows an increased drag coefficient for increasing orientation for all square leg geometries. The DnV method however, compares well with MMEC and BSI in the range of 15-75 degrees for the square geometry. The DnV method results assumes super critical flow and drag coefficient of 0.7 for all cylindrical members. The results of the all cylindrical member triangular geometry are given in fig. 4.19. The DnV results compare well with BSI and MMEC. The orientation of DnV, fig. 4.20 shows a minimum at 60 degrees.

4.4.2 BSI and MMEC Methods.

The BSI method compares favourably with the MMEC method for the two square leg geometries 3 and 4. This is surprising due to the different approaches of each method. There are differences however as can be seen in figs. 4.27-4.30 at wind velocities less than 20 m/s. This is due to the definitions of the domains of the sub and supercritical flow regimes. In the BSI method Appendix E, the Reynolds number or the transition of the flow regime is multiplied by a factor of 1.5. In the MMEC method the transition is calculated at actual Reynolds number. The transition Reynolds numbers were the same in both cases i.e. 4×10^5. The sub and supercritical drag coefficients for both methods are shown in figs. 4.26 and 4.32 for geometry 3 and 4 respectively. The subcritical drag coefficients shows clearly the large differences in the loading at the lower wind velocities. The supercritical drag coefficients show small differences.

The triangular lattice leg results are given in figs. 33-38 for leg geometries 5 and 6. The cornerposts are treated as flat plate in the BSI

method. In geometry 5, both methods compare well for supercritical behaviour and this is shown when comparing the drag coefficients, fig. 4.35. The MMEC method drag does not vary with orientation for triangular geometries. Geometry 6 shows much greater differences than in any of the previous geometries. On inspection of the drag coefficients, the subcritical drag coefficients compare better than the supercritical drag coefficients. A further investigation, shows the differences could be due to the lower cornerpost drag coefficients of windward and leeward faces as used by MMEC in geometry 6. These drag coefficients are given in Table 4.2 along with the flat plate drag coefficients obtained by BSI. The geometries 5 and 6 have the same solidity and hence flat plate drag coefficient.

4.4.3 MMEC Method and Marine Growth.

The MMEC calculation method was extended further to study the effects of marine growth or surface roughness on leg geometries 3 and 6. The values of the surface roughness examined were Mean Marine Growth (MMG) of 0.005m with Mean Roughness Height (MRH) of 0.00125m and also MMG 0.01m with MRH 0.0025m. The definitions of these quantities can be obtained from Ref. 4.10 and fig. 4.7. It is assumed that the marine growth is uniform over all the cylindrical members. The effect of marine growth is modelled as an increased drag coefficient and increased surface area as recommended by Pharr-Smith in Ref. 4.2. The effect of roughness appears to be quite dramatic as seen in figs. 4.39 and 4.41. It is noted that any further increase in marine growth and MRH only marginally increases the load on the leg. The results are however dependent upon the values chosen for the cylindrical member drag coefficients and transitional Reynolds numbers for supercritical flow. An example of experimental values from Ref. 4.3 can be seen in figures 4.8 and 4.9. The drag coefficient for a cylinder at sub critical flow was 1.25 and supercritical flow was 1.1. The transition Reynolds number was assumed as 1×10^5.

4.4.4 Variation of Drag Coefficient with Orientation for the Triangular Leg Geometry.

The prediction of wind loading on the triangular lattice leg geometry is more difficult than for the square geometry. In geometry 2 the DnV method, fig. 4.20 shows the minimum value of load occurring at 60 degrees.

In the MMEC method the orientation factor for the triangular legs is assumed as 1. In the MMEC experimental results Ref. 4.2 and figs. 4.10-4.11, the triangular drag coefficients have minimum values occurring approximately at 30 degrees. The use of the orientation factor of 1 was to ensure wind loading forces were not underestimated.

In the case of BSI, the orientation varies according to,

$$K_\theta = \frac{A_c + A_{c'}}{A_F} + \frac{A_f}{A_F}(1.0 - 0.1\sin^2 1.5\,\theta)$$

It can be seen from the above equation and fig. 4.12 and figs 4.34 and 4.37 that under the BSI method, the minimum value of wind loading will occur at 60 degrees only if there are flat sided members in the structure. If the structure is all cylindrical then the loading is constant for increasing wind incidence.

According to ESDU Data Item 81028 Ref. 4.7, the orientation factor for a triangular geometry indicates the minimum loading occurs at 30 degrees, and is shown in fig. 4.13

The above four calculation methods each give conflicting results about the location of the minimum value for loading on triangular lattice type structures.

Example Calculation for Estimate of Leg Member Dimensions from Ref.4.1
Square Gorilla Leg.
Assume members 2&3 have the same diameter.
Leg Dimensions and Component Projected Areas.

Component	Area(ft^2)	Area(m^2)
Total Cylinder Area	114.5	10.637
Total Gusset Area	15	1.394
Total Corner Post Area	102.81	9.551
Overall Projected Area	232.31	21.582
Length of bay (ft,m)	16.777	5.114
Width of Bay (ft,m)	46	14.021

Width of Corner Post=9.551m^2/(2*5.114m)=0.934m

Cylindrical Area=10.637m^2
Horizontal Brace= 1*(14.021-2*0.934)*DIAM= 12.159*DIAM
Vert. Brace= 2*((12.159/2)^2+5.114^2)^0.5)*DIAM= 15.883*DIAM
Total Area 28.042*DIAM

DIAM=10.637m^2/28.042m= 0.379m
Member 4 diameter is approximately 60% of diameters of members 2&3
Projected members per face.

Member	Length (m)	Diameter (m)	No.of Members
1	5.114	0.934	2
2	12.159	0.379	1
3	7.942	0.379	2

Example Calculation for Estimate of Leg Member Dimensions from Ref.4.2
Triangular Leg. Split Tube Opposed Rack.
Leg Dimensions and Component Projected Areas.

Component	Area(ft^2)	Area(m^2)
Total Cylinder Area (Windward)	49.8	4.627
Total Cylinder Area (Leeward)	61.79	5.740
Corner Post Area (Windward)	38.64	3.590
Corner Post Area (Leeward)	29.38	2.729
Length of bay (ft,m)	12	3.658
Width of Bay (ft,m)	34.11	10.397

Width of Corner Post =3.59m^2/(2*3.658m)=0.491m
Horizontal Brace Length=10.397m-2*0.491m=9.415m

Projected Member Lengths	
Windward	(3.658^2 + 9.415^2/4)^0.5=5.962m
Leeward	(3.658^2 + 9.415^2/16)^0.5=4.349m
Cylindrical Area	
Windward	4.627=9.415*DIAH + 2*5.962*DIAV
Leeward	5.74=9.415*DIAH + 4*4.349*DIAV
Lee-Wind	1.113=(17.396-11.923)*DIAV
	DIAV=0.204m
	DIAH=0.234m

Member 4 diameter is approximately 60% of diameters of members 2&3
Projected members per face.

Member	Length (m)	Diameter (m)	No.of Members
1	3.658	0.491	2
2	9.415	0.234	1
3	5.962	0.204	2

Table 4.1

Geometry1

Square. All Cylindrical Members

Member	Length (m)	Diameter (m)	No.of Members
1	4	0.7	4
2	8	0.25	4
3	5.66	0.25	8
4	5.66	0.15	4

Geometry 2

Triangular. All Cylindrical Members

Member	Length (m)	Diameter (m)	No.of Members
1	4	0.7	3
2	8	0.25	3
3	5.66	0.25	6
4	4	0.15	3

Geometry 3

Square. Gorilla Design.

MMEC Cornerpost Drag.			
Windward	1.882	Leg Solidity	0.3008
Leeward	1.573	BSI CNF	2.5313
Member	Length (m)	Diameter (m)	No.of Members
1	5.114	0.934	4
2	12.159	0.379	4
3	7.942	0.379	8
4	8.598	0.227	4

Geometry 4

Square. Triangular Corner Post Design.

MMEC Cornerpost Drag.			
Windward	2.012	Leg Solidity	0.3596
Leeward	1.625	BSI CNF	2.3359
Member	Length (m)	Diameter (m)	No.of Members
1	3.408	0.772	4
2	7.599	0.296	4
3	5.104	0.296	8
4	5.373	0.178	4

Geometry 5

Triangular. Circular with Opposed Racks.

MMEC Cornerpost Drag.			
Windward	0.9472	Leg Solidity	0.216
Leeward	1.7348	BSI CNF	2.489
Member	Length (m)	Diameter (m)	No.of Members
1	4.828	0.648	3
2	15.222	0.346	3
3	9.013	0.315	6
4	7.611	0.2	3

Geometry 6

Triangular. Split Tube Opposed Rack Chord.

MMEC Cornerpost Drag.			
Windward	0.8183	Leg Solidity	0.216
Leeward	1.3888	BSI CNF	2.488
Member	Length (m)	Diameter (m)	No.of Members
1	3.659	0.491	3
2	9.415	0.234	3
3	5.962	0.204	6
4	4.708	0.14	3

All members defined in Figures 4.3 & 4.6

Members 4 are hidden by members 2 and are approximately 60% diameter of members 2 & 3

Table 4.2

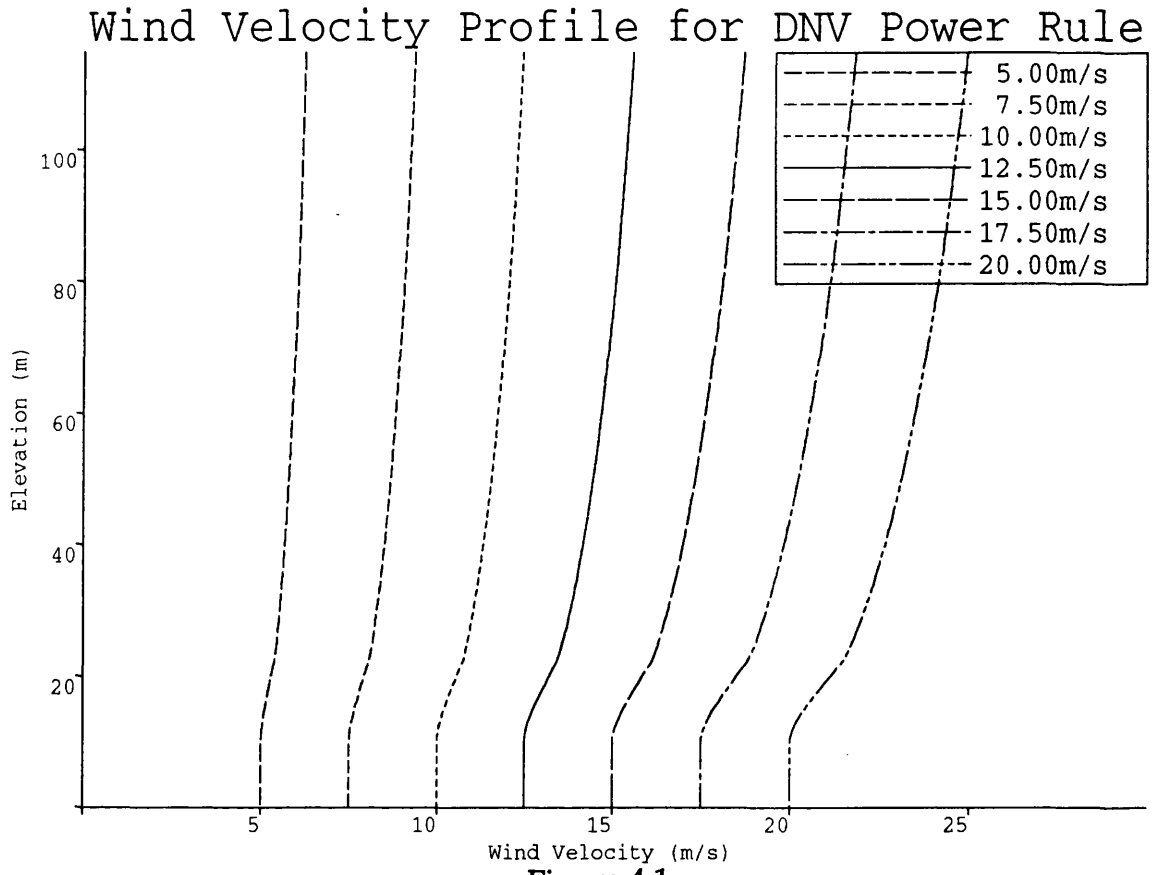

Figure 4.1

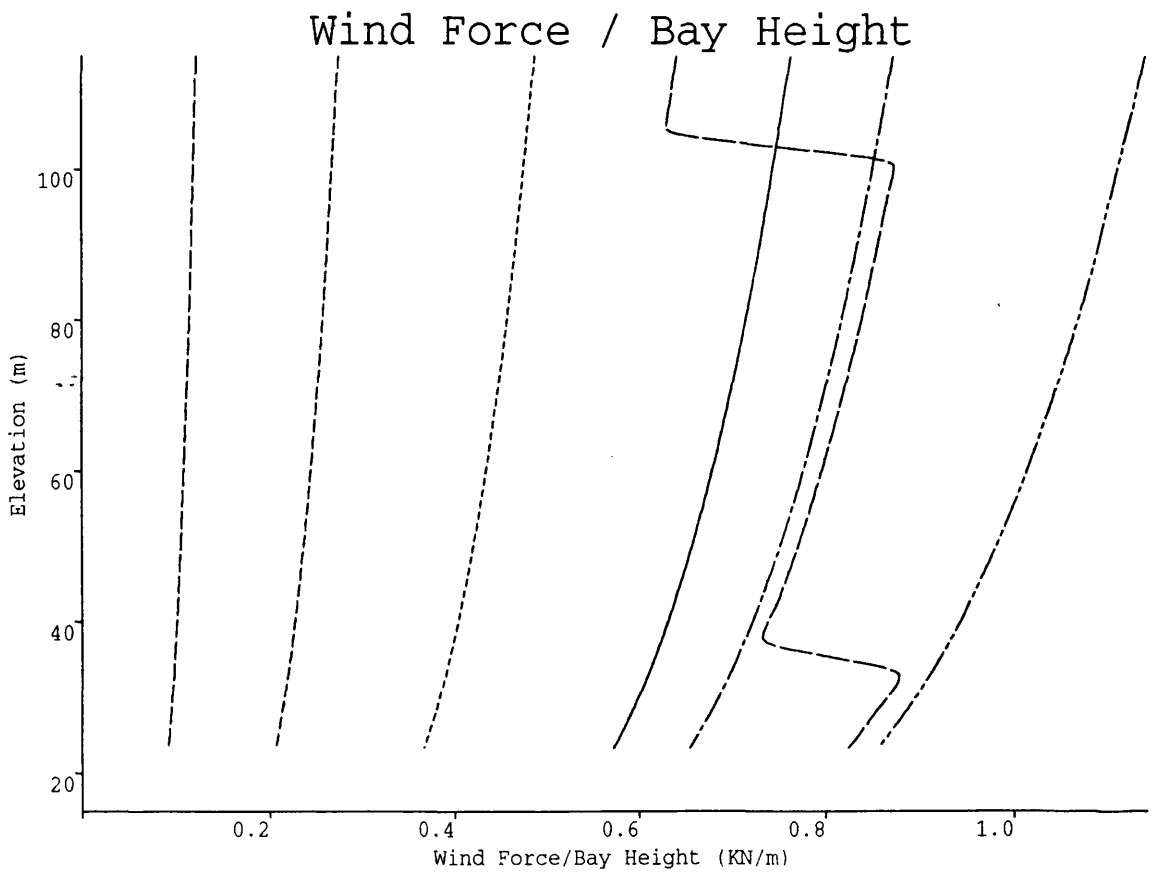

Figure 4.2

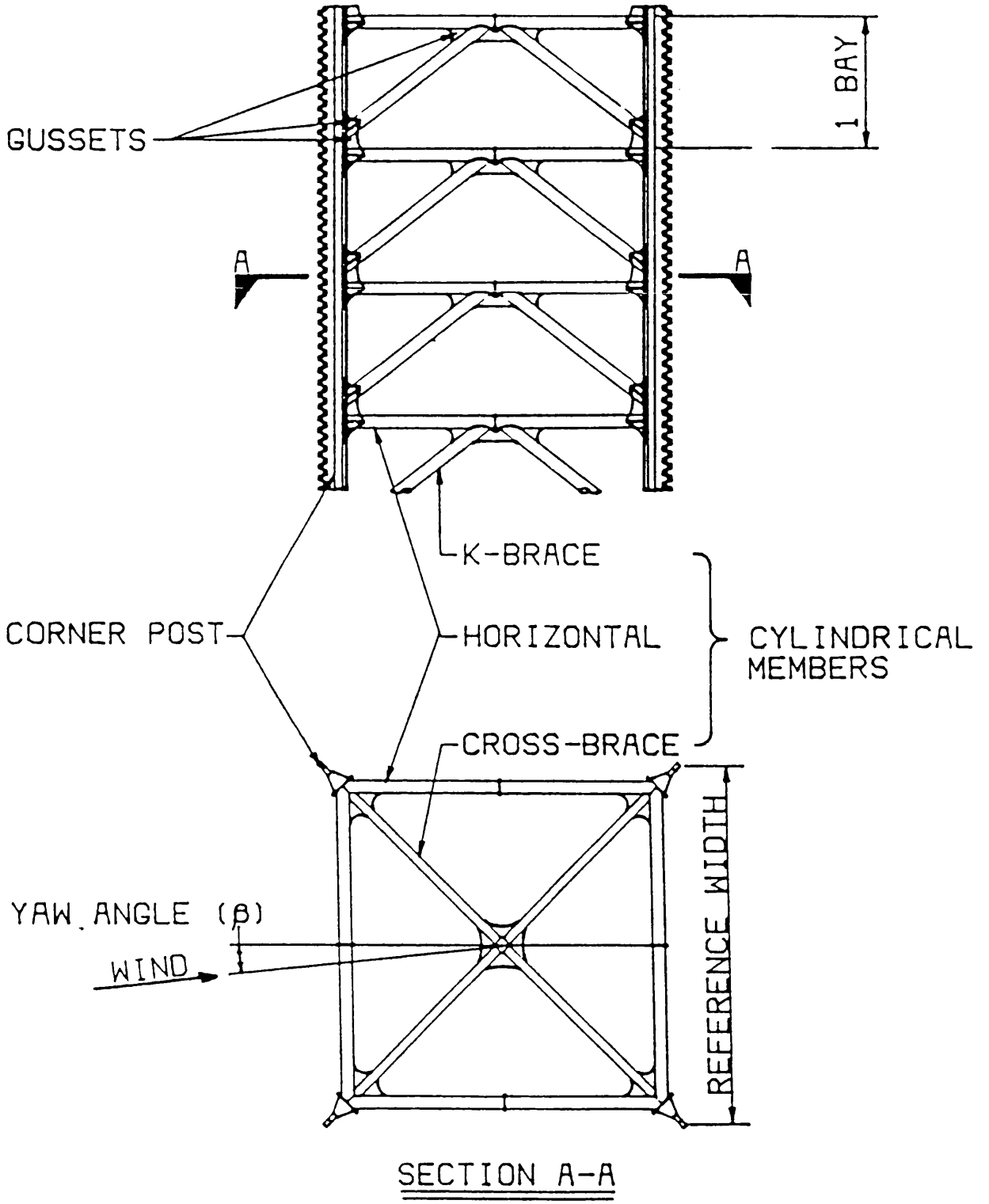

Generalized jackup truss leg (triangular corner posts with gussets shown)

Figures from Ref. 4.1

Figure 4.3

Leg Corner Post Cross Sections

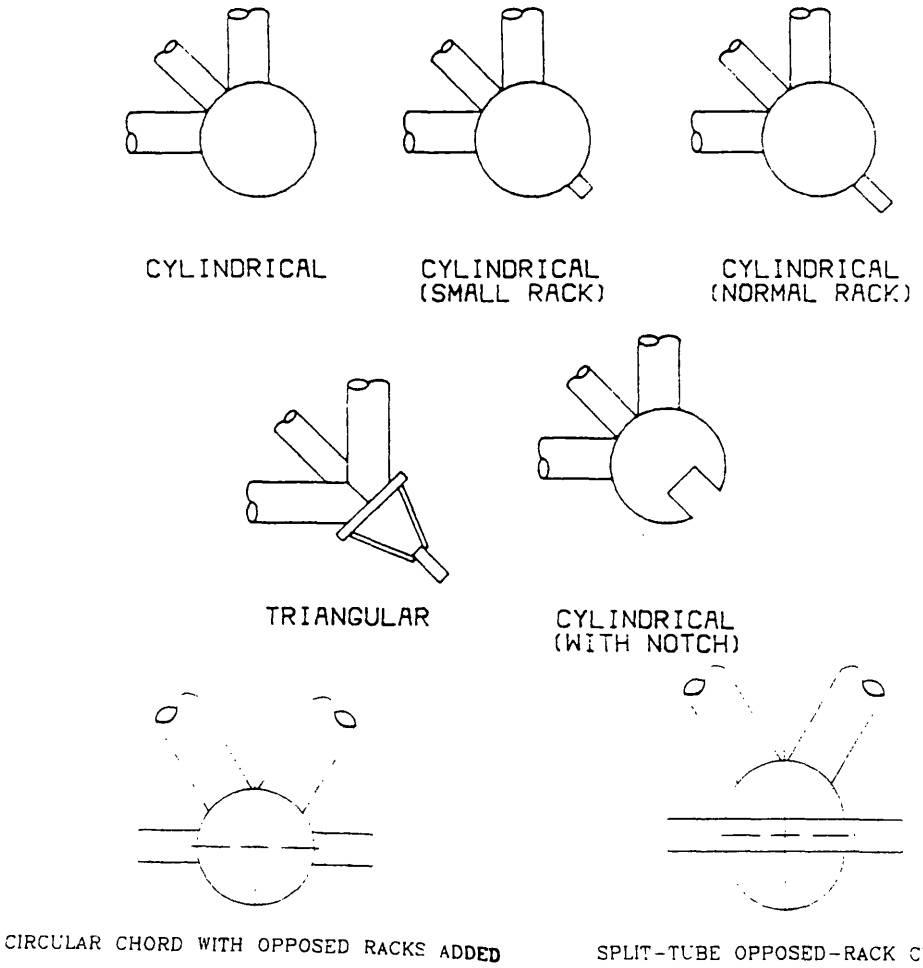

Figure 4.4

Figures from Ref. 4.1, 4.2

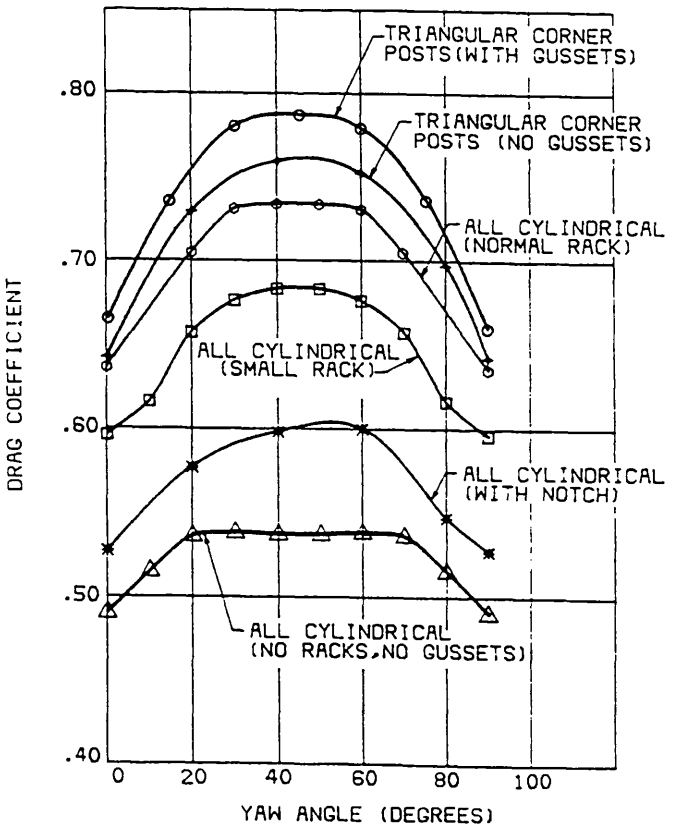

Variation of drag coefficient with yaw angle for various $1/12$-scale leg models

Figure 4.5

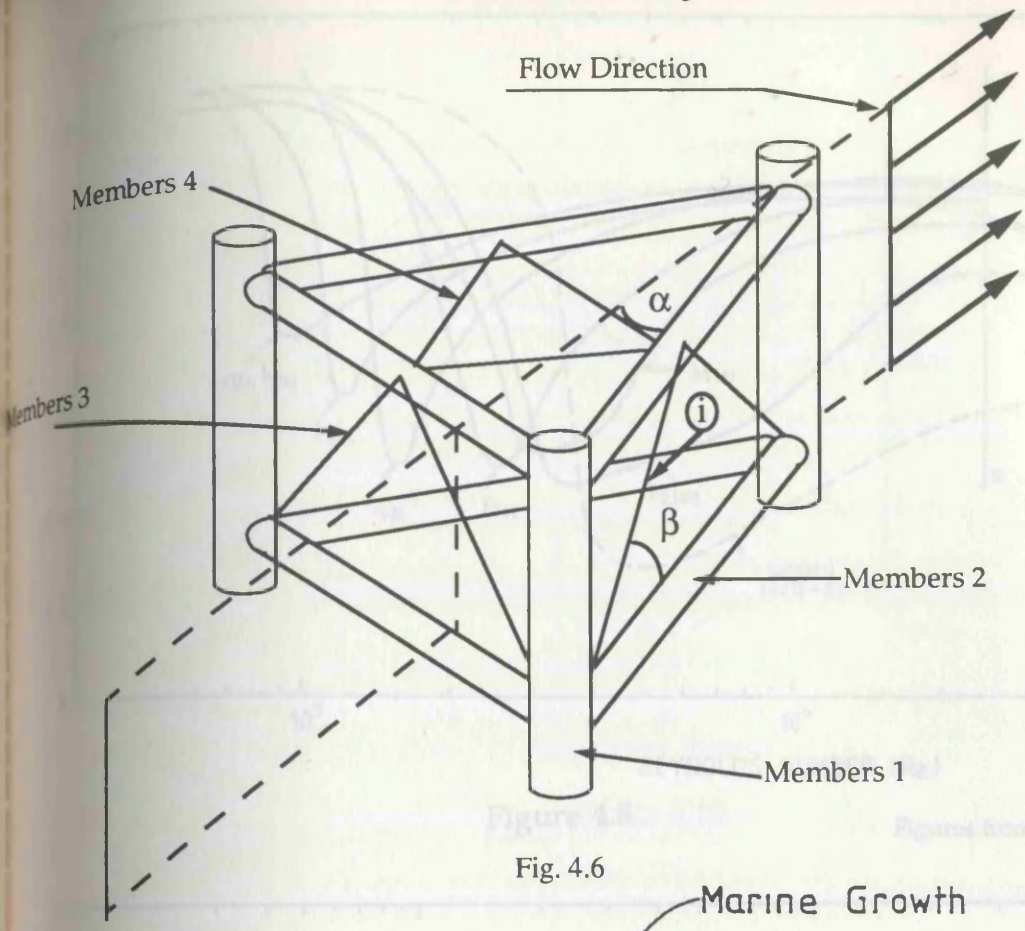

Fig. 4.6

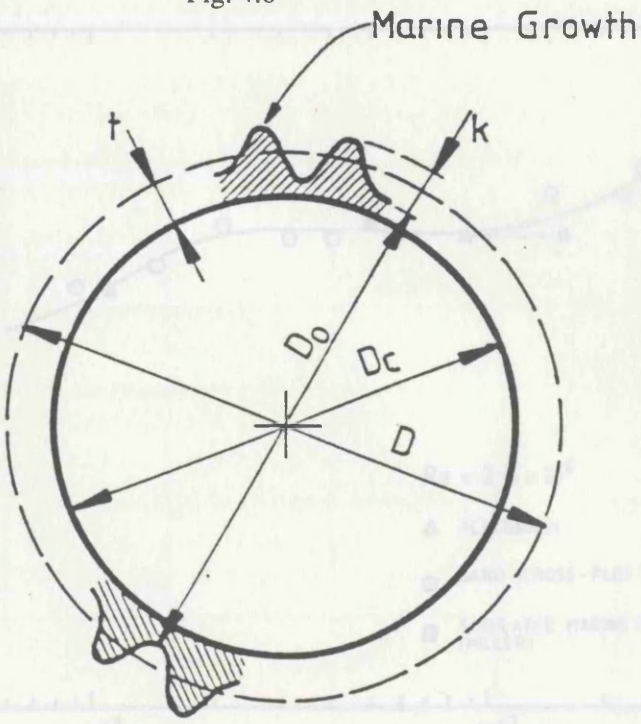

Figure from Ref. 4.10

D_C = cylinder diameter
$D_O = D_C - k + 2t$
D = mean diameter of cylinder and marine growth
t = mean marine growth thickness
k = mean roughness height
$A = \pi D^2/4$ = mean cross sectional area

Figure 4.7

Influence of Roughness Height with Reynolds Number on Drag Coefficient.

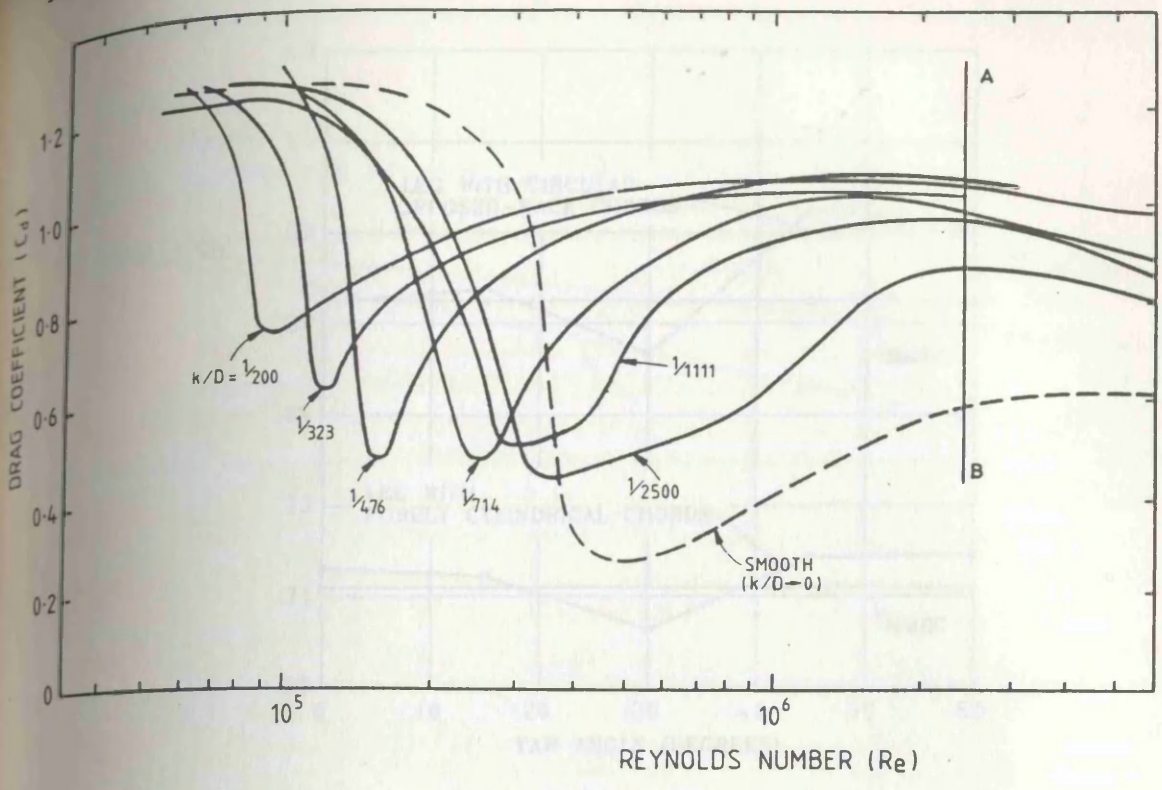

Figure 4.8

Figures from Refs. 4.3, 4.10

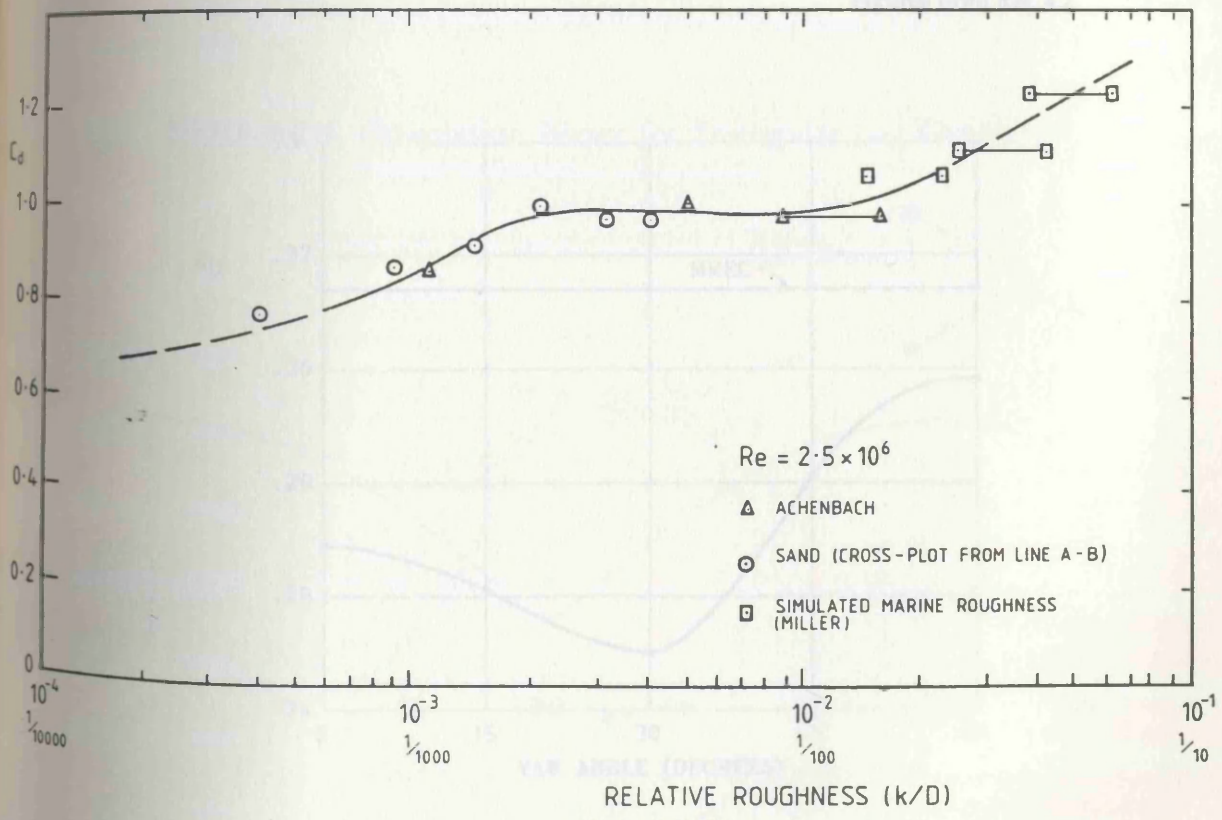

The influence of roughness height and Reynolds number on the drag coefficient for steady flow (Miller, 1976)

Figure 4.9

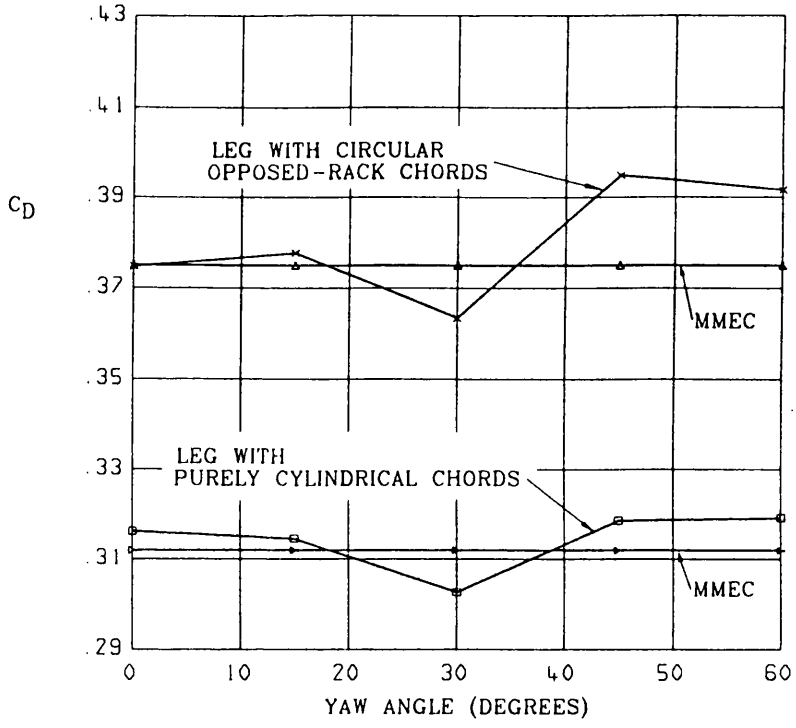

Figure 4.10

Figures from Ref. 4.2

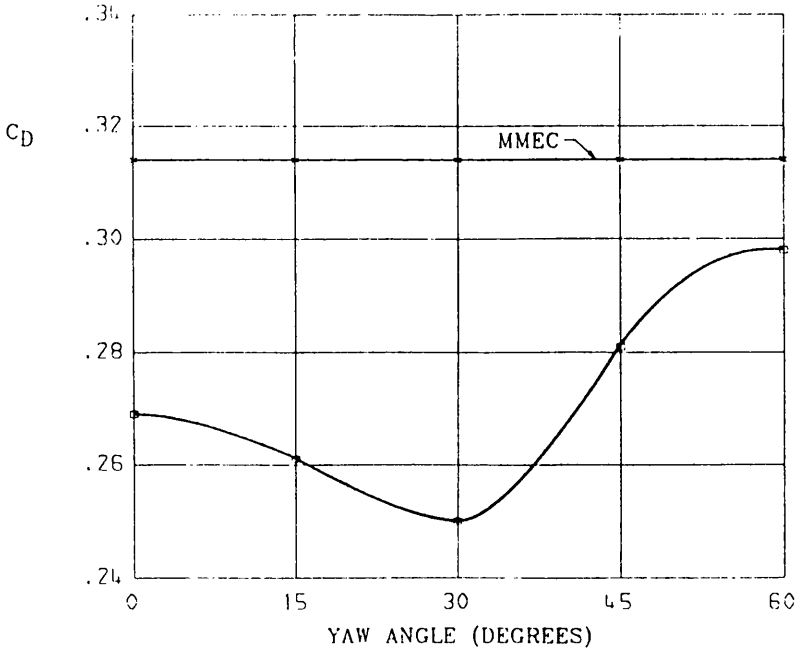

Figure 4.11

BSI 8100. Orientation Factors for Leg Geometries.

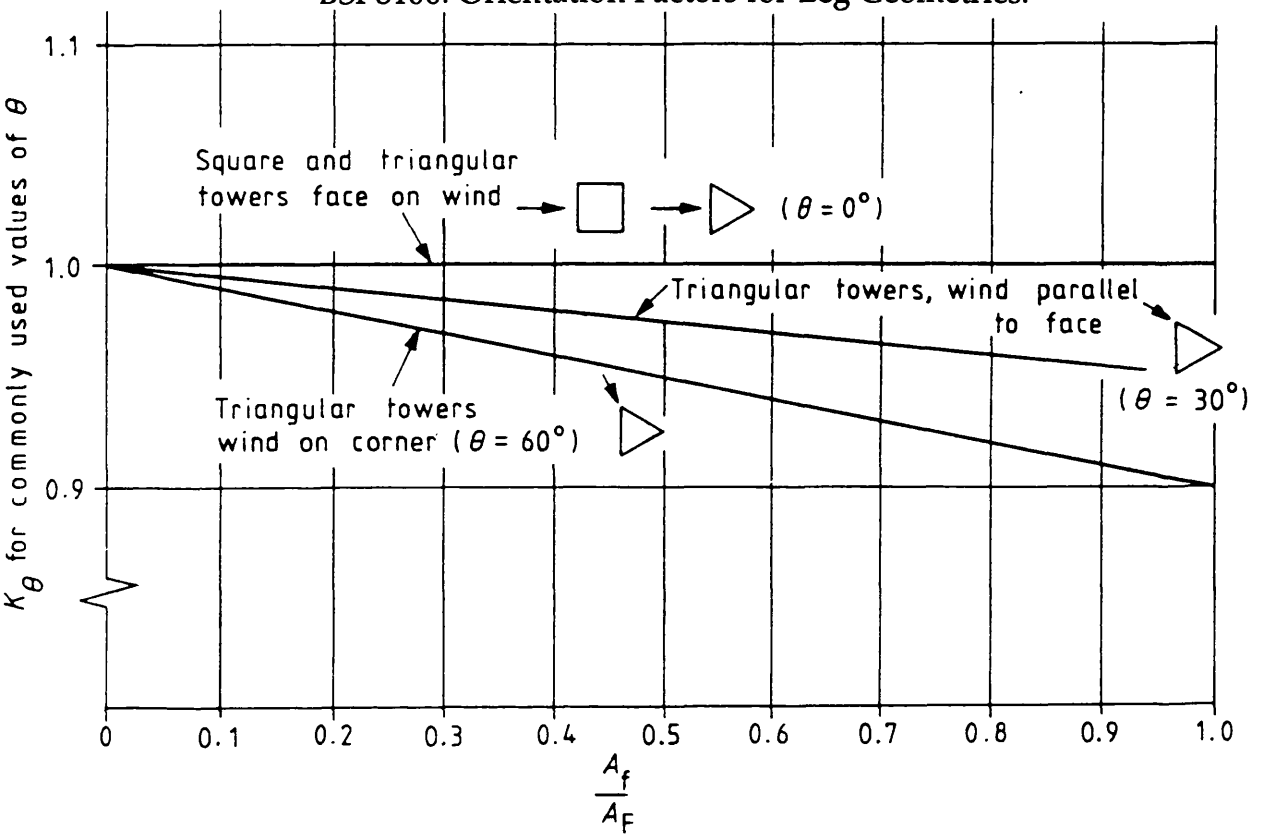

Figure 4.12

ESDU 81028. Orientation Factor for Triangular Leg Geometry.

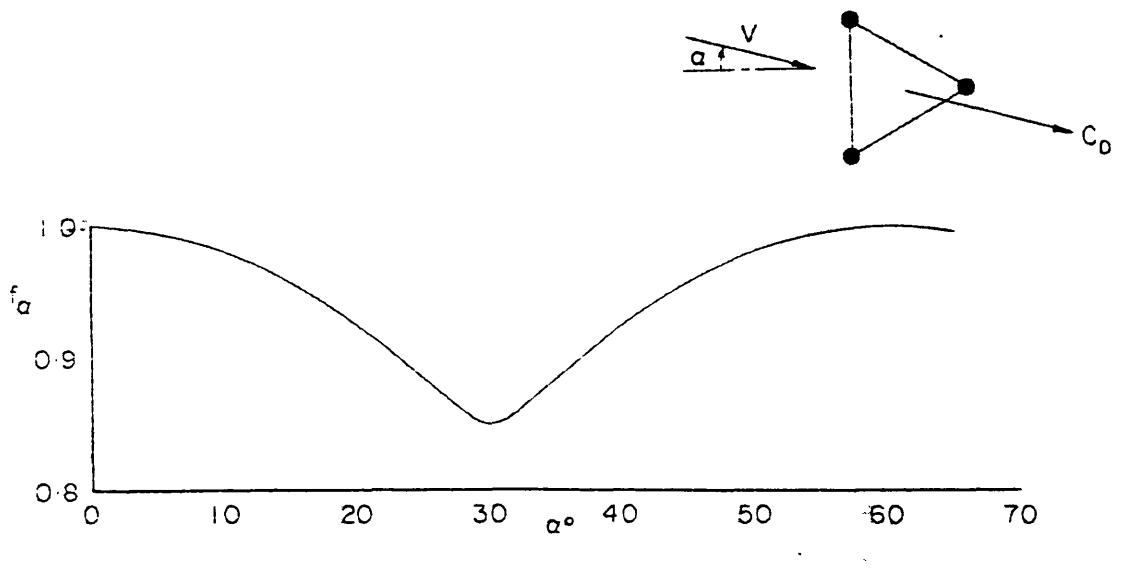

Figure 4.13

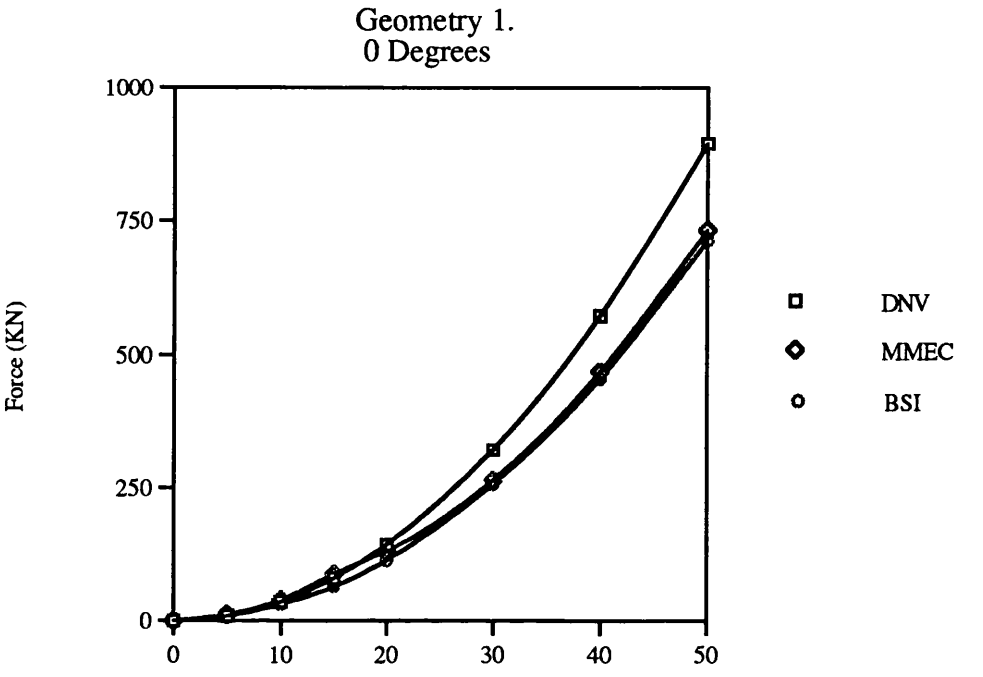

Figure.4.14

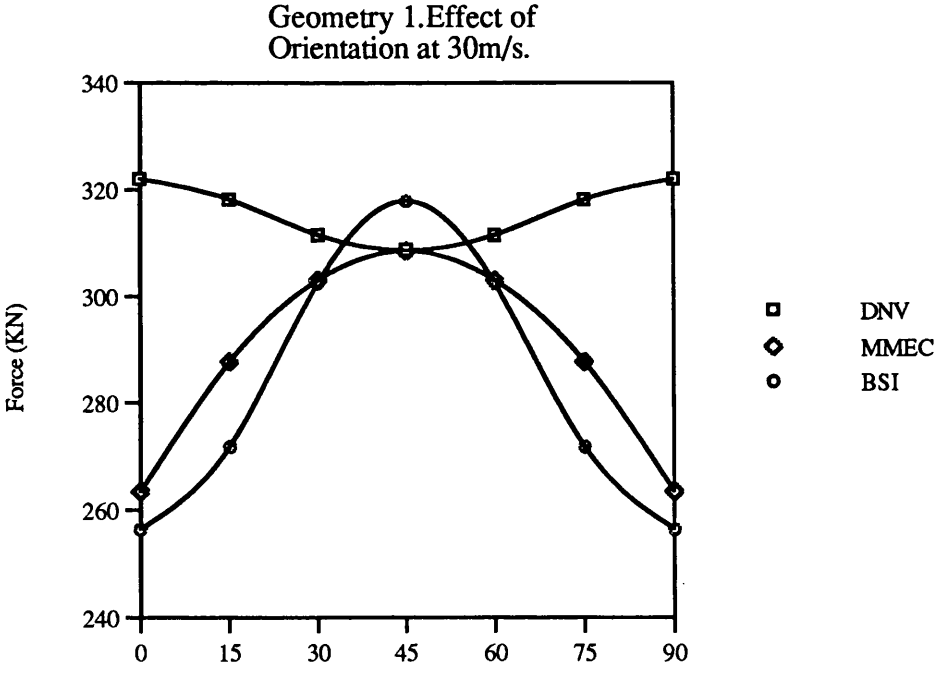

Fig.4.15

Geometry 1.
15 Degrees

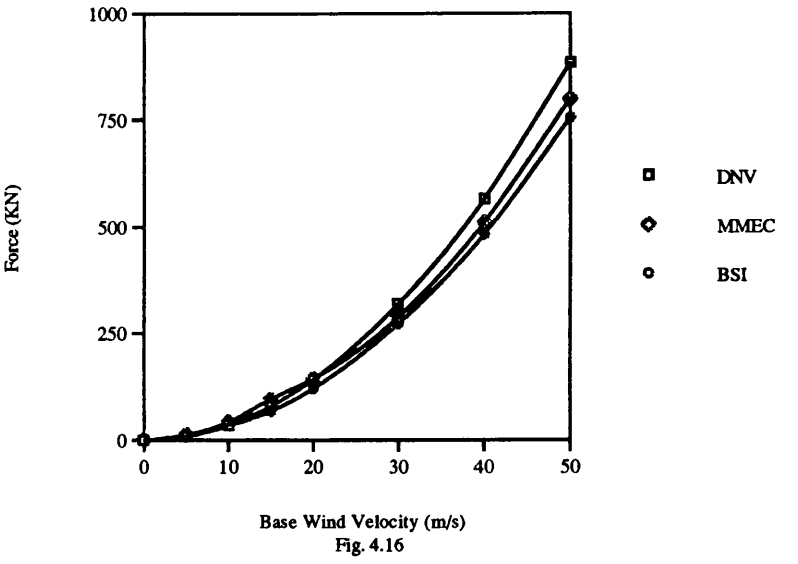

Fig. 4.16

Geometry 1.
30 Degrees

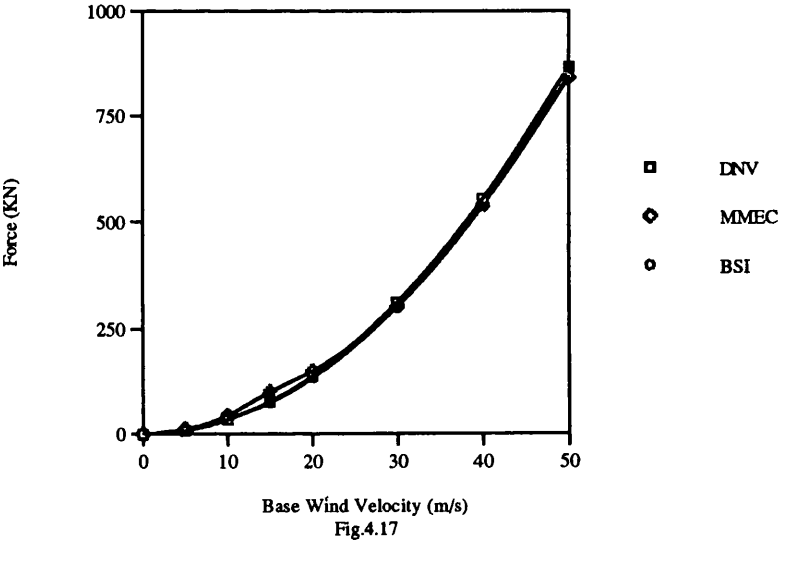

Fig.4.17

Geometry 1.
45 Degrees

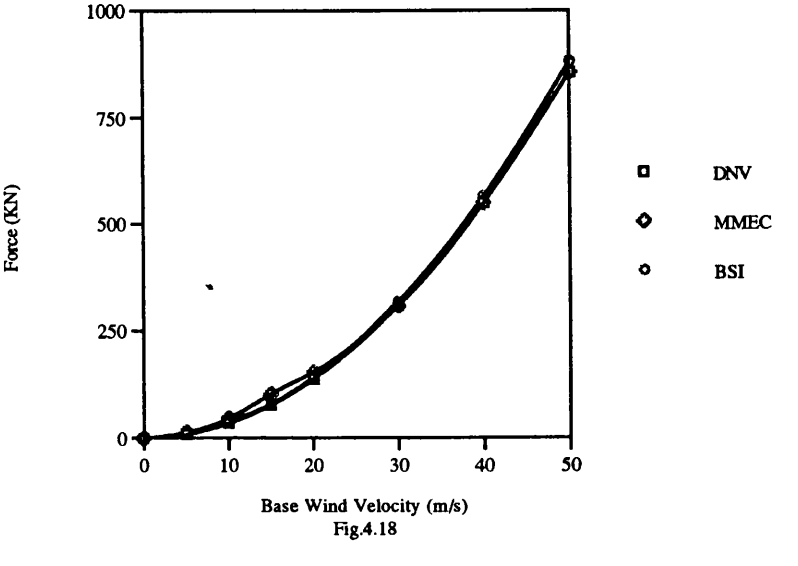

Fig.4.18

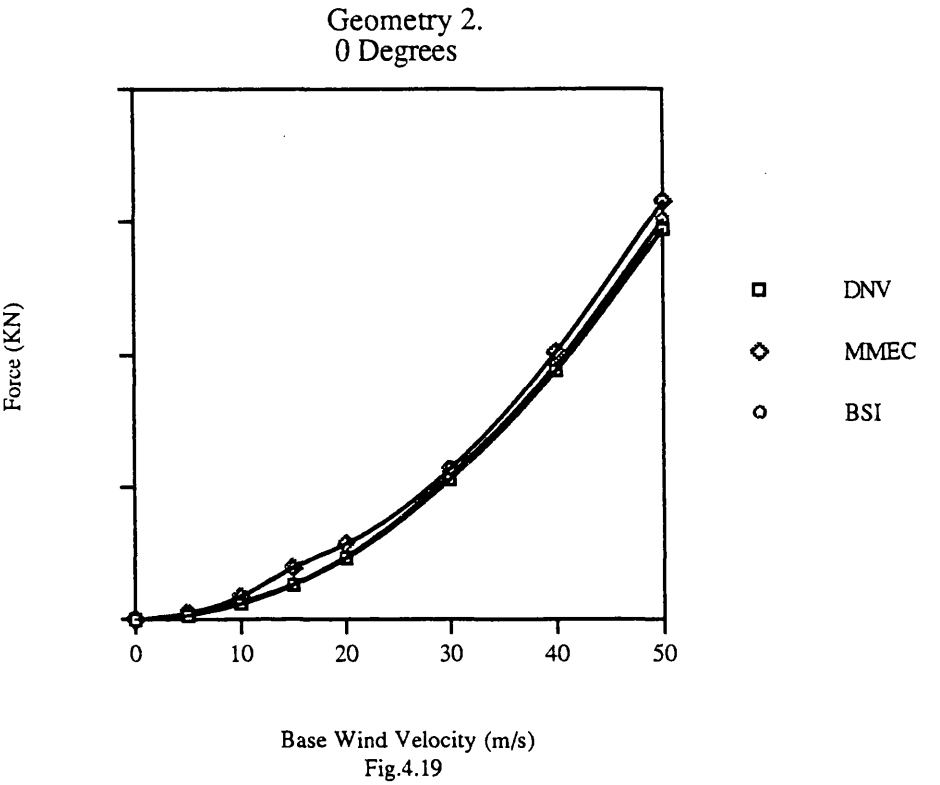

Fig.4.19

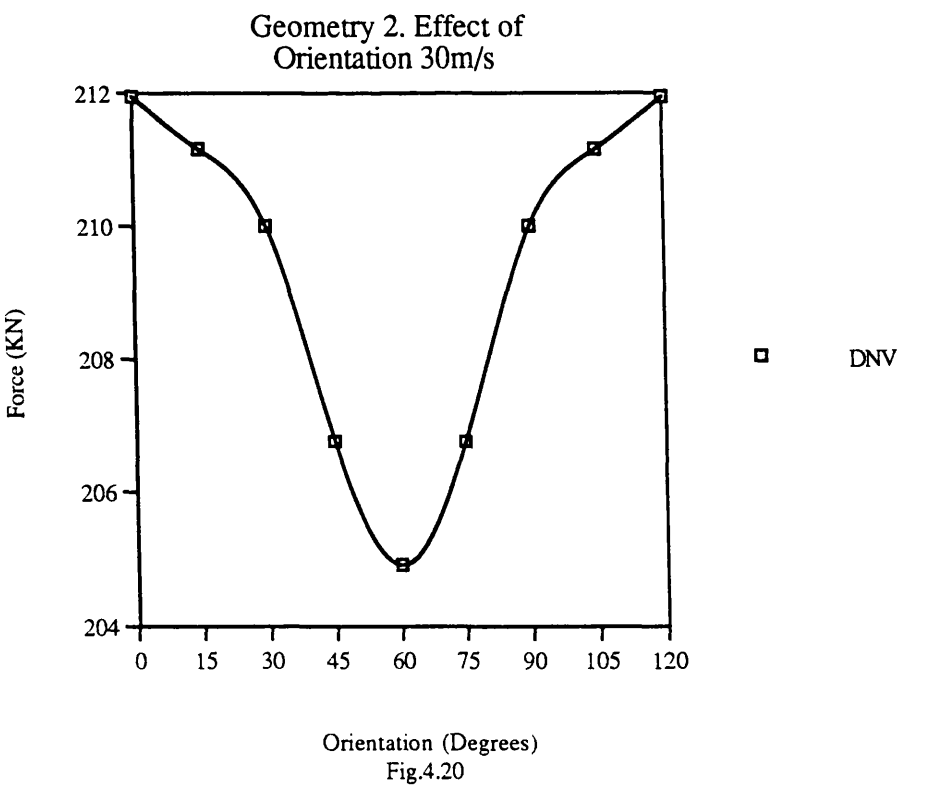

Fig.4.20

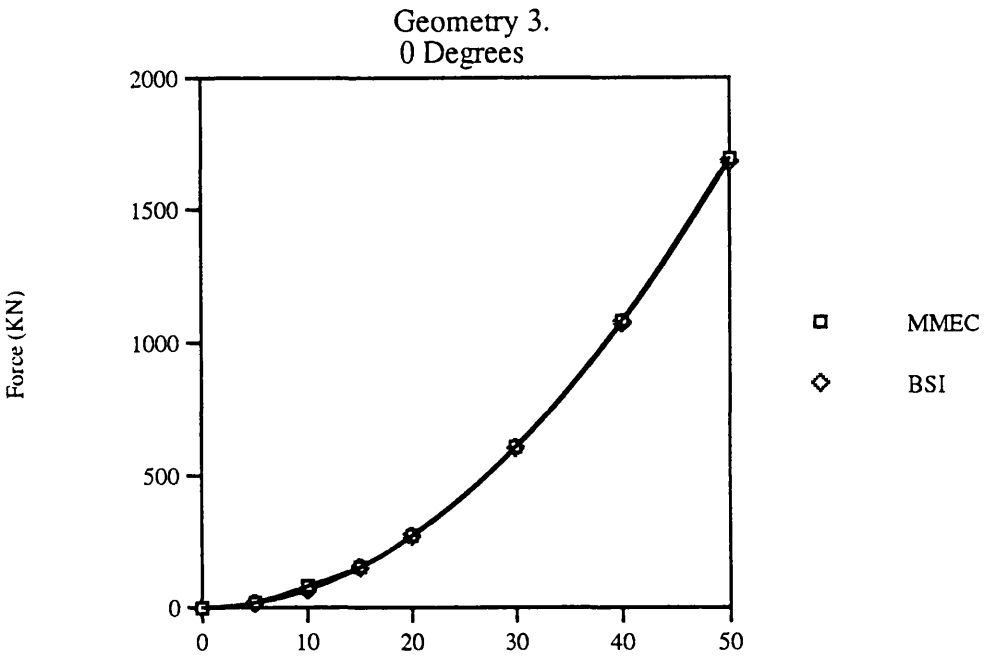

Fig.4.21

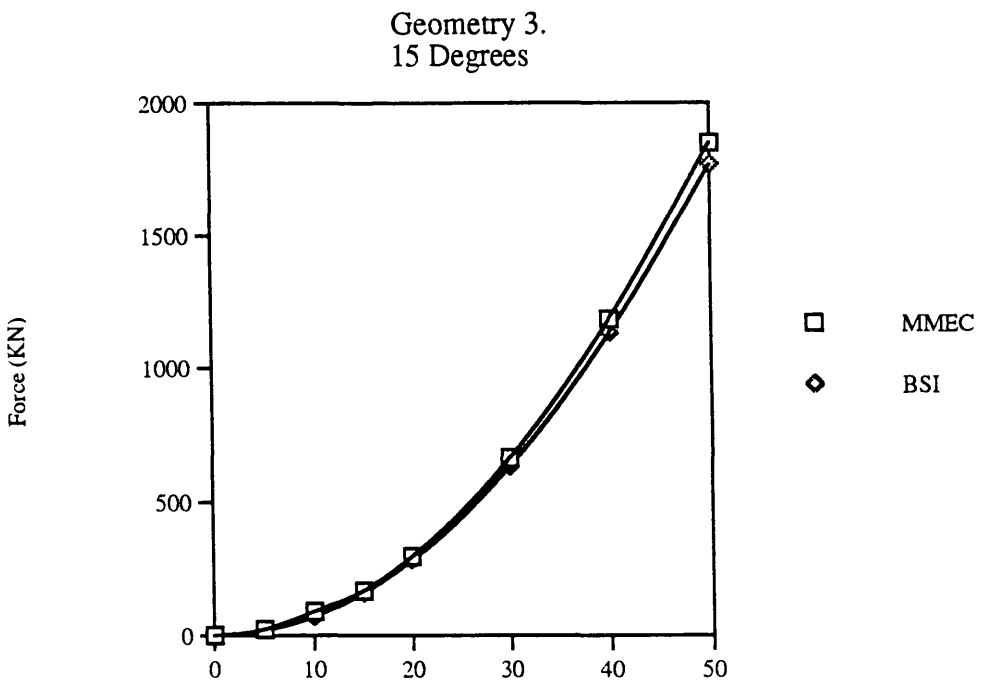

Fig.4.22

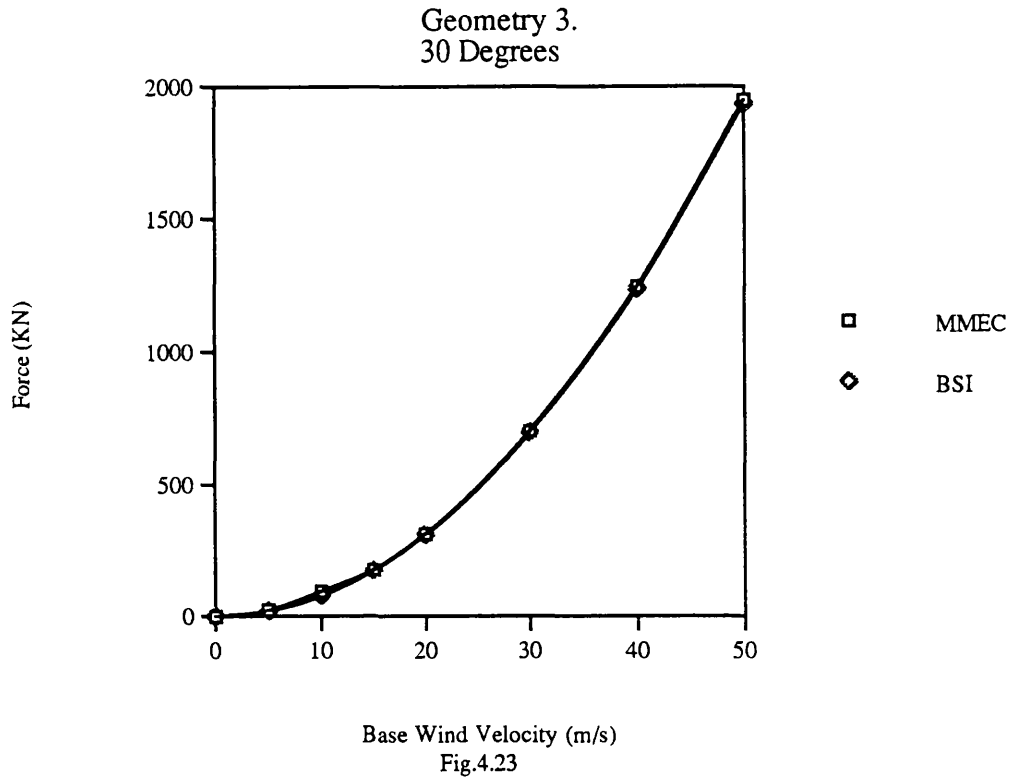

Fig.4.23

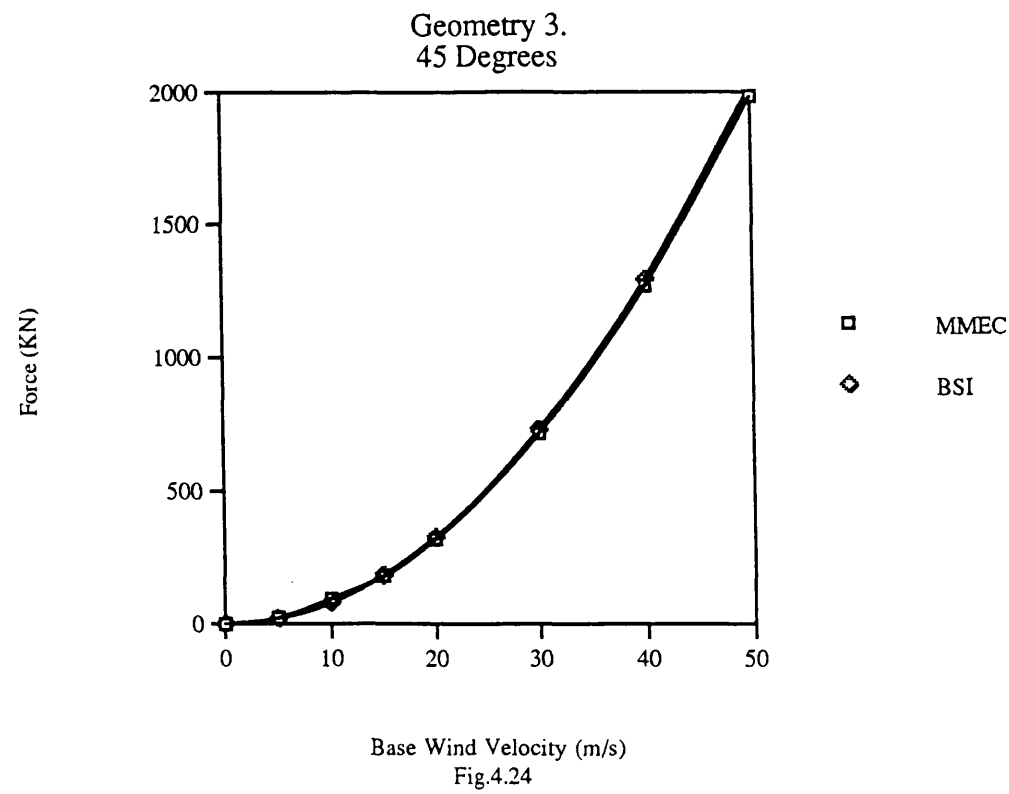

Fig.4.24

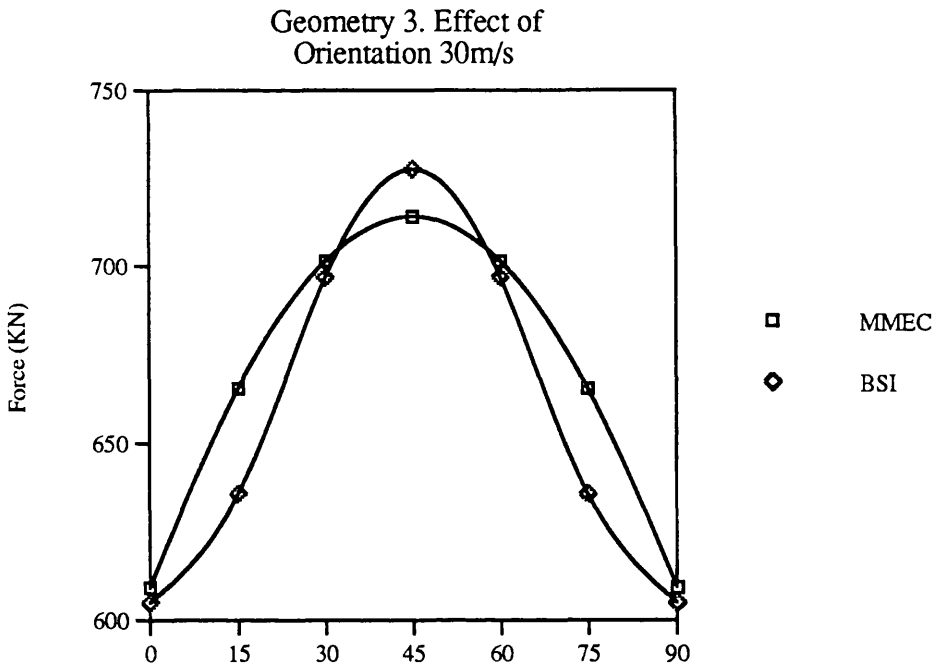

Fig.4.25

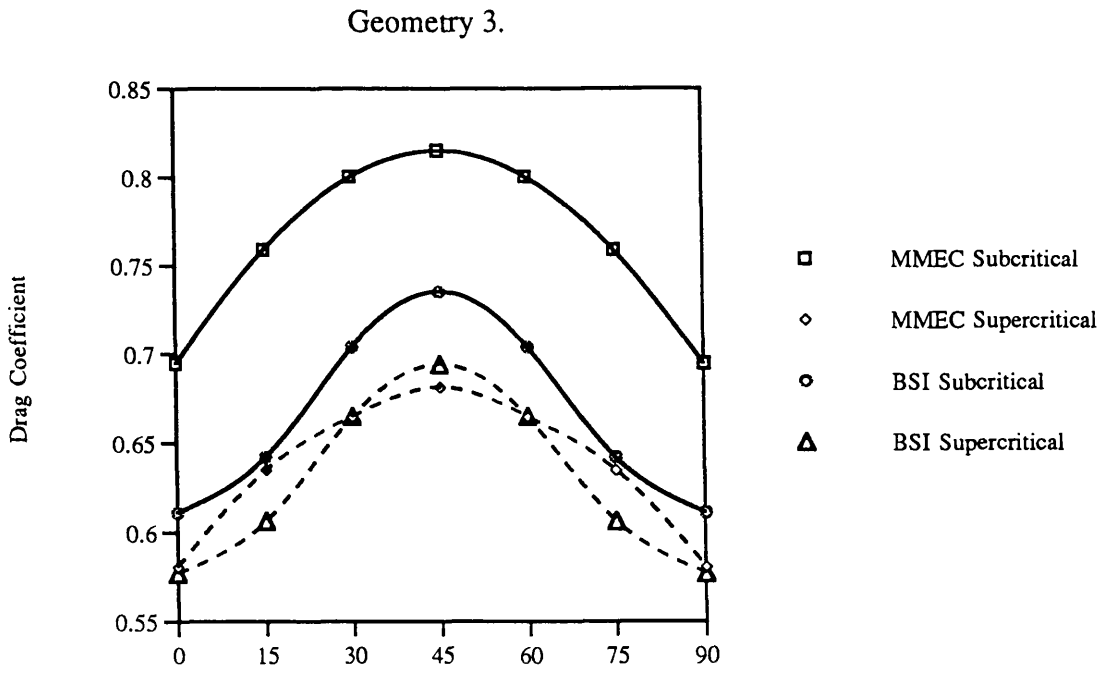

Fig.4.26

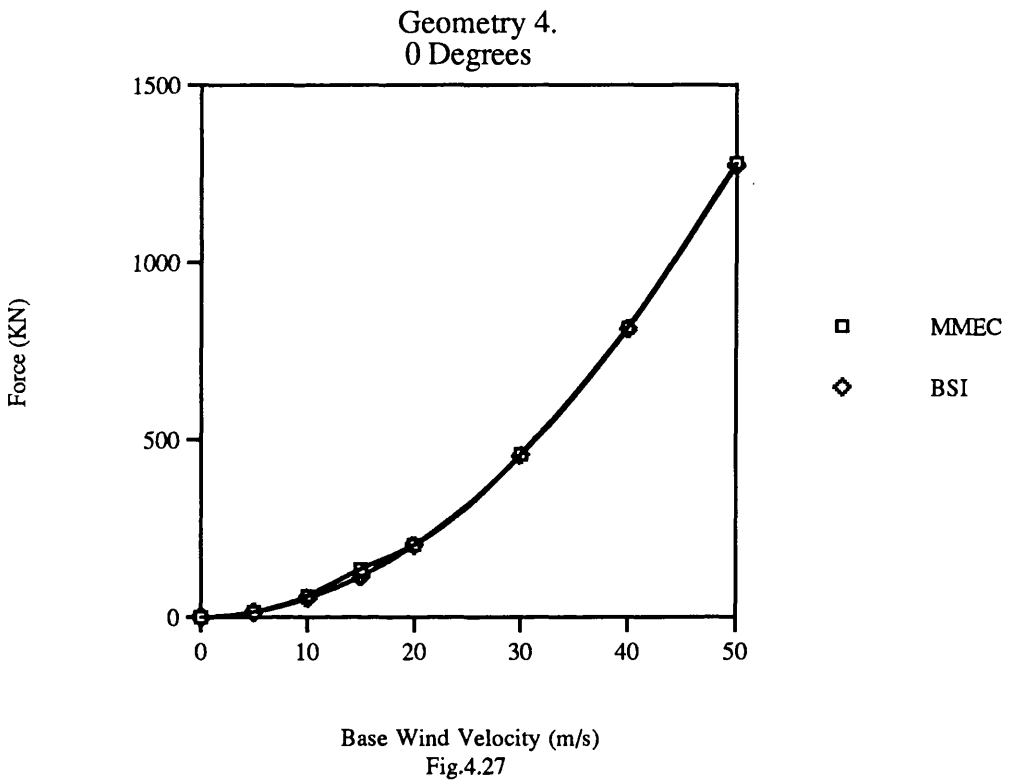

Fig.4.27

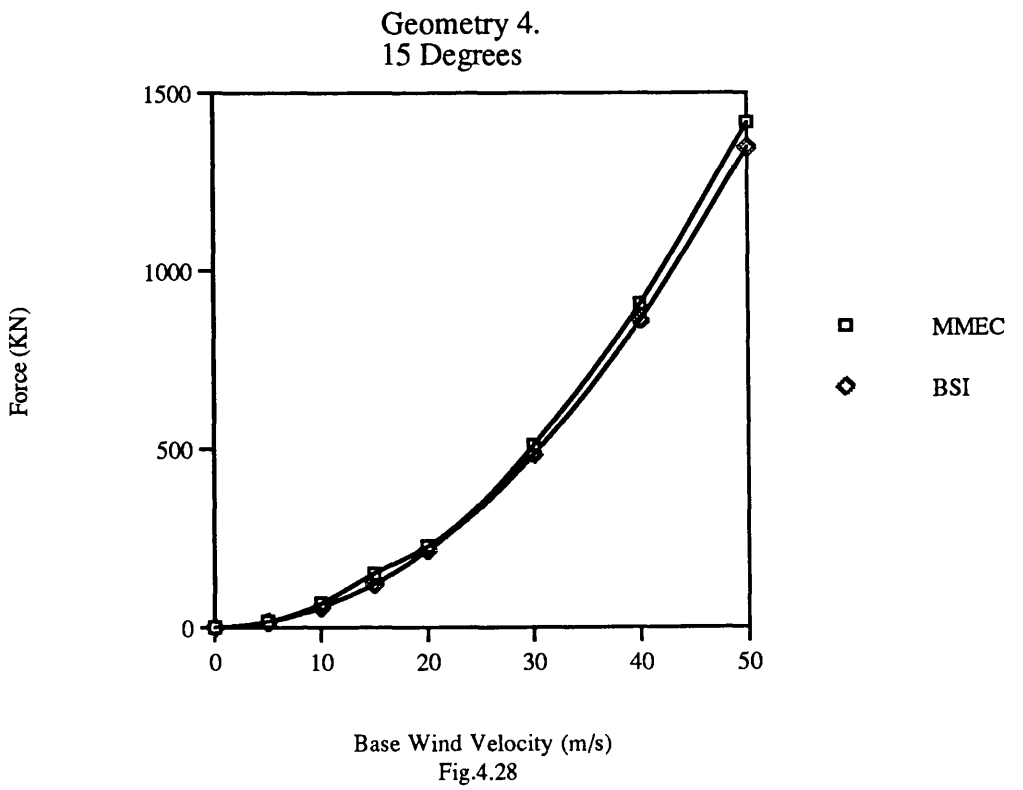

Fig.4.28

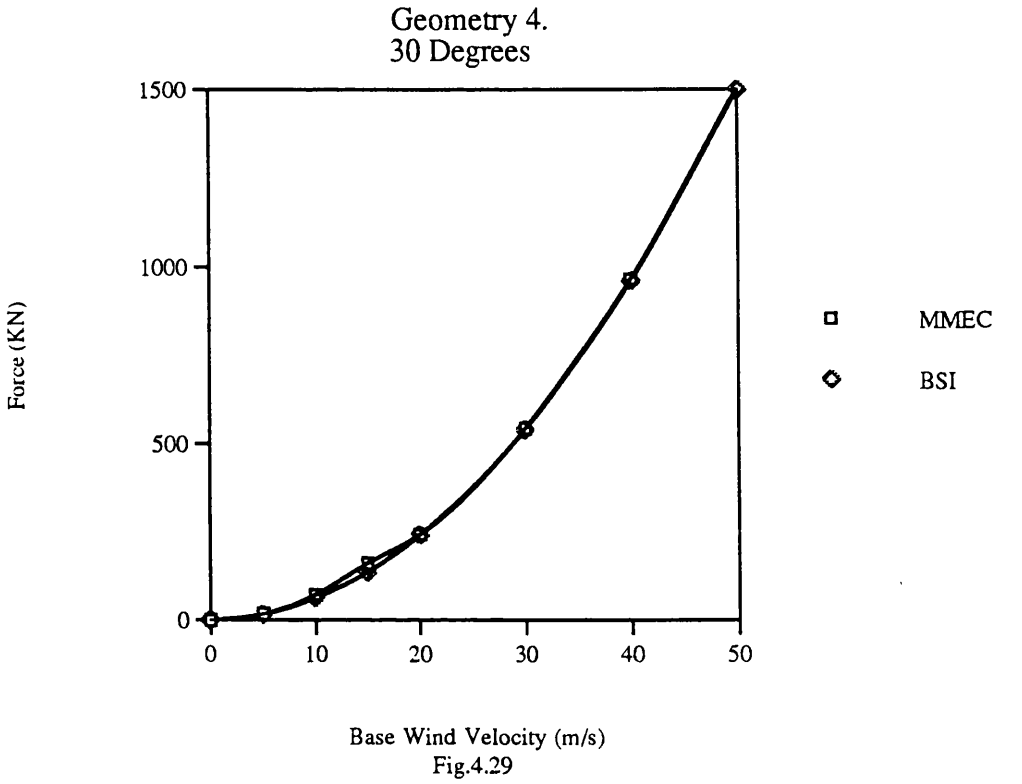

Fig.4.29

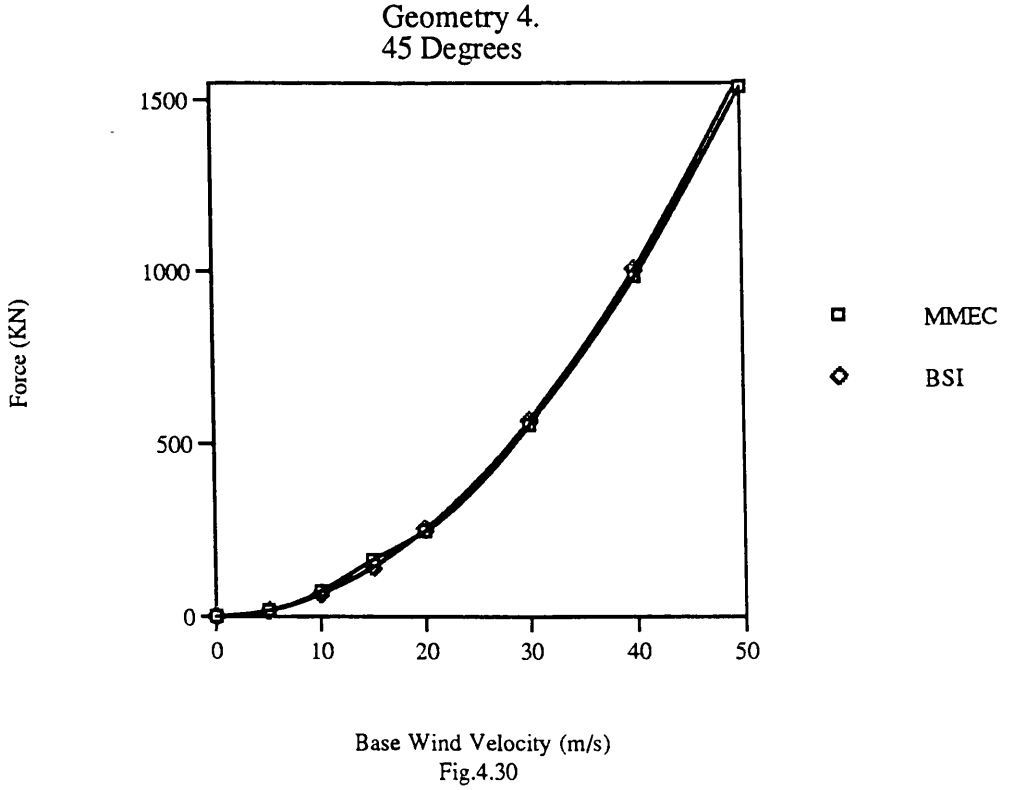

Fig.4.30

Geometry 4. Effect of Orientation 30m/s

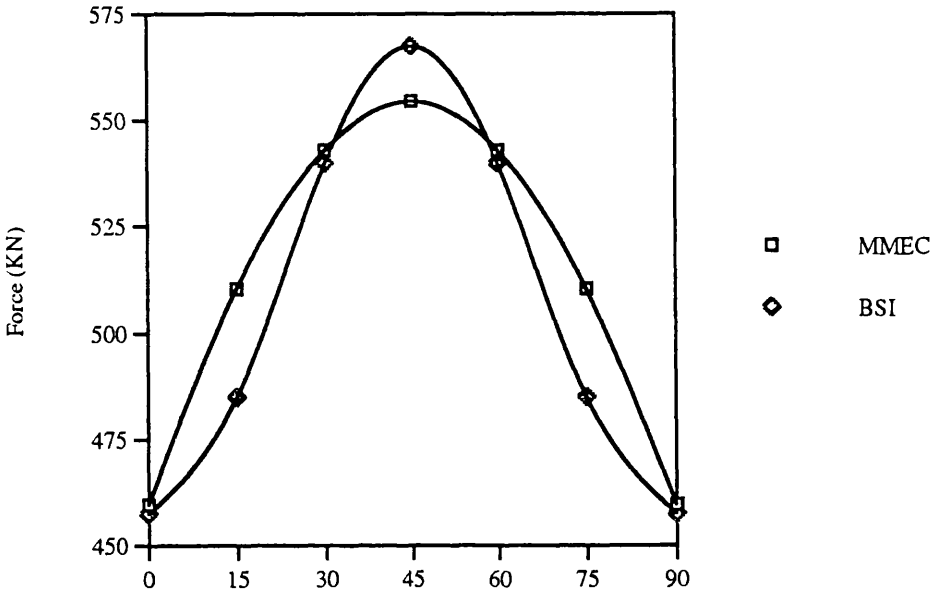

Orientation (Degrees)
Fig.4.31

Geometry 4.

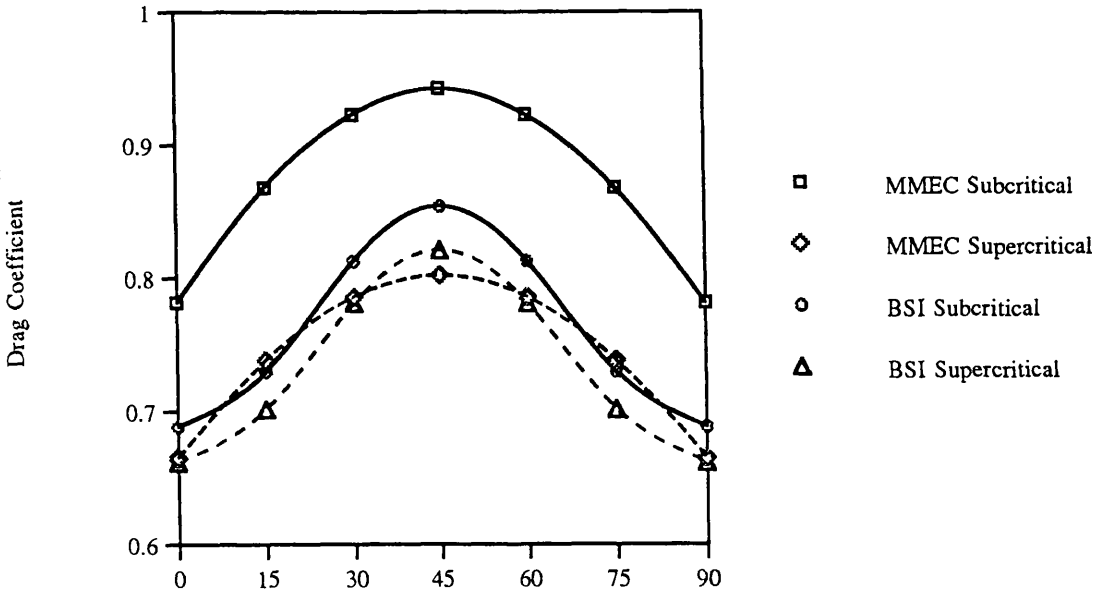

Orientation (Degrees)
Fig.4.32

Geometry 5.
0 Degrees

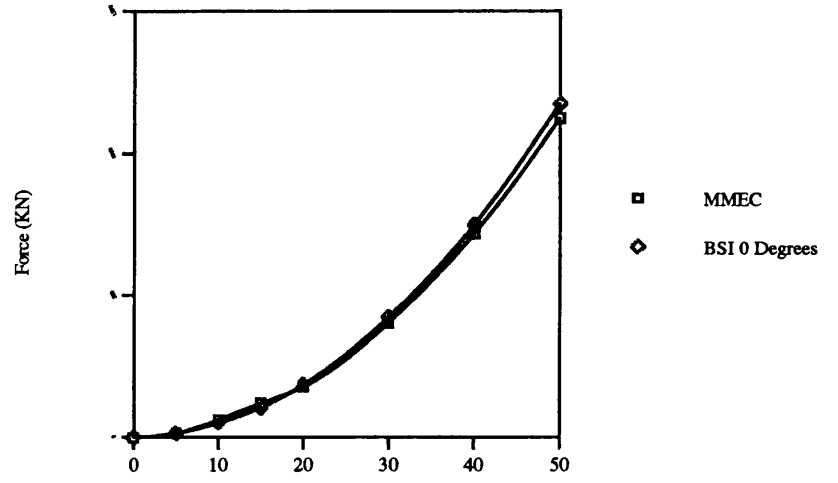

Fig.4.33

Geometry 5.Effect of
Orientation 30m/s

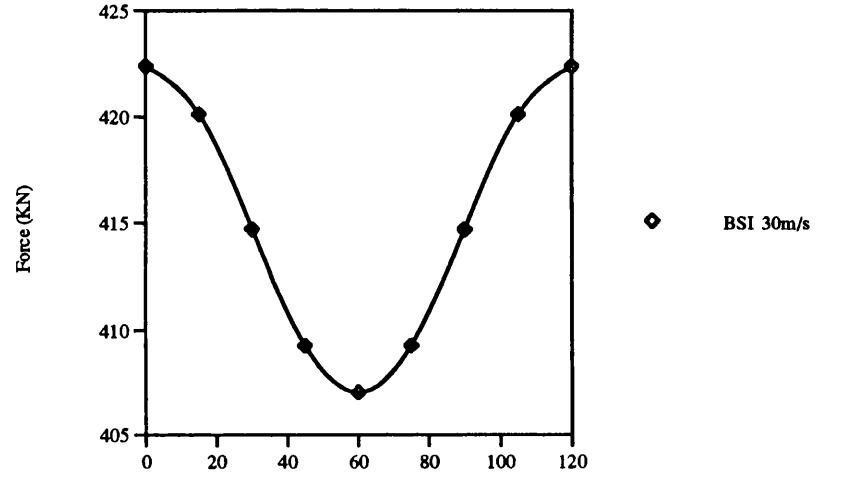

Fig.4.34

Geometry 5.

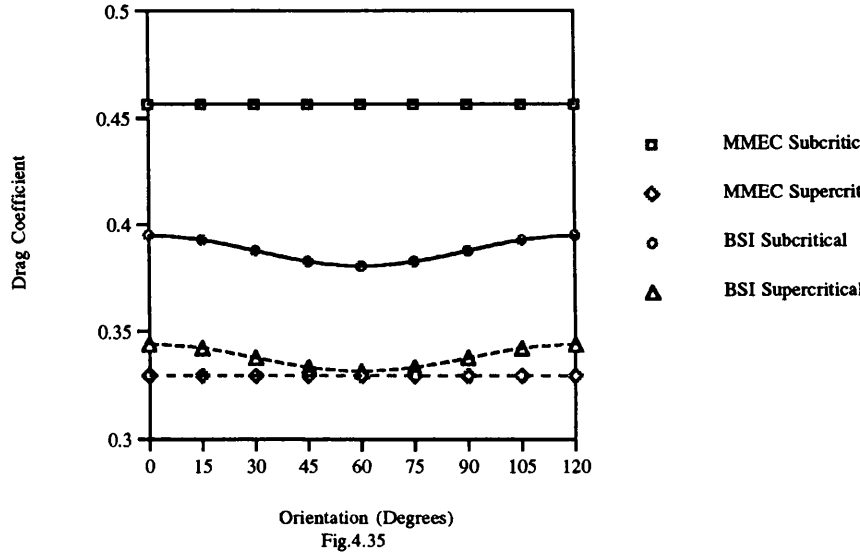

Fig.4.35

Geometry 6.
0 Degrees

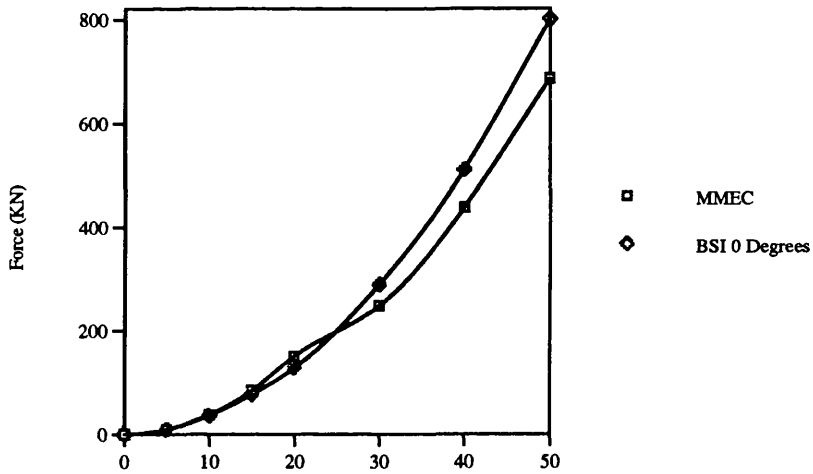

Fig.4.36

Geometry 6. Effect of
Orientation 30m/s

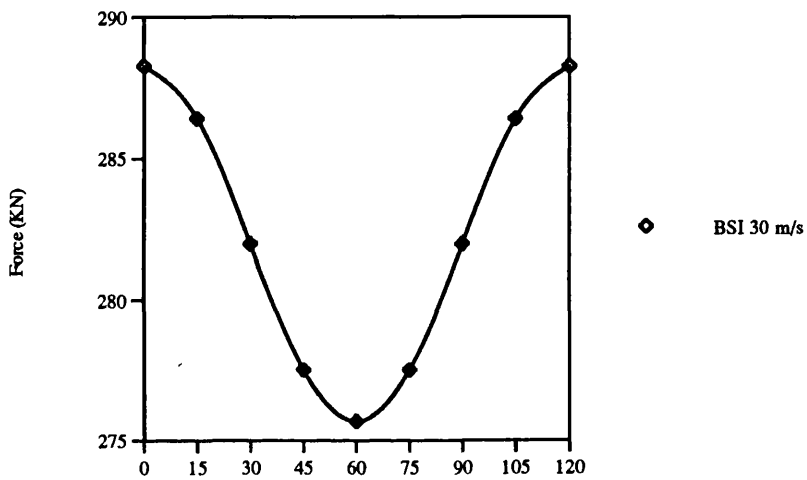

Fig.4.37

Geometry 6.

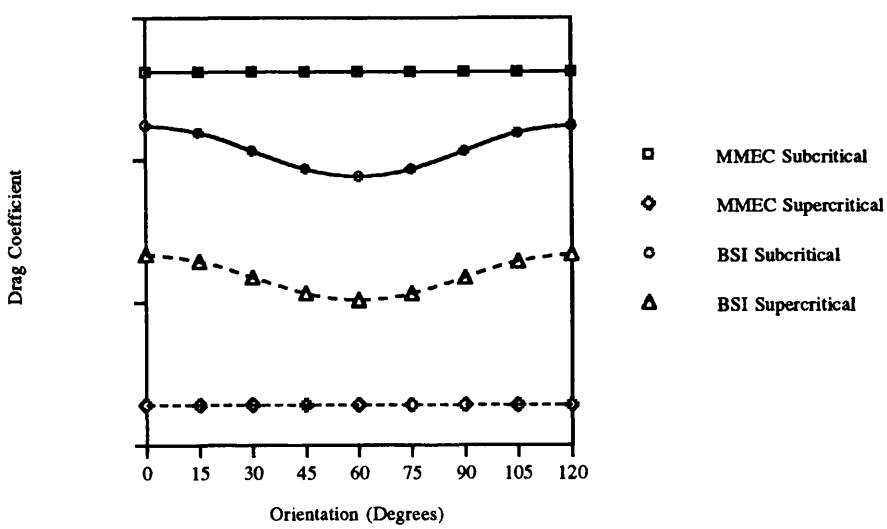

Fig.4.38

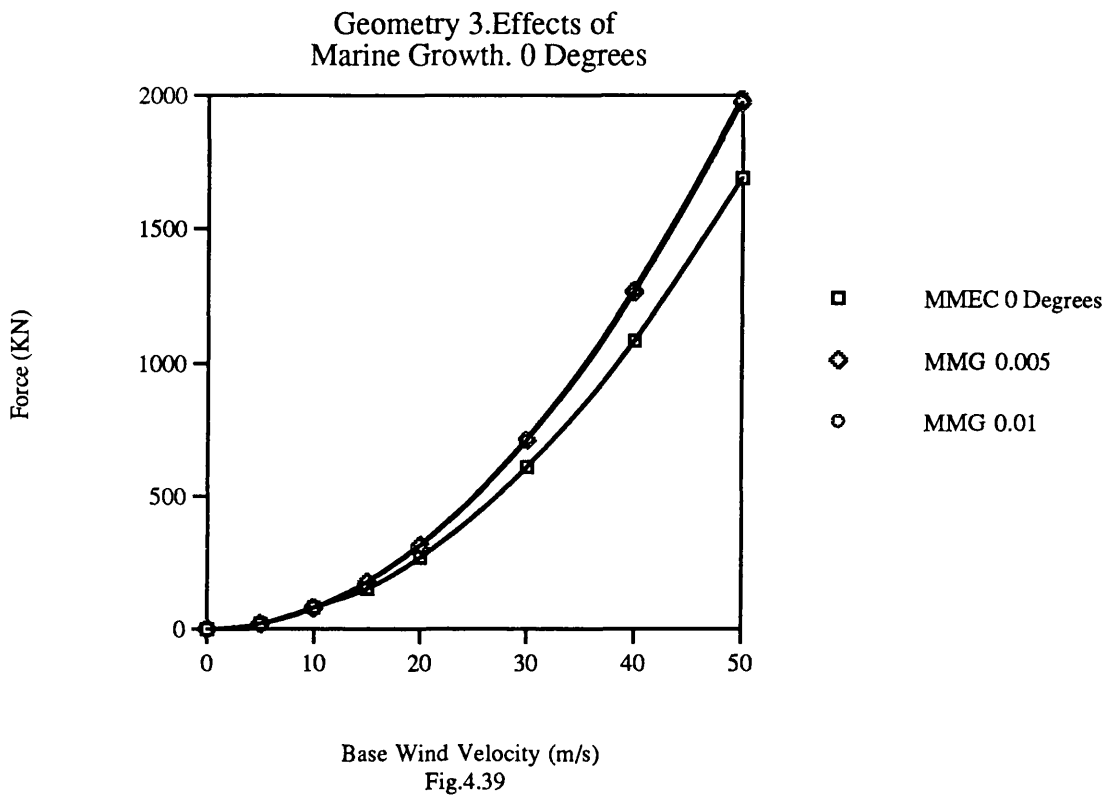

Fig.4.39

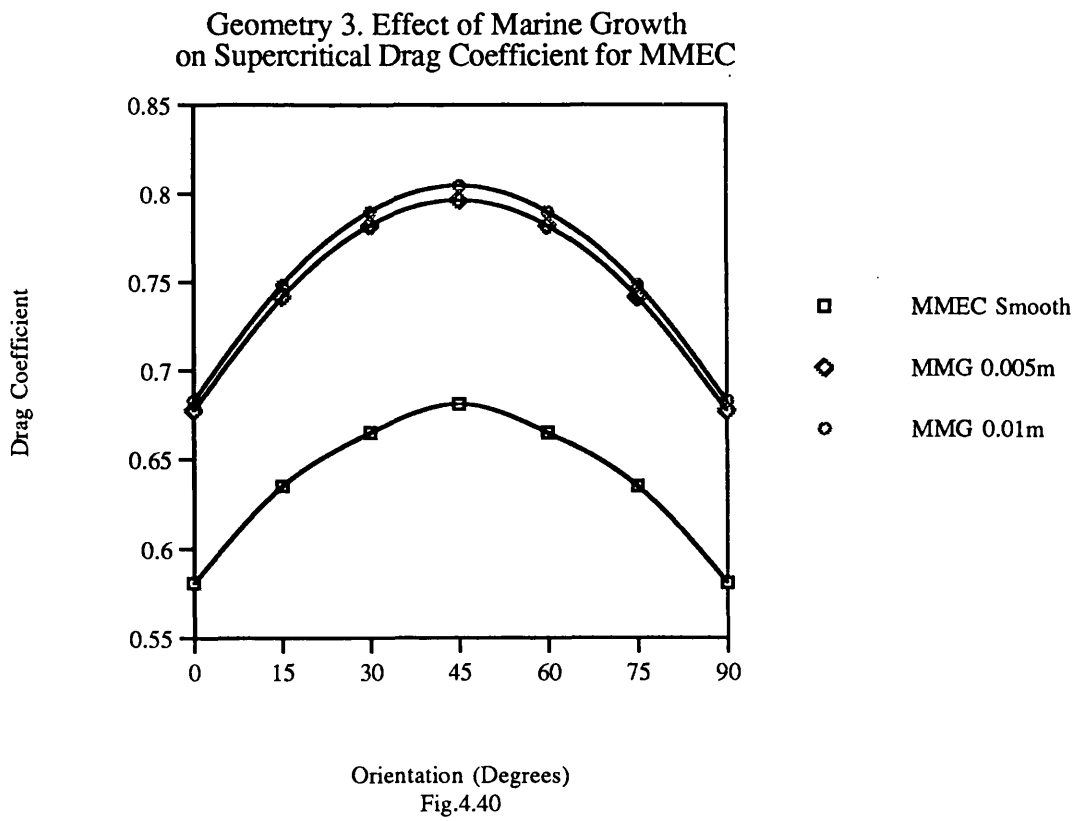

Fig.4.40

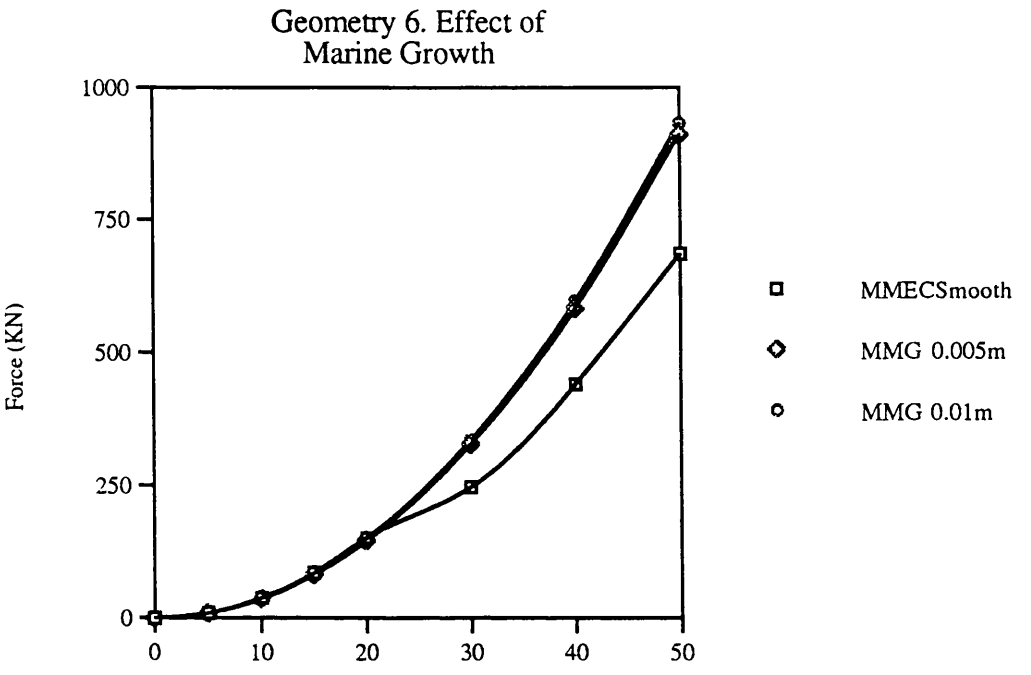

Fig.4.41

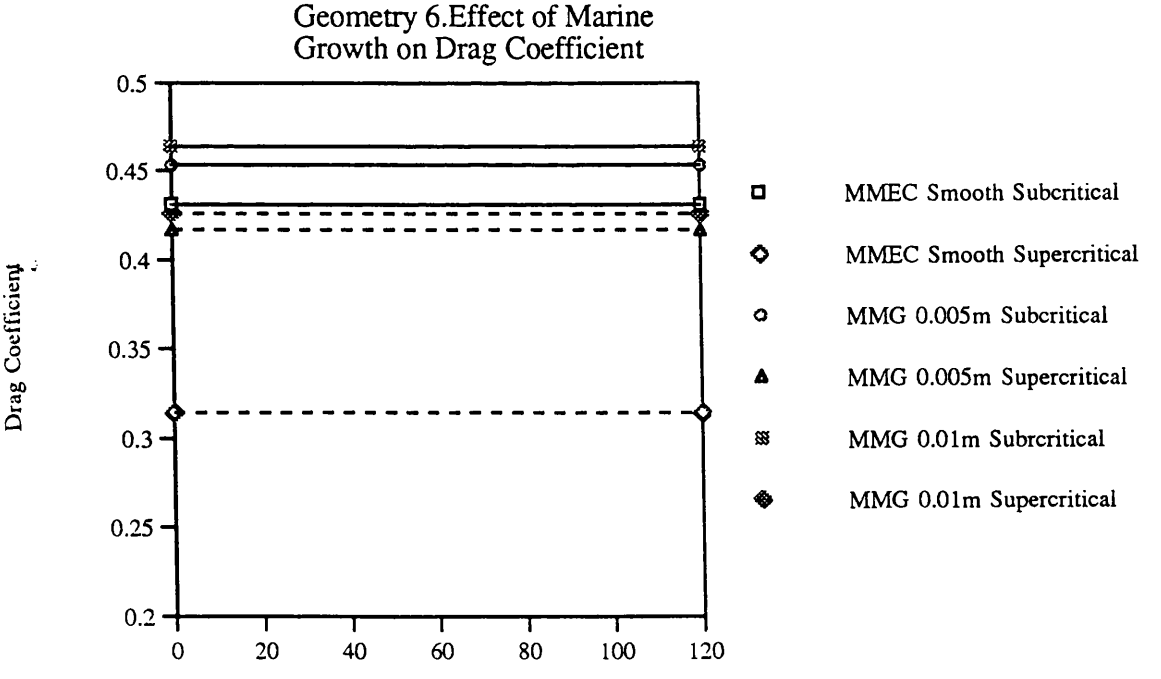

Fig.4.42

Chapter Five.

Study of the Dry Tow Simulation of a Heavy Lift Vessel and Jack Up with Wind Loading .

5.1 Introduction.

The simulation model described in Chapters Two and Three is now extended to study the dry tow simulation of a heavy lift vessel (HLV), with jack up under wind loading. The use of manoeuvring simulation will enable us to determine if the existing control devices such as rudder and skeg are adequate. It may also be possible to assess the manoeuvring capabilities for a new generation of heavy lift vessels which will be required for the transocean transportation of future designs of deep water jack up rigs. This will prove useful as an initial design tool to determine whether the control arrangements for the heavy lift vessel will satisfy any future IMO requirements for manoeuvring performance. The wind loads acting on the jack up legs will be determined using the MMEC calculation method detailed in Chapter Four. The wind loads acting on the jack up hull in the simulations were obtained from the current loading coefficients determined from the experiments in Chapter Six. No deck houses, drilling derricks were modelled.

In order to present an accurate simulation of the heavy lift vessel (HLV), with the jack up unit, it is necessary that the heavy lift vessel's manoeuvring characteristics in simulation should match the real behaviour of the full scale vessel. As a first step it was decided therefore to simulate the manoeuvring characteristics of the heavy lift vessel without the jack up and determine the appropriate interaction coefficients and propulsion characteristics as discussed in Chapter Two. This was achieved using the trials data of the 'Mighty Servant II' which was supplied by Wijsmuller, Ref. 5.1. The trials data contained information regarding the turning circle manoeuvres with additional data on the speed loss in the turn for both the starboard and port rudder, Table 5.2. This data is used as the basis for matching the simulation to the real manoeuvres without the

jack up. There are several approximations inherent in the simulation model. The first being the manoeuvring derivatives and the interaction coefficients were derived from model experiments for single screw vessels with relatively high block coefficient and scale effects are therefore present. Additionally, the propeller is ducted for the heavy lift vessel while the propulsion coefficients in the simulation model are derived for an open water propeller. The propeller bossings of the heavy lift vessel are also not taken into account. It was also necessary that the simulation should include a skeg. Two approaches of modelling the skeg lift and drag coefficients are studied and these will be detailed before the investigation of matching the simulation to the trials.

The dry tow simulation will include a combination of turning performance and automatic pilot control studies. The heavy lift vessel is the 'Mighty Servant I' and the jack up is based on the 'Ron Tappmeyer'. The simulations will investigate the manoeuvring performance of the heavy lift vessel system for wind velocity, rudder angle and variations in the longitudinal and transverse relative positioning of the jack up on the heavy lift vessel. Additionally the effects of leg length exposed, marine growth and orientation of the jack up rig will be studied. The heavy lift vessels have bow thrusters but these were not modelled as it is assumed that they are employed only in the positioning of the vessel when loading and unloading cargo.

5.2. Modelling the Skeg.

The heavy lift vessels of the 'Mighty Servant' class have a centerline skeg aft for increased dynamic stability. It was necessary to include the contribution of the skeg to the forces acting on the heavy lift vessel hull for the simulation. A review of literature on determining the aspect ratio of skegs introduced some debate on the appropriateness of the approach, (see section 5.2.1, Refs. 5.2, 5.3), and as a consequence of this uncertainty, two methods of determining the lift and drag coefficients were investigated and compared. The first method, using an extended

theoretical approach based on the work of Jacobs Ref. 5.2, with wing theory Ref. 5.4. The second approach of Harrington Ref. 5.5, using the lift and drag coefficients obtained from experiments with spade rudders which were then applied to the skeg.

This investigation of the two methods includes a comparison of the drag and lift coefficients and of the surge and sway coefficients for two skeg geometries which have the same area and maximum span but different taper ratios. These skegs can be seen in figures 5.1 and 5.2 and Table 5.1. The location and dimensions of the skegs were estimated from available literature on the heavy lift vessel.

The skeg in fig. 5.1 has the same taper ratio of 0.45 for which the experimental data for the spade rudder was obtained. The center of pressure of the skeg is assumed to be located at half the root chord. The two approaches are now detailed and the applicability of both approaches will be given in the discussion of the results.

5.2.1 Theoretical Approach using Low Aspect Ratio Wing Theory.

The approach developed by Jacobs Ref. 5.2, using low aspect ratio wing theory was initially studied. This work employs linear perturbation theory to determine the effect of a skeg on the dynamic stability of a vessel and as a result there was no investigation into the increased drag on the vessel due to the skeg. It is necessary however to include the drag of the skeg for the simulations as this will have a significant contribution at large drift angles. In Jacobs' work, the assumption which raised caution was that of the definition of the effective aspect ratio of the skeg. This was taken as its geometric aspect ratio for the skeg fully submerged. A review of Ref. 5.3, states that any low aspect ratio control surface will have an effective aspect ratio twice that of the geometric aspect ratio if flow is prevented from crossing its root. In the present study it is assumed the effective aspect ratio of the control surface to be double the maximum geometric span and that the control surface is fully submerged. The effective aspect ratio is then determined as,

$$AR = 2\frac{H^2}{A_S} \qquad 5.1$$

H Maximum span of the Skeg at the trailing edge.

A_S Area of Skeg

For low aspect ratio wings of AR less than unity, we determine the dimensionless lift rate per unit lateral area of skeg from the Jones formula,

$$\frac{\partial C_L}{\partial \beta} = \frac{\pi}{2} AR \qquad 5.2a$$

If however AR is greater than 1 then we must use,

$$\frac{\partial C_L}{\partial \beta} = \frac{2\pi AR}{2 + AR} \qquad 5.2b$$

$$L'_\beta = \frac{\partial C_L}{\partial \beta} \qquad 5.3$$

The above equation 5.3, is the non dimensionalised lift derivative of the skeg. If multiplied by the angle of incidence (in radians), it is approximately equal to the sway coefficient given in equation 5.4b.

If we define the lift and drag for the skegs with reference to figure 5.3, we obtain the equations for surge and sway coefficients as,

$$C_X = C_D \cos\beta - C_L \sin\beta \qquad 5.4a$$

$$C_Y = C_L \cos\beta + C_D \sin\beta \qquad 5.4b$$

In Jacobs' work the surge forces on the skeg were not included in the formulation. The above equations assume two dimensional flow, i.e. a wing of infinite span. The skeg is however of finite span and three dimensional flow will occur. The classical approach of Ref. 5.4 will be

adopted to account for the contribution of the three dimensional flow about the skeg. The three dimensional drag and lift coefficients are written as,

$$C_D = C_{Do}\cos\theta + C_{Lo}\sin\theta \qquad 5.5a$$

$$C_L = C_{Lo}\cos\theta - C_{Do}\sin\theta \qquad 5.5b$$

θ is the angle which the flow is deflected

C_{Do}, C_{Lo} are the drag and lift coefficients of the ideal two dimensional flow.

C_D, C_L are the true drag and lift coefficients of the three dimensional flow.

For small θ, $\cos\theta=1$, $\sin\theta=\theta$ (in radians), then the above equations 5.5 reduce to,

$$C_D = C_{Do} + C_{Lo}\theta \qquad 5.6a$$

$$C_L = C_{Lo} \qquad 5.6b$$

It can be shown from classical aerodynamic theory, Ref. 5.4 that,

$$\theta = \frac{C_L}{\pi AR} \qquad 5.7$$

Therefore the drag coefficient 5.6a can be rewritten in the form,

$$C_D = C_{Do} + \frac{C_L^2}{\pi AR} \qquad 5.8$$

The true three dimensional drag comprises of profile drag and induced drag. The induced drag is a function of the lift coefficient. It can be seen that the induced drag will decrease for increased aspect ratio. The

profile drag C_{Do} is made up of two components, the skin friction and form drag. The equation for the drag coefficient has the same form as that found in Ref. 5.3, except there is an 'efficiency factor' included in the denominator of the induced drag term which is named the Oswald efficiency factor e, and is assumed as 0.9. It is not stated whether this is an interaction coefficient and is also used by Whicker and Fehlner 1958 (see section 5.2.2). We will incorporate this into the formulation and note that Jacobs assumes that the local interaction effects between the hull and the skeg are negligible. The skin friction drag is determined from the 1957 ITTC model ship correction line equation. There is no contribution for form drag in the formulation as data for the form drag of a skeg was unattainable. The profile drag is therefore the skin friction drag and this acts only in the surge direction. The true drag equations 5.8 and lift coefficients 5.6b, are now placed back into the initial surge and sway equations 5.4 and we obtain,

$$C_X = C_{Do} + \frac{C_L^2}{\pi ARe}\cos\beta - C_L \sin\beta \qquad 5.9a$$

$$C_Y = C_L \cos\beta + \frac{C_L^2}{\pi ARe}\sin\beta \qquad 5.9b$$

5.2.2 Experimental Approach.

In the second approach the lift and drag coefficients for the skeg were obtained from the work of Harrington, Ref. 5.5. Harrington utilised the experimental data produced in the DTMB Report No. 933 written by Whicker and Fehlner in 1958. The information in Report No. 933 contains extensive experimental data on the lift, drag and centre of pressure of various rudder geometries of the NACA family of rudders as well as flat plates and elliptical sections as described in Ref. 5.3. The report also includes empirical formulae for the determination of the rudder forces, rudder torque and centre of pressure. Using the experimental data, Harrington reproduced the values of lift and drag coefficients and centre of

pressure in graphical form for various angles of attack against effective aspect ratio for a simple spade rudder geometry as shown in figs. 5.5 and 5.6. These lift and drag coefficients for the spade rudder were applied to the skeg geometries of figs. 5.1 and 5.2.

In the study we assume that the skeg is fully submerged and there is a uniform flow over the skeg. The lift and drag coefficients for the skeg are determined for a zero sweep angle. Harrington also includes the lift and drag coefficients for a rudder with a sweep angle of +11 degrees and recommends that an interpolation is carried out for the required sweep angle. The differences in the lift and drag are small however and so this was not considered necessary. The effective aspect ratio of the control surface is defined by Harrington as,

$$AR = \frac{X_3}{C_M}\left(2 - \frac{X_2}{X_1 + X_2}\frac{\alpha}{75}\right) \qquad 5.10$$

The definition of these quantities can be seen in figure 5.4

C_M Mean Chord

α angle of attack

X_3 Span of Skeg

The equation 5.10 applies to a rudder whose effective aspect ratio varies as the rudder is deflected through α degrees and flow crosses between the root of the rudder and the hull. In the case of the skeg there is no deflection of the skeg relative to the hull and therefore α=0. The above equation will therefore reduce to,

$$AR = 2\frac{H^2}{A_S} \qquad 5.1$$

After interpolating the lift C_{L1} and drag C_{D1} coefficients for the skeg obtained from figs. 5.5 and 5.6, it is then possible to determine their contribution to the skeg surge and sway coefficients. These are defined in terms of the drag and lift as,

$$C_X = C_D\cos\beta - C_L\sin\beta \qquad 5.4a$$

$$C_Y = C_L\cos\beta + C_D\sin\beta \qquad 5.4b$$

The rudder is however of a simple spade geometry with an unspecified NACA section. This presents a problem as the thickness of a skeg is small when compared with its chord and applying the rudder to a skeg of large chord may lead to inaccuracies in the drag coefficient. The experiments to obtain the lift and drag coefficients for the rudder were conducted for a control surface with a taper ratio of 0.45. The lift and drag coefficients are then corrected for differing taper ratios as,

$$\Delta C_L = \frac{1.63\lambda - 0.73}{AR}\left(\frac{\beta}{57.3}\right)^2 \qquad 5.11$$

λ Taper ratio

The corrected lift coefficient is then written as,

$$C_{L2} = C_{L1} + \Delta C_L \qquad 5.12$$

The drag coefficient is then corrected as,

$$\Delta C_D = \frac{C_{L2}^2 - C_{L1}^2}{2.83AR} \qquad 5.13$$

The corrected drag,

$$C_{D2} = C_{D1} + \Delta C_D \qquad 5.14$$

Where $C_{D2}=C_D$ and $C_{L2}=C_L$ in equations 5.4.

As mentioned previously the two skeg geometries of figs. 5.1 and 5.2 were studied. These skegs have the same area and maximum span ie the same effective aspect ratio but differing taper ratio. The first skeg taper ratio is 0.45 while the second is 0.87. The second skeg is the design skeg used in the simulation. The classical aerodynamic wing theory approach treats both skegs similarly as they have the same aspect ratios while the Harrington approach takes into account the taper ratio. These effects are discussed later.

5.3 Simulation of the Turning Manoeuvre of the Heavy Lift Vessel.

The aim of the following study is to match the simulation turning performance of the heavy lift vessel 'Mighty Servant II' to its sea trials data. This will be achieved by adjusting the interaction coefficients to obtain a reasonable match. This procedure was employed in Refs. 2.4 and 2.5. This combination of interaction coefficients will be used in the later simulations with the 'Mighty Servant I' and the jack up 'Ron Tappmeyer' under wind loading. Wind loading is also included in the 'Mighty Servant II' simulation with the wind angles and velocities as given at the trials. The contribution of the skeg forces acting on the vessel will now be detailed.

5.3.1 Skeg Derivatives and Forces.

In modelling the inclusion of the skeg for simulation, the method proposed by Jacobs Ref. 5.2, has been followed except for the definition of the effective span of the skeg as previously detailed. Additionally using the classical aerodynamic wing theory Ref. 5.4, the surge forces of the skeg and drag contribution to the sway forces on the skeg were included. In Jacobs' work the lift per unit area of skeg for small angles is written as,

$$L'_\beta\beta = Y'_\beta\beta \qquad 5.15a$$

This is now used to obtain the remaining derivatives for the skeg as,

$$N'_\beta = \frac{x_s}{L}Y'_\beta \qquad 5.15b$$

$$Y'_r = -\frac{x_s}{L}Y'_\beta \qquad 5.15c$$

$$N'_r = -\left(\frac{x_s}{L}\right)^2 Y'_\beta \qquad 5.15d$$

x_s Distance of centre of pressure of skeg to LCG (-ve aft)

L Vessel Length.

These derivatives are now added to obtain the total skeg forces in sway and yaw as,

$$C_Y = C_L\cos\beta + C_D\sin\beta + Y'_r r' \qquad 5.16$$

$$N' = N'_\beta\beta + N'_r r' \qquad 5.17$$

It is noted for the skeg at small angles of drift from 5.16

$$Y'_\beta\beta \approx C_L\cos\beta + C_D\sin\beta$$

In order that the contributions of the surge and sway coefficients of the skeg are added to the hull forces and moments, we must multiply the surge and sway coefficients and yaw derivative, by the area of the skeg and then dividing by the length and draft of the vessel as,

$$X'_{SKEG} = -\frac{A_S C_X}{LD} \qquad 5.18a$$

$$Y'_{SKEG} = \frac{A_S C_Y}{LD} \qquad 5.18b$$

$$N'_{SKEG} = \frac{A_S N'}{LD} \qquad 5.18c$$

A_S Area of Skeg

D Vessel Draft

5.3.2 Modelling the Wind Loading on the Heavy Lift Vessel.

The wind loading coefficients for the heavy lift vessel, figures 5.14 were adapted from Ref. 3.1 for the condition of a full loaded tanker. The same coordinate system applies from Chapter Three. There are several points to note about the applicability of using the wind loading coefficients of the tanker. The geometry of the HLV is very different as it has a large forward superstructure as well as the aft pontoons for increased stability when submerged. The ratio of the transverse/longitudinal windage area are significantly greater in the case of heavy lift vessel and as a result the longitudinal position of centre of windage area will be different. The location of the superstructure of the heavy lift vessel also meant that it was necessary to reverse the wind loading coefficients for sway and yaw. The surge and sway coefficients are relatively unaffected by this transformation, however the yaw moment sign is changed and acts in the same sense as the sway forces thus adding to the control requirements of the vessel.

5.3.3 Propulsion.

The value of the propeller advance coefficients C_1,C_2,C_3 are given in Table 5.2 and were chosen from the Wageningen Series B-4 propeller diagrams of Ref. 2.13. The simulation was carried out for a propeller with a P/D ratio of 0.6 and a disk area ratio of 0.7.

5.4 Simulation of the Dry Tow of a Jack Up.

The simulations carried out for the 'Mighty Servant II' are now extended to study the dry towing of a jack up rig on a heavy lift vessel. The interaction coefficients obtained from the trials comparison are applied to the heavy lift vessel 'Mighty Servant I'. The conditions for the dry tow simulations were determined from a transportation manual provided by Wijsmuller Ref. 5.1, and are given in Table 5.3. The dimensions for the initial conditions can be seen in figure 5.16. The skeg is included with its dimensions remaining the same as fig. 5.2. In the simulation study, the effects of wind velocity, location of the jack up transversely and longitudinally on the heavy lift vessel will be investigated. Additionally the orientation of the rig, the exposed leg length with marine growth and rudder angle will be studied. This study will provide useful information regarding the behaviour and sensitivity of the vessel to the parameters and the adequacy of the control devices. It may also be possible to produce recommendations regarding the location limits of the rig and acceptable leg length limits for any wind velocity. It is remembered however that the simulation model does not consider roll motion. A limit on the static wind heel moment will therefore need to be determined. This will be detailed in the next section of the chapter. It is assumed for all conditions of loading, the vessel has zero trim. This is a necessary assumption as details of ballast tank capacities and locations were not available in the literature provided. If there is any change in exposed leg lengths from the initial condition then the vessel displacement will remain the same and the ballast will be rearranged accordingly to obtain the zero trim condition. This assumption is reasonable for the tow system conditions as can be seen in Table 5.3.

5.4.1 Maximum Wind Heel Moment.

A limit of the wind heel moment for the simulation is necessary as the manoeuvring model does not include roll. In order to determine a maximum acceptable wind heel moment we must first have knowledge of the vessel righting lever. This information was provided in the

transportation manual for the initial load condition given in Table 5.3. If the tow system KG is known then the GZ value can be determined from KN static stability,

$$GZ = KN - KG\sin\varphi \qquad 5.19$$

φ Heel Angle. Maximum assumed at 5 Degrees.

The limiting wind heel angle was chosen as 5 degrees. It is assumed that the manoeuvring derivatives are unaffected up to this angle. Due to the asymmetry of the hull when heeling this will not be strictly correct. Additionally the jack up keel should not immerse before this angle. The limiting wind heel moment was determined from the value of the righting lever, GZ for the heavy lift vessel at 5 degrees. The contribution to this moment includes the heavy lift vessel, the jack up hull and the jack up legs. The wind heel moment on the HLV and jack up were obtained from the ABS guidelines on wind heeling Ref. 5.6 detailed in Appendix G. The moments on the legs were determined from the MMEC method. If varying the leg lengths the heeling moment will change as will the values of VCG of the system. Hence there will be a limiting envelope of maximum wind heel for wind velocity and exposed leg length. The leg loading model for the simulations will be detailed in the next section.

$$\text{Wind Heeling Arm} = \frac{\text{Wind Heeling Moment}}{g\Delta} \qquad 5.20$$

g Acceleration due to gravity

Δ Vessel Displacement.

5.4.2 Simulation of Wind Loading on the Jack Up Leg.

The wind loading forces on the jack up legs were determined using the MMEC method detailed in Chapter Four and Refs. 4.1, 4.2. The

design of the leg given in the transport manual is the Marathon Le Tourneau 116 class leg, which is square with triangular cornerposts. It was fortunate that this leg geometry was similar to the leg design given in Ref. 4.1 and the leg member dimensions for the simulation were scaled from this leg. The calculations for the leg member dimension and element areas and drag coefficients are given in Table 5.4.

The leg loading model is quite detailed as previously described. The legs are assumed to be orientated in the same direction. There are no interference or shielding effects between each of the legs, jack up hull and the HLV hull. We assume for the 5 degree heel that the levers about the waterline are constant and the drag coefficients are unaffected by the heel. The wind heel moments on the legs are therefore considered constant up to a 5 degree inclination. We shall assume the relative wind angle acting on the legs is taken at the base level, i.e. 10 meters above the mean still waterline. This assumption is useful as the relative wind angle does not vary significantly with elevation as described in Ref. 3.7. The wind heel is static only and no dynamic or second order effects are included. The variation of wind velocity with elevation is determined by the DNV power rule, equation 4.1. The total forces F_T acting on the legs is determined by summing the forces on each bay.

$$F_T = \frac{\rho_A A_B \sum_{j=1}^{N} U_{Zj}^2 C_{Dj}}{2} \qquad 5.21$$

N Number of Bays in the Leg.

A_B Projected Area of Bay

ρ_A Mass Density of Air

The forces acting in the surge and sway directions are then determined as,

$$F_X = F_T \cos\alpha \qquad 5.22a$$

$$F_Y = F_T \sin\alpha \qquad 5.22b$$

α Relative Angle of Wind Incidence

The output surge and sway and drag coefficients shown in figure 5.18c is obtained as,

$$C_X = \frac{2F_X}{\rho_A A_B N U_{10}^2} \qquad 5.23a$$

$$C_Y = \frac{2F_Y}{\rho_A A_B N U_{10}^2} \qquad 5.23b$$

$$C_D = \frac{2F_T}{\rho_A A_B N U_{10}^2} \qquad 5.23c$$

5.4.3 Simulation of Wind Loading on the Jack Up Hull.

The wind loads on the jack up hull used in the simulations were obtained from the experiments for the current loading coefficients described in Chapter Six. In the simulations no deck houses or top side structures on the jack up were included. The jack up hull current coefficients cannot strictly be applied to the wind coefficients as the Reynolds Numbers will not be similar, however wind loading data of this nature is unavailable. The local forces and moments on the jack up hull are small when compared with the heavy lift vessel and leg forces and moments. The jack up hull wind loading coefficients for forward and aft orientation are therefore assumed to be the same. The total yaw moment acting on the system due to the jack up hull is then determined from,

$$N_{JUTotal} = N_{JU} + X_{JU} l_T + Y_{JU} l_L \qquad 5.24$$

l_L Longitudinal distance of JU LCG to HLV system LCG

l_T Transverse distance of JU TCG to HLV system TCG

N_{JU} Local wind yaw moment acting on the jack up hull.

5.5. Discussion of Results.

The discussion of the results will be presented in two parts. The first part will include the study of the skeg coefficients and the matching of the simulations with trials data for the 'Mighty Servant II'. The second part concerns the simulations for the dry towing study for the 'Mighty Servant I'. These simulations were conducted for both the turning circle performance and for the automatic pilot control. The turning circles in general were for a starboard turn in a head wind. The auto pilot simulations were conducted in beam winds. The simulations of the initial conditions for turning circle and auto pilot are shown in figures 5.18 and 5.19 respectively. A selection of figures of both types of simulations are presented to illustrate the conclusions drawn.

5.5.1.1 Skeg Lift and Drag Coefficients.

The results of the theoretical approach linked with Jacobs' and the experimental results from Harrington for the drag and lift coefficients for the two skeg geometries are given in figures 5.7 and 5.8. The two approaches show similar characteristics for both the lift and drag coefficients. The experimental coefficients are less than the theoretical predicted values in both the lift and drag. The theoretical results are the same for the two skegs as they have the same aspect ratios.

5.5.1.2 Skeg Surge and Sway Coefficients.

The surge coefficients give an excellent match for both skegs as can be seen in fig. 5.9. It can be seen that the lift coefficient dominates in the surge direction fig. 5.3 and equation 5.4a.

$$C_X = C_D\cos\beta - C_L\sin\beta$$

The drag is negative and therefore the skeg is acting to increase the vessel speed. This may be due to the approximation of applying the lift and drag

of the NACA rudder section to the skeg, but we are unable to study this effect for an actual skeg as lift and drag coefficients are not available. It is also noted that the theoretical approach has no contribution from the form drag of the skeg.

The skeg sway force coefficients are given in figure 5.10. The sway coefficients are slightly larger than the lift coefficients because of the small contribution from the drag. For increased taper ratio Skeg 2, the sway coefficient increases. We can conclude therefore that the low aspect ratio wing theory and the Harrington method can be used equally well in modelling a skeg. The theoretical approach is naturally the easiest to implement.

5.5.1.3 Simulation of 'Mighty Servant II'.

The simulation results of the heavy lift vessel 'Mighty Servant II' are shown in figures 5.12-5.13. These can be compared with the actual trials trajectories in figure 5.11. It is encouraging to note that on inspection of the advance, transfer and tactical diameters given in Table 5.2, the differences between the simulation and trials on the whole are approximately only 5%. The time taken for the port and starboard turns in the simulations have increased however and the ratio of the velocity in the simulations is also greater. This can be due to several reasons mentioned previously such as the empirical derivatives and the modelling of the skeg. A further idea is that it is linked to the propeller P/D ratio chosen or the fact that the propeller is ducted for the actual vessel while the simulation model uses an open propeller. The strongest argument is that it may also be due to the scale effects which are inherent when using the interaction coefficients from model experiments. In order to match the simulation to the trials for the condition of the vessel, all the interaction coefficients were initially set to their empirical values. It became necessary however to adjust the rudder interaction coefficients to obtain a similar turning circle trajectory. The present simulation results with the skeg will have to suffice however.

5.5.2.1 Limit of Wind Heel Moment.

The limiting wind heel moment for the 5 degree inclination can be seen in figures 5.17a-d for the conditions of exposed leg length of 74.15m, 89.15m and 104.15m and marine growth of thickness 5.0 mm and height 1.25 mm. The leg limiting wind heel arm is determined as the initial arm obtained from equation 5.19 minus the wind heel arms for the contribution of the jack up hull and top side structures and the heavy lift vessel at 5 degrees inclination. It can be seen that the exposed leg length has a significant effect on the maximum allowable wind velocity. The wind heel levers will increase with increased leg lengths and additionally the system VCG will rise, thus reducing the static stability GZ at 5 degrees. The marine growth does affect the allowable maximum wind velocity and should be considered when designing limiting envelopes for exposed leg lengths and wind velocities.

5.5.2.2 Wind Loading on the Jack Up Leg.

An example of the output from the simulation for the leg drag and force coefficients of the jack up leg geometry is given in figure 5.18c. These results show a simulation of a starboard turn with a head wind. The overall drag coefficient is initially in the region of supercritical Reynolds numbers. As the turn progresses however, the drag coefficient then acts in the subcritical region. The change is caused by the reduced relative wind velocity caused by the following wind. The figure also shows the variation of the overall leg X and Y force coefficients of equation 5.23. The drag coefficient (supercritical) in the figure is the same as the drag coefficient detailed in Table 5.4. The difference in value is caused by the definition of the overall drag described in equation 5.23c and 5.21.

5.5.2.3 Longitudinal and Transverse Location of Jack Up on the Heavy Lift Vessel.

The longitudinal positioning of the jack up relative to the tow

system LCG has a significant effect on the trajectory of the tow system. It is apparent from figures 5.20a-b, that the advance, transfer and tactical diameter are increased for shifts of the jack up away from the tow system LCG. It can also be seen in figures 5.20e-f, that as the jack up shifts aft away from the system LCG, the magnitude of the total wind yaw moment increases significantly. This is due not only to the contribution of the legs but also to the total jack up hull wind yaw moment (equation 5.24). The wind yaw moment on the bow leg 1 when orientated aft, has the greatest influence on the total wind yaw moment figs. 5.18d and 5.20e-f.

In the auto pilot simulations figures 5.21, the rudder activity increases from -10.733 to -16.333 degrees for the -10 meter shift of centroid of the jack up from -11.96m. The negative rudder angle denotes a port rudder angle.

In simulations conducted but not presented, the trajectory of the tow system does not appear to be sensitive to the transverse positioning of the jack up on the heavy lift vessel. If we consider that the jack up is usually placed as close to the ship centerline from loading considerations then this effect will be negligible.

5.5.2.4 Variation in Exposed Leg Length.

The additional simulations for the variation in exposed leg lengths were conducted for exposed leg lengths of 74.15m and 104.15m. It is clear from figures 5.18d and 5.22e-f that the variation of leg length has a significant effect on the overall wind yaw moment for the condition of the vessel. The bow leg 1, dominates the total wind yaw moment for increasing leg lengths, fig. 5.22e-f. In figures 5.22c-d we see that the amplitude of the velocity ratio, the drift angle and angular velocity have increased for the increased leg lengths. If the location of the rig was strictly fixed at a significant distance from the system LCG and the wind yaw moments were to diminish the manoeuvring performance, then the exposed leg lengths could be varied to reduce the over all wind yaw moment.

The automatic pilot simulations show an increased rudder

deflection from -10.733 to -15.866 degrees for the increased leg lengths of 74.15m to 104.15m. The transverse displacement of the vessel course has also increased. In the auto pilot simulations the negative rudder angle denotes a port rudder.

5.5.2.5 Orientation of Jack Up Rig.

The jack up rig centerline was initially orientated aft with its bow facing 180 degrees relative to the heavy lift vessel centerline. In simulations where the rig is orientated forward figures 5.24, there does not appear to be any major effect on the trajectories of the turning circle performance. This is due to the design of the jack up, where the wind yaw moments due to the longitudinal and transverse locations of the legs and the hull, balance to produce a small net moment. Simulations were also conducted for the auto pilot and similar conclusions were drawn.

5.5.2.6 Marine Growth.

The inclusion of marine growth is important in the simulations when one considers the leg wind yaw moment and force. The significance depends however upon the degree of surface roughness modelled and the sub/super critical drag coefficients chosen. In the trajectory figure 5.25b for the auto pilot simulations, the transverse displacement has increased as has the rudder deflection and the drift angle when compared with the initial conditions of figures 5.19. It is noted in Ref. 5.1, the drag on the lattice type structure is assumed as 0.55. If we examine the value of the drag coefficient obtained from the MMEC method (0.663 without marine growth), we see that the assumed leg drag is 83% of the MMEC value and 72% with marine growth.

5.5.2.7 Wind Velocity.

The wind velocity has a major effect on the trajectory of the vessel. In the turning circle simulations of figures 5.26, with the wind velocity of 25m/s, the vessel may become unmanoeuvrable. The drift

angle has increased to 45 degrees and the non dimensional angular velocity has a peak value of 1.65. In the automatic pilot simulations of the variation in exposed leg lengths figures 5.23, the wind velocity acting on the system is also 30m/s. These simulations show a more realistic manoeuvring performance.

This raises some doubts about the accuracy of the turning circle simulation at the higher wind velocities. The empirical non linear manoeuvring derivative equations are applicable up to drift angles of approximately 25 degrees and for non dimensional angular velocities of approximately 1.1.

5.5.2.8 Rudder Angle.

The rudder angle has a significant effect on the predicted trajectory of the tow, figures 5.27. The drift angle and angular velocity for the 35 degree rudder appear to be excessive and out with the limits of the empirical derivative equations. A rudder angle of less than 10 degrees may be insufficient to turn the heavy lift vessel system in the wind. If the jack up was brought forward towards the tow system centroid then the manoeuvring performance would improve.

5.5.2.9 Automatic Pilot Rudder Constants.

The simulations for the variation of automatic pilot rudder constants are given in figures 5.28. It is apparent that the reduction of the constants 1, 2 from the initial values of 8, 5 to 4, 2.5 and 2, 1.25 decreases the transverse displacement of the simulation trajectory. The rudder deflection is -13.066 and -12.6 degrees respectively. The differences in the trajectories can be explained by the following. It is clear that when the heading angle equals the drift angle then the trajectory will follow a course angle of zero degrees, figure 5.28b. In the simulations of constants 8, 5 the course angle is approximately -6.5 degrees while for rudder constants 4, 2.5 it is at -5.5 degrees. The ratios of these angles are proportional to the ratios of their respective transverse displacements. The system optimum rudder control constants 1, 2 should be less than 2.0 and 1.25 respectively. These

conclusions are drawn for the automatic pilot model used. A more sophisticated auto pilot model could be applied which takes into account the global positioning of the heavy lift vessel system and the course angle of the tow system.

Skeg Dimensions	Skeg1	Skeg2
Maximum Span (m)	5.2	5.2
Root Chord (m)	9.469	9.7
Tip Chord (m)	4.261	8.4
Area (m^2)	35.7	35.7

Table 5.1

Heavy Lift Vessel Mighty Servant II
Official Trials. Nagasaki, Japan 2nd October, 1983.
Water Depth 70 m
Sea Condition Fine
Wind Velocity 8m/s Starboard Turn, 11m/s Port Turn
Wind Direction 8 Degrees off Starboard Bow, 355 Degrees of Port Bow

Length	160	m
L.B.P.	155	m
B mld	40	m
D mld	12	m
Draft Frd	8.477	m
Midships	8.47	m
Aft	8.562	m
Mean	8.52	m
Trim (stern)	0.085	m
Displacement	32164	tonnes

Midship Coeff	0.753	
Prismatic Coeff	0.79	
Block Coeff	0.595	
TPC	57.2	tonnes/cm
Vessel Velocity	15	knots
Wind Area (Trans	1067	m^2
Longitudinal	1618	m^2

Propellers		
Propeller Diam	4.3	m
P/D	0.6	
C1	0.246	
C2	-0.241	
C3	-0.225	
RPS	3.3	
Thrust Deduction	0.14	
ah	0.15	
xr'	-0.435	
xh'	1.6	

Rudder		
Span	5.4	m
Root Chord	4	m
Tip Chord	2.4	m
Area	34.56	m^2

	Port Turn 35 Degrees			Starboard Turn 35 Degrees		
	Simulation	Trials	% S/T	Simulation	Trials	% S/T
Advance	514	524	0.980916031	506.1	532	0.951315789
Transfer	257	234	1.098290598	249.4	236	1.056779661
Tactical Diameter	534.2	528	1.011742424	512.4	511	1.002739726

	Trials Port Turn		Trials Starboard Turn	
Heading Angle	Time (secs)	U/Uo	Time (secs)	U/Uo
0	0	1	0	1
5	17	1	17	0.993
15	29	0.98	29	0.973
30	43	0.96	44	0.934
60	65	0.88	66	0.849
90	87	0.78	88	0.756
120	109	0.673	109	0.658
150	133	0.567	131	0.553
180	160	0.44	157	0.434
210	188	0.36	185	0.349
240	216	0.32	215	0.303
270	246	0.313	244	0.283
300	275	0.313	273	0.283
330	304	0.313	302	0.283
360	333	0.313	332	0.283

Table 5.2

Ship	Mighty Servant I	Bow Leg Length	104.54 m
Cargo	Ron Tappmeyer	Stern Leg Port	104.54 m
Condition	Depart Ravenna	Stern Leg Stbd.	104.54 m
		Leg Mass/m	7 tonne/m

MIGHTY SERVANT I' initial loading condition.

ITEM	WEIGHT	VCG	V Mmt	LCG from AP	LMmt	Free Surface
Fresh Water	164	22.38	3670.32	146.99	24106.36	0
Fuel Oil	2388	6.66	15904.08	93.69	223731.72	3600
Gas Oil	102	1.88	191.76	125.54	12805.08	0
Lub Oil	107	9.54	1020.78	122.28	13083.96	0
Hydro Oil	17	8.69	147.73	132.28	2248.76	0
Bilge Tanks	55	0.93	51.15	132.75	7301.25	0
Cooling Water	39	2.57	100.23	17.85	696.15	0
Crib & Sea Fast	75	12.2	915	70	5250	0
Dead Water	330	0.1	33	70	23100	0
Stores	216	10.08	2177.28	109.77	23710.32	0
Casing Port	190	18.5	3515	6	1140	0
Casing Stbd.	190	18.5	3515	6	1140	0
Lightship	11718	10.84	127023.12	91.66	1074071.88	0
	15591	**10.151**	158264.45	**90.590**	1412385.48	0

Ron Tappmeyer

ITEM	WEIGHT	VCG	V Mmt	LCG from Bow	L Mmt	TCG	T Mmt
HULL	6953.66	7.457	51852.8682	44.816	311632.1664	0.039	274.47
BOW LEG	731.78	52.27	38250.1406	18.288	13382.79264	0	0
STERN LEG P	731.78	52.27	38250.1406	57.607	42155.65046	22.7	16611.406
STERN LEG S	731.78	52.27	38250.1406	57.607	42155.65046	-22.7	-16611.406
	9149	**18.21**	166603.29	**44.74**	409326.26	**0.03**	274.47

Total Tow System

Vertical Height of the Keel of the Jack Up above Keel of HLV. 12.3 m

Item	Mass	VCG	V Mmt	LCG from AP	L Mmt	TCG	T Mmt
Mighty Servant	15591	10.151	158264.45	90.590	1412385.48	0	0
Ballast 5D	1584	1.32	2091	**49.254**	78018.336		
Ballast 7W	384	6.59	2529	**15.42**	5921.28		
JU without Legs	6953.66	19.757	137382.8862	**59.496**	413711.8952	0.039	274.47
Bow Leg	731.78	64.57	47251.0346	**32.968**	24125.32304	0.039	28.8833566
Stern Leg Port	731.78	64.57	47251.0346	**72.287**	52898.18086	22.740	16640.6772
Stern Leg Stbd.	731.78	64.57	47251.0346	**72.287**	52898.18086	-22.66	-16582.1348
	26708	**16.550**	442020.44	**76.380**	2039958.676	**0.014**	361.8957566

LCG of JU relative to HLV System. -16.960 m

Table 5.3

Ron Tappmeyer Particulars

Marathon Le Tourneau 116 class Jack Up

Length	74.09	m
Breadth	61.11	m
Depth(at side)	7.92	
Leg No.	3	
Leg Length	104.54	m
Protrusion	0.46	m
Weight	9149	tonnes
Draft	4.57	m
VCG	18.21	m
LCG from bow	44.74	m
TCG (Port)	0.03	m

Mighty Servant 1

Length o.a.	160	m
Breadth	40	m
Depth	12	m
Draft(Submerged)	22	m
Max draft	9.16	
Deck Area	40*120	
Length WL	145	m
Breadth WL	35	m
Draft	7.92	m
Cb	0.648	
GZ at 5 degrees	0.658	m
KN at 5 degrees	2.1	m
KMt	23.79	m
LCB	76.38	m
LCF	71.1	m
MCT	510	tonnes/cm
Skeg	-68.409	m
Rudder	-66.909	m

Variation in Longitudinal Position of Jack Up on the Heavy Lift Vessel

Total Tow System

Vertical Height of the Keel of the Jack Up above Keel of HLV. 12.3 m

Item	Mass	VCG	V Mmt	LCG from AP	L Mmt	TCG	T Mmt
Mighty Servant	15591	10.151	158264.45	90.590	1412385.48	0	0
Ballast 5D	1700	1.32	2091	73.85	125545		
Ballast 7W	268	6.59	2529	15.42	4132.56		
JU without Legs	6953.66	19.757	137382.8862	54.496	378943.5952	0.039	274.47
Bow Leg	731.78	64.57	47251.0346	27.968	20466.42304	0.039	28.8833566
Stern Leg Port	731.78	64.57	47251.0346	67.287	49239.28086	22.740	16640.31131
Stern Leg Stbd.	731.78	64.57	47251.0346	67.287	49239.28086	-22.66	-16582.1348
	26708	16.550	442020.44	76.380	2039951.62	0.014	361.5298666

LCG of JU relative to HLV System. -21.960 m

Total Tow System

Vertical Height of the Keel of the Jack Up above Keel of HLV. 12.3 m

Item	Mass	VCG	V Mmt	LCG from AP	L Mmt	TCG	T Mmt
Mighty Servant	15591	10.151	158264.45	90.590	1412385.48	0	0
Ballast 5D	1584	1.32	2091	21	33264		
Ballast 7W	384	6.59	2529	12.85	4934.4		
JU without Legs	6953.66	19.757	137382.8862	64.496	448480.1952	0.039	274.47
Bow Leg	731.78	64.57	47251.0346	37.968	27784.22304	0.039	28.8833566
Stern Leg Port	731.78	64.57	47251.0346	77.287	56557.08086	22.740	16640.31131
Stern Leg Stbd.	731.78	64.57	47251.0346	77.287	56557.08086	-22.66	-16582.1348
	26708	16.550	442020.44	76.380	2039962.46	0.014	361.5298666

LCG of JU relative to HLV System. -11.960 m

Orientation of Jack Up on Heavy Lift Vessel : Forward

Bow Leg Length 104.54 m

Stern Leg Port 104.54 m

Stern Leg Stbd. 104.54 m

Leg Mass/m 7 tonne/m

Ron Tappmeyer

ITEM	WEIGHT	VCG	V Mmt	LCG from Bow	L Mmt	TCG	T Mmt
Hull	6953.66	7.457	51852.868	44.816	311632.166	.039	274.470
Bow Leg	731.78	52.27	38250.141	18.288	13382.793	.000	.000
Sten Leg Port	731.78	52.27	38250.141	57.607	42155.650	22.700	16611.406
Stern Leg Stbd.	731.78	52.27	38250.141	57.607	42155.650	-22.700	-16611.406
	9149	18.21	166603.29	44.74	409326.26	0.03	274.47

Total Tow System

Vertical Height of the Keel of the Jack Up above Keel of HLV. 12.3 m

Item	Mass	VCG	V Mmt	LCG from AP	L Mmt	TCG	T Mmt
Mighty Servant	15591	10.151	158264.450	90.590	1412385.480	.000	.000
Ballast 5D	1543	1.32	2091.000	49.254	75998.922		
Ballast 7W	425	6.59	2529.000	15.420	6553.500		
JU without Legs	6953.66	19.757	137382.886	59.496	413711.895	.039	274.470
Bow Leg	731.78	64.57	47251.035	86.024	62950.643	.039	28.883
Stern Leg Port	731.78	64.57	47251.035	46.705	34177.785	22.740	16640.677
Stern Leg Stbd.	731.78	64.57	47251.035	46.705	34177.785	-22.660	-16582.135
	26708	16.550	442020.44	76.380	2039956.01	0.014	361.90

LCG of JU relative to HLV System. -16.960 m

Table 5.3

Variation in Jack Up Leg Length.

Bow Leg Length 119.54 m
Stern Leg Port 119.54 m
Stern Leg Stbd. 119.54 m
Leg Mass/m 7 tonne/m
Ron Tappmeyer

Item	Mass	VCG	V Mmt	LCG from Bow	L Mmt	TCG	T Mmt
Hull	6953.66	7.457	51852.8682	44.816	311632.1664	0.039	274.47
Bow Leg	836.78	59.77	50014.3406	18.288	15303.03264	0	0
Stern Leg Port	836.78	59.77	50014.3406	57.607	48204.38546	22.7	18994.906
Stern Leg Stbd.	836.78	59.77	50014.3406	57.607	48204.38546	-22.7	-18994.906
	9464	**21.333**	201895.89	**44.732**	423343.97	**0.03**	283.92

Total Tow System
Vertical Height of the Keel of the Jack Up above Keel of HLV. 12.3 m

Item	Mass	VCG	V Mmt	LCG from AP	L Mmt	TCG	T Mmt
Mighty Servant	15591	10.151	158264.241	90.590	1412388.69	0	0
Ballast 5D	1480	1.32	2091	42.31	62618.8		
Ballast 7W	173	6.59	2529	15.42	2667.66		
JU without Legs	6953.66	19.757	137382.8862	59.496	413711.8952	0.039	274.47
Bow Leg	836.78	72.07	60306.7346	32.968	27586.96304	0.039	33.0277066
Stern Leg Port	836.78	72.07	60306.7346	72.287	60488.31586	22.740	19027.95881
Stern Leg Stbd.	836.78	72.07	60306.7346	72.287	60488.31586	-22.66	-18961.4348
	26708	**18.017**	481187.331	**76.380**	2039950.64	**0.014**	374.0217166

CoG of JU relative to HLV System. -16.968 m

Bow Leg Length 89.54 m
Stern Leg Port 89.54 m
Stern Leg Stbd. 89.54 m
Leg Mass/m 7 tonne/m
Ron Tappmeyer

Item	Mass	VCG	V Mmt	LCG from Bow	L Mmt	TCG	T Mmt
Hull	6953.66	7.457	51852.8682	44.816	311632.1664	0.039	274.47
Bow Leg	626.78	44.77	28060.9406	18.288	11462.55264	0	0
Stern Leg Port	626.78	44.77	28060.9406	57.607	36106.91546	22.7	14227.906
Stern Leg Stbd.	626.78	44.77	28060.9406	57.607	36106.91546	-22.7	-14227.906
	8834	**15.399**	136035.69	**44.749**	395308.55	**0.03**	265.02

Total Tow System
Vertical Height of the Keel of the Jack Up above Keel of HLV. 12.3 m

Item	Mass	VCG	V Mmt	LCG from AP	L Mmt	TCG	T Mmt
Mighty Servant	15591	10.151	158264.241	90.590	1412388.69	0	0
Ballast 5D	1760	1.32	2091	53	93280		
Ballast 7W	523	6.59	2529	17.8	9309.4		
JU without Legs	6953.66	19.757	137382.8862	59.496	413711.8952	0.039	274.47
Bow Leg	626.78	57.07	35770.3346	32.968	20663.68304	0.039	24.7390066
Stern Leg Port	626.78	57.07	35770.3346	72.287	45308.04586	22.740	14252.66381
Stern Leg Stbd.	626.78	57.07	35770.3346	72.287	45308.04586	-22.66	-14202.8348
	26708	**15.261**	407578.131	**76.380**	2039969.76	**0.013**	349.0380166

CoG of JU relative to HLV System. -16.952 m

Table 5.3

Calculation of Leg Member Dimensions and Drag Coefficients

Marathon Le Tourneau 116c Class Leg

Example Calculation for estimate of Leg Member dimensions.

Data scaled from Ref.4.2

Leg Dimensions and Component Projected Areas.

Component	Area(ft^2)	Area(m^2)
Total Cylinder Area	64.374	5.981
Total Gusset Area	6.396	0.594
Total Corner Post Area	65.817	6.115
Overall Projected Area	136.587	12.689
Length of bay (ft,m)	11.92	3.633
Width of Bay (ft,m)	31.98	9.748

Width of Corner Post=6.115m^2/(2*3.633m)=0.842m

Cylindrical Area=5.981m^2

Assume members 2&3 have the same diameter.

Horizontal Brace= 1*(9.748-2*0.842)*DIAM= 8.064*DIAM

Vert. Brace= 2*((8.064/2)^2+3.633^2)^0.5)*DIAM= 10.855*DIAM

Total Area 18.919*DIAM

DIAM=5.981m^2/18.919m= 0.316m

Member 4 diameter is approximately 60% of diameters of members 2&3

Marine Growth Height and Thickness (mm) 0.00, 0.00

MMEC Cornerpost Drag		Member Drag Coefficients	
Windward	2.012	Flat Plate	2
Leeward	1.625	Cylindrical	0.7
Member	Length (m)	Diameter (m)	No.of Members/Face
1	3.633	0.842	2
2	8.064	0.316	1
3	5.427	0.316	2
4	5.702	0.19	1

All members defined in Fig 4.

Members 4 are hidden by members 2 and are 60% diameter of members 2 &3

Assume Angle of Wind Incidence (beta) is zero degrees

Solidity= 12.689/(3.633*9.748)= 0.358

Shielding= 1.1-2.012*0.3583= 0.379

Orientation= 1+0.5728*Solidity*sin(2beta)^0.09= 1

Drag Coefficient= (6.115*2.012+2*0.594+0.7*5.981+0.397*
(6.115*1.625+2*0.594+0.7*5.981))/(L*W)= 0.633

Marine Growth Height and Thickness (mm) 1.25, 5.0

MMEC Cornerpost Drag		Member Drag Coefficients	
Windward	2.012	Flat Plate	2
Leeward	1.625	Cylindrical	1.1
Member	Length (m)	Diameter (m)	No.of Members
1	3.633	0.85075	2
2	8.064	0.32475	1
3	5.427	0.32475	2
4	5.702	0.19875	1

Solidity= 12.919/35.454 = 0.3644

Shielding= 1.1-2.012*0.3644 = 0.3668

Orientation= 1+0.5728*solidity*sin(2beta)^0.09 = 1

Drag Coefficient= (6.1816*2.012+2*0.594+1.1*6.1436+0.397*
(6.1816*1.625+2*0.594+1.1*6.1436))/(L*W) = 0.761

Table 5.4

Skeg Geometries.

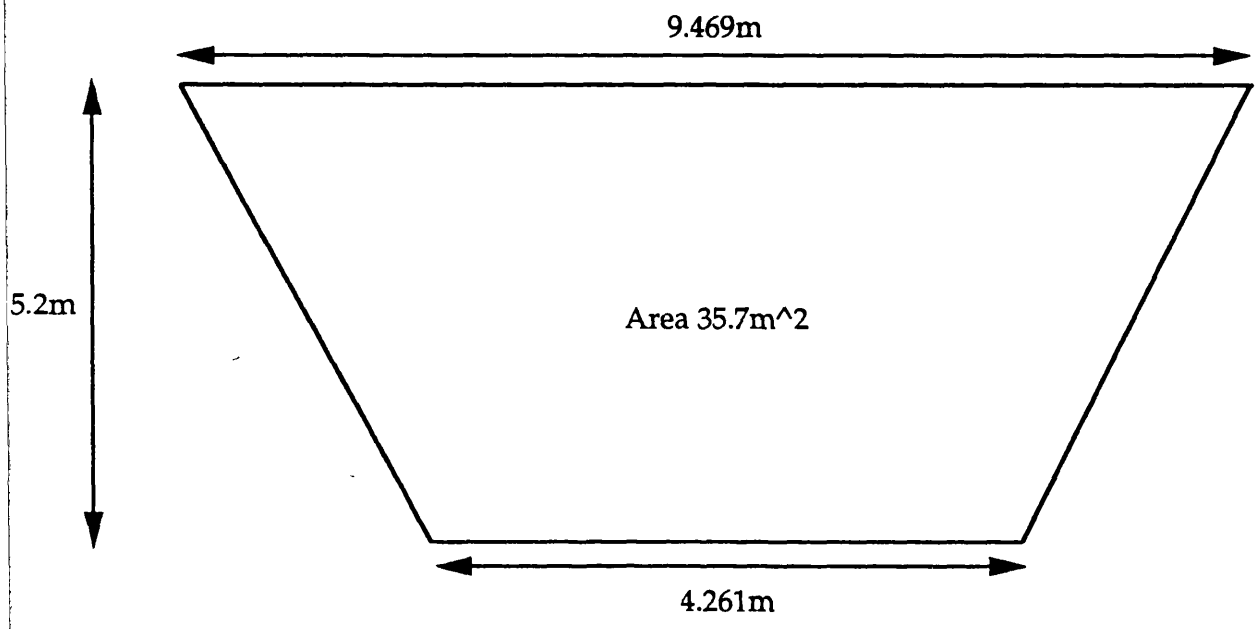

Skeg 1

Figure 5.1

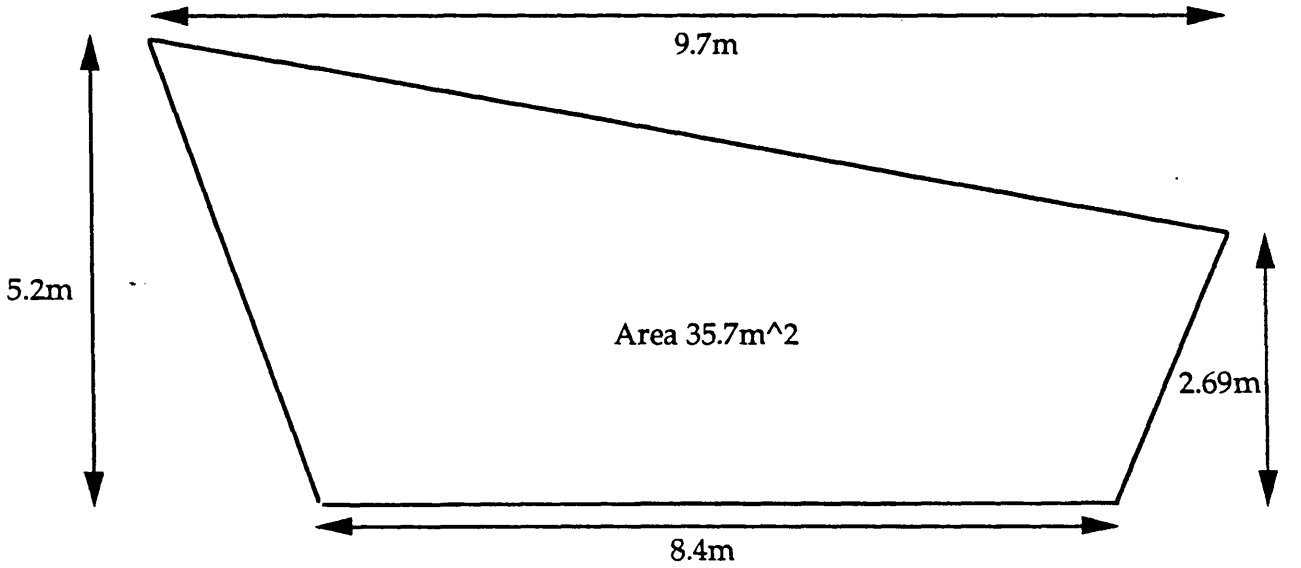

Skeg 2

Not to Scale

Figure 5.2

Definition of Lift and Drag Coefficients for the Skeg.

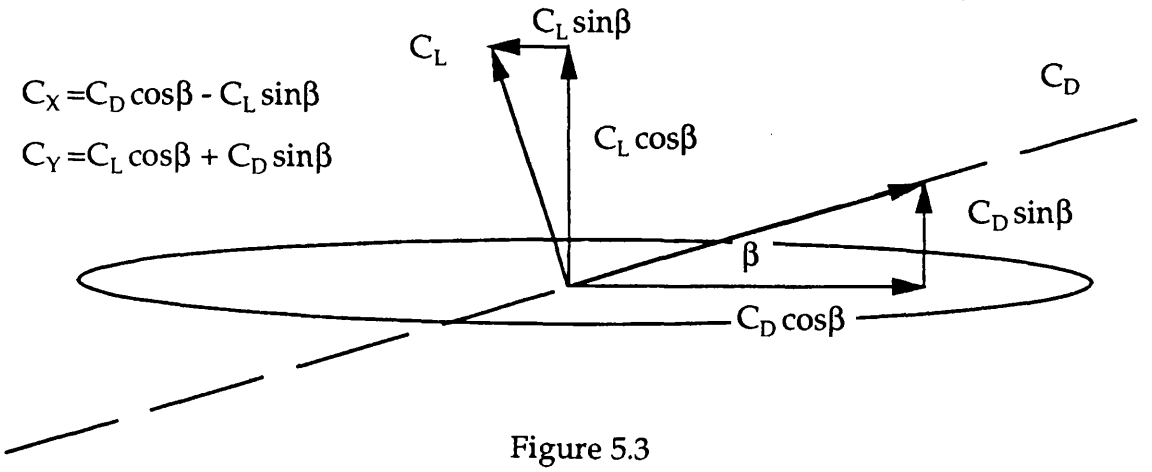

Figure 5.3

Rudder Definitions

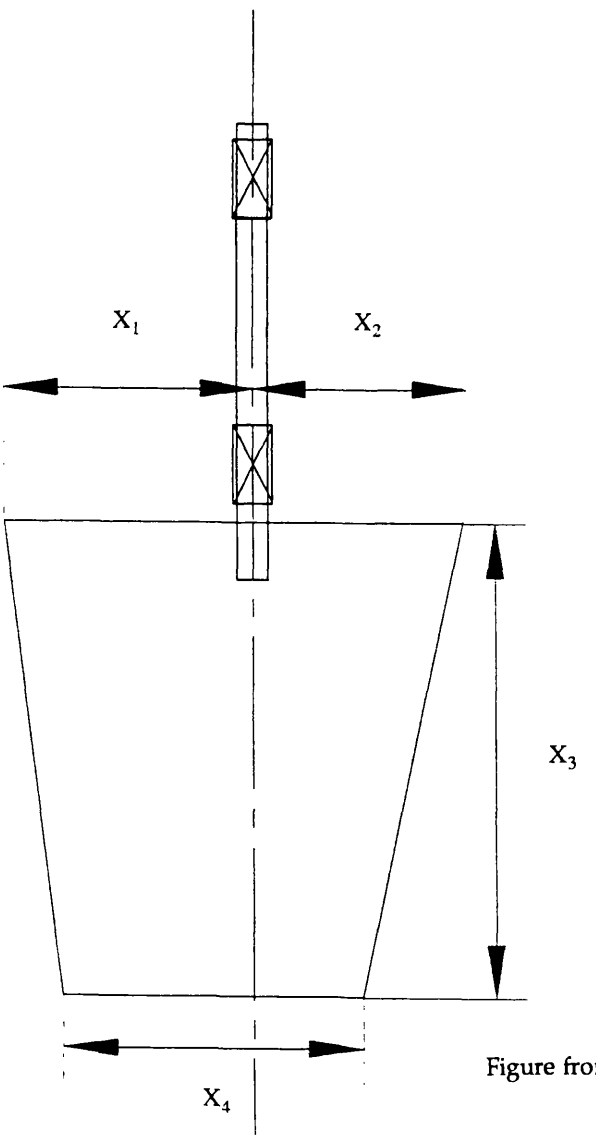

Figure from Ref. 5.5

Figure 5.4

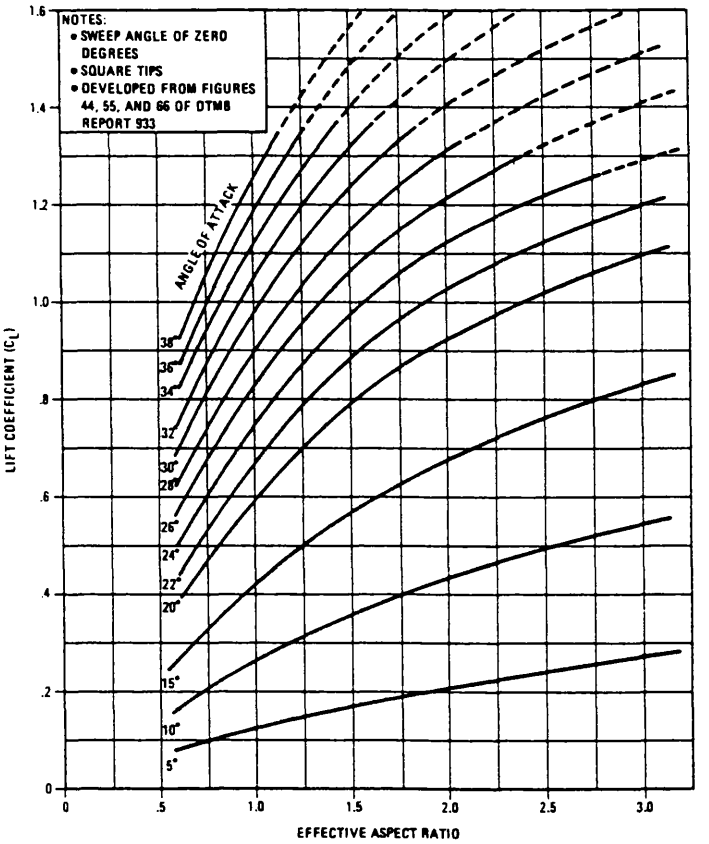

Figure 5.5

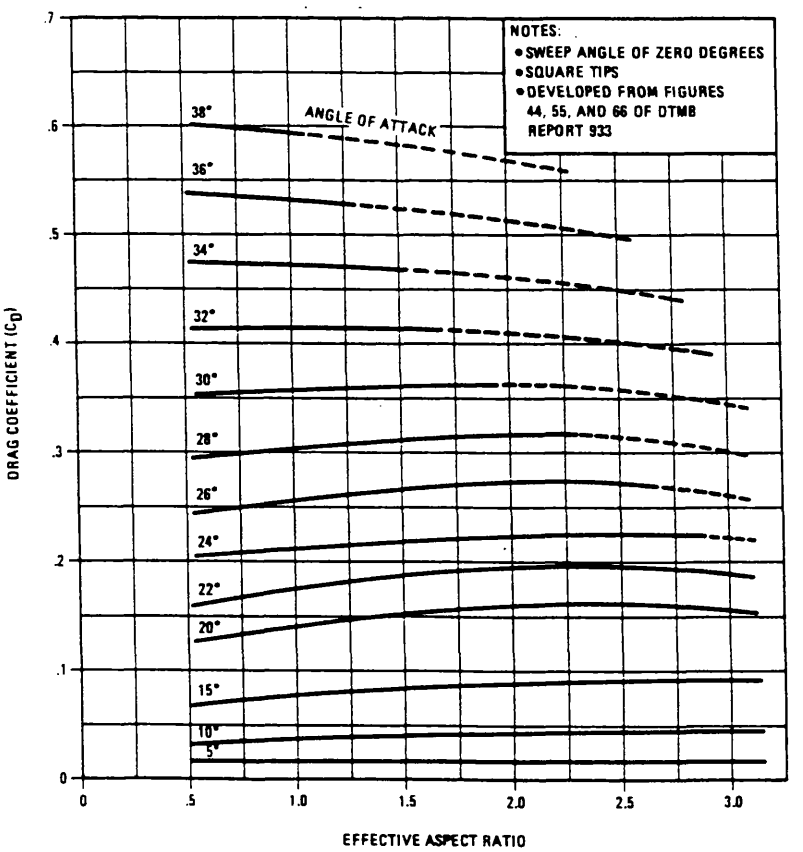

Figure 5.6

Comparison of Skeg Drag Coefficient

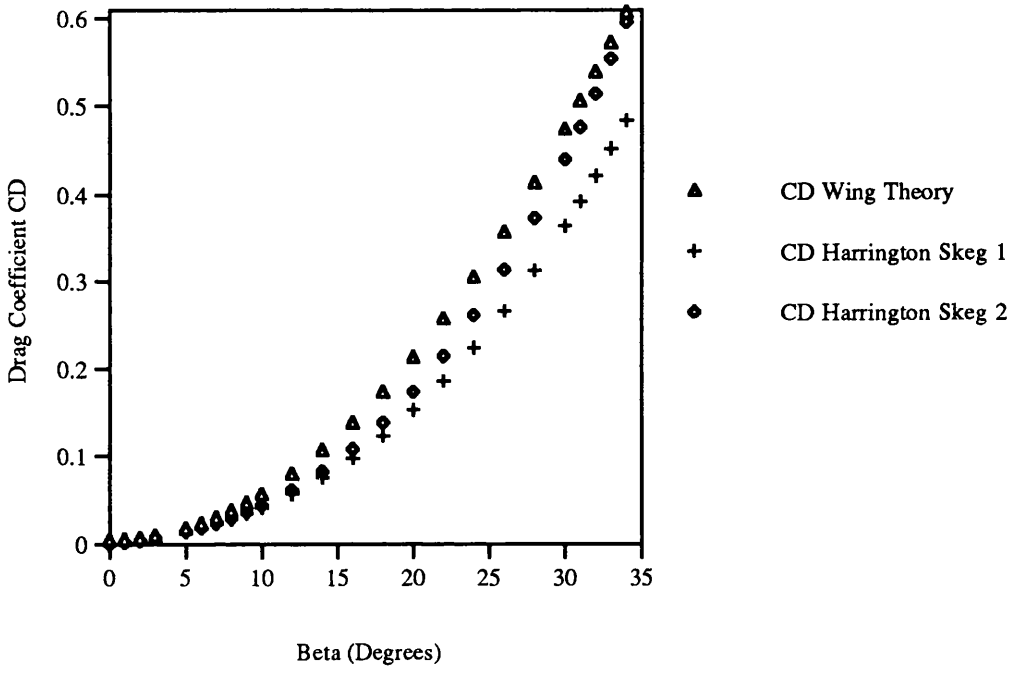

Figure 5.7

Comparison of Skeg Lift Coefficient.

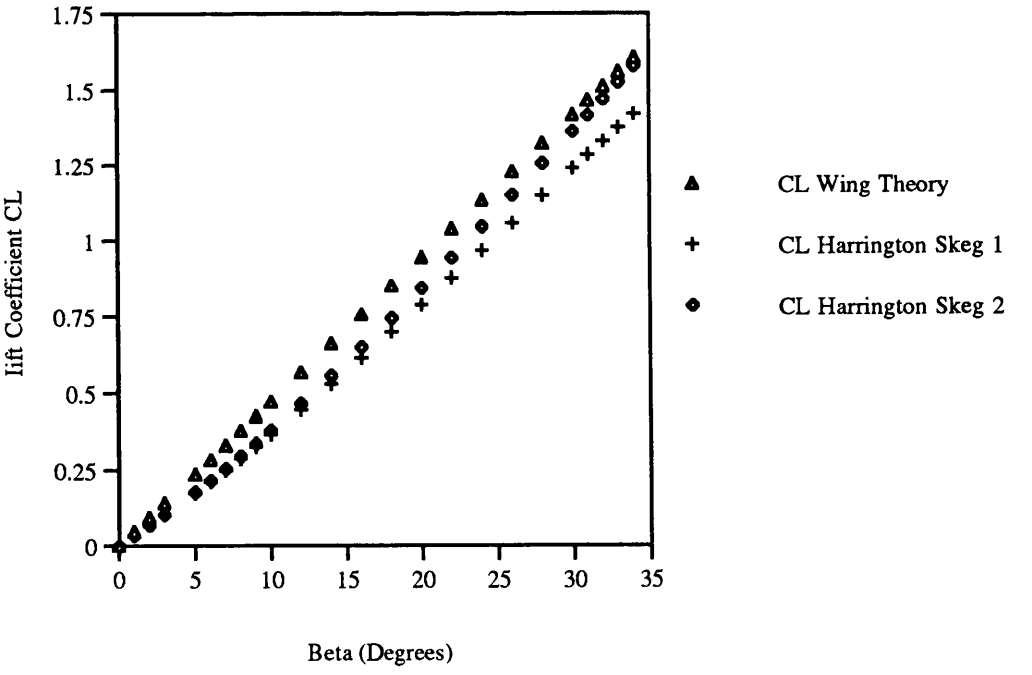

Figure 5.8

Comparison of Skeg Surge Forces

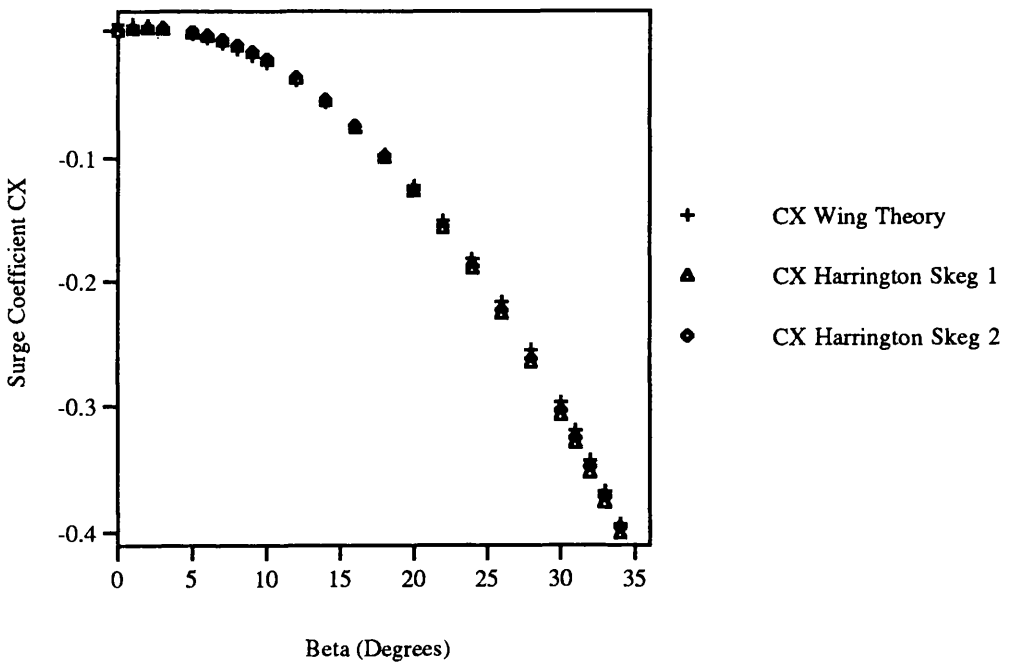

Figure 5.9

Comparison of Skeg Sway Force

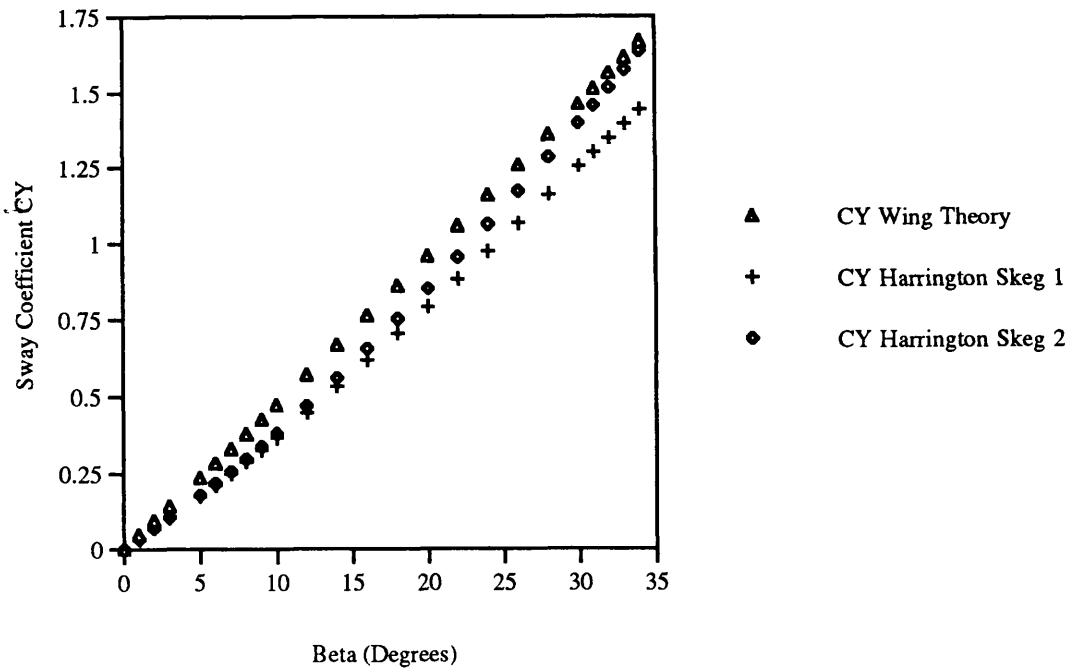

Figure 5.10

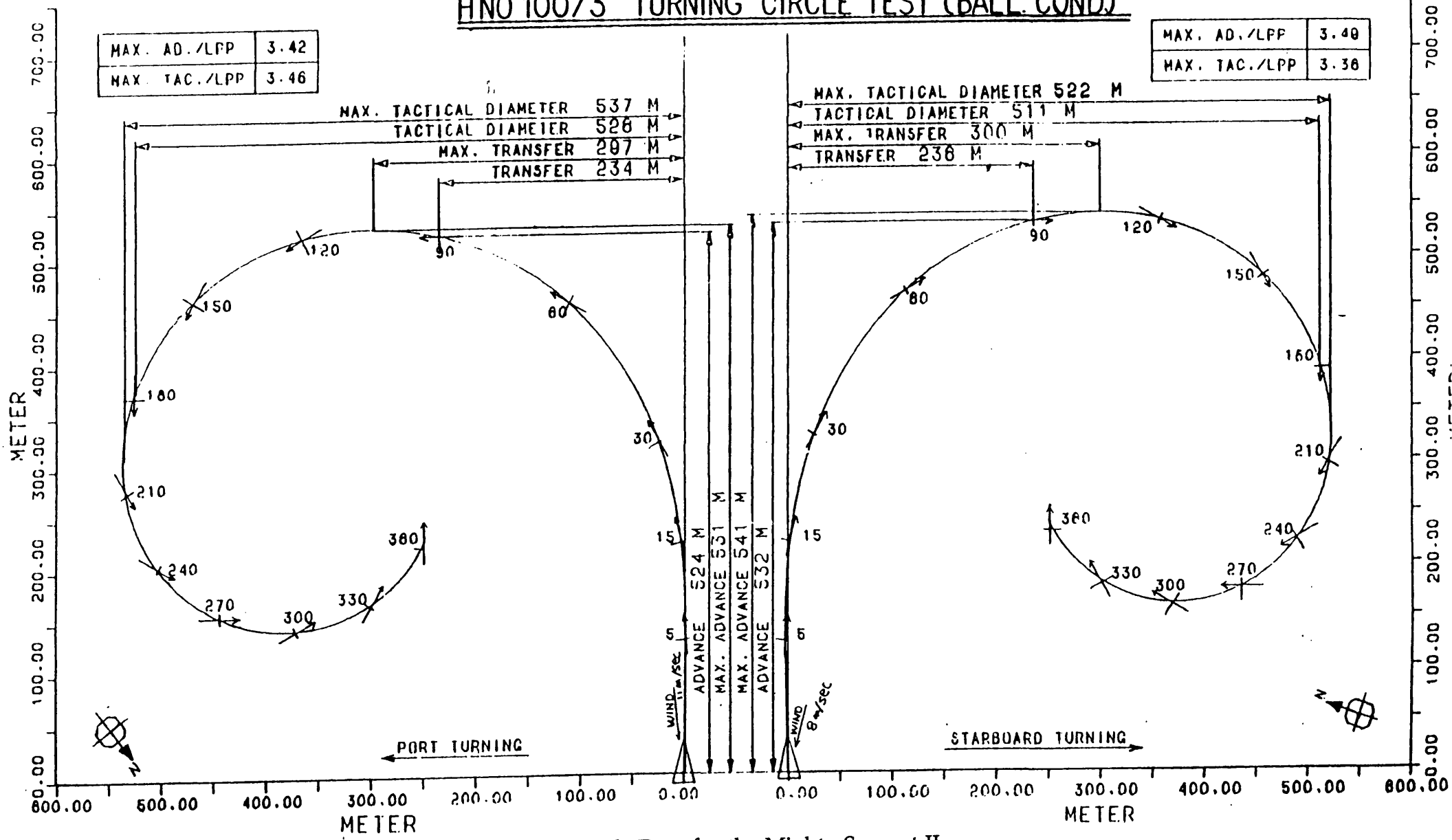

Trials Data for the Mighty Servant II.

Figure 5.11

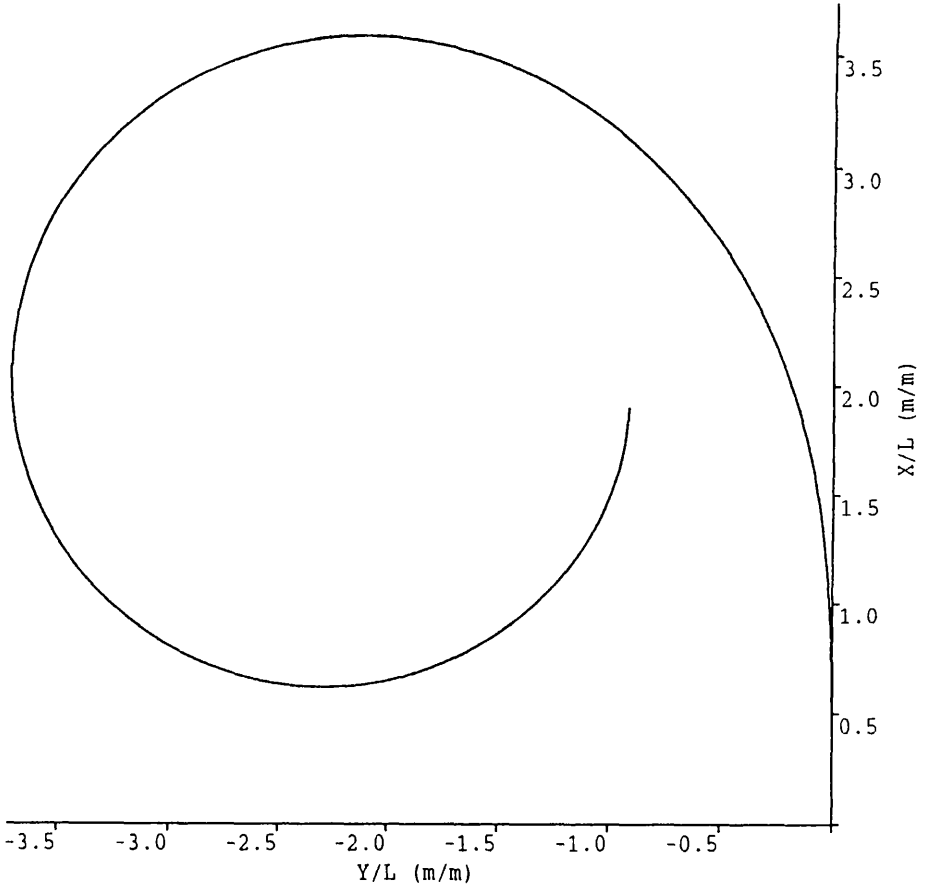

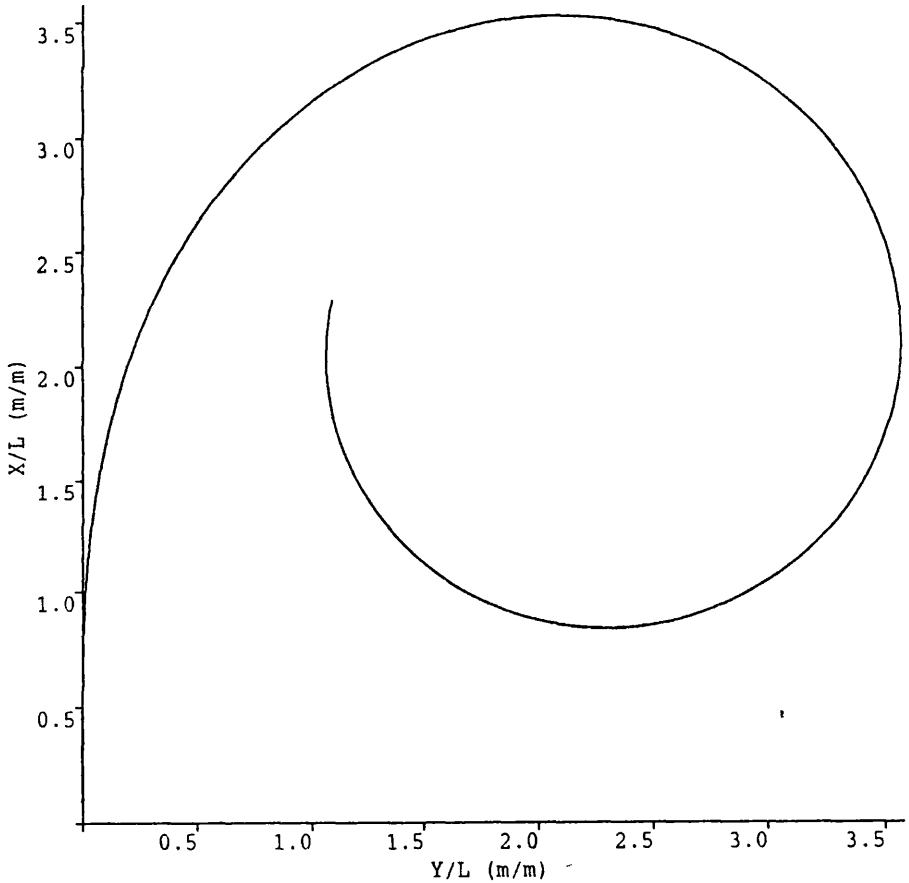

Vessel Velocity : 15.0 Knots
Rudder Angle : -35.0 Degrees
Advance : 514.4 m
Transfer : 257.0 m
Tactical Diameter : 534.2 m
Wind Velocity,Angle : 21.4,355.0 Knots,Deg

Vessel Velocity : 15.0 Knots
Rudder Angle : 35.0 Degrees
Advance : 506.1 m
Transfer : 249.4 m
Tactical Diameter : 512.4 m
Wind Velocity,Angle : 15.6, 8.0 Knots,Deg

Figure 5.12

Mighty Servant II

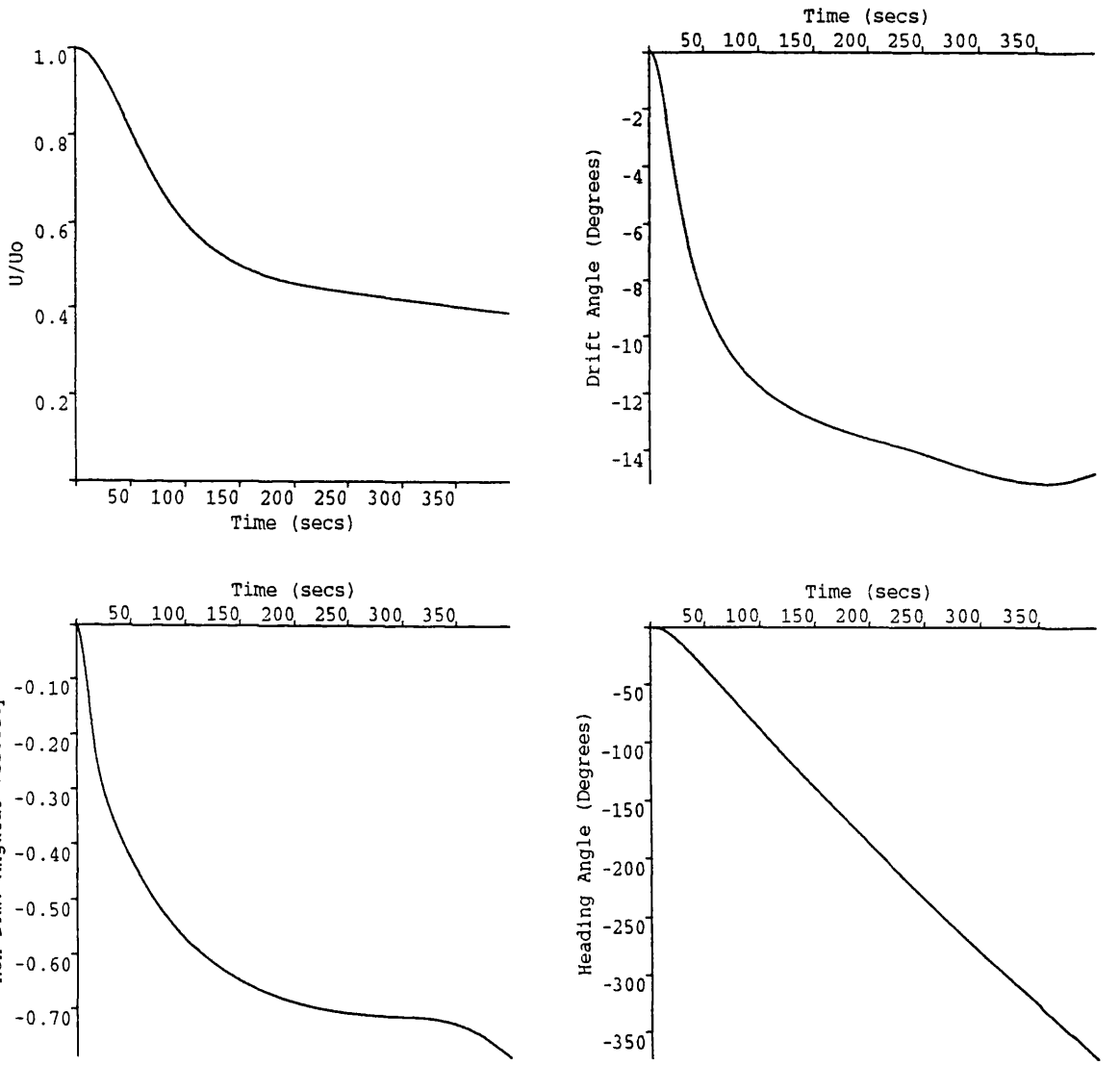

Vessel Velocity : 15.0 Knots
Rudder Angle : -35.0 Degrees
Advance : 514.4 m
Transfer : 257.0 m
Tactical Diameter : 534.2 m
Wind Velocity,Angle : 21.4,355.0 Knots,Deg

Figure 5.13a

Mighty Servant II

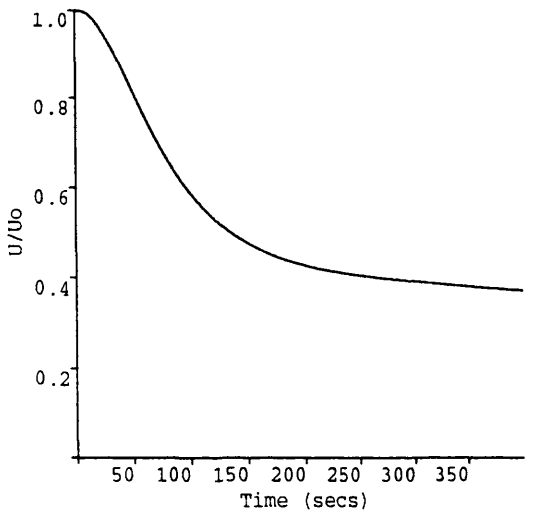

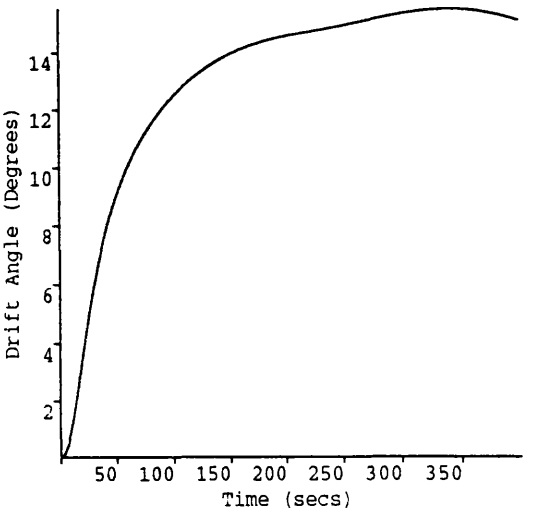

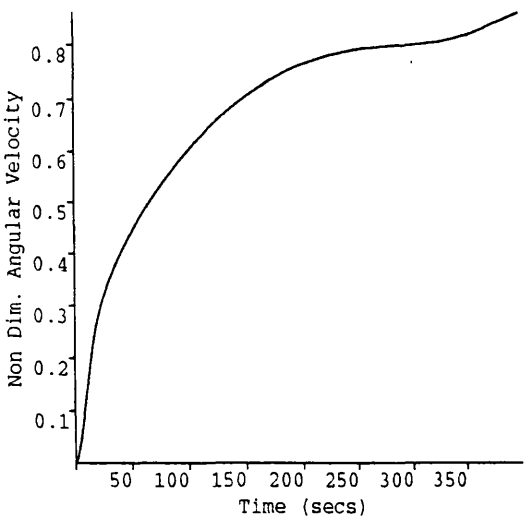

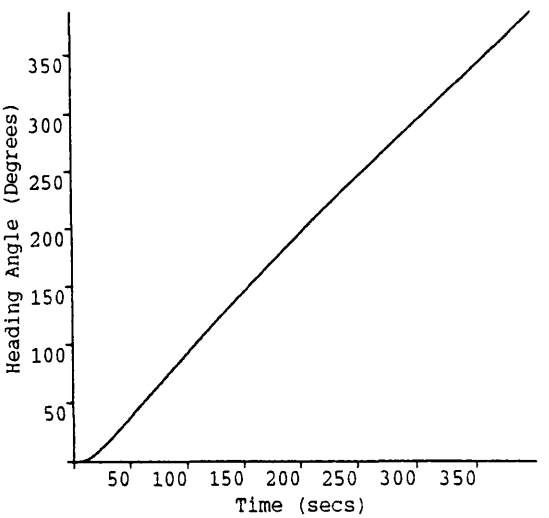

Vessel Velocity : 15.0 Knots
Rudder Angle : 35.0 Degrees
Advance : 506.1 m
Transfer : 249.4 m
Tactical Diameter : 512.4 m
Wind Velocity,Angle : 15.6, 8.0 Knots,Deg

Figure 5.13b

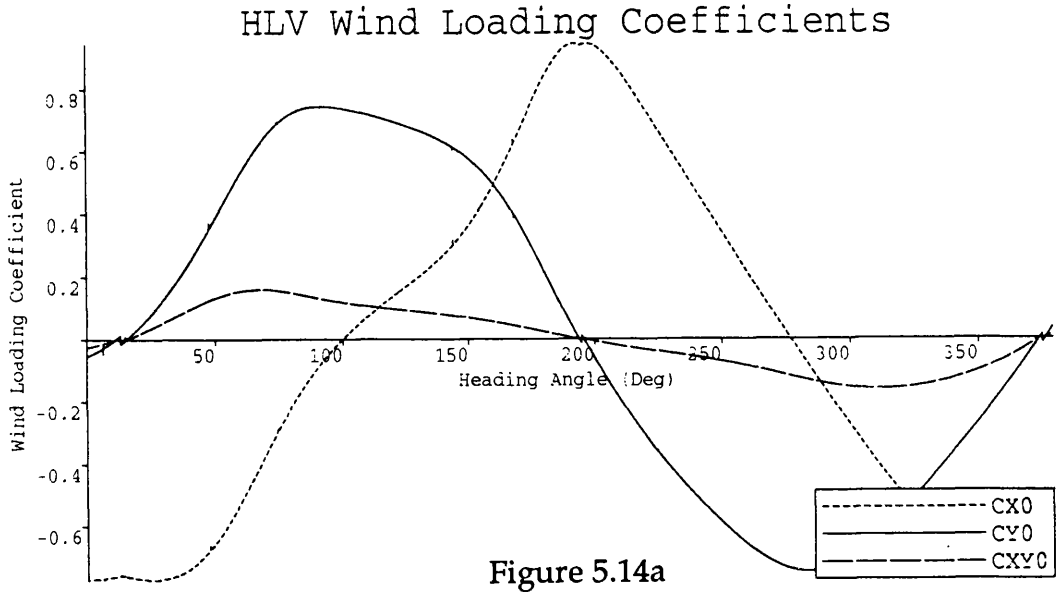

Figure 5.14a

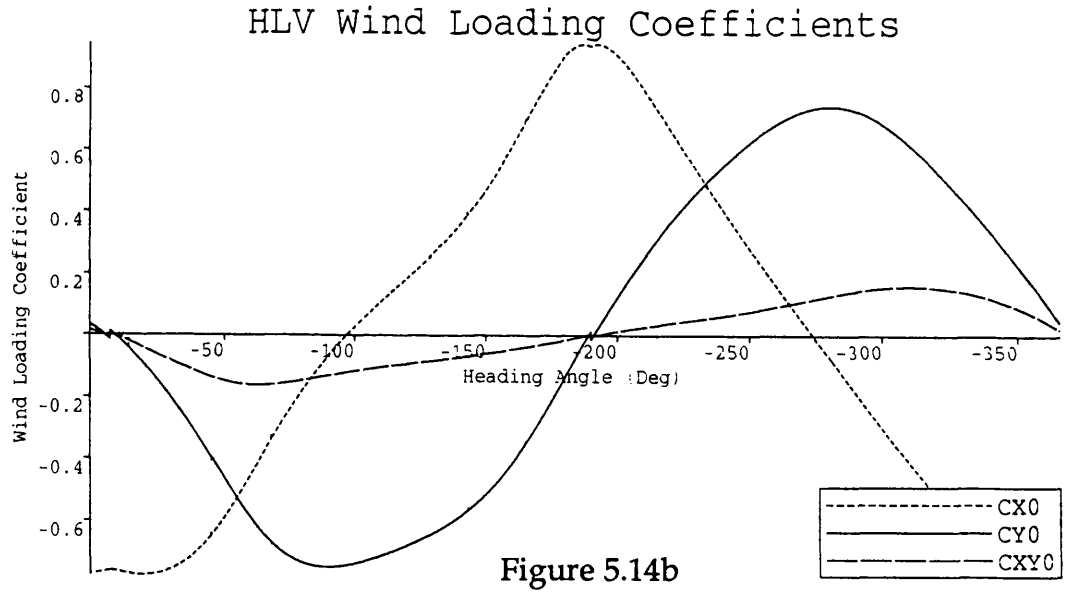

Figure 5.14b

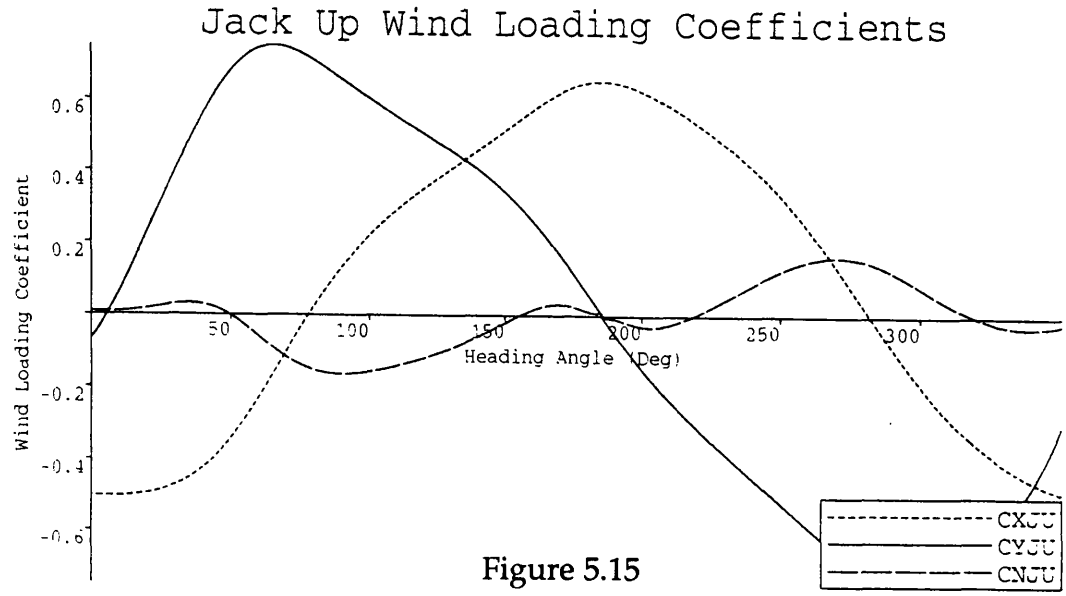

Figure 5.15

Condition of the Dry Tow System.

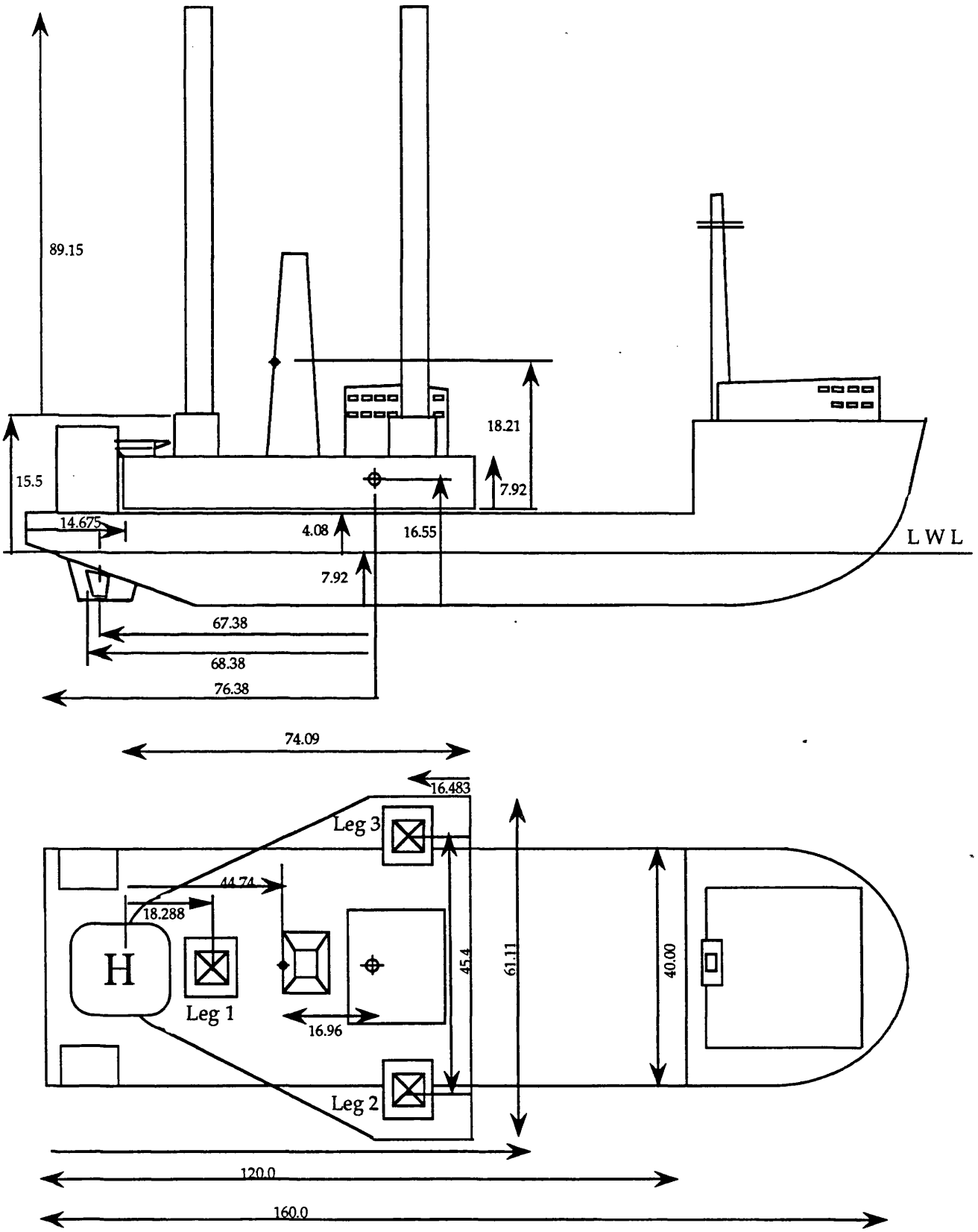

Figure 5.16

All dims. in meters

◆ COG of Jack Up

⊕ COG of Tow System

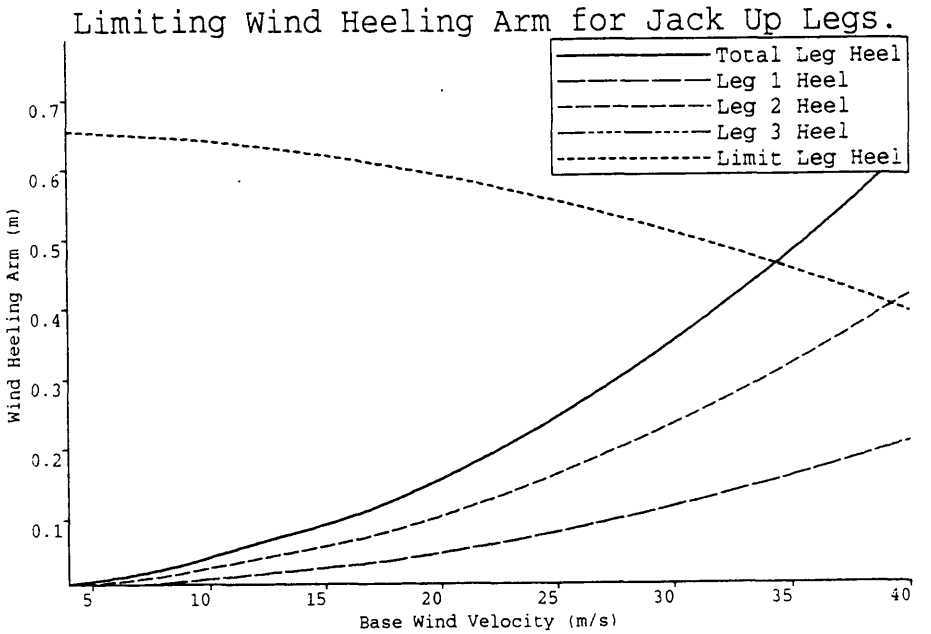

Base Height of Exposed Leg : 19.58m
Marine Growth Height & Thickness: 0.00, 0.00mm,mm
Leg Drag Coefficient : 0.663
GZ at 5 Degrees Heel : 0.658m
Leg Geometry : Square
Leg Type : 116 Marathon
Leg Length Exposed : 89.15 m

Figure 5.17a

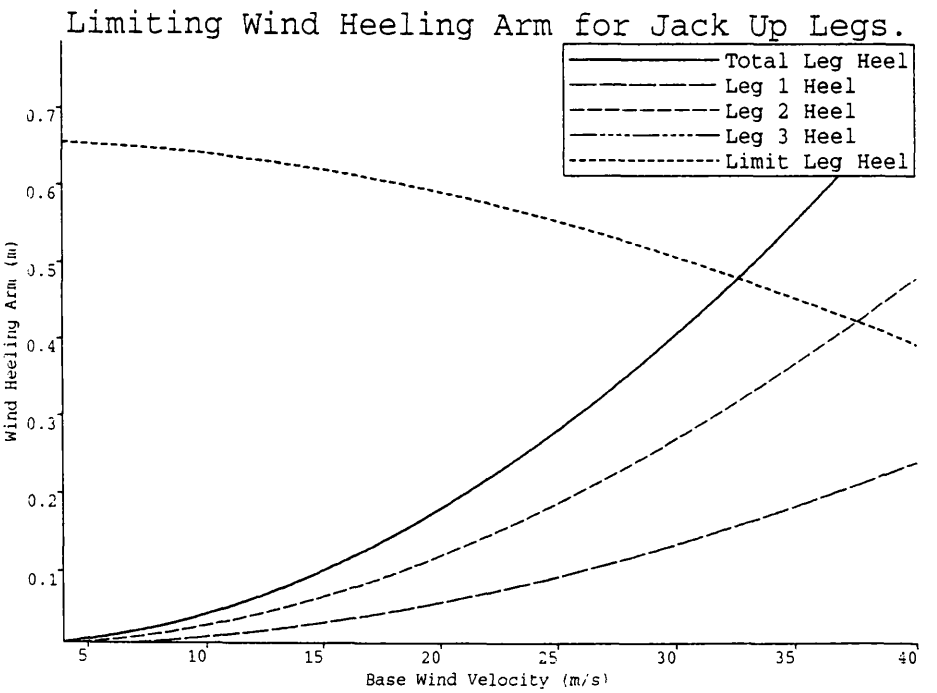

Base Height of Exposed Leg : 19.58m
Marine Growth Height & Thickness: 1.25, 5.00mm,mm
Leg Drag Coefficient : 0.761
GZ at 5 Degrees Heel : 0.658m
Leg Geometry : Square
Leg Type : 116 Marathon
Leg Length Exposed : 89.15 m

Figure 5.17b

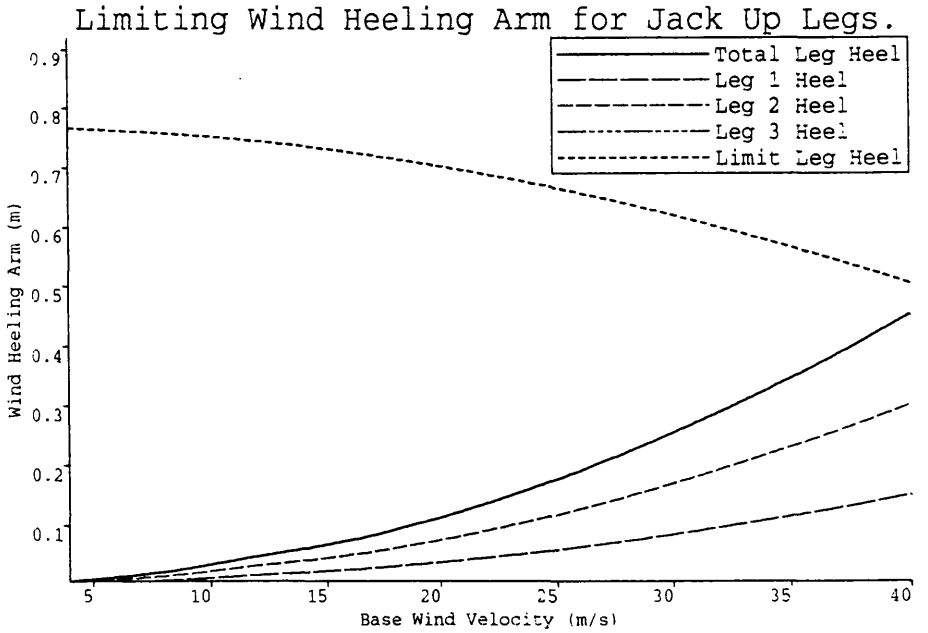

Base Height of Exposed Leg : 19.58m
Marine Growth Height & Thickness: 0.00, 0.00mm,mm
Leg Drag Coefficient : 0.663
GZ at 5 Degrees Heel : 0.770m
Leg Geometry : Square
Leg Type : 116 Marathon
Leg Length Exposed : 74.15 m

Figure 5.17c

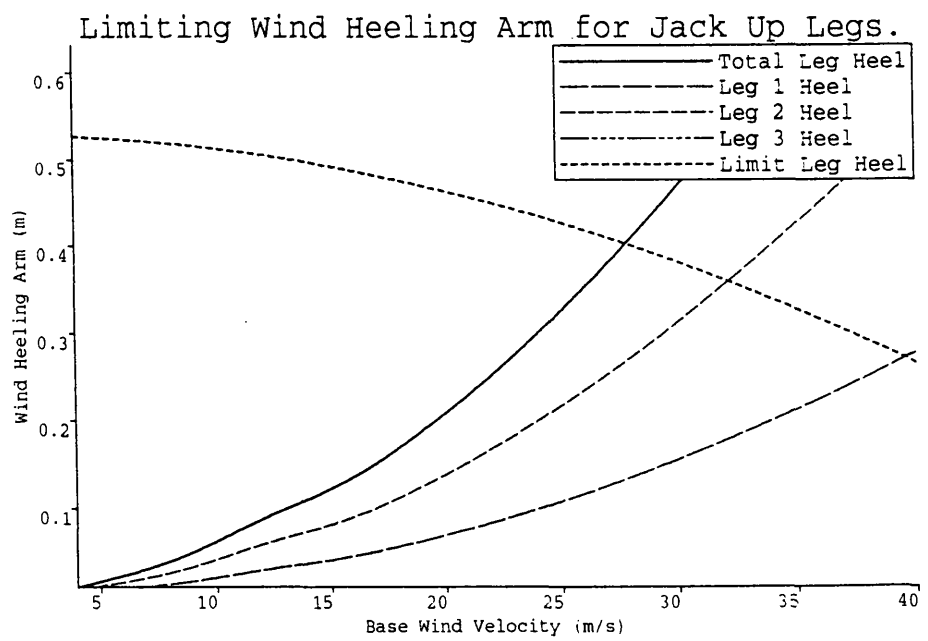

Base Height of Exposed Leg : 19.58m
Marine Growth Height & Thickness: 0.00, 0.00mm,mm
Leg Drag Coefficient : 0.663
GZ at 5 Degrees Heel : 0.530m
Leg Geometry : Square
Leg Type : 116 Marathon
Leg Length Exposed :104.15 m

Figure 5.17d

Mighty Servant I

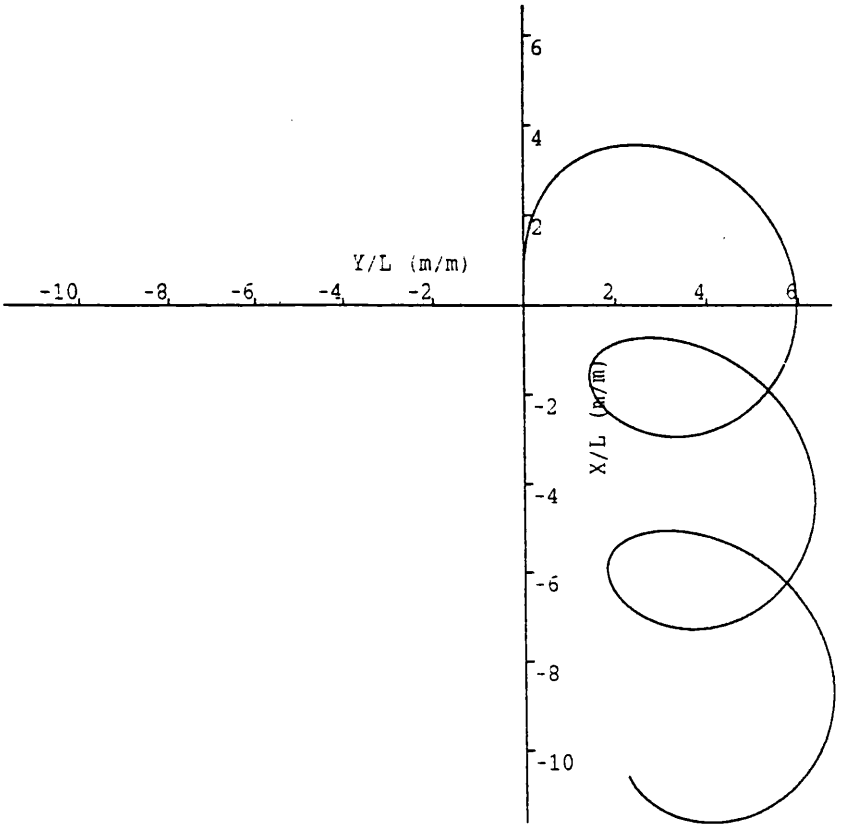

Figure 5.18a

Vessel Velocity : 15.0 Knots
Orientation of Jack Up on HLV : Aft
JU CoG with System CoG (X,Y) :-16.96, 0.04m,m
Bow & Stern Leg Longitudinal: 26.7 12.8m,m
Bow & Stern Leg Transverse: 0.0 22.7m,m
Rudder Angle : 20.0 Degrees
Advance : 517.0 m
Transfer : 338.0 m
Tactical Diameter : 859.7 m
Wind Velocity,Angle : 38.9, 0.0 Knots,Deg
Leg Length Exposed : 89.15 m

Mighty Servant I

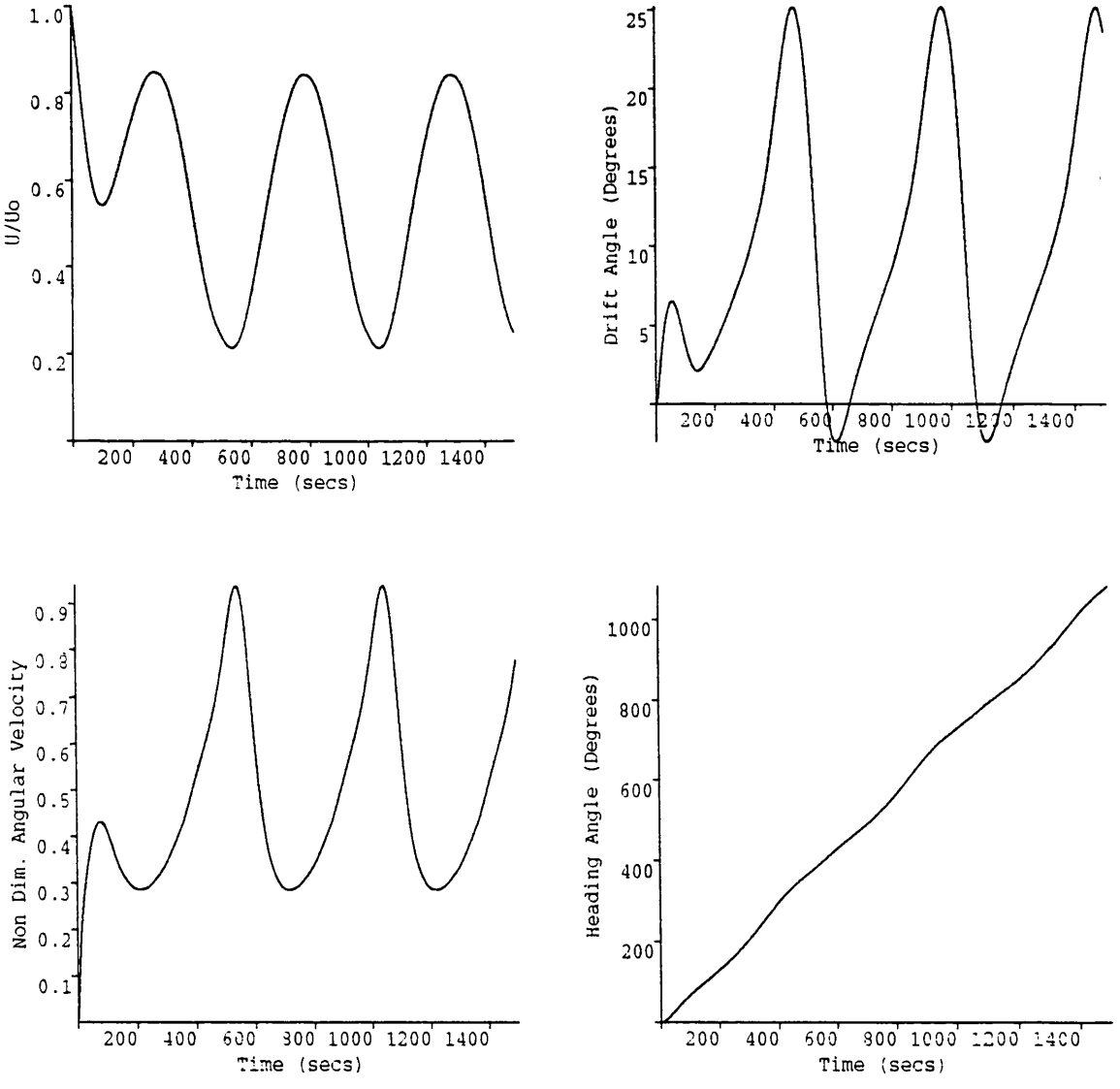

Figure 5.18b

Vessel Velocity : 15.0 Knots
Orientation of Jack Up on HLV : Aft
JU CoG with System CoG (X,Y) :-16.96, 0.04m,m
Bow & Stern Leg Longitudinal: 26.7 12.8m,m
Bow & Stern Leg Transverse: 0.0 22.7m,m
Rudder Angle : 20.0 Degrees
Advance : 517.0 m
Transfer : 338.0 m
Tactical Diameter : 859.7 m
Wind Velocity,Angle : 38.9, 0.0 Knots,Deg
Leg Length Exposed : 89.15 m

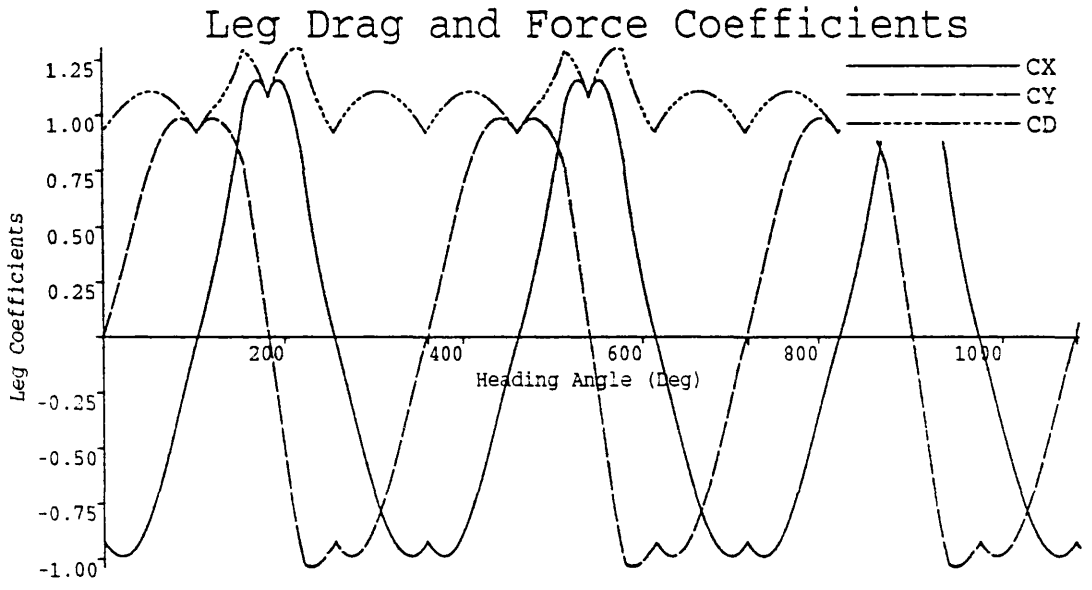

Figure 5.18c

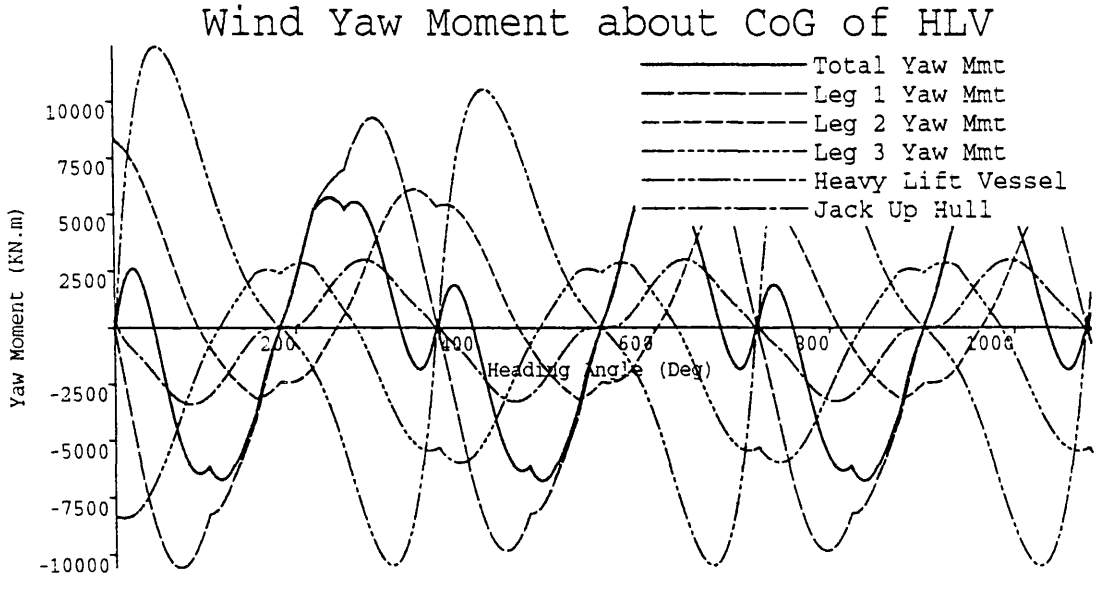

Figure 5.18d

Base Height of Exposed Leg : 19.58m
Marine Growth Height&Thickness: 0.00, 0.00mm,mm
Leg Drag Coefficient :0.663
Wind Velocity,Angle :38.9, 0.0Knots,Deg
Leg Geometry : Square
Leg Type : 116 Marathon
Orientation of Jack Up on HLV : Aft
JU CoG with System CoG (X,Y) :-16.96, 0.04m,m
Bow & Stern Leg Longitudinal: 26.7 12.8m,m
Bow & Stern Leg Transverse: 0.0 22.7m,m
Leg Length Exposed : 89.15 m

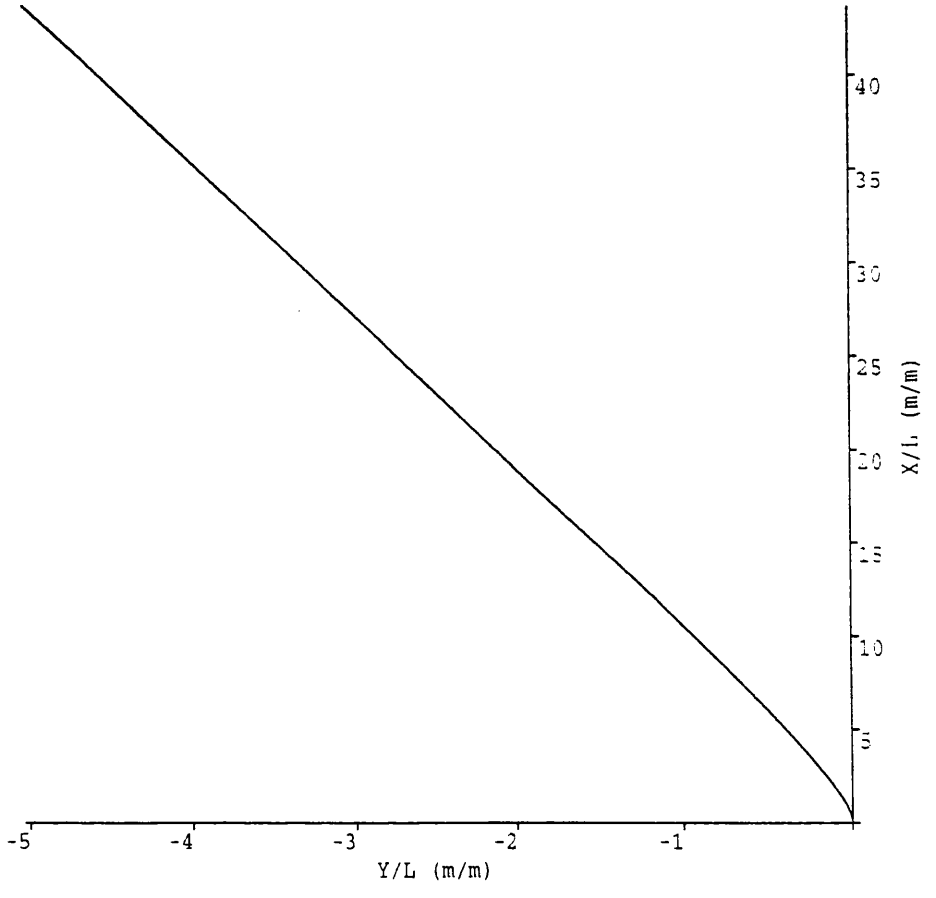

Figure 5.19a

Vessel Velocity : 15.0 Knots
Orientation of Jack Up on HLV : Aft
JU CoG with System CoG (X,Y) :-16.96, 0.04m,m
Bow & Stern Leg Longitudinal: 26.7 12.8m,m
Bow & Stern Leg Transverse: 0.0 22.7m,m
Rudder Constants 1,2 : 8.0,5.0
Maximum Deflection : -13.066 Degrees
Wind Velocity,Angle : 58.4, 90.0 Knots,Deg
Leg Length Exposed : 89.15 m

Mighty Servant I

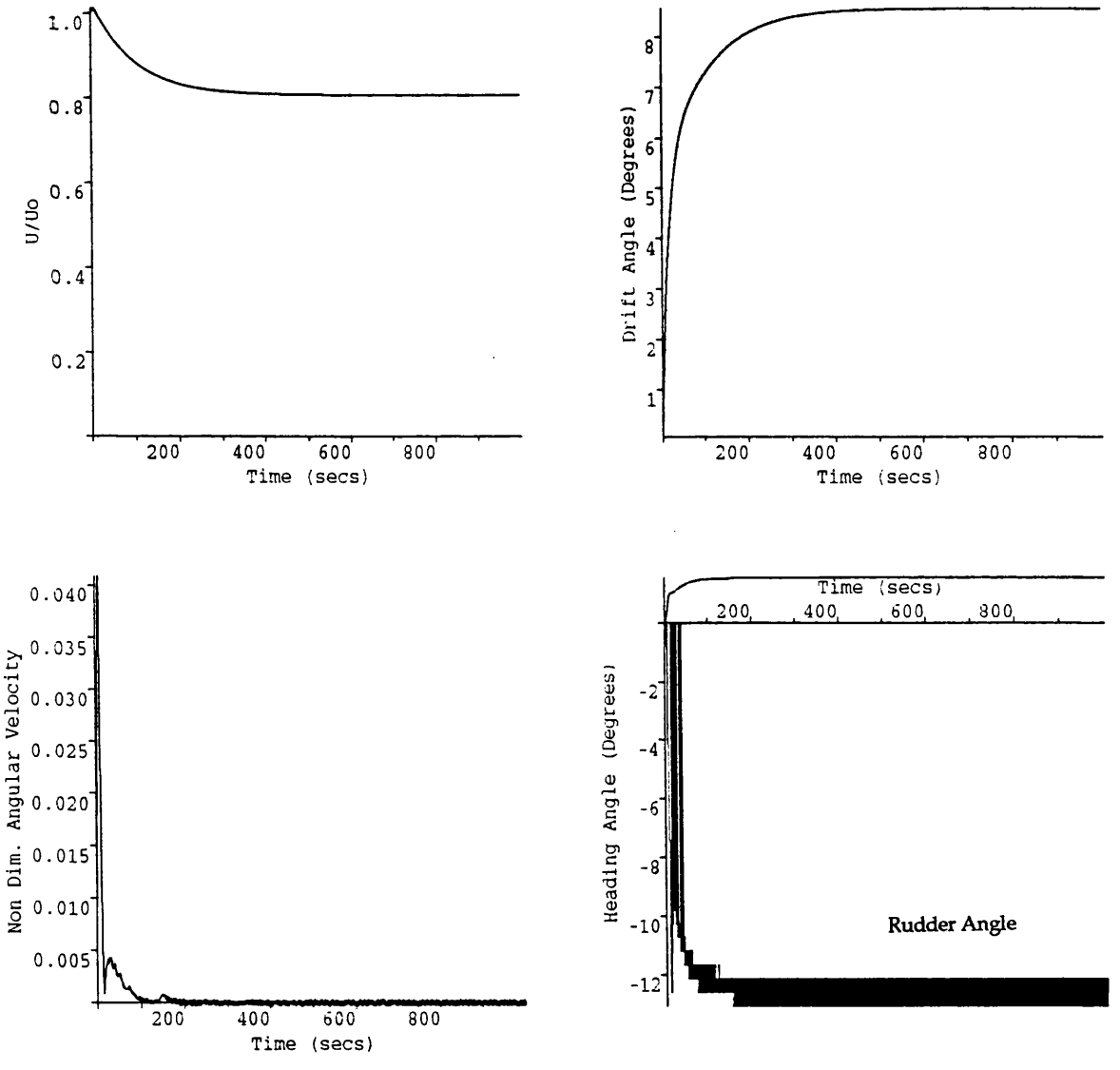

Figure 5.19b

Vessel Velocity : 15.0 Knots
Orientation of Jack Up on HLV : Aft
JU CoG with System CoG (X,Y) :-16.96, 0.04m,m
Bow & Stern Leg Longitudinal: 26.7 12.8m,m
Bow & Stern Leg Transverse: 0.0 22.7m,m
Rudder Constants 1,2 : 8.0,5.0
Maximum Deflection : -13.066 Degrees
Wind Velocity,Angle : 58.4, 90.0 Knots,Deg
Leg Length Exposed : 89.15 m

Mighty Servant I

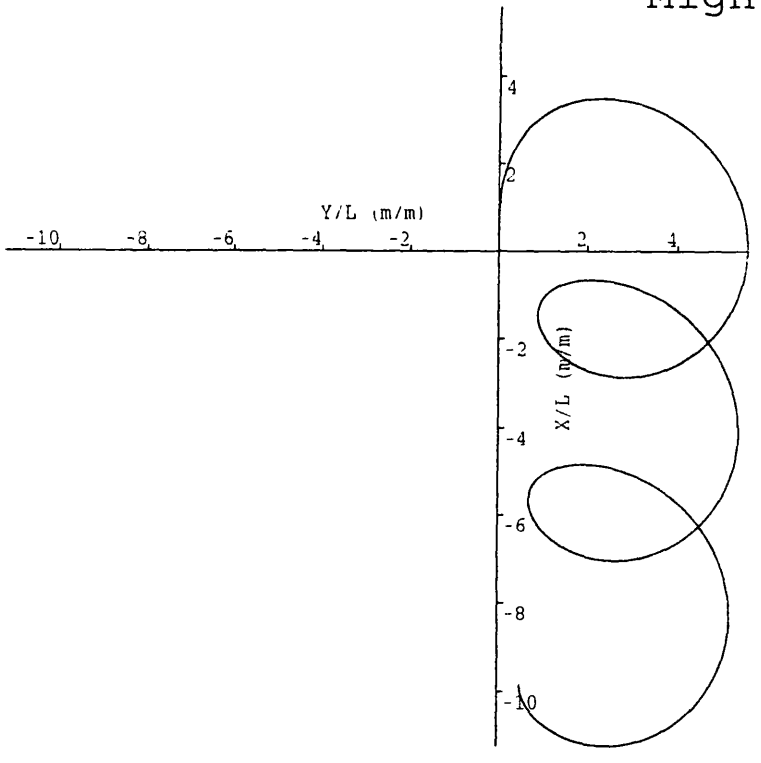

Figure 5.20a

Vessel Velocity : 15.0 Knots
Orientation of Jack Up on HLV : Aft
JU CoG with System CoG (X,Y) :-11.96, 0.04m,m
Bow & Stern Leg Longitudinal: 26.7 12.8m,m
Bow & Stern Leg Transverse: 0.0 22.7m,m
Rudder Angle : 20.0 Degrees
Advance : 505.4 m
Transfer : 315.4 m
Tactical Diameter : 800.8 m
Wind Velocity,Angle : 38.9, 0.0 Knots,Deg
Leg Length Exposed : 89.15 m

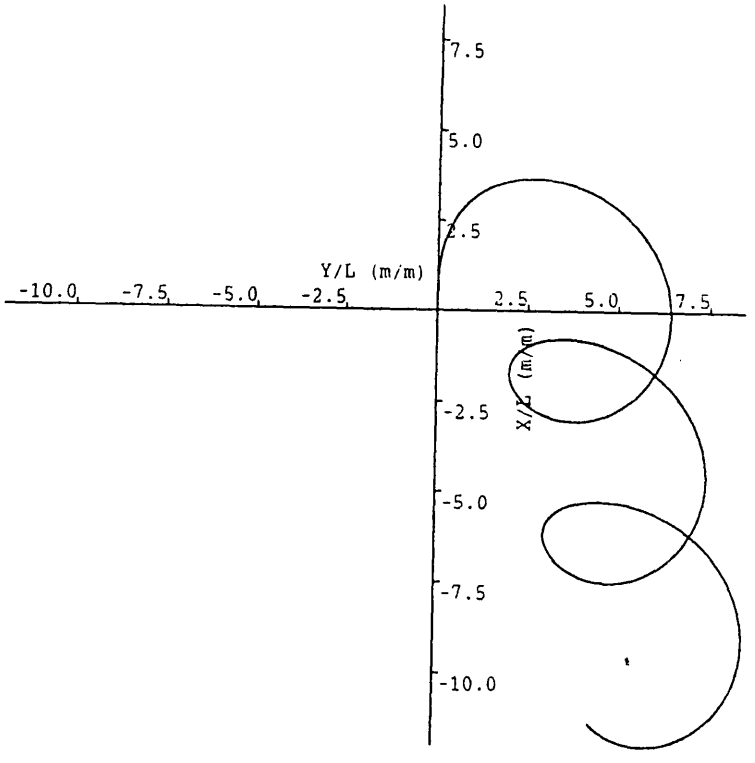

Figure 5.20b

Vessel Velocity : 15.0 Knots
Orientation of Jack Up on HLV : Aft
JU CoG with System CoG (X,Y) :-21.96, 0.04m,m
Bow & Stern Leg Longitudinal: 26.7 12.8m,m
Bow & Stern Leg Transverse: 0.0 22.7m,m
Rudder Angle : 20.0 Degrees
Advance : 529.8 m
Transfer : 365.1 m
Tactical Diameter : 928.6 m
Wind Velocity,Angle : 38.9, 0.0 Knots,Deg
Leg Length Exposed : 89.15 m

Mighty Servant I

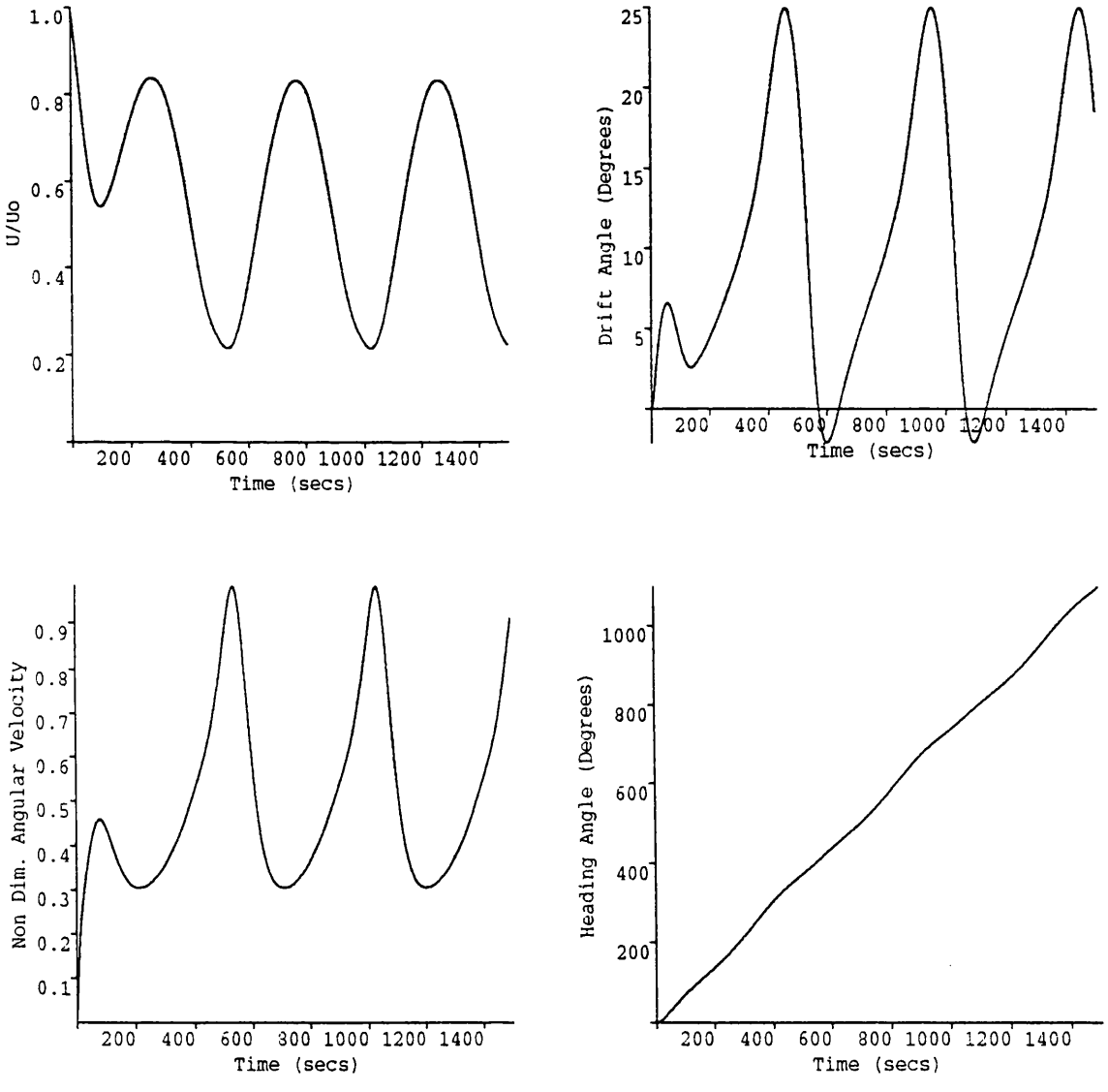

Figure 5.20c

Vessel Velocity : 15.0 Knots
Orientation of Jack Up on HLV : Aft
JU CoG with System CoG (X,Y) :-11.96, 0.04m,m
Bow & Stern Leg Longitudinal: 26.7 12.8m,m
Bow & Stern Leg Transverse: 0.0 22.7m,m
Rudder Angle : 20.0 Degrees
Advance : 505.4 m
Transfer : 315.4 m
Tactical Diameter : 800.8 m
Wind Velocity,Angle : 38.9, 0.0 Knots,Deg
Leg Length Exposed : 89.15 m

Mighty Servant I

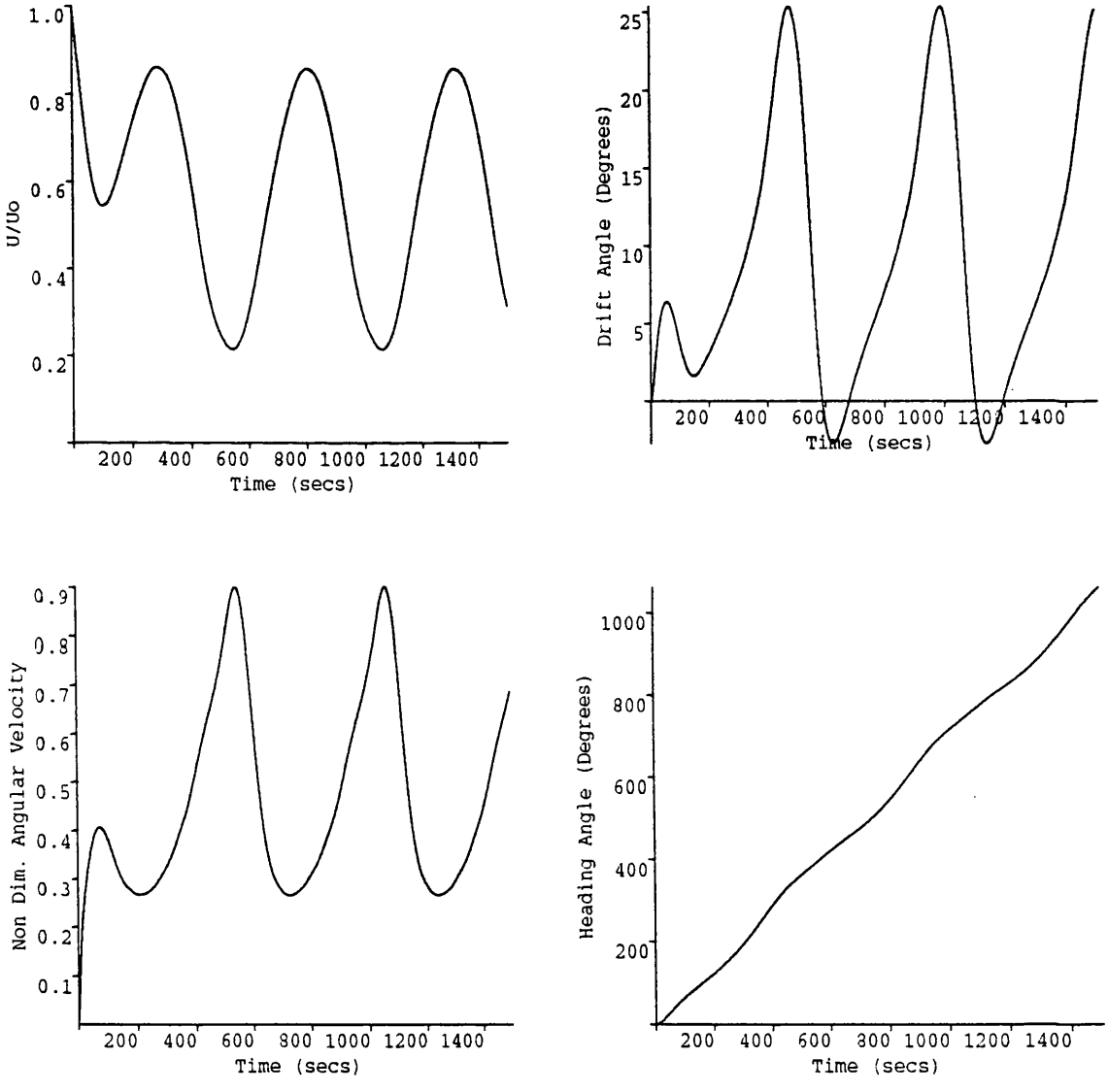

Figure 5.20d

Vessel Velocity : 15.0 Knots
Orientation of Jack Up on HLV : Aft
JU CoG with System CoG (X,Y) :-21.96, 0.04m,m
Bow & Stern Leg Longitudinal: 26.7 12.8m,m
Bow & Stern Leg Transverse: 0.0 22.7m,m
Rudder Angle : 20.0 Degrees
Advance : 529.8 m
Transfer : 365.1 m
Tactical Diameter : 928.6 m
Wind Velocity,Angle : 38.9, 0.0 Knots,Deg
Leg Length Exposed : 89.15 m

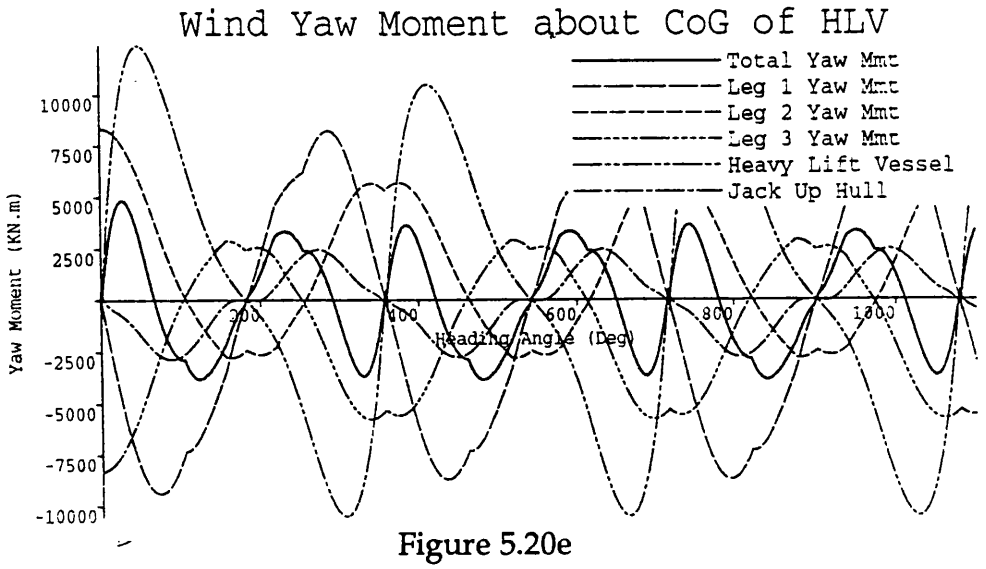

Figure 5.20e

JU CoG with System CoG (X,Y) :-11.96, 0.04m,m
Bow & Stern Leg Longitudinal: 26.7 12.8m,m
Bow & Stern Leg Transverse: 0.0 22.7m,m
Leg Length Exposed : 89.15 m

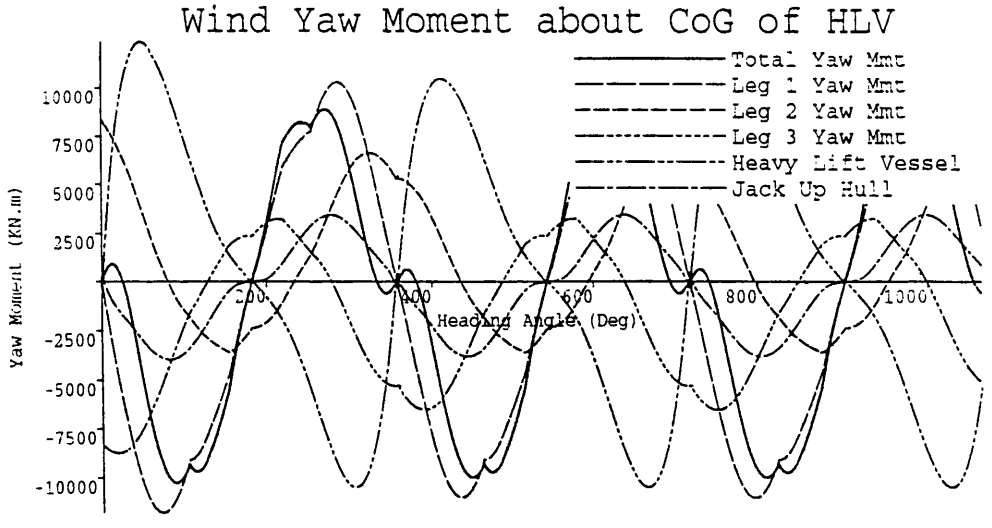

Figure 5.20f

Base Height of Exposed Leg : 19.58m
Marine Growth Height&Thickness: 0.00, 0.00mm,mm
Leg Drag Coefficient :0.663
Wind Velocity,Angle :38.9, 0.0Knots,Deg
Leg Geometry : Square
Leg Type : 116 Marathon
Orientation of Jack Up on HLV : Aft
JU CoG with System CoG (X,Y) :-21.96, 0.04m,m
Bow & Stern Leg Longitudinal: 26.7 12.8m,m
Bow & Stern Leg Transverse: 0.0 22.7m,m
Leg Length Exposed : 89.15 m

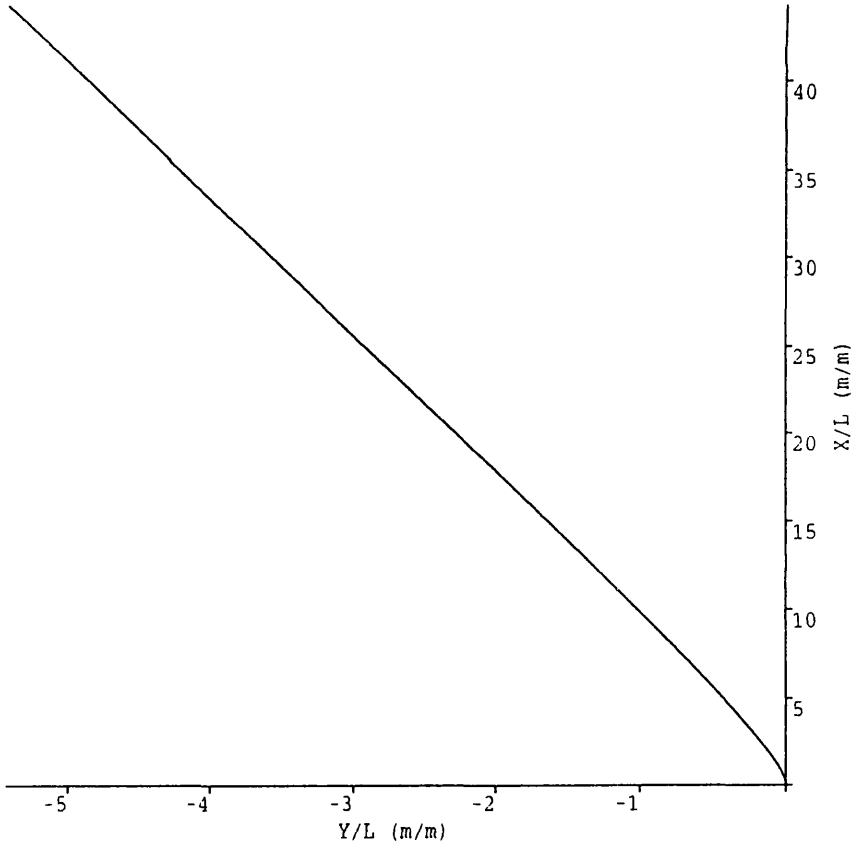

Figure 5.21a

Vessel Velocity : 15.0 Knots
Orientation of Jack Up on HLV : Aft
JU CoG with System CoG (X,Y) :-11.96, 0.04m,m
Bow & Stern Leg Longitudinal: 26.7 12.8m,m
Bow & Stern Leg Transverse: 0.0 22.7m,m
Rudder Constants 1,2 : 8.0,5.0
Maximum Deflection : -10.733 Degrees
Wind Velocity,Angle : 58.4, 90.0 Knots,Deg
Leg Length Exposed : 89.15 m

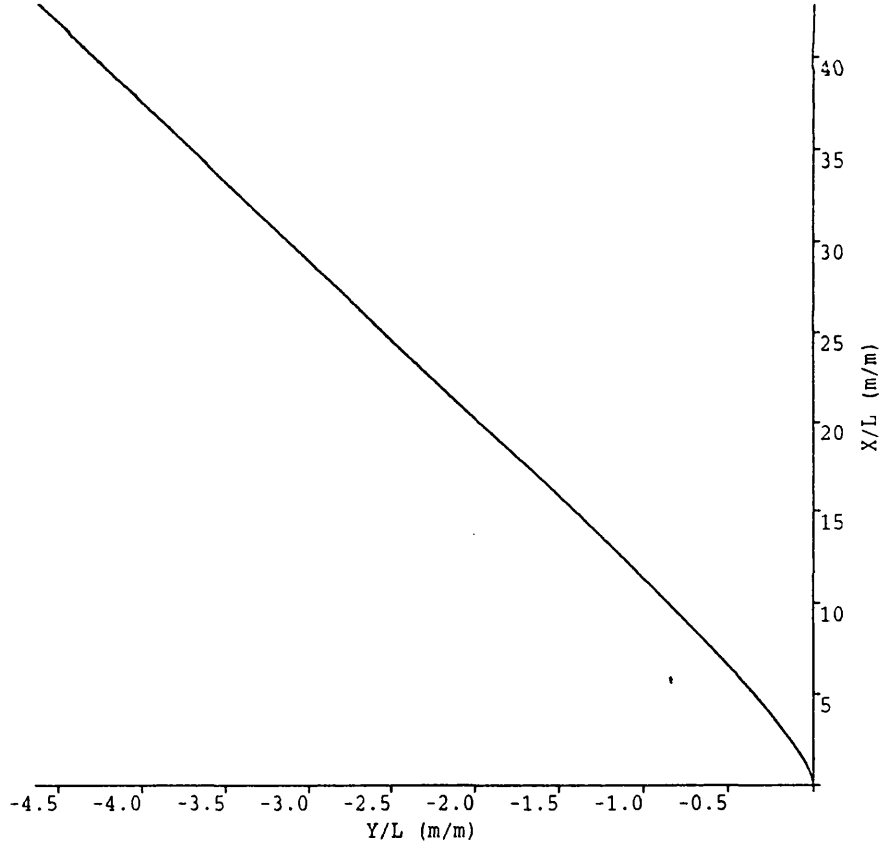

Figure 5.21b

Vessel Velocity : 15.0 Knots
Orientation of Jack Up on HLV : Aft
JU CoG with System CoG (X,Y) :-21.96, 0.04m,m
Bow & Stern Leg Longitudinal: 26.7 12.8m,m
Bow & Stern Leg Transverse: 0.0 22.7m,m
Rudder Constants 1,2 : 8.0,5.0
Maximum Deflection : -16.333 Degrees
Wind Velocity,Angle : 58.4, 90.0 Knots,Deg
Leg Length Exposed : 89.15 m

Mighty Servant I

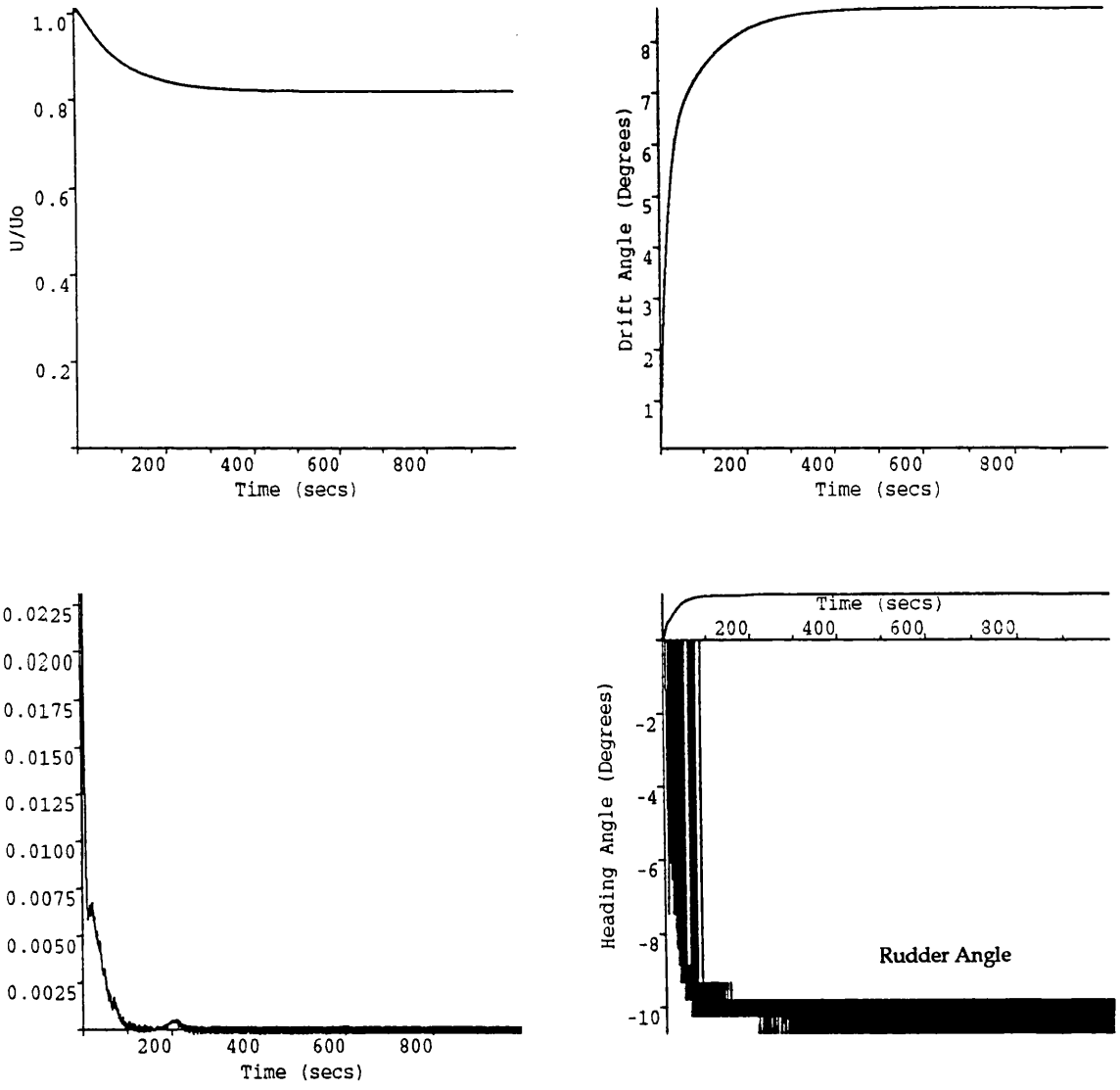

Figure 5.21c

Vessel Velocity : 15.0 Knots
Orientation of Jack Up on HLV : Aft
JU CoG with System CoG (X,Y) :-11.96, 0.04m,m
Bow & Stern Leg Longitudinal: 26.7 12.8m,m
Bow & Stern Leg Transverse: 0.0 22.7m,m
Rudder Constants 1,2 : 8.0,5.0
Maximum Deflection : -10.733 Degrees
Wind Velocity,Angle : 58.4, 90.0 Knots,Deg
Leg Length Exposed : 89.15 m

Mighty Servant I

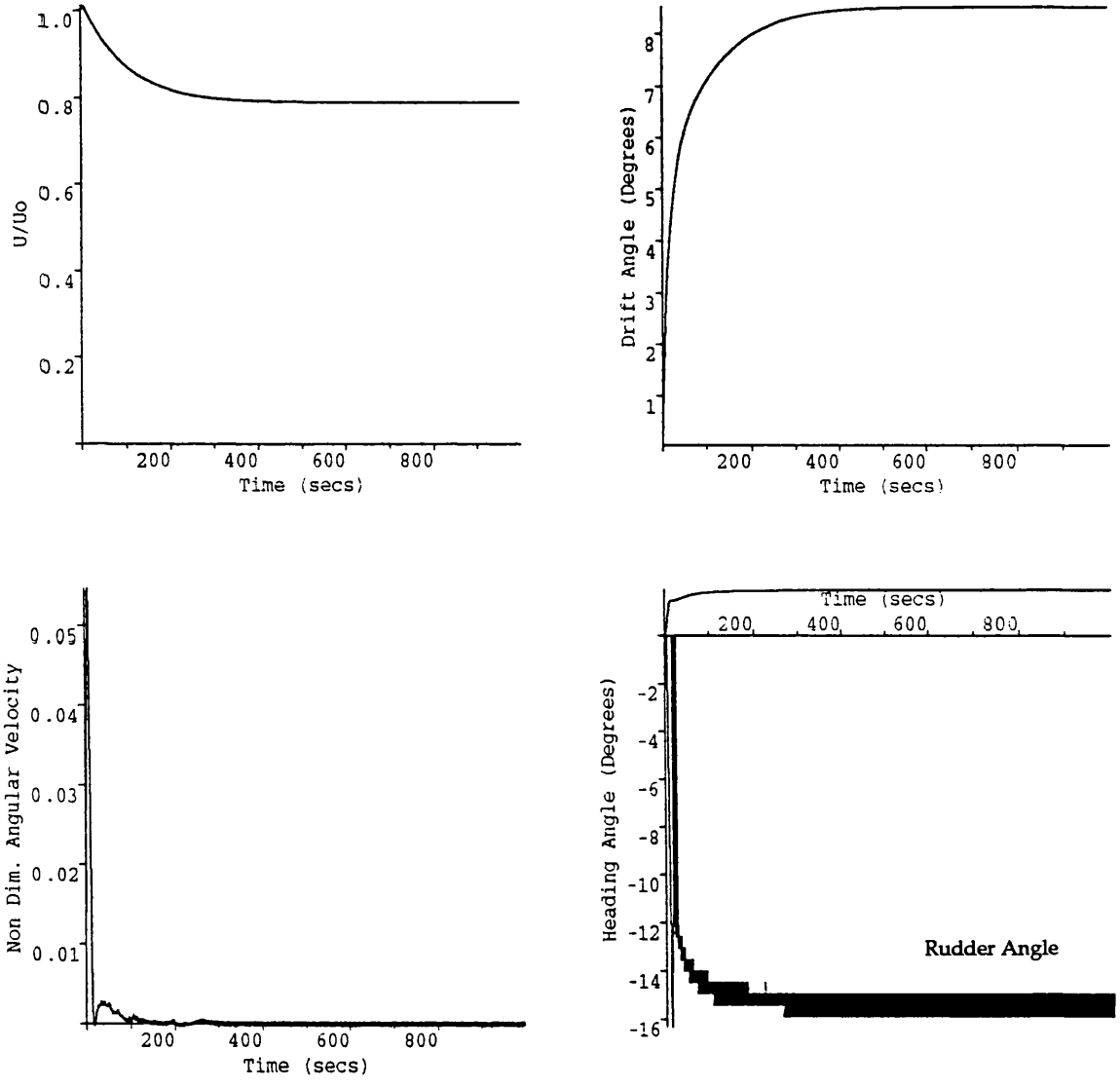

Figure 5.21d

Vessel Velocity : 15.0 Knots
Orientation of Jack Up on HLV : Aft
JU CoG with System CoG (X,Y) :-21.96, 0.04m,m
Bow & Stern Leg Longitudinal: 26.7 12.8m,m
Bow & Stern Leg Transverse: 0.0 22.7m,m
Rudder Constants 1,2 : 8.0,5.0
Maximum Deflection : -16.333 Degrees
Wind Velocity,Angle : 58.4, 90.0 Knots,Deg
Leg Length Exposed : 89.15 m

Mighty Servant I

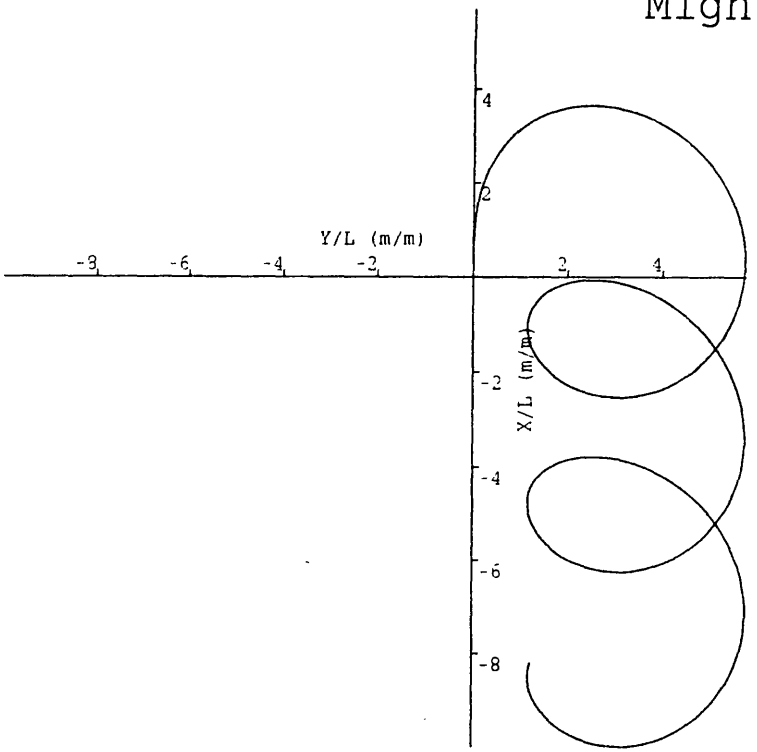

Figure 5.22a

Vessel Velocity : 15.0 Knots
Orientation of Jack Up on HLV : Aft
JU CoG with System CoG (X,Y) :-16.96, 0.04m,m
Bow & Stern Leg Longitudinal: 26.7 12.8m,m
Bow & Stern Leg Transverse: 0.0 22.7m,m
Rudder Angle : 20.0 Degrees
Advance : 528.5 m
Transfer : 334.4 m
Tactical Diameter : 824.4 m
Wind Velocity,Angle : 38.9, 0.0 Knots,Deg
Leg Length Exposed : 74.15 m

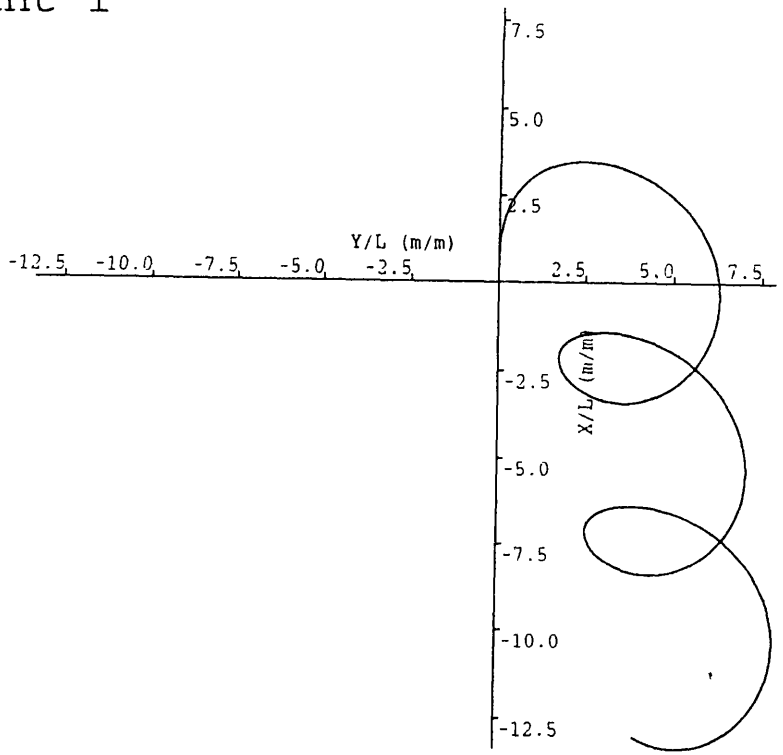

Figure 5.22b

Vessel Velocity : 15.0 Knots
Orientation of Jack Up on HLV : Aft
JU CoG with System CoG (X,Y) :-16.96, 0.04m,m
Bow & Stern Leg Longitudinal: 26.7 12.8m,m
Bow & Stern Leg Transverse: 0.0 22.7m,m
Rudder Angle : 20.0 Degrees
Advance : 503.8 m
Transfer : 344.4 m
Tactical Diameter : 906.8 m
Wind Velocity,Angle : 38.9, 0.0 Knots,Deg
Leg Length Exposed :104.15 m

Mighty Servant I

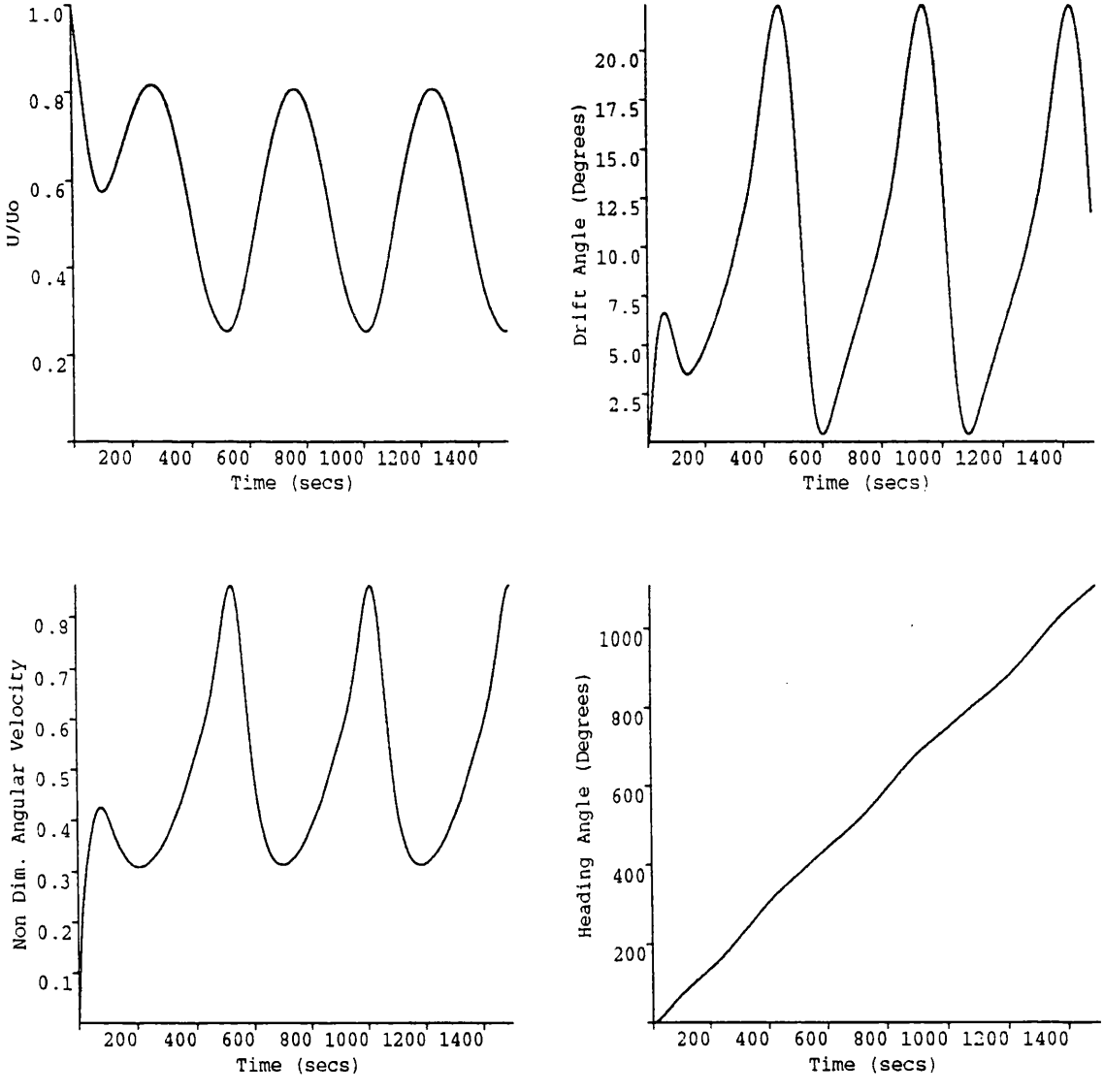

Figure 5.22c

Vessel Velocity : 15.0 Knots
Orientation of Jack Up on HLV : Aft
JU CoG with System CoG (X,Y) :-16.96, 0.04m,m
Bow & Stern Leg Longitudinal: 26.7 12.8m,m
Bow & Stern Leg Transverse: 0.0 22.7m,m
Rudder Angle : 20.0 Degrees
Advance : 528.5 m
Transfer : 334.4 m
Tactical Diameter : 824.4 m
Wind Velocity,Angle : 38.9, 0.0 Knots,Deg
Leg Length Exposed : 74.15 m

Mighty Servant I

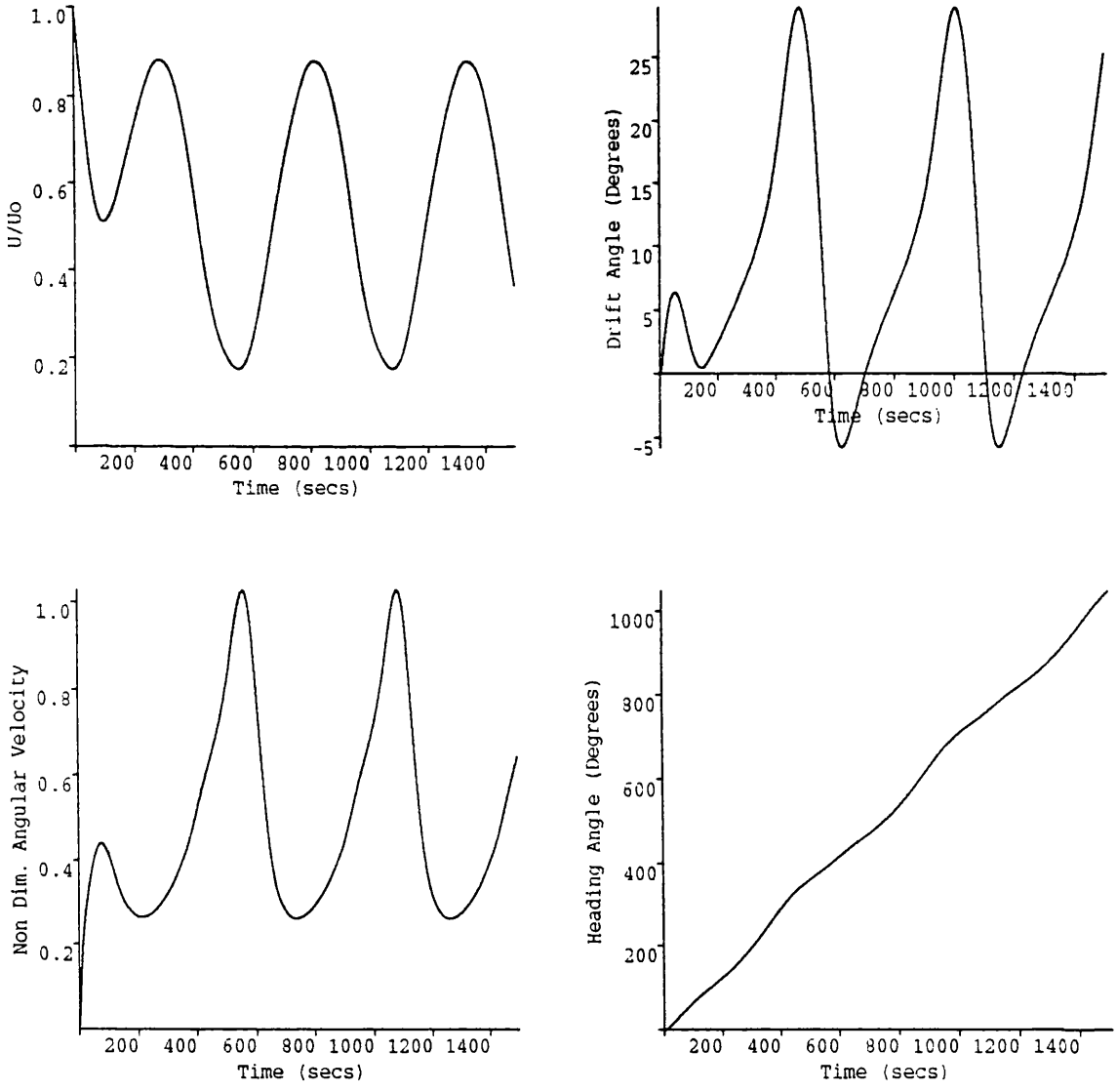

Figure 5.22d

Vessel Velocity : 15.0 Knots
Orientation of Jack Up on HLV : Aft
JU CoG with System CoG (X,Y) :-16.96, 0.04m,m
Bow & Stern Leg Longitudinal: 26.7 12.8m,m
Bow & Stern Leg Transverse: 0.0 22.7m,m
Rudder Angle : 20.0 Degrees
Advance : 503.8 m
Transfer : 344.4 m
Tactical Diameter : 906.8 m
Wind Velocity,Angle : 38.9, 0.0 Knots,Deg
Leg Length Exposed :104.15 m

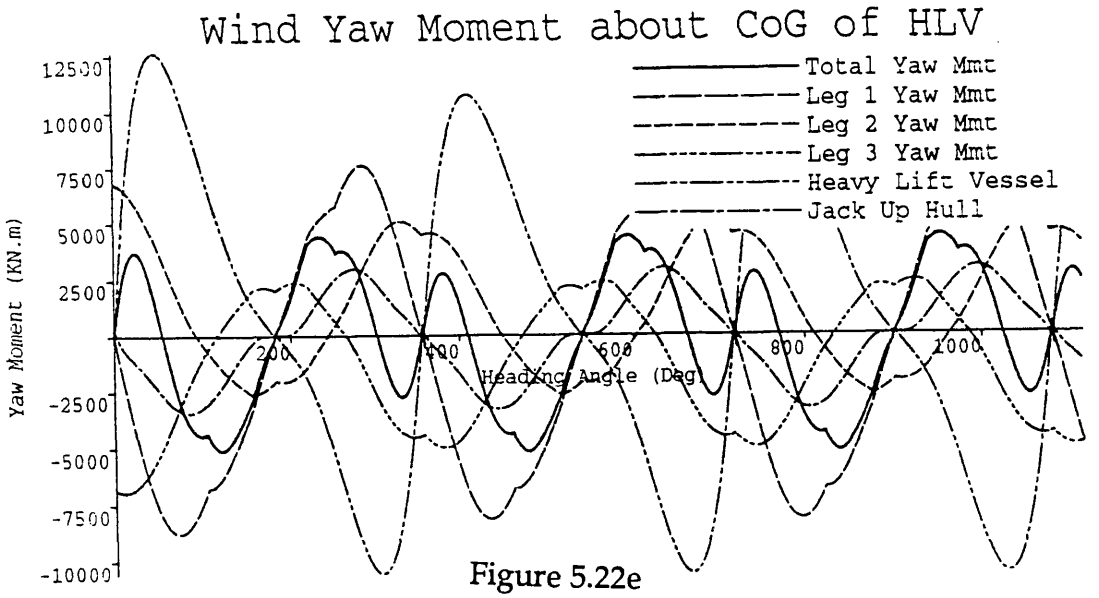

Figure 5.22e

JU CoG with System CoG (X,Y) :-16.96, 0.04m,m
Bow & Stern Leg Longitudinal: 26.7 12.8m,m
Bow & Stern Leg Transverse: 0.0 22.7m,m
Leg Length Exposed : 74.15 m

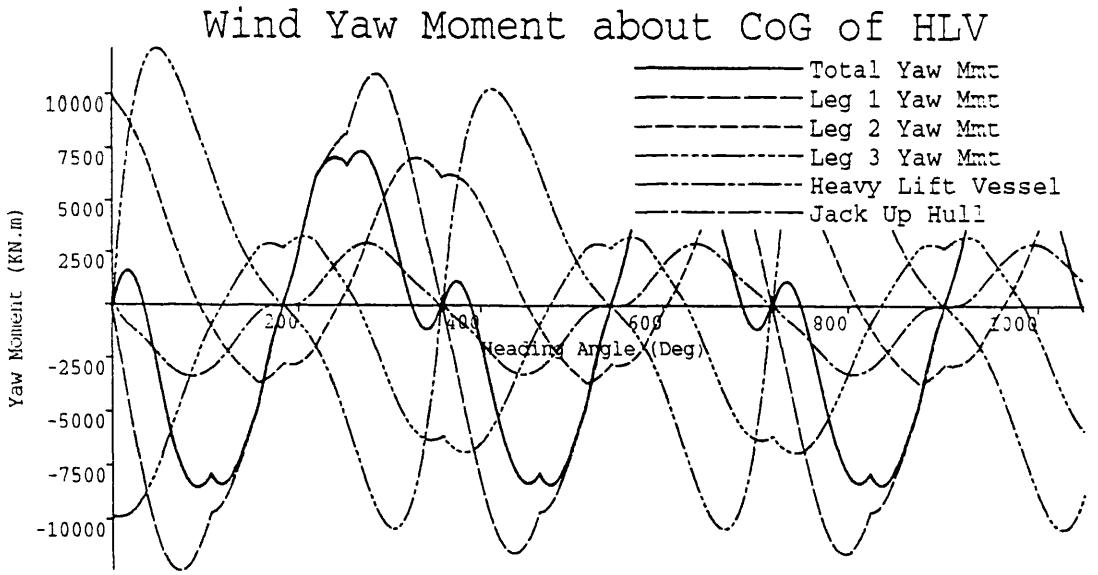

Figure 5.22f

Base Height of Exposed Leg : 19.58m
Marine Growth Height&Thickness: 0.00, 0.00mm,mm
Leg Drag Coefficient :0.663
Wind Velocity,Angle :38.9, 0.0Knots,Deg
Leg Geometry : Square
Leg Type : 116 Marathon
Orientation of Jack Up on HLV : Aft
JU CoG with System CoG (X,Y) :-16.96, 0.04m,m
Bow & Stern Leg Longitudinal: 26.7 12.8m,m
Bow & Stern Leg Transverse: 0.0 22.7m,m
Leg Length Exposed :104.15 m

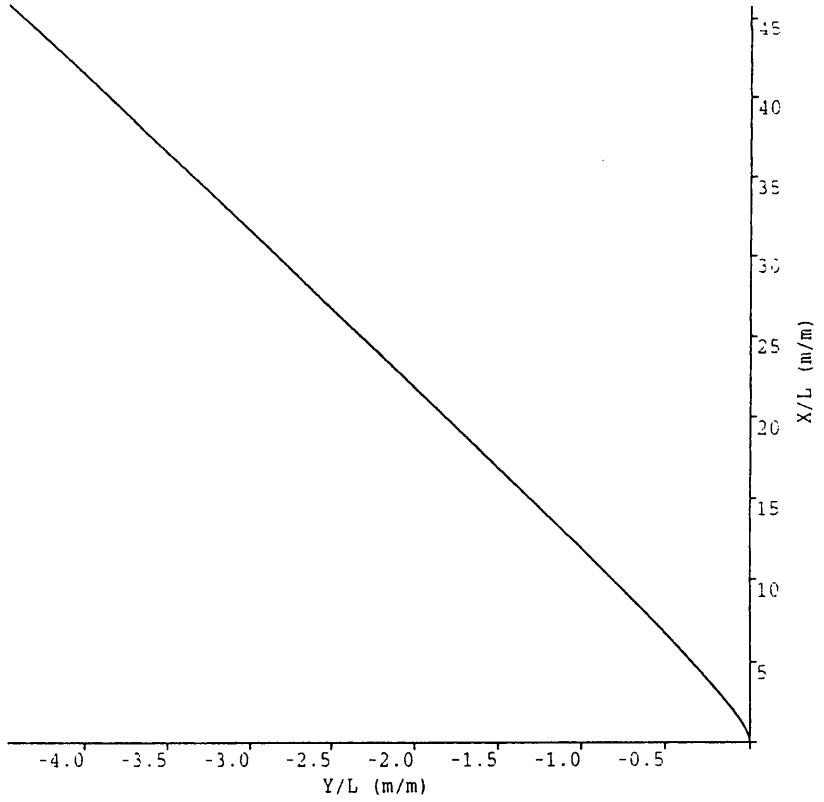

Figure 5.23a

Vessel Velocity : 15.0 Knots
Orientation of Jack Up on HLV : Aft
JU CoG with System CoG (X,Y) :-16.96, 0.04m,m
Bow & Stern Leg Longitudinal: 26.7 12.8m,m
Bow & Stern Leg Transverse: 0.0 22.7m,m
Rudder Constants 1,2 : 8.0,5.0
Maximum Deflection : -10.733 Degrees
Wind Velocity,Angle : 58.4, 90.0 Knots,Deg
Leg Length Exposed : 74.15 m

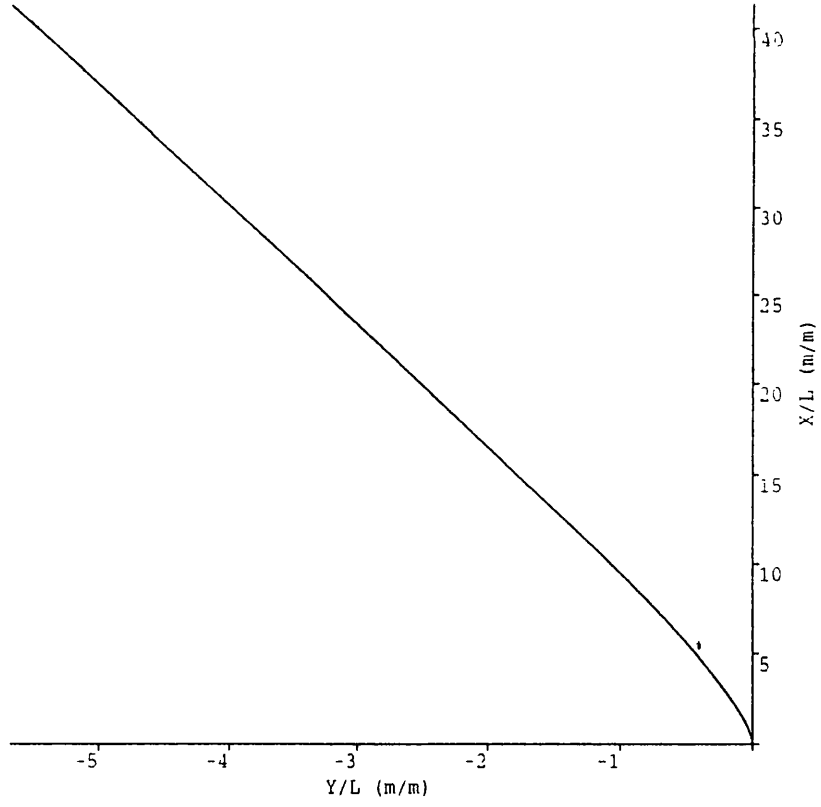

Figure 5.23b

Vessel Velocity : 15.0 Knots
Orientation of Jack Up on HLV : Aft
JU CoG with System CoG (X,Y) :-16.96, 0.04m,m
Bow & Stern Leg Longitudinal: 26.7 12.8m,m
Bow & Stern Leg Transverse: 0.0 22.7m,m
Rudder Constants 1,2 : 8.0,5.0
Maximum Deflection : -15.866 Degrees
Wind Velocity,Angle : 58.4, 90.0 Knots,Deg
Leg Length Exposed :104.15 m

Mighty Servant I

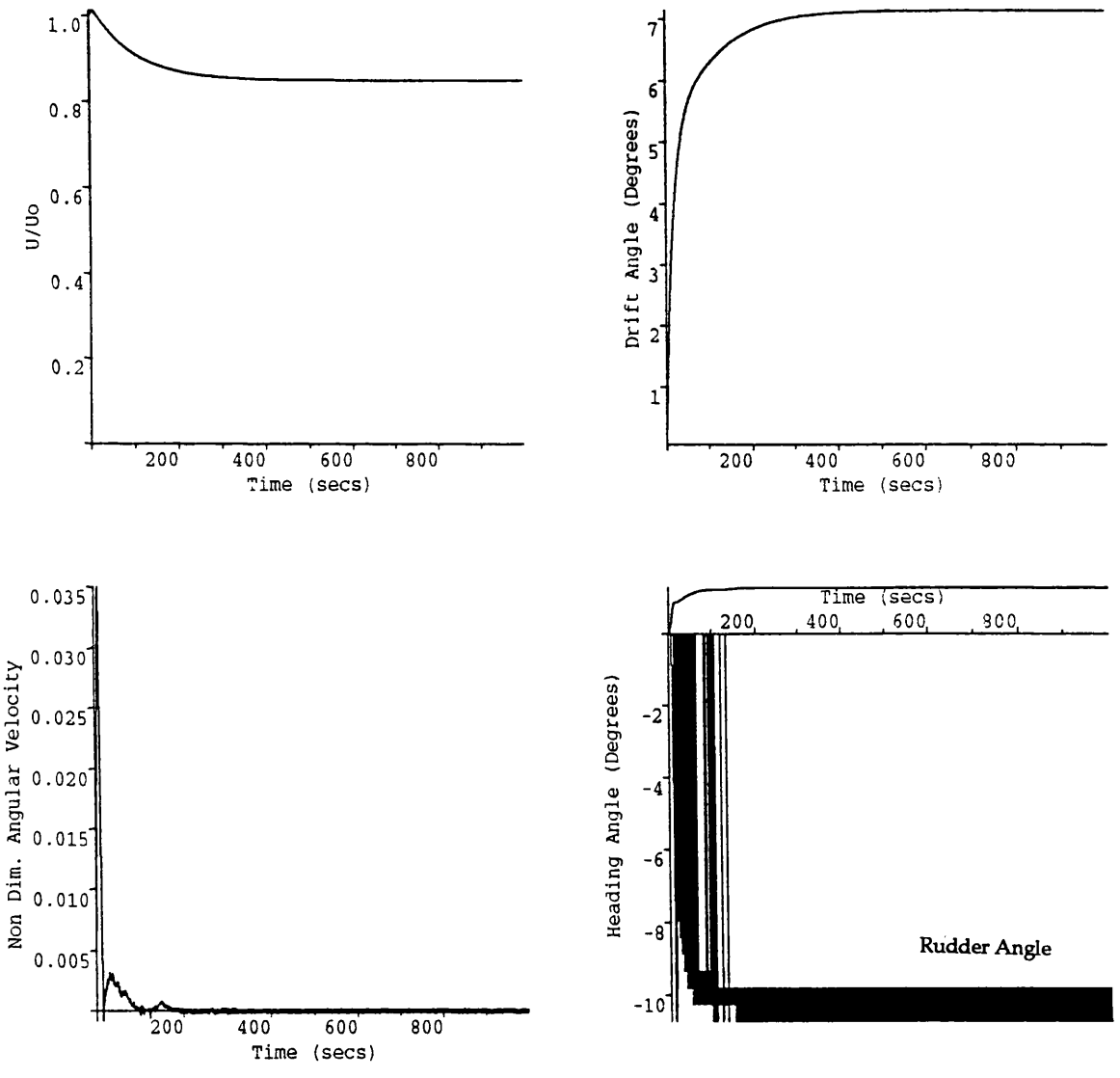

Figure 5.23c

Vessel Velocity : 15.0 Knots
Orientation of Jack Up on HLV : Aft
JU CoG with System CoG (X,Y) :-16.96, 0.04m,m
Bow & Stern Leg Longitudinal: 26.7 12.8m,m
Bow & Stern Leg Transverse: 0.0 22.7m,m
Rudder Constants 1,2 : 8.0,5.0
Maximum Deflection : -10.733 Degrees
Wind Velocity,Angle : 58.4, 90.0 Knots,Deg
Leg Length Exposed : 74.15 m

Mighty Servant I

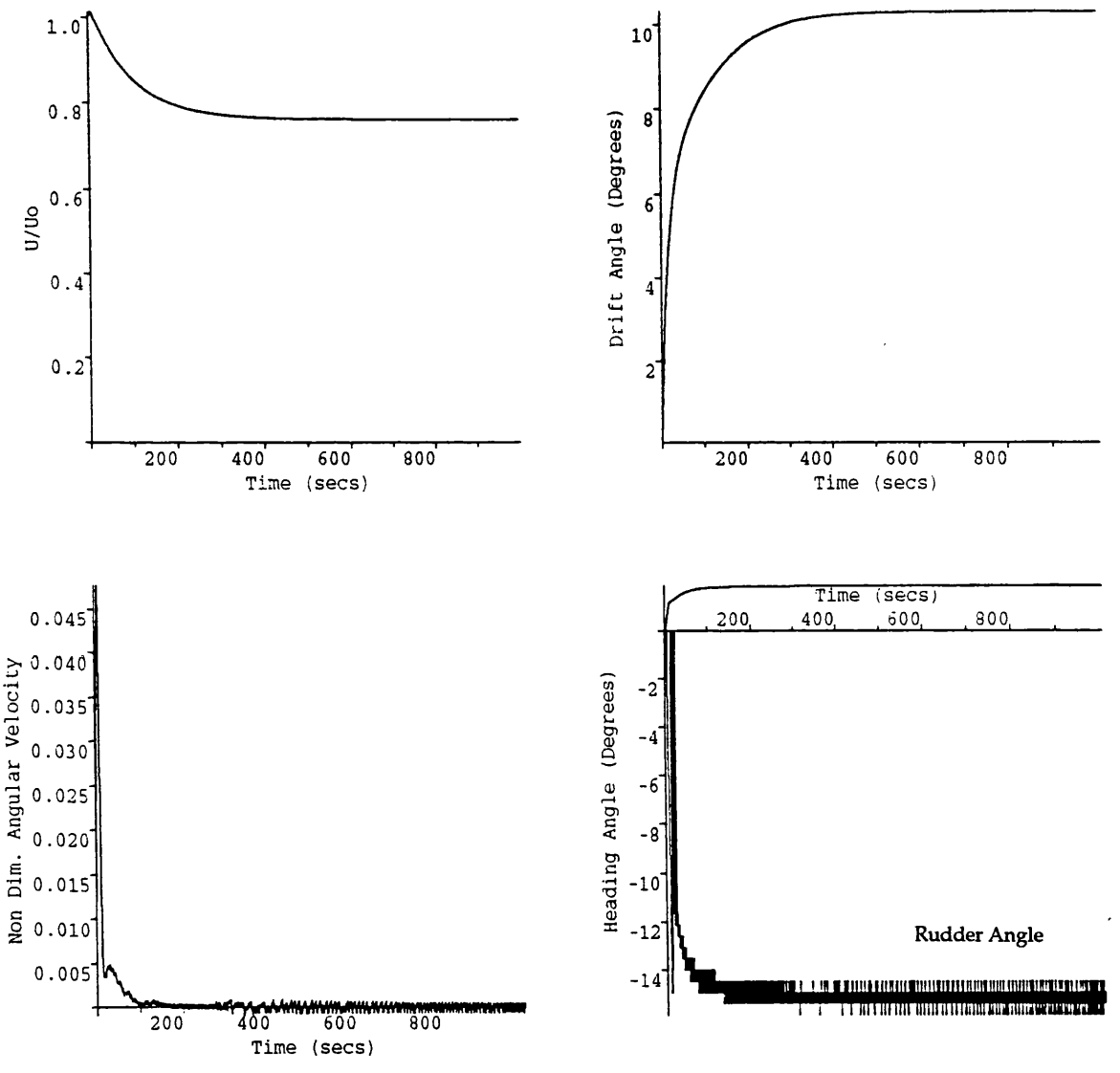

Figure 5.23d

Vessel Velocity : 15.0 Knots
Orientation of Jack Up on HLV : Aft
JU CoG with System CoG (X,Y) :-16.96, 0.04m,m
Bow & Stern Leg Longitudinal: 26.7 12.8m,m
Bow & Stern Leg Transverse: 0.0 22.7m,m
Rudder Constants 1,2 : 8.0,5.0
Maximum Deflection : -15.866 Degrees
Wind Velocity,Angle : 58.4, 90.0 Knots,Deg
Leg Length Exposed :104.15 m

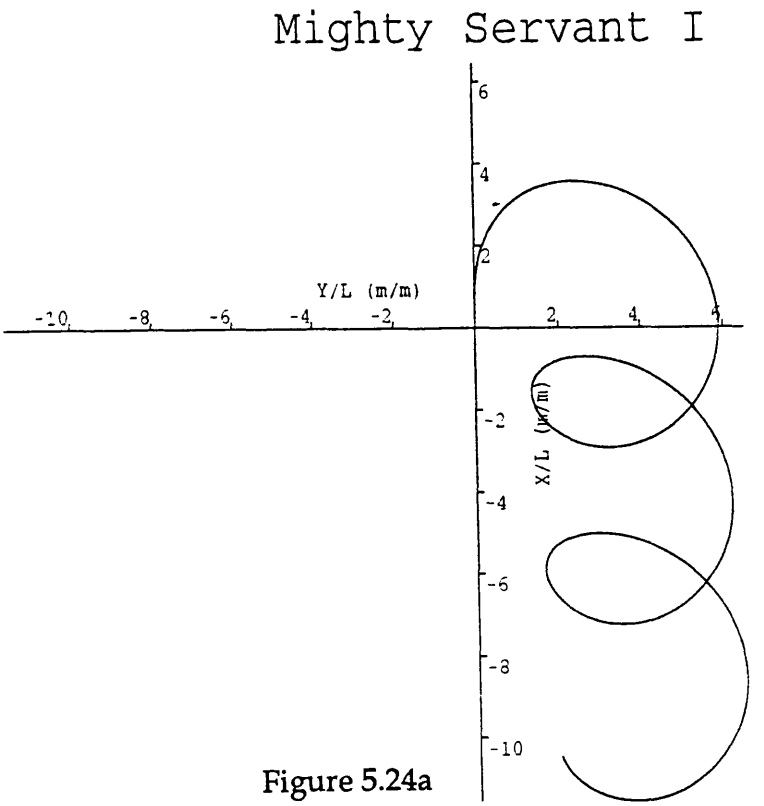

Figure 5.24a

Vessel Velocity : 15.0 Knots
Orientation of Jack Up on HLV : Forward
JU CoG with System CoG (X,Y) :-16.96, 0.04m,m
Bow & Stern Leg Longitudinal: 26.7 12.8m,m
Bow & Stern Leg Transverse: 0.0 22.7m,m
Rudder Angle : 20.0 Degrees
Advance : 515.5 m
Transfer : 334.9 m
Tactical Diameter : 851.1 m
Wind Velocity,Angle : 38.9, 0.0 Knots,Deg
Leg Length Exposed : 89.15 m

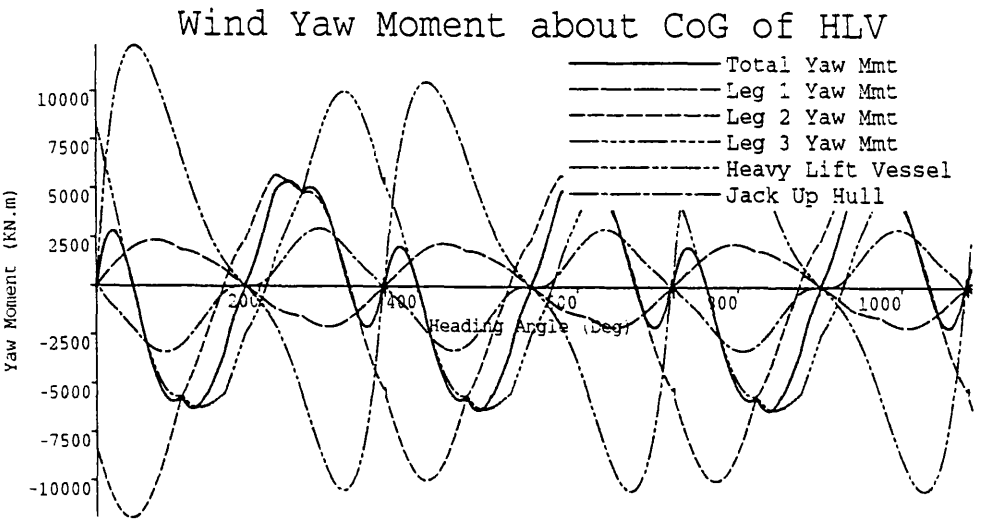

Figure 5.24b

Base Height of Exposed Leg : 19.58m
Marine Growth Height&Thickness: 0.00, 0.00mm,mm
Leg Drag Coefficient :0.663
Wind Velocity,Angle :38.9, 0.0Knots,Deg
Leg Geometry : Square
Leg Type : 116 Marathon
Orientation of Jack Up on HLV : Forward

Mighty Servant I

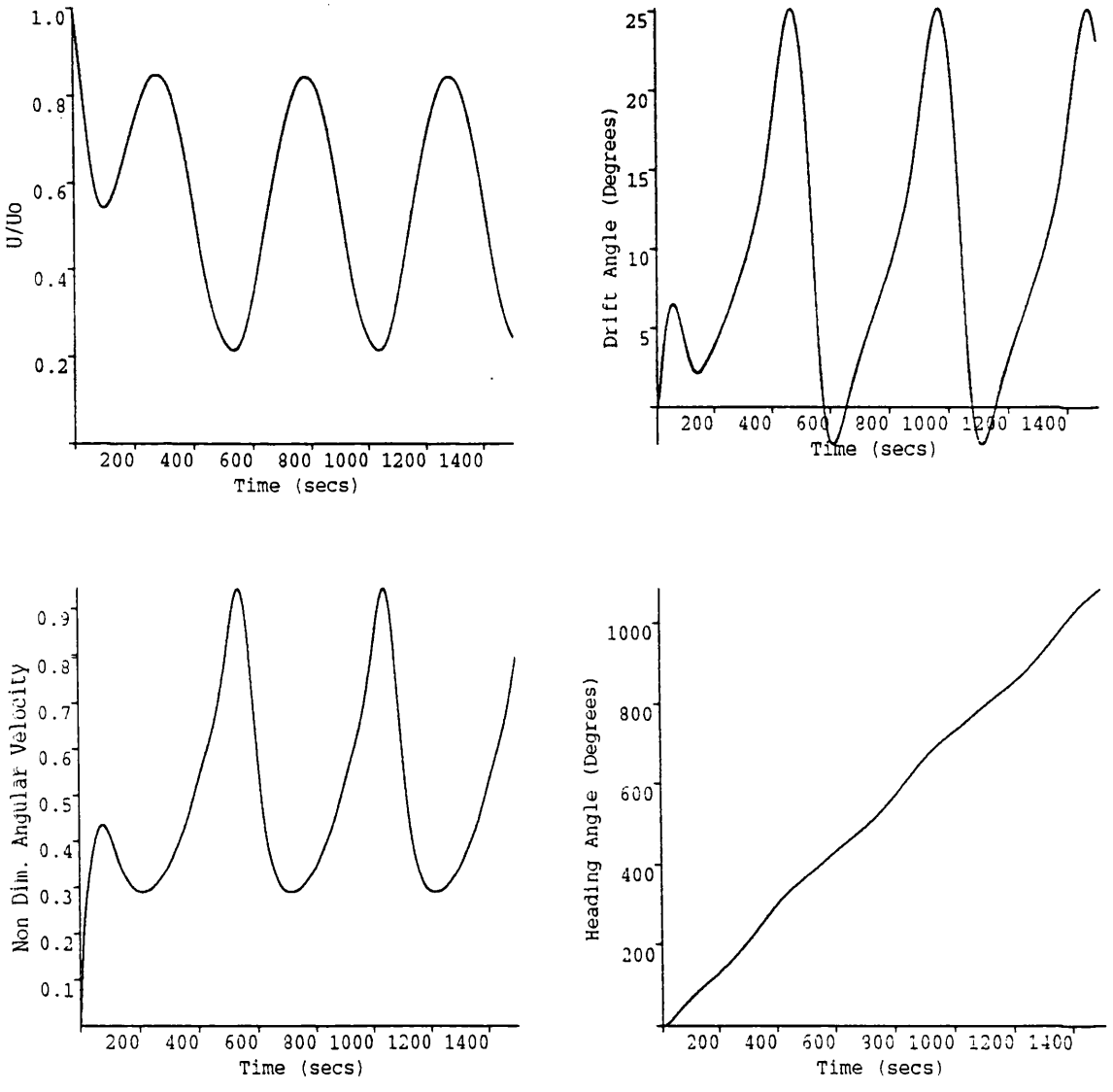

Figure 5.24c

Vessel Velocity : 15.0 Knots
Orientation of Jack Up on HLV : Forward
JU CoG with System CoG (X,Y) :-16.96, 0.04m,m
Bow & Stern Leg Longitudinal: 26.7 12.8m,m
Bow & Stern Leg Transverse: 0.0 22.7m,m
Rudder Angle : 20.0 Degrees
Advance : 515.5 m
Transfer : 334.9 m
Tactical Diameter : 851.1 m
Wind Velocity,Angle : 38.9, 0.0 Knots,Deg
Leg Length Exposed : 89.15 m

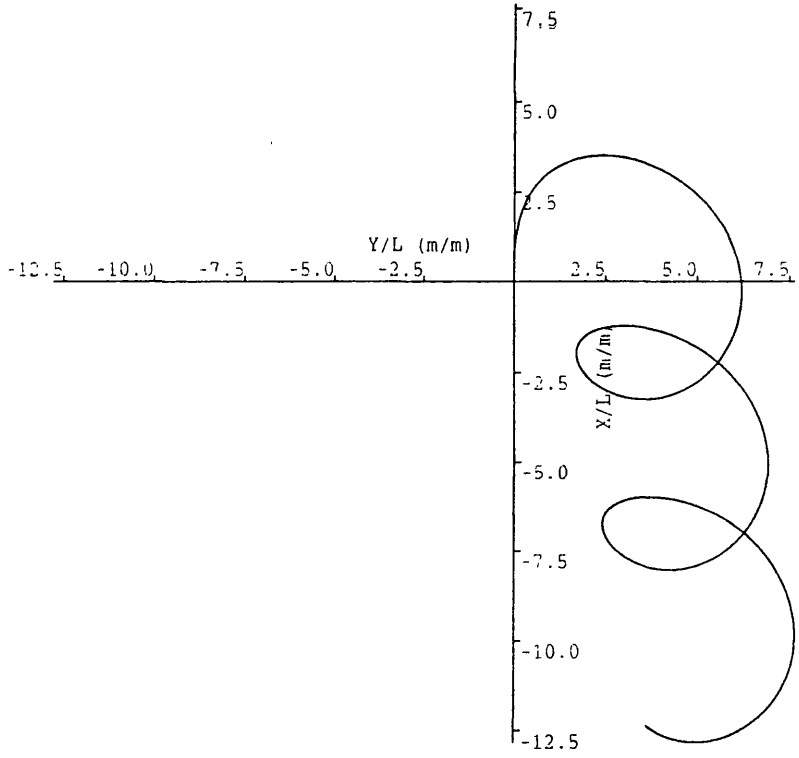

Figure 7.25a

Vessel Velocity : 15.0 Knots
Orientation of Jack Up on HLV : Aft
JU CoG with System CoG (X,Y) :-16.96, 0.04m,m
Bow & Stern Leg Longitudinal: 26.7 12.8m,m
Bow & Stern Leg Transverse: 0.0 22.7m,m
Rudder Angle : 20.0 Degrees
Advance : 506.6 m
Transfer : 343.3 m
Tactical Diameter : 895.2 m
Wind Velocity,Angle : 38.9, 0.0 Knots,Deg
Leg Length Exposed : 89.15 m

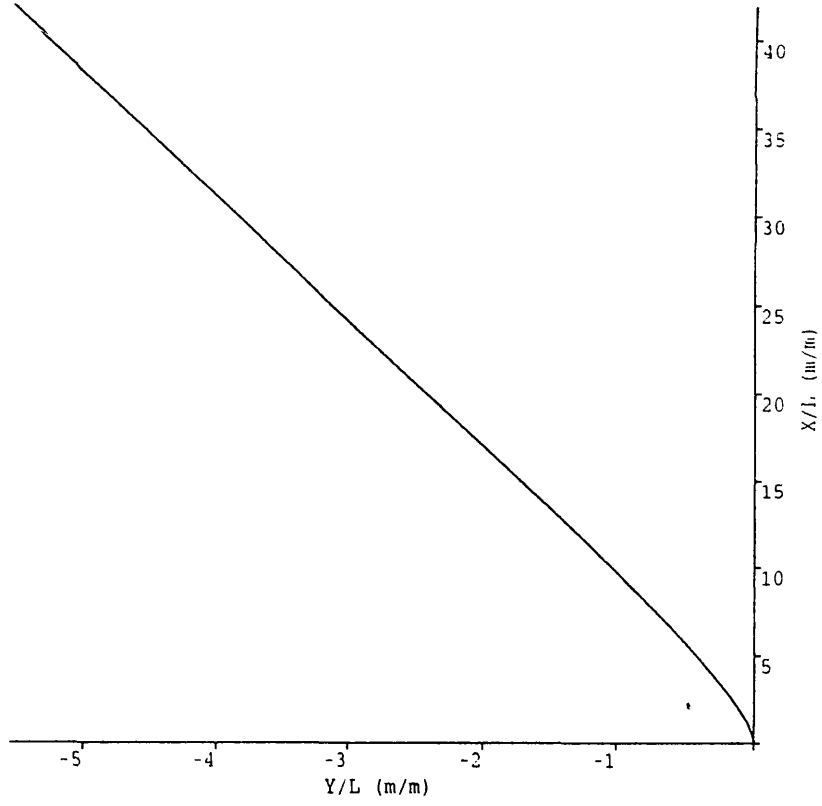

Figure 5.25b

Vessel Velocity : 15.0 Knots
Orientation of Jack Up on HLV : Aft
JU CoG with System CoG (X,Y) :-16.96, 0.04m,m
Bow & Stern Leg Longitudinal: 26.7 12.8m,m
Bow & Stern Leg Transverse: 0.0 22.7m,m
Rudder Constants 1,2 : 8.0,5.0
Maximum Deflection : -15.400 Degrees
Wind Velocity,Angle : 58.4, 90.0 Knots,Deg
Leg Length Exposed : 89.15 m

Mighty Servant I

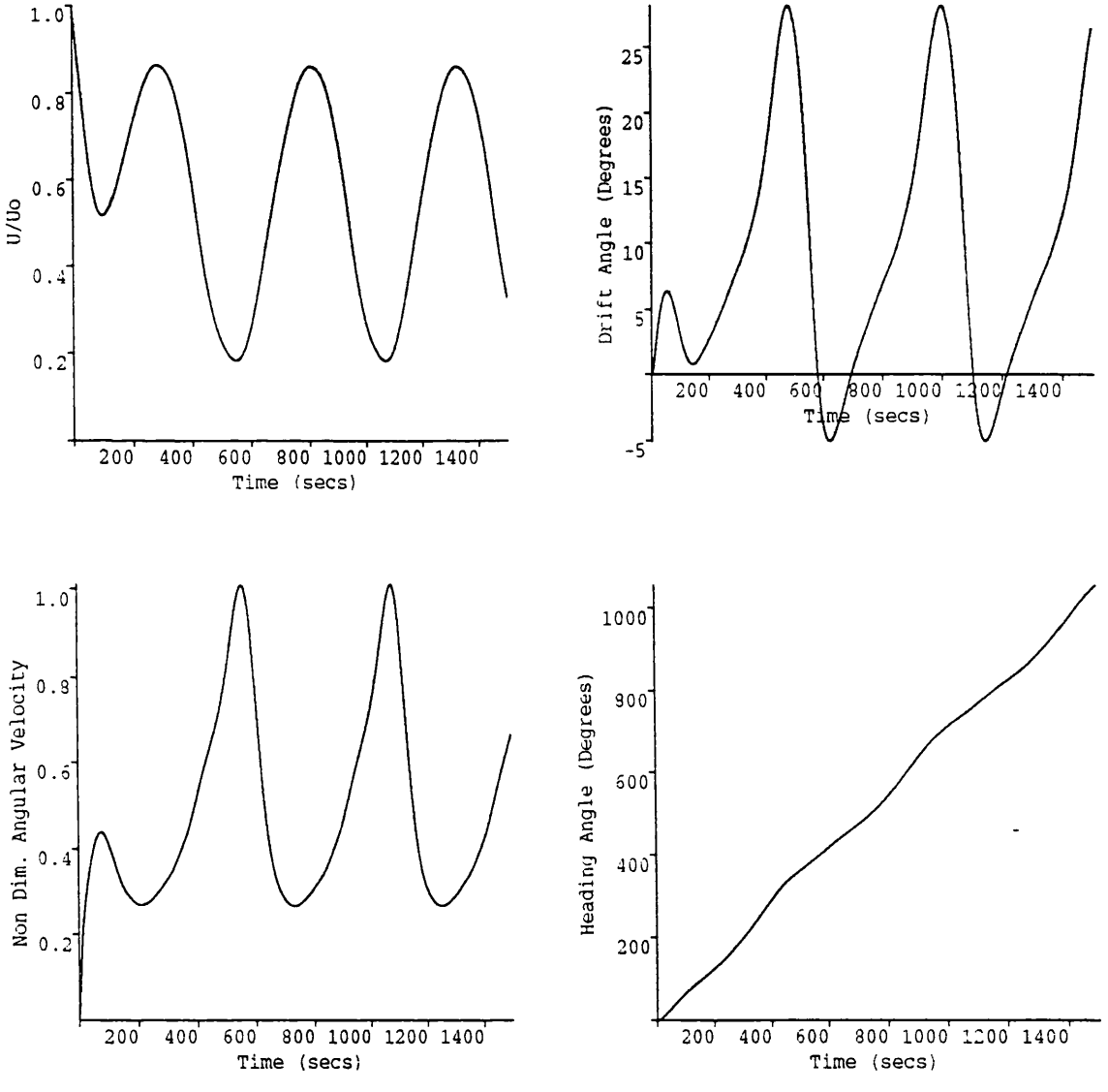

Figure 5.25c

Vessel Velocity : 15.0 Knots
Orientation of Jack Up on HLV : Aft
JU CoG with System CoG (X,Y) :-16.96, 0.04m,m
Bow & Stern Leg Longitudinal: 26.7 12.8m,m
Bow & Stern Leg Transverse: 0.0 22.7m,m
Rudder Angle : 20.0 Degrees
Advance : 506.6 m
Transfer : 343.3 m
Tactical Diameter : 895.2 m
Wind Velocity,Angle : 38.9, 0.0 Knots,Deg
Leg Length Exposed : 89.15 m

Mighty Servant I

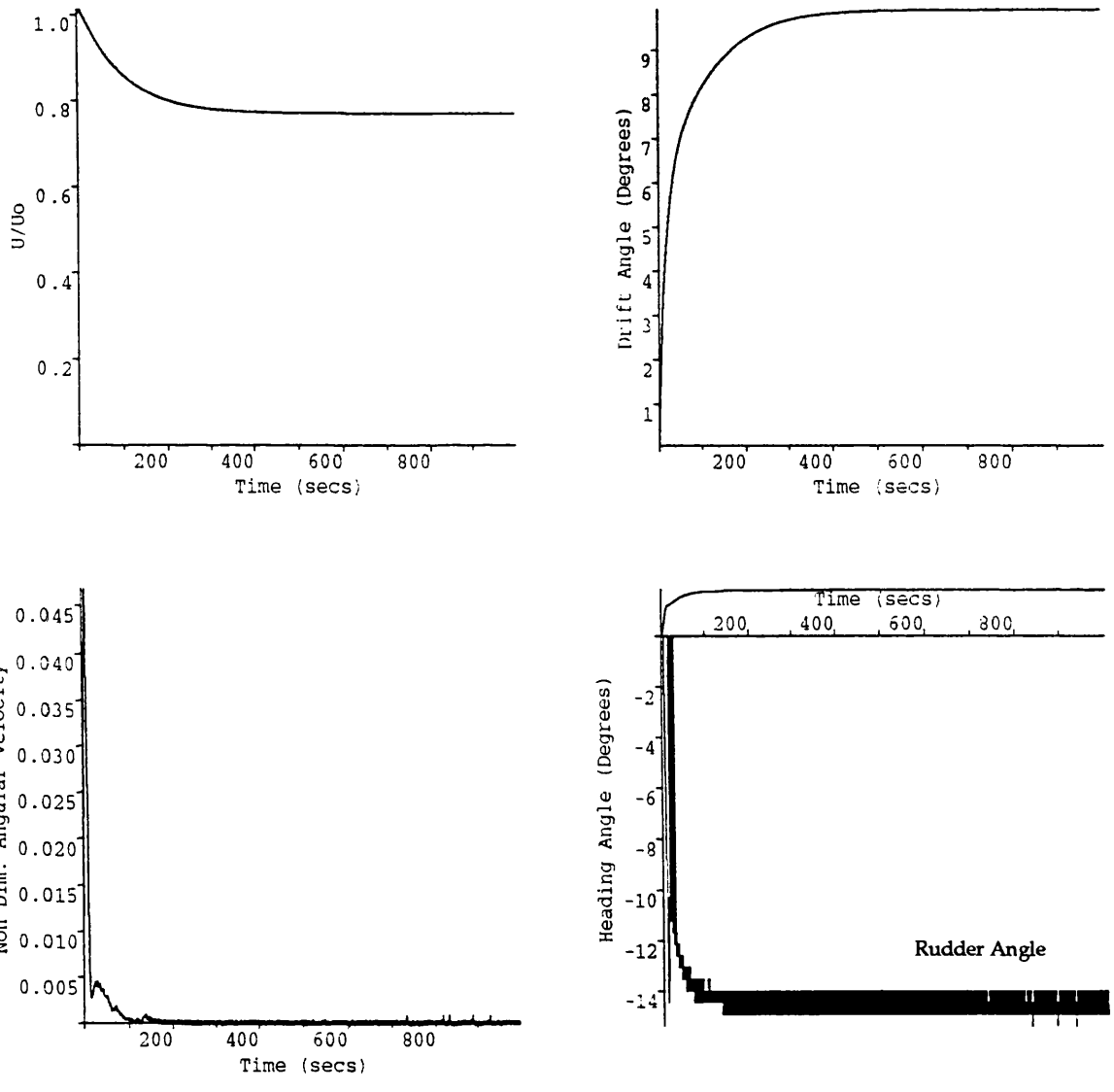

Figure 5.25d

Vessel Velocity : 15.0 Knots
Orientation of Jack Up on HLV : Aft
JU CoG with System CoG (X,Y) :-16.96, 0.04m,m
Bow & Stern Leg Longitudinal: 26.7 12.8m,m
Bow & Stern Leg Transverse: 0.0 22.7m,m
Rudder Constants 1,2 : 8.0,5.0
Maximum Deflection : -15.400 Degrees
Wind Velocity,Angle : 58.4, 90.0 Knots,Deg
Leg Length Exposed : 89.15 m

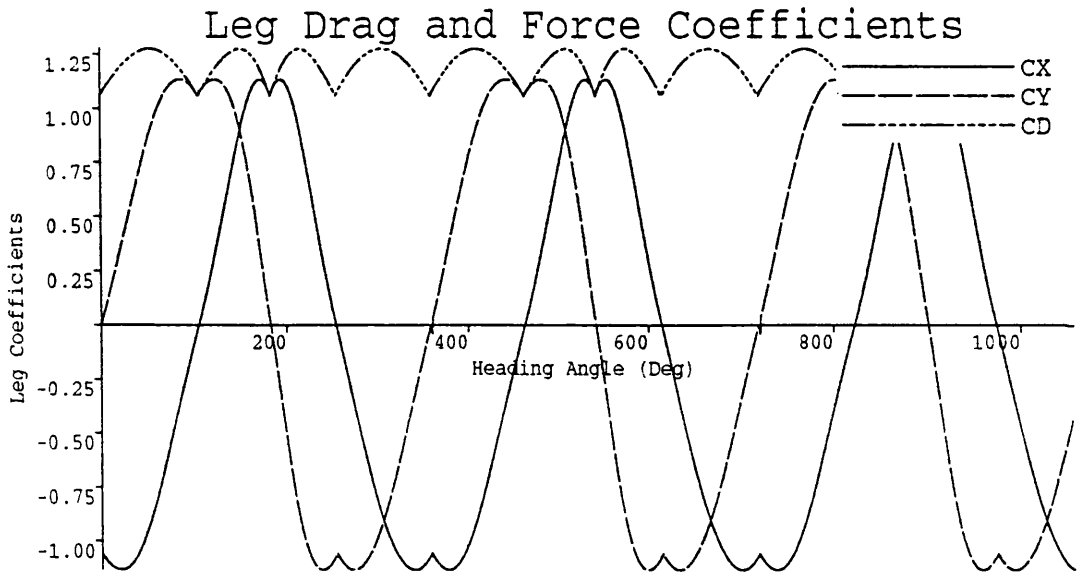

Figure 5.25e

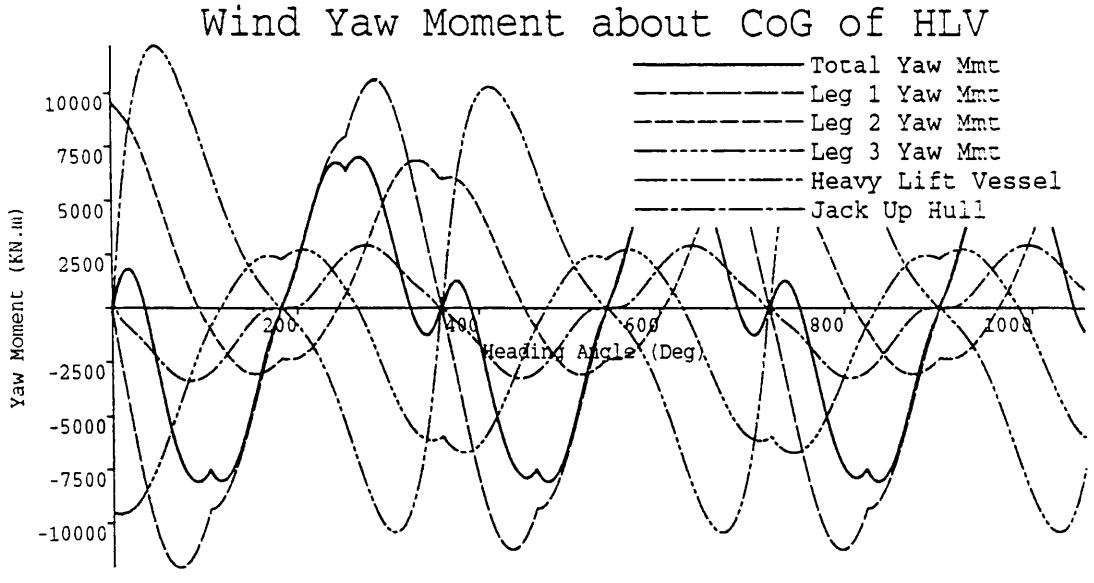

Figure 5.25f

Base Height of Exposed Leg : 19.58m
Marine Growth Height&Thickness: 1.25, 5.00mm,mm
Leg Drag Coefficient :0.761
Wind Velocity,Angle :38.9, 0.0Knots,Deg
Leg Geometry : Square
Leg Type : 116 Marathon
Orientation of Jack Up on HLV : Aft
JU CoG with System CoG (X,Y) :-16.96, 0.04m,m
Bow & Stern Leg Longitudinal: 26.7 12.8m,m
Bow & Stern Leg Transverse: 0.0 22.7m,m
Leg Length Exposed : 89.15 m

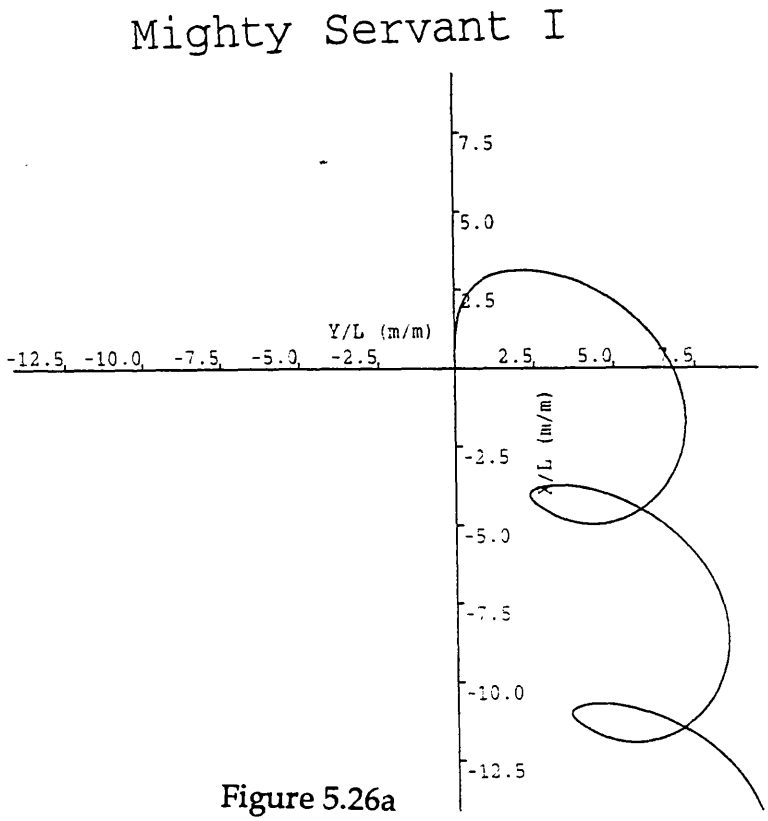

Figure 5.26a

Vessel Velocity : 15.0 Knots
Orientation of Jack Up on HLV : Aft
JU CoG with System CoG (X,Y) :-16.96, 0.04m,m
Bow & Stern Leg Longitudinal: 26.7 12.8m,m
Bow & Stern Leg Transverse: 0.0 22.7m,m
Rudder Angle : 20.0 Degrees
Advance : 450.8 m
Transfer : 347.1 m
Tactical Diameter : 1041.5 m
Wind Velocity,Angle : 48.6, 0.0 Knots,Deg
Leg Length Exposed : 89.15 m

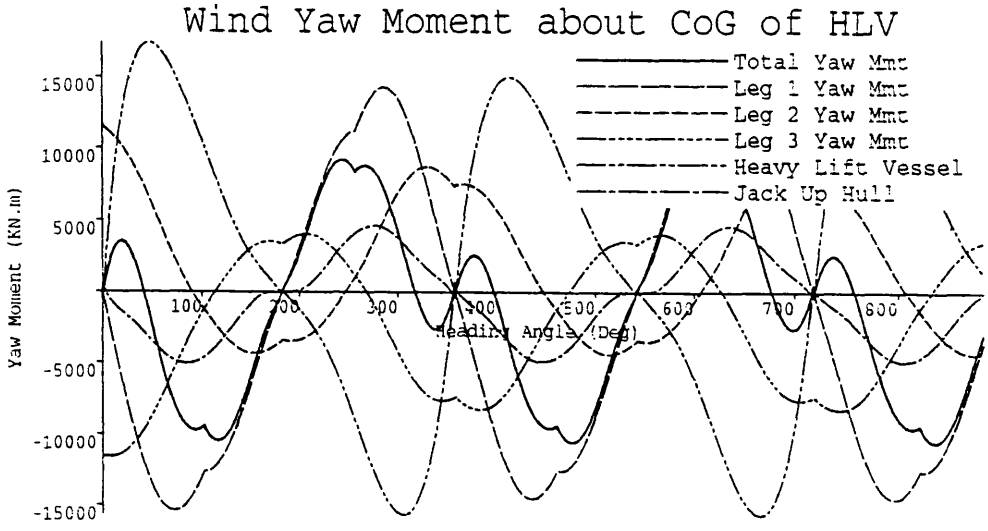

Figure 5.26b

Base Height of Exposed Leg : 19.58m
Marine Growth Height&Thickness: 0.00, 0.00mm,mm
Leg Drag Coefficient :0.663
Wind Velocity,Angle :48.6, 0.0Knots,Deg
Leg Geometry : Square
Leg Type : 116 Marathon

Mighty Servant I

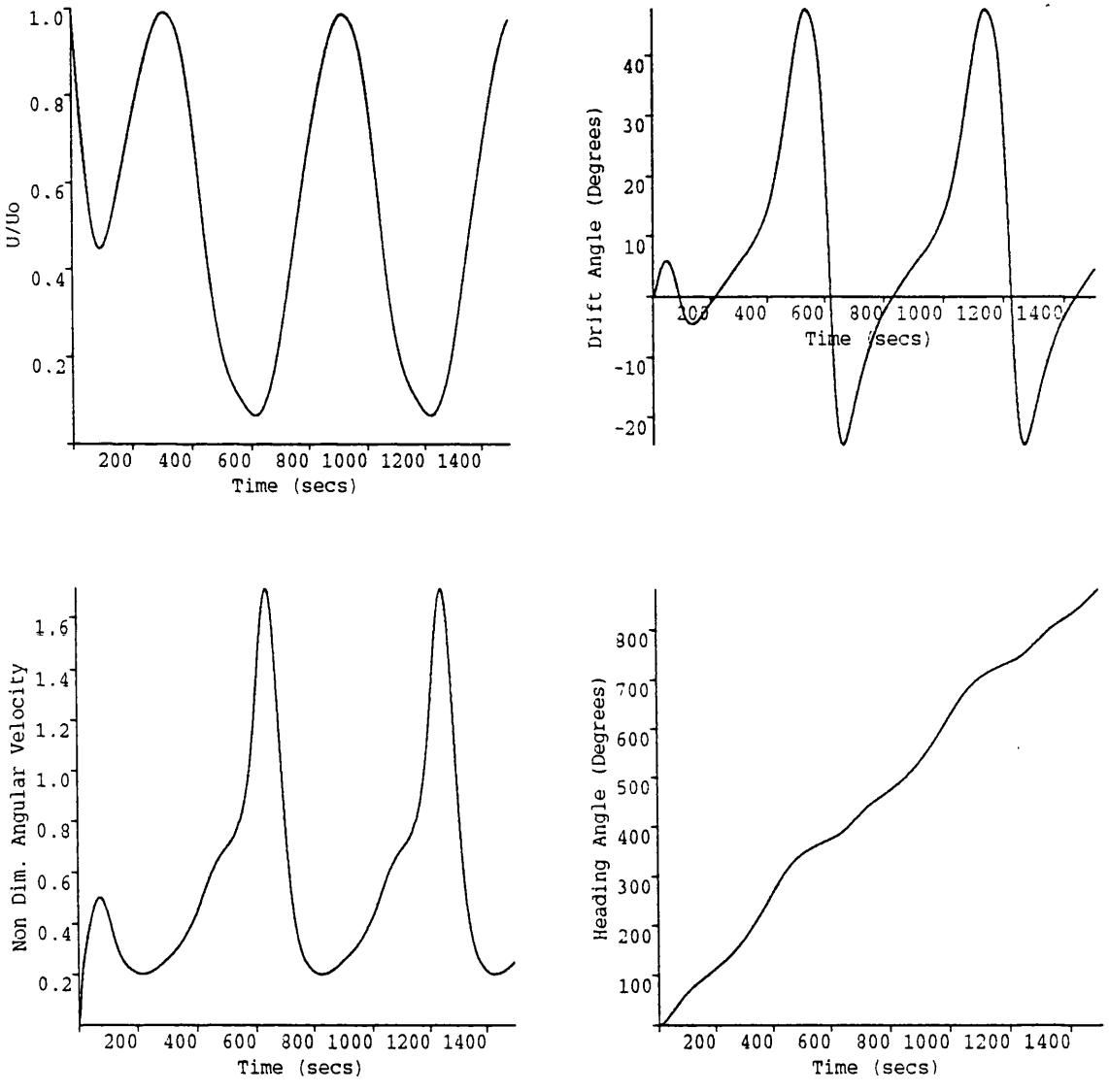

Figure 5.26c

Vessel Velocity : 15.0 Knots
Orientation of Jack Up on HLV : Aft
JU CoG with System CoG (X,Y) :-16.96, 0.04m,m
Bow & Stern Leg Longitudinal: 26.7 12.8m,m
Bow & Stern Leg Transverse: 0.0 22.7m,m
Rudder Angle : 20.0 Degrees
Advance : 450.8 m
Transfer : 347.1 m
Tactical Diameter : 1041.5 m
Wind Velocity,Angle : 48.6, 0.0 Knots,Deg
Leg Length Exposed : 89.15 m

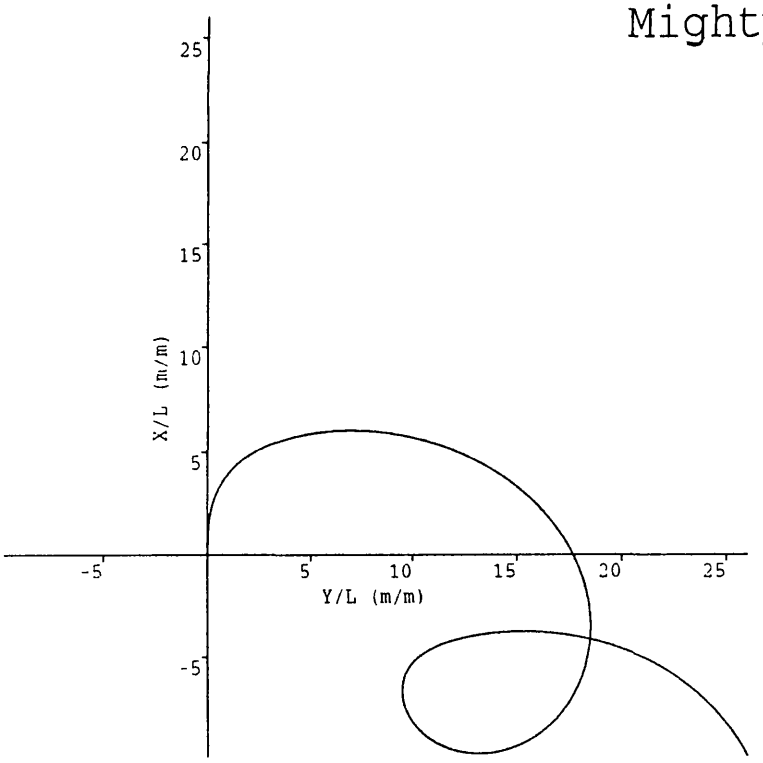

Figure 5.27a

Vessel Velocity : 15.0 Knots
Orientation of Jack Up on HLV : Aft
JU CoG with System CoG (X,Y) :-16.96, 0.04m,m
Bow & Stern Leg Longitudinal: 26.7 12.8m,m
Bow & Stern Leg Transverse: 0.0 22.7m,m
Rudder Angle : 10.0 Degrees
Advance : 871.6 m
Transfer : 1091.6 m
Tactical Diameter : 2681.4 m
Wind Velocity,Angle : 38.9, 0.0 Knots,Deg
Leg Length Exposed : 89.15 m

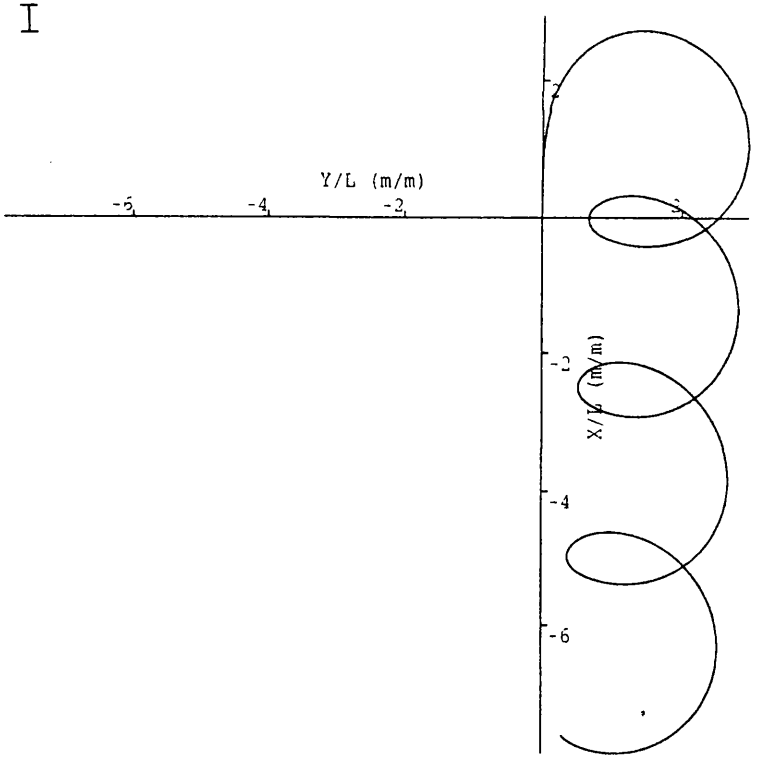

Figure 5.27b

Vessel Velocity : 15.0 Knots
Orientation of Jack Up on HLV : Aft
JU CoG with System CoG (X,Y) :-16.96, 0.04m,m
Bow & Stern Leg Longitudinal: 26.7 12.8m,m
Bow & Stern Leg Transverse: 0.0 22.7m,m
Rudder Angle : 35.0 Degrees
Advance : 393.9 m
Transfer : 180.5 m
Tactical Diameter : 422.4 m
Wind Velocity,Angle : 38.9, 0.0 Knots,Deg
Leg Length Exposed : 89.15 m

Mighty Servant I

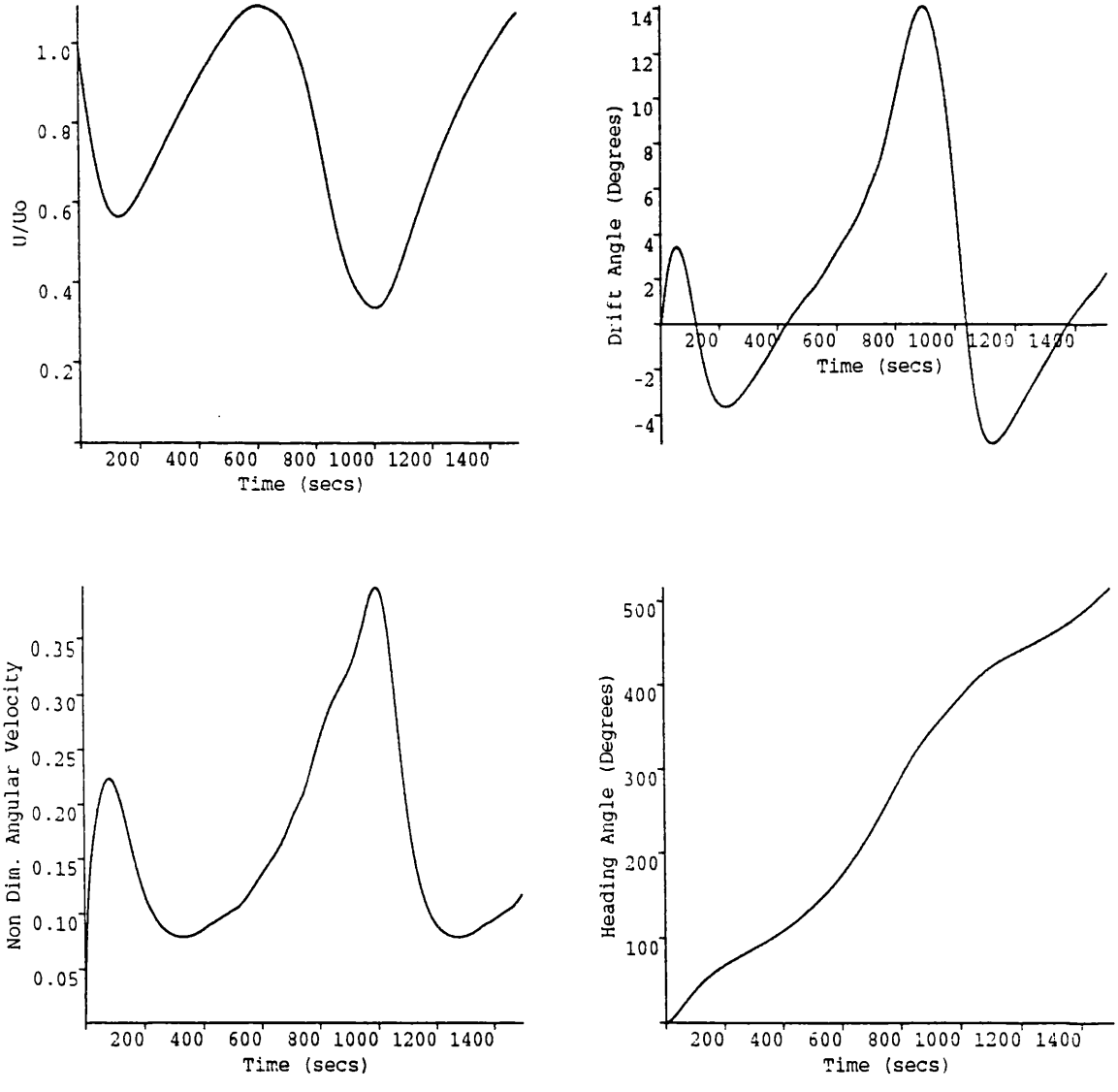

Figure 5.27c

Vessel Velocity : 15.0 Knots
Orientation of Jack Up on HLV : Aft
JU CoG with System CoG (X,Y) :-16.96, 0.04m,m
Bow & Stern Leg Longitudinal: 26.7 12.8m,m
Bow & Stern Leg Transverse: 0.0 22.7m,m
Rudder Angle : 10.0 Degrees
Advance : 871.6 m
Transfer : 1091.6 m
Tactical Diameter : 2681.4 m
Wind Velocity,Angle : 38.9, 0.0 Knots,Deg
Leg Length Exposed : 89.15 m

Mighty Servant I

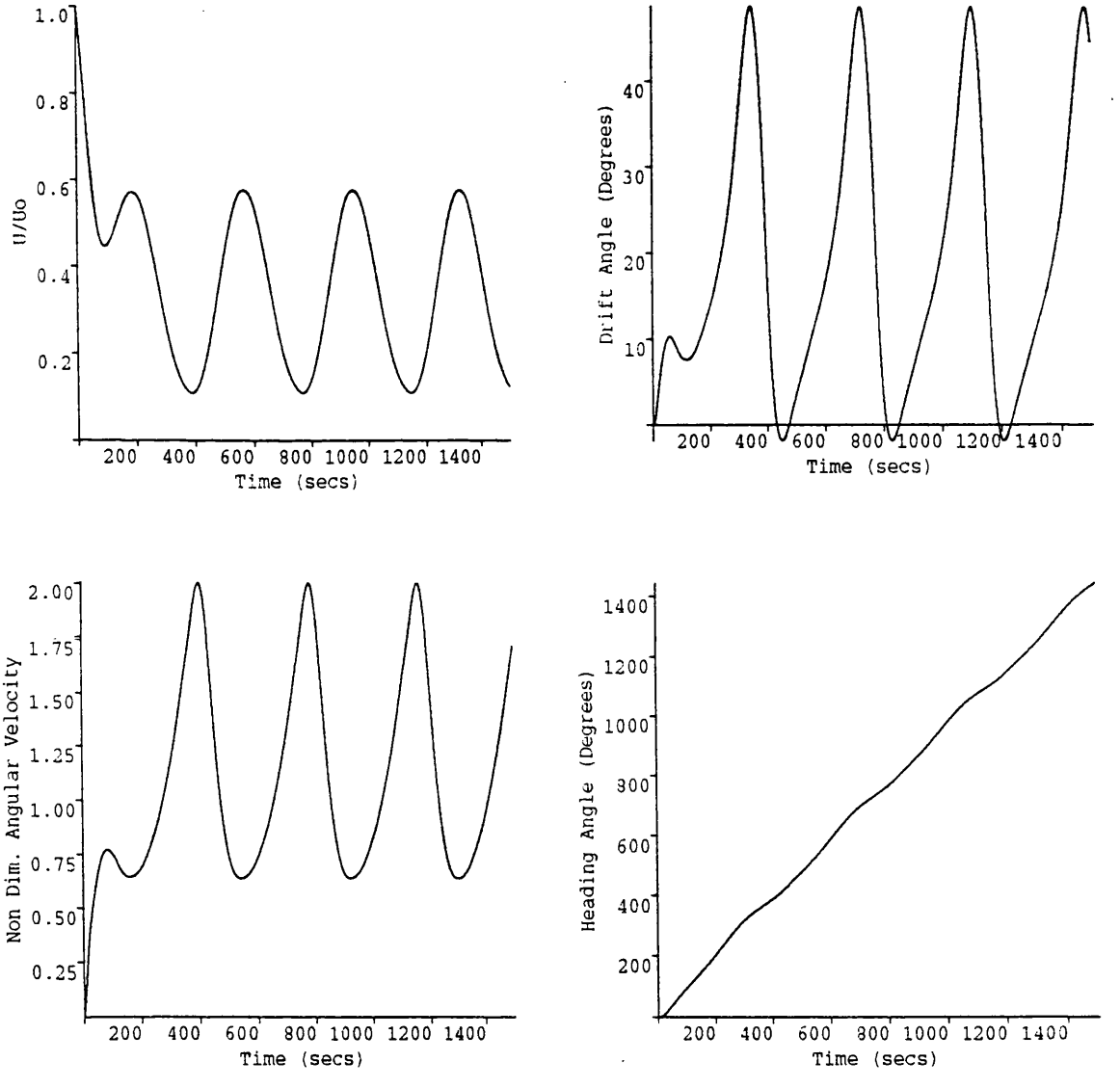

Figure 5.27d

Vessel Velocity : 15.0 Knots
Orientation of Jack Up on HLV : Aft
JU CoG with System CoG (X,Y) :-16.96, 0.04m,m
Bow & Stern Leg Longitudinal: 26.7 12.8m,m
Bow & Stern Leg Transverse: 0.0 22.7m,m
Rudder Angle : 35.0 Degrees
Advance : 393.9 m
Transfer : 180.5 m
Tactical Diameter : 422.4 m
Wind Velocity,Angle : 38.9, 0.0 Knots,Deg
Leg Length Exposed : 89.15 m

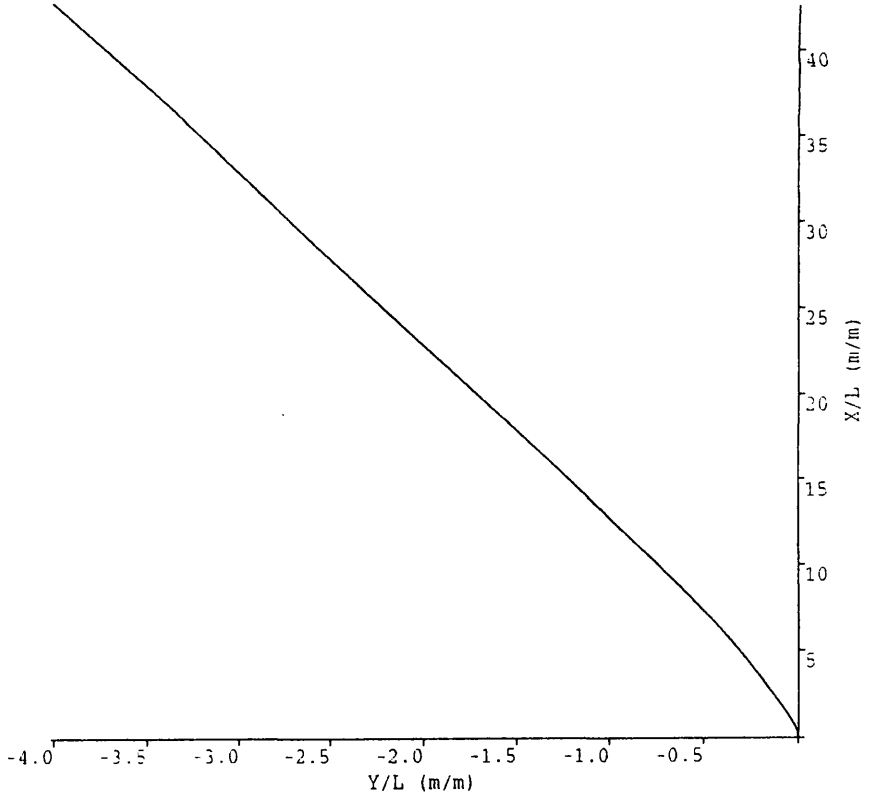

Figure 5.28a

Vessel Velocity : 15.0 Knots
Orientation of Jack Up on HLV : Aft
JU CoG with System CoG (X,Y) :-16.96, 0.04m,m
Bow & Stern Leg Longitudinal: 26.7 12.8m,m
Bow & Stern Leg Transverse: 0.0 22.7m,m
Rudder Constants 1,2 : 4.0,2.5
Maximum Deflection : -13.066 Degrees
Wind Velocity,Angle : 58.4, 90.0 Knots,Deg
Leg Length Exposed : 89.15 m

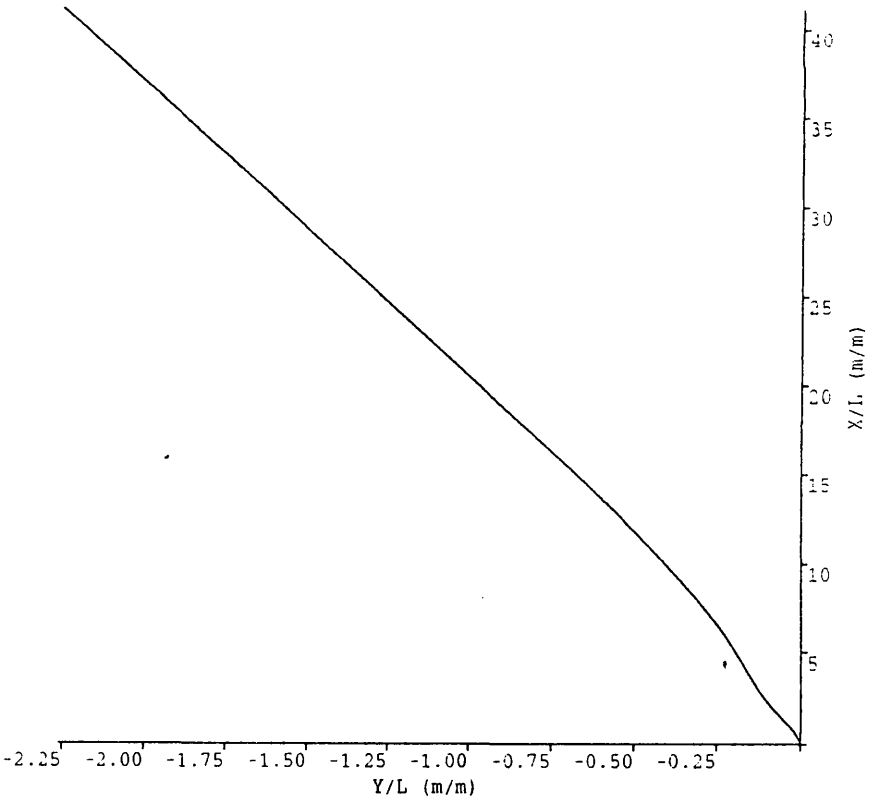

Figure 5.28b

Vessel Velocity : 15.0 Knots
Orientation of Jack Up on HLV : Aft
JU CoG with System CoG (X,Y) :-16.96, 0.04m,m
Bow & Stern Leg Longitudinal: 26.7 12.8m,m
Bow & Stern Leg Transverse: 0.0 22.7m,m
Rudder Constants 1,2 : 2.0,1.3
Maximum Deflection : -12.600 Degrees
Wind Velocity,Angle : 58.4, 90.0 Knots,Deg
Leg Length Exposed : 89.15 m

Mighty Servant I

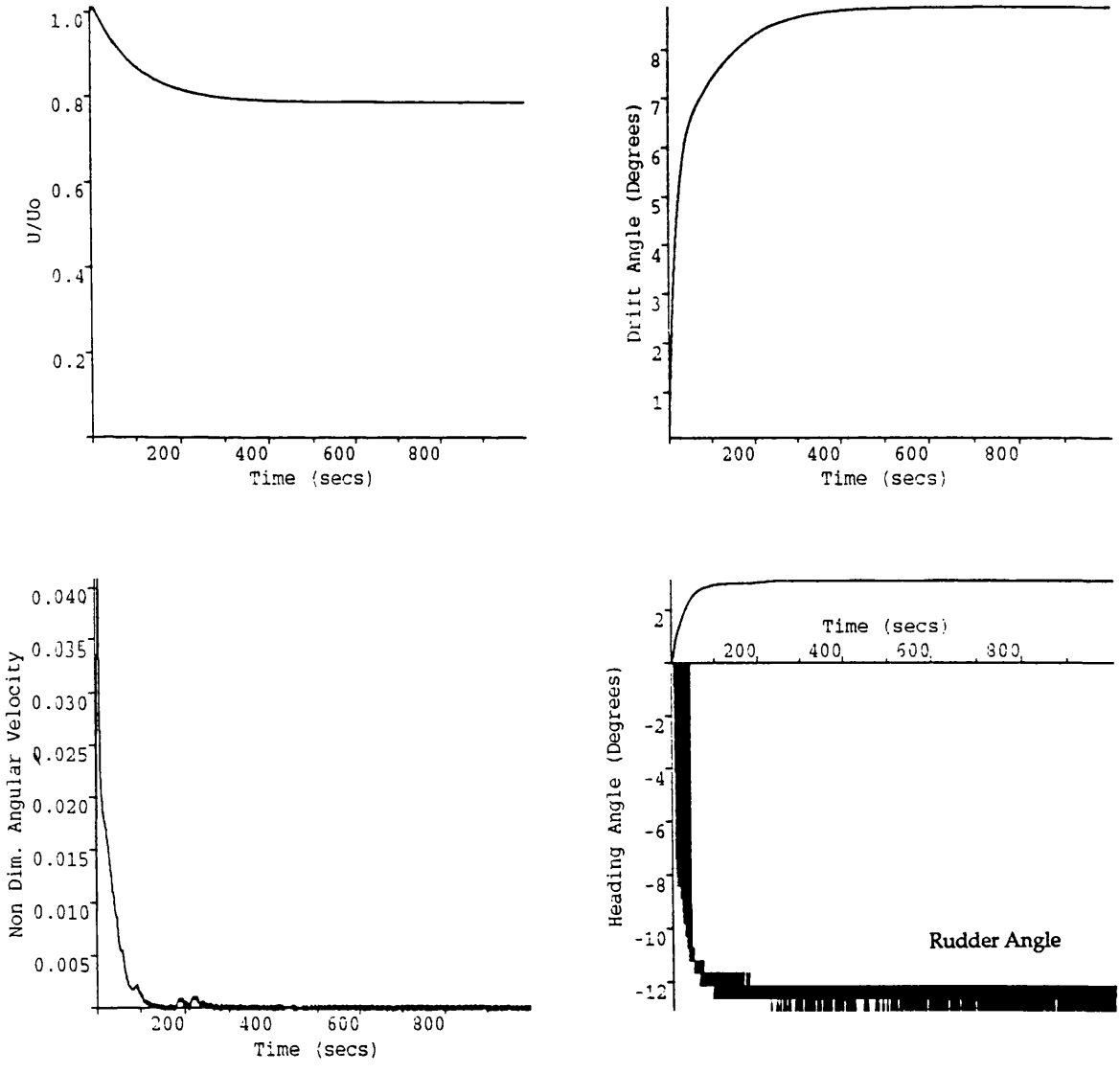

Figure 5.28c

Vessel Velocity : 15.0 Knots
Orientation of Jack Up on HLV : Aft
JU CoG with System CoG (X,Y) :-16.96, 0.04m,m
Bow & Stern Leg Longitudinal: 26.7 12.8m,m
Bow & Stern Leg Transverse: 0.0 22.7m,m
Rudder Constants 1,2 : 4.0,2.5
Maximum Deflection : -13.066 Degrees
Wind Velocity,Angle : 58.4, 90.0 Knots,Deg
Leg Length Exposed : 89.15 m

Mighty Servant I

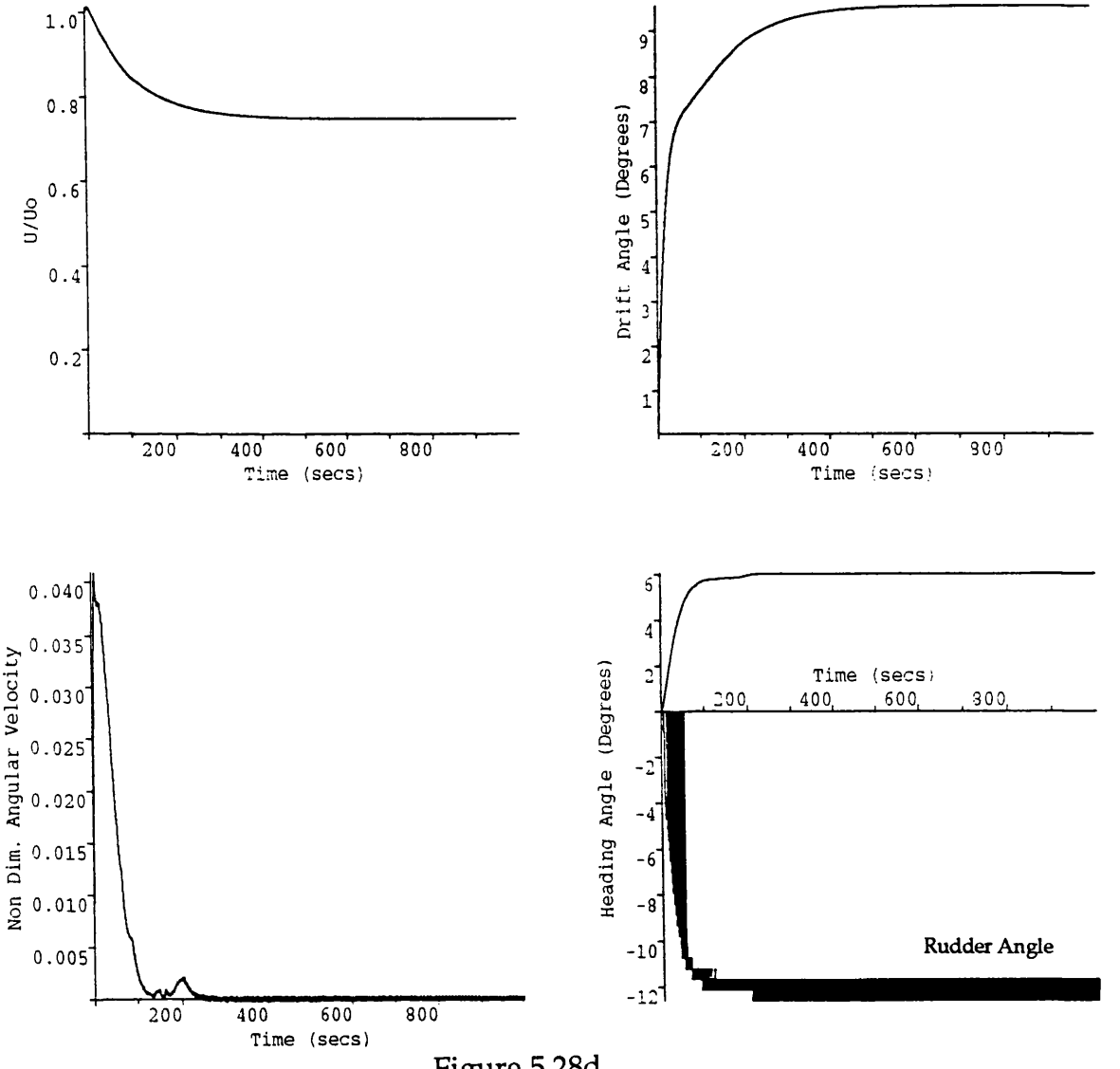

Figure 5.28d

Vessel Velocity : 15.0 Knots
Orientation of Jack Up on HLV : Aft
JU CoG with System CoG (X,Y) :-16.96, 0.04m,m
Bow & Stern Leg Longitudinal: 26.7 12.8m,m
Bow & Stern Leg Transverse: 0.0 22.7m,m
Rudder Constants 1,2 : 2.0,1.3
Maximum Deflection : -12.600 Degrees
Wind Velocity,Angle : 58.4, 90.0 Knots,Deg
Leg Length Exposed : 89.15 m

Chapter Six.

6.1 Jack Up Design and Oblique Towing Experiments.

The experimental program described in this chapter is the first stage in obtaining the necessary manoeuvring derivatives for a jack up hull which can be incorporated into a tow system simulation program. The experiments were carried out to determine the linear sway and yaw drift derivatives and the current force and moment coefficients for the conditions described.

The geometry for the jack up model is based on 'Galaxy 1', the first of the new generation of deep water 'Universe Class' jack ups. Permission was granted by the owners Santa Fe Drilling Company and the plans were supplied by Noble Denton Associates. The model scale is approximately 1:89 and this scale was chosen with several factors in mind. One important factor was the size of the model had to be sufficiently large enough to give validity to the experimental data obtained in the oblique towing experiments. The second factor, was the restriction imposed by the width of the experiment tank where the model would be towed. In the case of oblique (constrained) towing, the model was confined within a working bay and sufficient room had to be given for the model to rotate through 180 degrees. This would have proved difficult if a larger scale model were used. There was also a limiting factor arising from the size of standard diameter pipe for the leg well. The main dimensions of the model jack up is given in figure 6.1. The hull of the model was fabricated from PVC sheet as were the spud cans. The legwells were modelled using PVC pipe. The model can be modified to include the upper legs. These legs can be modelled using PVC pipe and the dimensions should be selected to give a similar mass per unit length as the full scale legs as well as a similar inertia. The lower legs were modelled in brass tube with a K brace triangular lattice configuration. This is to take a true account of the interactions between the leg, spud can and leg well. The effects of scale make this impossible however. The cornerpost rack was not modelled

because it would have a minimal effect on the final results. The lower legs can be extended to include additional bays and this enables the effects of leg submergence to be studied. Ballast may be added as required for trim and heel for the main hull. The spud cans are also able to be ballasted. Photographs of the model construction are shown. Only the hull and leg structure were modelled i.e. no deck houses, drilling derrick or helipad were included.

6.2 Oblique Towing Experiments.

The experiments described in this chapter were carried out to determine the linear drift manoeuvring derivatives and the current loading coefficients for the jack up model. Both of these experimental values were obtained by oblique towing of the model.

The oblique towing experiments were carried out in the University of Glasgow Hydrodynamics Laboratory. The experimental tank is 77.0m long, 4.6m wide and 2.7m deep. In the oblique towing experiments, the model is constrained at various heading angles and is towed along the tank in calm water. It was not necessary therefore to include the upper legs in the experiments to obtain the drift hydrodynamic derivatives and current loading coefficients as they would have no effect on the overall results. All the experiment conditions were carried out for two speeds of approximately 0.4m/s and 0.7m/s which correspond to full scale tow speed of 7.3 knots and 13 knots. The latter velocity is slightly larger than that normally undertaken for wet ocean tow but due to the high sensitivity of the apparatus and the signal interference generated from the noise of the carriage it was felt that the slightly increased velocity would give more accurate results. All the experiments were carried out at two conditions of leg submergence and extension. The first condition was the complete leg and spud can housed inside the leg well. The second was the spud can top, level with the base of the jack up and without any leg bays exposed. The experiments were carried out to investigate the effect of the spud can and leg appendages on the drift

manoeuvring derivatives and current loading coefficients. The model freeboard was very small, 4.5cm and as the frame structure was designed for ship models, it was necessary to add packing between the model and the turntable frame and secure rigidly.

6.2.1 Drift Manoeuvring Derivatives.

The angles chosen to obtain the drift derivatives for the two towing speeds were -4, -2, 0, 2, 4, 6, 8, 10, 12 and 15 degrees. These specific angles were obtained using a turntable mechanism. The drift forces and moments were non dimensionalised in order to obtain the non dimensionalised derivatives of the same form as the derivatives of Chapter Two.

$$Y' = \frac{Y}{\frac{\rho LDU^2}{2}}, \quad N' = \frac{N}{\frac{\rho L^2 DU^2}{2}}$$

$$Y'_\beta = \frac{Y_\beta}{\frac{\rho LDU^2}{2}}, \quad N'_\beta = \frac{N_\beta}{\frac{\rho L^2 DU^2}{2}}$$

The above derivative representation are derived for the Japanese modular manoeuvring model.

6.2.2 Current Loading Coefficients.

The experimental set up for the drift derivatives was also used to obtain the current loading coefficients for the same towing velocities and angles of 20,30,40,....,170,180 degrees. These larger angles of incidence were obtained by replacing the drift turntable with a second current loading turntable. The current force and moment coefficients for angles less than 20 degrees were derived from the forces and moments obtained for the derivative results. These coefficients could then be used in modelling the current loading on the towing simulation of the jack up. The current loading coefficients are non dimensionalised in the same manner as for

the current loading coefficients of Ref. 3.1 in Chapter Three. The current loading coefficients were employed in the previous chapter to model the wind loading on the jack up hull as wind loading coefficients for such units are unavailable. This is obviously incorrect because of the flow regimes are different as is the hull form.

$$C_X = \frac{X}{\frac{\rho B\, DU^2}{2}} \quad C_Y = \frac{Y}{\frac{\rho L\, DU^2}{2}} \quad C_N = \frac{N}{\frac{\rho L^2 DU^2}{2}}$$

In all the experimental runs, the sampling rate was 100 samples per second per channel for 20 seconds. The velocity of the carriage was averaged over the length of the run.

6.3 Experimental Apparatus and Calibration Procedure.

The forces and moments acting on the jack up model were calculated using the experimental set up shown in photographs 6.1-6.4. The system consists of a 2 bar aluminium frame which, after calibration is fixed to the model. A turntable is then bolted to the top of the frame. This whole system is then bolted securely to the frame work of the main carriage. To obtain the required heading angle, the turntable is rotated through the desired angle.

The forces acting on the hull were derived from measurements obtained from strain gauges which were fitted to the faces of the two aluminium bars as shown in figs. 6.2.

To measure the sway force, 2 pairs of opposite strain gauges are fitted to faces 2 and 4 on each of the aluminium bars. Likewise the surge is determined from 2 pairs of opposite strain gauges fitted to faces 1 and 3 on each bar. This gives a total of 16 strain gauges. Each of these sets of four strain gauges form a bridge circuit or Wheatstone Bridge. The forward bar and after bar are aligned along the centerline of the model. It was necessary to calibrate the 2 bar system to determine the relationship between the strain gauge readings and the loadings imposed by the oblique towing of

the model.

Before the system is loaded, the Wheatstone bridge should be balanced as the output voltage is zero. As the system is loaded a change in resistance will unbalance the bridge and induce an output voltage across the output terminal. By measuring this voltage and using the calibration curve, the voltage readout can be converted into the corresponding load value.

The calibration procedure was carried out prior to fixing the model and bolting the complete system to the main carriage. Ten separate calibrations were needed to determine the resistance, the sway force and the yaw moment. The calibrations include,

Top and Bottom of Bars 1 and 2 (faces 1&3), 4 calibrations for surge forces
Top and Bottom of Bars 1 and 2 (faces 2&4), 4 calibrations for sway forces
Torques on Bar 1 and 2, 2 calibrations for the yaw moments.

with reference to figure 6.2 the pair of strain gauges were placed as,

Channel 1	Torque in Bar 1 (M_1)
Channel 2	Torque in Bar 2 (M_2)
Channel 3	Moment on Face 1,3 at Bottom of Bar 1 (M_3)
Channel 4	Moment on Face 1,3 at Top of Bar 1 (M_4)
Channel 5	Moment on Face 1,3 at Bottom of Bar 2 (M_5)
Channel 6	Moment on Face 1,3 at Top of Bar 2 (M_6)
Channel 7	Moment on Face 2,4 at Bottom of Bar 1 (M_7)
Channel 8	Moment on Face 2,4 at Top of Bar 1 (M_8)
Channel 9	Moment on Face 2,4 at Bottom of Bar 2 (M_9)
Channel 10	Moment on Face 2,4 at Top of Bar 2 (M_{10})

All of these calibrations produced linear relationships. The units for the calibrations were moments [kg. m]. The masses used were from 0.5kg to 2kg in 0.25 kg intervals for the force calibrations and 0.5 kg up to 3kg in 0.5 kg intervals for the torques. The surge and sway force and yaw

moment were obtained from the moments from the ten channels on the bars as,

$$X = \frac{(M_4 - M_3) + (M_6 - M_5)}{0.2} \qquad 6.1$$

$$Y = \frac{(M_7 - M_8) + (M_9 - M_{10})}{0.2} \qquad 6.2$$

The yaw moment is corrected as the moments produced on bar 2 and bar 1 are the local yaw moments acting on the two aluminium bars. The sway forces acting on bar 2 and 1 make additional contributions to the overall yaw moment as,

$$N = M_1 + M_2 + F_2x_2 - F_1x_1 \qquad 6.3$$

6.4 Discussion of Results.

6.4.1 Surge Force.

The results from the resistance are given in figures 6.3-6.6. It will be necessary to repeat these experiments as these initial investigations show very poor consistency especially with the spud can exposed.

6.4.2 Sway Drift Derivative.

The non dimensionalised sway drift derivatives results produced from the experiments using the 2 bar system are given in figures 6.7-6.10 for the zero leg and spud can exposed conditions for the velocities of approximately 0.4 and 0.7 m/s. It can be seen that the experiment results produced a very good linear relationships for the sway derivatives.

6.4.3 Yaw Drift Derivative.

The non dimensionalised yaw drift derivative using the two bar system show less encouraging results. In the case of the zero leg position figures 6.11-6.12 the results can be assumed as linear. The results for the

spud can exposed figures 6.13-6.14 shows greater scatter even after a careful re examination of the experimental data. After breaking down the contributions of yaw moment equation 6.3, it became apparent that the large scatter is due to the contribution of the additional yaw moment from sway forces acting on bars 2 and 1. The experimental set up had originally been designed for conventional ship models. The local yaw moment contribution to the total yaw moment is more significant in the ship models than in the case of the jack up model.

6.4.4 Current Loading Coefficients.

The current loading coefficients are shown in Figs. 6.15 - 6.17 for the two velocities in the zero leg position and with the leg extended for 0.4 m/s. The coefficients show good repeatability.

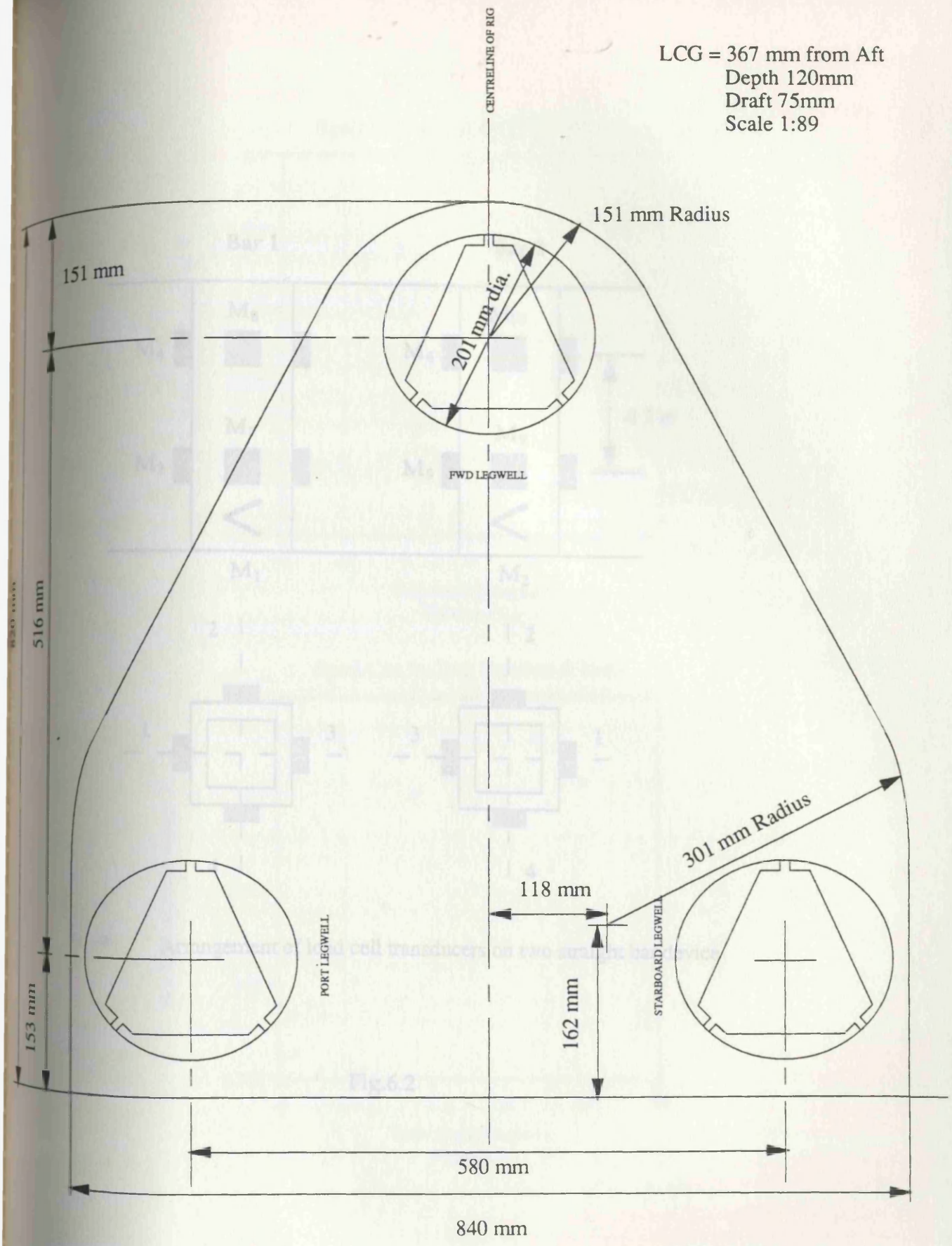
LCG = 367 mm from Aft
Depth 120mm
Draft 75mm
Scale 1:89
CENTRELINE OF RIG
151 mm Radius
151 mm
201 mm dia.
FWD LEGWELL
516 mm
301 mm Radius
118 mm
PORT LEGWELL
STARBOARD LEGWELL
153 mm
162 mm
580 mm
840 mm

Fig.6.1

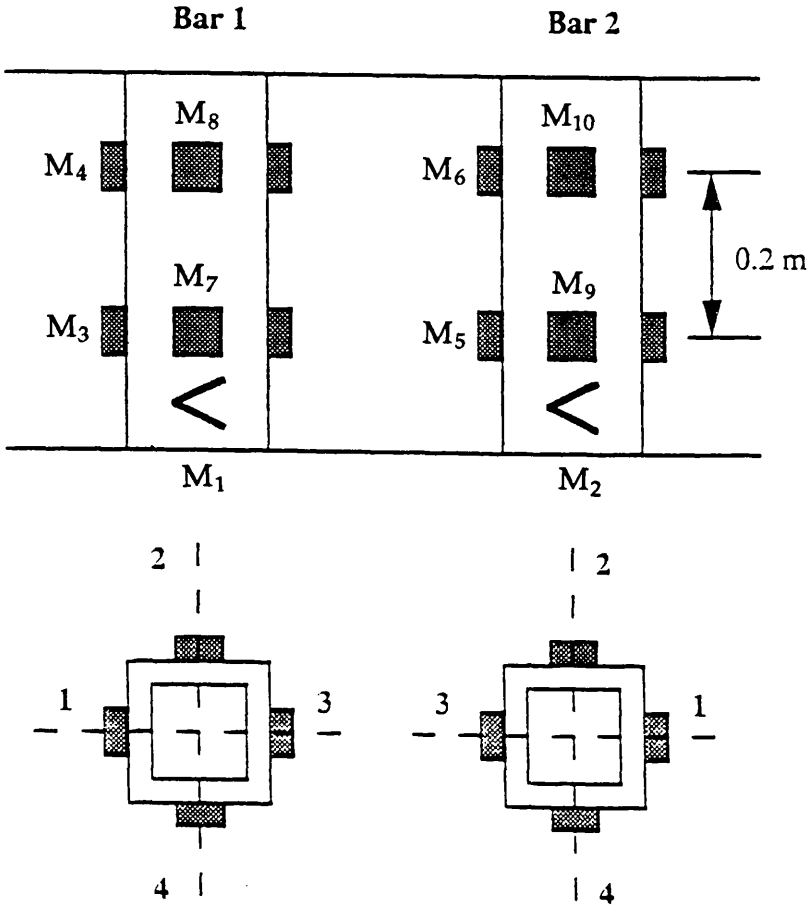

Arrangement of load cell transducers on two straight bar device

Fig.6.2

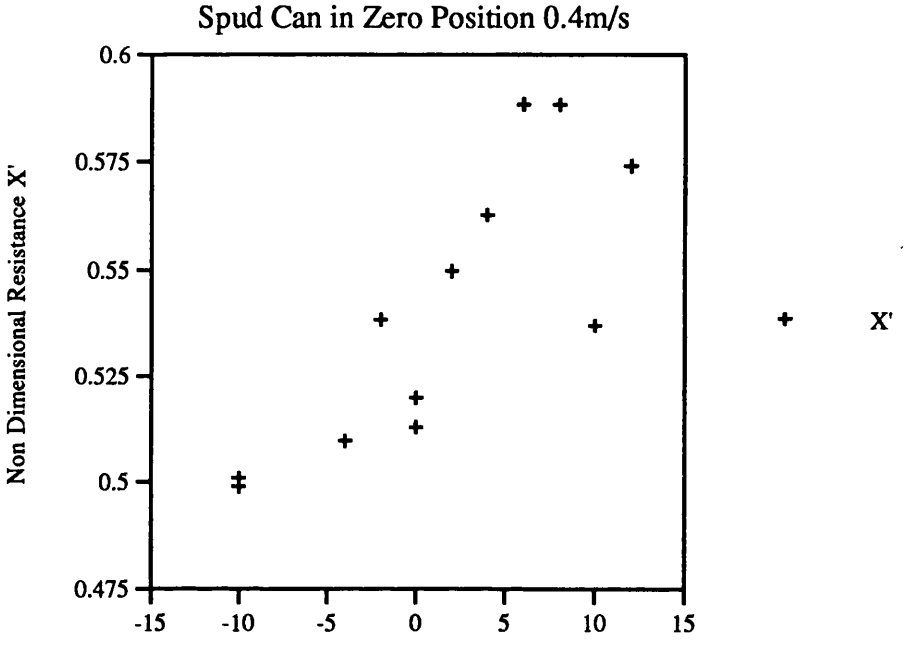

Figure 6.3

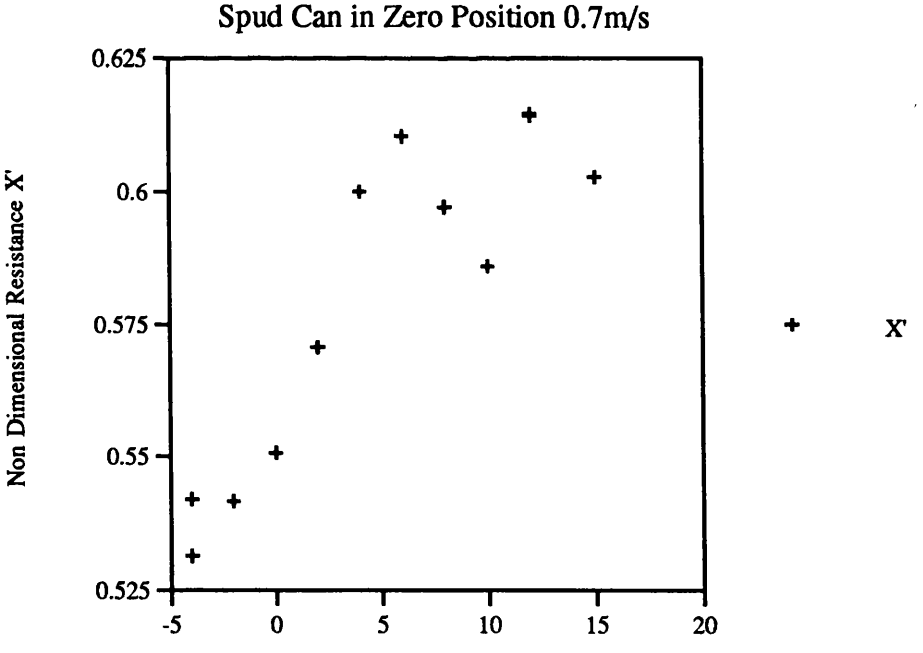

Figure 6.4

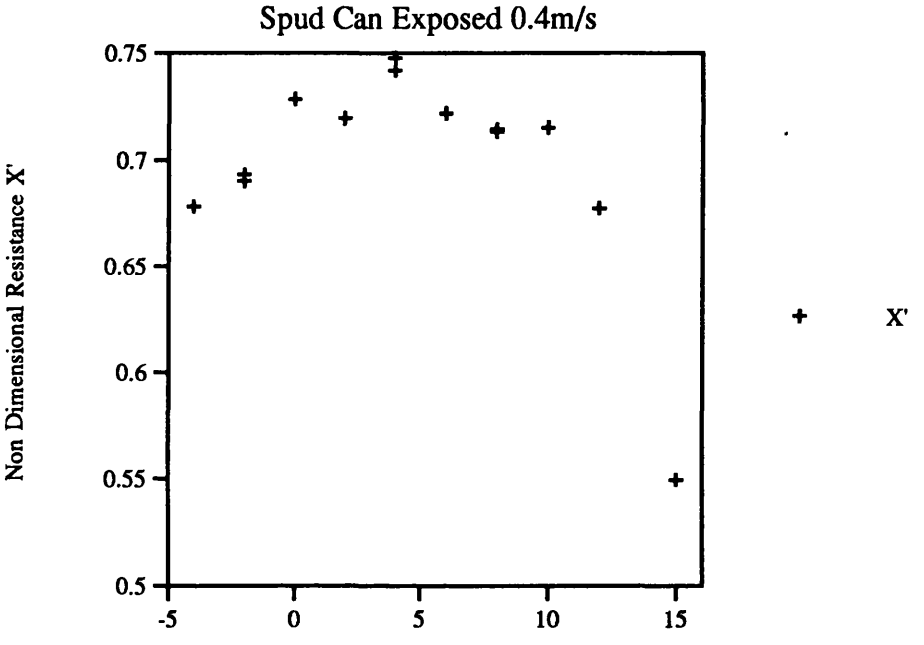

Figure 6.5

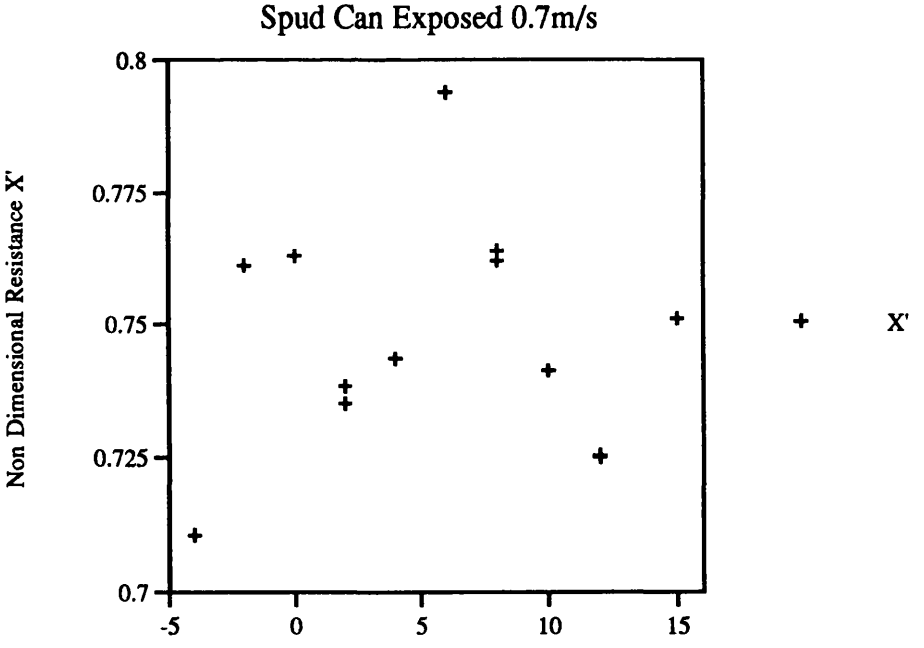

Figure 6.6

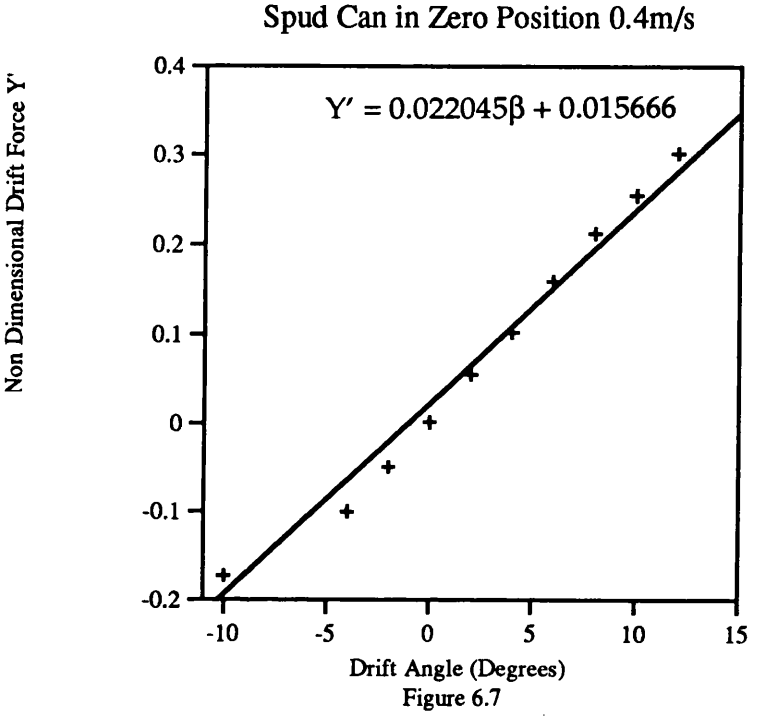

Figure 6.7

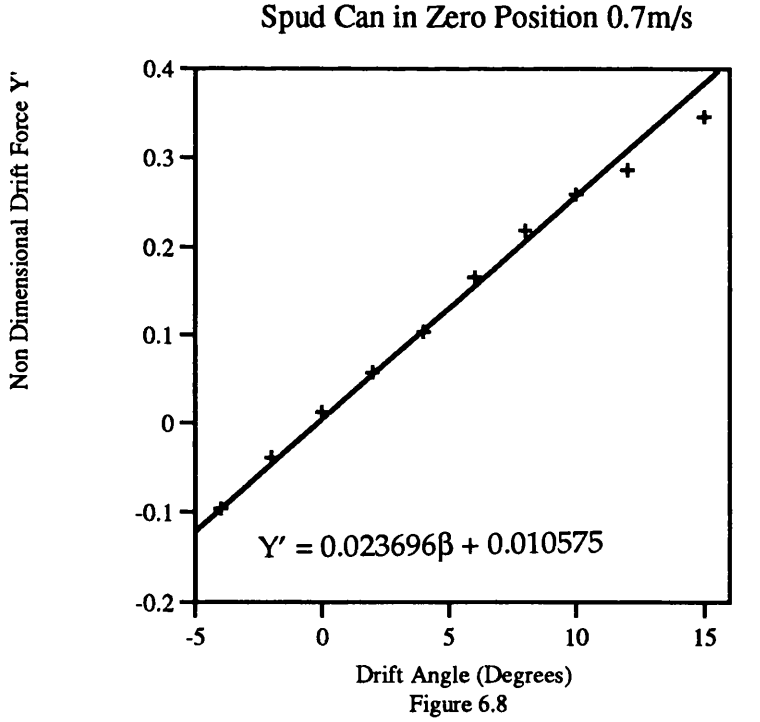

Figure 6.8

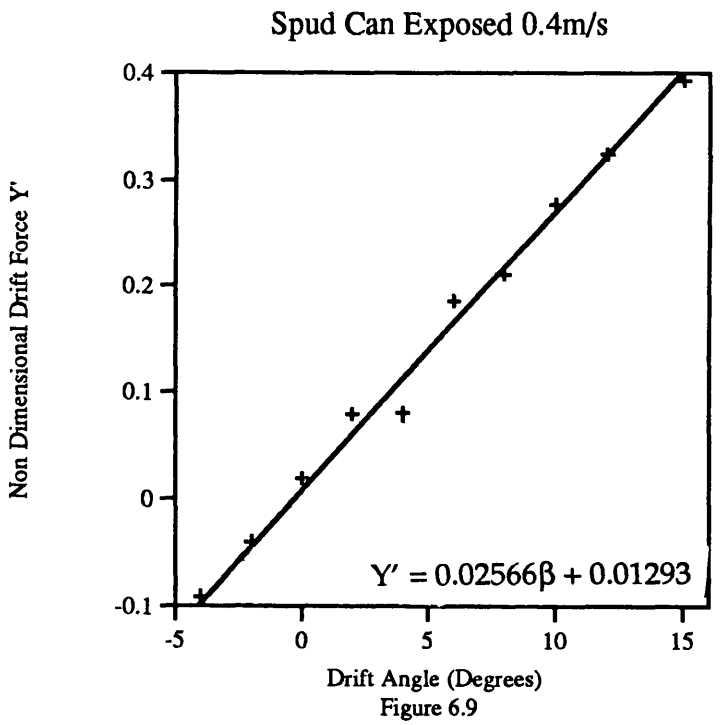

Figure 6.9

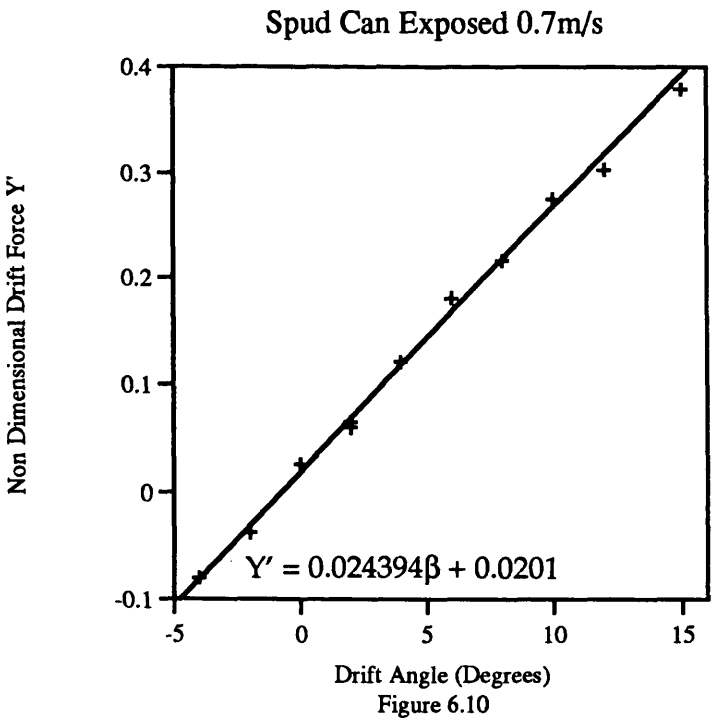

Figure 6.10

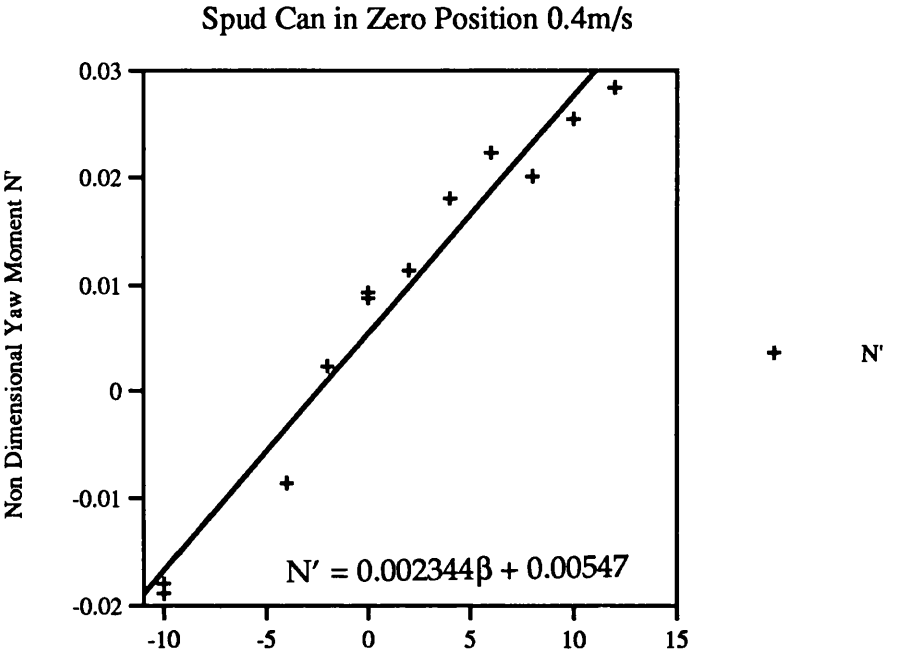

Figure 6.11

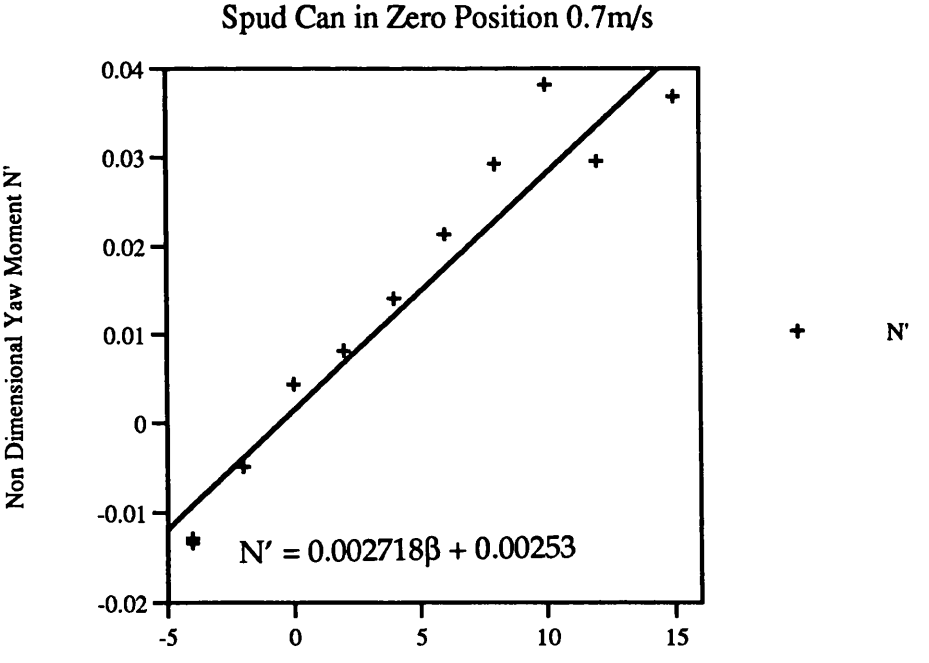

Figure 6.12

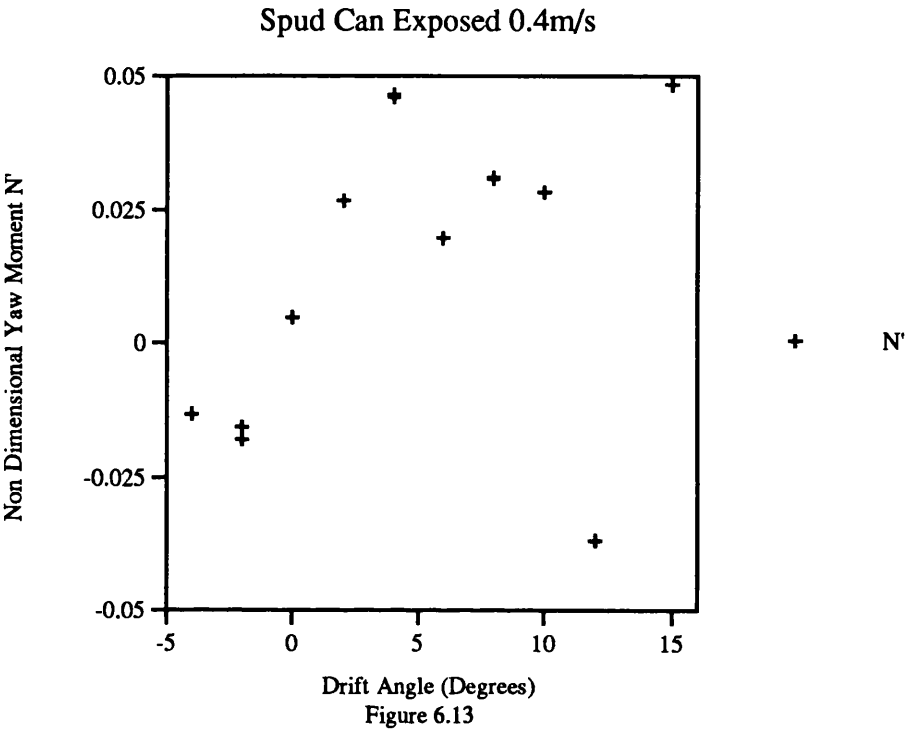

Figure 6.13

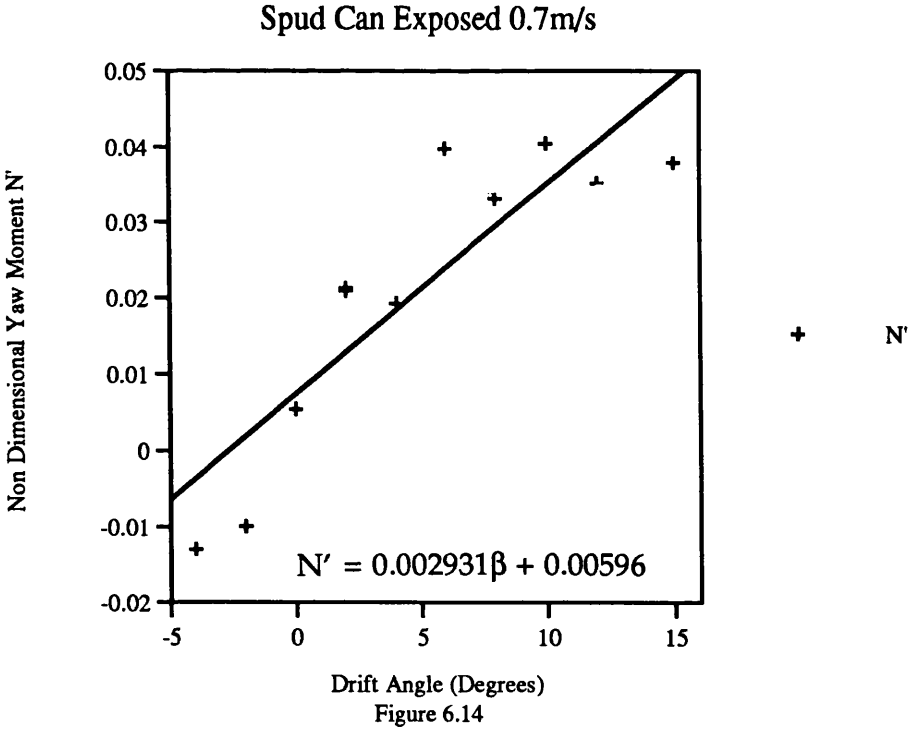

Figure 6.14

Spud Can in Zero Position 0.4m/s

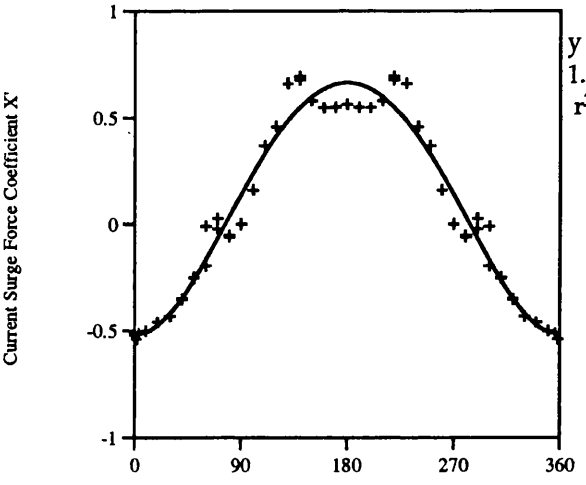

$y = 1.196E\text{-}09x^4 - 8.607E\text{-}07x^3 + 1.572E\text{-}04x^2 - 8.323E\text{-}04x - 5.126E\text{-}01$
$r^2 = 9.632E\text{-}01$

\+ X'

Figure 6.15a

Spud Can in Zero Position 0.7m/s

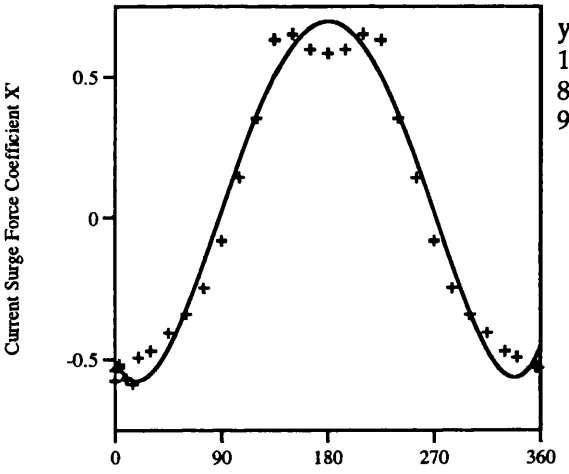

$y = 5.300E\text{-}13x^5 + 1.459E\text{-}09x^4 - 1.237E\text{-}06x^3 + 2.544E\text{-}04x^2 - 8.089E\text{-}03x - 5.054E\text{-}01$ $r^2 = 9.791E\text{-}01$

\+ X'

Figure 6.15b

Spud Can Exposed 0.4m/s

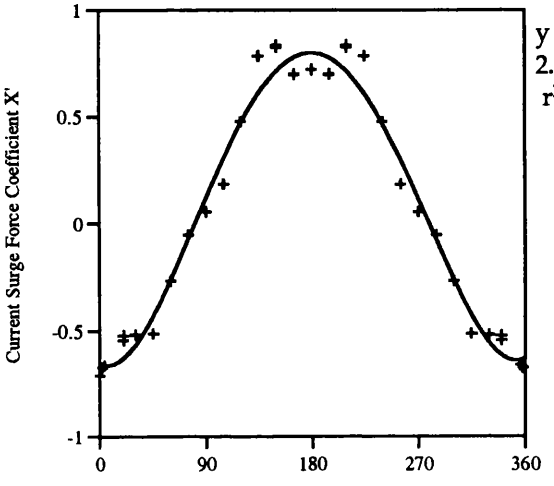

$y = 1.606E\text{-}09x^4 - 1.151E\text{-}06x^3 + 2.132E\text{-}04x^2 - 2.344E\text{-}03x - 6.578E\text{-}01$
$r^2 = 9.798E\text{-}01$

\+ X'

Figure 6.15c

Spud Can in Zero Position 0.4m/s

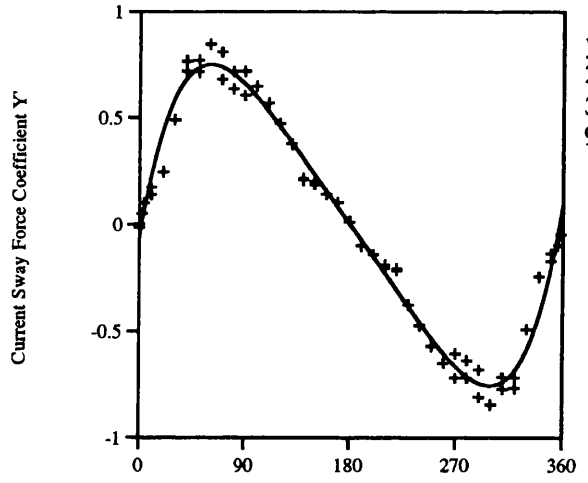

$y = 8.465E\text{-}12x^5 - 7.566E\text{-}09x^4 + 2.683E\text{-}06x^3 - 4.728E\text{-}04x^2 + 3.380E\text{-}02x - 6.594E\text{-}02$ $r^2 = 9.833E\text{-}01$

\+ Y'

Figure 6.16a

Spud Can in Zero Position 0.7m/s

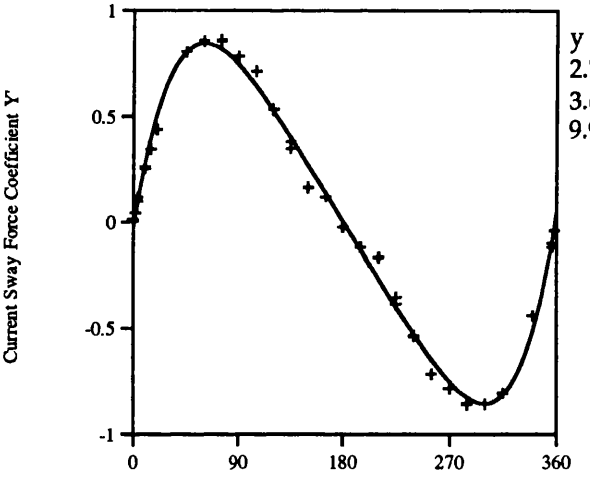

$y = 8.687E\text{-}12x^5 - 7.788E\text{-}09x^4 + 2.793E\text{-}06x^3 - 5.019E\text{-}04x^2 + 3.635E\text{-}02x - 3.703E\text{-}02$ $r^2 = 9.919E\text{-}01$

\+ Y'

Figure 6.16b

Spud Can Exposed 0.4m/s

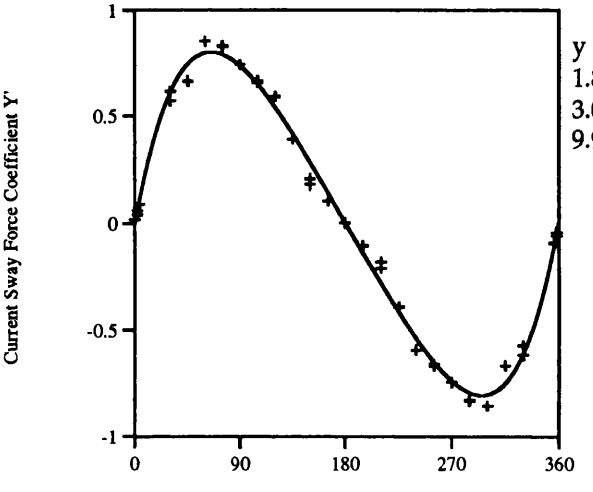

$y = 5.490E\text{-}12x^5 - 4.918E\text{-}09x^4 + 1.880E\text{-}06x^3 - 3.799E\text{-}04x^2 + 3.041E\text{-}02x - 4.880E\text{-}03$ $r^2 = 9.931E\text{-}01$

\+ Y'

Figure 6.16c

Spud Can in Zero Position 0.4m/s

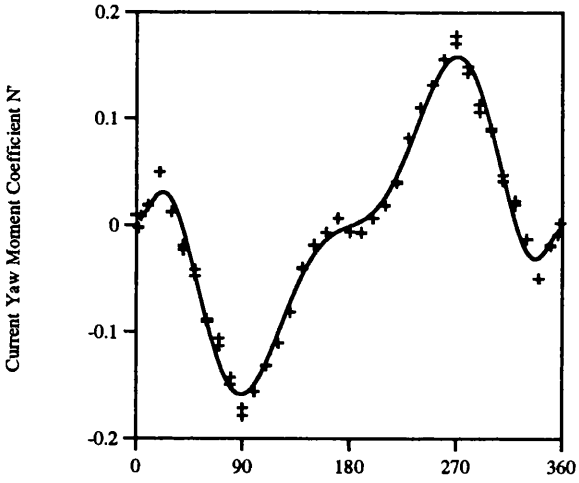

$y = -2.983E\text{-}20x^9 + 4.831E\text{-}17x^8 - 3.231E\text{-}14x^7 + 1.149E\text{-}11x^6 - 2.328E\text{-}09x^5 + 2.650E\text{-}07x^4 - 1.532E\text{-}05x^3 + 3.357E\text{-}04x^2 - 1.280E\text{-}03x + 8.043E\text{-}03 \quad r^2 = 9.848E\text{-}01$

\+ N'

Figure 6.17a

Spud Can in Zero Position 0.7m/s

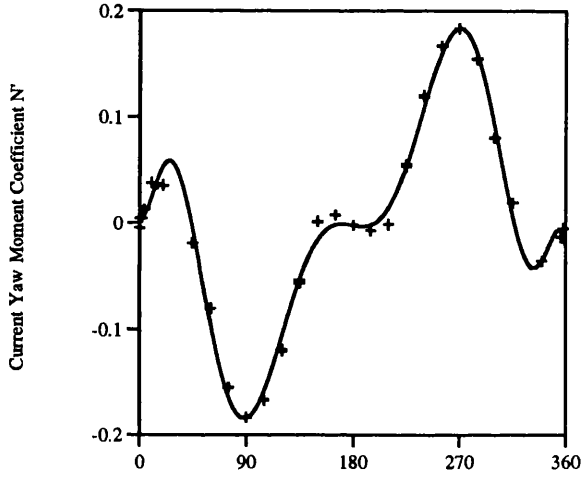

$y = -4.665E\text{-}20x^9 + 7.510E\text{-}17x^8 - 4.995E\text{-}14x^7 + 1.769E\text{-}11x^6 - 3.572E\text{-}09x^5 + 4.067E\text{-}07x^4 - 2.371E\text{-}05x^3 + 5.346E\text{-}04x^2 - 1.589E\text{-}03x + 7.080E\text{-}03 \quad r^2 = 9.872E\text{-}01$

\+ N'

Figure 6.17b

Spud Can Exposed 0.4m/s

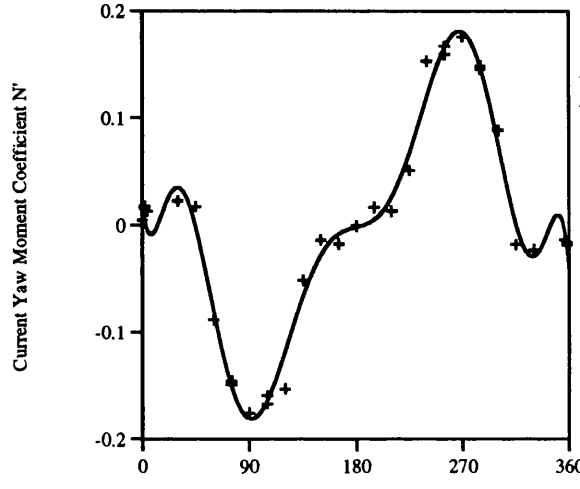

$y = -5.263E\text{-}20x^9 + 8.486E\text{-}17x^8 - 5.678E\text{-}14x^7 + 2.037E\text{-}11x^6 - 4.216E\text{-}09x^5 + 5.027E\text{-}07x^4 - 3.223E\text{-}05x^3 + 9.358E\text{-}04x^2 - 9.166E\text{-}03x + 1.997E\text{-}02 \quad r^2 = 9.799E\text{-}01$

\+ N'

Figure 6.17c

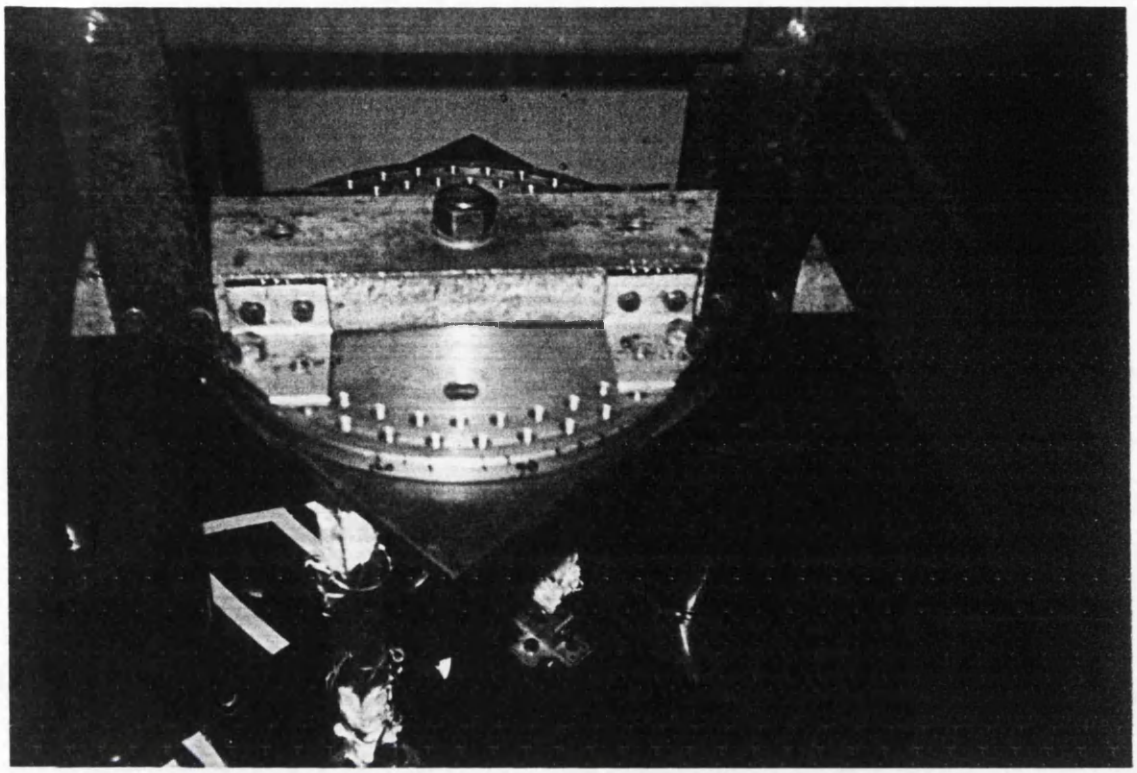

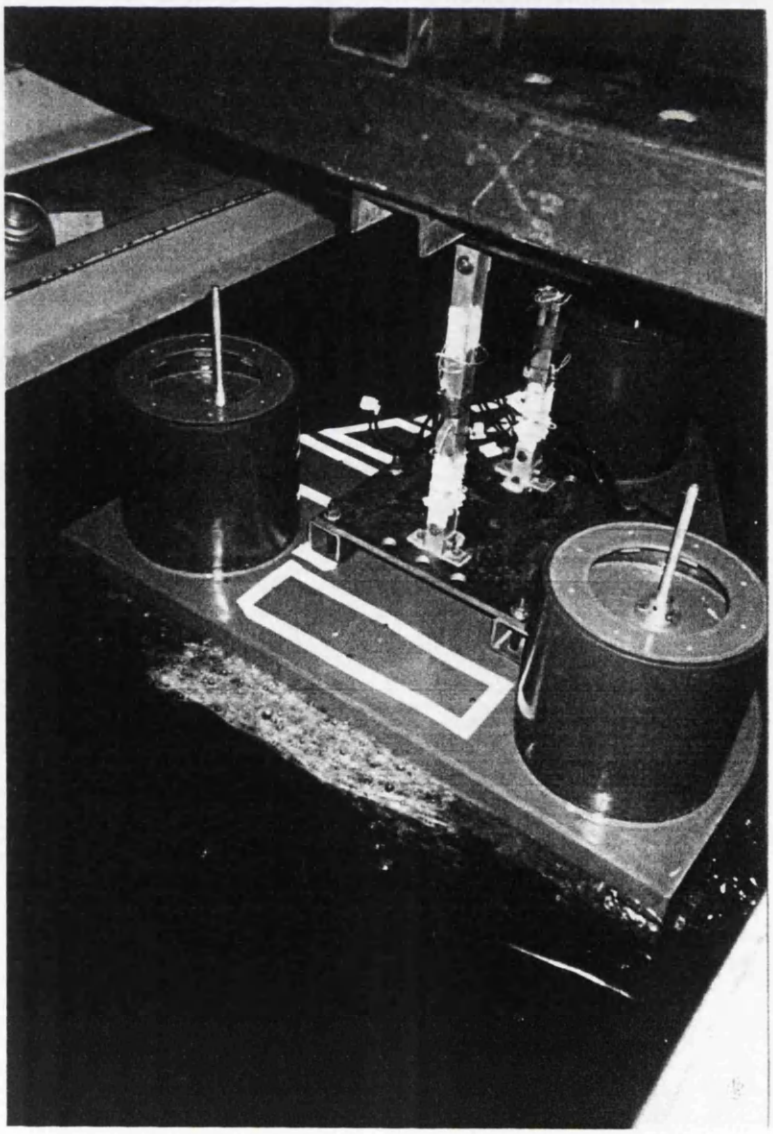

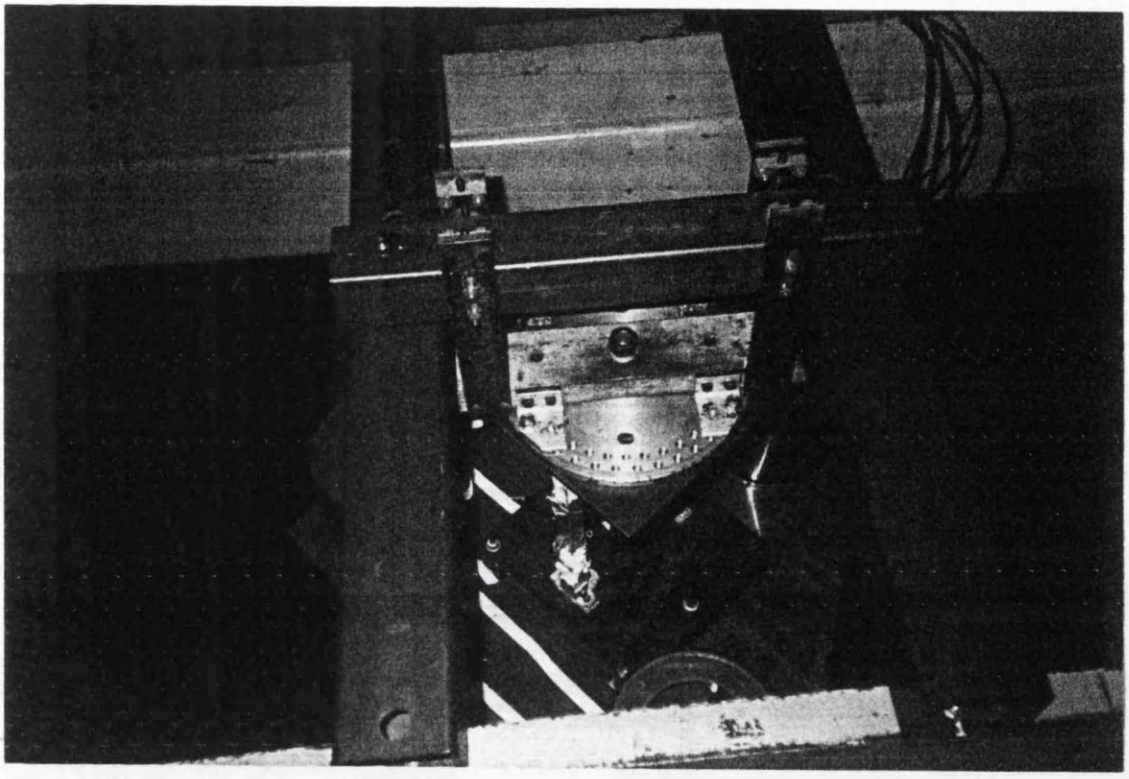

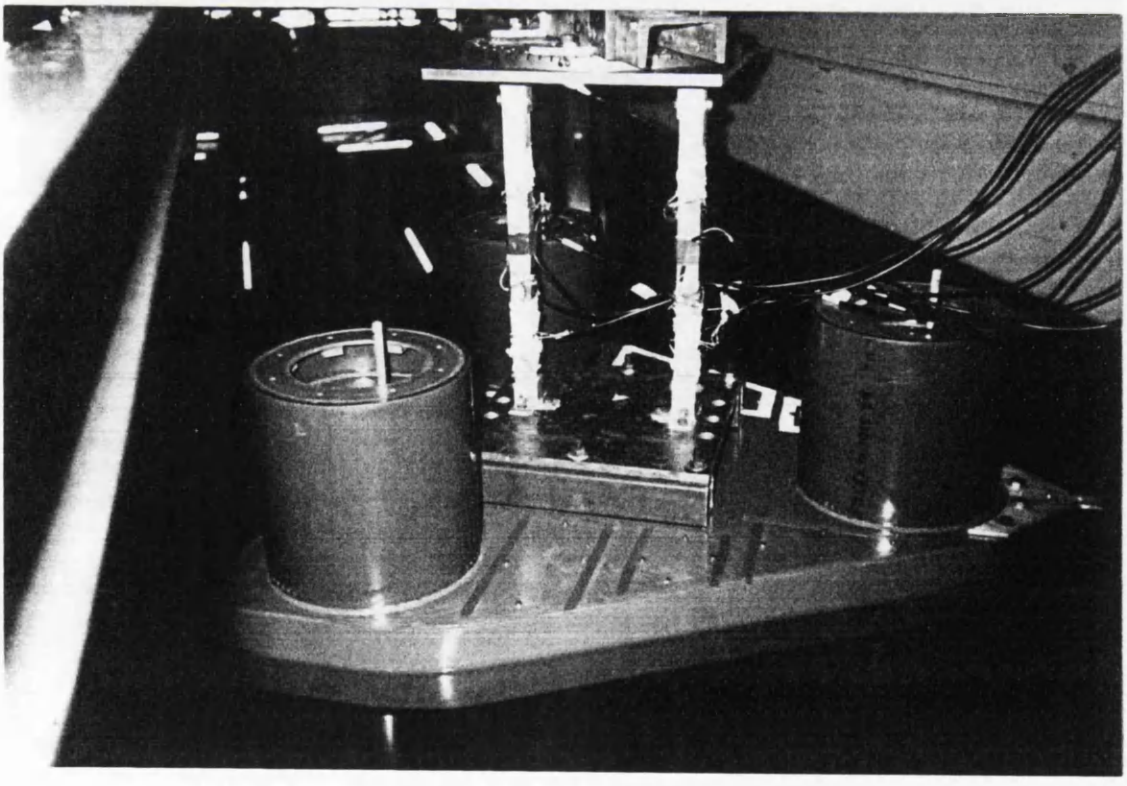

Chapter Seven.

Theoretical and Simulation Towing Studies.

7.1 Introduction and Literature Review.

It is necessary in towing operations to determine the directional stability of tow configurations from the aspects of safety and economy. Unstable motions in crowded seaways and canals may result in collisions and capsizing. It is also important as minimum resistance is experienced when the vessel tows in a straight line. When the towed vessel yaws the speed of the whole tow is reduced and the increased tow rope tension may also cause fatigue and breaking of the tow line.

The understanding and prediction of towed system behaviour has developed steadily from the early work of Strandhagen et al. in 1950, Ref. 7.1. Using a linear theoretical approach the authors developed the mathematical formulation to predict the directional stability of single point towing systems and this is detailed in the following section and Appendix H. In the mid to late 1970's, studies in Japan furthered the understanding of towing through the work of Takekawa et al., Ref. 7.2 and Tanaka et al. Ref. 7.17. These authors under took experimental studies of the effects of skegs and bridles on the directional stability of towed barges. Arguably the major contribution of this period in Japan was produced by Lim, Ref. 7.9. In this work on multi vessel tow systems, Lim presented equations for the prediction of the directional stability of tow systems. Studies were also conducted to predict the conditions for steady turning of the tow systems with experiments. He also considered the effects of shallow and restricted water on the towed system behaviour. There have been several experimental investigations on the towing of barges since by Latorre et al., Refs. 7.12, 7.13, 7.14 and 7.18. These experimental investigations are very useful in increasing our knowledge of towing but are expensive and are often limited due to the length of the testing facilities.

Due to the evolution in computing over the last two decades,

significant progress has been made in the prediction of tow system behaviour using theoretical and simulation models. Bernitsas et al. Refs. 7.3, 7.4 and 7.19 have developed non linear prediction methods employing bifurcation theory in the study of single point and multi point tow and mooring systems. This work has also been augmented with simulation studies employing the elastic tow rope of Ref. 7.11. The particular towing simulation model detailed in Ref. 7.3 assumes that the tow vessel advances along a straight path and the heading is unaffected by the towed vessels motions. There have been various other tow rope simulation models published some with catenary solutions. A very different model common to Japanese simulation studies is the rigid tow rope model, Kijima et al. Ref. 7.8, which is detailed in this chapter.

The elastic tow simulation model developed and described in this chapter is a hybrid of the two simulation models described above. It employs the best features of the two models and as a result it has enabled the study of wind loading and bridle towing. It will also be possible to develop this model to predict the conditions for the steady turning of a tow system. A two tug towing simulation and catenary solutions are also possible.

In this chapter, a study of the directional stability of three single point towing systems is presented using both a linear theoretical approach and using manoeuvring simulation. The first tow system is a tug towing a vessel of similar size, Vessel A. The second tow system is the tug towing Vessel B, a Mariner hull form used in Ref. 7.3. This vessel is then used in a theoretical study of the effects of shallow water on the directional stability of the tow system. The change in the linear manoeuvring derivatives were obtained from the Kijima shallow water correcting factors Ref. 2.5, detailed in Appendix B. The third vessel is a heavy lift vessel or barge type vessel and a study is carried out with and without the skeg of Chapter Five for this system. The skeg derivatives are added to the linear hull derivatives in the same method as Jacobs, Ref. 5.2. The theoretical study uses the classical Routh Hurwitz stability criteria, Refs.

2.1, 7.1, 7.2 and this stability analysis is then extended in the same manner as Bernitsas, Refs. 7.3, 7.4.

The conditions which result in stable and unstable tow configurations from this theoretical analysis for Tow Systems B and C are then placed in the two tow simulation models and are compared with and without wind loading. Further studies are conducted on the elastic model only for the effects of location of the towed vessel superstructure. The elastic tow rope model in then extended to study the tow system behaviour with a bridle. Both the tow rope models require the use of an automatic pilot to keep a steady straight course. The equations for the hull, propeller, rudder and the rigid tow rope forces used in the formulation are those commonly found in many Japanese manoeuvring simulation studies. The chapter will conclude with discussions and some recommendations for towing operations. It is emphasised that the theoretical and simulation studies presented here are for wet towing of conventional hull forms. The study of the wet towing of jack ups was not conducted as it was not possible to obtain the necessary linear rotary manoeuvring derivatives.

7.2.1 Directional Stability of a Towed System.

The tow system for the theoretical directional stability study is shown in figure 7.1a. The figure shows a towed vessel after it has deviated from its steady course and the path of the tow ship. The steady course conditions assume the tow and towed vessel's to advance along a straight path with velocity U where the yaw angles of both vessel's are zero. The origin of the towed vessel is located at its centre of gravity. The tow vessel is assumed to remain on the steady course and to maintain a steady velocity even after the towed vessel has began to yaw. The motion is considered to take place in the horizontal plane. Any possible roll or pitch of either the tow or towed vessel is assumed to have no influence on the yawing motion. The towed vessel is without an active rudder or propeller. The tow line is assumed massless, inextensible and lies in the plane of motion. Most important is that yaw angles and velocities remain small.

These assumptions are necessary to linearise the problem.

The equations of motion for the towed vessel can be written with reference to the body axes as,

$$m_X\dot{u} - m_Y vr = X_H + T\cos(\varepsilon_0 - \theta_1) \qquad 7.1a$$

$$m_Y\dot{v} + m_X ur = Y_\beta\beta + Y_r r + T\sin(\varepsilon_0 - \theta_1) \qquad 7.1b$$

$$I_Z\dot{r} = N_\beta\beta + N_r r + Tx_P\sin(\varepsilon_0 - \theta_1) \qquad 7.1c$$

The linear derivatives above should contain the contributions of the skeg derivatives if the skeg is included in the theoretical analysis. The method of Jacobs is used to obtain the skeg derivatives as detailed in Chapter Five. The equations 7.1 when linearised and the determinant found, produce the conditions of equations 7.3 and 7.4 for directional stability of the towed system. A full description is given in the Appendix H.

$$A = \frac{Y_\beta}{m_Y u} - \frac{N_r}{I} \qquad 7.2a$$

$$B = \frac{N_\beta(Y_r - m_X u) - Y_\beta N_r}{I_Z m_Y u} + \frac{T}{I_Z l}\left(\frac{I_Z}{m_Y} + x_P{}^2 + x_P l\right) \qquad 7.2b$$

$$C = \frac{T}{I_Z m_Y}\left[-\frac{1}{u}(N_\beta - x_P Y_\beta) + \frac{x_P}{l}(Y_r - m_X u + m_Y u) + \frac{x_P}{ul}(x_P Y_\beta - N_\beta) - \frac{N_r}{l}\right] \qquad 7.2c$$

$$D = \frac{T}{I_Z m_Y l}(x_P Y_\beta - N_\beta) \qquad 7.2d$$

The above equations are in a dimensional form. If the tow system is directionally stable then all the roots must either be negative real numbers

or complex numbers with negative real parts. This requirement will be fulfilled if equations 7.2 meet the following 4 requirements,

$$A,B,C,D > 0 \qquad 7.3$$

and the additional requirement,

$$ABC - C^2 - A^2D > 0 \qquad 7.4$$

The last condition, equation 7.4, is commonly called the Routh Hurwitz Stability criteria. If these 5 conditions are satisfied then the towed vessel will tend to assume a steady straight course.

The stability criteria analysis can be extended following the work of Bernitsas, Refs. 7.3, 7.4, 7.12-7.14. In single point towing, the most important parameters are the tow point attachment, the tow rope length and the tow rope tension which are functions of the tow velocity. If we rewrite the equations 7.2 in a form where functions of tow rope tension have subscript 1 and the ratio of tow rope tension/tow rope length have subscript 2 then,

$$A = A_0 \qquad 7.5a$$

$$B = B_0 + T\left(B_1 + \frac{B_2}{l}\right) \qquad 7.5b$$

$$C = T\left(C_1 + \frac{C_2}{l}\right) \qquad 7.5c$$

$$D = \frac{T}{l}D_2 \qquad 7.5d$$

The terms in these equations are then written as,

$$B_0 = \frac{N_\beta(Y_r - m_X u) - Y_\beta N_r}{I_Z m_Y u} \qquad 7.6a$$

$$B_1 = \frac{x_P}{I_Z} \qquad 7.6b$$

$$B_2 = \frac{1}{m_Y} + \frac{x_P^{\,2}}{I_Z} \qquad 7.6c$$

$$C_1 = \frac{-1}{I_Z m_Y u}(N_\beta - x_P Y_\beta) \qquad 7.6d$$

$$C_2 = \frac{x_P}{I_Z m_Y}(Y_r - m_X u + m_Y u) + \frac{x_P}{I_Z m_Y u}(x_P Y_\beta - N_\beta) - \frac{N_r}{I_Z m_Y} \qquad 7.6e$$

$$D_2 = \frac{1}{I_Z m_Y}(x_P Y_\beta - N_\beta) \qquad 7.6f$$

It has be shown in Refs. 2.1, 7.3, that A is always greater than zero. If we examine D, we find that the condition where D>0 is true if,

$$x_P > \frac{N_\beta}{Y_\beta} \qquad 7.7$$

We will call the above condition R1. It is noted that if R1 is satisfied then condition C will also be satisfied, Ref. 7.3. The Routh Hurwitz criteria, equation 7.4 can be rewritten in the following form as,

$$T\alpha_1 + \alpha_2 > 0 \qquad 7.8$$

where on expansion,

$$\alpha_1 = A_0B_1C_1 - C_1^2 + \frac{1}{1}(A_0B_1C_2 + A_0B_2C_1 - 2C_1C_2) + \frac{1}{1^2}(A_0B_2C_2 - C_2^2) \qquad 7.9a$$

$$\alpha_2 = A_0B_0C_1 + \frac{1}{1}(A_0B_0C_2 - A_0^2D_2) \qquad 7.9b$$

It can be deduced that α_1 will always be positive Ref. 7.4, and therefore the following condition R2, should be satisfied.

$$T > \frac{-\alpha_2}{\alpha_1} \qquad 7.10$$

The right hand side of the equation is referred to as the critical tow rope tension and if it is negative then R2 is satisfied.

7.2.2 Shallow Water.

The shallow water study was conducted for two water depth to draft ratios of 3 and 1.5 for the Mariner hull form only, System B . The towed tug and heavy lift barge type vessel were not considered as appropriate vessels with which to apply the Kijima shallow water correcting factors. It was stated previously that the empirical deep water derivatives apply to high block coefficient hull forms. As the shallow water derivatives will be affected greatly by scale effects, any results obtained for a barge form for shallow water may be suspect. The changes to the linear deep water manoeuvring derivatives were obtained from the Kijima shallow water correcting factors given in Appendix B. These new derivative values for the depth to draft ratios are shown in Table 7.2. The increase in hull resistance or tow line tension, was determined from the approach proposed by Schlicting detailed in Ref. 7.5. The increase in the coefficients of accession to inertia were obtained from Ref. 7.20. No simulations were conducted for the effect of shallow water as data essential for the simulations is unfortunately unattainable.

7.2.3 Effect of a Skeg.

The effect of a skeg on the directional stability is investigated on the heavy lift vessel hull form, System C. The hull is essentially a barge form and is therefore directionally unstable. The addition of the skeg for increased directional stability requires us to modify the hull derivatives

using the method of Jacobs and was previously detailed in Chapter Five with the skeg dimensions remaining the same.

7.3. Simulation Model and Vessel Dimensions.

The configurations for the single point tow simulations were decided from the results of the theoretical study. The simulation variants include tow rope model, tow point location on tow and towed vessels, tow rope length, elastic tow rope type and vessel speed. Additionally studies on inclusion of a skeg, wind velocity, wind angle and location of superstructure are investigated. Additional simulations were conducted for an elastic bridle model.

In order to give the tow simulation some degree of reality it is necessary that we consider the limits of the bollard pull of the tug and the limit of the tow rope diameters. The dimensions of the tug used in the simulations are based on the escort tug 'Thorax' of Ref. 7.6. A review of literature showed the largest bollard pull of present tug designs are of the order of 90 tonnes. In the simulation of the mariner and heavy lift vessel, the resistance at moderate towing speeds will exceed this value. If the towed system is operating outside the limits of the tug bollard pull then the simulation results will become inaccurate. An example is the size of the rudders which are a function of the tug dimensions, may be inadequate to control the tow system. There will also be an increased yawing of the tow vessel and hence rudder activity. In such cases the tow velocity should be reduced or the size of the tug should be increased. In towing of offshore rigs, anchor handling tug supply vessels may also be employed, Ref. 7.7. These vessels can offer the higher bollard pulls required. Additionally we must consider the maximum tow rope diameters which appear to be around 80mm. This can be due to the design limits of the handling equipment on board the tugs. In the case of a single tug towing a large vessel at moderate speeds, the tension in the tow rope would exceed the recommended load levels and the rope would need to be replaced more frequently as it would become damaged and unsafe for

towing operations. The values of the tow rope diameters given in Table 7.3 for the elastic tow rope simulations assume the towed vessel resistance to be equal to 10% of the minimum breaking strength of the tow rope.

7.4.1 Forces acting on the Tow System.

The total forces and moments acting on the tow and towed vessels include contributions from hull, rudder, propeller, tow line tension and external forces due to wind. These forces are shown with subscripts H, R, P, and E. The tow rope forces are included in the external forces. We assume the towed vessel has no propulsion or rudder control and the tow points lie along the centre lines of the vessels. The tow vessel can navigate a straight course by activating an automatic pilot to control its heading.

The forces and moments acting on the tow vessel are,

$$X = X_P + X_H + X_R + X_E$$

$$Y = Y_H + Y_R + Y_E \qquad 7.11$$

$$N = N_H + N_R + N_E.$$

The towed vessel forces and moments are identical except that there is no contribution from propeller forces in the surge equation or rudder forces.

7.4.2 Hull Forces.

7.4.2.1 Surge Forces.

The hull forces acting on the vessels in surge are written in the same form as equation 2.9

$$X_{Hi} = -m_{xi}\dot{u}_i + (m_{yi} + X_{vri})v_i r_i + X_i(u_i) \qquad 7.12$$

If we consider the same assumptions stated in Chapter Two then the non dimensionalised surge hull forces can be written as,

$$X'_{H_i} = m'_{y_i}(1-C_{m_i})r'_i \sin\beta_i - C_{t_i}\left(1.7+\frac{B_iC_{B_i}}{D_i}\right) \qquad 7.13$$

In much of the Japanese literature on towing Ref. 7.8, the increased hull resistance due to the drift angle is expressed more simply as,

$$X'_{Hi} = -R'_i(1+13\beta_i{}^2)$$

where,

$$R'_i = C_{t_i}\left(1.7+\frac{B_iC_{B_i}}{D_i}\right)$$

7.4.2.2 Sway and Yaw Manoeuvring Derivatives.

The hull sway force and yaw moments acting on the tow and towed vessels are described by the vessels manoeuvring derivatives. These forces are represented by the nonlinear deep water derivatives already described.

7.4.2.3 Propeller Forces.

The propeller model described in Chapter Two is again used in the towing simulation study. The propeller chosen is a Wageningen Series B-4, constant pitch, with a P/D ratio of 0.8. The area ratio is 0.7. The data was obtained from reference 2.13. The propulsion characteristics of the tug are C_1=0.366, C_2=-0.374, C_3=-0.063. It is noted that this form of modelling the propulsive forces is common to a single vessel simulation. In the Japanese literature on towing simulation, the propeller forces are modelled as a balance of the total resistance of the tow system and is less sophisticated, Refs. 7.8, 7.9. It is also noted that the rudder model requires knowledge of the propeller revolutions n, pitch P and diameter D_P and so it is as easy to

employ the former propulsion model than develop the latter.

7.4.2.4 Rudder Forces.

A detail of the formulation of the rudder force and moment equations can be found in Chapter Two. The rudder area is again determined from the DNV minimum rudder area equation in the case of a single conventional vessel, equation 2.29. The tug used in the simulation model is based on the escort tug 'Thorax' of Ref. 7.6. The actual vessel is a Voith tractor and has no rudder but it was necessary to include a rudder in the design for simulation. The minimum rudder area obtained from equation 2.29 was increased by 130% and corresponds to 4.5 % of the product of length and draft. A suggested design value of the rudder area for tugs as a percentage of LT is recommended between 3 and 6% which is given in Ref. 7.10.

7.4.2.5 Tow and Towed Vessel Tow Rope Forces.

The rigid and elastic tow rope models introduced in Section 7.1 employ different methods to determine both the tension of the tow rope and the tow rope angle and these are described in the section 7.5.

The formulation of the non dimensionalised tow rope forces acting on the tow and towed vessels is common to both the rigid and elastic tow rope models. With reference to the towed system figure 7.1b, when the towed vessel moves away from a straight path, we can use empirical expressions to describe the component non dimensionalised tow line forces in surge, sway and yaw on the towed vessel as,

$$X'_{T1} = T'_1 \cos\varepsilon_1 \qquad 7.14.a$$

$$Y'_{T1} = T'_1 \sin\varepsilon_1 \qquad 7.14.b$$

$$N'_{T1} = \frac{f_1}{L_1} T'_1 \sin\varepsilon_1 \qquad 7.14.c$$

The non dimensional towed vessel tow rope tension for the rigid tow rope model is determined from equation 7.18. In order to determine the component tow rope forces acting on the tow vessel we must first dimensionalise the tow rope tension with respect to the towed vessel and then non dimensionalise once again with respect to the tow vessel.

$$T'_0 = -T'_1 \frac{L_1 D_1 U_1^2}{L_0 D_0 U_0^2} \qquad 7.15$$

The components of the tow rope force acting on the tow vessel can be represented by,

$$X'_{T0} = T'_0 \cos(\theta_0 - \theta_1 - \varepsilon_1) \qquad 7.16.a$$

$$Y'_{T0} = -T'_0 \sin(\theta_0 - \theta_1 - \varepsilon_1) \qquad 7.16.b$$

$$N'_{T0} = -T'_0 \frac{a_0}{L_0} \sin(\theta_0 - \theta_1 - \varepsilon_1) \qquad 7.16.c$$

a_0 distance between LCG and aft tow point on the tow vessel (-ve aft).

f_1 distance between LCG and forward tow point on the towed vessel.

7.5.1 Rigid and Elastic Towing Simulation Models.

The essential differences between the rigid and elastic tow rope models stem from the different methods of determining the tow rope tensions and the angle which the tow rope makes with the towed vessel. The formulations for the simulation programs are therefore very much different and some of these programming requirements are discussed in the following sections. In both the tow rope models we assume the towed ship systems are floating on the surface of still water. Actions due to waves and ship wakes are neglected. We are further required to employ an automatic pilot which will keep the tow vessel on a straight course. The

rudder angle will thus change to correct the heading angle of the tow vessel. The results obtained from the tow simulation without an automatic pilot are unrealistic not only in the output obtained but also in the events of an actual tow where the rudder will be constantly employed to keep a straight course.

7.5.2 Rigid Tow Rope Model.

In the rigid tow rope model, the velocity of the tow vessel is determined using the formulation detailed in Chapter Two and Appendix A with the NAG routine Ref. 2.16. The velocity of the towed vessel is determined from a knowledge of the motions of the vessels and is directly related to the tow vessel velocity, see Appendix I and Ref. 7.9. The towed vessel velocity is not directly influenced by the tow rope tension, equation I 6.

7.5.2.1 Rigid Tow Rope Angle.

The tow rope angle in the rigid model is obtained from the tow rope angular velocity detailed in Appendix J and Ref. 7.9.

$$\dot{\varepsilon}_1 = \frac{1}{l_T}\left\{\begin{array}{l} \overline{U}_1\left[\sin(\varepsilon_1+\beta_1) - f_1\frac{r_1'}{L_1}\cos\varepsilon_1 - \frac{r_1' l_T}{L_1}\right] \\ -\overline{U}_0\left[\sin(\theta_1+\varepsilon_1-\theta_0+\beta_0) - a_0\frac{r_0'}{L_0}\cos(\theta_1+\varepsilon_1-\theta_0)\right] \end{array}\right\} \qquad 7.17$$

The NAG routine is then used to obtain the tow rope angle and is represented by the simplified Euler integration below.

$$\varepsilon_{1i} = \varepsilon_{1i-1} + \dot{\varepsilon}_{1i}\Delta t$$

The position of the towed vessel in the global coordinate system is found directly from a knowledge of the position of the tow ship, the tow point locations, the tow rope length and the angle of the tow rope as shown in equations 7.19.

7.5.2.2 Rigid Tow Rope Force.

The formulation of the tow rope forces with the rigid tow rope includes the contributions for wind loading acting on the towed system. The rigid tow rope assumption is crude and assumes the tow rope is always in tension although the tension will vary. It is also assumed that the tow rope is massless, inextensible and has a straight line configuration when projected in the horizontal plane. The rigid tow rope model is common in many Japanese publications on towing, Refs. 7.8, 7.9 and would appear not to permit the study of the tow system behaviour for a turning manoeuvre. It will only allow a straight tow. With reference to the towed system figure 7.1b, when the towed vessel moves away from this straight path, we can use the empirical expression based on equation 7.13 to describe the non dimensionalised towline tension as,

$$T_1' = -m_{y1}'(1-C_{m1})r_1' \sin(\beta_1+\varepsilon_1) + C_{t1}\left(1.7+\frac{B_1 C_{B1}}{D_1}\right) - \frac{X_{W1}'}{\cos\varepsilon_1} \qquad 7.18$$

The first term describes the oblique motion of the towed vessel due to drift and tow rope angle. The second term is the resistance of the vessel advancing along a straight path. The third is the contribution of wind resistance to the tow rope tension. It is noted that the X wind force acting on the towed vessel is included in the tow rope tension. The wind forces and moment also act on the tow and towed vessels and are included externally in the equations of the force summation.

7.5.3 Elastic Tow Rope Model.

In the elastic tow rope simulation model we determine the velocity of the towed vessel with the same formulation as the velocity of the tow vessel detailed in Chapter Two and Appendix A. The positions of the tow and towed vessels is dependent only upon the summations of the forces and moments acting on the system. The component forces of the tow rope on the tow and towed vessels for the elastic tow rope are the

same as the component force equations in the rigid tow rope, equations 7.14 and 7.16. The tension in the tow rope is not found from equation 7.18 but from a knowledge of the positions of the tow point locations on the vessels in the global coordinate system. The towed vessel of the elastic model therefore has greater 'independence' than the towed vessel in the rigid tow rope model it is able to have zero tension. The form of the elastic tow rope model is the same as that employed in the towing studies of Bernitsas et al, Refs. 7.3, 7.4. The tow rope is considered as massless and buoyant and that it is 'used' or 'stabilised', Ref. 7.11. The definition of a 'used' rope is one which has been loaded to 20% of its breaking strength for fifty cycles. There are three different tow ropes considered, each with varying properties. These ropes are nylon, polypropylene, and polyester. The nylon rope has different properties when it is wet and therefore only the wet rope is applicable in a towing simulation. The polyester rope has similar strength properties to nylon and does not shrink and is approximately twice as stiff. Polypropylene is the weakest of the three and is less resistant to abrasion. The average breaking strength for fully shrunk, wet nylon ropes are about 15% less than the values for new dry nylon ropes. The values of the average breaking strength for the three ropes for various rope diameters are given in Table 7.3. Also shown in this table are the values of minimum breaking strength which are approximately 15% lower than the average breaking strength values. Long term loads of 40% breaking strength for 10^4 cycles has been shown to be detrimental to the tow ropes and at 10^5 cycles, failure is expected. The static loading recommendations state the working load should never exceed 20% of the tow rope breaking strength but danger of abrasion and cutting can lower this value. The simulation tow rope diameters given in Table 7.4, assume a towed vessel resistance as 10% of the minimum breaking strength for the tow conditions. The relationships between the rope diameter and minimum breaking strength for each rope are shown in figures 7.2. Using these power relationship derived for each rope we can then easily determine the required rope diameter. The values of the tow

rope diameter will therefore be conservative due to the 10% load and the minimum breaking strength. As noted earlier, the maximum tow rope diameter which tugs are able to handle appears to be about 80mm diameter. Thus a single tug towing a larger vessel will induce higher tensions in the tow ropes than may be designed for in normal operations.

7.5.3.1 Elastic Tow Rope Angle.

The tow rope angle, the length and hence the strain and the tension of the tow rope is dependent upon the relative positions of the tow points on the tow and towed vessels. In order to determine the tow rope angle with respect to the towed vessel we use the relationship of the tow and towed vessels positions,

$$Y_1 = Y_0 - a_0 \sin\theta_0 - l_T \sin(\theta_1 + \varepsilon_1) - f_1 \sin\theta_1 \qquad 7.19.a$$

$$X_1 = X_0 - a_0 \cos\theta_0 - l_T \cos(\theta_1 + \varepsilon_1) - f_1 \cos\theta_1 \qquad 7.19.b$$

and rearranging,

$$l_T \sin(\theta_1 + \varepsilon_1) = Y_0 - a_0 \sin\theta_0 - f_1 \sin\theta_1 - Y_1 \qquad 7.20a$$

$$l_T \cos(\theta_1 + \varepsilon_1) = X_0 - a_0 \cos\theta_0 - f_1 \cos\theta_1 - X_1 \qquad 7.20b$$

$$\tan(\theta_1 + \varepsilon_1) = \frac{Y_0 - a_0 \sin\theta_0 - f_1 \sin\theta_1 - Y_1}{X_0 - a_0 \cos\theta_0 - f_1 \cos\theta_1 - X_1} \qquad 7.21$$

$$\varepsilon_1 = \tan^{-1}\left(\frac{Y_0 - a_0 \sin\theta_0 - f_1 \sin\theta_1 - Y_1}{X_0 - a_0 \cos\theta_0 - f_1 \cos\theta_1 - X_1}\right) - \theta_1 \qquad 7.22$$

X_i, Y_i are the X and Y positions of the centre of gravity of the vessels in the earth fixed coordinate system. (i=0,1)

7.5.3.2 Elastic Tow Rope Length and Tension.

The true tow rope length determined from the relative positions of the tow points in the global coordinate system is obtained by squaring equations 7.20a and b and then adding to give,

$$l_T = \sqrt{(X_0 - a_0\cos\theta_0 - f_1\cos\theta_1 - X_1)^2 + (Y_0 - a_0\sin\theta_0 - f_1\sin\theta_1 - Y_1)^2} \qquad 7.23$$

From a knowledge of the true tow rope length we are then able to determine the strain in the tow rope,

$$\varepsilon_w = \frac{l_T - l_T}{l_T} = \frac{\Delta l_T}{l_T} \qquad 7.24$$

If the distance between the tow points on the two vessels is less than the initial tow rope length, l_T then there will be no strain in the tow rope and hence no tension.

ε_w working strain in the tow rope
l_T variable tow rope length. (This is a function of time).
l_T initial tow rope length unstrained and stabilised.

The tension force can be described by the nonlinear equation of the form (equation 7.25) where A and m are constants of the tow rope properties and were determined experimentally.

$$\tau = A(\varepsilon_W)^m \qquad 7.25$$

τ Specific Tension= T / S_b
S_b Breaking Strength
T Actual Tension
A, m Experimentally determined constants.

The tension in the tow rope is therefore,

$$T = S_b A(\varepsilon_W)^m \qquad 7.26$$

The experimental constants A and m, for each tow rope type are reproduced from Ref. 7.11 and are,

nylon(wet): $\tau = 9.78\ (\varepsilon_W)^{1.93}$

nylon(dry): $\tau = 14.2\ (\varepsilon_W)^{1.71}$

polyester: $\tau = 176\ (\varepsilon_W)^{1.86}$

polypropylene: $\tau = 40.9\ (\varepsilon_W)^{1.73}$

7.6 Towing with a Bridle.

In towing operations a bridle is often used as opposed to a single towing line. The theoretical approach of Routh Hurwitz using linear theory cannot be used to describe the effect of the bridle on the directional stability. This is shown below and similar conclusions were drawn by Lim, Ref. 7.9. The equations of motion for the towed vessel may be written with reference to figure 7.1.c as,

$$m_X\dot{u} - m_Y vr = X_H + T_1\cos\alpha_1 + T_2\cos\alpha_2 \qquad 7.27a$$

$$m_Y\dot{v} + m_X ur = Y_\beta\beta + Y_r r + T_1\sin\alpha_1 - T_2\sin\alpha_2 \qquad 7.27b$$

$$I_Z\dot{r} = N_\beta\beta + N_r r + T_1\frac{y}{2}\cos\alpha_1 + T_1 x_P\sin\alpha_1 - T_2\frac{y}{2}\cos\alpha_2 - T_2 x_P\sin\alpha_2 \qquad 7.27c$$

$T_{1,2}$ Tensions in the Bridle ropes

$\alpha_{1,2}$ Angle of Bridle ropes

If we assume $T_1 \approx T_2$ and $\alpha_1 \approx \alpha_2$ then the sway and yaw equations above reduce to the single towed vessel equations of motion of Appendix H.

It has been shown that linear theory is unable to describe the effects of a bridle on the directional stability of a towed vessel. The

simulation model has therefore been extended in an attempt to show the effects of the bridle on the stability of the tow configuration. The simulations will be conducted to investigate the effects of varying the length of the bridle, the transverse location of tow points and the distance of the tow points from the LCG of the towed vessel. The effects of the skeg was also investigated.

In the bridle simulation model it is assumed that the bridle tow points are located at the same longitudinal distance from the towed vessel LCG. The tow rope is also assumed to imaginarily extend to the centerline of the towed vessel at the same longitudinal distance where the bridles are fixed to the vessel. The angles of the bridles are then determined from the geometrical conditions and the tow rope angle which are shown in figure 7.1c. As the tow rope stretches and contracts, it is assumed the point where the tow rope is attached to the bridle ropes also extends under the same strain. The bridle angles will therefore change accordingly. It will become apparent that there will be no equilibrium of tension between the bridles and the tow rope due to the non linearities of the elastic rope dynamics. The tension in the bridle ropes are therefore determined from a knowledge of the tow rope tension, the tow rope angle and the bridle angles. The equations from the equilibrium of tension are,

$$T_1 \cos\varepsilon_1 = T_{11}\cos\alpha_1 + T_{12}\cos\alpha_2 \qquad 7.28a$$

$$T_1 \sin\varepsilon_1 = T_{11}\sin\alpha_1 - T_{12}\sin\alpha_2 \qquad 7.28b$$

After solving these equations simultaneously the bridle tensions are determined from,

$$T_{11} = \frac{T_1 \sin(\varepsilon_1 + \alpha_2)}{\sin(\alpha_1 + \alpha_2)} \qquad 7.29$$

$$T_{12} = \frac{T_1 \cos\varepsilon_1 - T_{11}\cos\alpha_1}{\cos\alpha_2} \qquad 7.30$$

The bridle ropes can be loaded with higher tensions than the tow ropes. This is shown in figures 7.29c-7.32c and is due to the larger oblique towing angles. It is suggested therefore that the bridle rope diameters are different from the tow rope diameter. It would seem more sensible and economical to design the tow system to allow the bridle rope to break first and replace them rather than a complete tow rope. If the bridle rope diameters are not considered carefully for a given configuration then the tow rope tensions may cause the tow rope to break. The bridle tension equation of 7.29 can be used to estimate the maximum bridle rope diameters in the same manner the tow rope diameters were determined from figures 7.2. If we write the ratio of the tow rope diameters as,

$$\frac{\phi_T}{\phi_B} = \frac{a_T S_{bT}^{b_T}}{a_B\left[\frac{S_{bT}\sin(\alpha_2+\varepsilon_1)}{\sin(\alpha_1+\alpha_2)}\right]^{b_B}} \qquad 7.31$$

If the bridle rope and the tow rope have the same properties then 7.31 reduces to,

$$\phi_B = \phi_T\left[\frac{\sin(\alpha_2+\varepsilon_1)}{\sin(\alpha_1+\alpha_2)}\right]^{b} \qquad 7.32$$

ϕ_B Bridle Diameter

ϕ_T Tow Rope Diameter

$\alpha_{1,2}$ Bridle Angles

ε_1 Tow Rope Angle

b Constant of Elastic Rope. This constant will depend upon the rope type and the type of loading i.e. average or minimum breaking strength and the design loads on the ropes as 10% etc. (See Figures 7.2)

The bridle diameters used in the simulations obtained from equation 7.32 are given in Table 7.5.

7.7 Discussion of Results.

7.7.1 Theoretical Analysis.

Three tow systems are analysed. The details of these systems are given in Table 7.1. The results for the theoretical analysis are given in figures 7.3-7.6. The figures show the directional stability for variations of tow point location with tow line length. The effects of tow velocity, vessel types, shallow water and the inclusion of skeg are studied. The tow rope length varies as a function of the tug length. The towing velocities for the systems were analysed at 3, 5, and 7 m/s (5.84, 9.72, 13.6 knots).

In using the Routh Hurwitz Stability Criteria figures 7.3a, 7.4a, the stable region is determined as any condition which gives the Routh Hurwitz criteria greater than zero and tow point greater than condition R1, equation 7.7.

The R2 Stability Criteria figures show the stable region as any condition where the tow point location is greater than R1 and additionally lies below the line of towline tension. The vertical axis is measured as tension [KN]. This form of stability diagram therefore gives more insight when compared with the Routh Hurwitz diagram.

7.7.1.1 Tow Point Location.

Generally we can say that the tow stability is sensitive to the location of the tow point. The greatest tow stability occurs at a point just ahead of the condition R1, i.e. on the limit of $x_P > N_\beta/Y_\beta$. This is at 17.42 m forward of the towed vessel LCG for System A, 72.68 m for System B and 63.33m for System C without skegs. The maximum values of $ABC - C^2 - A^2D > 0$ used in the Routh Hurwitz analysis for a given tow rope length occurs along these limits. When the tow point is brought forward, the area of the stability region decreases. This is because A, equation 7.5a is always positive Ref. 7.3, and therefore the minimum value of D remembering D>0, is just ahead of the centre of lateral resistance.

7.7.1.2 Tow Rope Length.

In general, it cannot be said that any increase in the tow rope length will result in a greater degree of directional stability. If the towed vessel is operating in an unstable region a decrease in tow rope length may also take the tow system to a stable domain.

7.7.1.3 Tow Velocity.

In an initial inspection of the results for the variation of velocity for Systems A,B and C, figures 7.3, 7.4, 7.6 it cannot be said in general, that an increase in the tow velocity will increase the region of stability. However if the ratio of residuary resistance to skin friction coefficient given in Table 7.1 is equated to R2 as shown in the equation below we can begin to understand why the region of stability of System A increases while System B decreases marginally with increased tow velocity.

$$\frac{C_r}{C_f} > \frac{-2\alpha_2}{\alpha_1 \rho S U^2 C_f} - 1$$

It can be seen that the residuary resistance coefficient which has the greatest effect on the tow directional stability with the increase in tow velocity.

7.7.1.4 Effect of Water Depth.

The decrease in water depth increases the values of the linear derivatives as can be seen in Refs. 7.14, 7.15. In Table 7.2 it can be seen that the values of the shallow water linear derivatives Y'_β, N'_β, N'_r for H/d=3 are decreasing when compared with their respective deep water derivatives. This behaviour is obviously incorrect and suggests the shallow water correcting factors obtained from Ref. 2.4 and reproduced in the Appendix B are incorrect or are limited in their applicability. The case for the water depth of H/d =1.5 does however give an increase in the magnitude of the derivatives as expected. It is noted the effect of these errors will not affect the R1 condition using the Kijima derivatives as the

correcting factors are the same but it will affect the R2 condition. The increase in the tow rope tension with decreasing water depth will increase the stability region.

7.7.1.5 Effect of Skeg.

The tow System C is analysed further with the addition of the skeg detailed in Chapter Five. The stability figure 7.6.b shows that the skeg has a dramatic effect on the stability of the tow system. The resistance of the vessel remains unchanged as the only contribution to the skeg resistance is from skin friction and this is considered negligible. The addition of the skeg shifts the limit of R1 aft, towards the LCG of the towed vessel as seen in Table 7.1.

7.7.2 Towing Simulation.

The single point tow simulation figures are given in figures 7.7 onwards. These simulations were conducted for tow systems B and C only. The tow conditions simulated can be compared with the corresponding theoretical studies in figures 7.4 a-c and 7.6 a-b for tow point location on the towed vessel and tow rope length and the stable and unstable conditions can be clearly identified. The simulation conditions are given in Table 7.4. The figures for the simulation without wind are identified by a, b and c. The figures a depict the trajectory of the tow and towed vessel in the global coordinate system. Figures b show the tension, propulsion and the hull resistance. The total hull resistance will be equal and opposite to the propulsion. The tension will be equal and opposite the towed vessel resistance. Also shown on these figures are the bridle tensions where applicable. Figures c show the velocity ratio of the vessels, the drift angles and the tow rope angle, the non dimensional angular velocities and the heading angles with automatic pilot rudder deflection. This gives an insight into the system behaviour and shows the activity of the rudder.

7.7.2.1 Time Step.

The effect of the time step was investigated initially to determine which time step would ensure convergence of the results while minimising the cpu time. Various time steps were investigated ranging from 0.05 to 0.5 seconds. The results presented here were based upon the time step for 0.1 seconds. The larger time steps were unsatisfactory as the behaviour of the tow system had not converged.

7.7.2.2 Tow Point Location on Towed Vessel.

The tow points on the towed vessel B were selected as 81.82m and 77.25m for tow rope length of $4L_0$ figures 7.8 and 7.9. Increasing the tow point location decreases the degree of directional stability. If we examine the corresponding R2 figure 7.4b, for the tow system conditions we see the simulation behaviour agrees with the theoretical results. The tow point on the tug is located at its LCG.

7.7.2.3 Tow Rope Length.

A comparison of figures 7.7 and 7.8 show that an increase in the tow rope length has reduced the degree of directional stability. This is also the same result as predicted using the theoretical analysis. However the shorter tow rope length has increased the period of towed vessel oscillations and this could not be predicted by the theoretical analysis. It is important to note that in general, every towing system will not experience an increase in directional stability for decreasing tow rope length and it depends entirely upon the conditions for the tow.

7.7.2.4 Comparison of Towed System Behaviour for the Rigid and Elastic Tow Rope Assumptions.

The conditions of the tow system simulations for the rigid tow rope assumption figure 7.9, were simulated for the three elastic tow ropes as shown in figures 7.10- 7.12. We can see that the rigid tow rope model compares well with the elastic tow rope model. The trajectory figures show the same behaviour as do the figures for the velocity, drift/tow rope angle, angular velocity and heading angles. The automatic pilot rudder

activity shows some noted differences initially but the magnitude and time axis crossing are very similar.

The comparison of rigid and elastic tow rope models is further studied with wind loading on the simulations in sections 7.7.3.1 and 7.7.3.2.

7.7.2.5 Elastic Tow Rope Type.

The variation of elastic tow rope has no effect on the final tow trajectories of the tow and towed vessels, figures 7.10 7.12. The initial disturbances of the tow vessel trajectory and the tow rope tension figures b, are due to the tow system reaching an equilibrium condition for the initial inputs. Decreasing the time step further will reduce these features of the simulations.

7.7.2.6 Tow Velocity.

In figure 7.13 we see that the increased tow velocity of 5m/s does not appear to affect the final trajectory of the tow system simulation. This suggests that trajectory is independent of towing velocity. However if we examine the R2 stability figures 7.4b and c we see that this behaviour is predicted. As indicated previously the tow velocity will affect the residual resistance coefficient and hence the hull forces on the system.

7.7.2.7 Tow Point Location on Tow Vessel.

The simulation for the variation of the aft tow point location - $0.4L_0$, on the tow vessel is given in figure 7.14. The effect of shifting the tow point aft is to destablise the trajectories of both vessels. It is apparent that the dynamics of the tow vessel acts to increase the motions of the towed vessel. The increased motions are due to the tow rope yaw moment on the tow vessel which was previously zero. We are unable to compare simulation with the theoretical study as we assume the tow vessel to have a steady straight course. Increasing the rudder constants should increase the directionally stability of the system.

7.7.2.8 Comparison of Theoretical and Simulation Prediction Methods.

The predictions for directional stability obtained from the simulations and theoretical approaches compare well. The theoretical approaches gives great insight to the directional stability of a single point tow configuration. It is a linear model and does not require a great knowledge of manoeuvring or towing and can easily be computed. The towing simulation model however gives a great deal of information as to the trajectory and magnitude of the motions and forces on the system and is non linear. It requires a powerful computer however and the modular model has several input variables to describe the forces on the system. A knowledge of towing, manoeuvring and computing is therefore essential. It is recommended to use the theoretical study initially to determine the stability regions and then if possible, use a simulation model to define the tow system configuration. The simulation program can be used to model many of the factors which affect the directional stability such as environmental loading, towing with a bridle or manoeuvring devices such as bow thrusters provided that they are modelled accurately.

7.7.3 Wind Loading Effects.

The tow system behaviour with wind loading was studied for tow system C only. The wind loading coefficients for the fully loaded tanker were employed with the load line windage areas of the heavy lift vessel. The initial simulations were conducted with the towed vessel superstructure located aft. These simulations employed the rigid and elastic tow rope models in head, following and beam winds.

Simulations were then conducted for the elastic tow rope model only with a forward superstructure in beam winds.

7.7.3.1 Head and Following Wind.

It is apparent from the trajectory figures that the inclusion of wind is important when considering towing. In figures 7.17 and 7.19 a head

wind will increase the directional stability of the tow. The wind acts to increase the vessel resistance and hence the tow rope tension which will favour R2 stability criteria. The result of this is to increase the region of directional stability.

A following wind will act to decrease the stability region and this is apparent in the trajectory figures of 7.18 and 7.20. The degree of instability will depend upon the system conditions and the wind velocity.

If we compare the trajectories of the head wind simulations figures 7.17 and 7.19, there are apparent differences in the advances of the tow systems. The rigid model advance is approximately 400m behind the elastic over 5000m. The transverse trajectory also show differences but if we consider these against the longitudinal axes then it is clear that such effects are negligible. The figures 7.17c and 7.19c all compare favourably. The following wind figures 7.18 and 7.20 give an excellent match.

7.7.3.2 Beam Winds on Towed System Behaviour.

On first inspection of figures 7.21, 7.22, 7.23 and 7.24 for the condition of an aft superstructure it is apparent that towing in 10 m/s beam winds produces significant lateral shifts of the tow system. The wind acting on the aft superstructure pushes the towed vessel into the wind. The towed vessel then pulls the tow vessel along its own heading.

The rigid tow rope model vessels' transverse shifts are less than the elastic tow rope trajectories. It can be deduced that these differences are a direct result of the relative magnitudes of the vessel course angles. The velocity ratio of the rigid tow rope model has increased slightly while the elastic model is less than unity. The differences in rudder deflection are due to the differences in the heading angles.

7.7.3.3 Trajectory and Location of Superstructure of the Towed Vessel.

The figures 7.25 and 7.26 show the trajectories for a forward superstructure in 10 m/s beam wind for the elastic tow rope model. It is clear the lateral shifts predicted are greatly reduced when compared with figures 7.23 and 7.24 for the aft superstructures. The trajectory figures for

forward superstructure show the towed vessel heading away from the wind and pulling the tow vessel along its course as expected. The towed vessels' trajectories oscillate about the tow vessels' trajectories. This behaviour is very different from the case of an aft superstructure. These differences raised some debate on the possible causes. One possible explanation is linked to the behaviour of the towed vessel drift angle. On the towed vessel with superstructure aft and wind 90 degrees, the drift angle increases in wind fig. 7.23b, when compared with fig. 7.25b. The hull and skeg forces which are functions of drift therefore increase in this condition. The wind is acting in the same sense as the hull moments and the tow rope moment is greatly increased to counter these. If we examine the contributions of the hull, skeg, wind and tow line to the total yaw moment acting on the towed vessel figures d, we see the tow rope acts to produce a net zero yaw moment.

In the condition with the superstructure forward figure 7.25b, the drift angle is decreased when compared with figure 7.23b and the wind is acting against the hull moments. When the superstructure is forward, the required tow rope yaw moment is therefore reduced. The difference in the trajectories for superstructure location is caused by the course angle.

Further work would need to be undertaken to establish the nature of the relationship between the transverse displacement and superstructure location while towing. The greater the control one has over the tow then the less sea room is required for the tow. This will greatly reduce the risk of collisions which can lead to capsize. Such a study will have prove useful and provide insight in the case of wet towing of a jack up rig.

7.7.3.4 Effect of Beam Wind Velocity.

The simulations for forward and aft superstructures were conducted for beam wind velocities of 20m/s. The increased wind velocity has a dramatic effect on the tow system behaviour. In figures 7.27 for the superstructure aft, the trajectories of the tow and towed vessels are very

different. The velocity of the tow system has significantly decreased from its original value, figures 7.27b. If we examine the same simulations for the superstructure forward figures 7.28 and 7.25, the velocity of the tow system has remained almost constant while the transverse displacements have increased four times. These differences in superstructure location are very dramatic.

7.7.4 Towing with a Bridle.

The simulations with the bridle can be seen in figures 7.29 to 7.32. These were conducted for Tow System C only as this vessel has the greatest directional instability. The simulations were carried out for 3m/s tow without wind and fixed tow rope length. The investigations considered the effects of bridle length to breadth ratio, bridle tow point locations and the effects of the skeg. The definitions of the bridle dimensions are given in figure 7.1c.

7.7.4.1 Effect of Bridle Dimensions.

If we compare figures 7.29 and 7.30 for the effects of bridle length to breadth there are some interesting points to note. If the ratio of the bridle length to breadth is decreased, then the directional stability of the tow increases. It was further noted in additional simulations that fixing the bridle length to breadth ratio and varying the lengths and breadths of the bridles accordingly, the directional stability is relatively unchanged. It is concluded therefore that for increased bridle angles, the directional stability increases. The decrease in tow rope length and increased breadth will achieve this effect.

7.7.4.2 Effects of Skegs and Longitudinal Tow Point Locations.

The results for the bridle simulations without the skegs are given in figures 7.32. When the simulations with the bridle are compared with those of the single point tow without skegs figure 7.15. It is clear that the bridle has dramatically increased the directional stability but that the

towed vessel trajectory still sways although these motions are relatively small however.

Also comparing the results of the bridle figures 7.29 and 7.31, with those of the single point towing for the variation of longitudinal tow point location, we see the tow point location seems to have a less significant effect with the bridle configuration. These simulation results are very interesting and experiments should be conducted to determine if these conclusions are correct.

Theoretical Stability Conditions

Towed Vessel	A	B	C	C
Vessel Type	Tug	Mariner	Heavy Lift Vessel	HLV with Skeg
Length B.P. (m)	43.586	182.88	155	155
Breadth (m)	10.058	24.704	40	40
Draft (m)	3.886	10.973	8.52	8.52
Block Coefficient	0.514	0.6	0.595	0.595
Prismatic Coefficient	0.65	0.7	0.8	0.8
Length/Volume^0.333	4.566	5.923	4.928	4.928
Y'b	0.4462	0.3020	0.3877	0.4609
Y'r	0.0756	0.0517	0.0979	0.1298
N'b	0.1783	0.1200	0.1099	0.0781
N'r	-0.0645	-0.0504	-0.0473	-0.0611
Length*N'b/Y'b (m)	17.420	72.676	43.957	26.253
Froude Number 3m/s	0.145	0.071	0.077	0.077
Towed Vessel Cr	7.00E-04	4.50E-04	8.00E-04	8.00E-04
Cf	2.19E-03	1.79E-03	1.83E-03	1.83E-03
Cr/Cf	3.20E-01	2.52E-01	4.38E-01	4.38E-01
Tow Rope Tension [K.N.]	6.84	63.19	81.54	81.54
Froude Number 5m/s	0.242	0.118	0.128	0.128
Towed Vessel Cr	1.60E-03	4.50E-04	8.00E-04	8.00E-04
Cf	2.03E-03	1.67E-03	1.71E-03	1.71E-03
Cr/Cf	7.88E-01	2.69E-01	4.68E-01	4.68E-01
Tow Rope Tension [K.N.]	23.88	166.39	217.36	217.36
Froude Number 7m/s	0.338	0.166	0.179	0.179
Towed Vessel Cr	6.00E-03	4.60E-04	1.10E-03	1.10E-03
Cf	1.94E-03	1.60E-03	1.63E-03	1.63E-03
Cr/Cf	3.10E+00	2.87E-01	6.73E-01	6.73E-01
Tow Rope Tension [K.N.]	102.305	316.808	459.86	459.86

Table 7.1

Shallow Water Study Vessel B Towed at 5m/s		
Water Depth/Draft	3	1.5
Tow Rope Tension [K.N.]	175	200
Y'b	.27527	.34561
Y'r	.11269	.10904
N'b	.10939	.13733
N'r	-.04595	-.05768
Length*N'b/Y'b (m)	72.678	72.668

Table 7.2

Average Breaking Strength (Minimum Breaking Strength)				
Rope Diameter	Dry Nylon	Wet Nylon	Polyester	Polypropylene
24mm	149 (129.6)	129.6 (112.7)	140 (121.7)	116 (100.9)
48mm	583 (507)	507 (440.9)	520 (452.2)	331 (287.8)
73mm	1270 (1104)	1104 (960)	1110 (965.2)	694 (603.5)
120mm	3025 (2630.4)	2630.4 (2287.3)	2700 (2347.8)	1720 (1495.7)
168mm	5600 (4869.6)	4869.6 (4234.4)	5115 (4447.8)	3110 (2704.3)

Minimum Breaking Strength is 15% less than Average Breaking Strength

Table 7.3

Simulation Conditions for Chapter Seven
Single Tug Simulations.

Tug Dimensions	
Length (m)	41.12
Breadth (m)	13.8
Draught (m)	5.8
Block Coefficient	0.58
Length/Vol^0.333	3.3156
Wind Area T (m^2)	50
Wind Area L (m^2)	160

Tug Propulsion	
Diameter (m)	3.2
Pitch (m)	2.56
Number of	2
C1	0.366
C2	-0.374
C3	-0.063

Tug Interaction	
ah	0.3
xr (m)	-24
xh'	-1.5
tr	0.2876
gamma	-0.1572
wpo	0.24
wro	0.6813

Variables/Figure Number	7.7	7.8	7.9	7.10	7.11	7.12	7.13	7.14	7.15	7.16	7.29	7.30	7.31	7.32
Tow System	B	B	B	B	B	B	B	B	C	C with SKEG	C with SKEG	C with SKEG	C with SKEG	C
Simulation Run (secs)	2500	2500	2500	2500	2500	2500	2500	2500	2500	2500	2500	2500	2500	2500
Time Step (secs)	0.1	0.1	0.1	0.1	0.1	0.1	0.1	0.1	0.1	0.1	0.1	0.1	0.1	0.1
Tow Velocity (m/s)	3	3	3	3	3	3	5	3	3	3	3	3	3	3
Froude Number	0.1494	0.1494	0.1494	0.1494	0.1494	0.1494	0.2489	0.1494	0.1494	0.1494	0.1494	0.1494	0.1494	0.1494
Tow Vessel Cr	8.00E-04	8.00E-04	8.00E-04	8.00E-04	8.00E-04	8.00E-04	2.10E-03	8.00E-04	8.00E-04	8.00E-04	8.00E-04	8.00E-04	8.00E-04	8.00E-04
Tow Vessel Resistance [K.N.]	10.4	10.4	10.4	10.4	10.4	10.4	39.098	10.4	10.4	10.4	10.4	10.4	10.4	10.4
Tow Vessel RPS	1.49	1.49	1.49	1.49	1.49	1.49	2.49	1.49	1.61	1.61	1.61	1.61	1.61	1.61
Rudcon 1,2	8,5	8,5	8,5	8,5	8,5	8,5	8,5	8,5	8,5	8,5	8,5	8,5	8,5	8,5
Maximum Rudder Deflection	2.1	2.1	2.1	-2.8	-2.567	-2.8	-2.567	-5.367	-35.233	-2.567	-2.917	-2.917	-2.917	-2.917
Tow Rope Model	Rigid	Rigid	Rigid	Elastic PY	Elastic NW	Elastic PP	Elastic PP	Elastic NW	Elastic NW	Elastic NW	Bridle PY	Bridle PY	Bridle PY	Bridle PY
Rope Diameter (mm)	-	-	-	59	61	74	131	70	70	70	59	56	59	59
Aft Tow Point on Tug (m)	0	0	0	0	0	0	0	-16.448	0	0	0	0	0	0
Tow Rope Length (m)	51.4	164.48	164.48	164.48	164.48	164.48	164.48	164.48	133.64	133.64	133.64	133.64	133.64	133.64
Forward Tow Point (m)	81.82	81.82	77.25	77.25	77.25	77.25	77.25	77.25	63.3	63.3	63.3	63.3	73.3	63.3
Tow Rope Angle (degree)	5	5	5	5	5	5	5	5	5	5	5	5	5	5
									Bridle Length, Breadth (m,m)	20,40	20,10	20,40	20,40	

Variables/Figure Number	7.17	7.18	7.19	7.20	7.21	7.22	7.23	7.24	7.25	7.26	7.27	7.28
Tow System	C with SKEG	C with SKEG	C with SKEG	C with SKEG	C with SKEG	C with SKEG	C with SKEG	C with SKEG	C with SKEG	C with SKEG	C with SKEG	C with SKEG
Simulation Run (secs)	2500	2500	2500	2500	2500	2500	2500	2500	2500	2500	2500	2500
Time Step (secs)	0.1	0.1	0.1	0.1	0.1	0.1	0.1	0.1	0.1	0.1	0.1	0.1
Tow Velocity (m/s)	3	3	3	3	3	3	3	3	3	3	3	3
Froude Number	0.1494	0.1494	0.1494	0.1494	0.1494	0.1494	0.1494	0.1494	0.1494	0.1494	0.1494	0.1494
Tow Vessel Cr	8.00E-04	8.00E-04	8.00E-04	8.00E-04	8.00E-04	8.00E-04	8.00E-04	8.00E-04	8.00E-04	8.00E-04	8.00E-04	8.00E-04
Tow Vessel Resistance [K.N.]	10.4	10.4	10.4	10.4	10.4	10.4	10.4	10.4	10.4	10.4	10.4	10.4
Tow Vessel RPS	1.61	1.61	1.61	1.61	1.61	1.61	1.61	1.61	1.61	1.61	1.61	1.61
Rudcon 1,2	8,5	8,5	8,5	8,5	8,5	8,5	8,5	8,5	8,5	8,5	8,5	8,5
Maximum Rudder Deflection	-2.567	1.867	-2.8	-2.567	21.233	-20.3	23.1	-21.233	-7.7	5.367	22.4	-23.8
Tow Rope Model	Rigid	Rigid	Elastic PY	Elastic PY	Rigid	Rigid	Elastic PY	Elastic PY	Elastic PY	Elastic PY	Elastic PY	Elastic PY
Rope Diameter (mm)	-	-	68	68	-	-	68	68	68	68	68	68
Aft Tow Point on Tug (m)	0	0	0	0	0	0	0	0	0	0	0	0
Tow Rope Length (m)	133.64	133.64	133.64	133.64	133.64	133.64	133.64	133.64	133.64	133.64	133.64	133.64
Forward Tow Point (m)	63.3	63.3	63.3	63.3	63.3	63.3	63.3	63.3	63.3	63.3	63.3	63.3
Tow Rope Angle (degree)	5	5	5	5	5	5	5	5	5	5	5	5
Superstructure	Aft	Aft	Aft	Aft	Aft	Aft	Aft	Aft	Forward	Forward	Aft	Forward
Wind Area T (m^2)	1063	1063	1063	1063	1063	1063	1063	1063	1063	1063	1063	1063
Wind Area L (m^2)	1672	1672	1672	1672	1672	1672	1672	1672	1672	1672	1672	1672
Wind Velocity (m/s)	10	10	10	10	10	10	10	10	10	10	20	20
Wind Angle (degrees)	0	180	0	180	90	270	90	270	90	270	90	90

Skeg Dimensions are given in Table 5.2
PY Polyester, PP Polypropylene, NW Nylon Wet

Coordinate System.

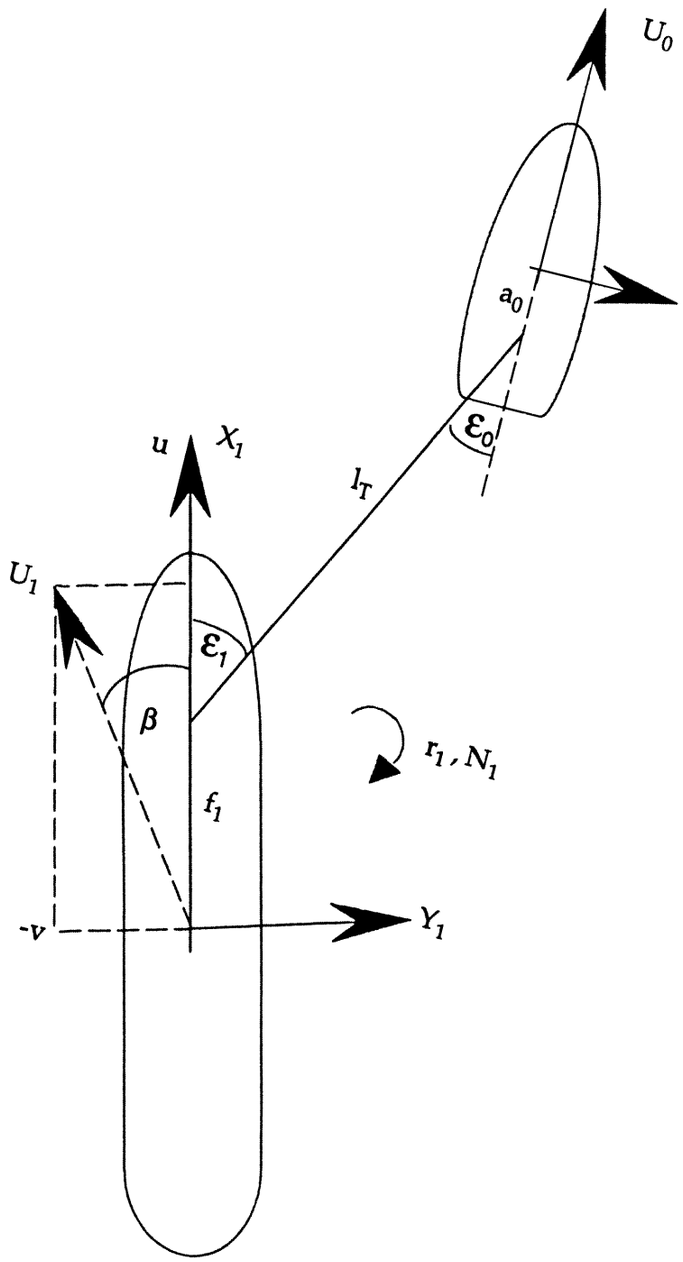

Figure 7.1.a

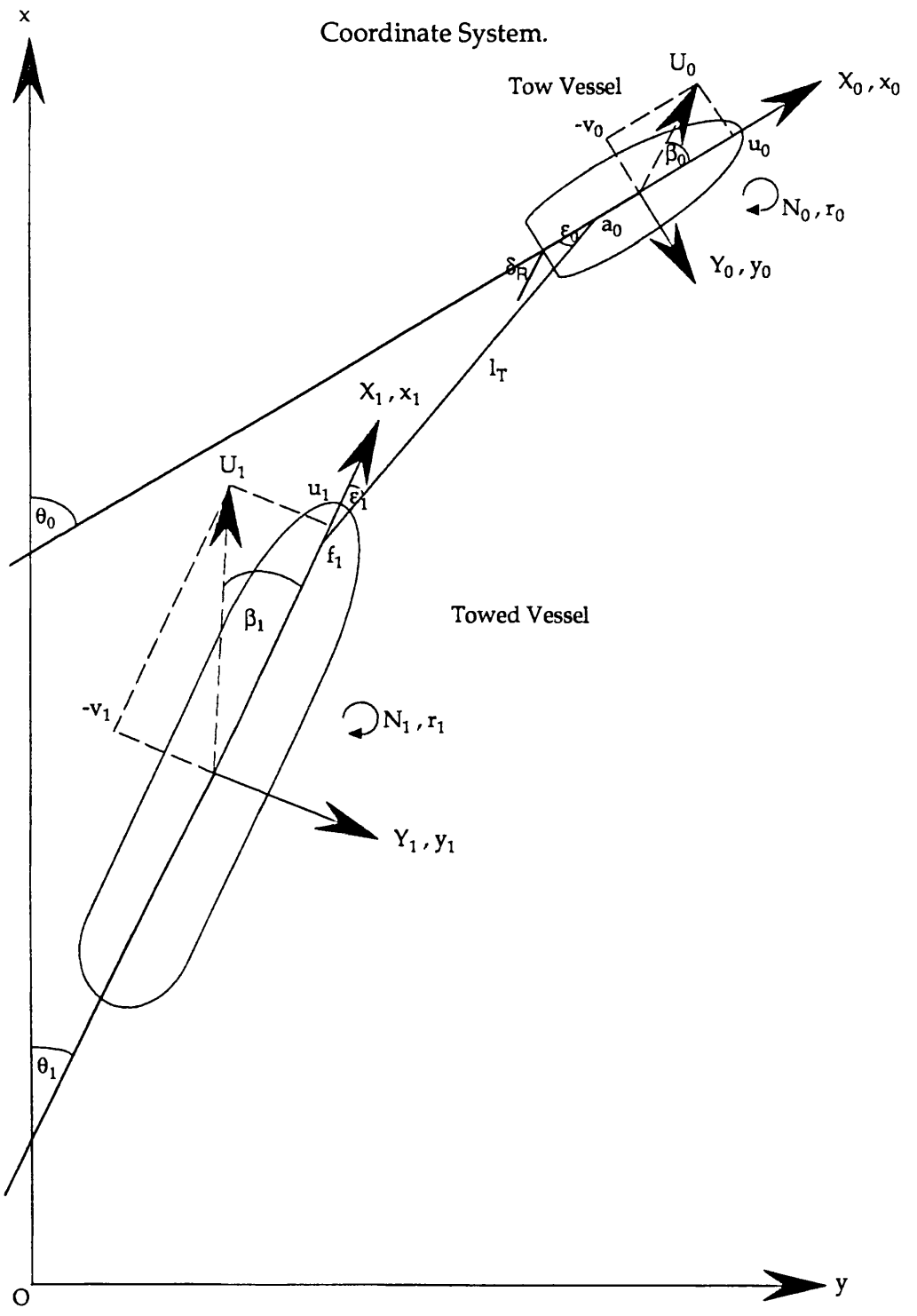
Coordinate System.
x
Tow Vessel
U_0
X_0, x_0
$-v_0$
β_0
u_0
N_0, r_0
ε_0
a_0
δ_R
Y_0, y_0
l_T
X_1, x_1
U_1
u_1
ε_1
θ_0
f_1
β_1
Towed Vessel
$-v_1$
N_1, r_1
Y_1, y_1
θ_1
O
y

Figure 7.1.b

Configuration for Bridle

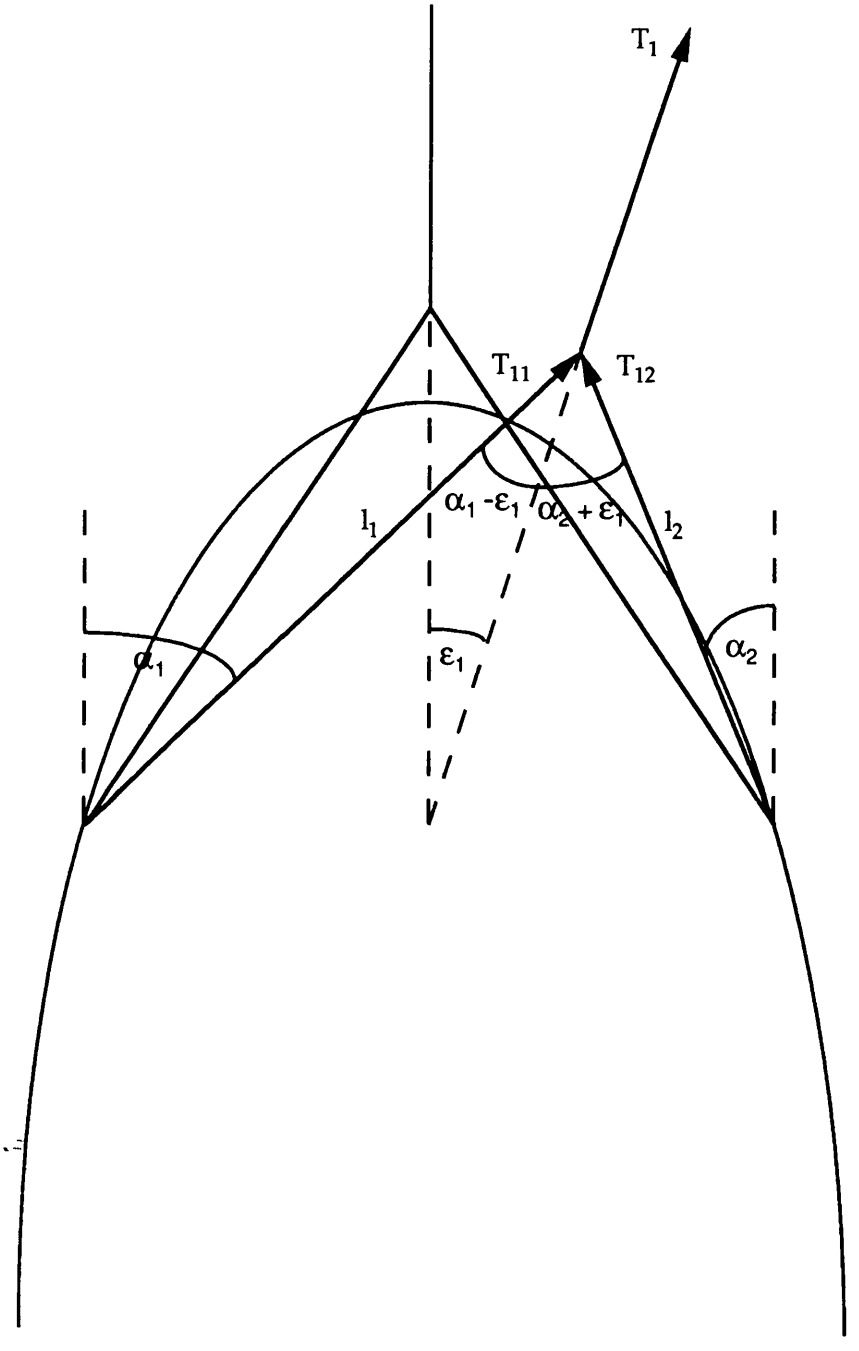

Figure 7.1c

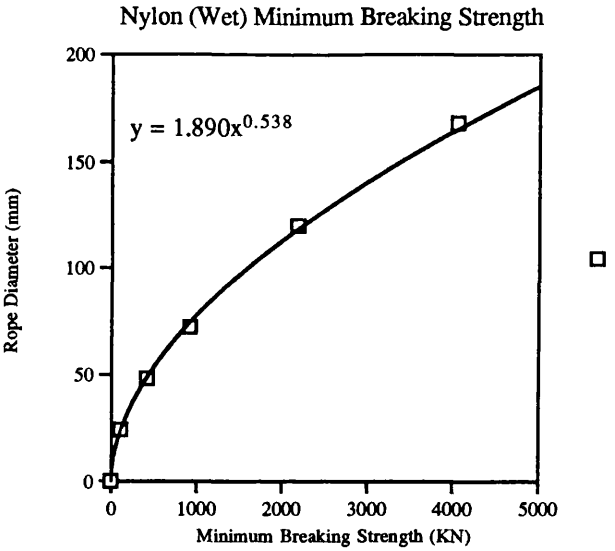

Figure 7.2a

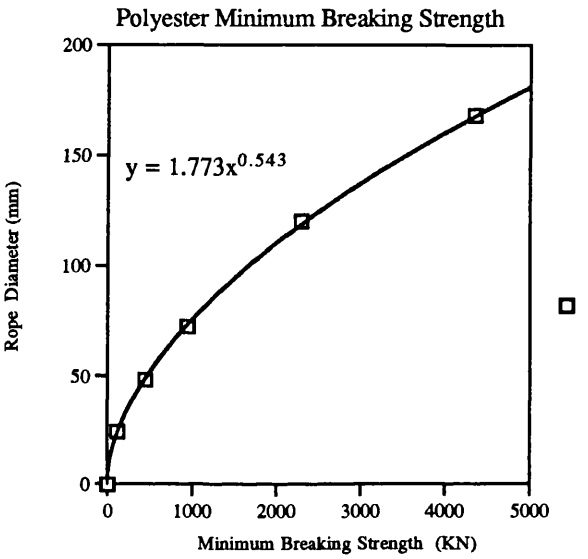

Figure 7.2b

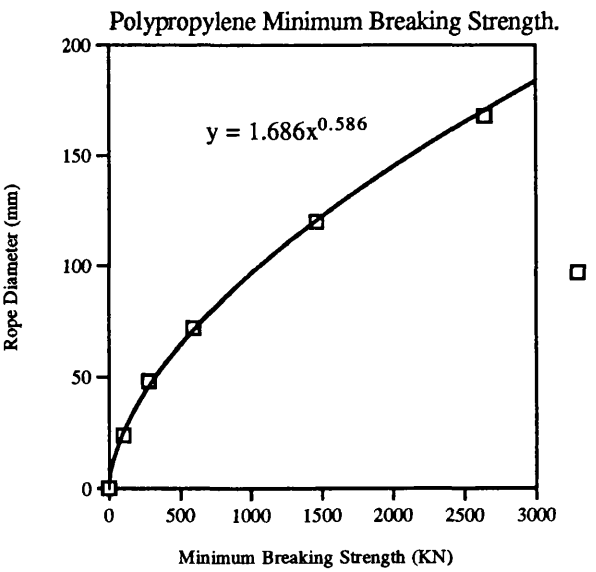

Figure 7.2c

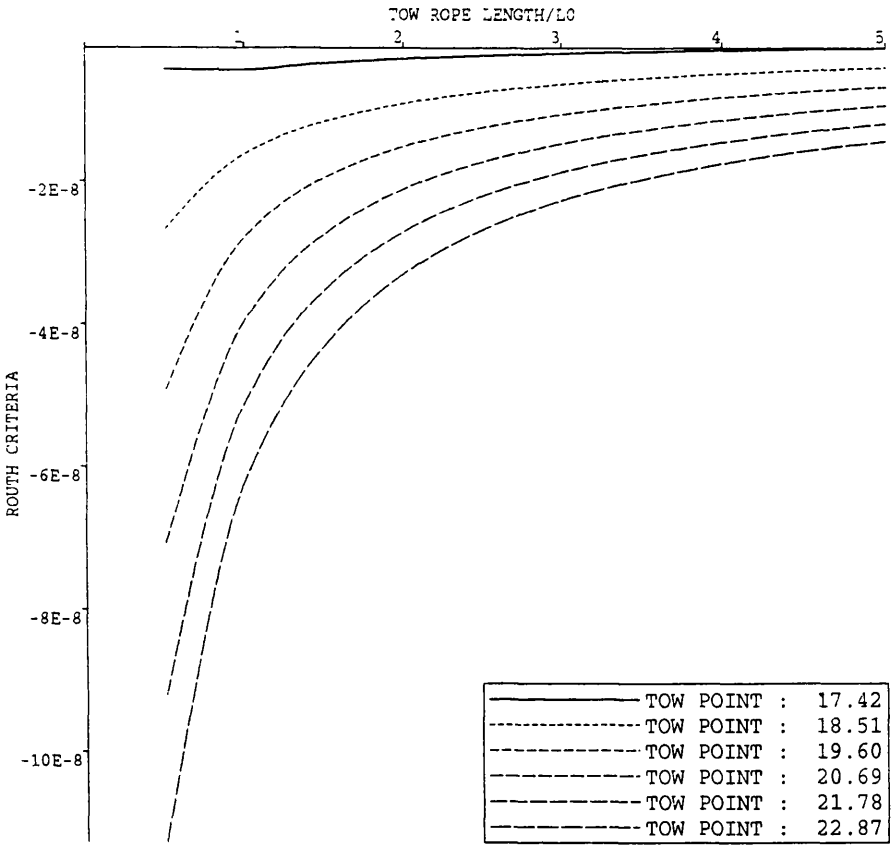

Figure 7.3a

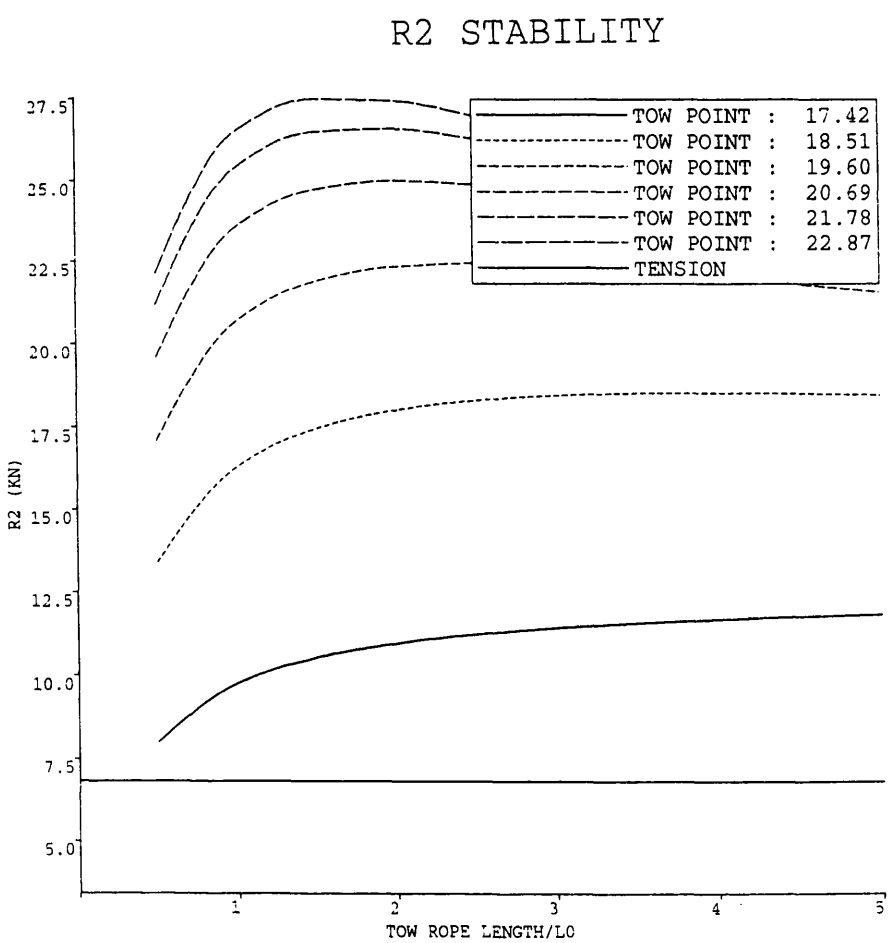

Figure 7.3b

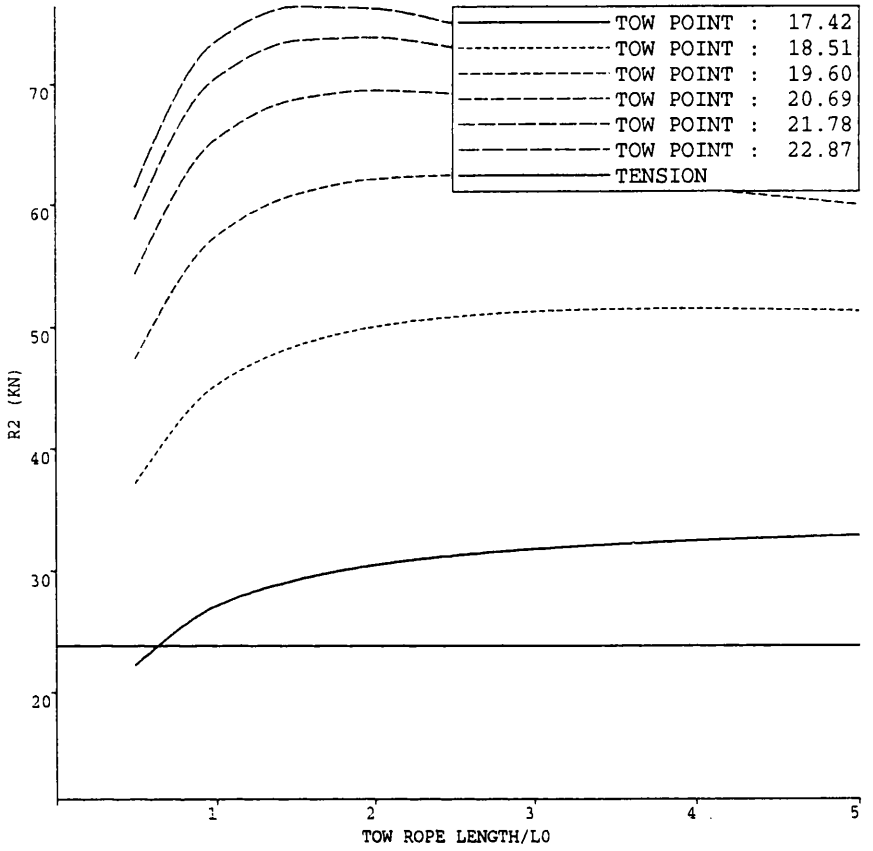

Figure 7.3c

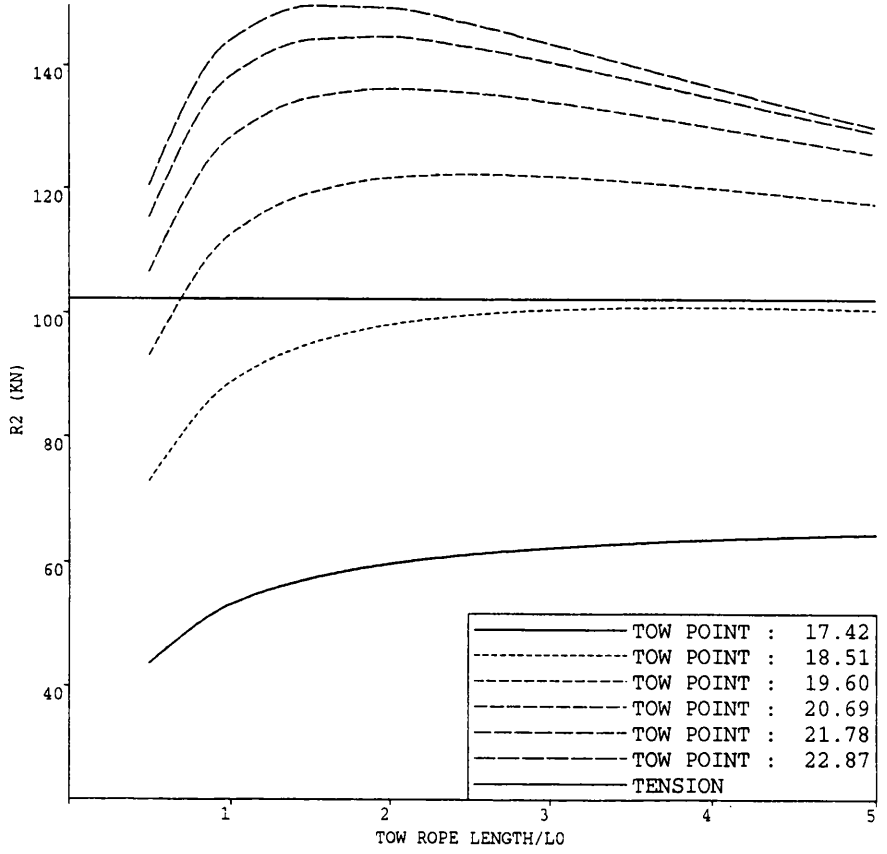

Figure 7.3d

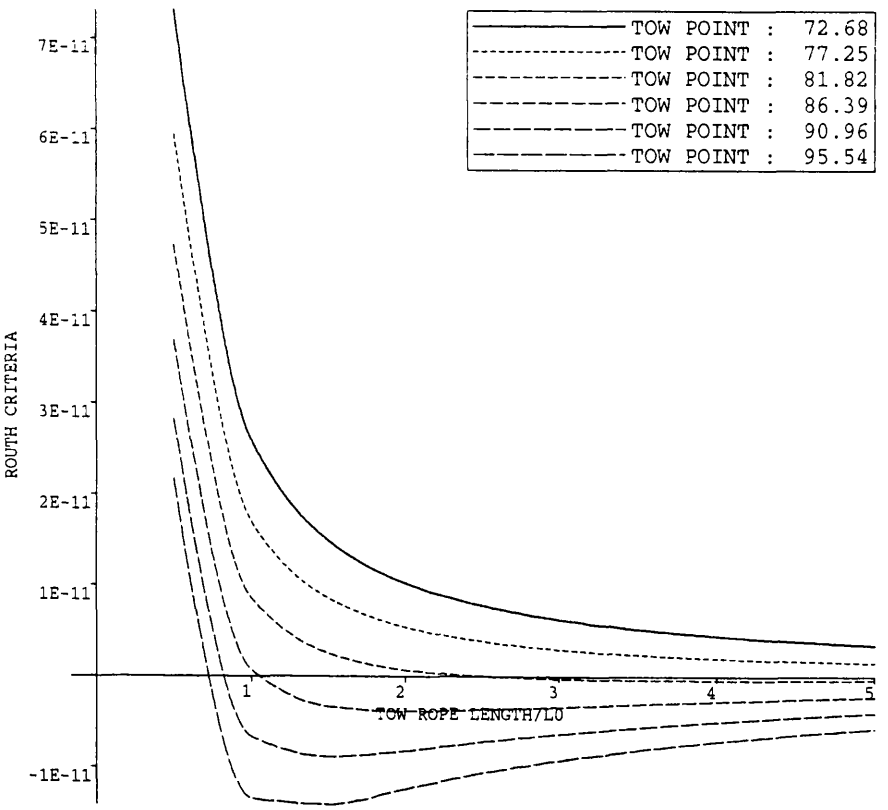

Figure 7.4a

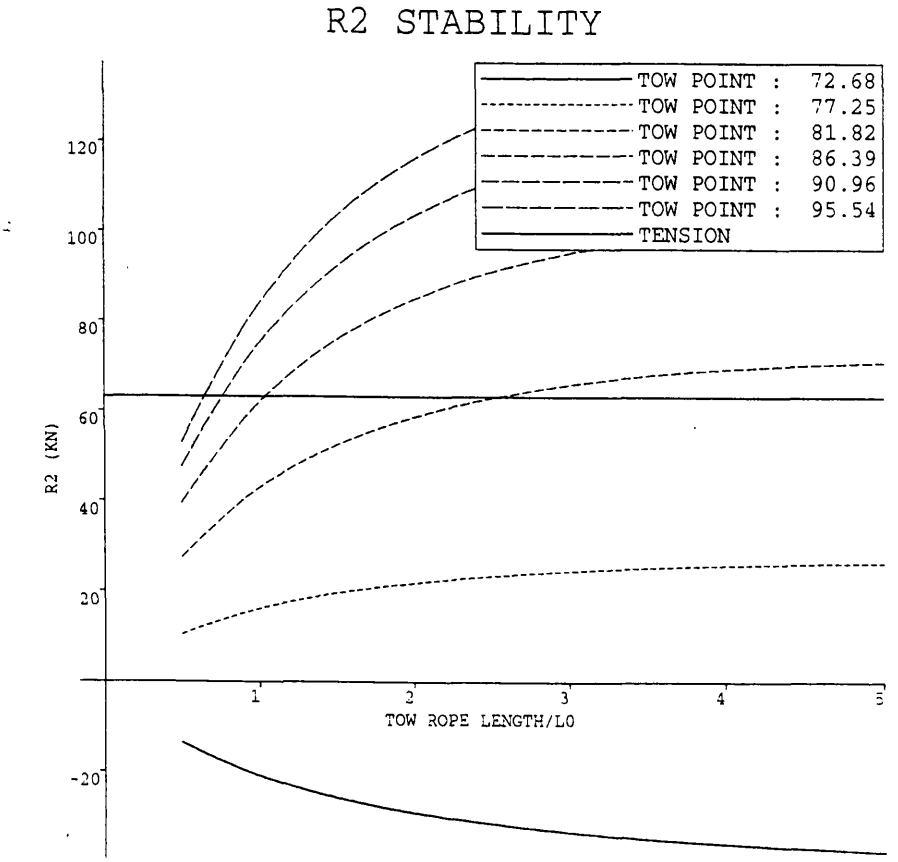

Figure 7.4b

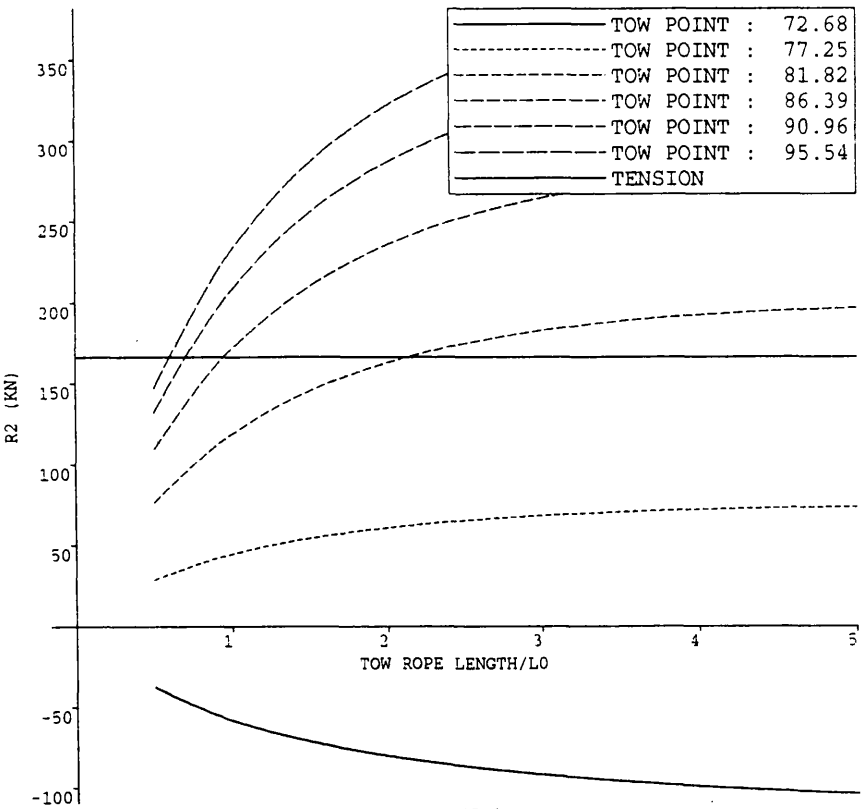

Figure 7.4c

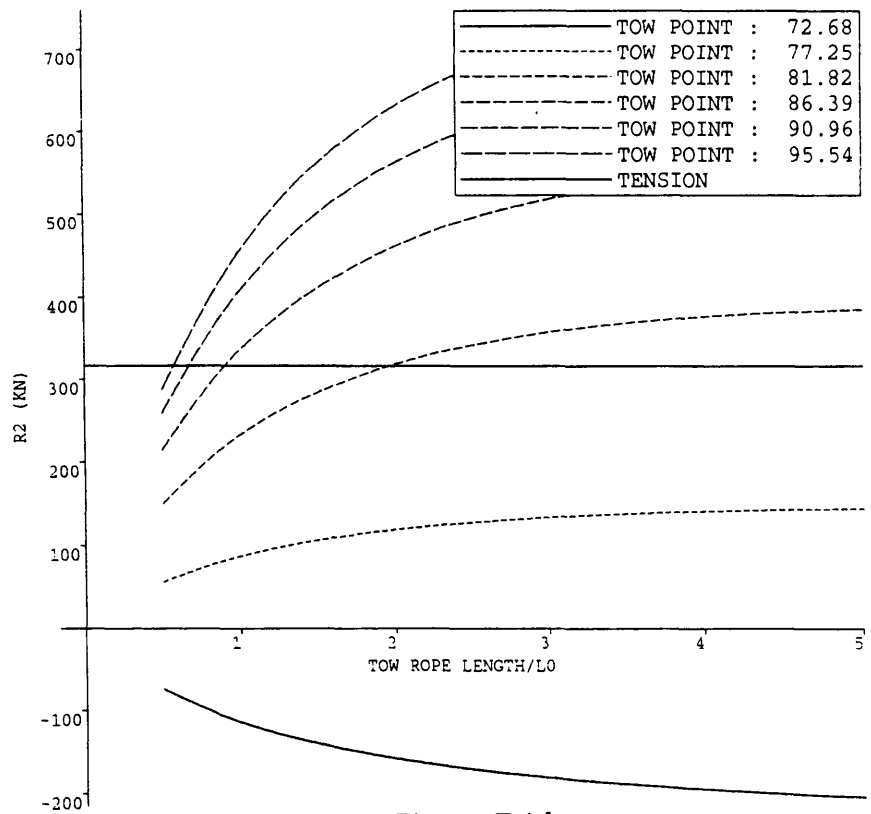

Figure 7.4d

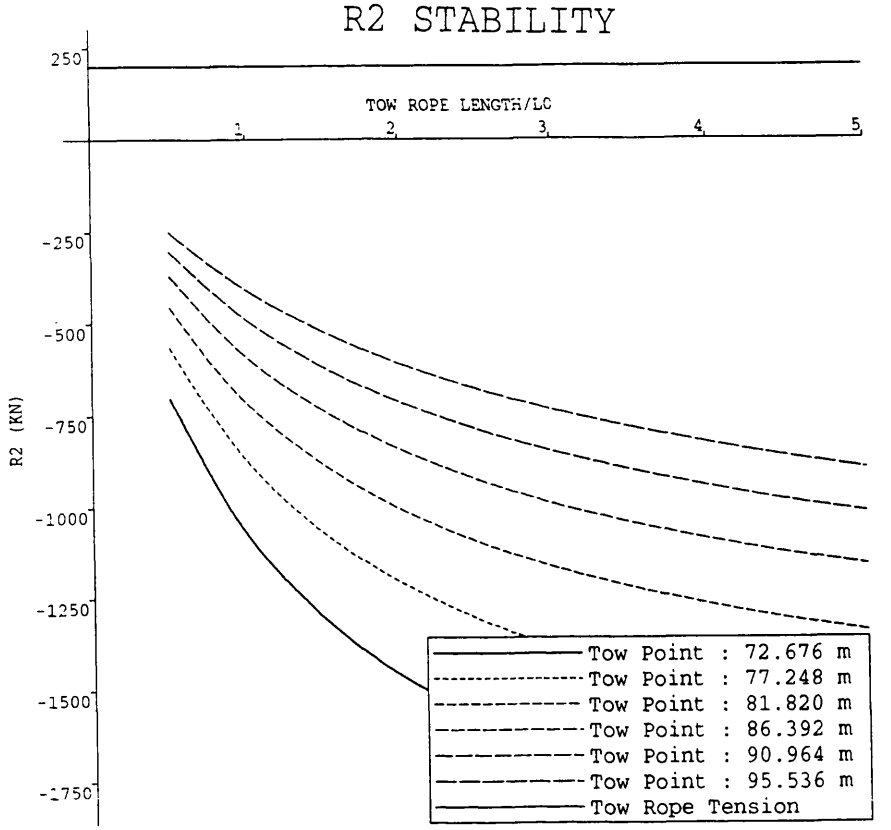

Figure 7.5a

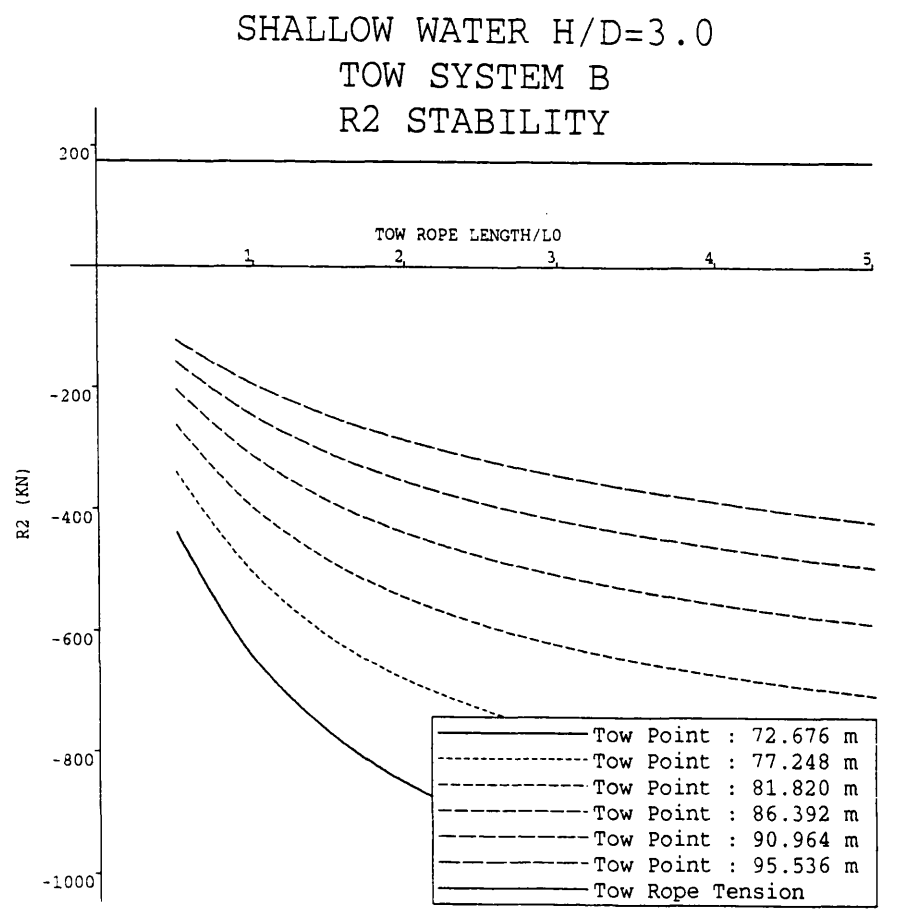

Figure 7.5b

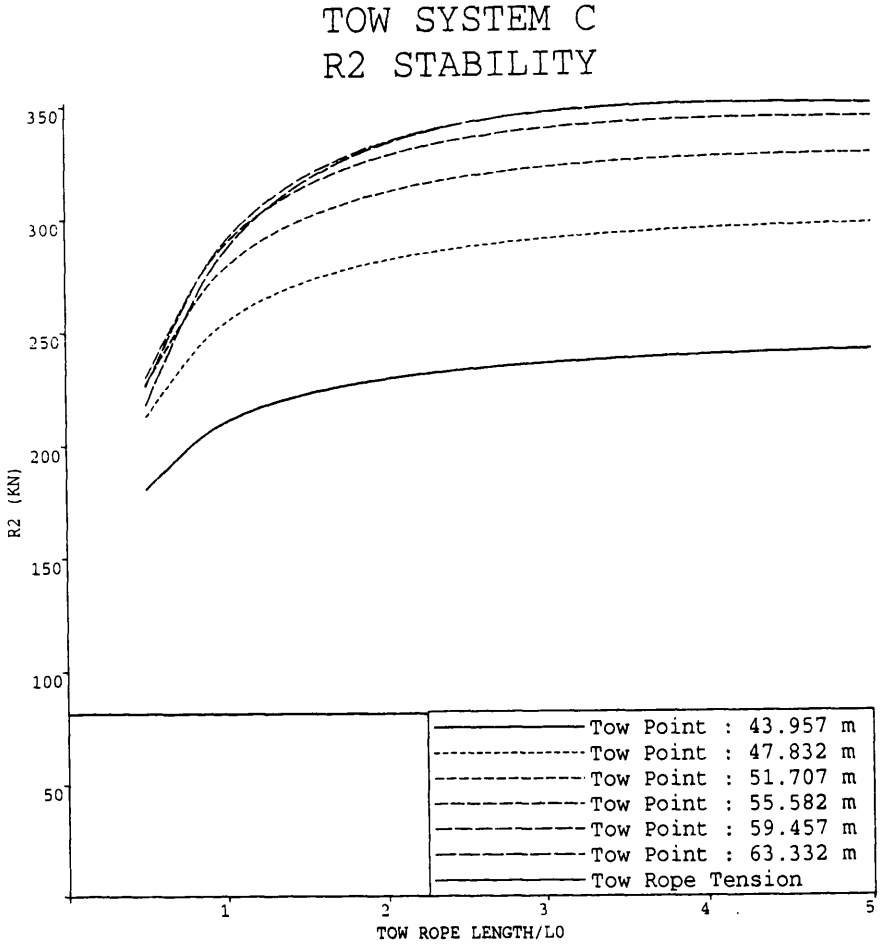

Figure 7.6a

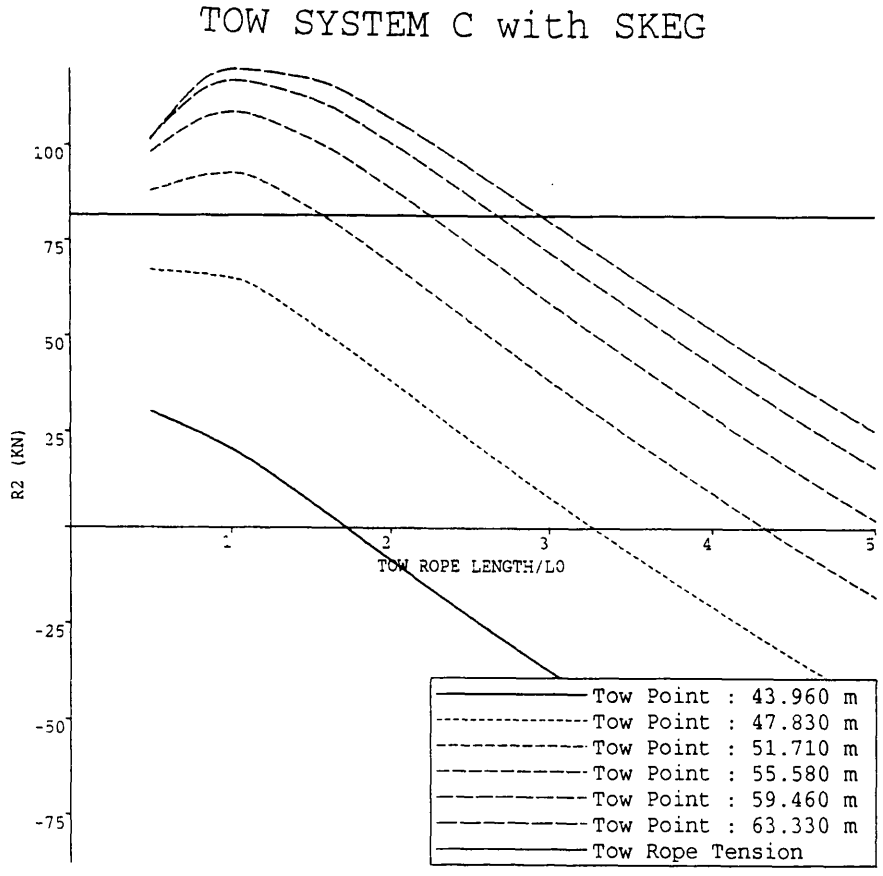

Figure 7.6b

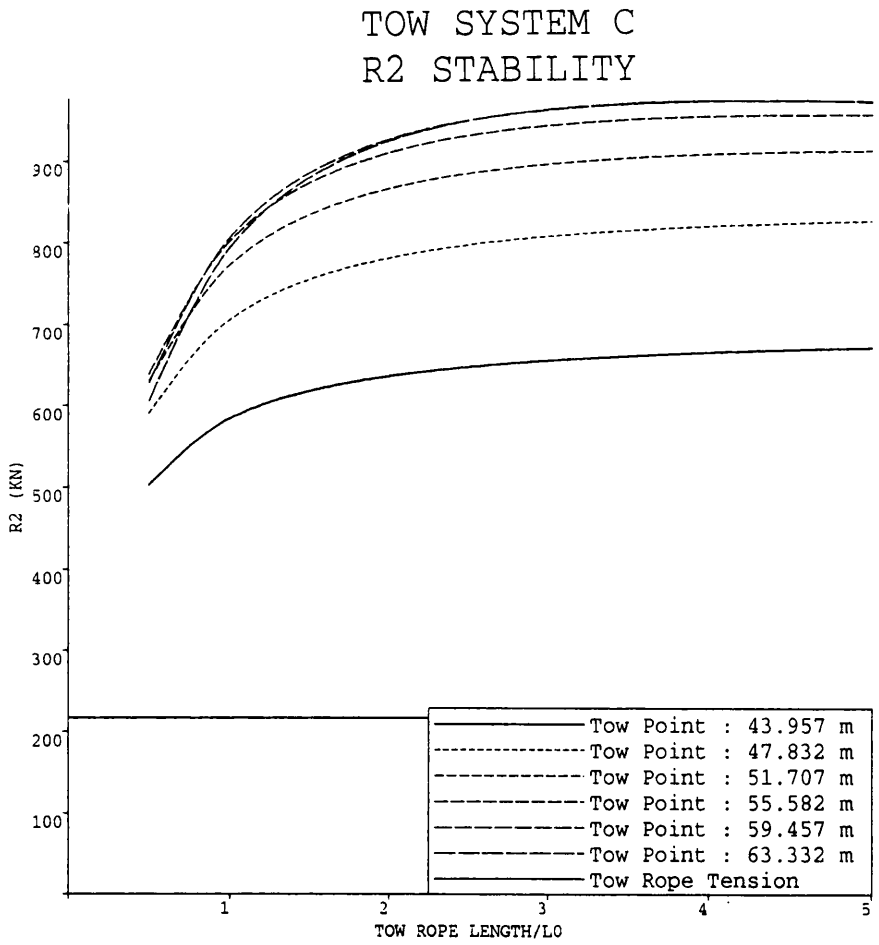

Figure 7.6c

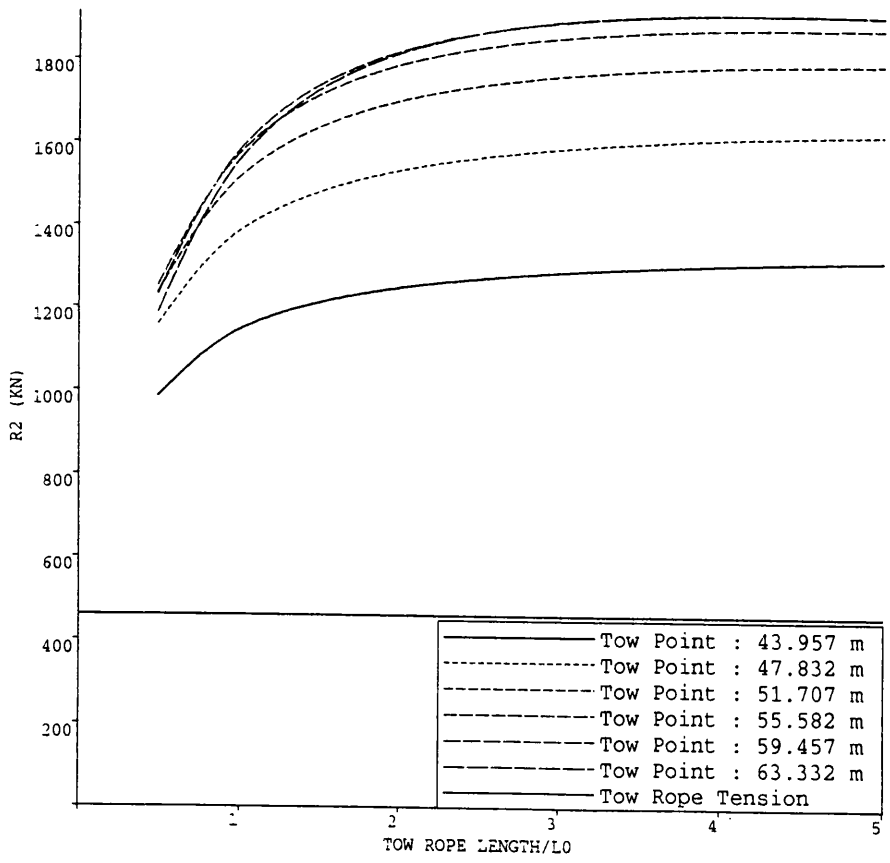

Figure 7.6d

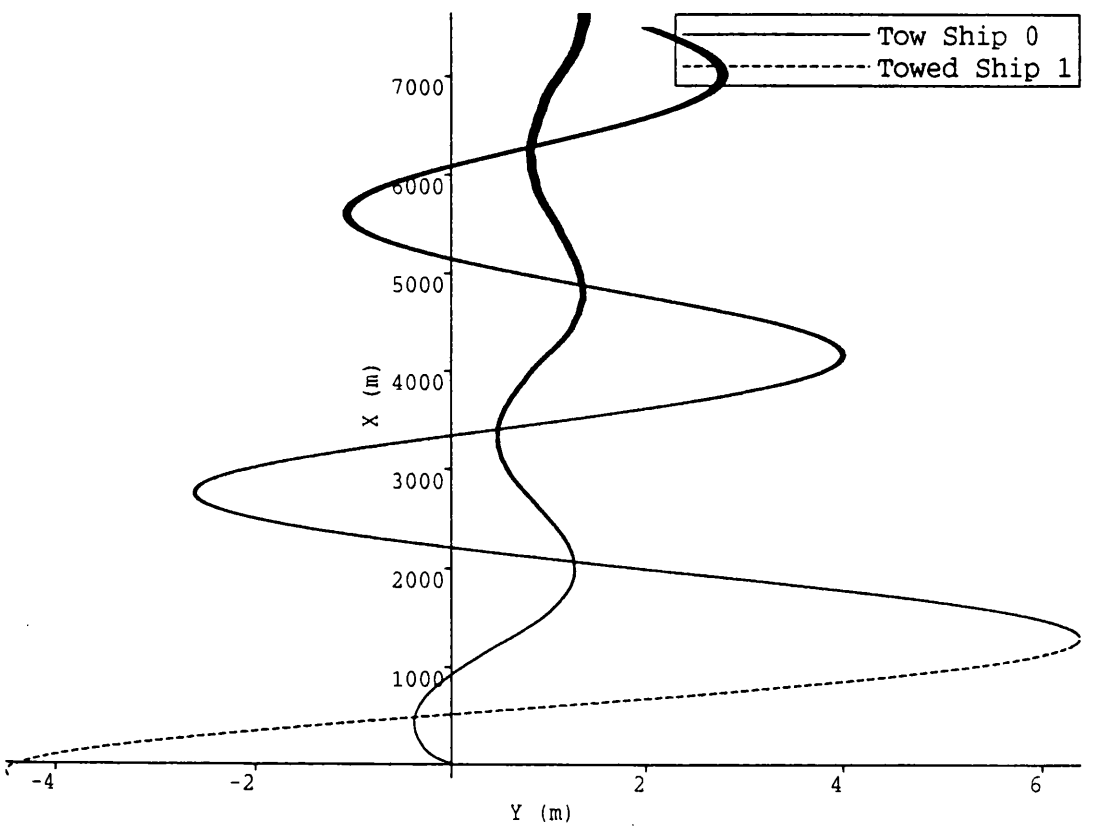

Figure 7.7a

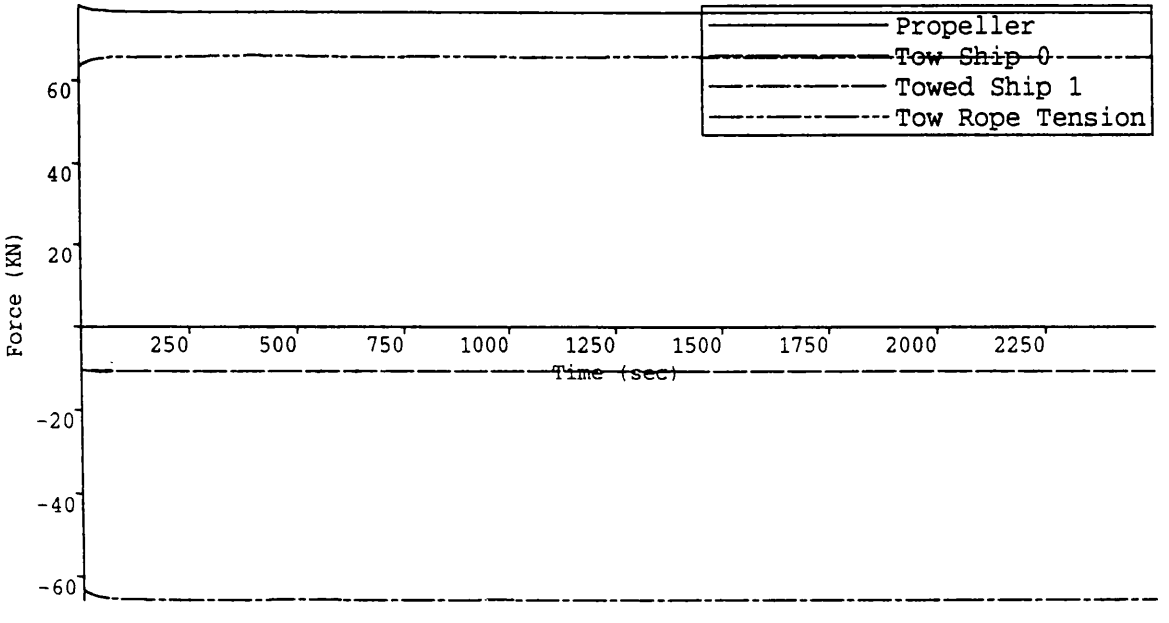

Figure 7.7b

```
Tow Velocity :  5.837 Knots
Rudder Constants 1,2 : 8.0,5.0
Tow Point 0 :   0.000 m
Tow Rope Length/L0 :  1.250 m/m
Tow Point 1 : 81.820 m
Tow Rope : Rigid
Maximum Deflection :  2.100 Degrees
```

Tow System B.

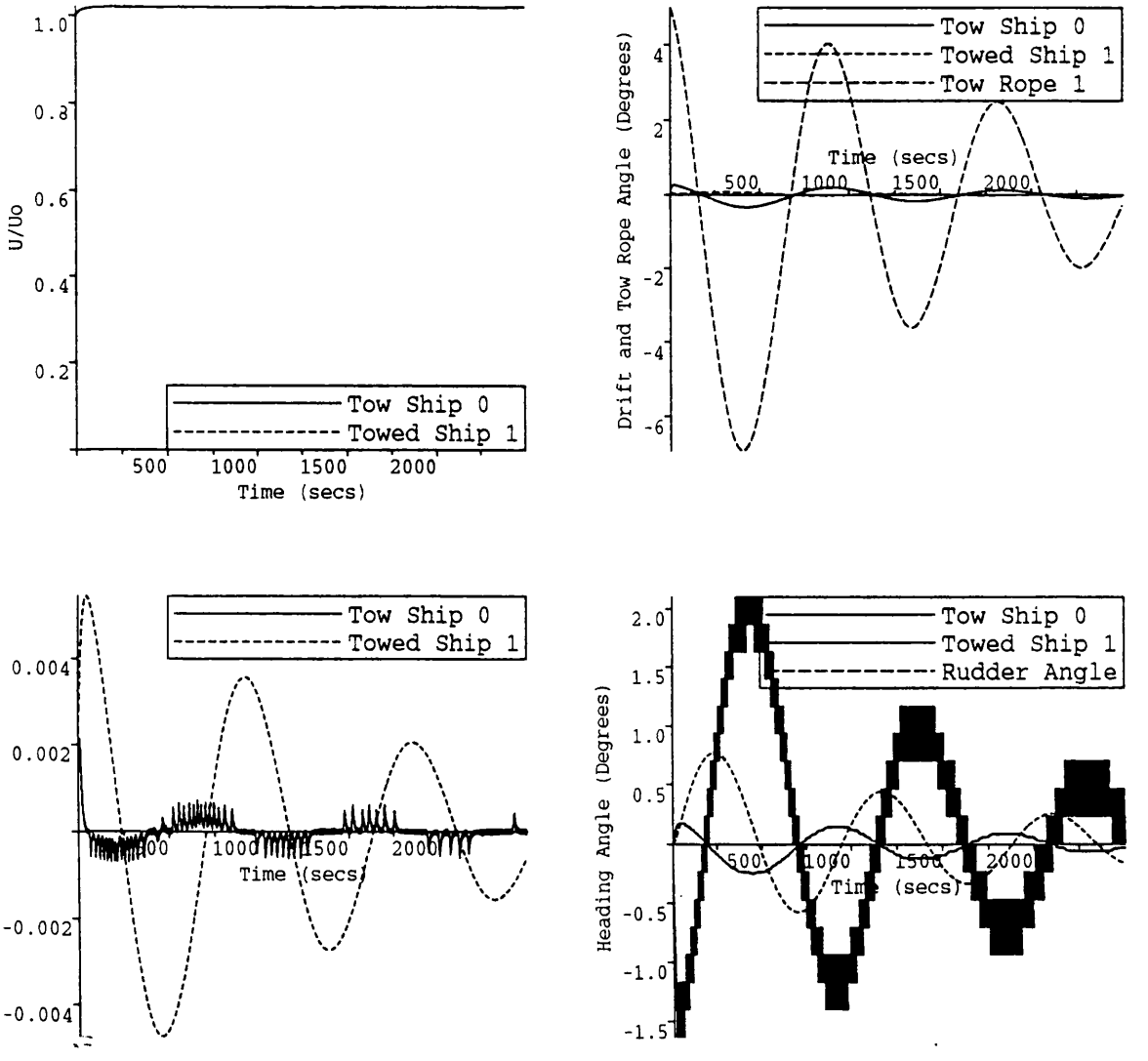

Figure 7.7c

Tow Velocity : 5.837 Knots
Rudder Constants 1,2 : 8.0,5.0
Tow Point 0 : 0.000 m
Tow Rope Length/L0 : 1.250 m/m
Tow Point 1 : 81.820 m
Tow Rope : Rigid
Maximum Deflection : 2.100 Degrees

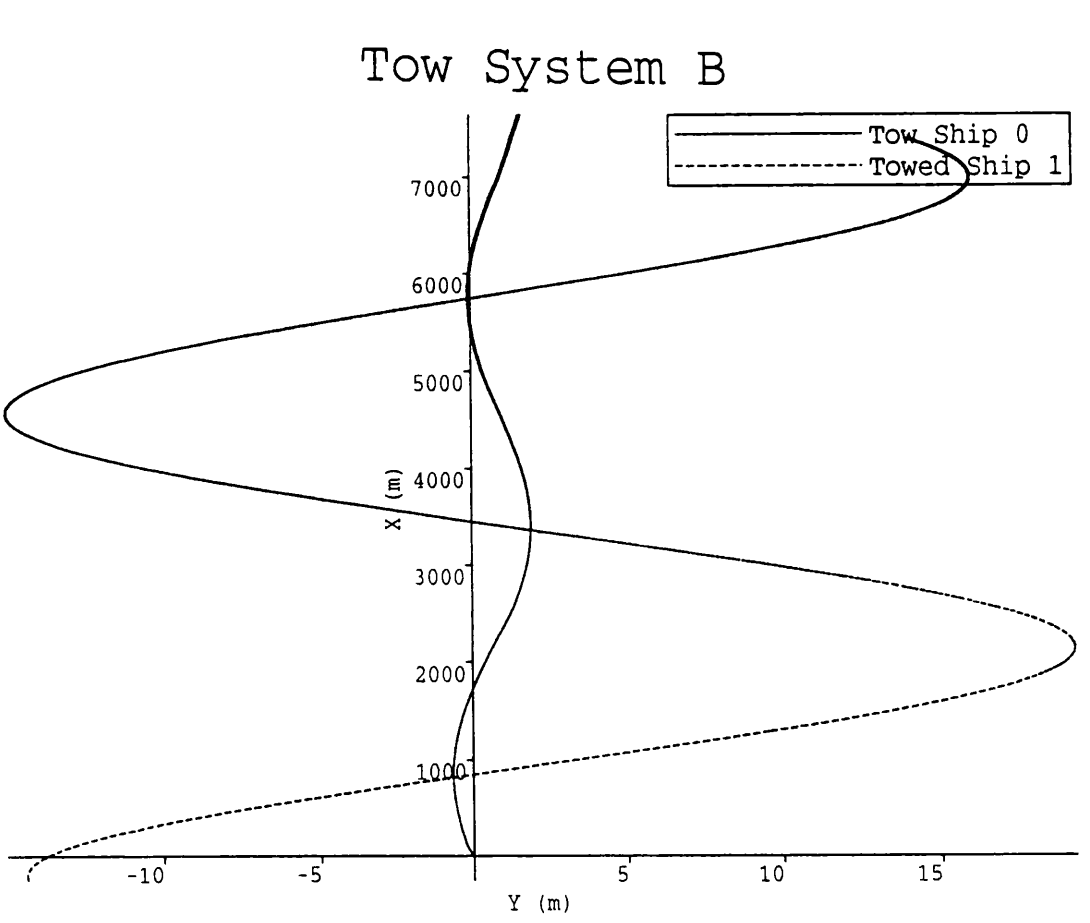

Figure 7.8a

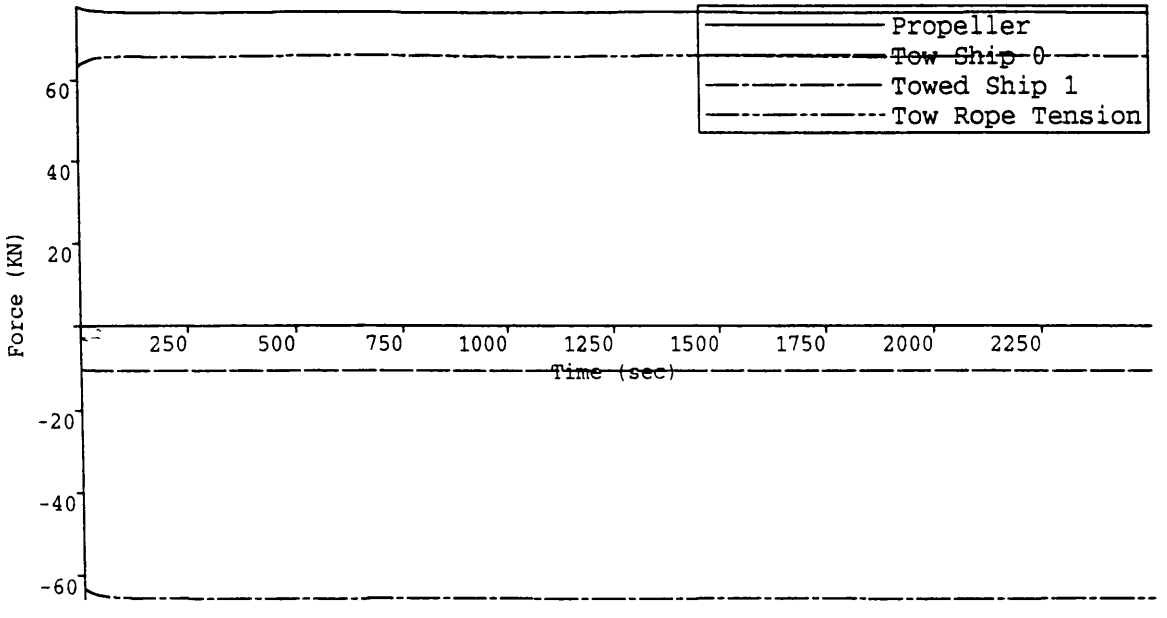

Figure 7.8b

```
Tow Velocity :  5.837 Knots
Rudder Constants 1,2 : 8.0,5.0
Tow Point 0 :   0.000 m
Tow Rope Length/L0 :  4.000 m/m
Tow Point 1 : 81.820 m
Tow Rope : Rigid
Maximum Deflection :  2.100 Degrees
```

Tow System B.

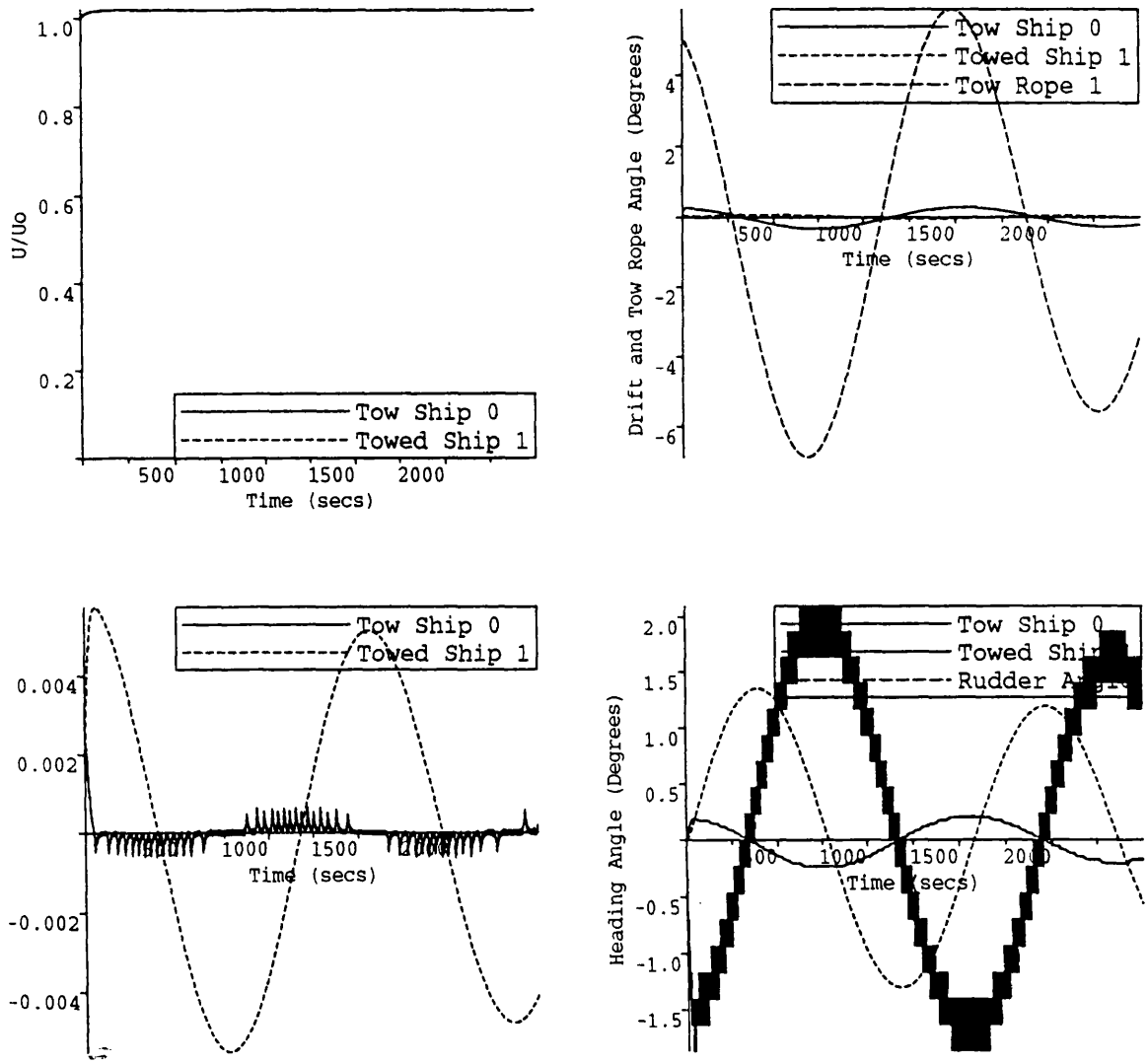

Figure 7.8c

Tow Velocity : 5.837 Knots
Rudder Constants 1,2 : 8.0,5.0
Tow Point 0 : 0.000 m
Tow Rope Length/L0 : 4.000 m/m
Tow Point 1 : 81.820 m
Tow Rope : Rigid
Maximum Deflection : 2.100 Degrees

Tow System B.

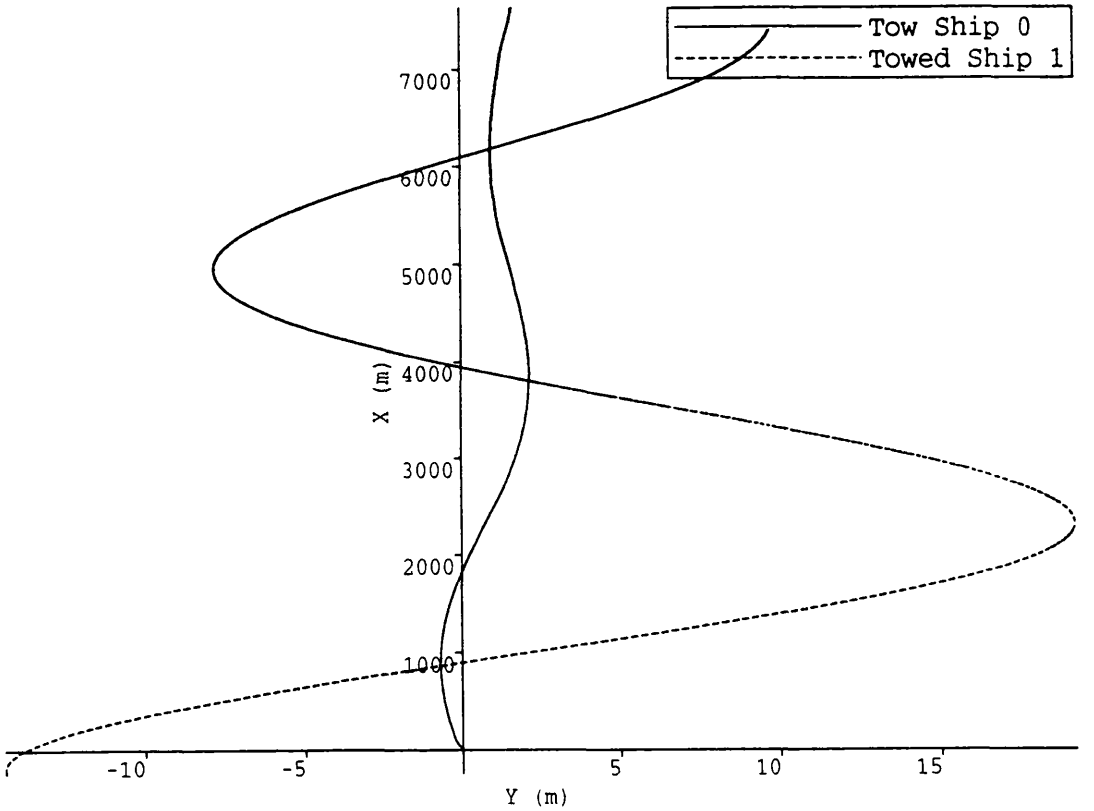

Figure 7.9a

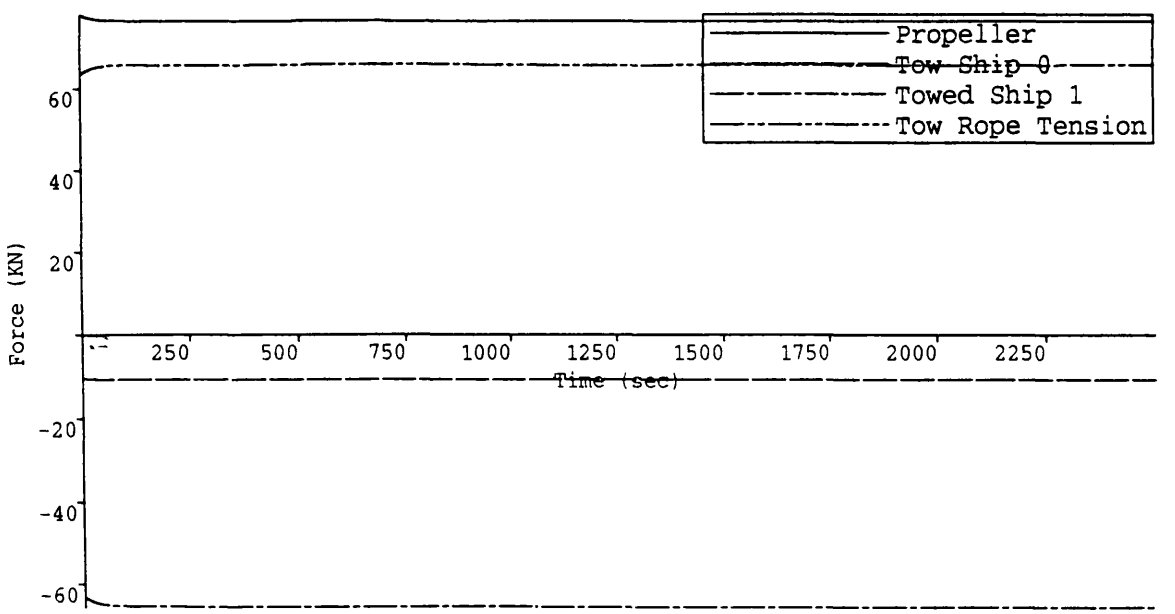

Figure 7.9b

Tow Velocity : 5.837 Knots
Rudder Constants 1,2 : 8.0,5.0
Tow Point 0 : 0.000 m
Tow Rope Length/L0 : 4.000 m/m
Tow Point 1 : 77.250 m
Tow Rope : Rigid
Maximum Deflection : 2.100 Degrees

Tow System B.

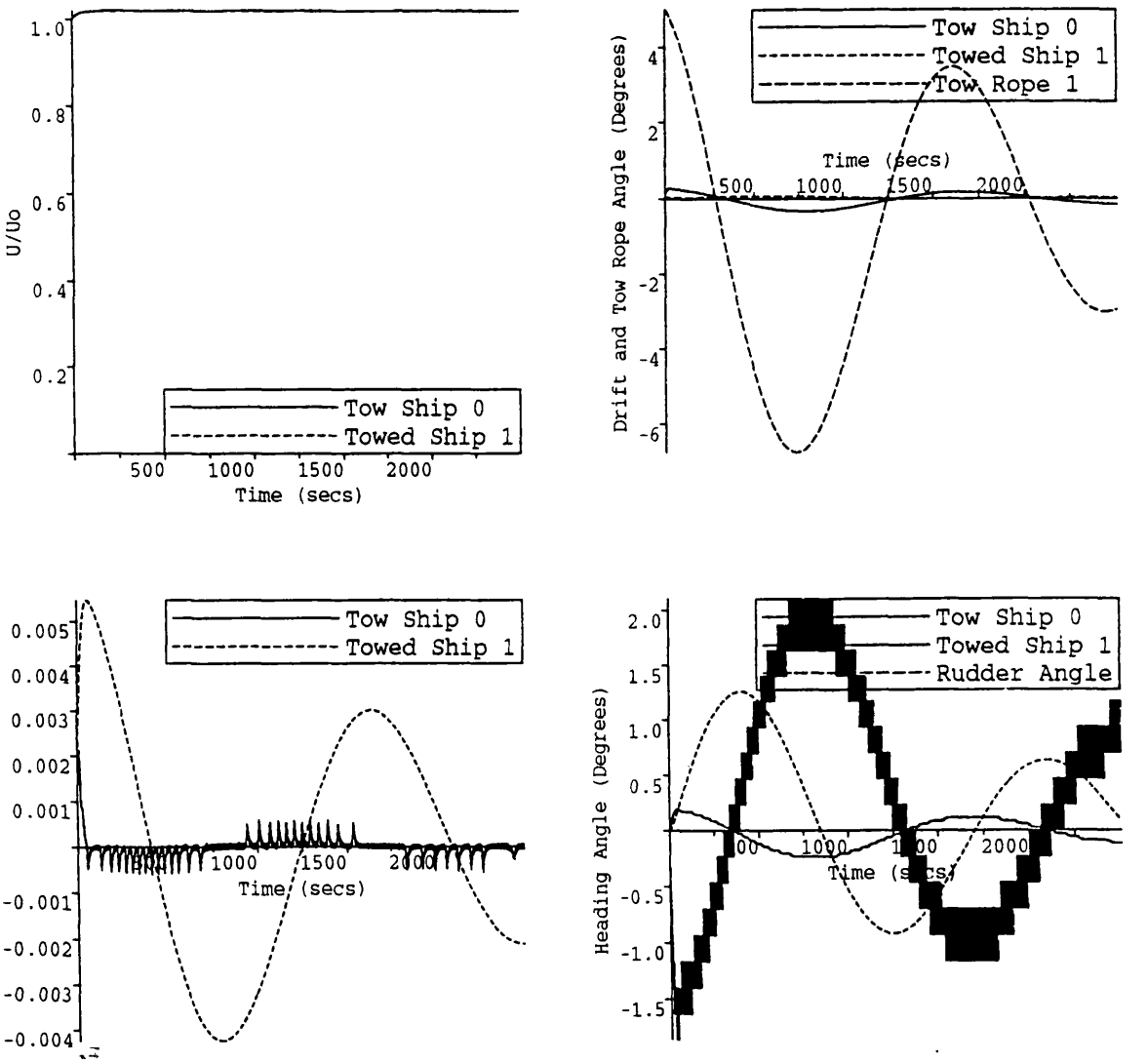

Figure 7.9c

Tow Velocity : 5.837 Knots
Rudder Constants 1,2 : 8.0,5.0
Tow Point 0 : 0.000 m
Tow Rope Length/L0 : 4.000 m/m
Tow Point 1 : 77.250 m
Tow Rope : Rigid
Maximum Deflection : 2.100 Degrees

Tow System B.

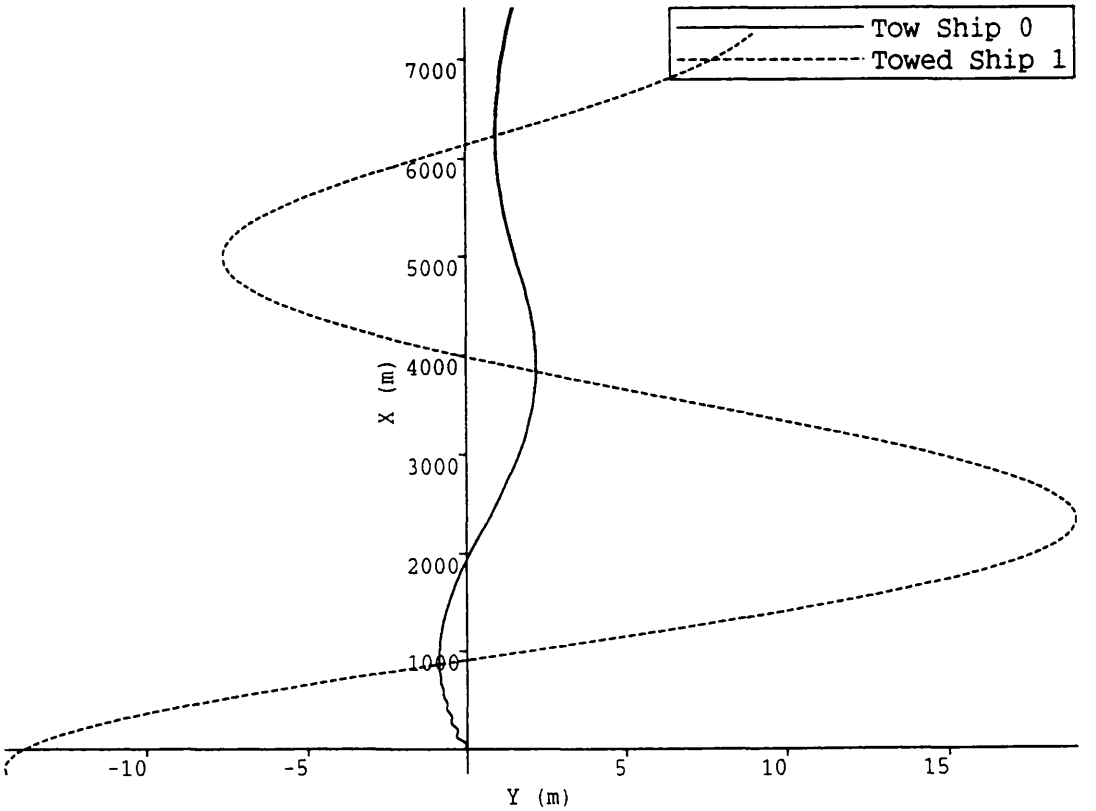

Figure 7.10a

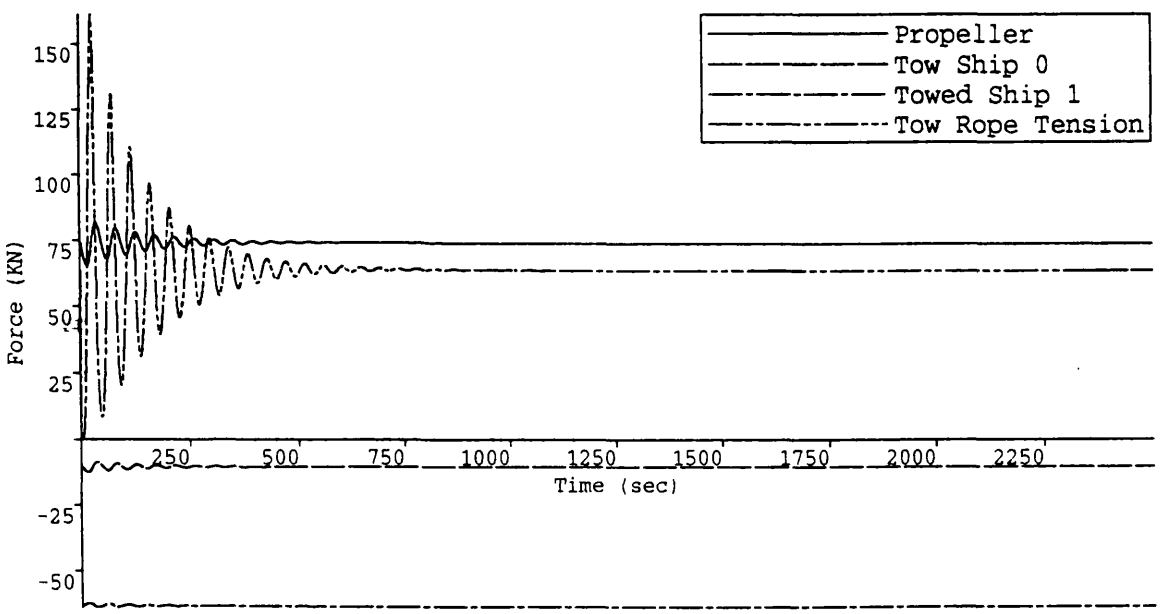

Figure 7.10b

Tow Velocity : 5.837 Knots
Rudder Constants 1,2 :8.0,5.0
Tow Point 0 : 0.000m
Tow Rope Length/L0 : 4.000m/m
Tow Point 1 :77.250m
Tow Rope :PY
Maximum Deflection :-2.800 Degrees

Tow System B.

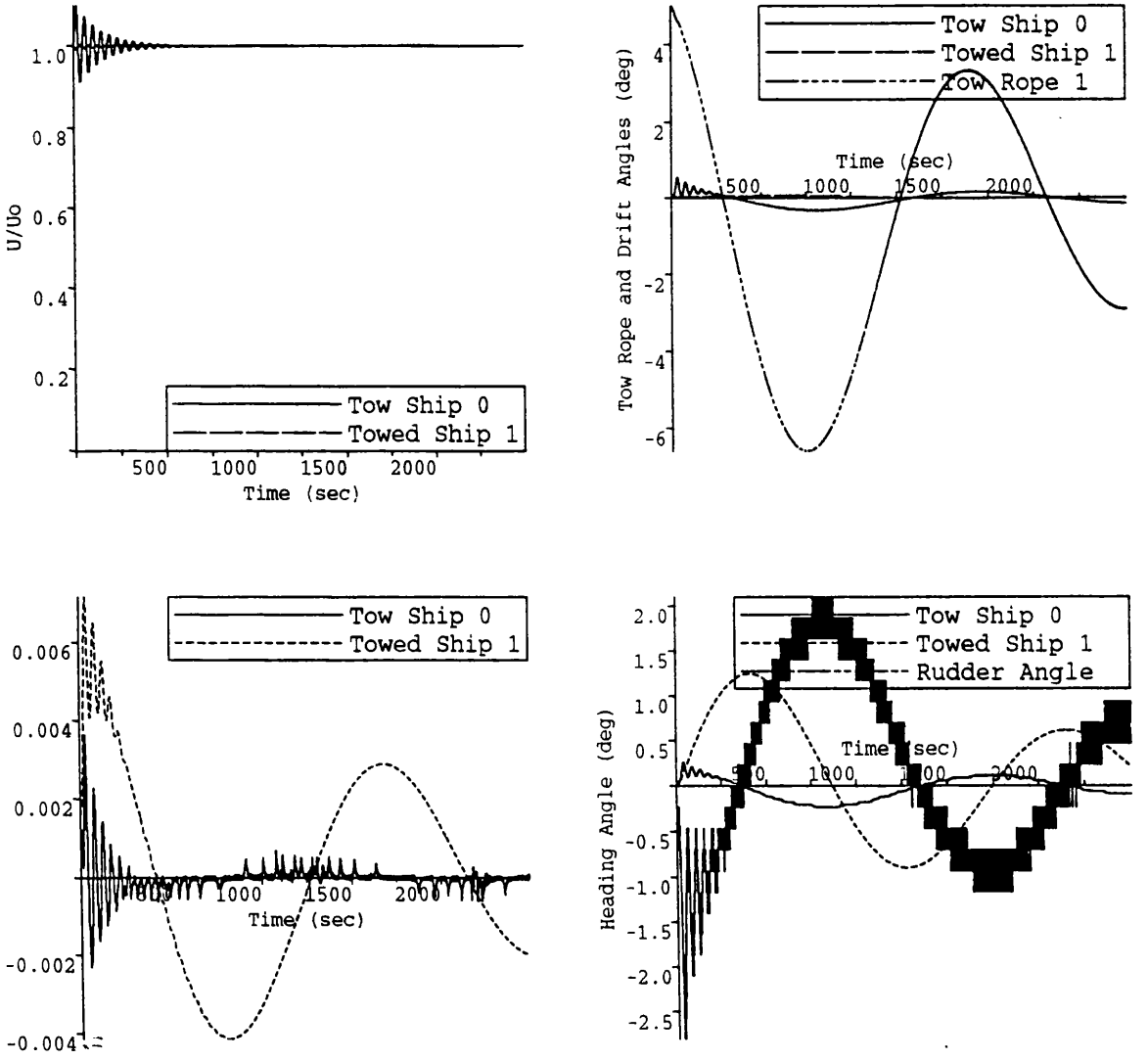

Figure 7.10c

Tow Velocity : 5.837 Knots
Rudder Constants 1,2 :8.0,5.0
Tow Point 0 : 0.000m
Tow Rope Length/L0 : 4.000m/m
Tow Point 1 :77.250m
Tow Rope :PY
Maximum Deflection :-2.800 Degrees

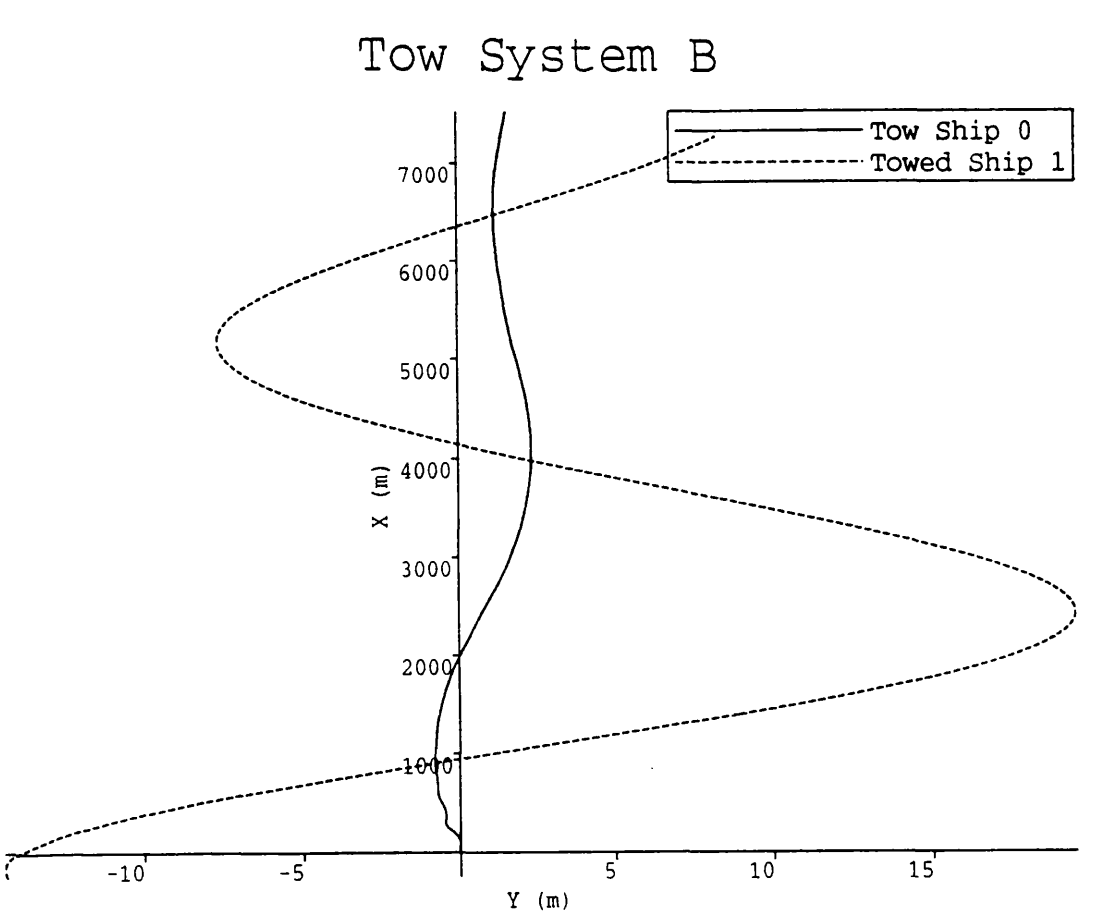

Figure 7.11a

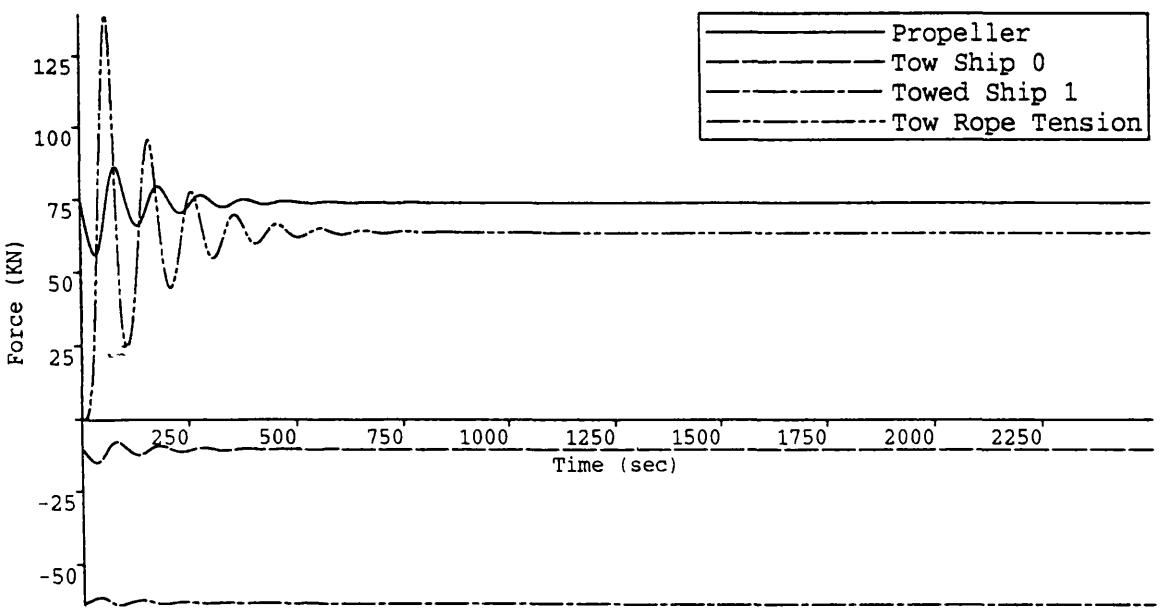

Figure 7.11b

```
Tow Velocity :  5.837 Knots
Rudder Constants 1,2 :8.0,5.0
Tow Point 0 : 0.000m
Tow Rope Length/L0 : 4.000m/m
Tow Point 1 :77.250m
Tow Rope :NW
Maximum Deflection :-2.567 Degrees
```

Tow System B.

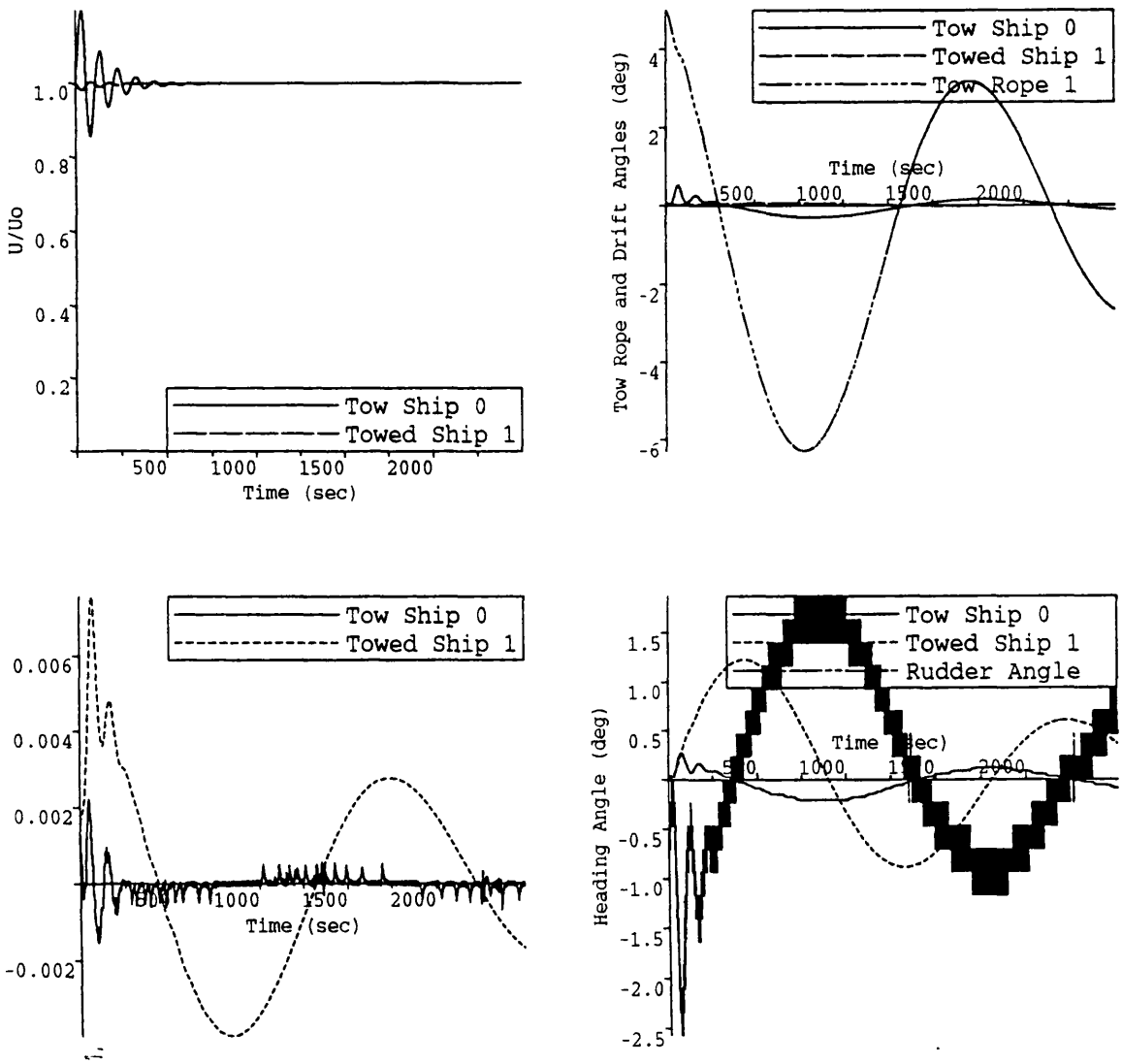

Figure 7.11c

Tow Velocity : 5.837 Knots
Rudder Constants 1,2 :8.0,5.0
Tow Point 0 : 0.000m
Tow Rope Length/L0 : 4.000m/m
Tow Point 1 :77.250m
Tow Rope :NW
Maximum Deflection :-2.567 Degrees

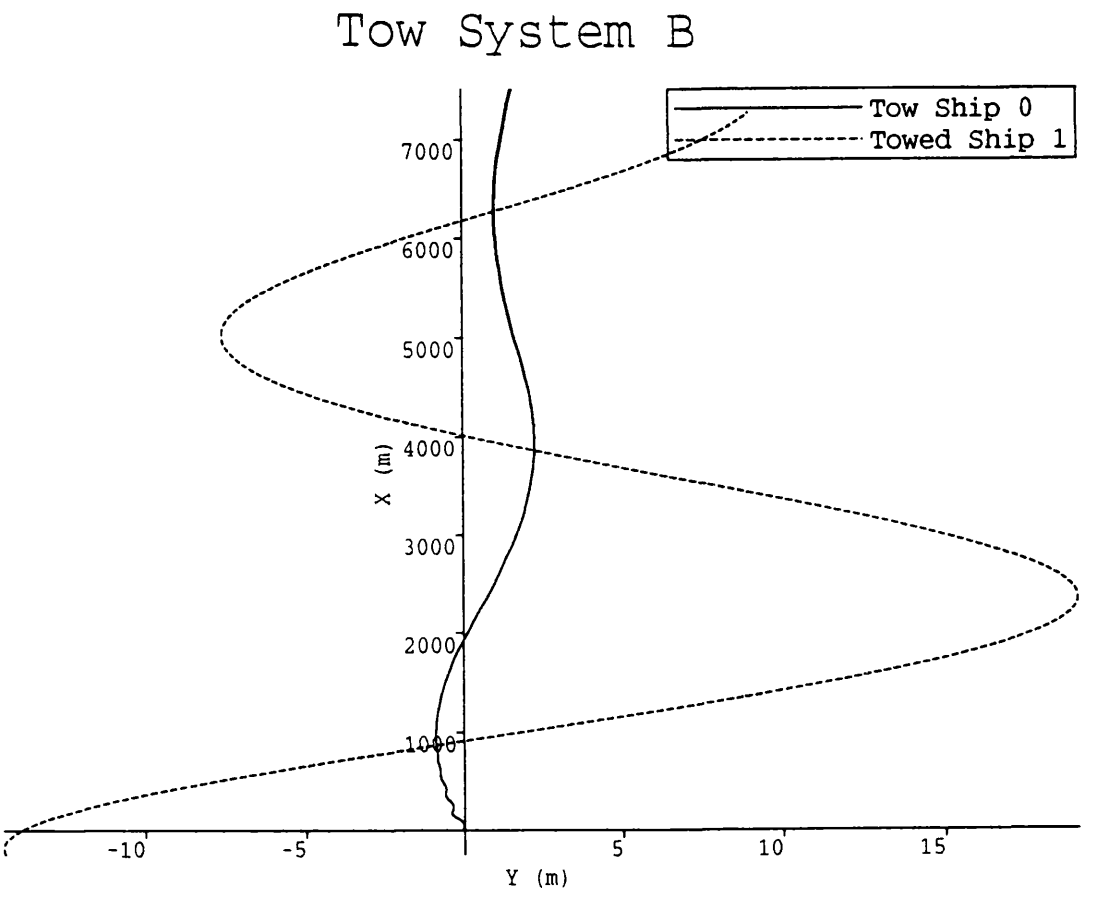

Figure 7.12a

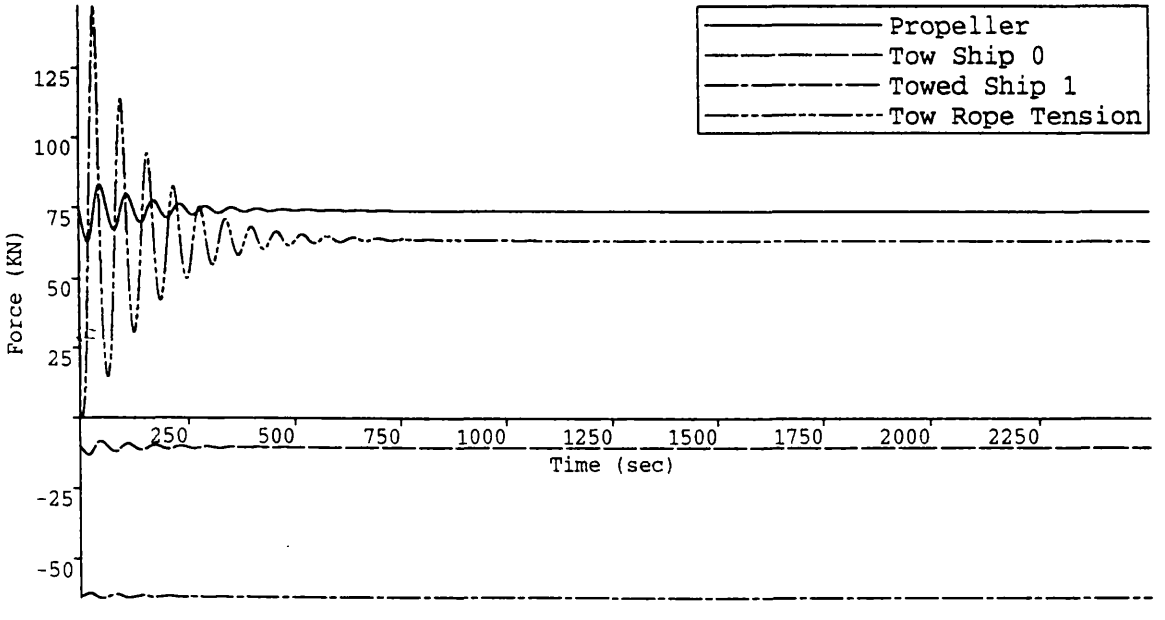

Figure 7.12b

```
Tow Velocity :  5.837 Knots
Rudder Constants 1,2 :8.0,5.0
Tow Point 0 : 0.000m
Tow Rope Length/L0 : 4.000m/m
Tow Point 1 :77.250m
Tow Rope :PP
Maximum Deflection :-2.800 Degrees
```

Tow System B.

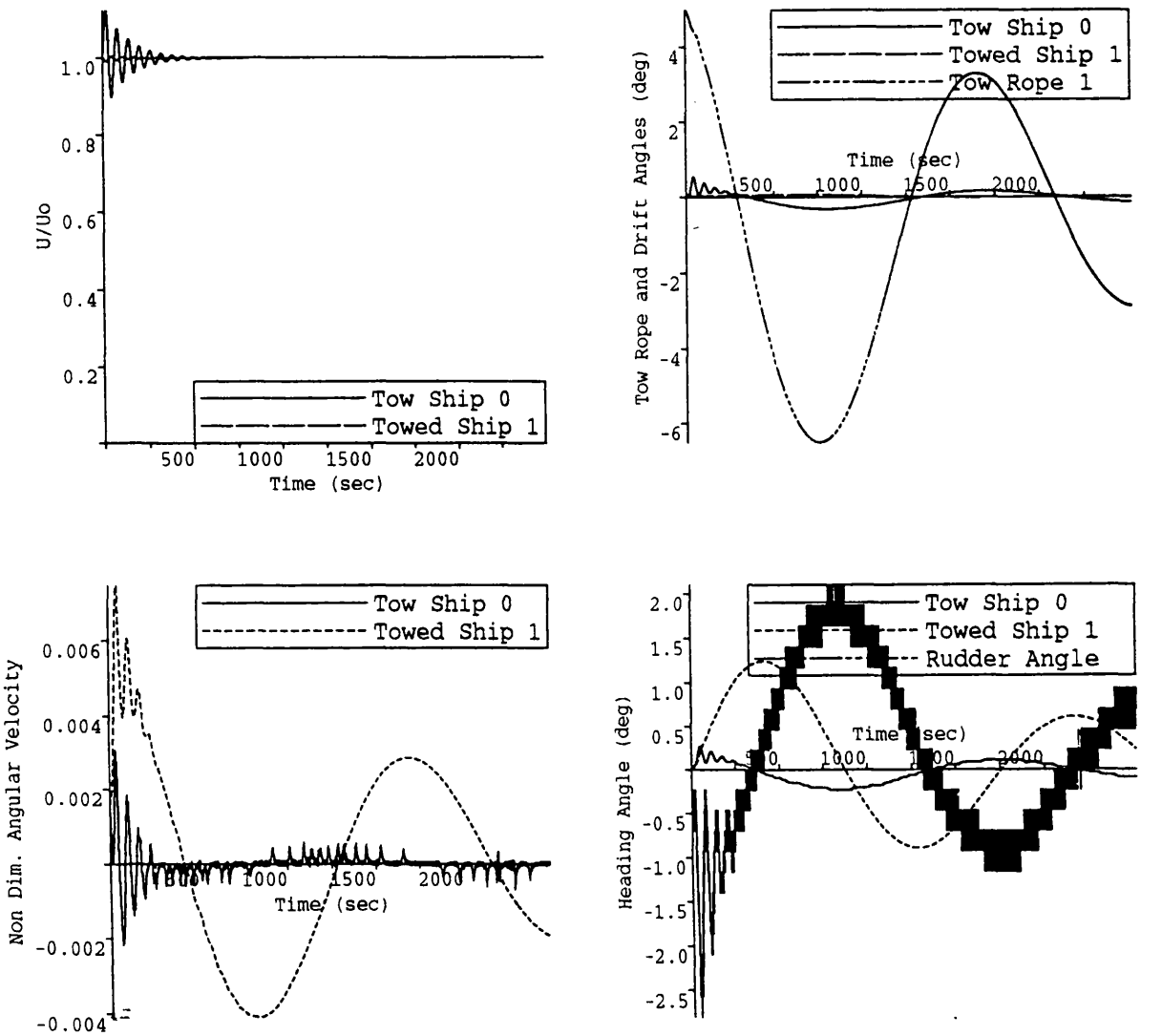

Figure 7.12c

Tow Velocity : 5.837 Knots
Rudder Constants 1,2 :8.0,5.0
Tow Point 0 : 0.000m
Tow Rope Length/L0 : 4.000m/m
Tow Point 1 :77.250m
Tow Rope :PP
Maximum Deflection :-2.800 Degrees

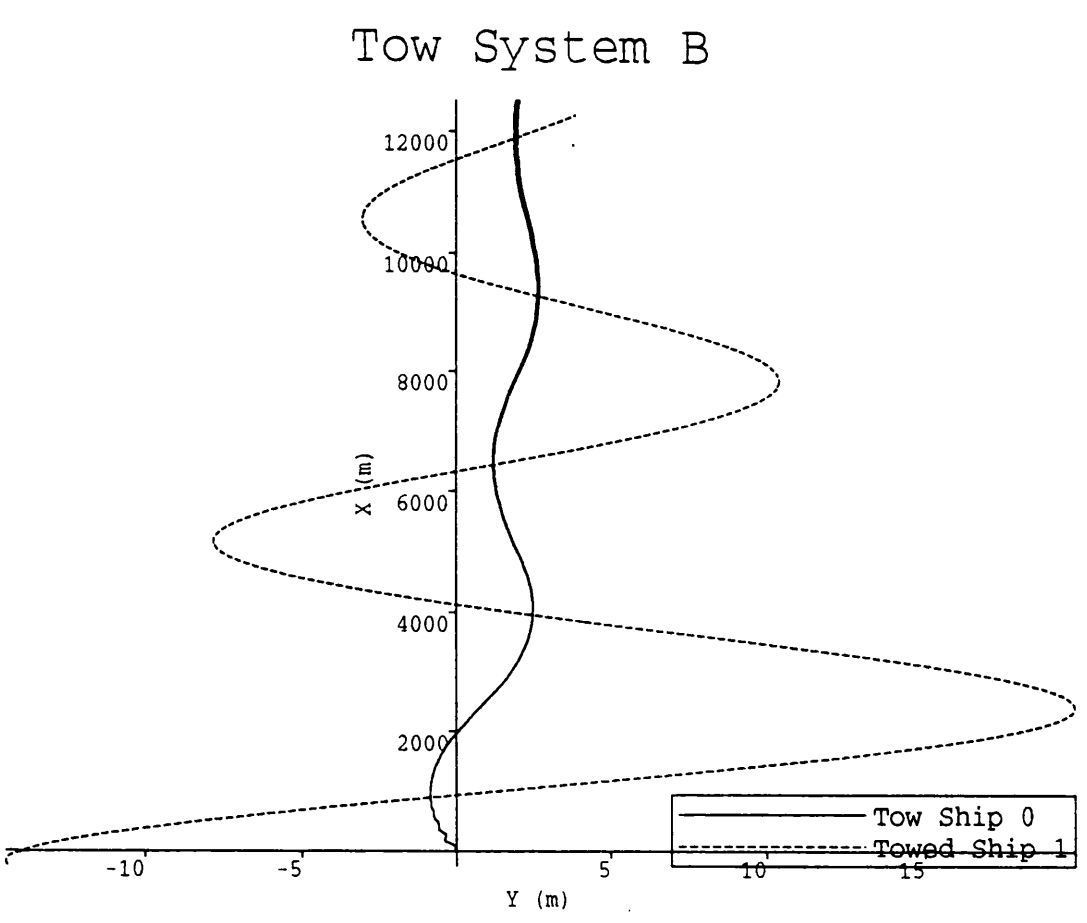

Figure 7.13a

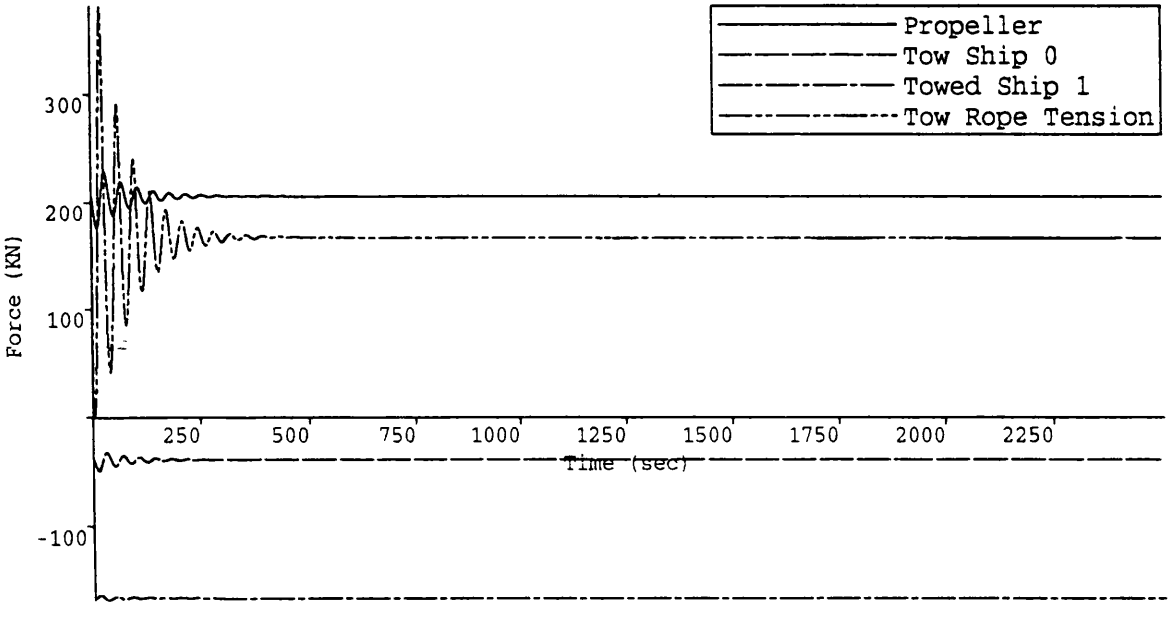

Figure 7.13b

```
Tow Velocity :  9.728 Knots
Rudder Constants 1,2 :8.0,5.0
Tow Point 0 : 0.000m
Tow Rope Length/L0 : 4.000m/m
Tow Point 1 :77.250m
Tow Rope :PP
Maximum Deflection :-2.567 Degrees
```

Tow System B.

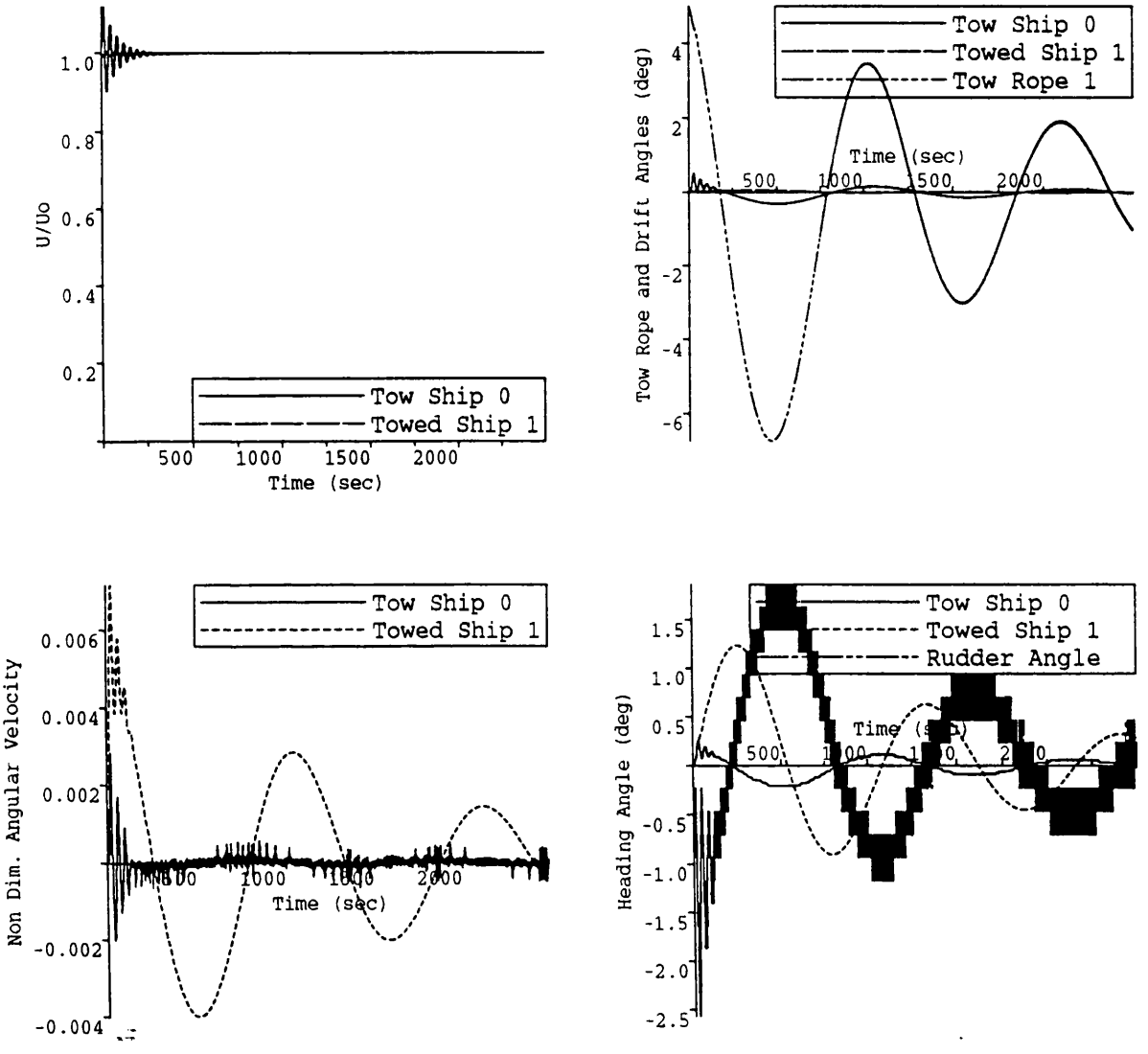

Figure 7.13c

Tow Velocity : 9.728 Knots
Rudder Constants 1,2 :8.0,5.0
Tow Point 0 : 0.000m
Tow Rope Length/L0 : 4.000m/m
Tow Point 1 :77.250m
Tow Rope :PP
Maximum Deflection :-2.567 Degrees

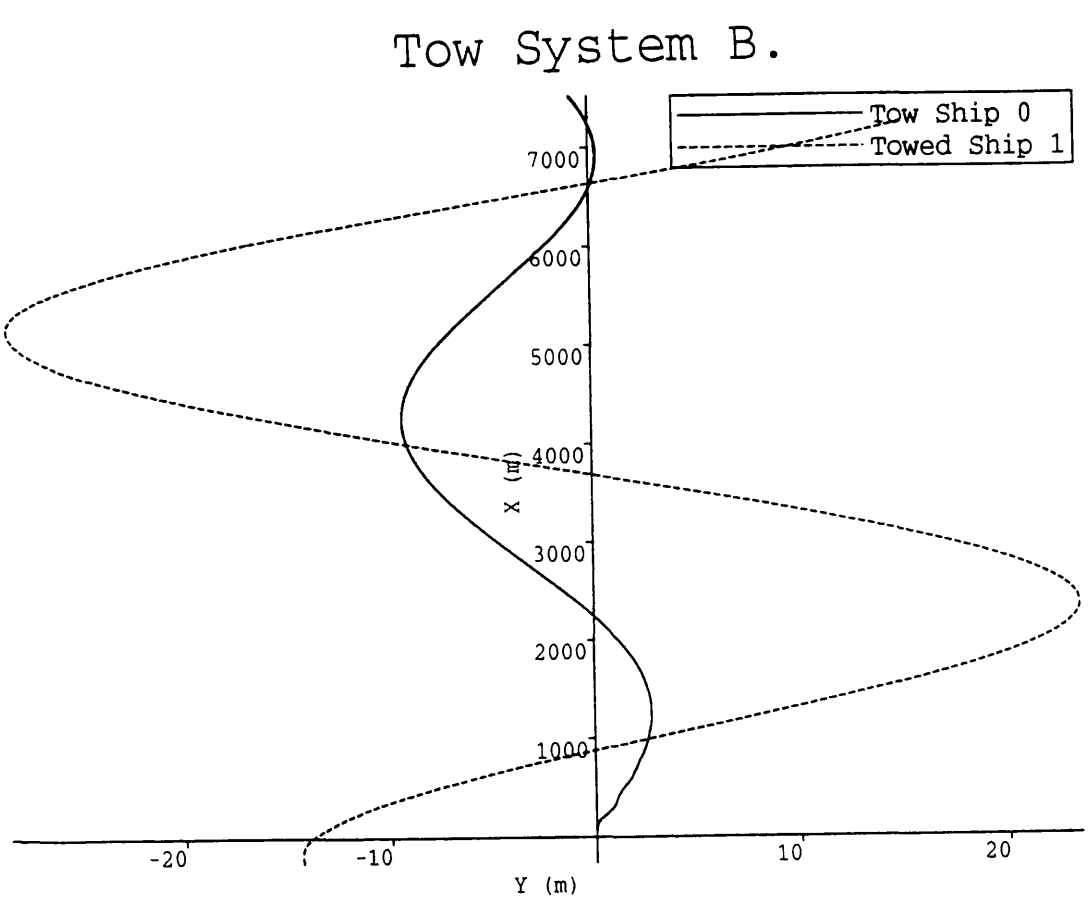

Figure 7.14a

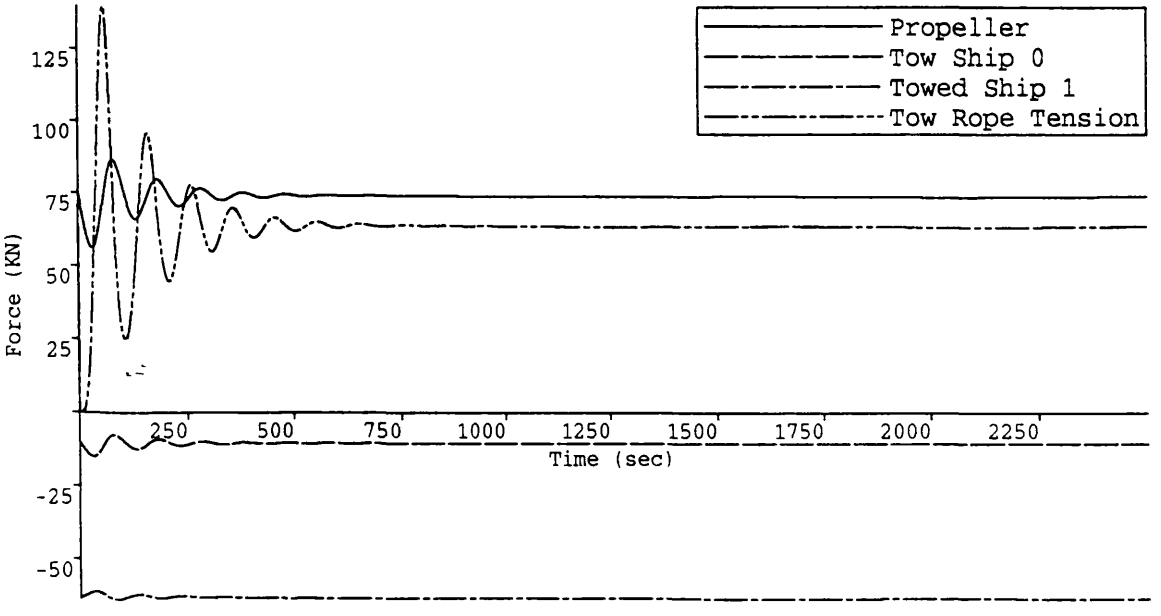

Figure 7.14b

```
Tow Velocity :  5.837 Knots
Rudder Constants 1,2 :8.0,5.0
Tow Point 0 :-16.448m
Tow Rope Length/L0 : 4.000m/m
Tow Point 1 :77.250m
Tow Rope :NW
Maximum Deflection :-5.367 Degrees
```

Tow System B

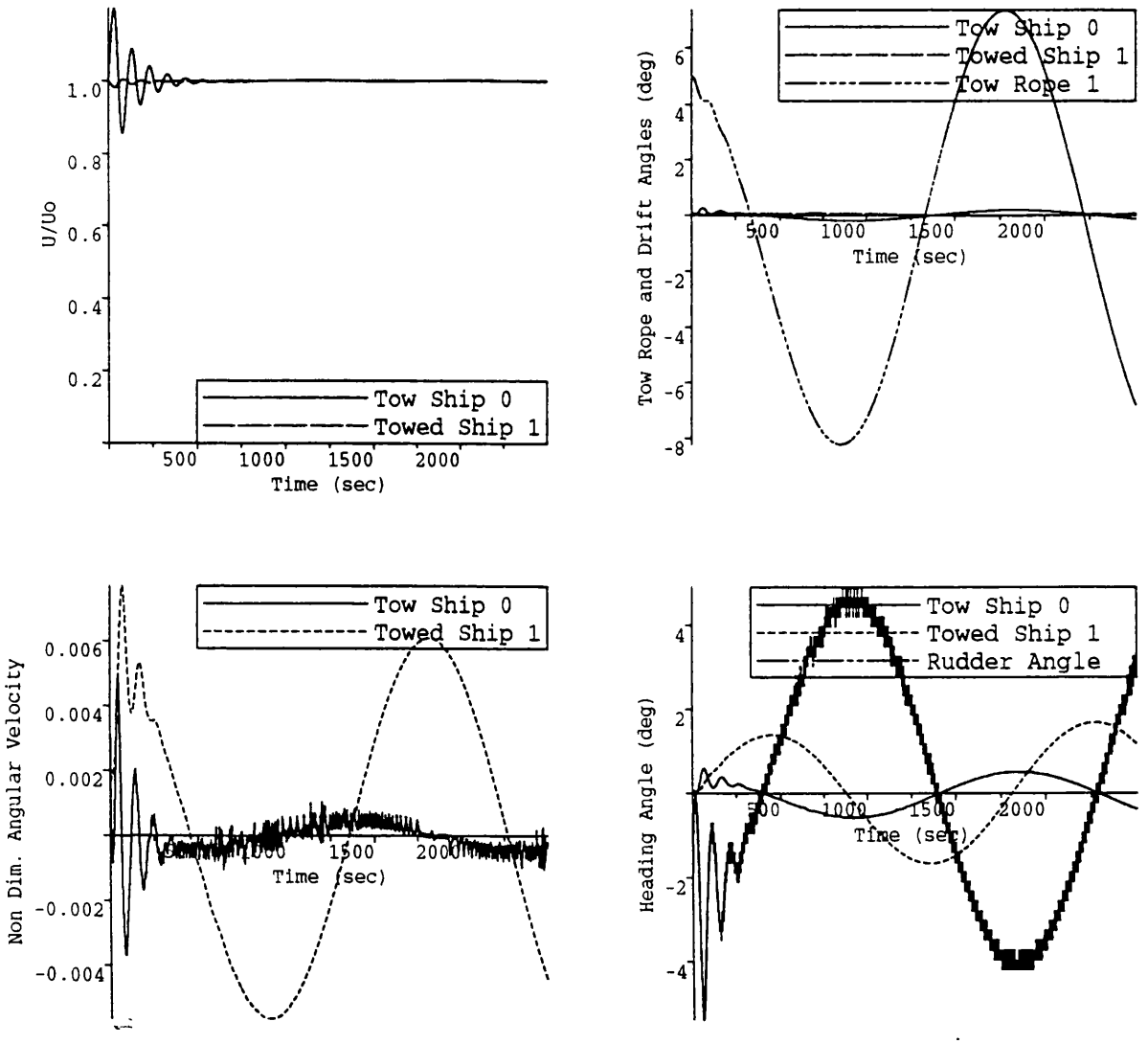

Figure 7.14c

Tow Velocity : 5.837 Knots
Rudder Constants 1,2 :8.0,5.0
Tow Point 0 :-16.448m
Tow Rope Length/L0 : 4.000m/m
Tow Point 1 :77.250m
Tow Rope :NW
Maximum Deflection :-5.367 Degrees

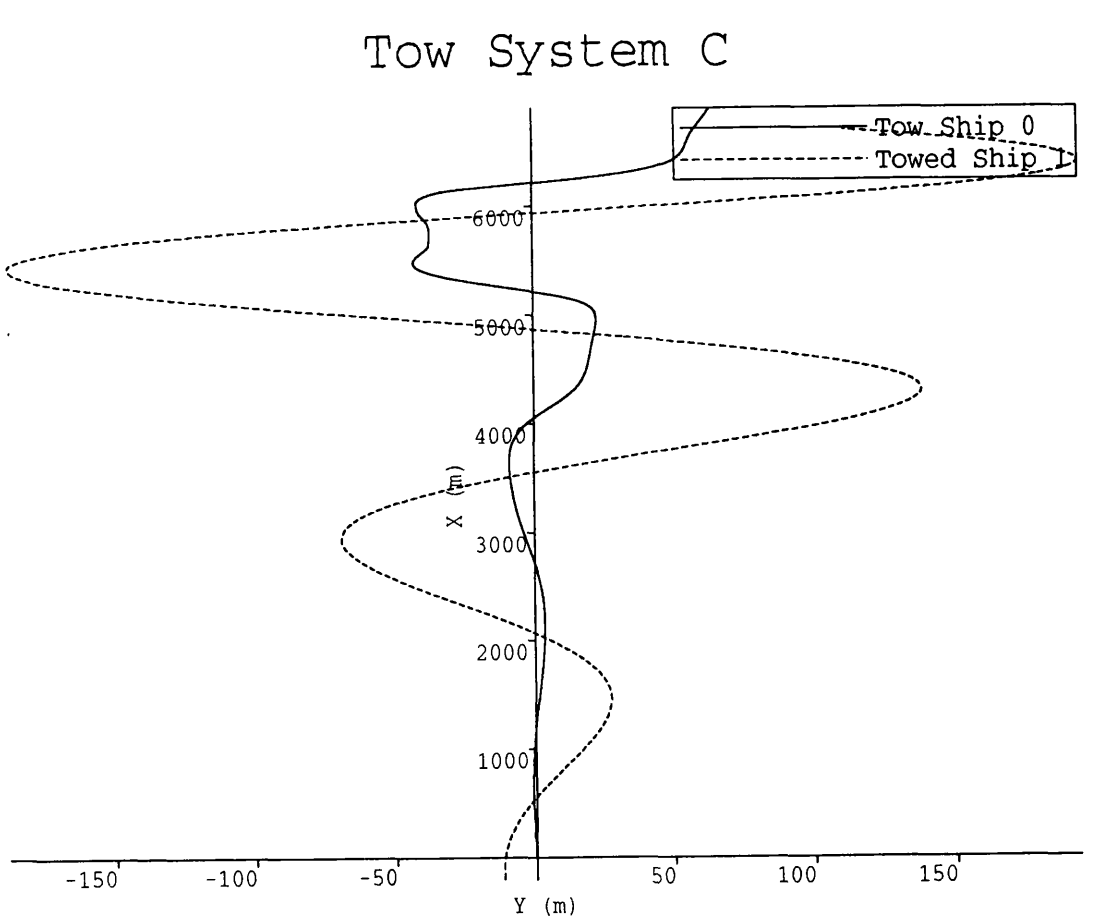

Figure 7.15a

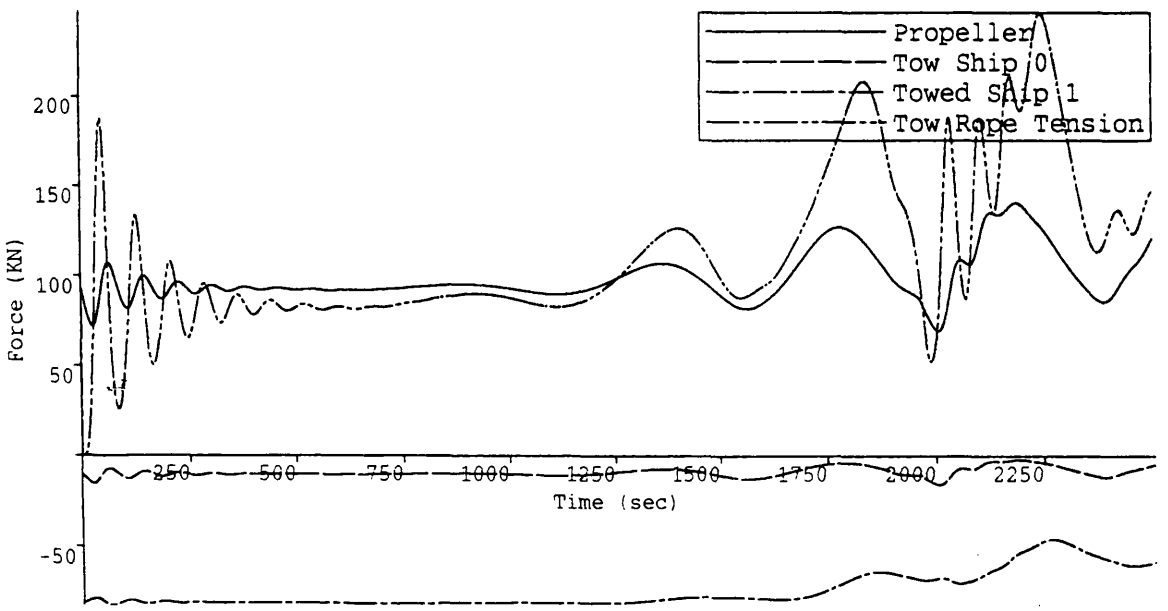

Figure 7.15b

Tow Velocity : 5.837 Knots
Rudder Constants 1,2 :8.0,5.0
Tow Point 0 : 0.000m
Tow Rope Length/L0 : 3.250m/m
Tow Point 1 :63.300m
Tow Rope :NW
Maximum Deflection :-35.233 Degrees

Tow System C.

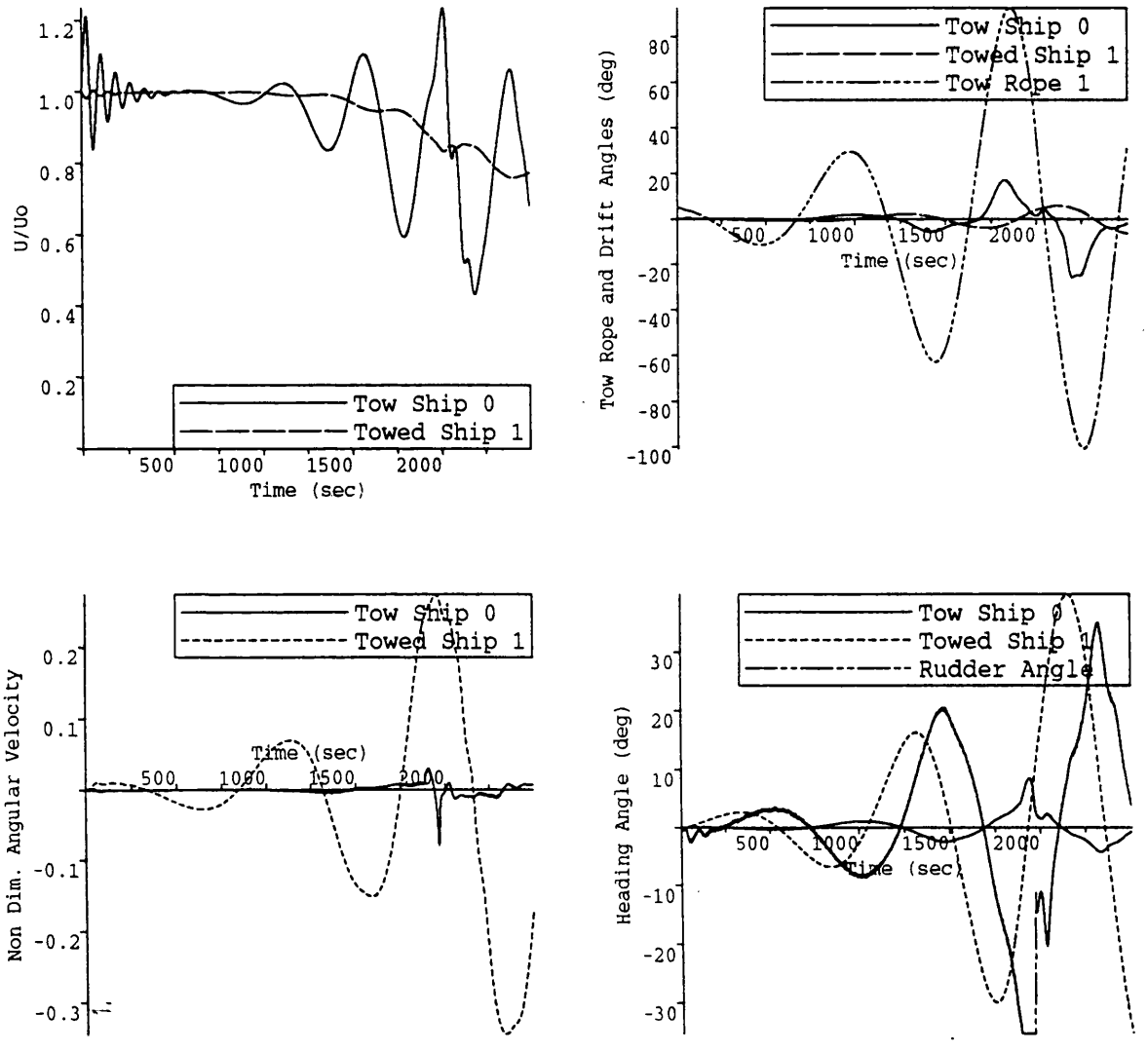

Figure 7.15c

Tow Velocity : 5.837 Knots
Rudder Constants 1,2 :8.0,5.0
Tow Point 0 : 0.000m
Tow Rope Length/L0 : 3.250m/m
Tow Point 1 :63.300m
Tow Rope :NW
Maximum Deflection :-35.233 Degrees

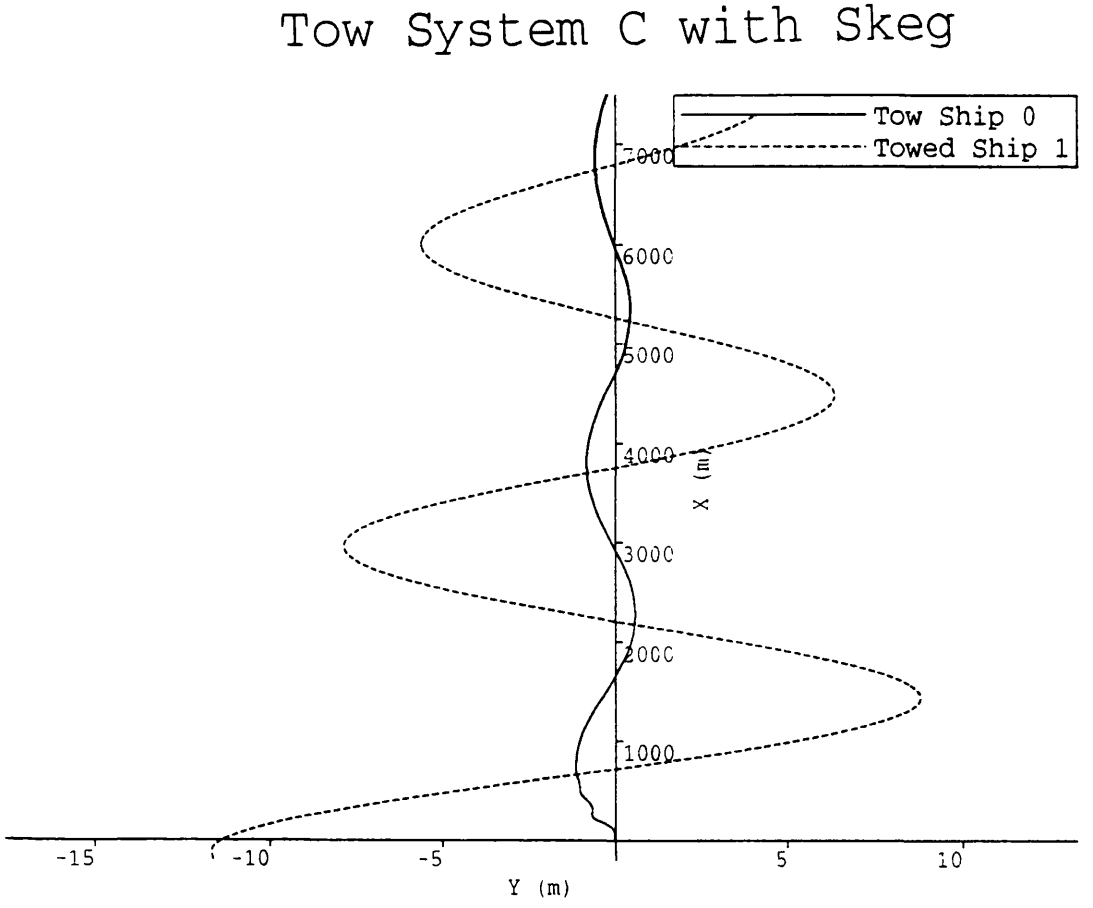

Figure 7.16a

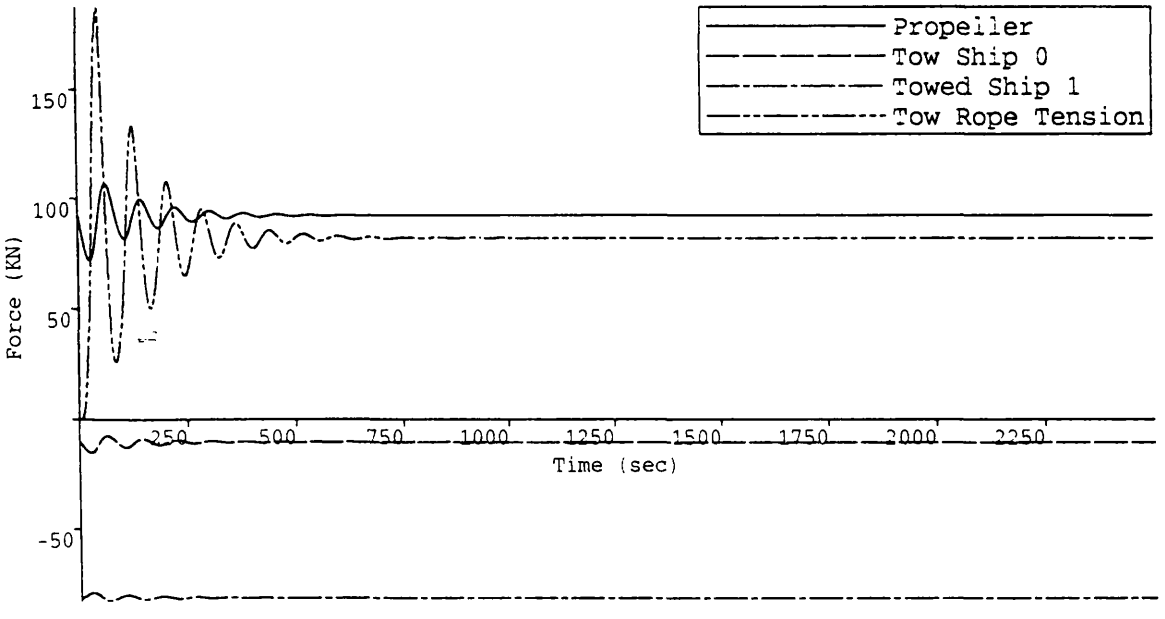

Figure 7.16b

Tow Velocity : 5.837 Knots
Rudder Constants 1,2 :8.0,5.0
Tow Point 0 : 0.000m
Tow Rope Length/L0 : 3.250m/m
Tow Point 1 :63.300m
Tow Rope :NW
Maximum Deflection :-2.567 Degrees

Tow System C with SKEG.

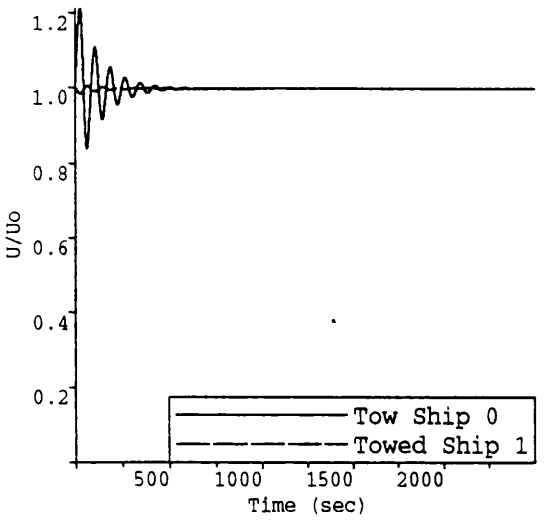

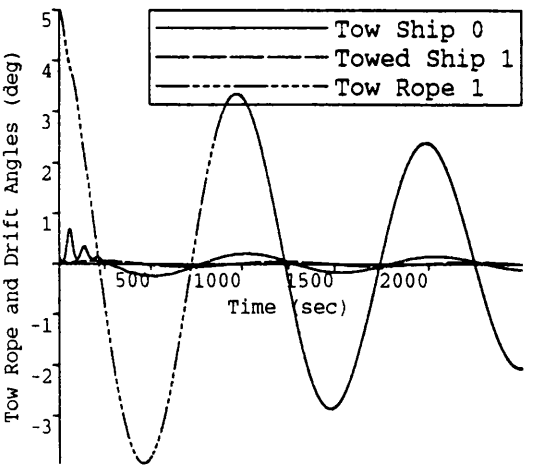

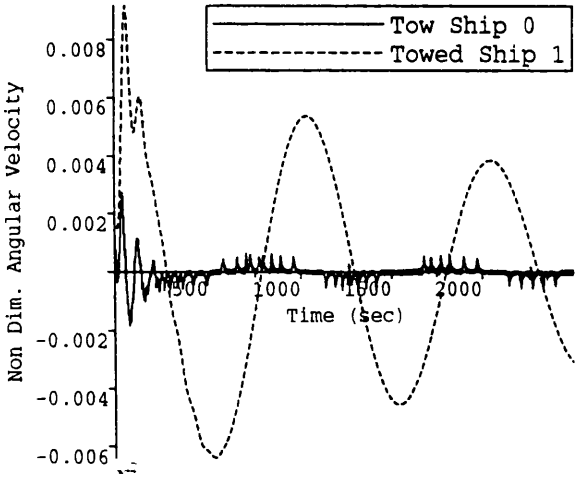

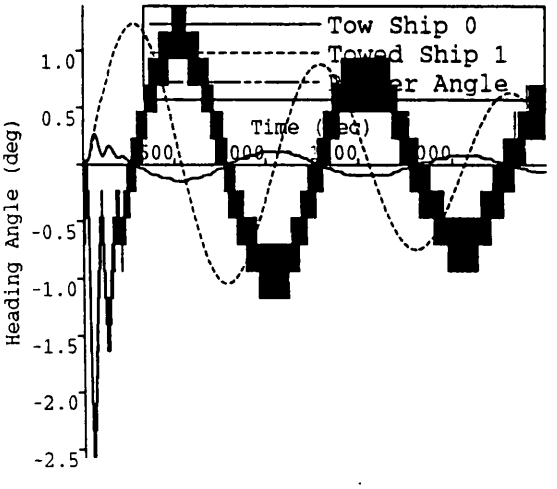

Figure 7.16c

Tow Velocity : 5.837 Knots
Rudder Constants 1,2 :8.0,5.0
Tow Point 0 : 0.000m
Tow Rope Length/L0 : 3.250m/m
Tow Point 1 :63.300m
Tow Rope :NW
Maximum Deflection :-2.567 Degrees

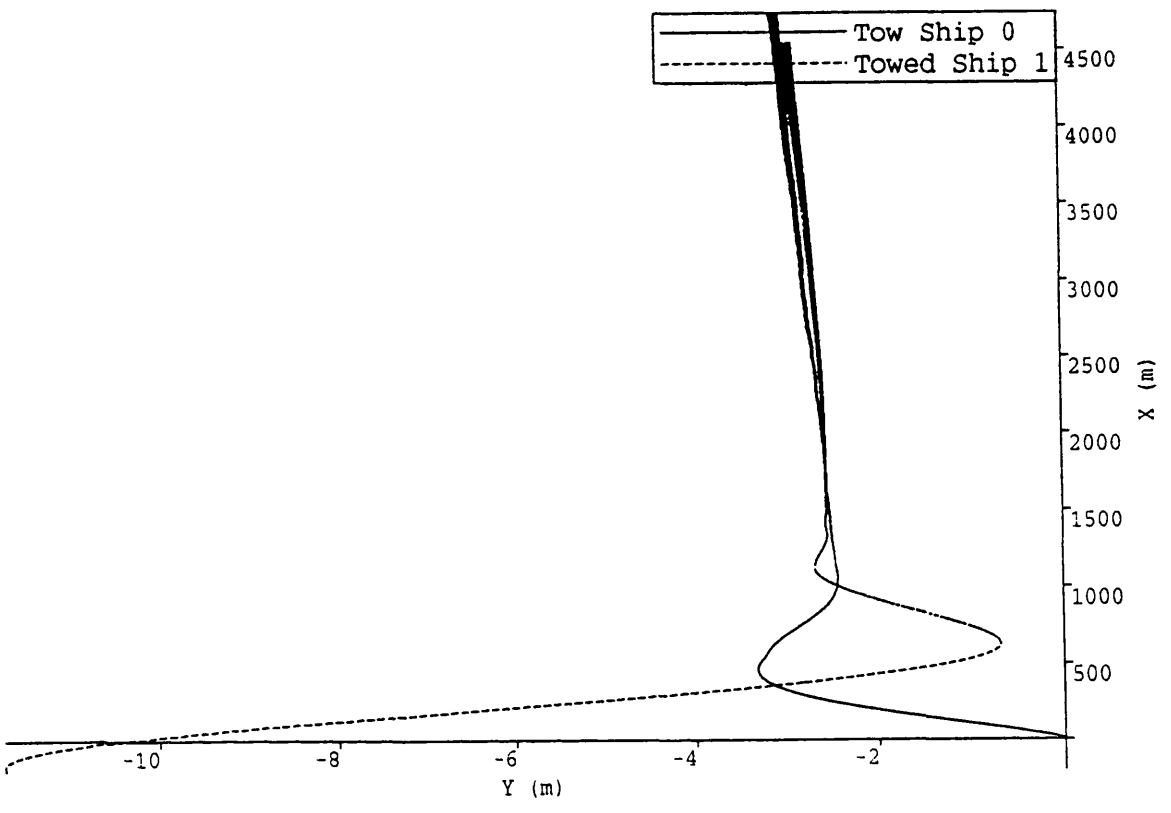

Figure 7.17a

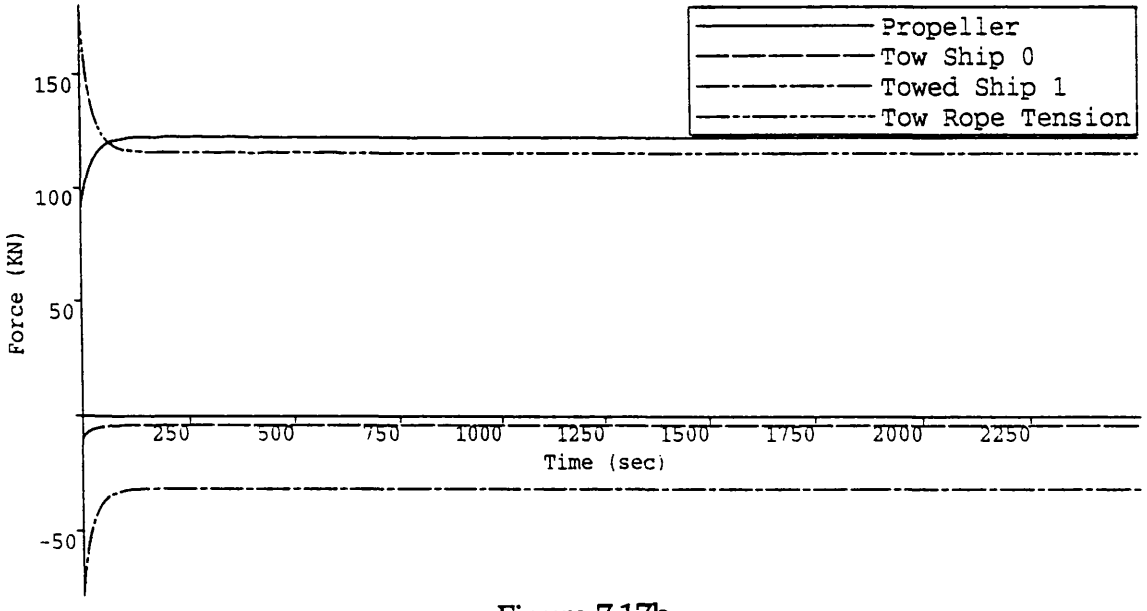

Figure 7.17b

Tow Velocity : 5.837 Knots
Rudder Constants 1,2 : 8.0,5.0
Tow Point 0 : 0.000 m
Tow Rope Length/L0 : 3.250 m/m
Tow Point 1 : 63.300 m
Tow Rope : Rigid
Maximum Deflection : -2.567 Degrees
Wind Velocity,Angle : 19.5, 0.0 Knots,Deg

Tow System C with Skeg.

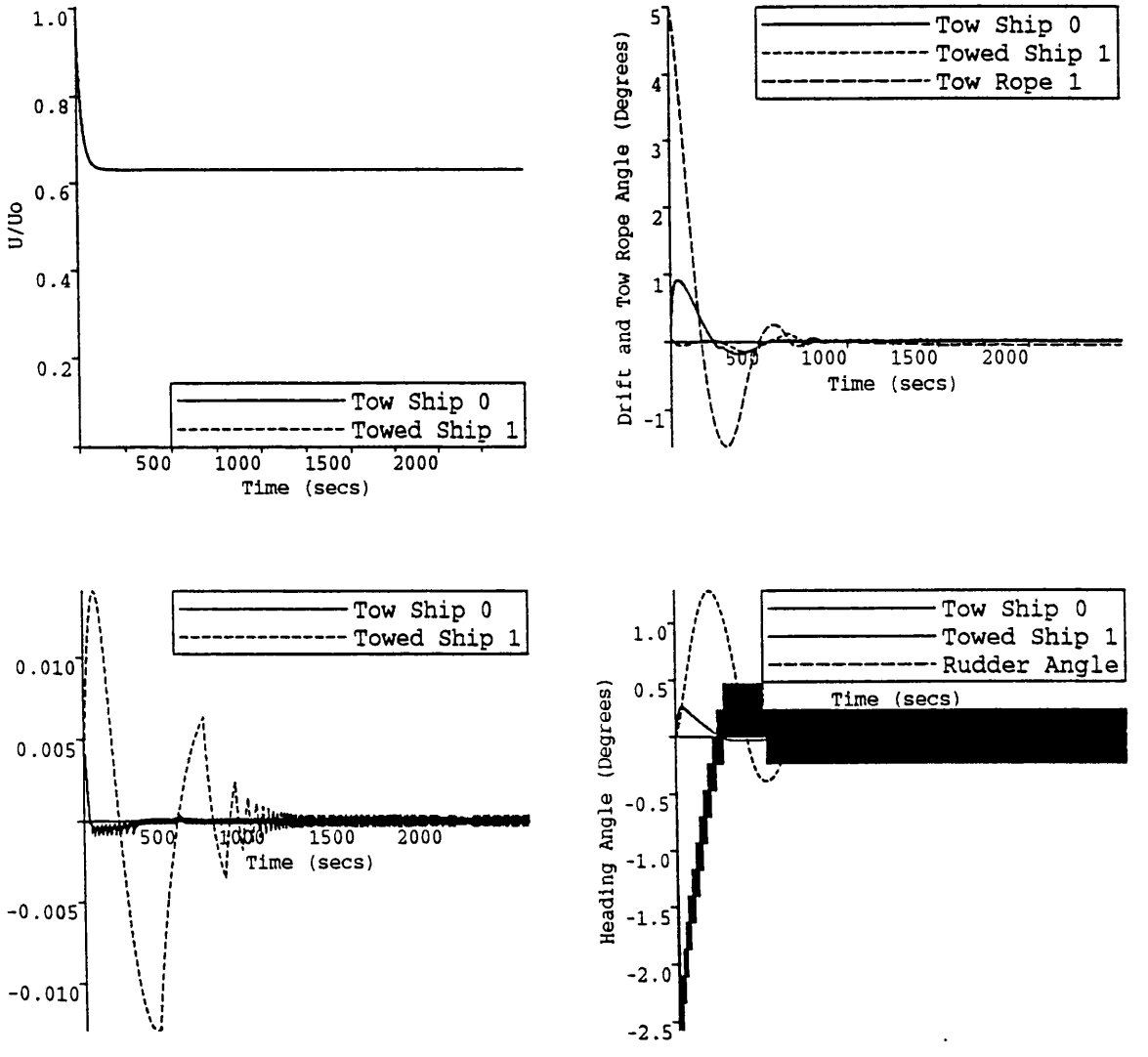

Figure 7.17c

Tow Velocity : 5.837 Knots
Rudder Constants 1,2 : 8.0,5.0
Tow Point 0 : 0.000 m
Tow Rope Length/L0 : 3.250 m/m
Tow Point 1 : 63.300 m
Tow Rope : Rigid
Maximum Deflection : -2.567 Degrees
Wind Velocity,Angle : 19.5, 0.0 Knots,Deg

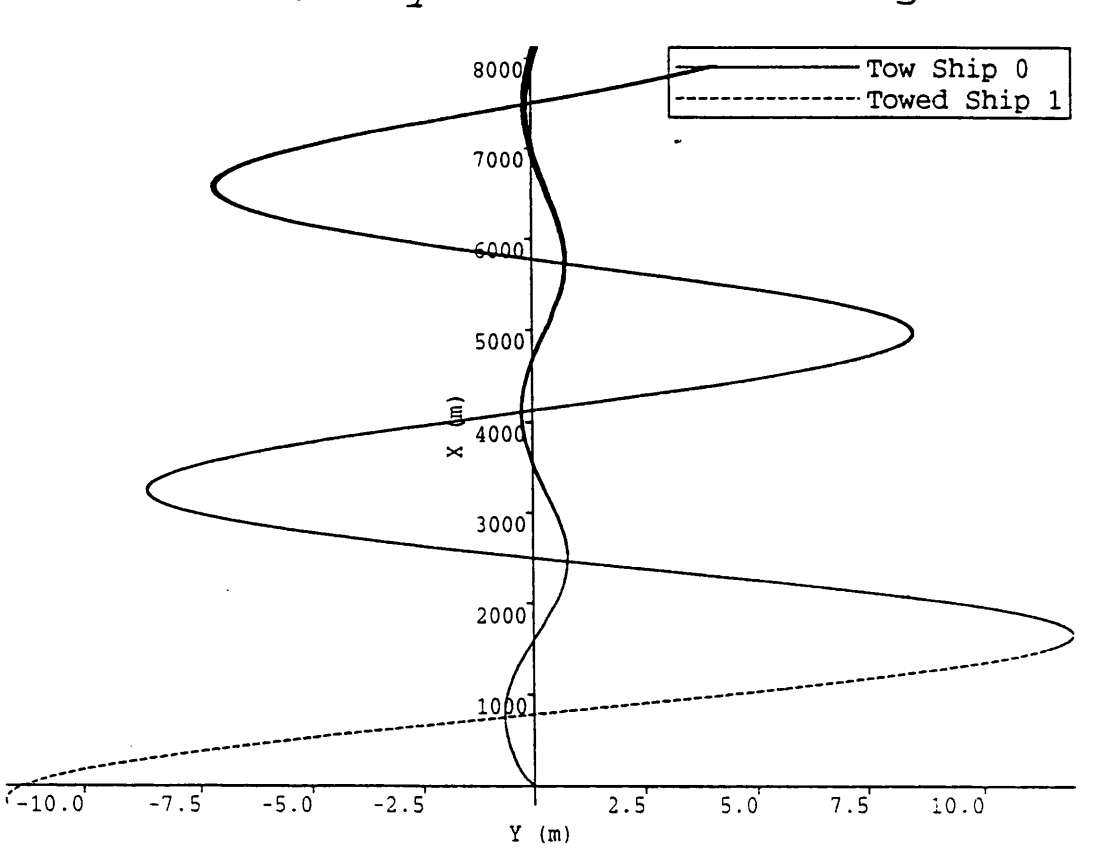

Figure 7.18a

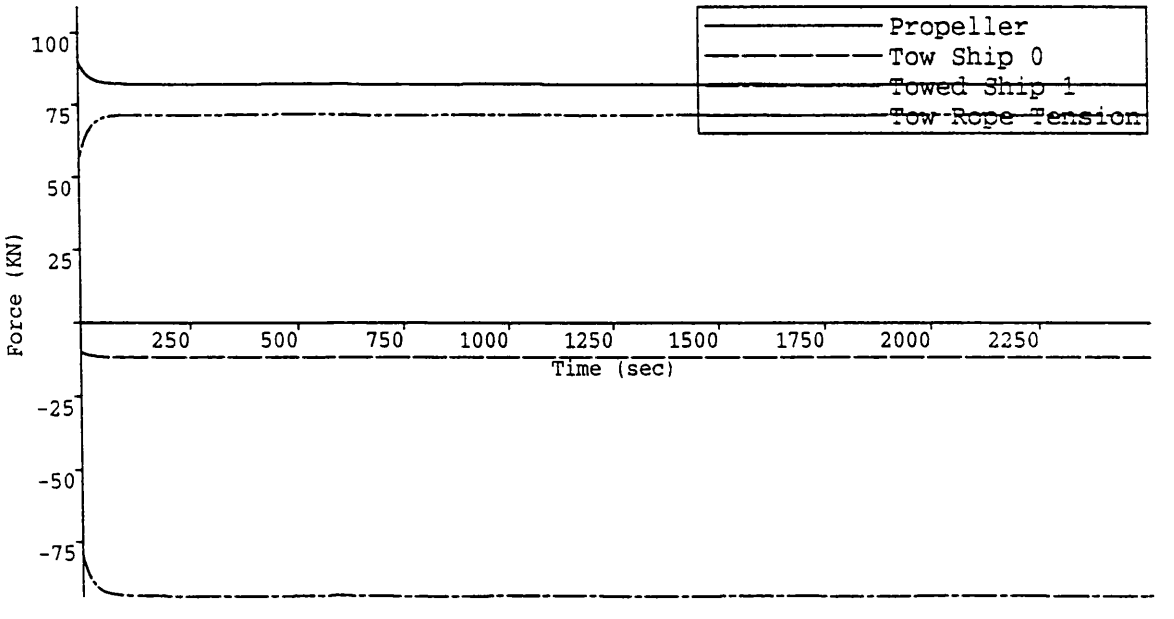

Figure 7.18b

```
Tow Velocity :  5.837 Knots
Rudder Constants 1,2 : 8.0,5.0
Tow Point 0 :   0.000 m
Tow Rope Length/L0 :  3.250 m/m
Tow Point 1 : 63.300 m
Tow Rope : Rigid
Maximum Deflection :   1.867 Degrees
Wind Velocity,Angle : 19.5,180.0 Knots,Deg
```

Tow System C with Skeg.

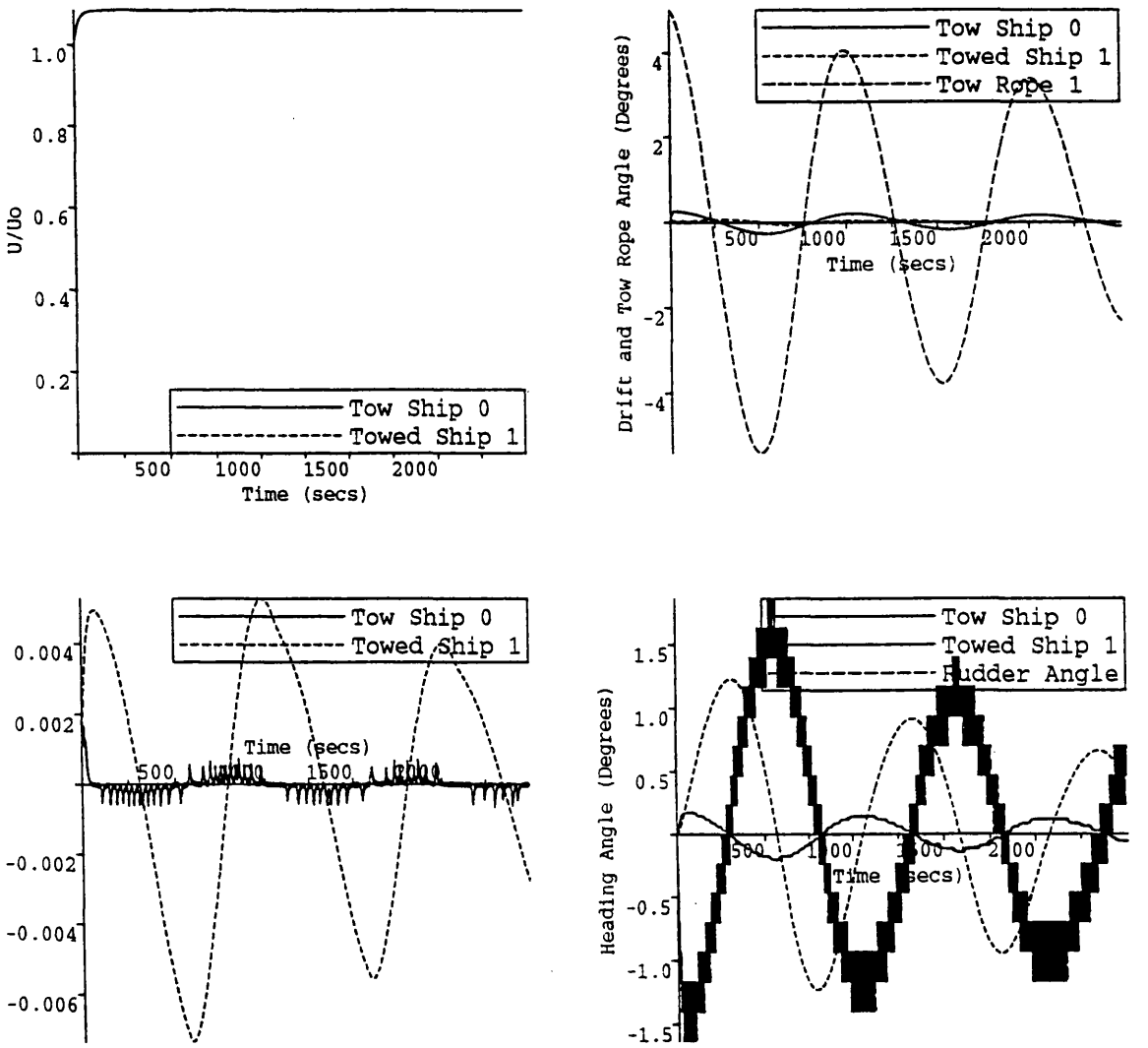

Figure 7.18c

Tow Velocity : 5.837 Knots
Rudder Constants 1,2 : 8.0,5.0
Tow Point 0 : 0.000 m
Tow Rope Length/L0 : 3.250 m/m
Tow Point 1 : 63.300 m
Tow Rope : Rigid
Maximum Deflection : 1.867 Degrees
Wind Velocity,Angle : 19.5,180.0 Knots,Deg

Tow System C with Skeg.

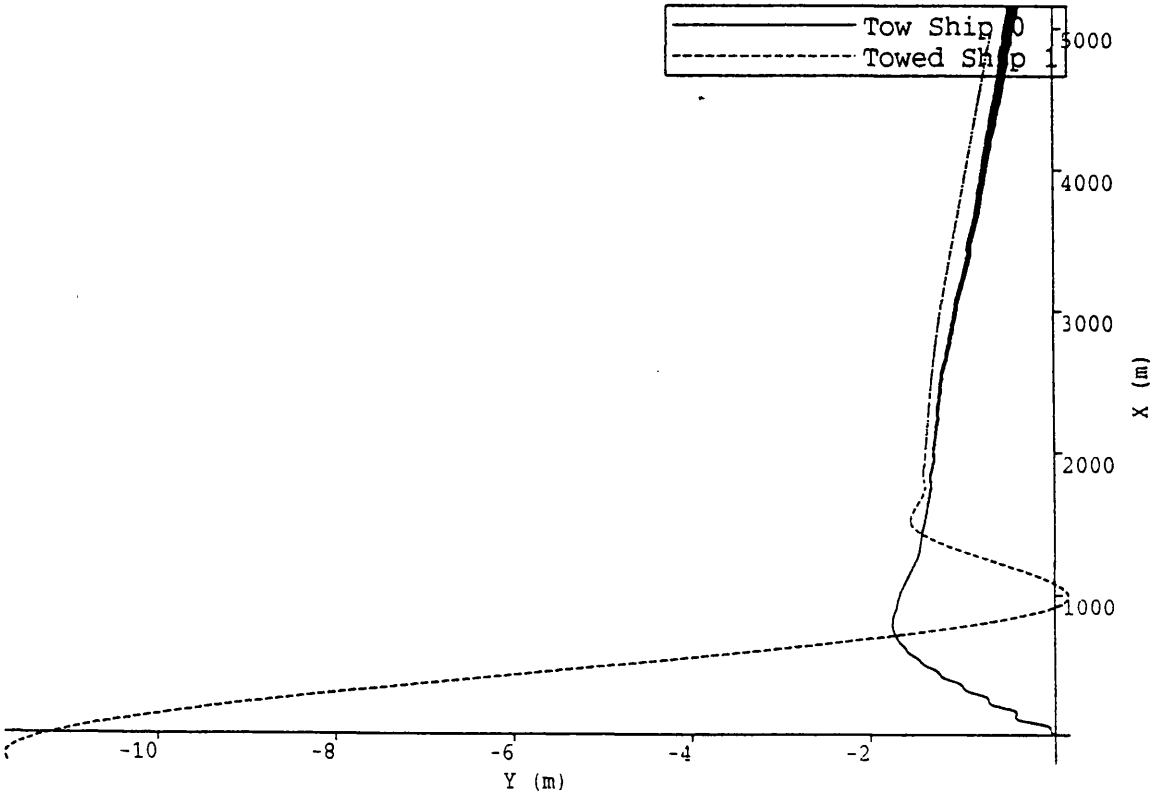

Figure 7.19a

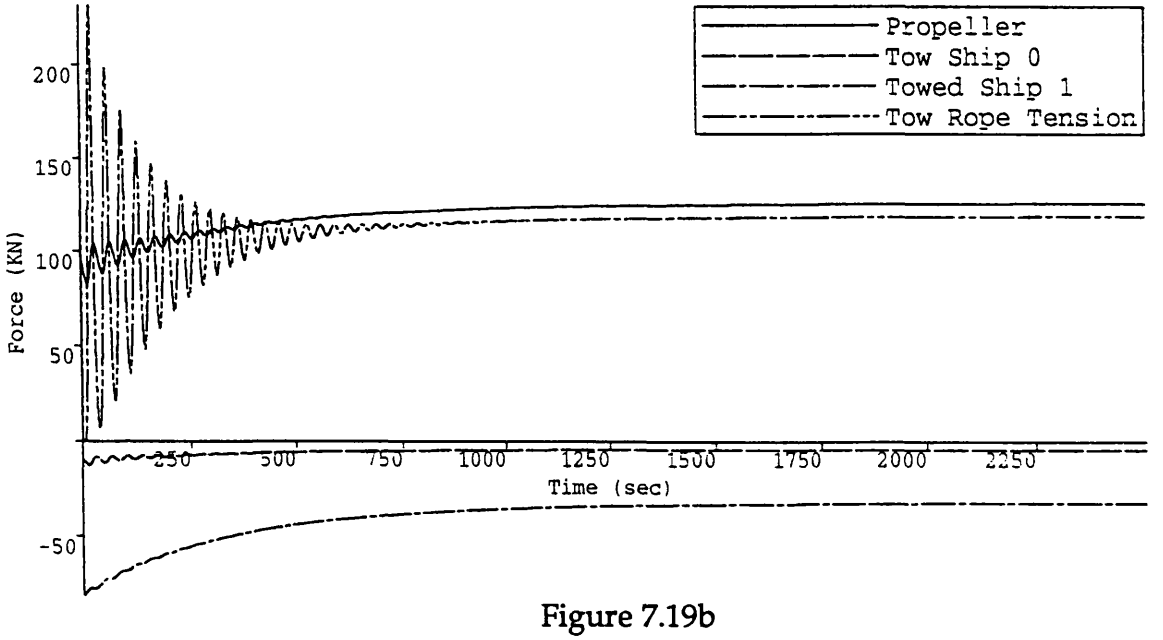

Figure 7.19b

Tow Velocity : 5.837 Knots
Rudder Constants 1,2 :8.0,5.0
Tow Point 0 : 0.000m
Tow Rope Length/L0 : 3.250m/m
Tow Point 1 :63.300m
Tow Rope :PY
Maximum Deflection : -2.800 Degrees
Wind Velocity,Angle :19.46, 0.0 Knots,Deg

Tow System C with Skeg

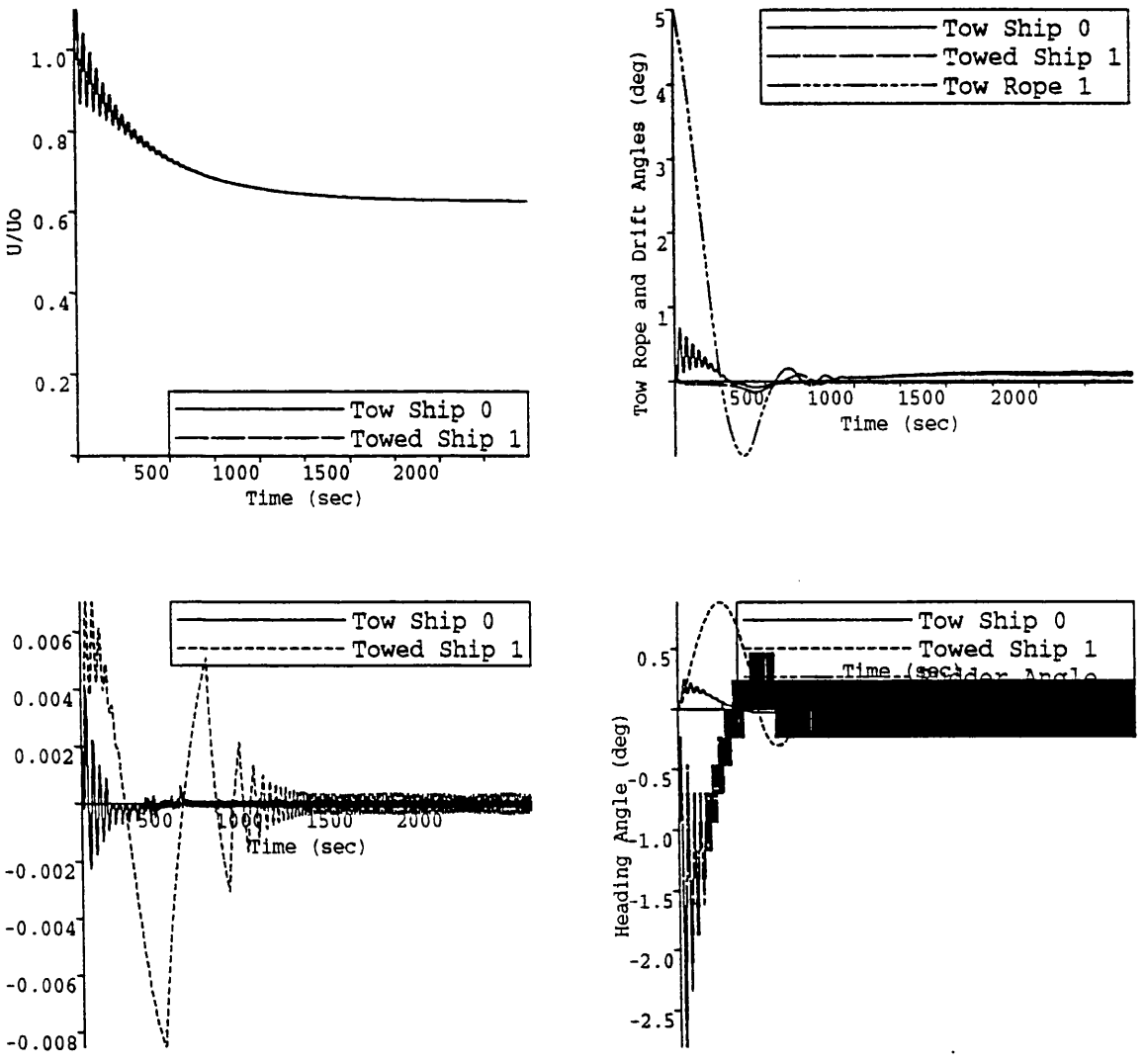

Figure 7.19c

```
Tow Velocity :  5.837 Knots
Rudder Constants 1,2 :8.0,5.0
Tow Point 0 :  0.000m
Tow Rope Length/L0 : 3.250m/m
Tow Point 1 :63.300m
Tow Rope :PY
Maximum Deflection : -2.800 Degrees
Wind Velocity,Angle :19.46, 0.0 Knots,Deg
```

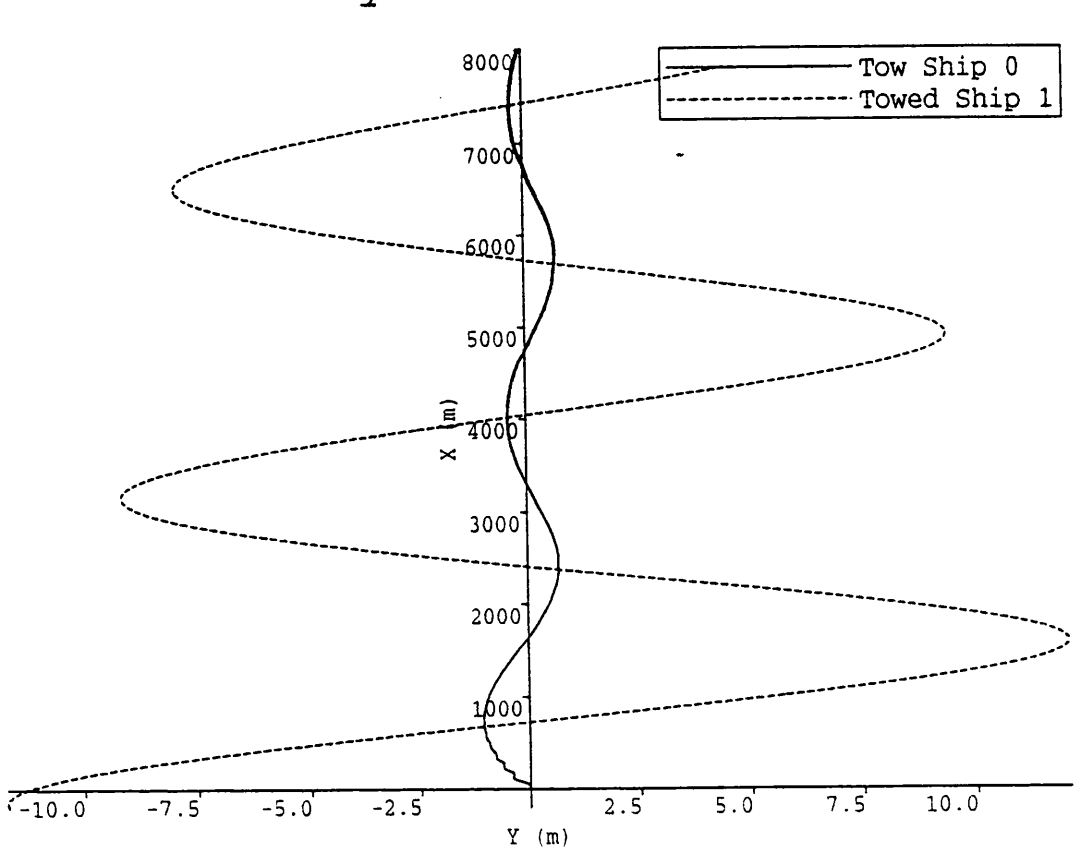

Figure 7.20a

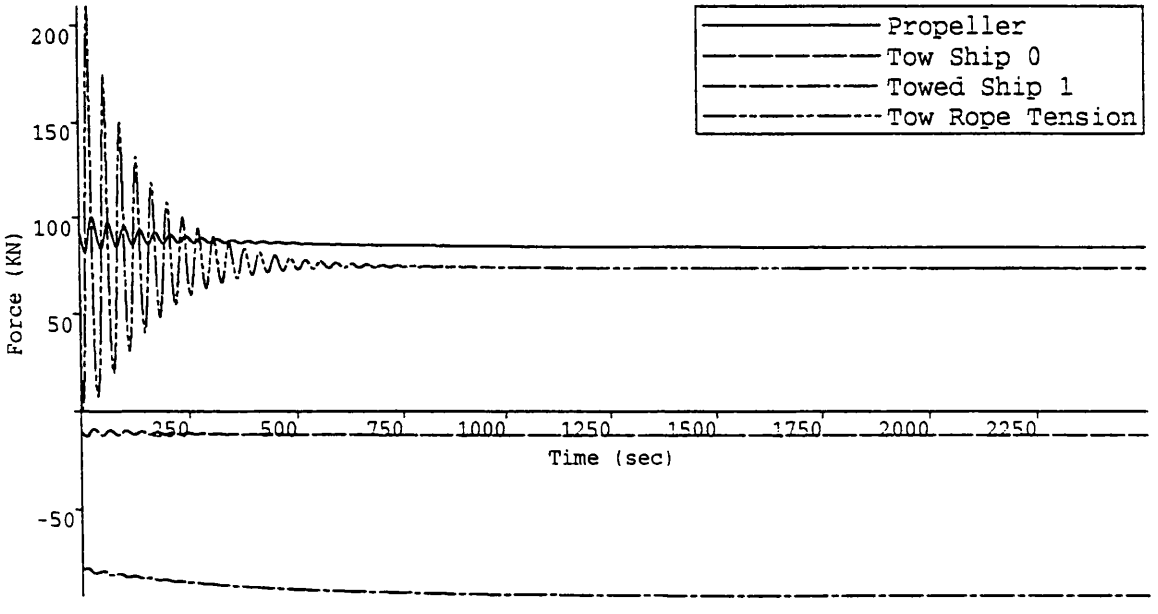

Figure 7.20b

```
Tow Velocity :  5.837 Knots
Rudder Constants 1,2 :8.0,5.0
Tow Point 0 :  0.000m
Tow Rope Length/L0 : 3.250m/m
Tow Point 1 :63.300m
Tow Rope :PY
Maximum Deflection : -2.567 Degrees
Wind Velocity,Angle :19.46, 180  Knots,Deg
```

Tow System C with Skeg

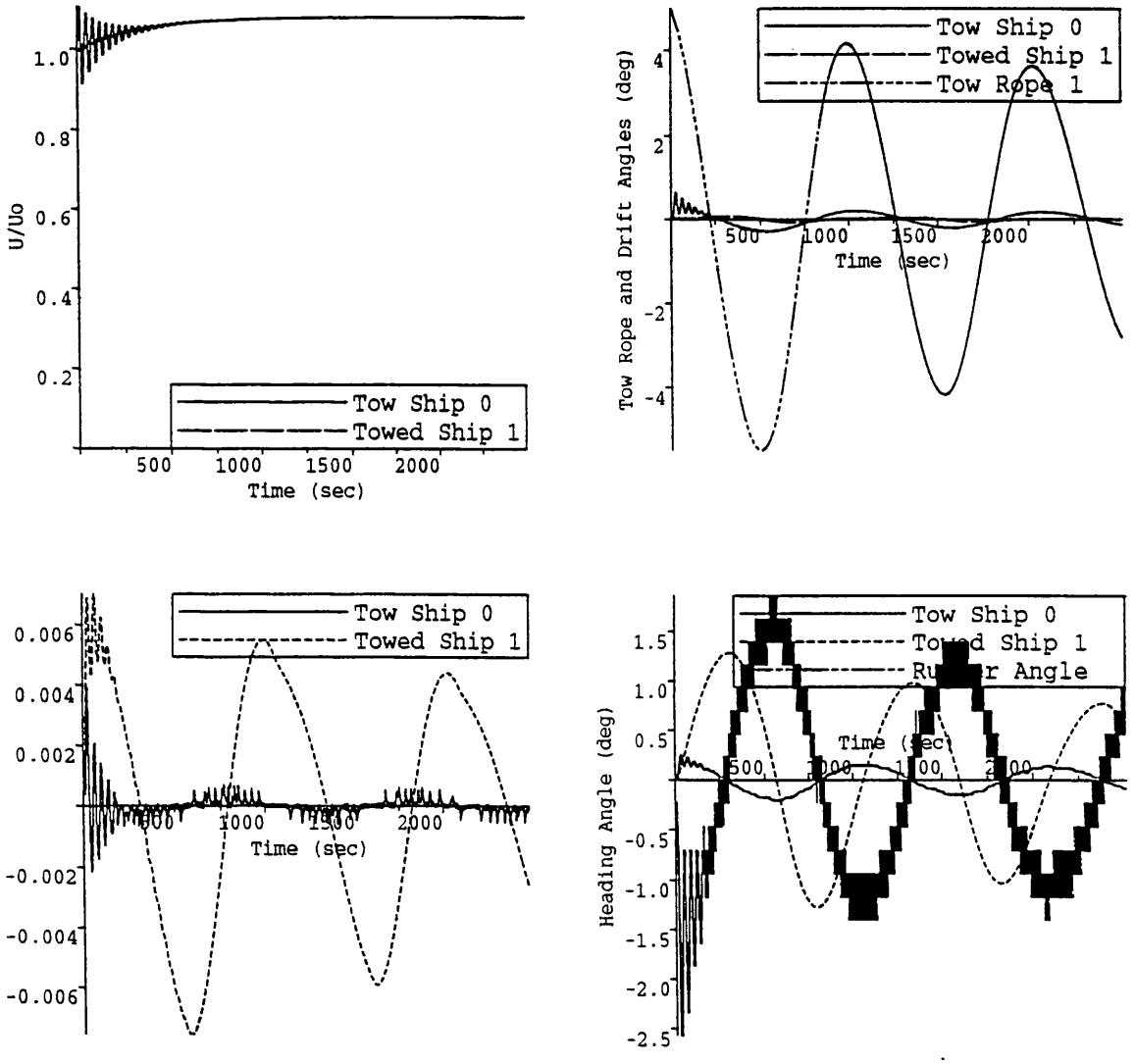

Figure 7.20c

Tow Velocity : 5.837 Knots
Rudder Constants 1,2 :8.0,5.0
Tow Point 0 : 0.000m
Tow Rope Length/L0 : 3.250m/m
Tow Point 1 :63.300m
Tow Rope :PY
Maximum Deflection : -2.567 Degrees
Wind Velocity,Angle :19.46, 180 Knots,Deg

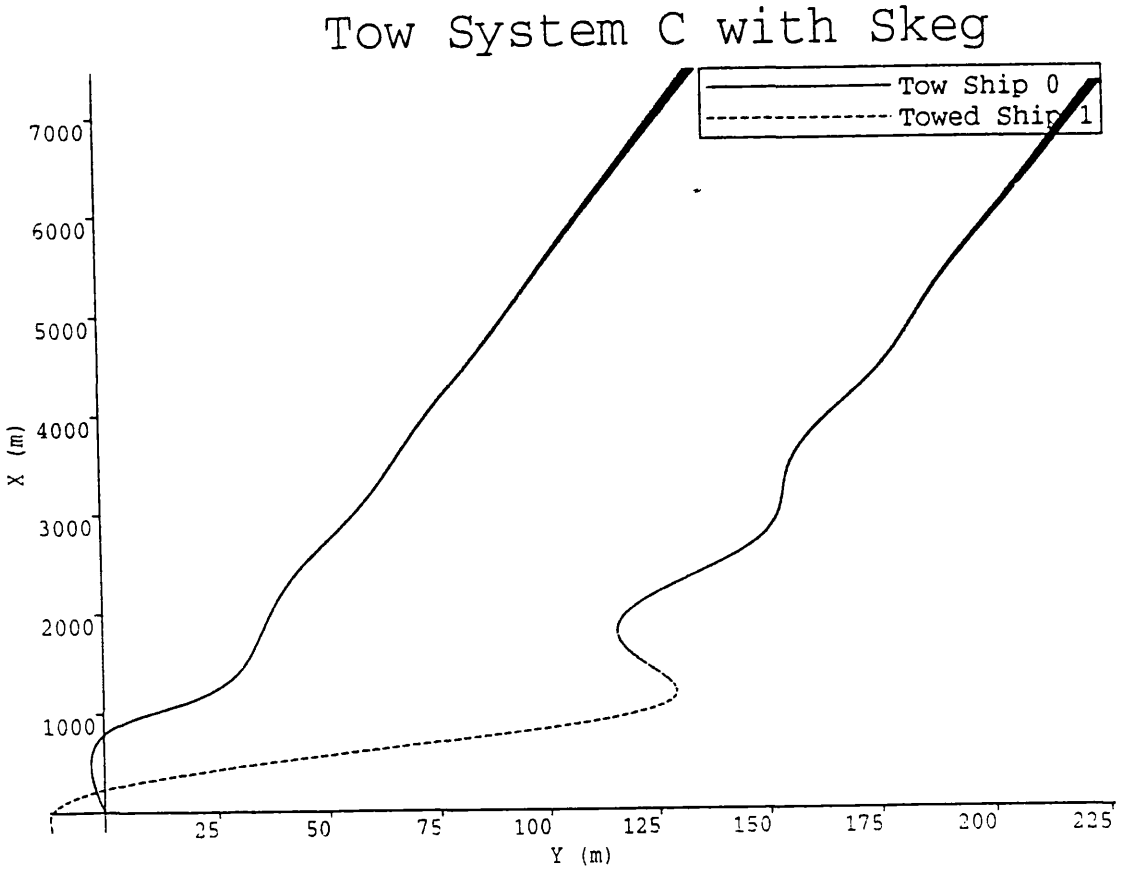

Figure 7.21a

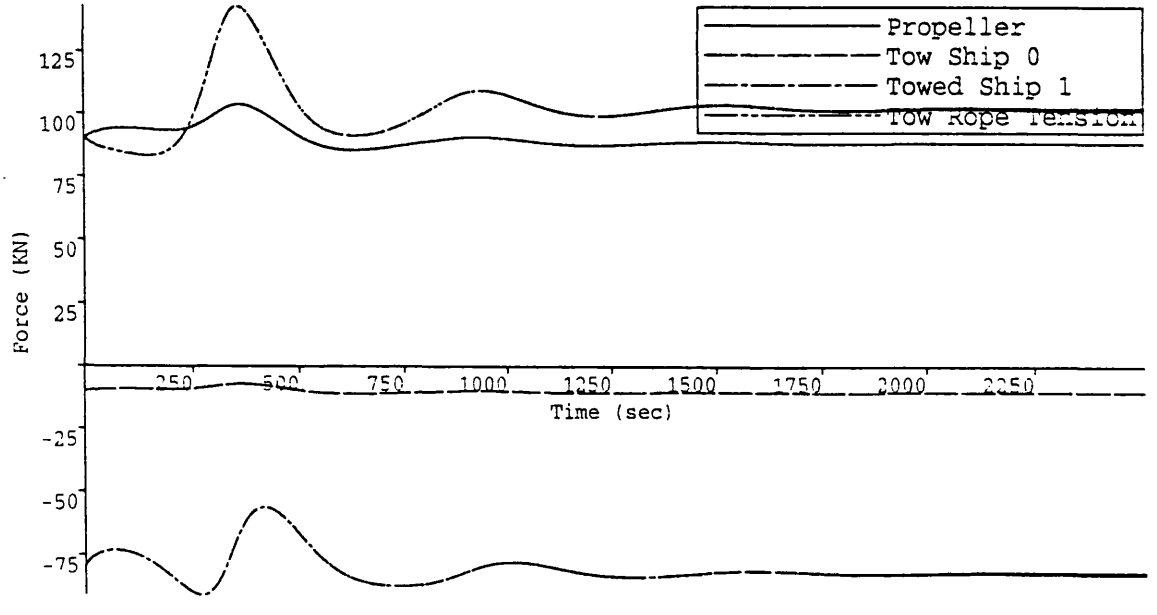

Figure 7.21b

```
Tow Velocity :  5.837 Knots
Rudder Constants 1,2 : 8.0,5.0
Tow Point 0 :   0.000 m
Tow Rope Length/L0 :  3.250 m/m
Tow Point 1 : 63.300 m
Tow Rope : Rigid
Maximum Deflection :  21.233 Degrees
Wind Velocity,Angle : 19.5, 90.0 Knots,Deg
```

Tow System C with Skeg.

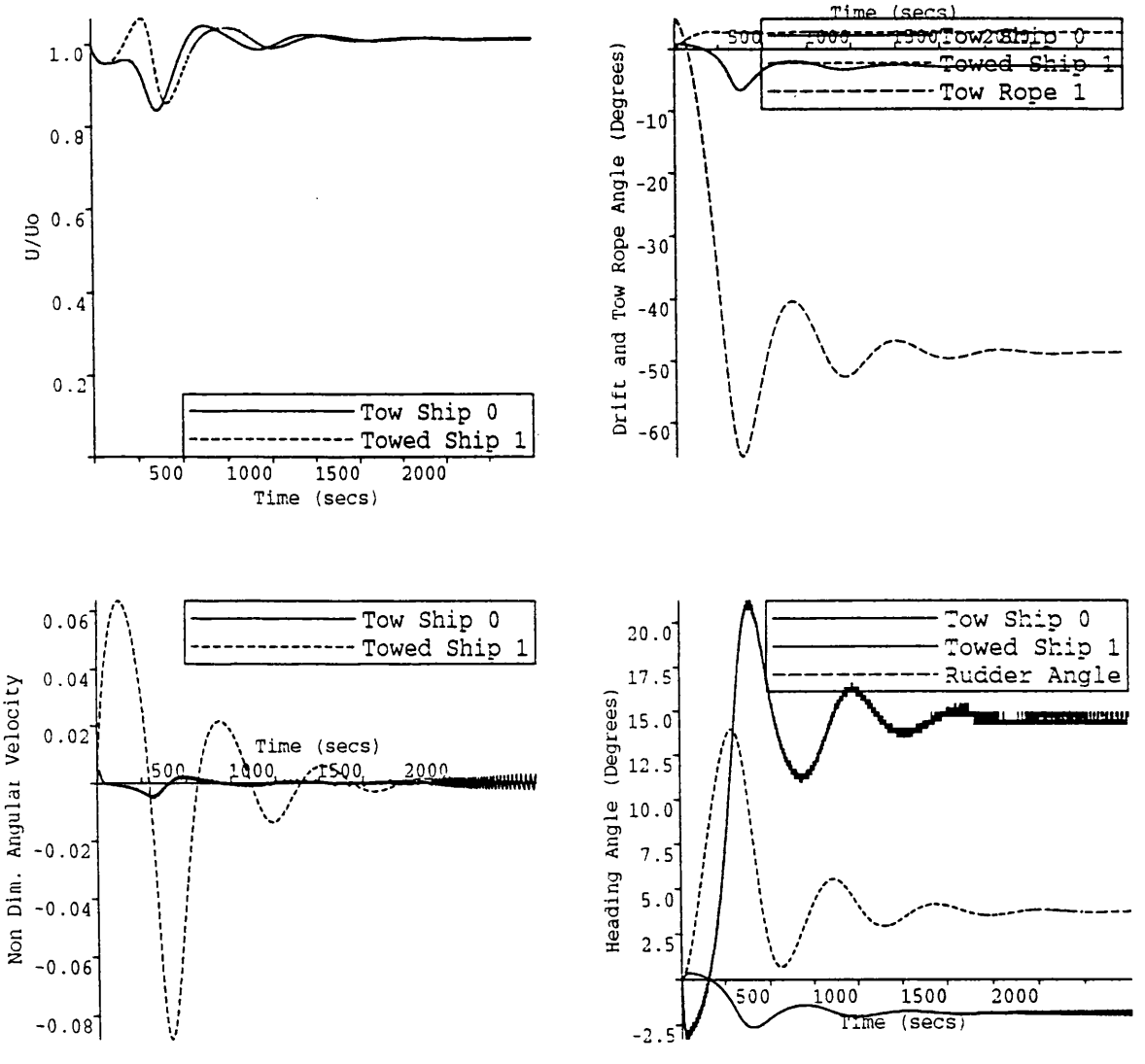

Figure 7.21c

Tow Velocity : 5.837 Knots
Rudder Constants 1,2 : 8.0,5.0
Tow Point 0 : 0.000 m
Tow Rope Length/L0 : 3.250 m/m
Tow Point 1 : 63.300 m
Tow Rope : Rigid
Maximum Deflection : 21.233 Degrees
Wind Velocity,Angle : 19.5, 90.0 Knots,Deg

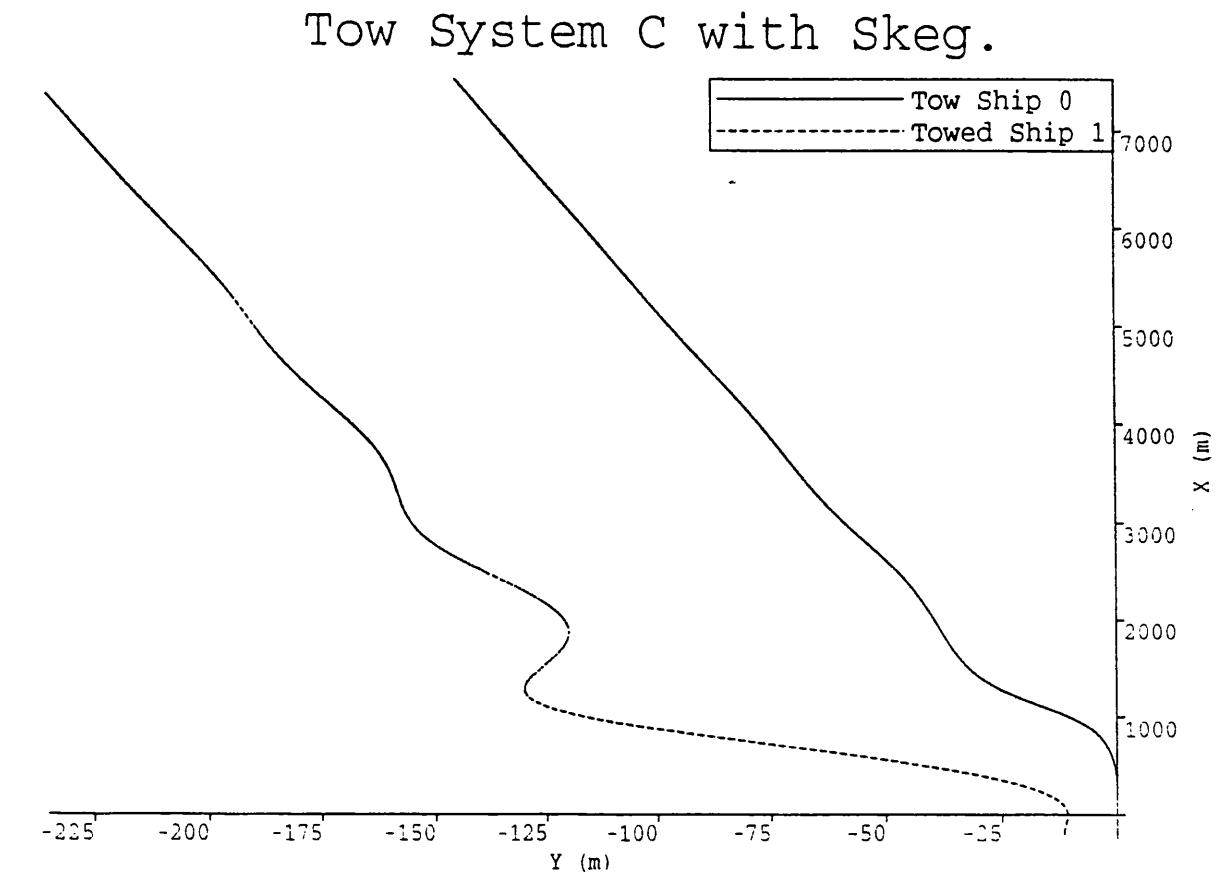

Figure 7.22a

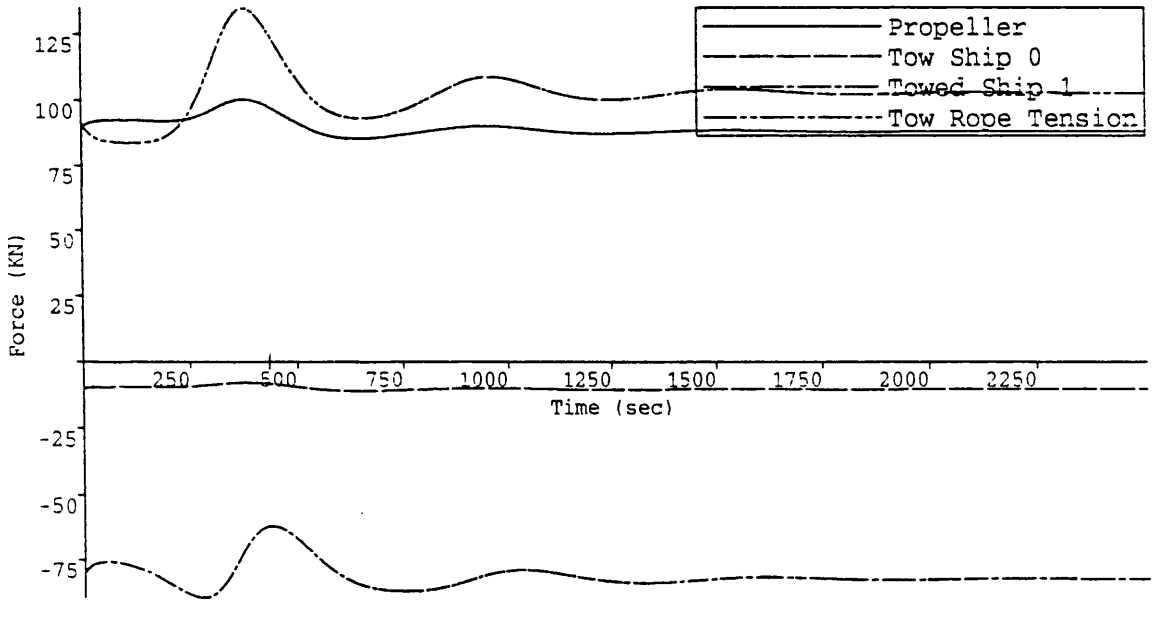

Figure 7.22b

```
Tow Velocity :  5.837 Knots
Rudder Constants 1,2 : 8.0,5.0
Tow Point 0 :   0.000 m
Tow Rope Length/L0 :  3.250 m/m
Tow Point 1 : 63.300 m
Tow Rope : Rigid
Maximum Deflection : -20.300 Degrees
Wind Velocity,Angle : 19.5,270.0 Knots,Deg
```

Tow System C with Skeg.

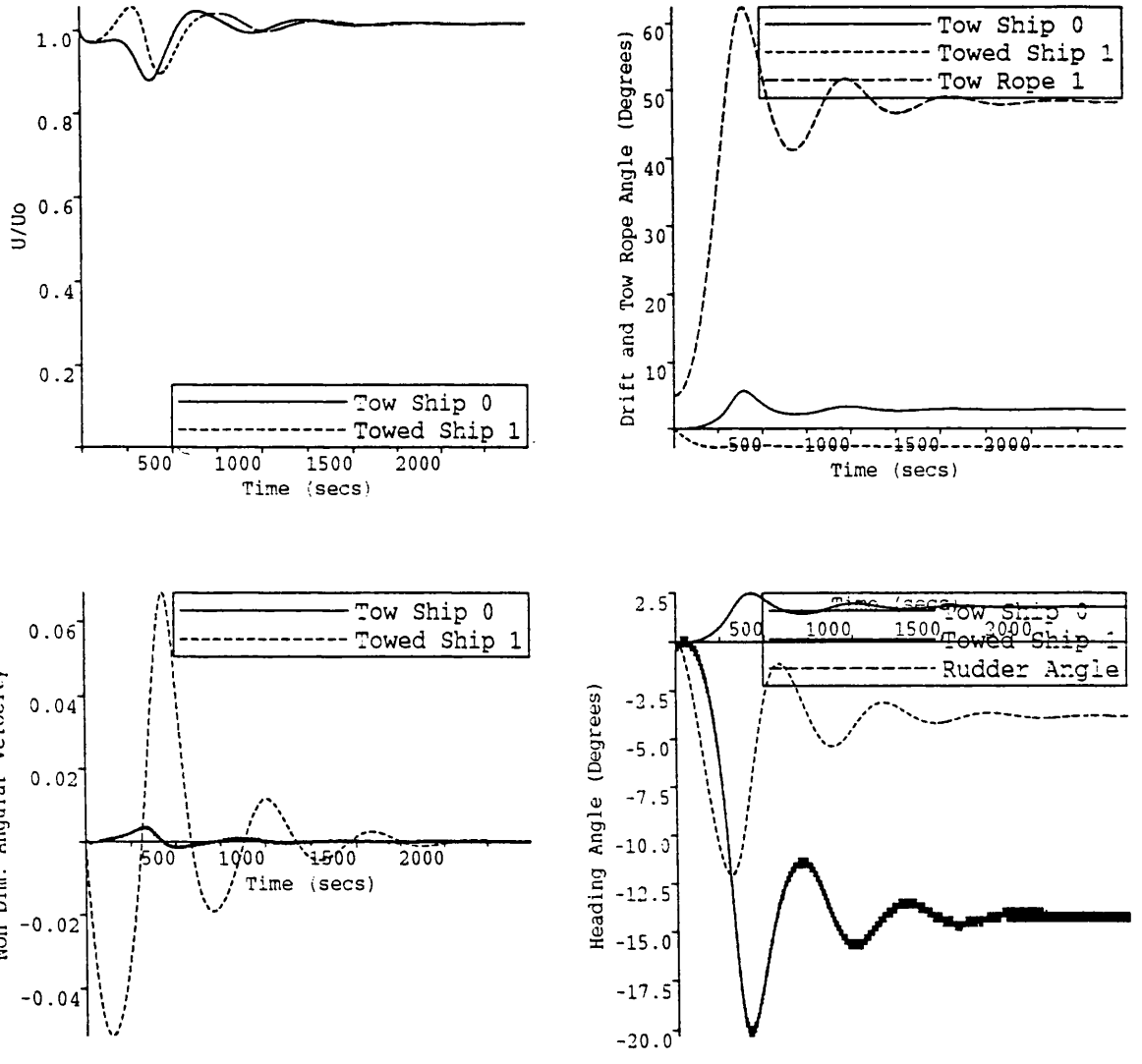

Figure 7.22c

Tow Velocity : 5.837 Knots
Rudder Constants 1,2 : 8.0,5.0
Tow Point 0 : 0.000 m
Tow Rope Length/L0 : 3.250 m/m
Tow Point 1 : 63.300 m
Tow Rope : Rigid
Maximum Deflection : -20.300 Degrees
Wind Velocity,Angle : 19.5,270.0 Knots,Deg

Tow System C with Skeg

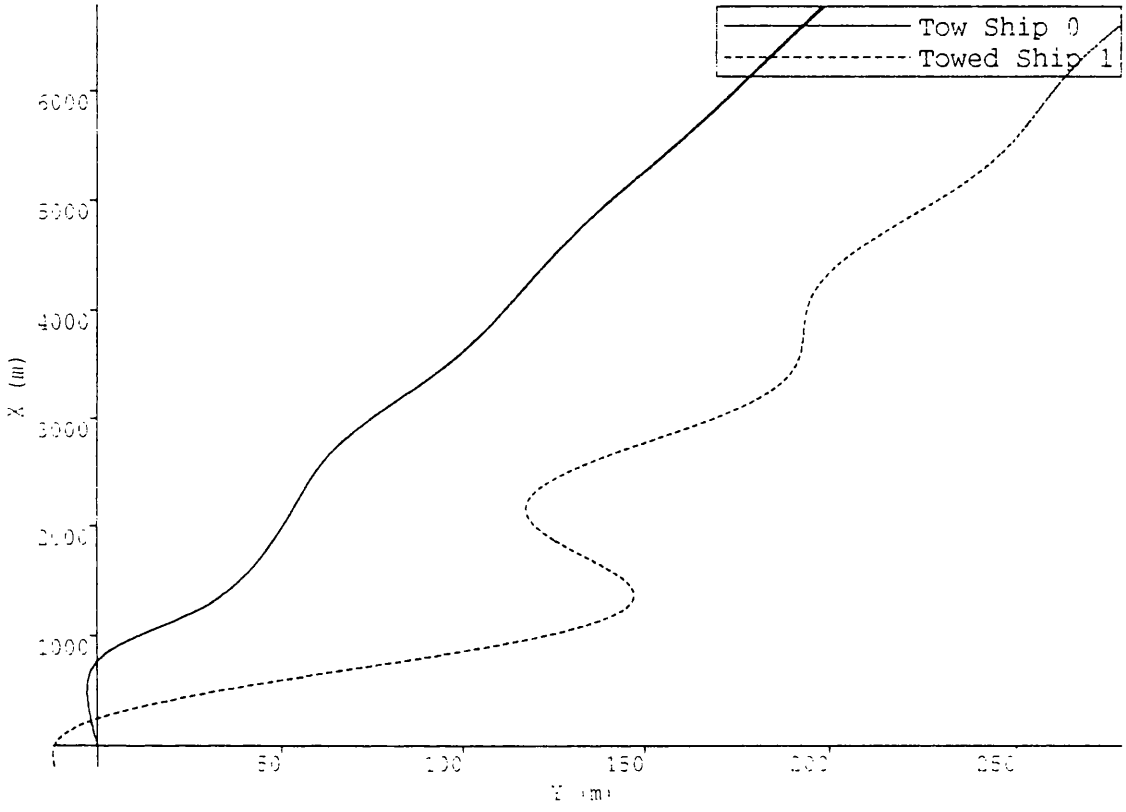

Figure 7.23a

Tow Velocity : 5.837 Knots
Rudder Constants 1,2 :8.0,5.0
Tow Point 0 : 0.000 m
Tow Rope Length/L0 : 3.250 m/m
Tow Point 1 :63.300m
Tow Rope : PY
Maximum Deflection : 23.100 Degrees
Wind Velocity,Angle : 19.46, 90.0 Knots,De

Tow System C with Skeg

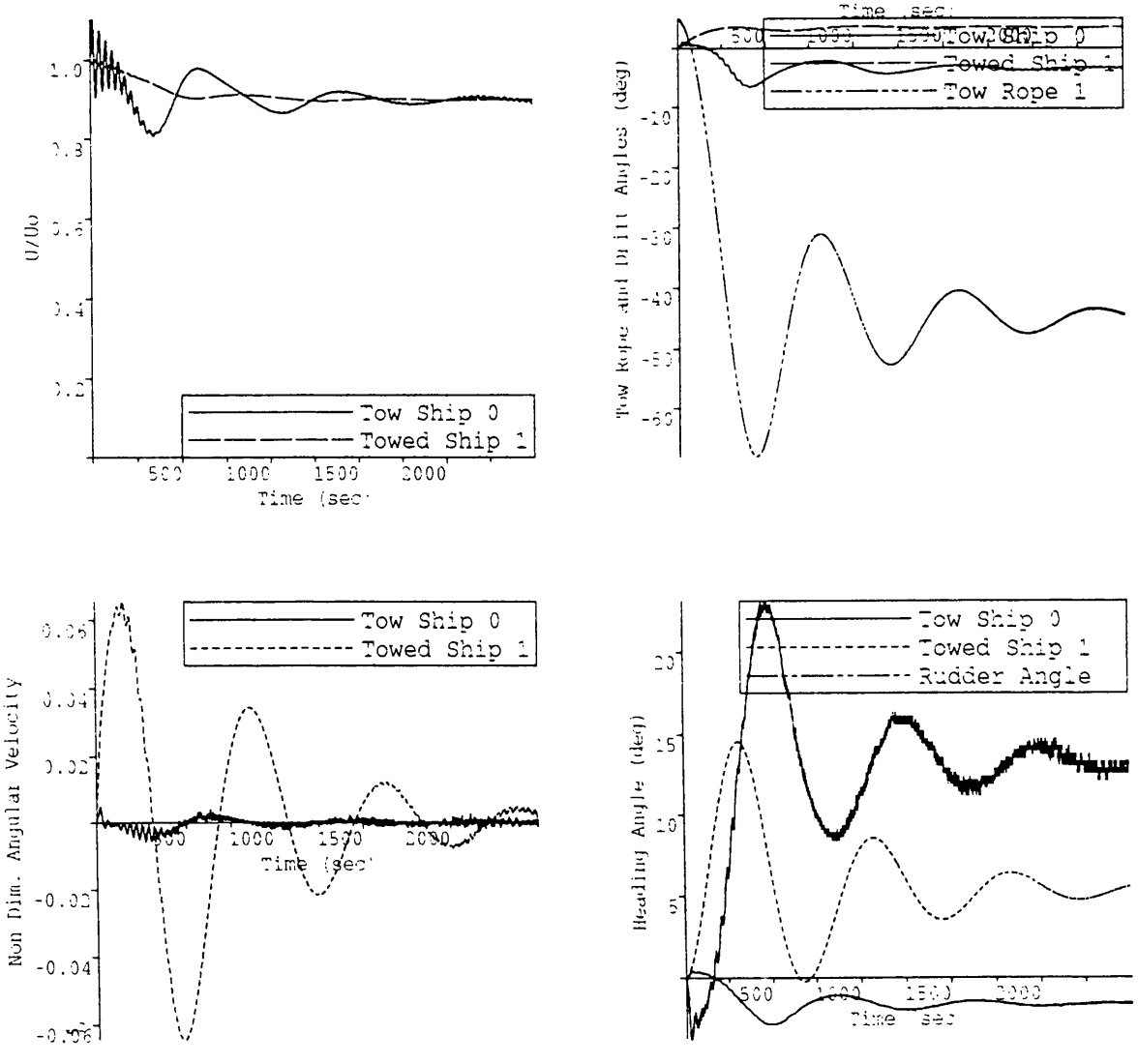

Figure 7.23b

Tow Velocity : 5.837 Knots
Rudder Constants 1,2 :8.0,5.0
Tow Point 0 : 0.000m
Tow Rope Length/L0 : 3.250m/m
Tow Point 1 :63.300m
Tow Rope :PY
Maximum Deflection : 23.100 Degrees
Wind Velocity,Angle :19.46, 90.0 Knots,Deg

Tow System C with Skeg

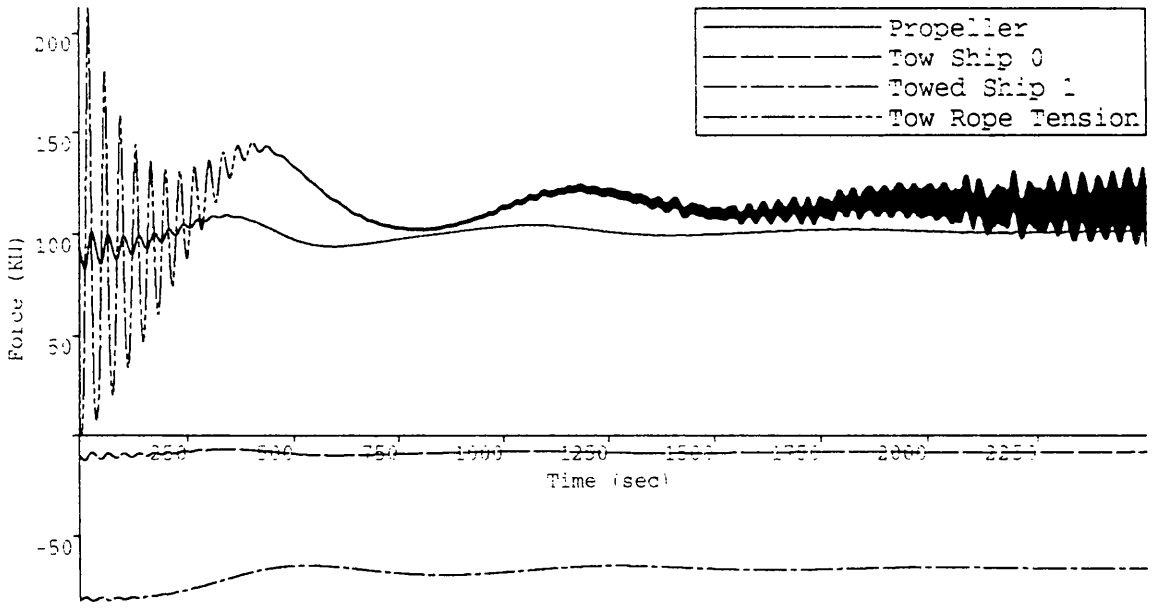

Figure 7.23c

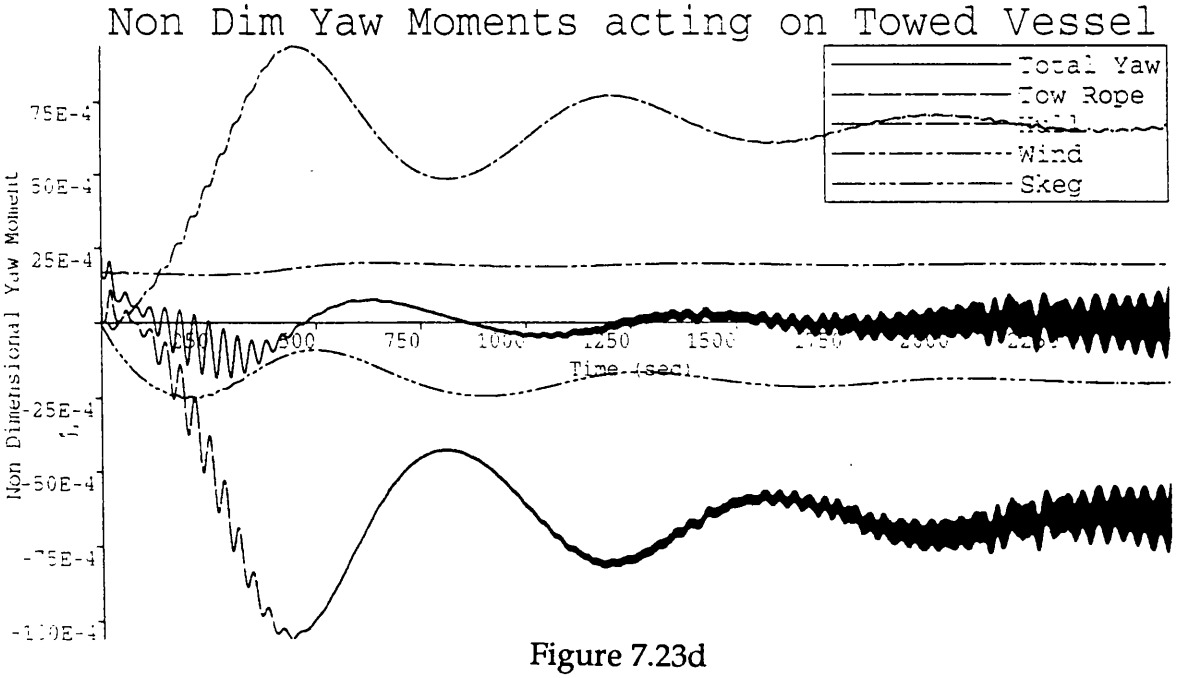

Figure 7.23d

Tow Velocity : 5.837 Knots
Rudder Constants 1,2 :8.0,5.0
Tow Point 0 : 0.000m
Tow Rope Length/L0 : 3.250m/m
Tow Point 1 :63.300m
Tow Rope :PY
Maximum Deflection : 23.100 Degrees
Wind Velocity,Angle :19.46, 90.0 Knots,Deg

Tow Wind Loading Coefficients

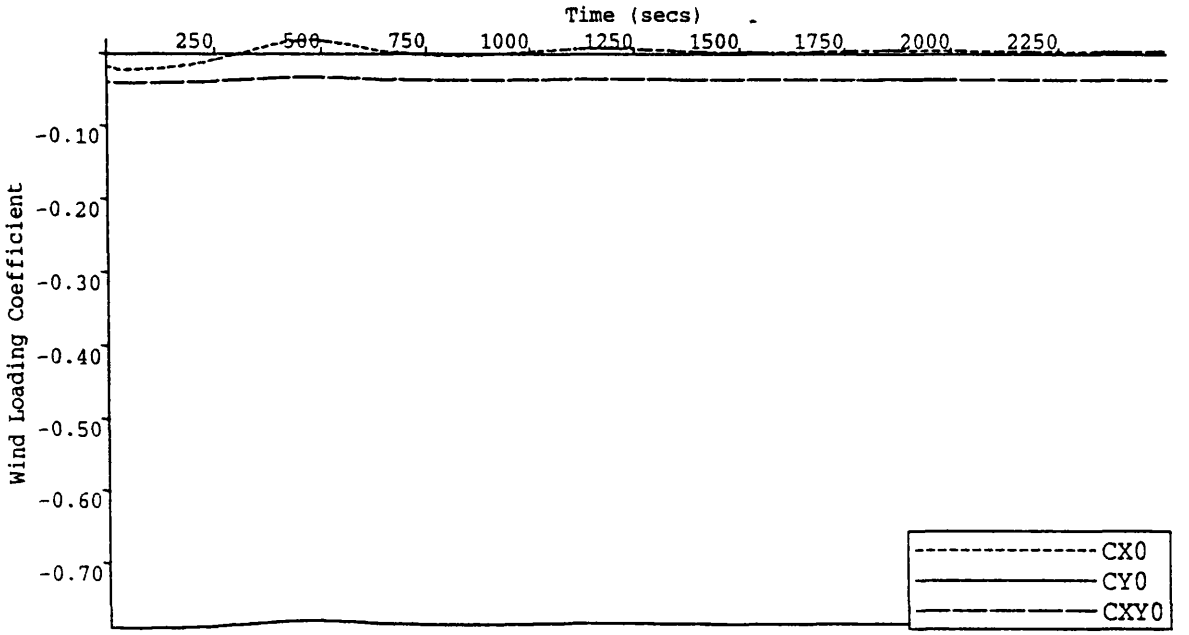

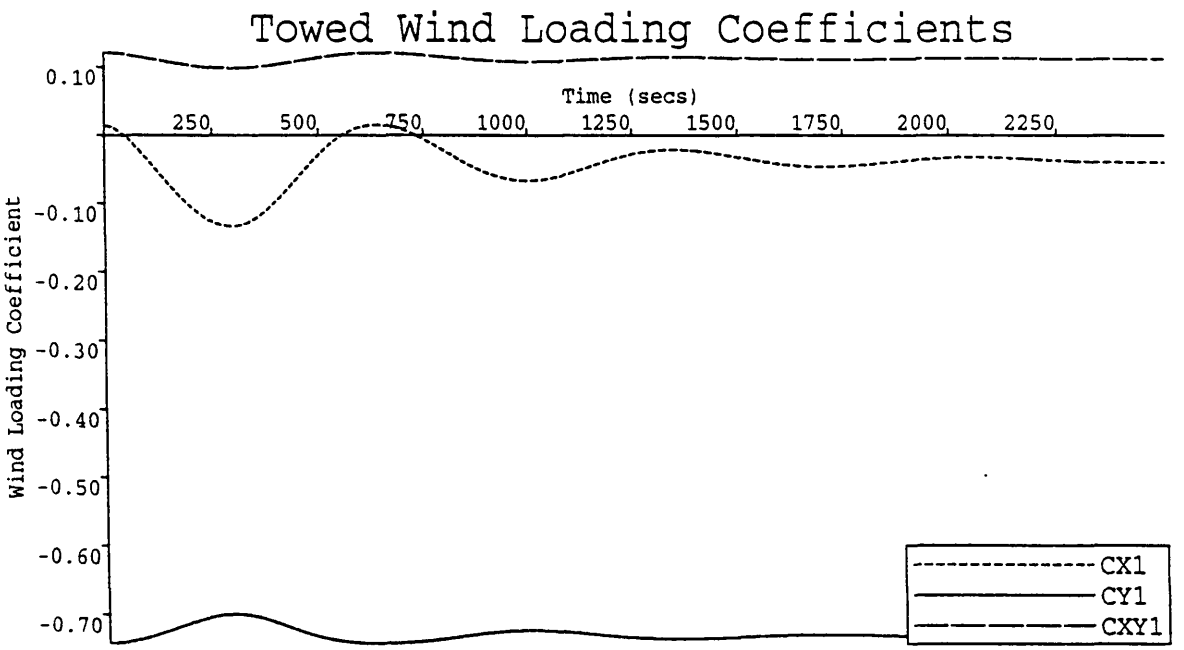

Figure 7.23e

Tow Velocity : 5.837 Knots
Rudder Constants 1,2 :8.0,5.0
Tow Point 0 : 0.000m
Tow Rope Length/L0 : 3.250m/m
Tow Point 1 :63.300m
Tow Rope :PY
Maximum Deflection : 23.100 Degrees
Wind Velocity,Angle :19.46, 90.0 Knots,Deg

Tow System C with Skeg

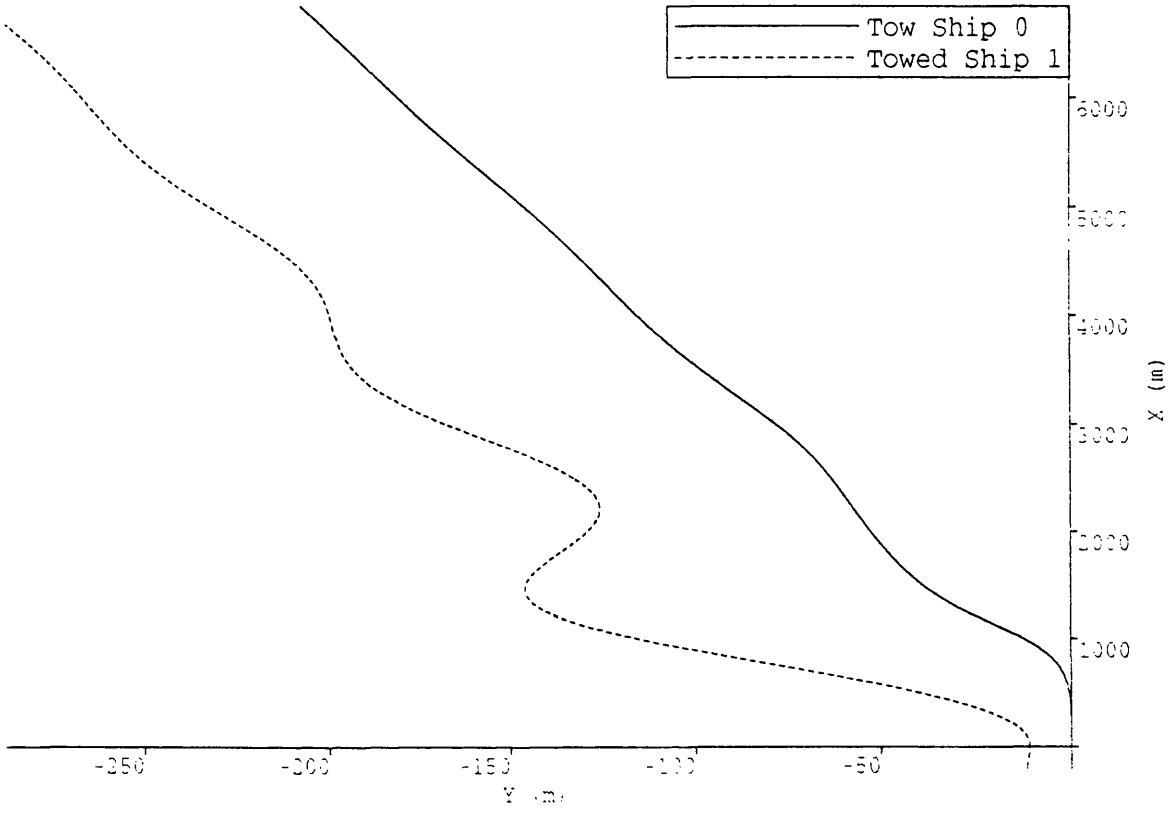

Figure 7.24a

Tow Velocity : 5.837 Knots
Rudder Constants 1,2 :8.0,5.0
Tow Point 0 : 0.000 m
Tow Rope Length/L0 : 3.250 m/m
Tow Point 1 :63.300m
Tow Rope : PY
Maximum Deflection :-21.233 Degrees
Wind Velocity,Angle : 19.46,270.0 Knots,De

Tow System C with Skeg

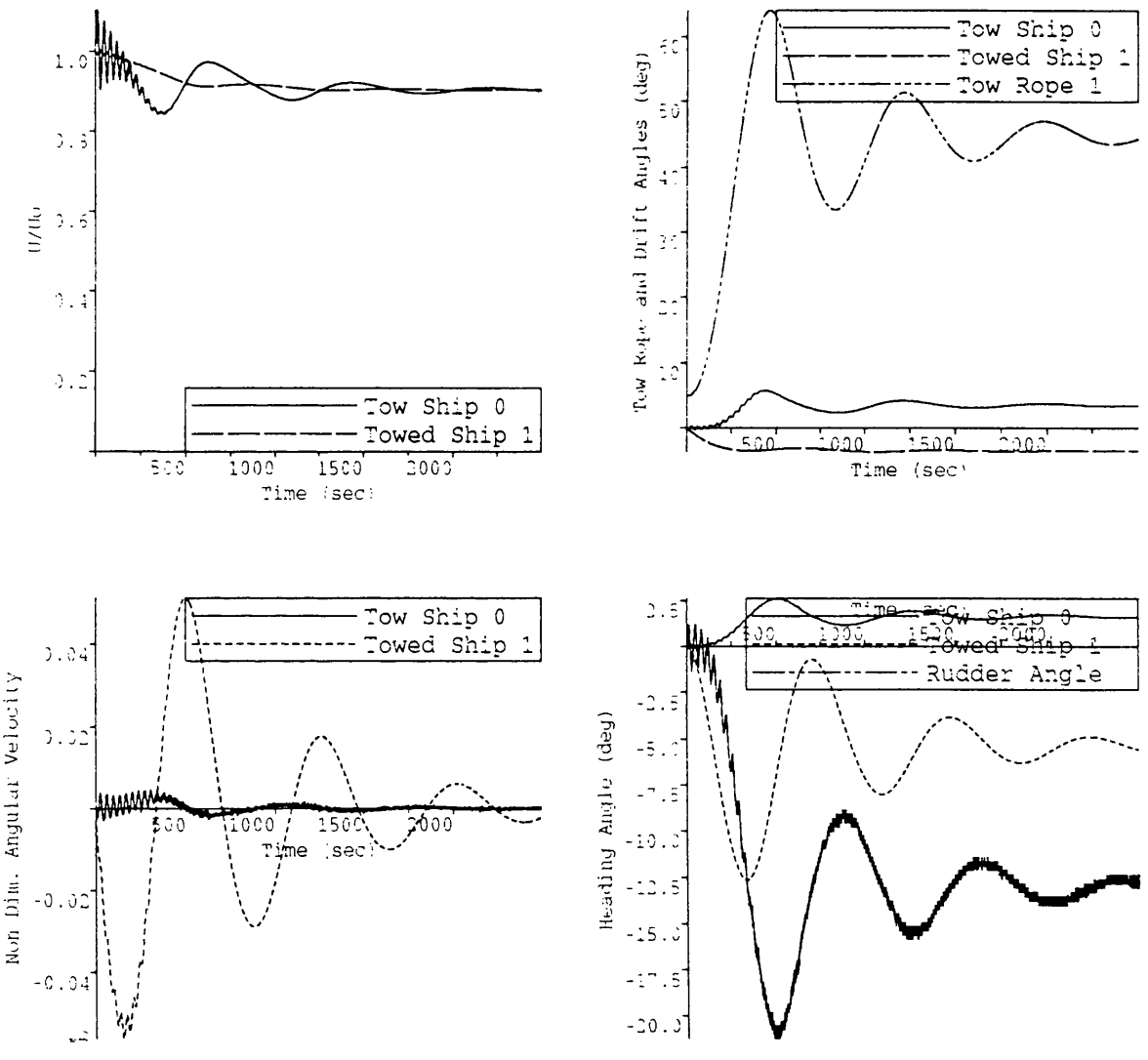

Figure 7.24b

Tow Velocity : 5.837 Knots
Rudder Constants 1,2 :8.0,5.0
Tow Point 0 : 0.000m
Tow Rope Length/L0 : 3.250m/m
Tow Point 1 :63.300m
Tow Rope :PY
Maximum Deflection :-21.233 Degrees
Wind Velocity,Angle :19.46,270.0 Knots,Deg

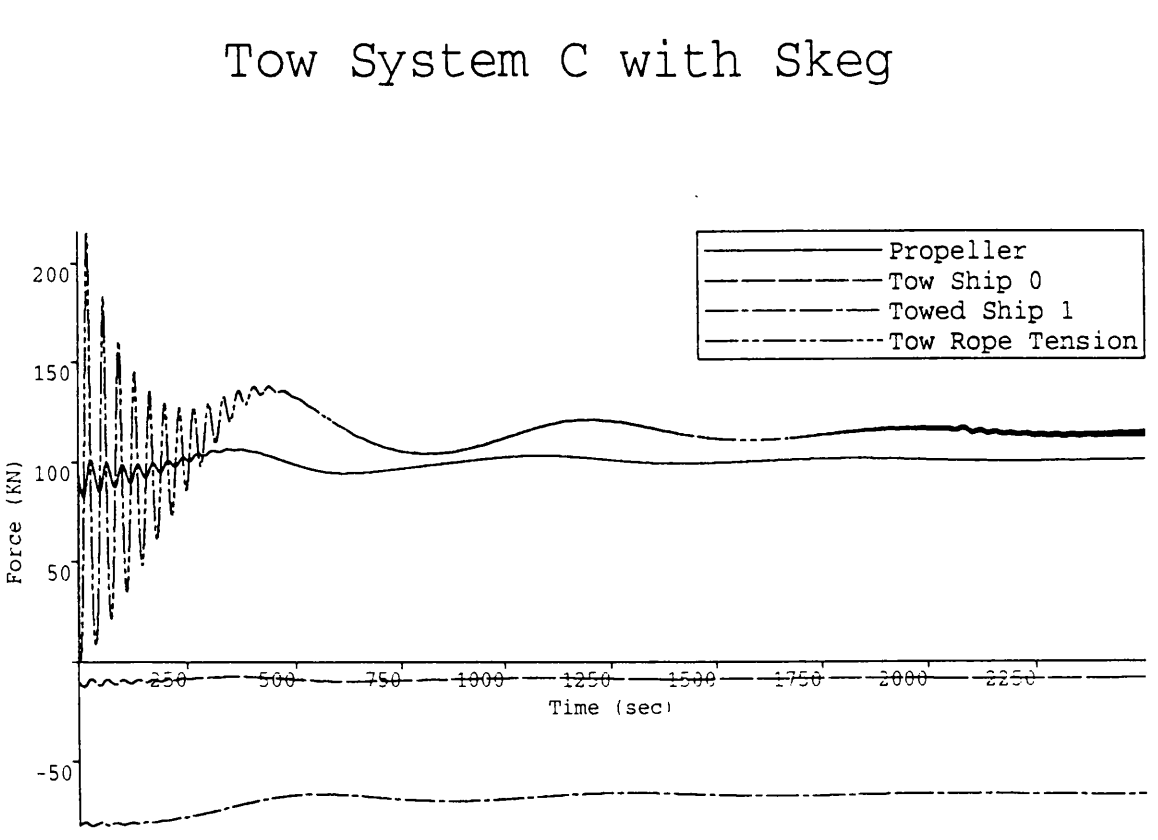

Figure 7.24c

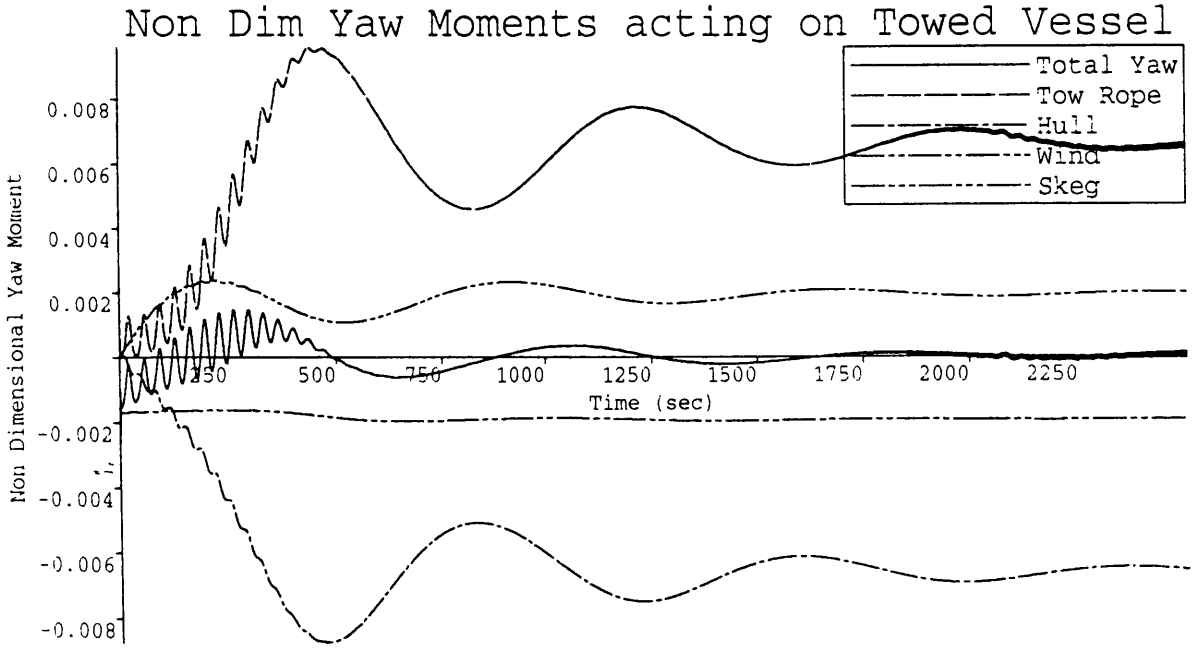

Figure 7.24d

Tow Velocity : 5.837 Knots
Rudder Constants 1,2 :8.0,5.0
Tow Point 0 : 0.000m
Tow Rope Length/L0 : 3.250m/m
Tow Point 1 :63.300m
Tow Rope :PY
Maximum Deflection :-21.233 Degrees
Wind Velocity,Angle :19.46,270.0 Knots,Deg

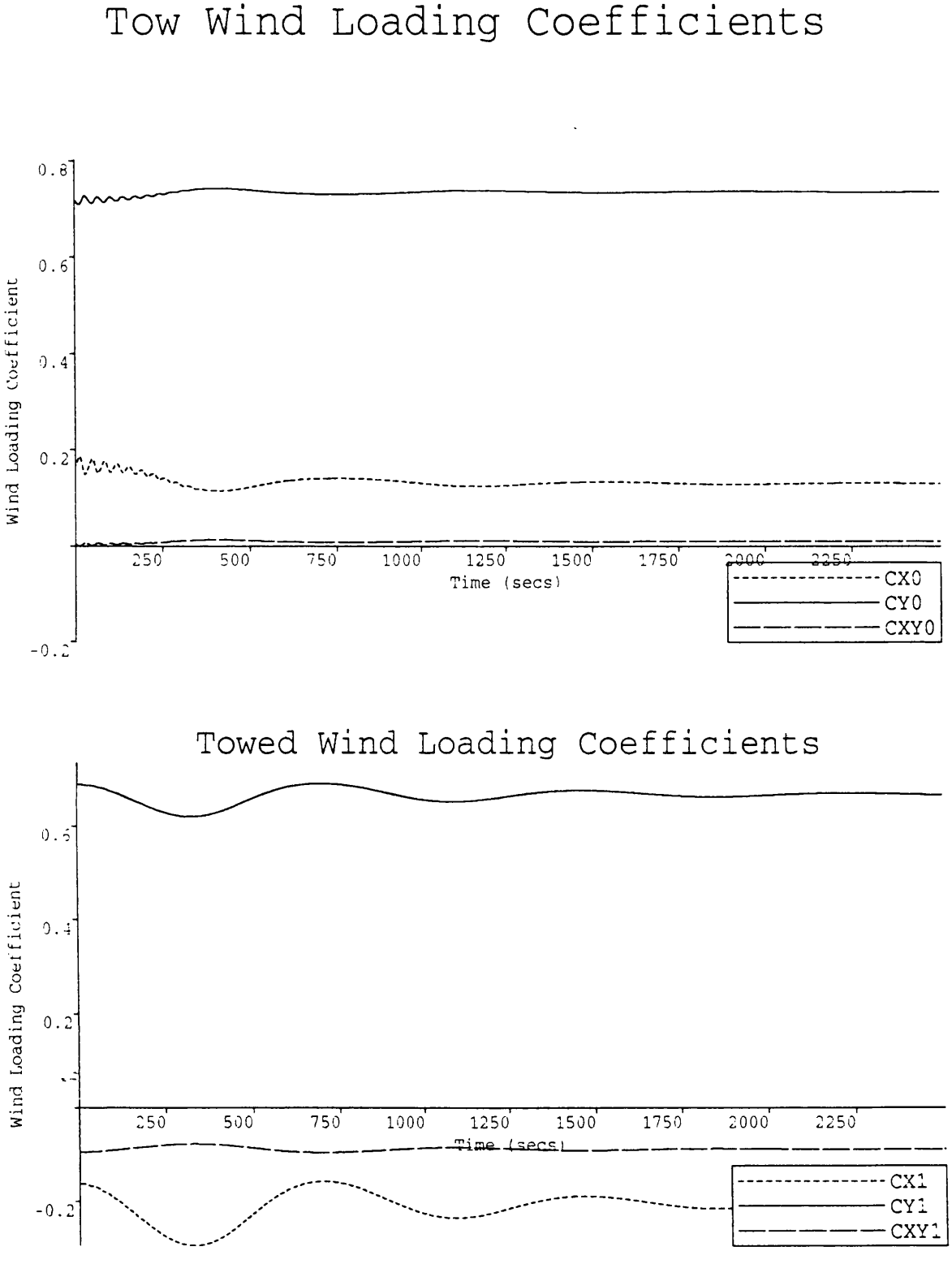

Figure 7.24e

```
Tow Velocity :  5.837 Knots
Rudder Constants 1,2 :8.0,5.0
Tow Point 0 :  0.000m
Tow Rope Length/L0 : 3.250m/m
Tow Point 1 :63.300m
Tow Rope :PY
Maximum Deflection :-21.233 Degrees
Wind Velocity,Angle :19.46,270.0 Knots,Deg
```

Tow System C with Skeg

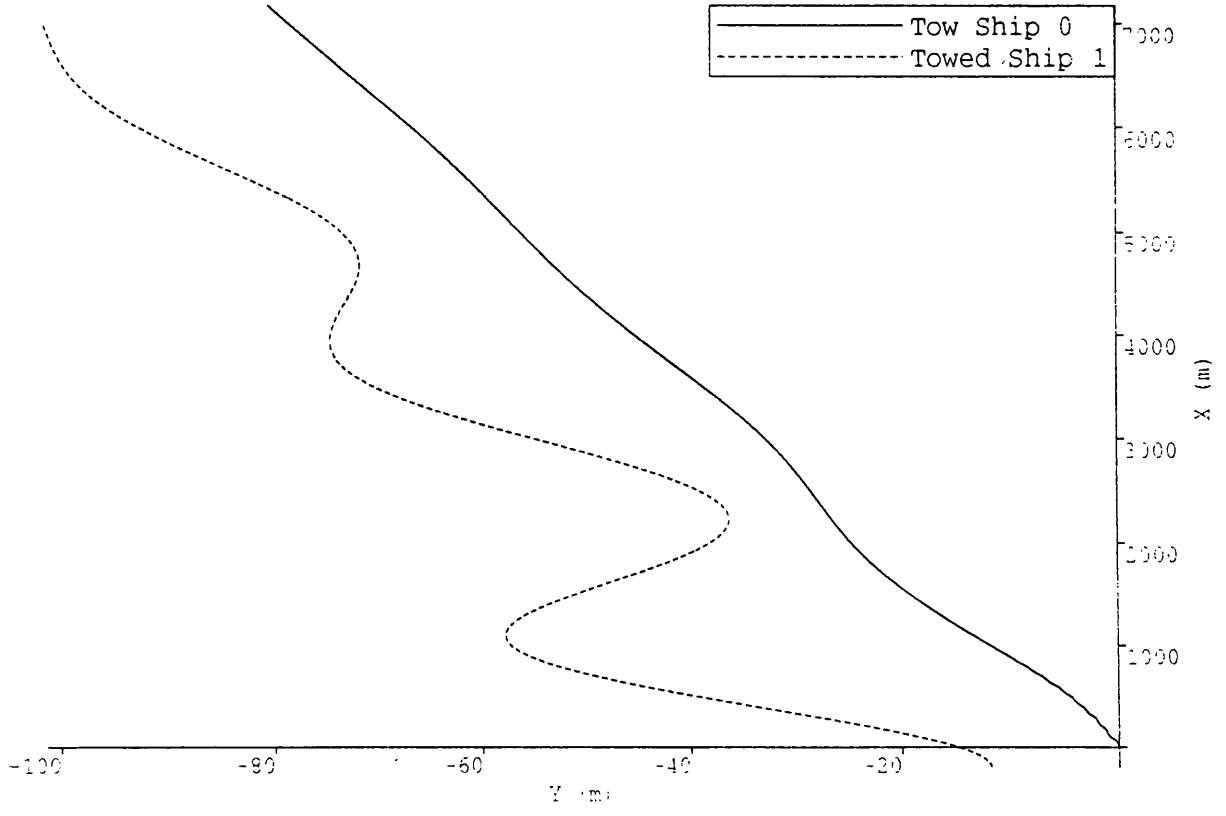

Figure 7.25a

Tow Velocity : 5.837 Knots
Rudder Constants 1,2 :8.0,5.0
Tow Point 0 : 0.000 m
Tow Rope Length/L0 : 3.250 m/m
Tow Point 1 :63.300m
Tow Rope : PY
Maximum Deflection : -7.700 Degrees
Wind Velocity,Angle : 19.46, 90.0 Knots,De

Tow System C with Skeg

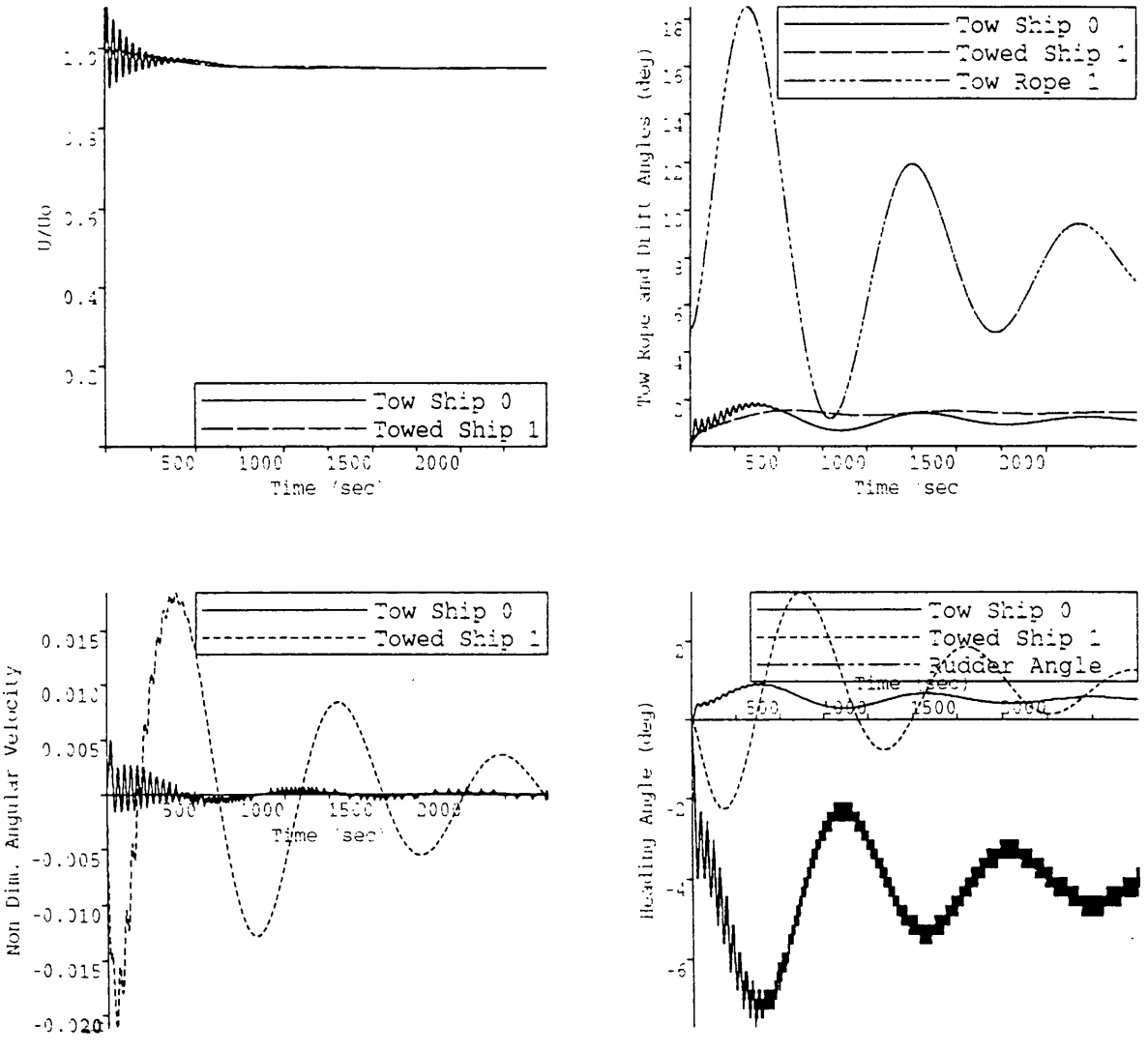

Figure 7.25b

Tow Velocity : 5.837 Knots
Rudder Constants 1,2 :8.0,5.0
Tow Point 0 : 0.000m
Tow Rope Length/L0 : 3.250m/m
Tow Point 1 :63.300m
Tow Rope :PY
Maximum Deflection : -7.700 Degrees
Wind Velocity,Angle :19.46, 90.0 Knots,Deg
Superstructure : Forward

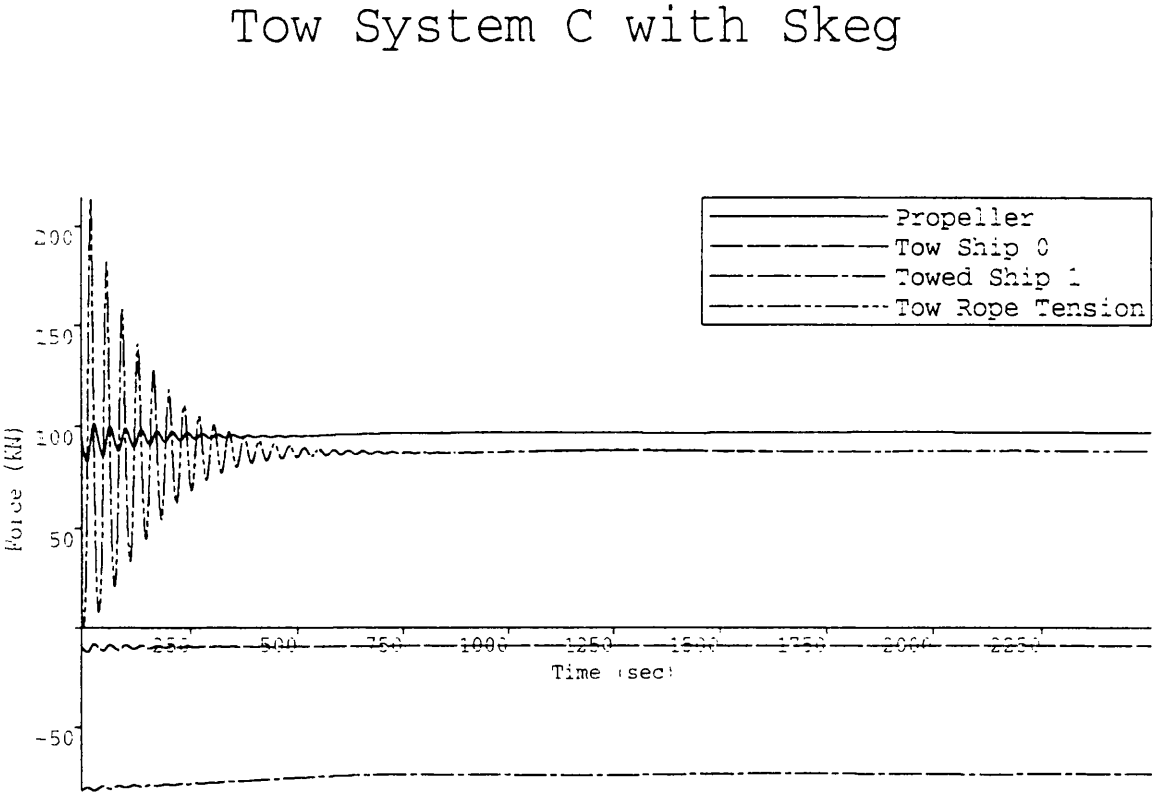

Figure 7.25c

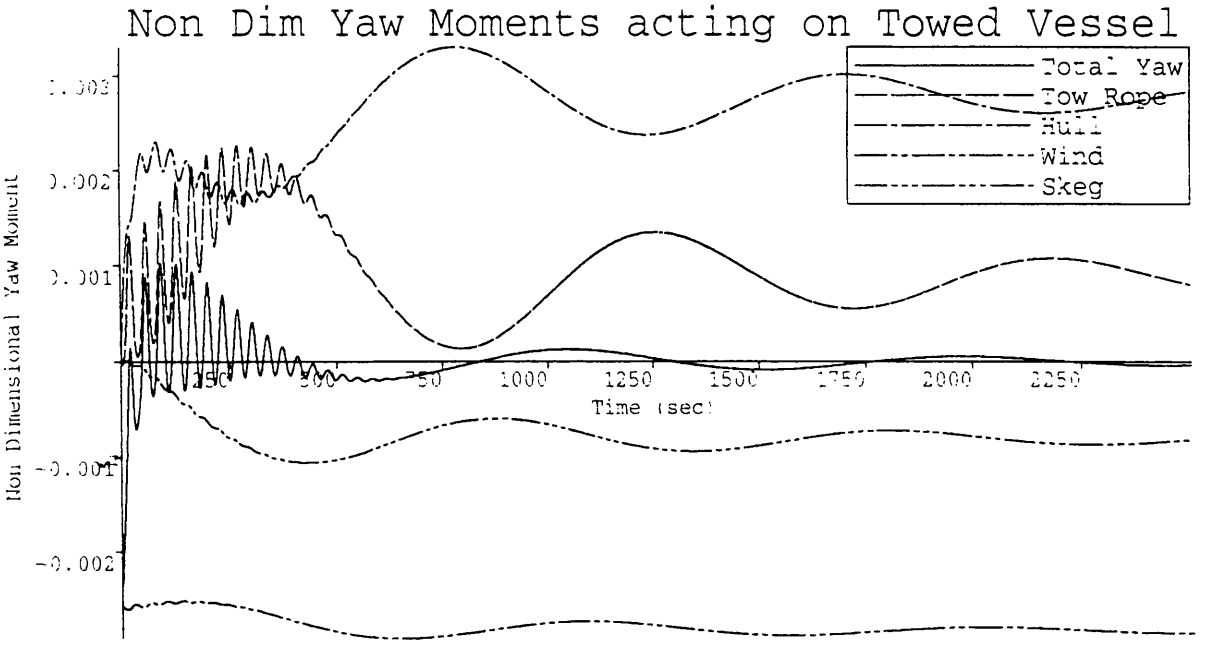

Figure 7.25d

Tow Velocity : 5.837 Knots
Rudder Constants 1,2 :8.0,5.0
Tow Point 0 : 0.000m
Tow Rope Length/L0 : 3.250m/m
Tow Point 1 :63.300m
Tow Rope :PY
Maximum Deflection : -7.700 Degrees
Wind Velocity,Angle :19.46, 90.0 Knots,Deg
Superstructure : Forward

Tow Wind Loading Coefficients

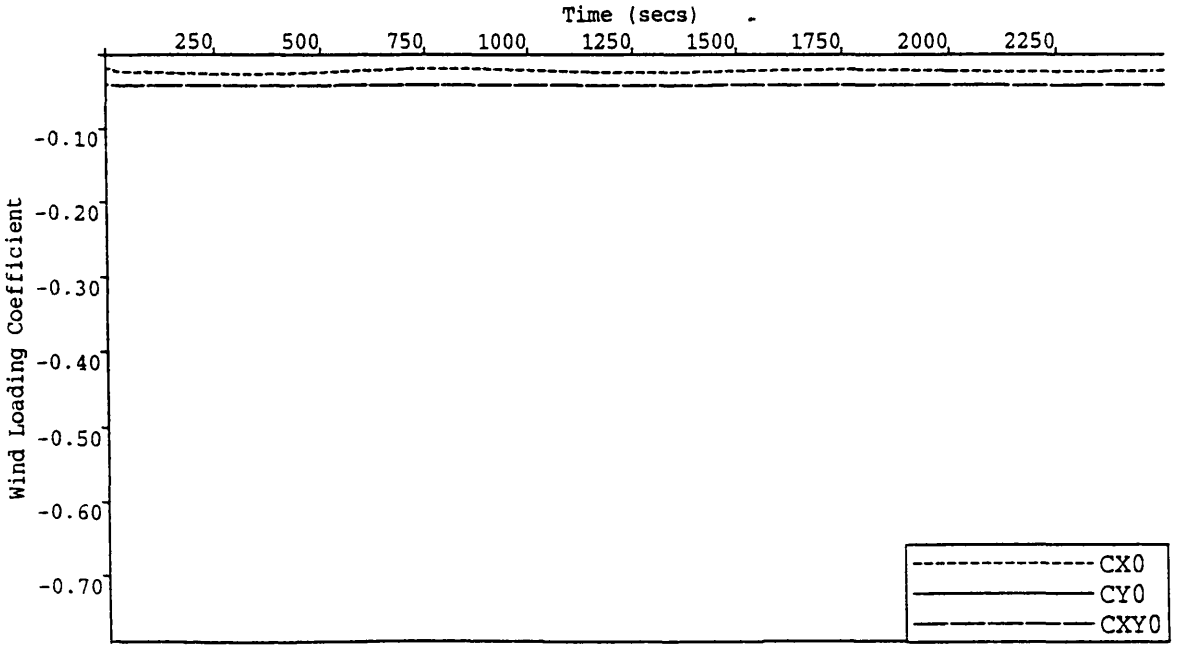

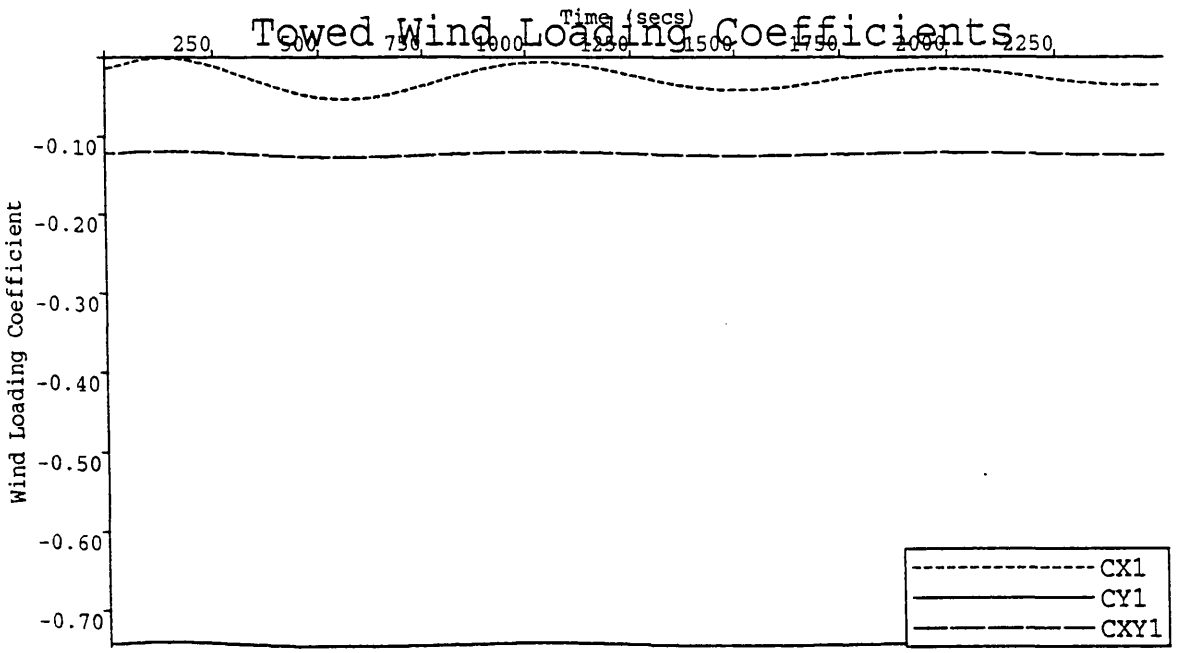

Figure 7.25e

Tow Velocity : 5.837 Knots
Rudder Constants 1,2 :8.0,5.0
Tow Point 0 : 0.000m
Tow Rope Length/L0 : 3.250m/m
Tow Point 1 :63.300m
Tow Rope :PY
Maximum Deflection : -7.700 Degrees
Wind Velocity,Angle :19.46,90.0 Knots,Deg

Tow System C with Skeg

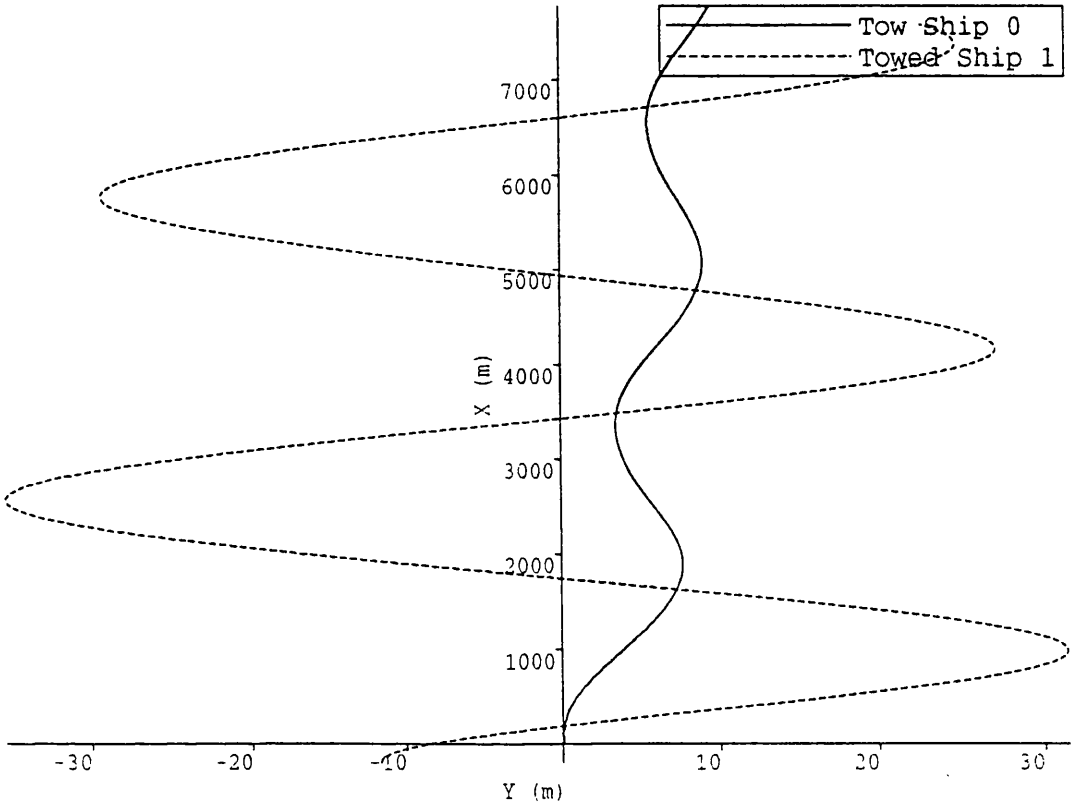

Figure 7.26a

Tow Velocity : 5.837 Knots
Rudder Constants 1,2 :8.0,5.0
Tow Point 0 : 0.000 m
Tow Rope Length/L0 : 3.250 m/m
Tow Point 1 :63.300m
Tow Rope : PY
Maximum Deflection : 5.367 Degrees
Wind Velocity,Angle : 19.46,270.0 Knots,De

Tow System C with Skeg

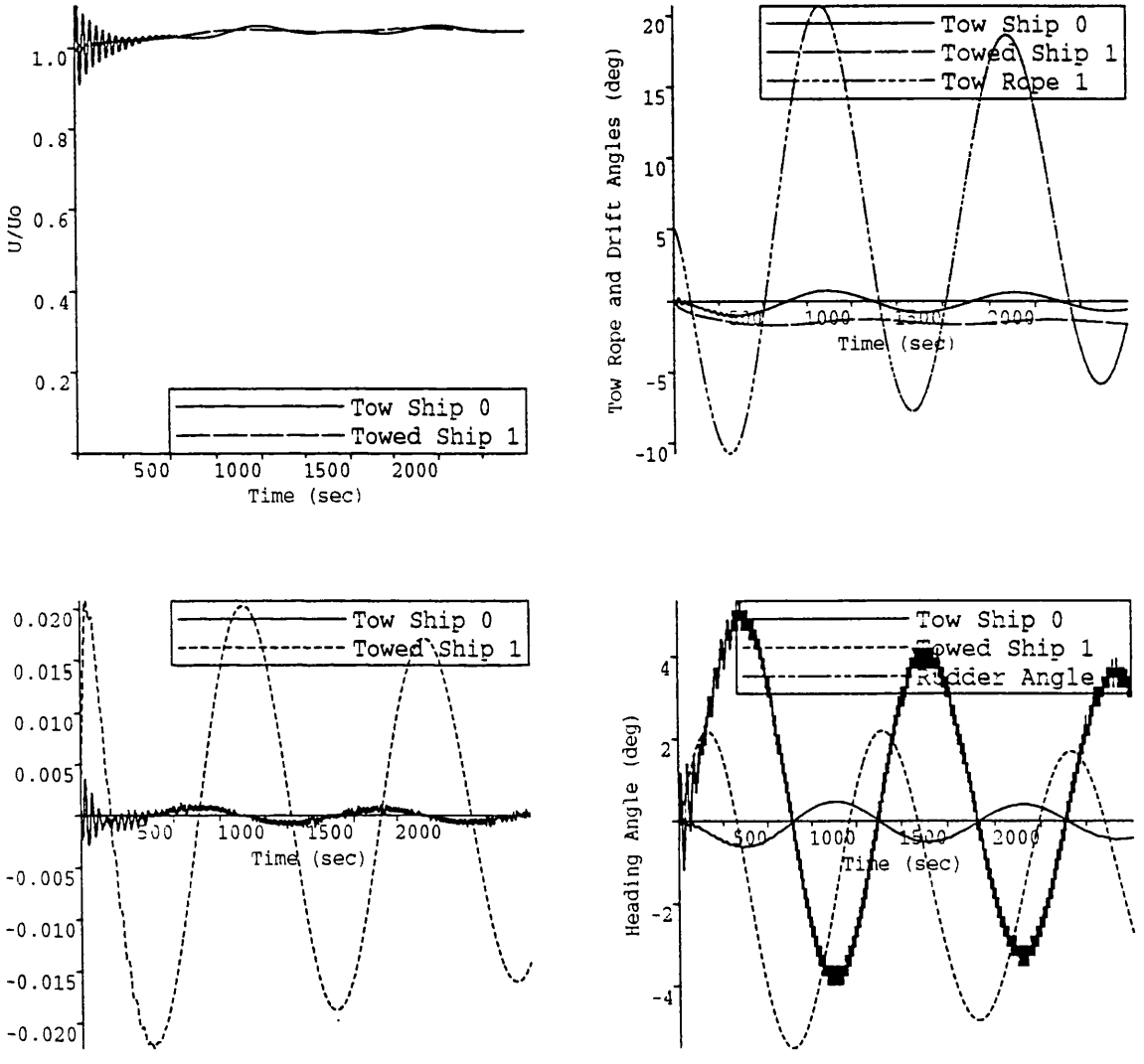

Figure 7.26b

Tow Velocity : 5.837 Knots
Rudder Constants 1,2 :8.0,5.0
Tow Point 0 : 0.000m
Tow Rope Length/L0 : 3.250m/m
Tow Point 1 :63.300m
Tow Rope :PY
Maximum Deflection : 5.367 Degrees
Wind Velocity,Angle :19.46,270.0 Knots,Deg
Superstructure : Forward

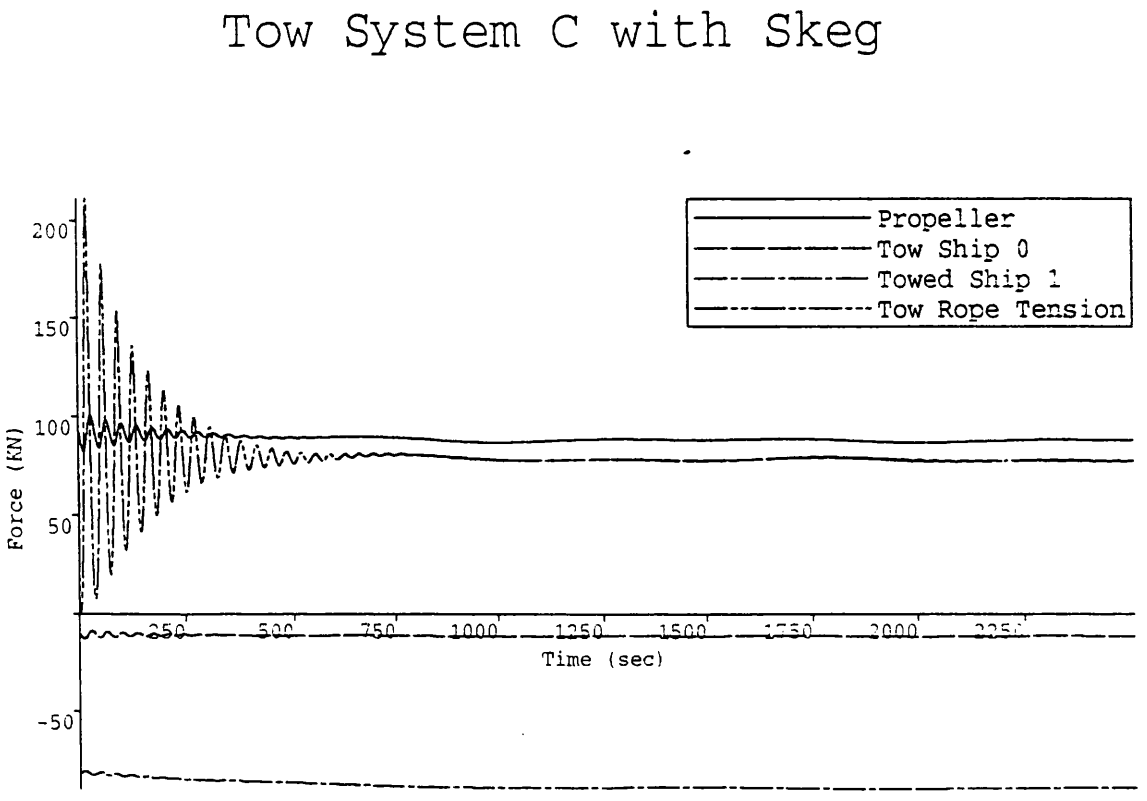

Figure 7.26c

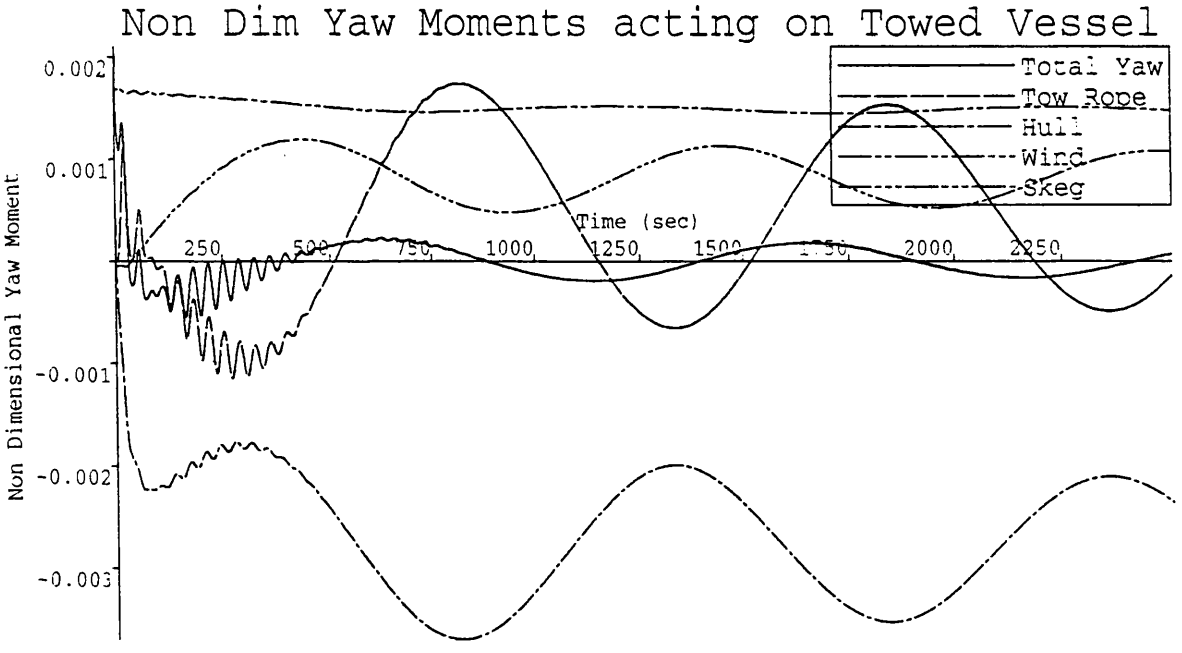

Figure 7.26d

Tow Velocity : 5.837 Knots
Rudder Constants 1,2 :8.0,5.0
Tow Point 0 : 0.000m
Tow Rope Length/L0 : 3.250m/m
Tow Point 1 :63.300m
Tow Rope :PY
Maximum Deflection : 5.367 Degrees
Wind Velocity,Angle :19.46,270.0 Knots,Deg
Superstructure : Forward

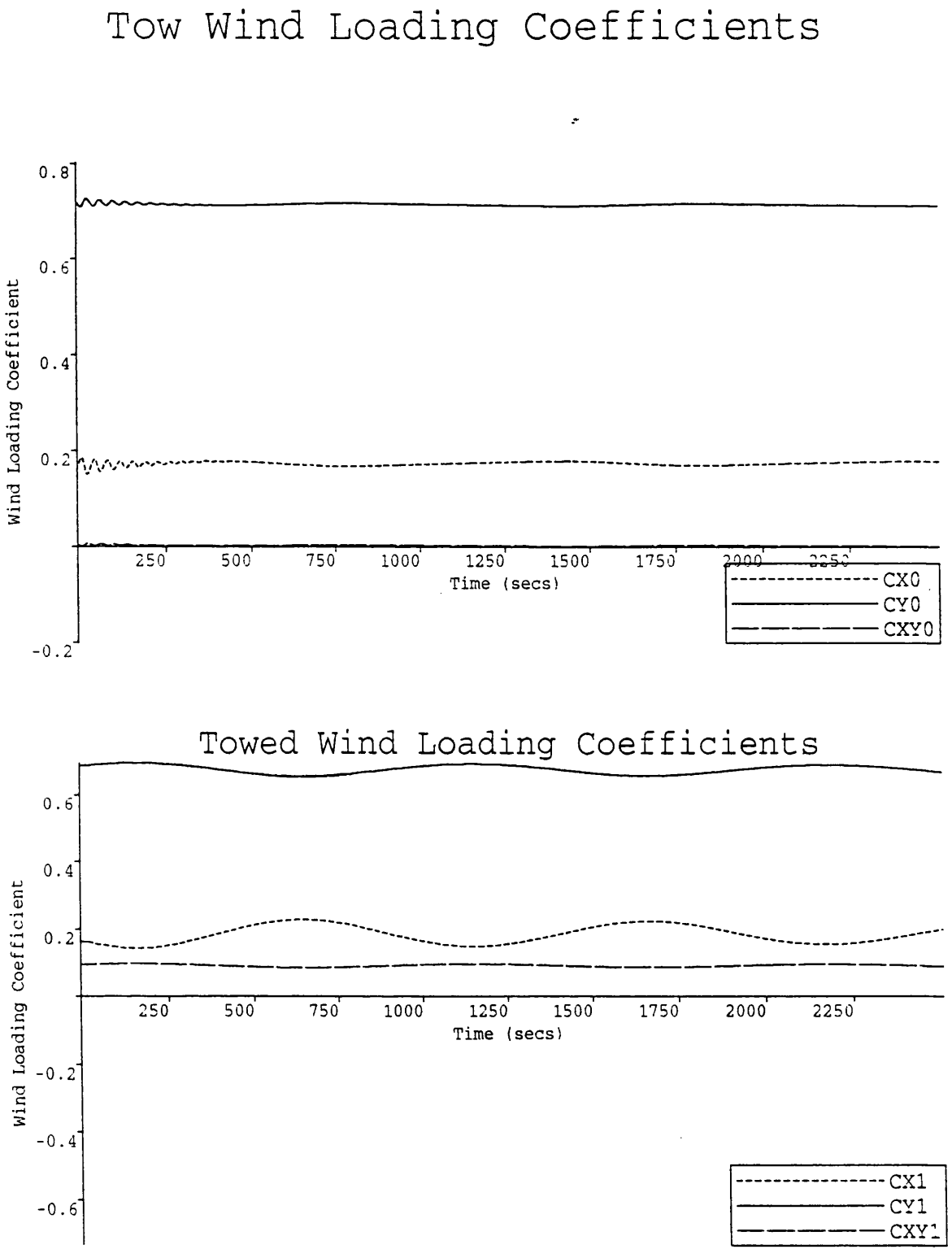

Figure 7.26e

```
Tow Velocity :  5.837 Knots
Rudder Constants 1,2 :8.0,5.0
Tow Point 0 :  0.000m
Tow Rope Length/L0 : 3.250m/m
Tow Point 1 :63.300m
Tow Rope :PY
Maximum Deflection :  5.367 Degrees
Wind Velocity,Angle :19.46,270.0 Knots,Deg
Superstructure : Forward
```

Tow System C with Skeg

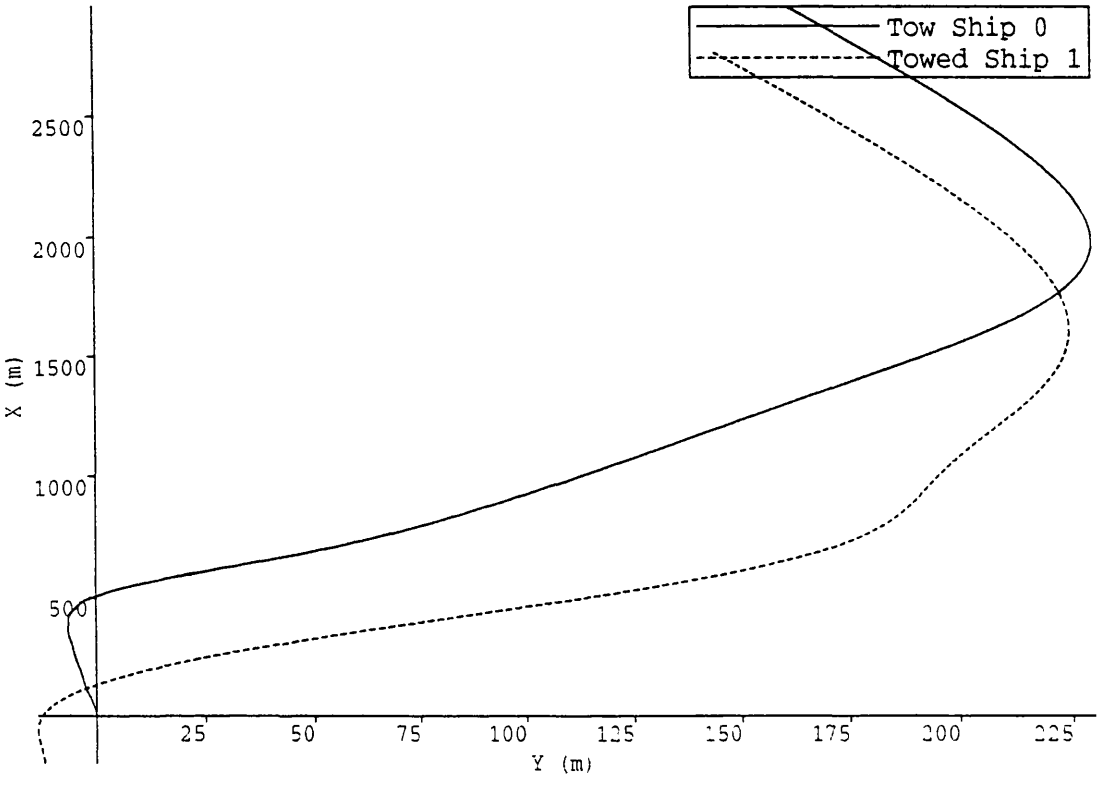

Figure 7.27a

Tow Velocity : 5.837 Knots
Rudder Constants 1,2 :8.0,5.0
Tow Point 0 : 0.000 m
Tow Rope Length/L0 : 3.250 m/m
Tow Point 1 :63.300m
Tow Rope : PY
Maximum Deflection : 22.400 Degrees
Wind Velocity,Angle : 38.91, 90.0 Knots,De

Tow System C with Skeg

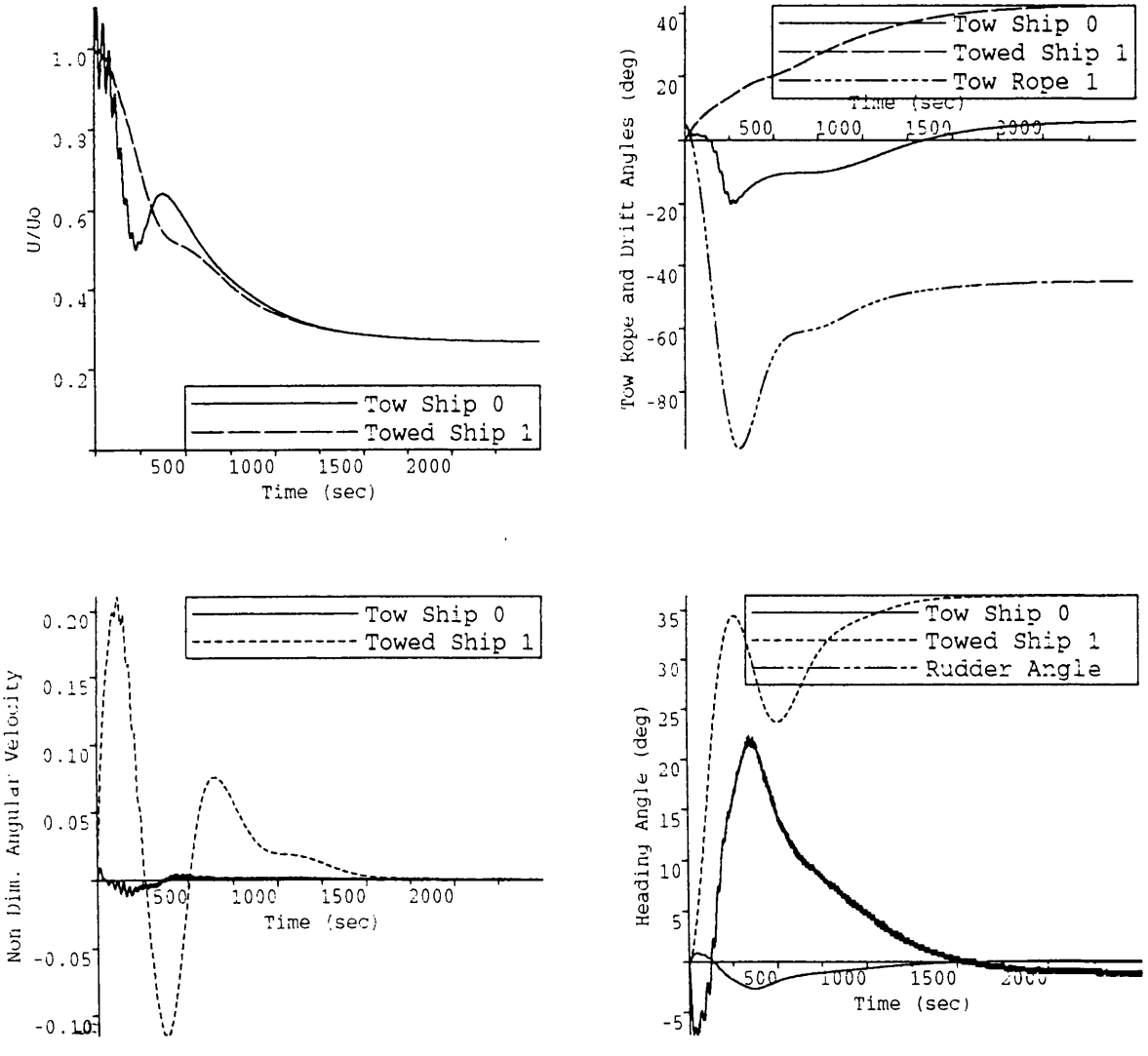

Figure 7.27b

Tow Velocity : 5.837 Knots
Rudder Constants 1,2 :8.0,5.0
Tow Point 0 : 0.000m
Tow Rope Length/L0 : 3.250m/m
Tow Point 1 :63.300m
Tow Rope :PY
Maximum Deflection : 22.400 Degrees
Wind Velocity,Angle :38.91, 90.0 Knots,Deg

Tow System C with Skeg

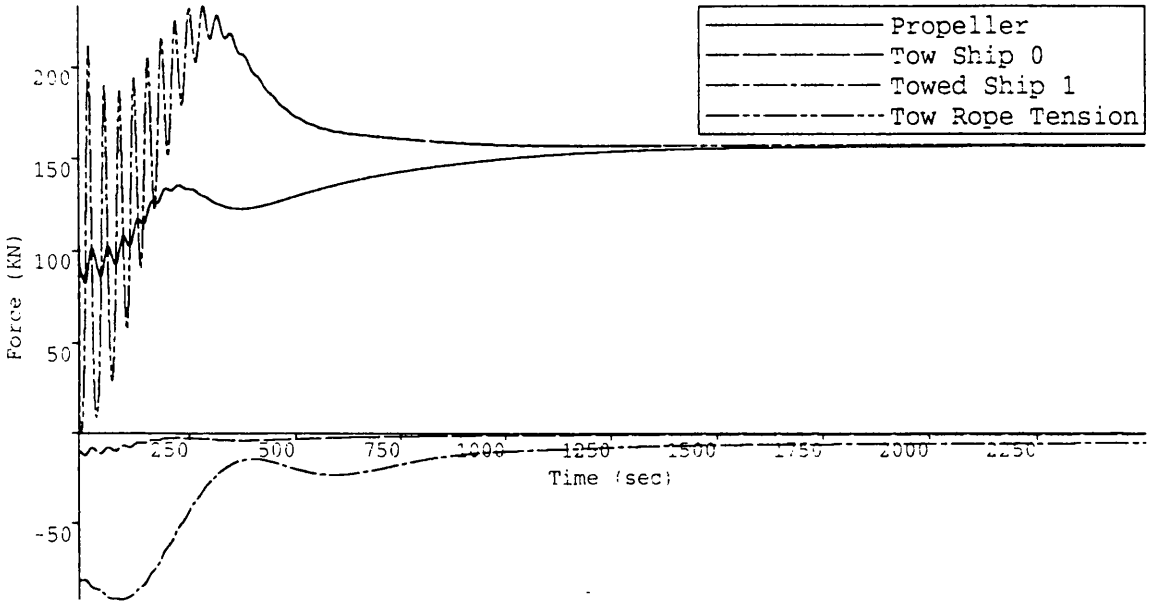

Figure 7.27c

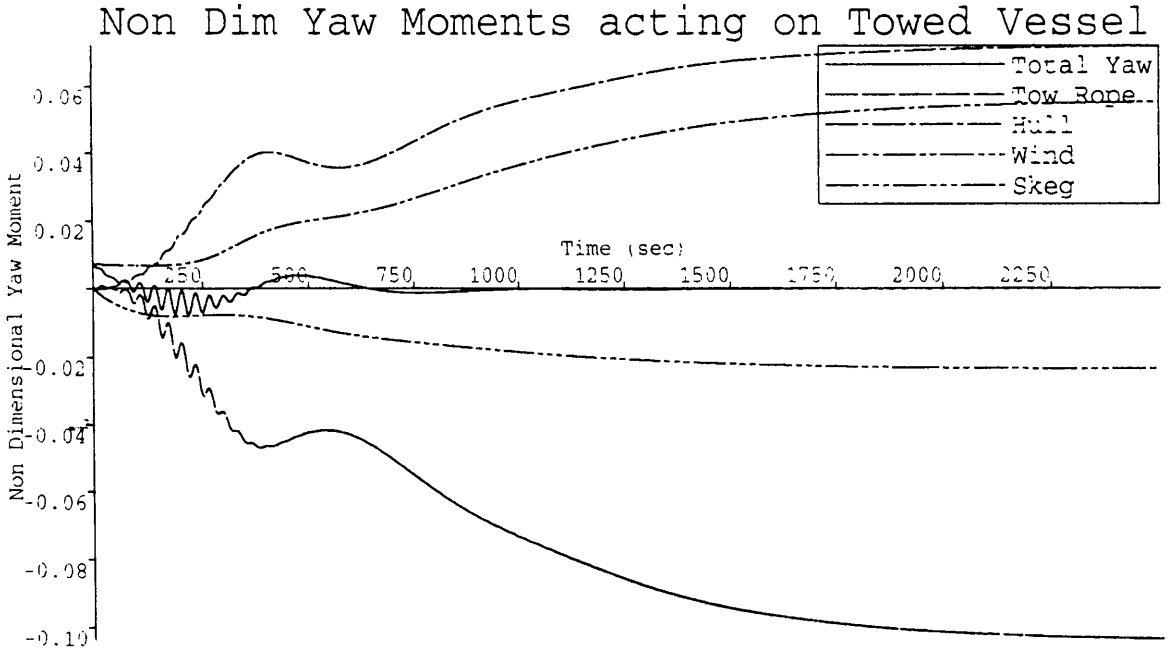

Figure 7.27d

```
Tow Velocity :  5.837 Knots
Rudder Constants 1,2 :8.0,5.0
Tow Point 0 :  0.000m
Tow Rope Length/L0 : 3.250m/m
Tow Point 1 :63.300m
Tow Rope :PY
Maximum Deflection : 22.400 Degrees
Wind Velocity,Angle :38.91, 90.0 Knots,Deg
```

Tow Wind Loading Coefficients

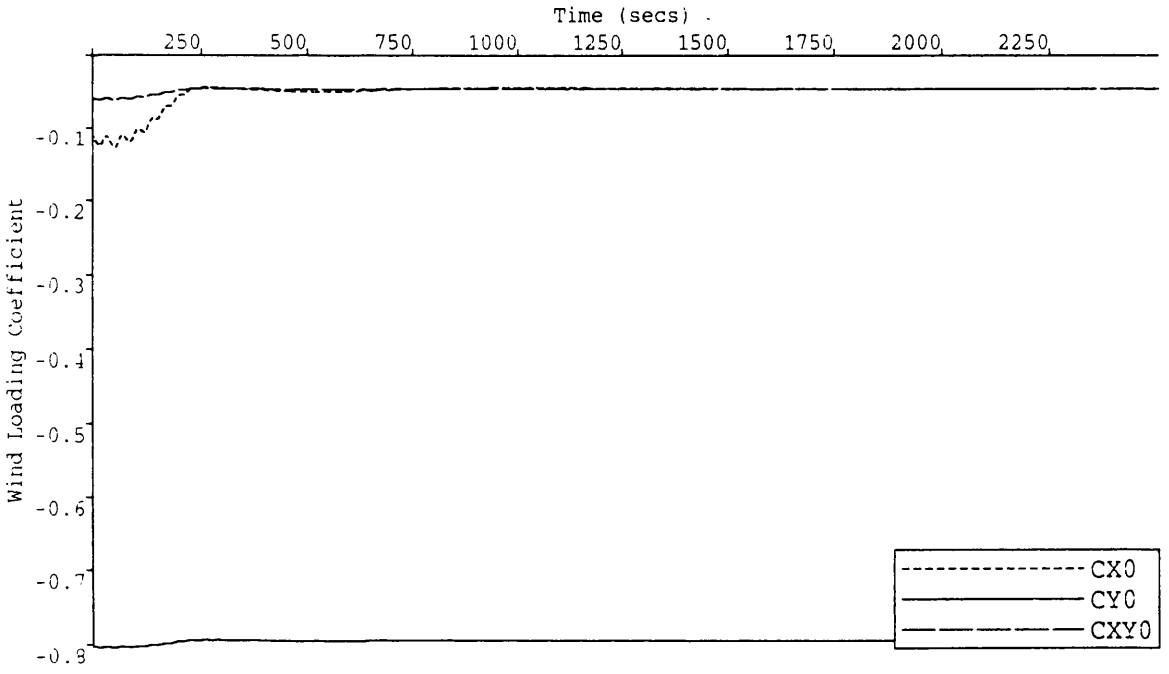

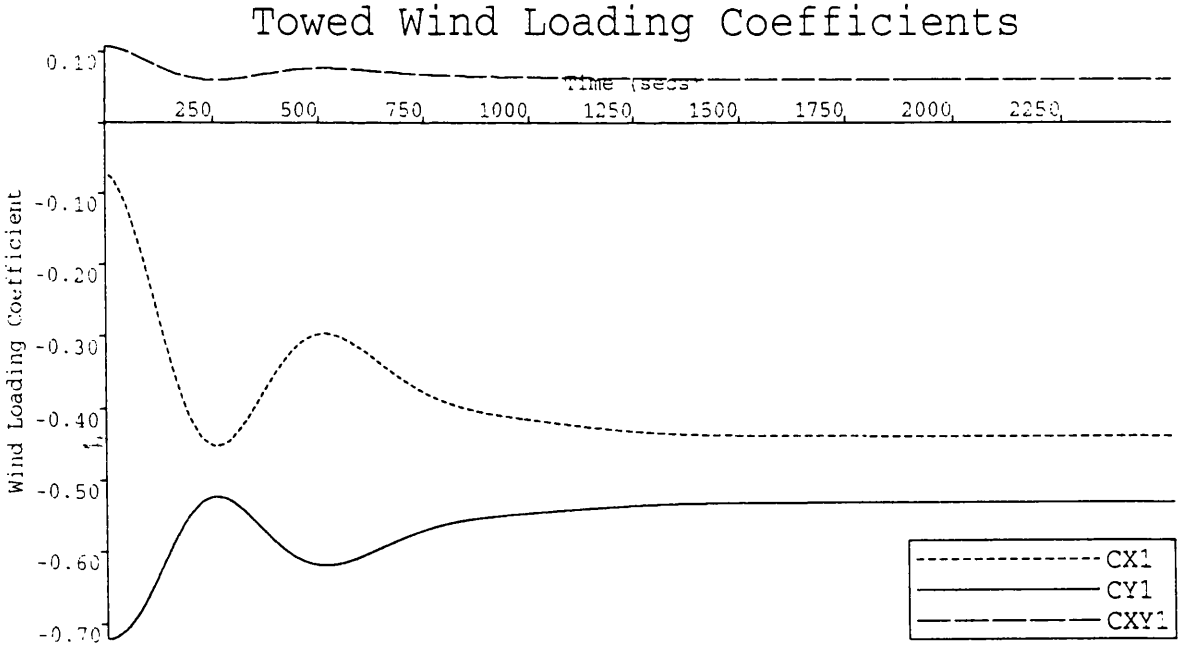

Figure 7.27e

```
Tow Velocity :  5.837 Knots
Rudder Constants 1,2 :8.0,5.0
Tow Point 0 :  0.000m
Tow Rope Length/L0 : 3.250m/m
Tow Point 1 :63.300m
Tow Rope :PY
Maximum Deflection : 22.400 Degrees
Wind Velocity,Angle :38.91, 90.0 Knots,Deg
```

Tow System C with Skeg

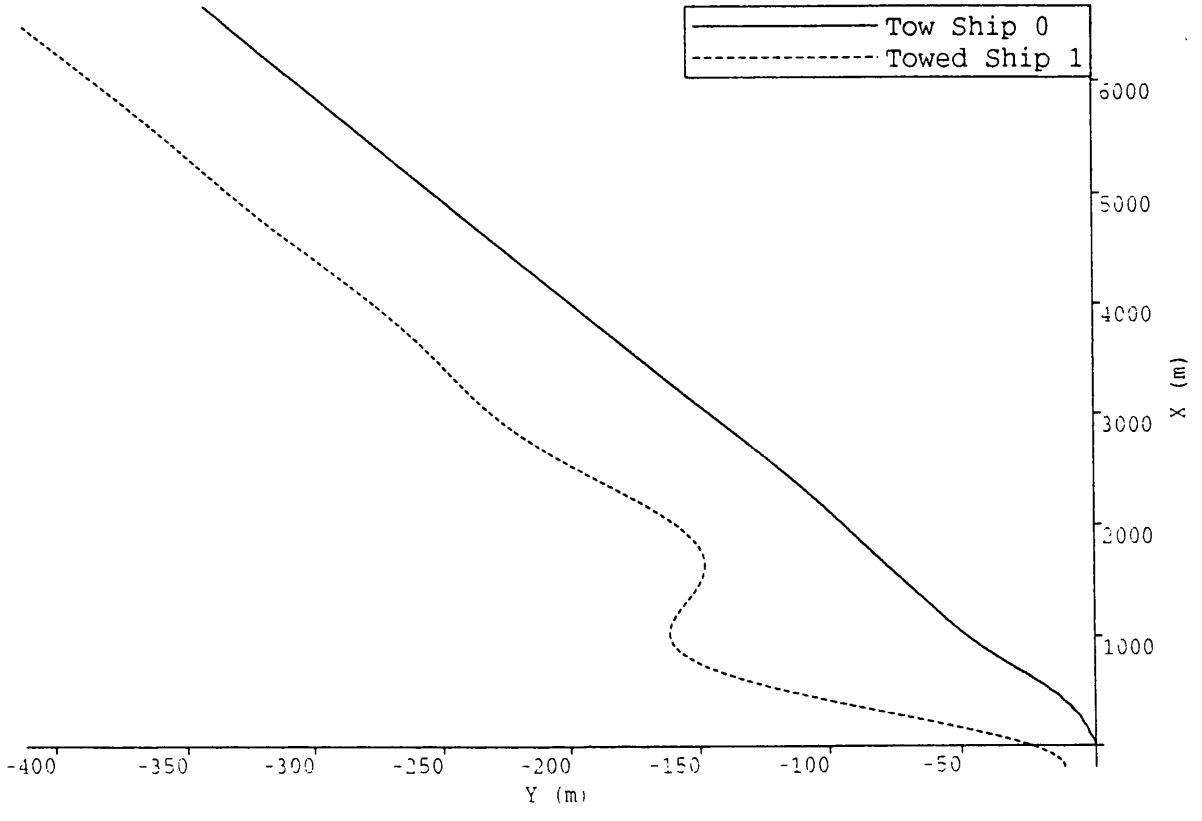

Figure 7.28a

Tow Velocity : 5.837 Knots
Rudder Constants 1,2 :8.0,5.0
Tow Point 0 : 0.000 m
Tow Rope Length/L0 : 3.250 m/m
Tow Point 1 :63.300m
Tow Rope : PY
Maximum Deflection :-23.800 Degrees
Wind Velocity,Angle : 38.91, 90.0 Knots,De

Tow System C with Skeg

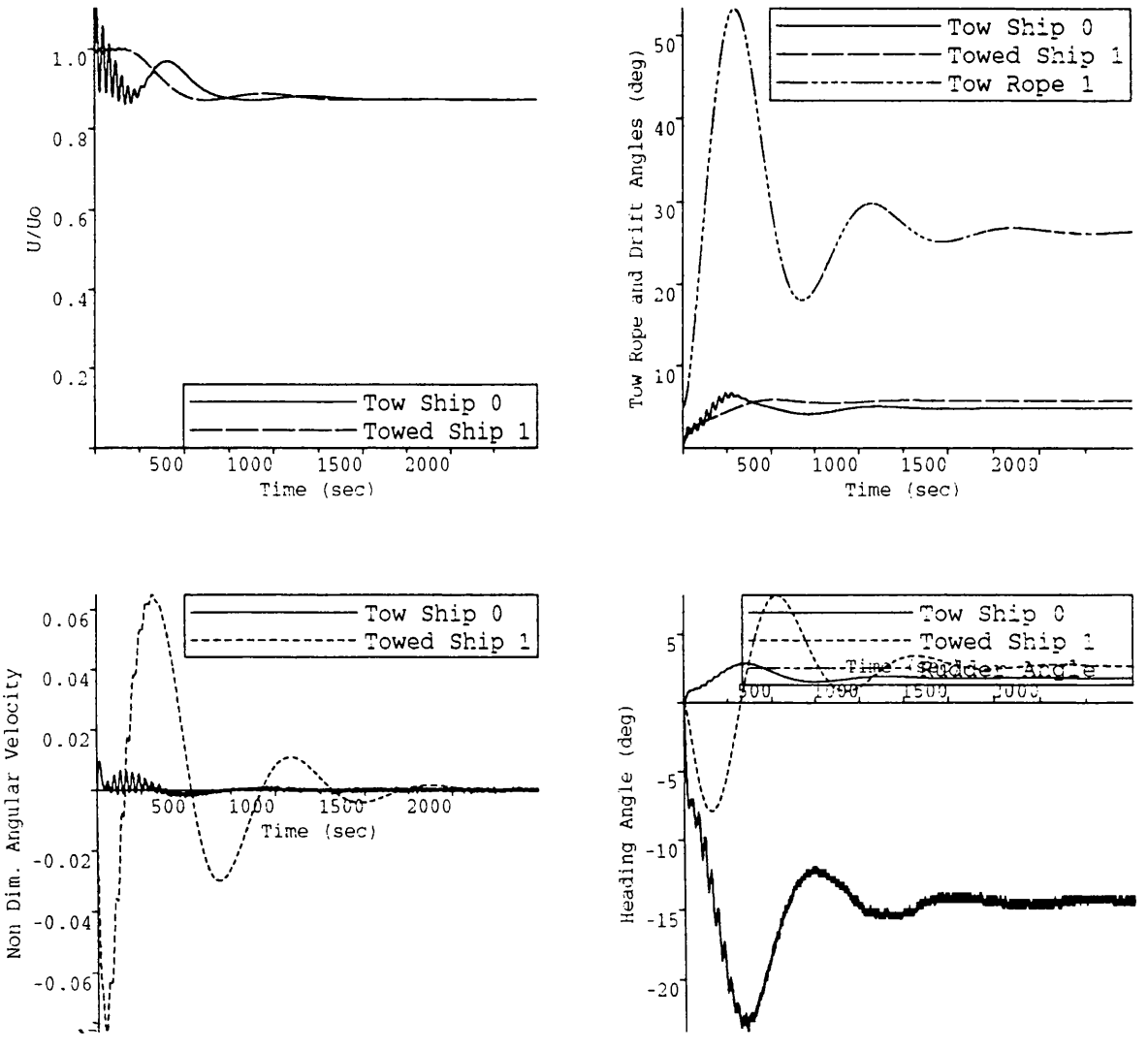

Figure 7.28b

Tow Velocity : 5.837 Knots
Rudder Constants 1,2 :8.0,5.0
Tow Point 0 : 0.000m
Tow Rope Length/L0 : 3.250m/m
Tow Point 1 :63.300m
Tow Rope :PY
Maximum Deflection :-23.800 Degrees
Wind Velocity,Angle :38.91, 90.0 Knots,Deg
Superstructure : Forward

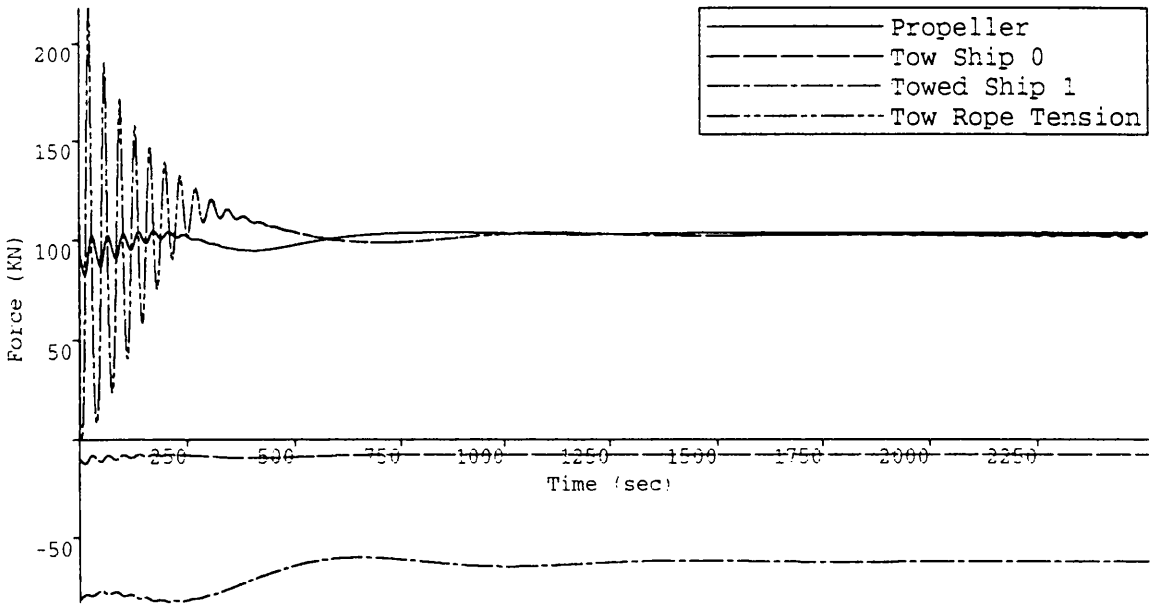

Figure 7.28c

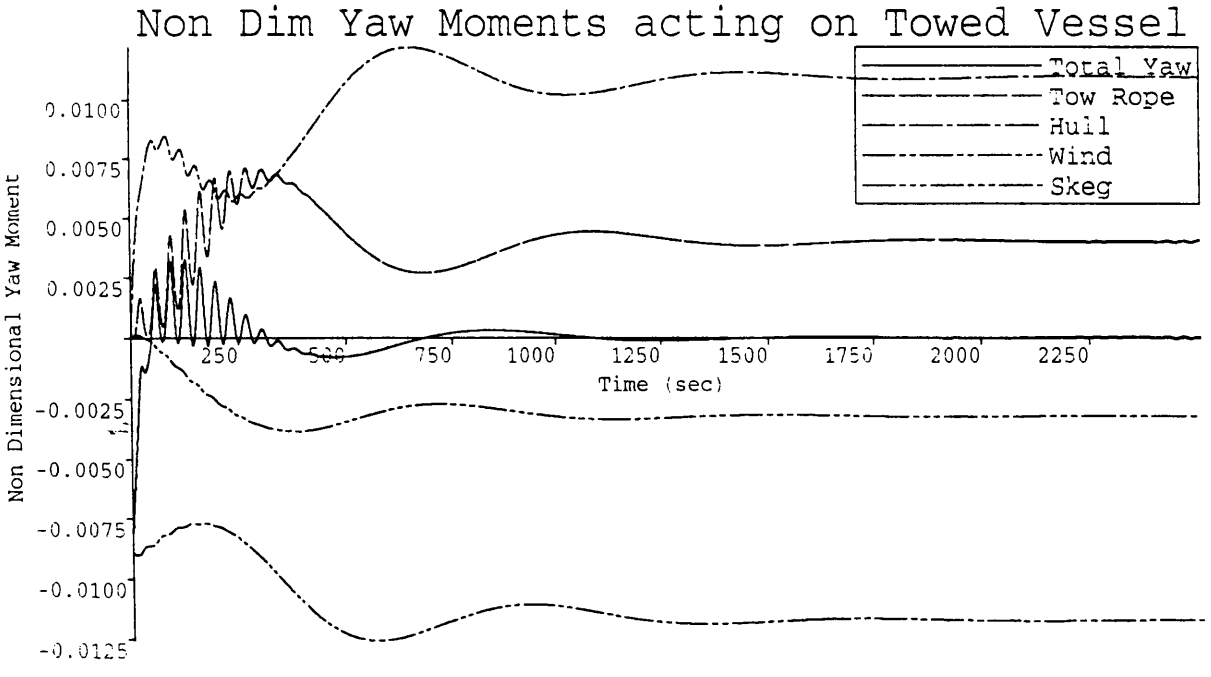

Figure 7.28d

Tow Velocity : 5.837 Knots
Rudder Constants 1,2 :8.0,5.0
Tow Point 0 : 0.000m
Tow Rope Length/L0 : 3.250m/m
Tow Point 1 :63.300m
Tow Rope :PY
Maximum Deflection :-23.800 Degrees
Wind Velocity,Angle :38.91, 90.0 Knots,Deg
Superstructure : Forward

Tow Wind Loading Coefficients

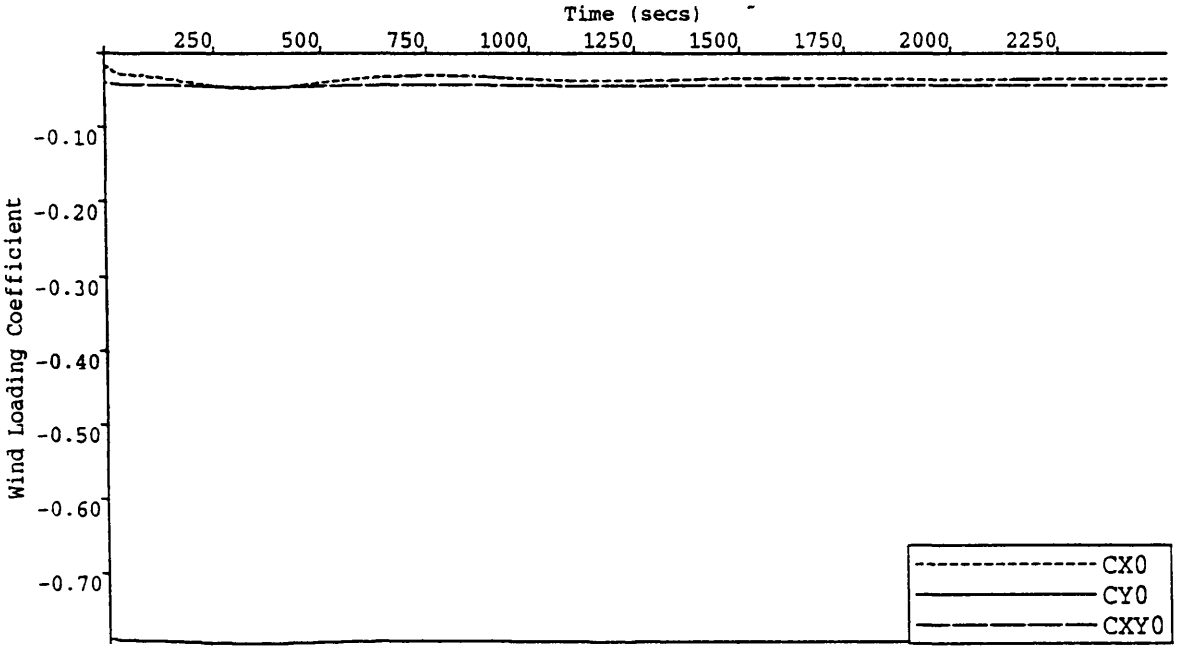

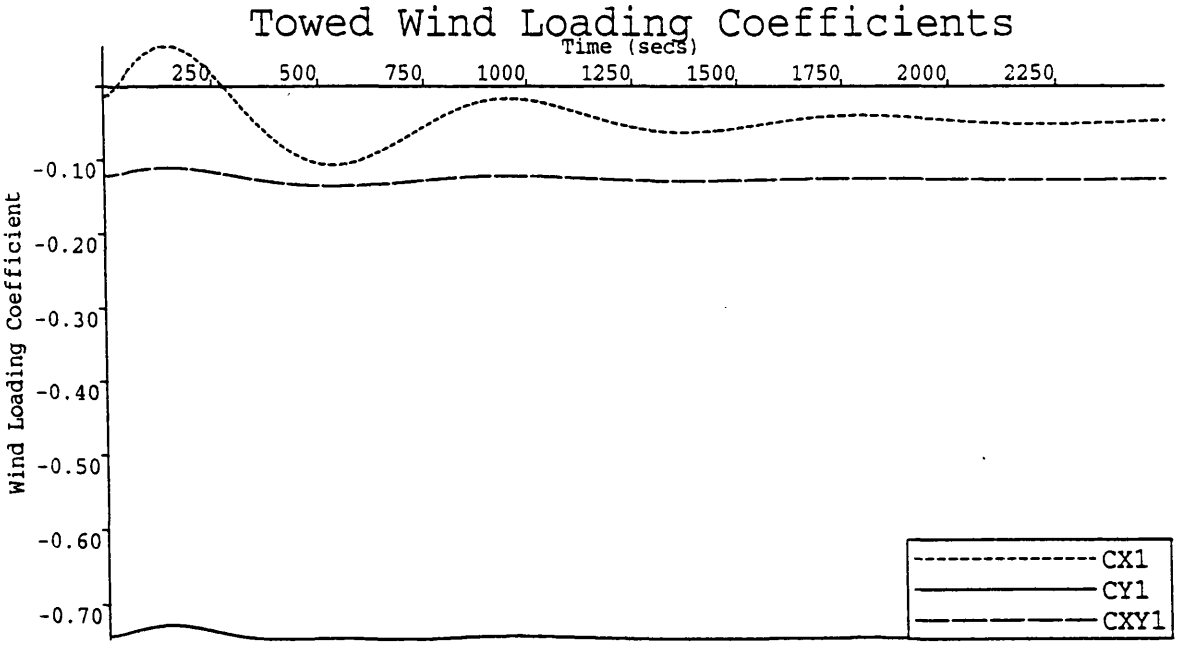

Figure 7.28e

Tow Velocity : 5.837 Knots
Rudder Constants 1,2 :8.0,5.0
Tow Point 0 : 0.000m
Tow Rope Length/L0 : 3.250m/m
Tow Point 1 :63.300m
Tow Rope :PY
Maximum Deflection : -23.800 Degrees
Wind Velocity,Angle :38.91, 90.0 Knots,Deg
Superstructure : Forward

Tow System C with Bridle

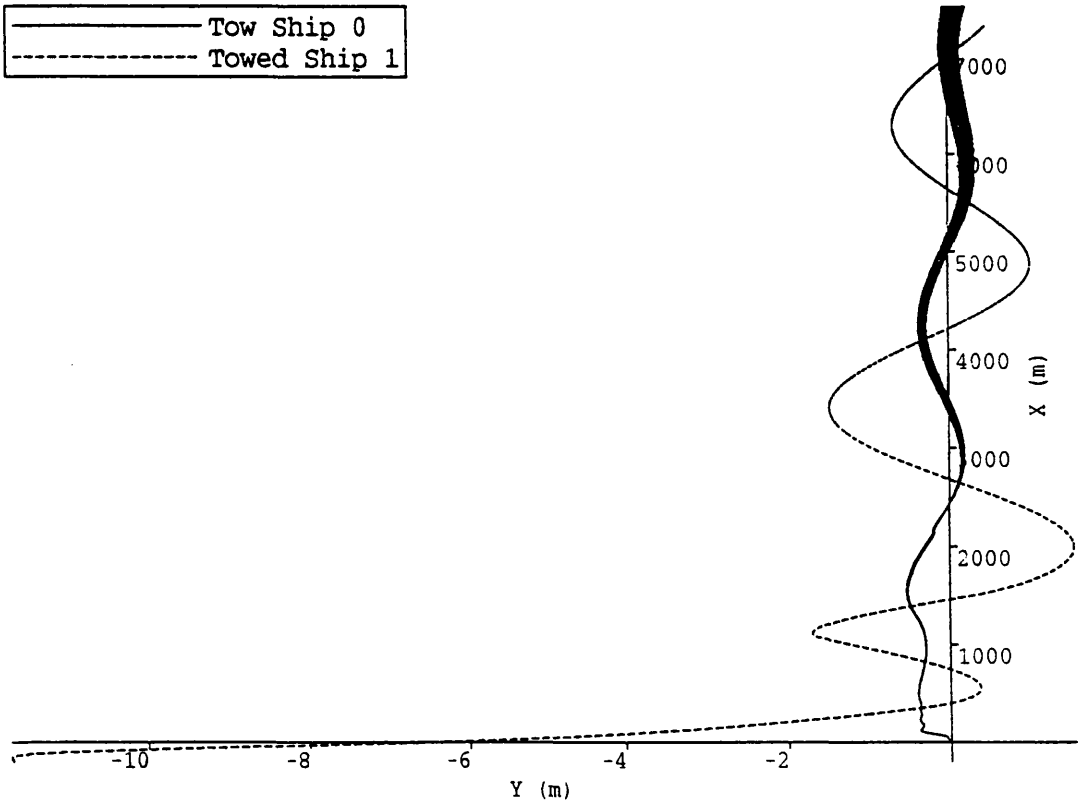

Figure 7.29a

Tow Velocity : 5.837 Knots
Rudder Constants 1,2 :8.0,5.0
Tow Point 0 : 0.000 m
Tow Rope Length/L0 : 3.250 m/m
Tow Point 1 :63.300m
Tow Rope : PY
Maximum Deflection : -2.917 Degrees
Bridle Length,Width :20.00,40.00 m,m

Tow System C with Bridle

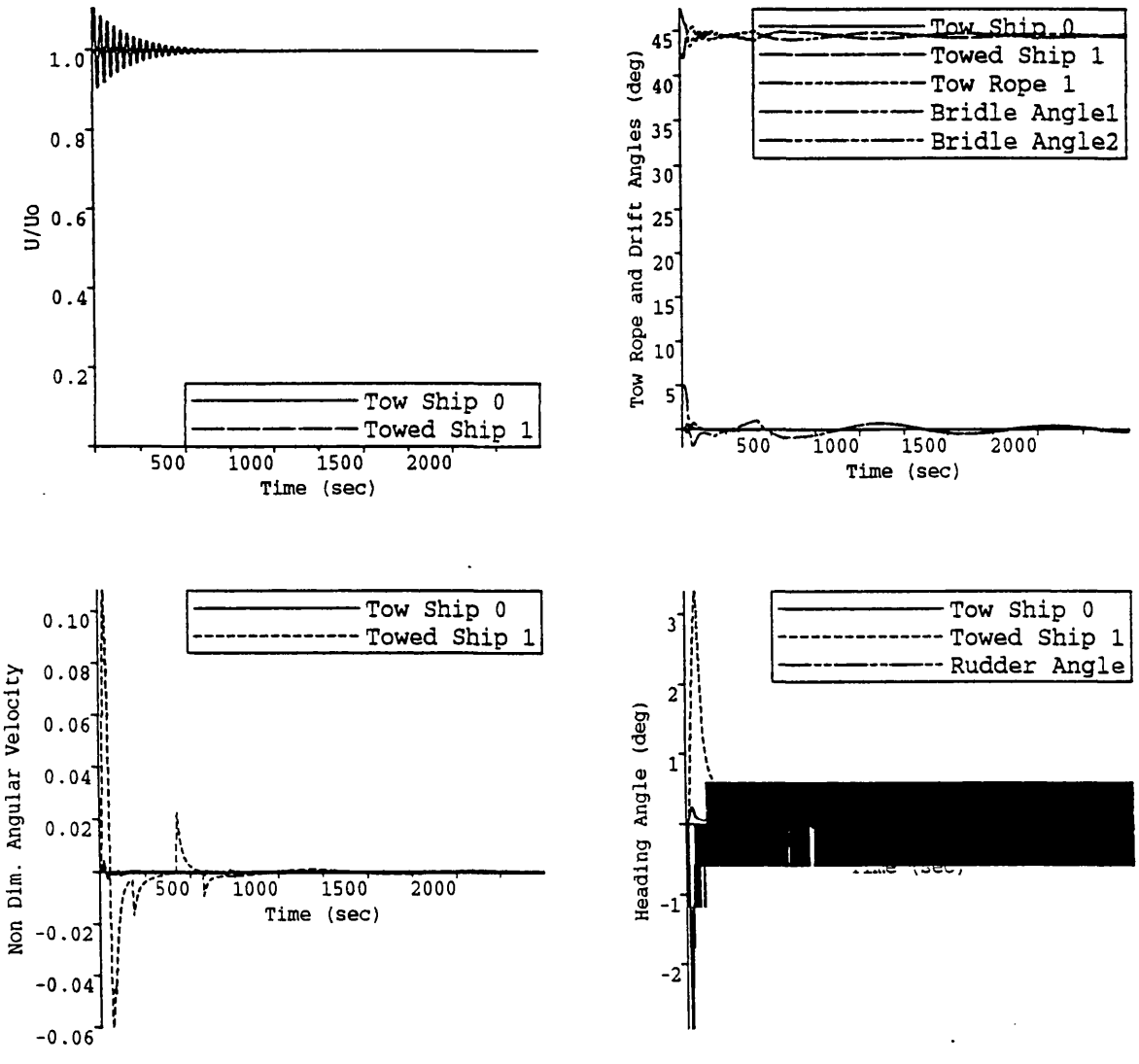

Figure 7.29b

Tow Velocity : 5.837 Knots
Rudder Constants 1,2 :8.0,5.0
Tow Point 0 : 0.000m
Tow Rope Length/L0 : 3.250m/m
Tow Point 1 :63.300m
Tow Rope :PY
Maximum Deflection : -2.917 Degrees
Bridle Length,Width :20.00, 40.0 m,m

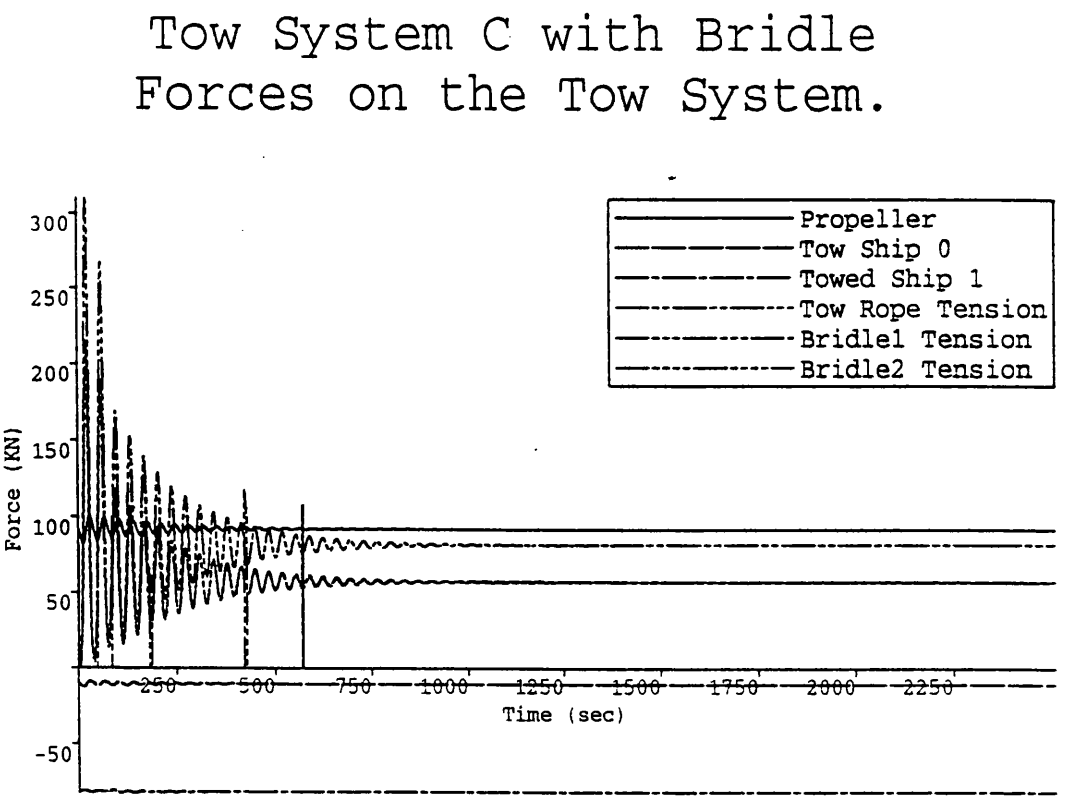

Figure 7.29c

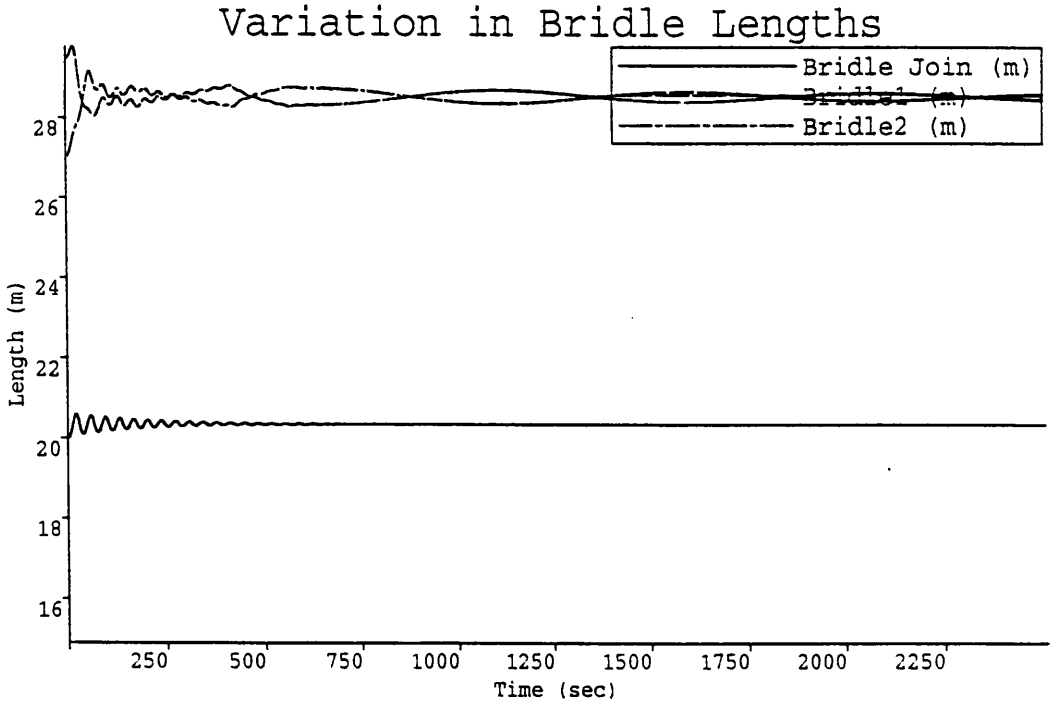

Figure 7.29d

Tow Velocity : 5.837 Knots
Rudder Constants 1,2 :8.0,5.0
Tow Point 0 : 0.000m
Tow Rope Length/L0 : 3.250m/m
Tow Point 1 :63.300m
Tow Rope :PY
Maximum Deflection : -2.917 Degrees
Bridle Length,Width :20.00, 40.0 m,m

Tow System C with Bridle

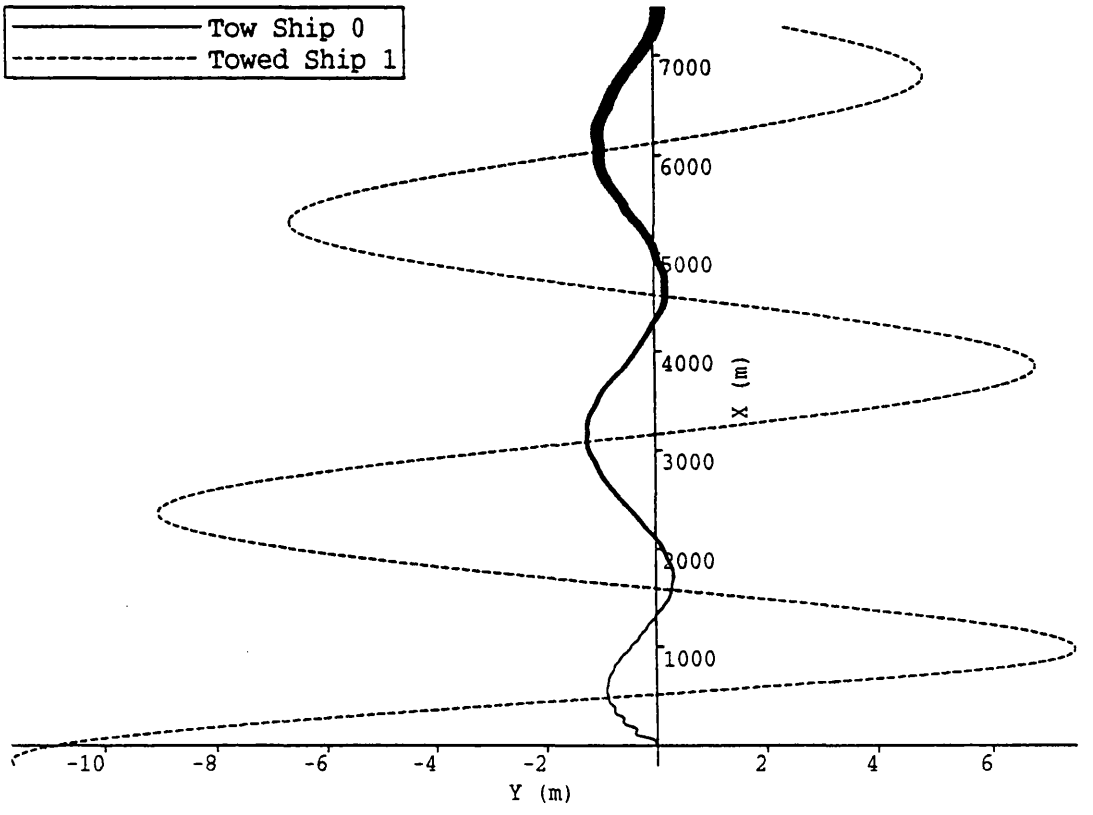

Figure 7.30a

Tow Velocity : 5.837 Knots
Rudder Constants 1,2 :8.0,5.0
Tow Point 0 : 0.000 m
Tow Rope Length/L0 : 3.250 m/m
Tow Point 1 :63.300m
Tow Rope : PY
Maximum Deflection : -2.917 Degrees
Bridle Length,Width :20.00,10.00 m,m

Tow System C with Bridle

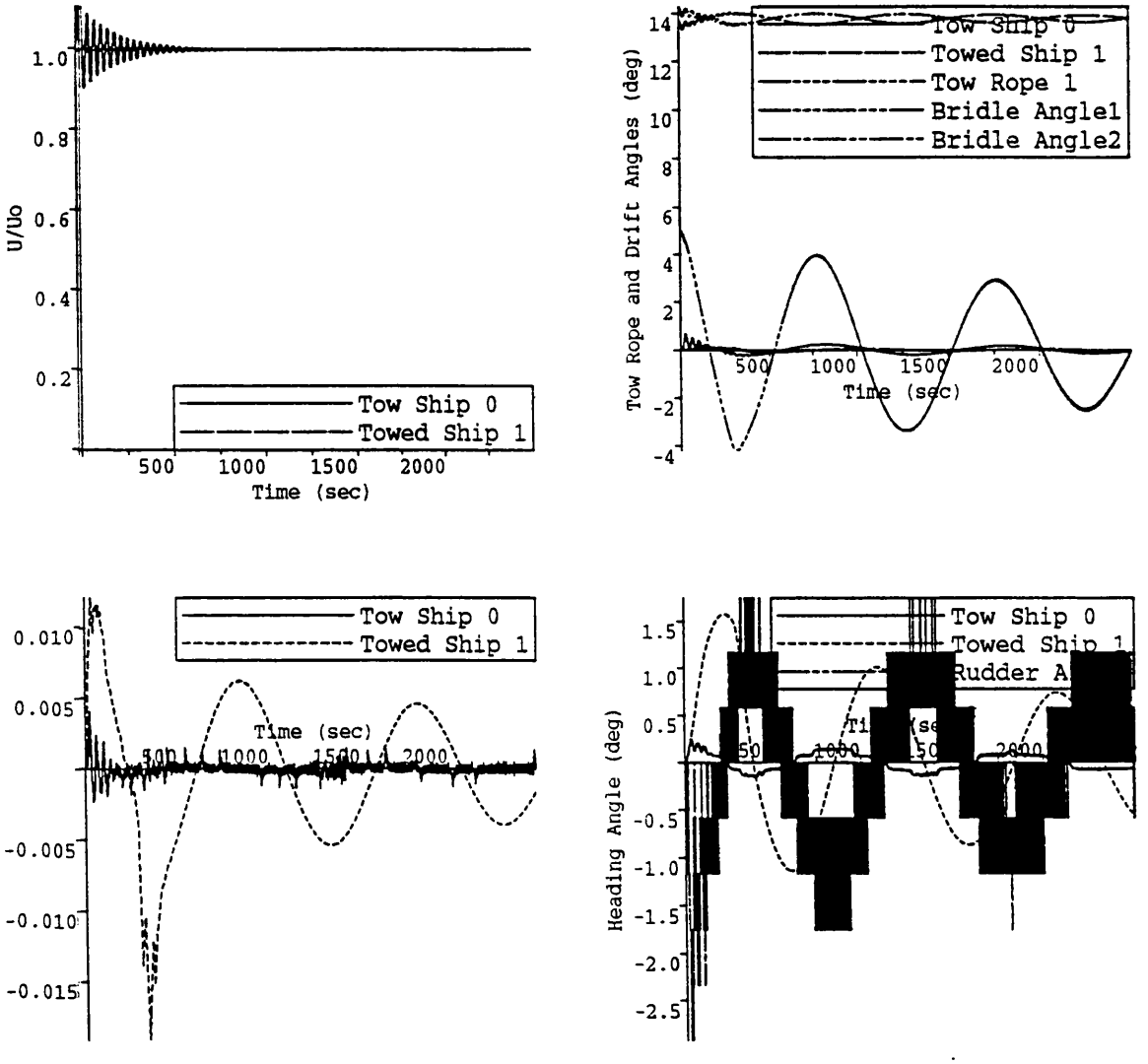

Figure 7.30b

Tow Velocity : 5.837 Knots
Rudder Constants 1,2 :8.0,5.0
Tow Point 0 : 0.000m
Tow Rope Length/L0 : 3.250m/m
Tow Point 1 :63.300m
Tow Rope :PY
Maximum Deflection : -2.917 Degrees
Bridle Length,Width :20.00, 10.0 m,m

Tow System C with Bridle
Forces on the Tow System.

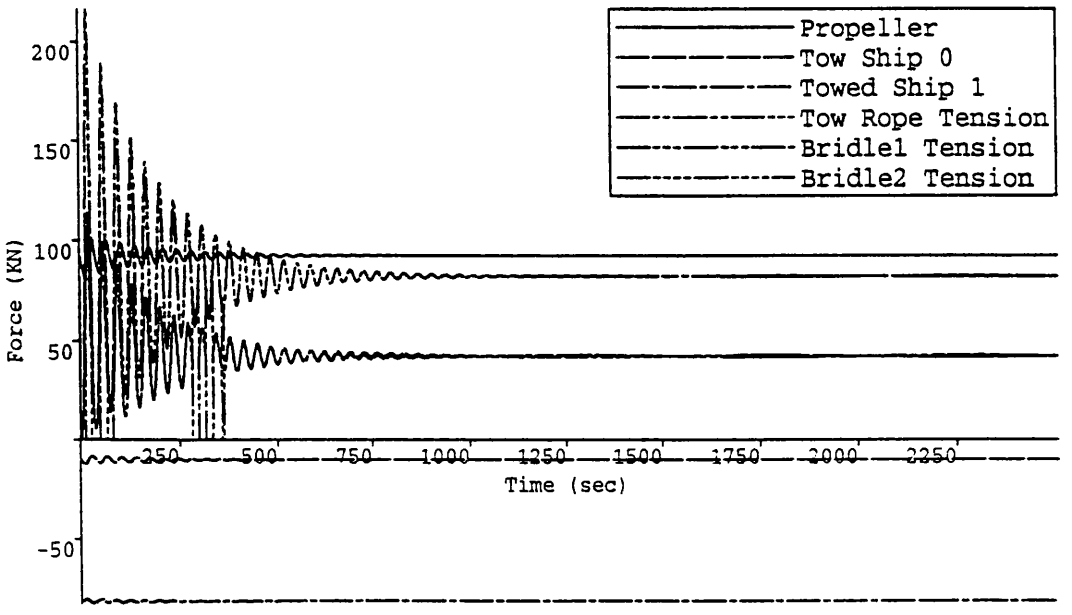

Figure 7.30c

Variation in Bridle Lengths

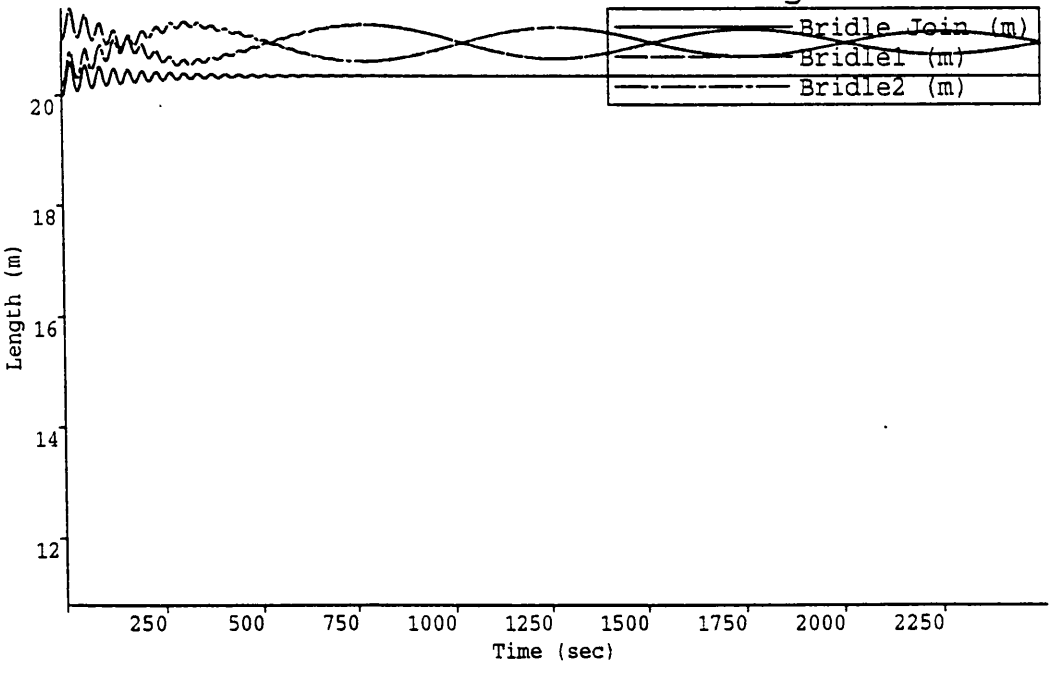

Figure 7.30d

Tow Velocity : 5.837 Knots
Rudder Constants 1,2 :8.0,5.0
Tow Point 0 : 0.000m
Tow Rope Length/L0 : 3.250m/m
Tow Point 1 :63.300m
Tow Rope :PY
Maximum Deflection : -2.917 Degrees
Bridle Length,Width :20.00, 10.0 m,m

Tow System C with Bridle

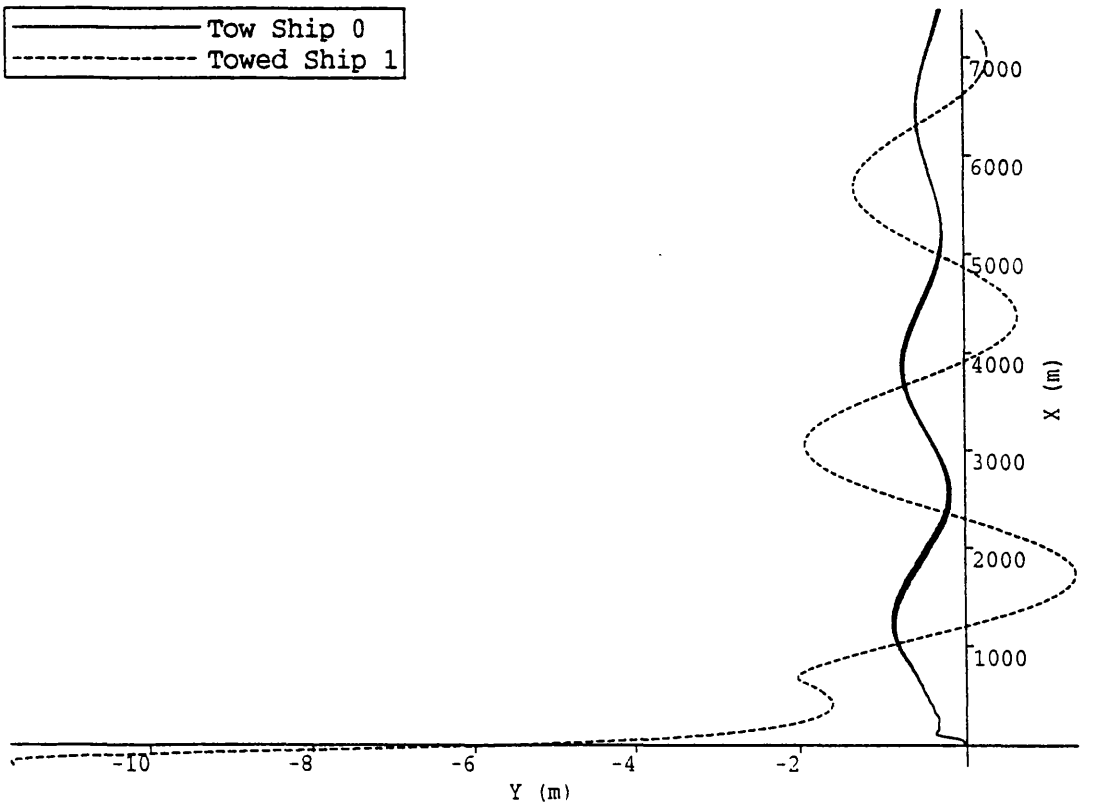

Figure 7.31a

Tow Velocity : 5.837 Knots
Rudder Constants 1,2 :8.0,5.0
Tow Point 0 : 0.000 m
Tow Rope Length/L0 : 3.250 m/m
Tow Point 1 :73.300m
Tow Rope : PY
Maximum Deflection : -2.917 Degrees
Bridle Length,Width :20.00,40.00 m,m

Tow System C with Bridle

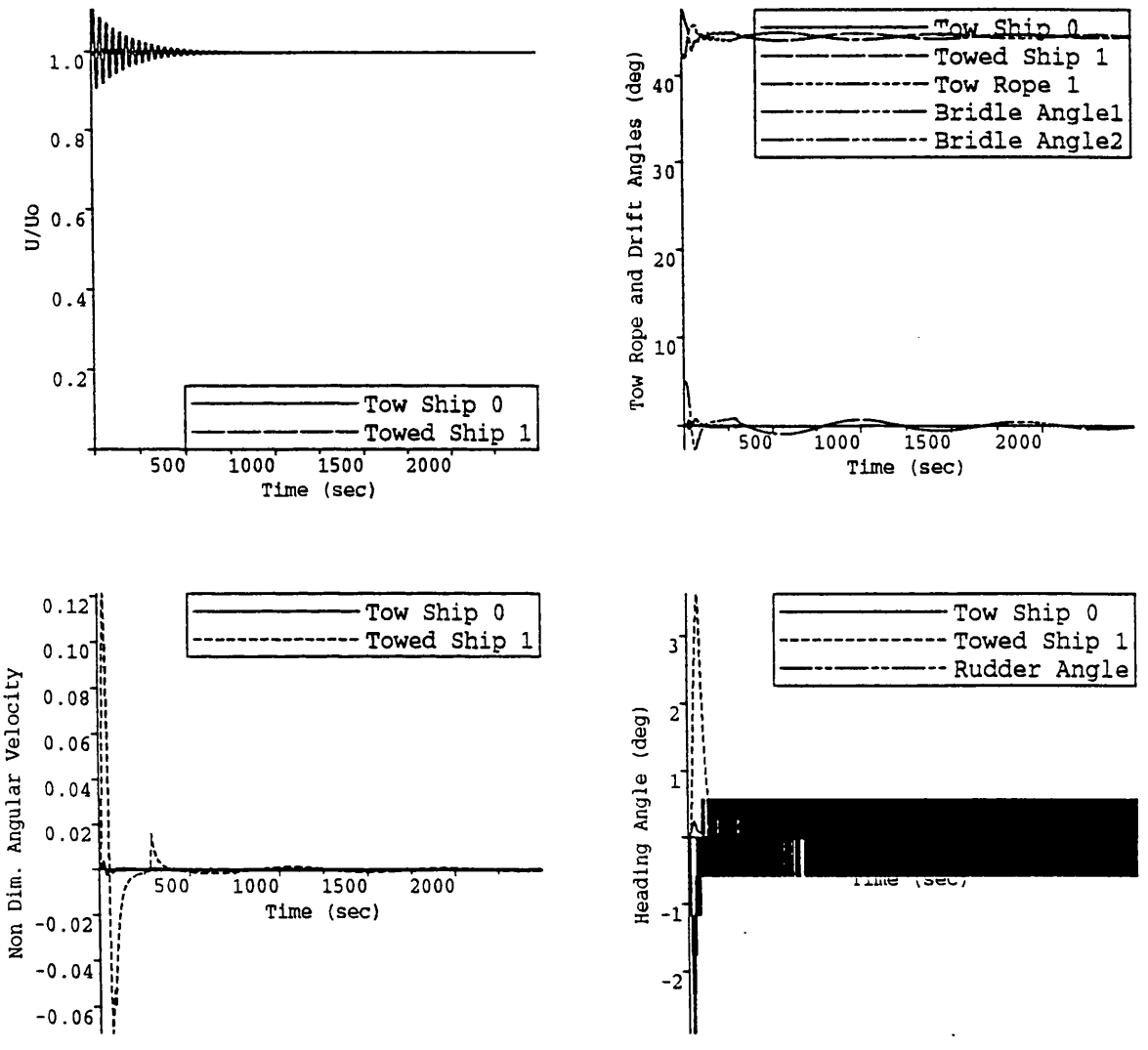

Figure 7.31b

Tow Velocity : 5.837 Knots
Rudder Constants 1,2 :8.0,5.0
Tow Point 0 : 0.000m
Tow Rope Length/L0 : 3.250m/m
Tow Point 1 :73.300m
Tow Rope :PY
Maximum Deflection : -2.917 Degrees
Bridle Length,Width :20.00, 40.0 m,m

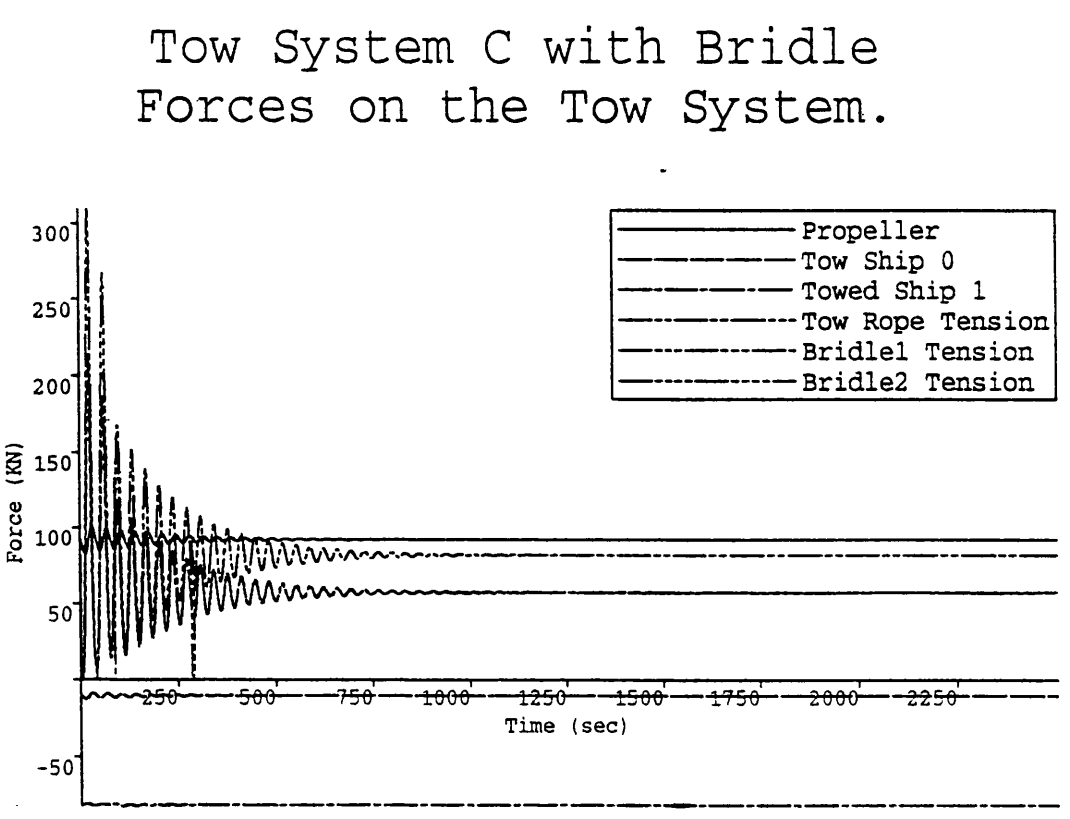

Figure 7.31c

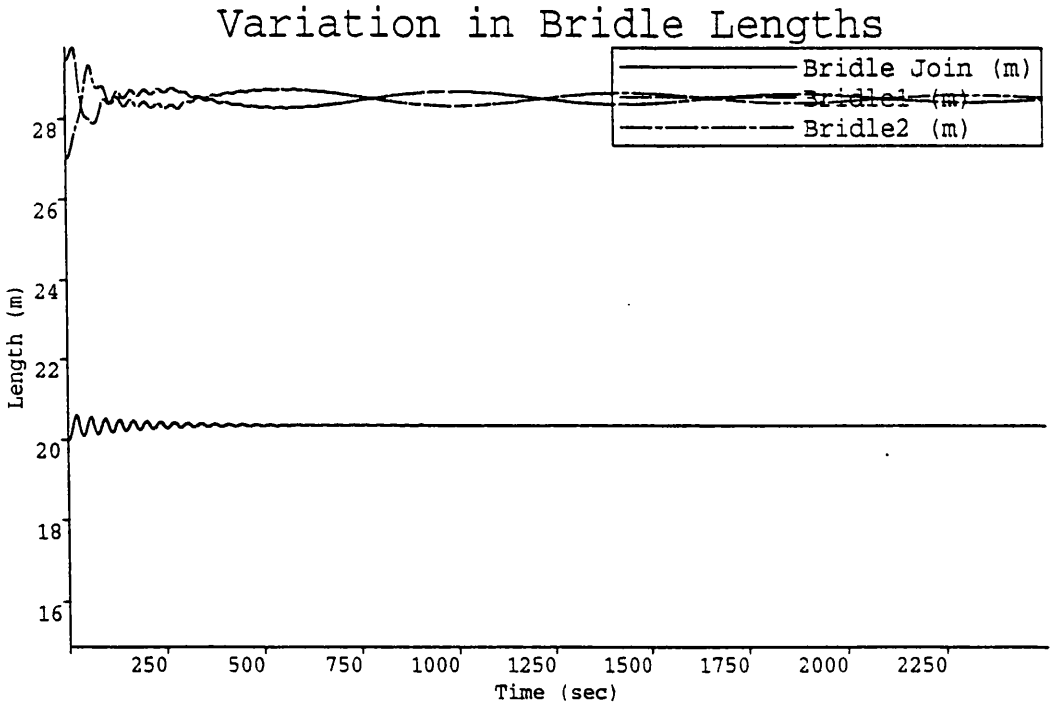

Figure 7.31d

Tow Velocity : 5.837 Knots
Rudder Constants 1,2 :8.0,5.0
Tow Point 0 : 0.000m
Tow Rope Length/L0 : 3.250m/m
Tow Point 1 :73.300m
Tow Rope :PY
Maximum Deflection : -2.917 Degrees
Bridle Length,Width :20.00, 40.0 m,m

Tow System C with Bridle

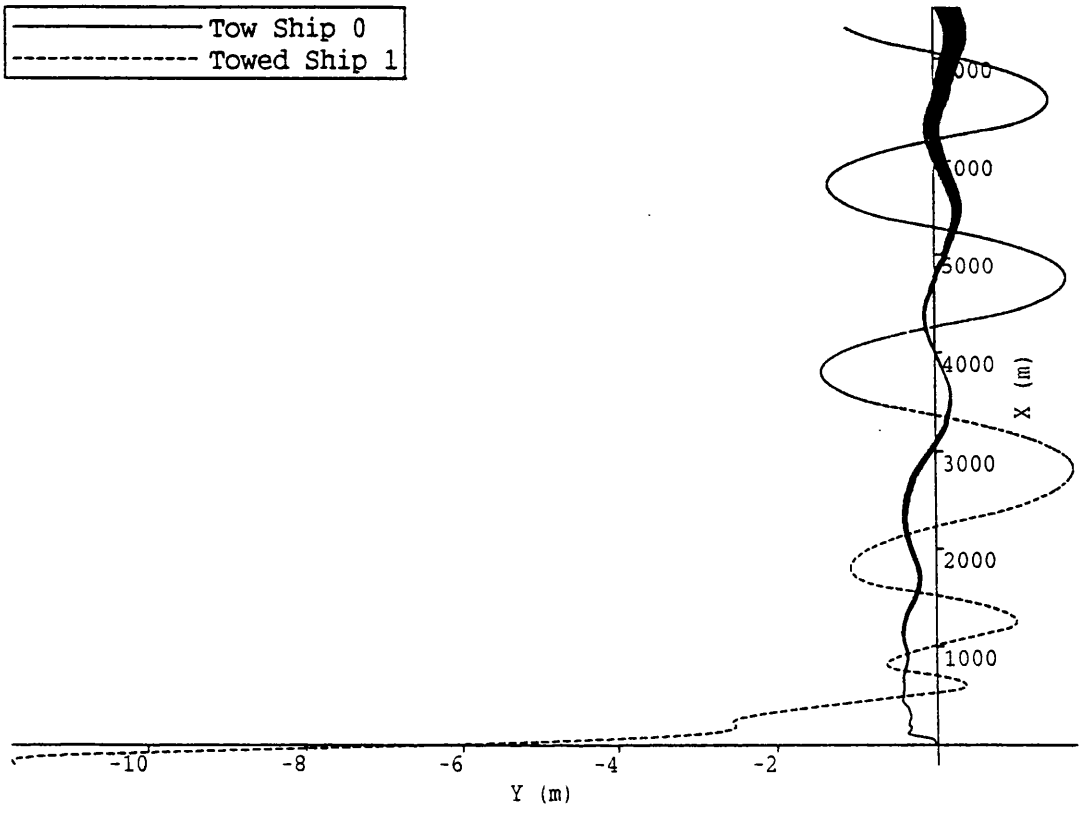

Figure 7.32a

Tow Velocity : 5.837 Knots
Rudder Constants 1,2 :8.0,5.0
Tow Point 0 : 0.000 m
Tow Rope Length/L0 : 3.250 m/m
Tow Point 1 :63.300m
Tow Rope : PY
Maximum Deflection : -2.917 Degrees
Bridle Length,Width :20.00,40.00 m,m

Tow System C with Bridle

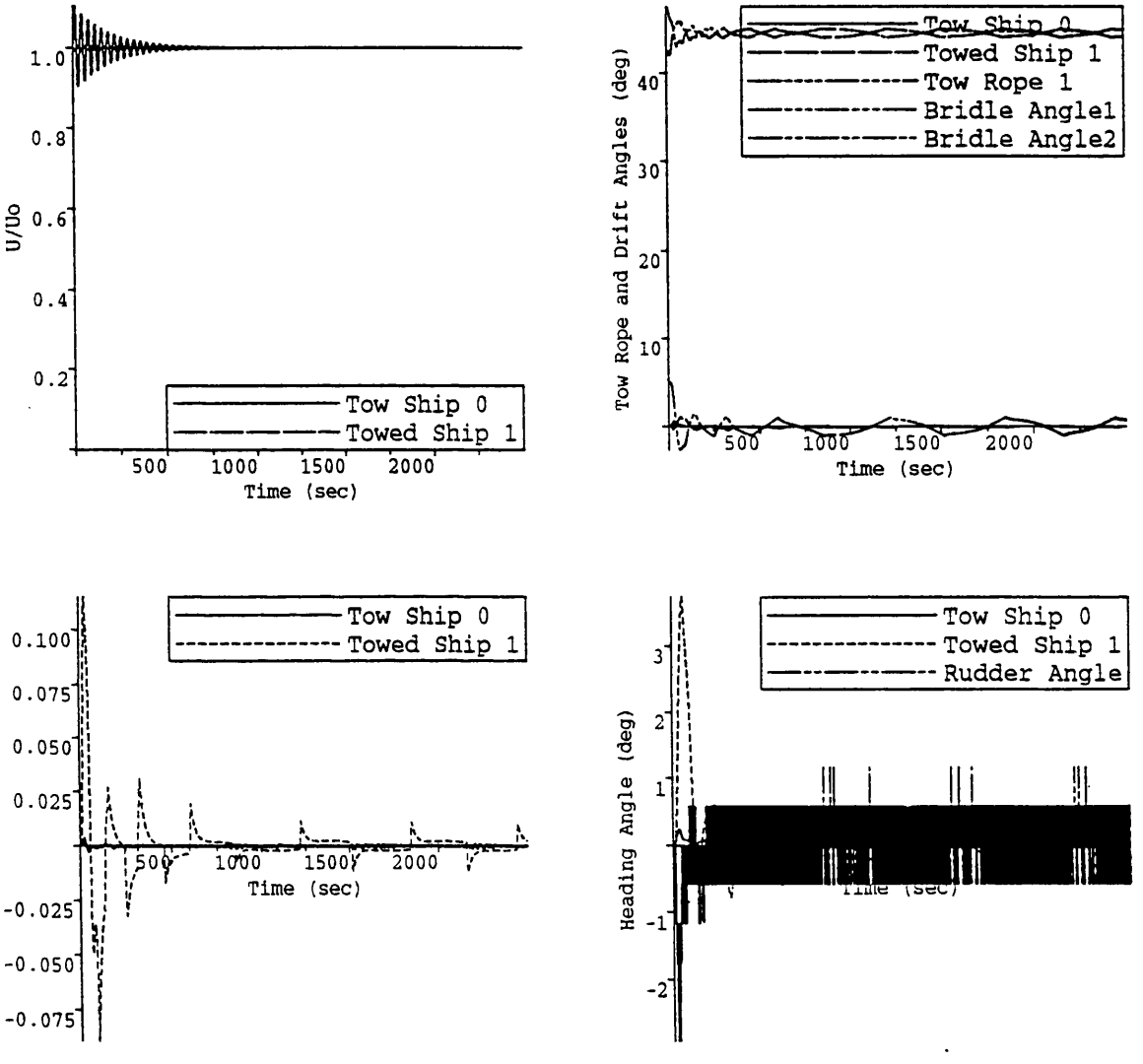

Figure 7.32b

Tow Velocity : 5.837 Knots
Rudder Constants 1,2 :8.0,5.0
Tow Point 0 : 0.000m
Tow Rope Length/L0 : 3.250m/m
Tow Point 1 :63.300m
Tow Rope :PY
Maximum Deflection : -2.917 Degrees
Bridle Length,Width :20.00, 40.0 m,m

Tow System C with Bridle
Forces on the Tow System.

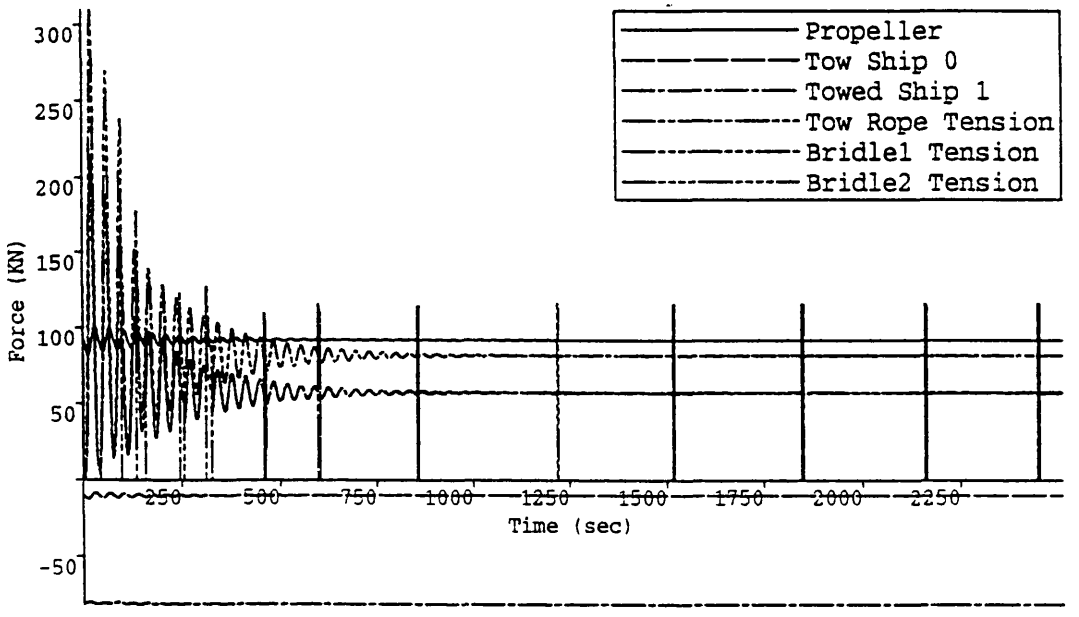

Figure 7.32c

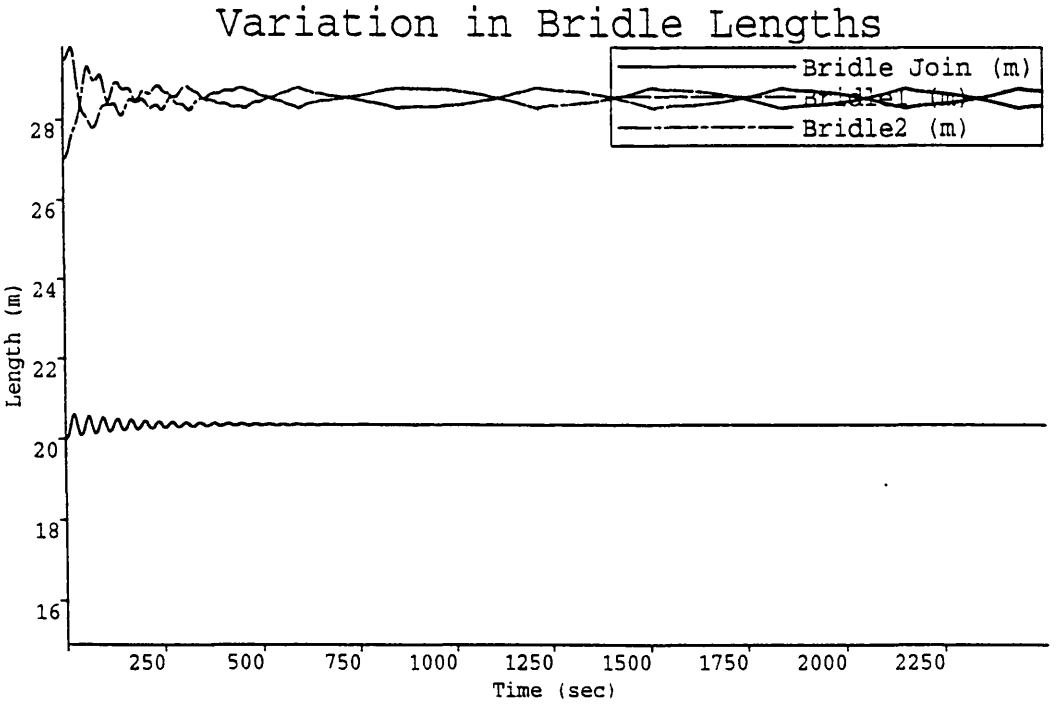

Figure 7.32d

Tow Velocity : 5.837 Knots
Rudder Constants 1,2 :8.0,5.0
Tow Point 0 : 0.000m
Tow Rope Length/L0 : 3.250m/m
Tow Point 1 :63.300m
Tow Rope :PY
Maximum Deflection : -2.917 Degrees
Bridle Length,Width :20.00, 40.0 m,m

Chapter Eight.

8.1 Main Conclusions to the Chapters.

The modular manoeuvring simulation model described in Chapter Two has proven to be accurate when comparing the results of model simulations with free running model tests Refs. 2.3, 2.4. The simulation model will also predict the manoeuvring performance of full scale vessels provided the full scale interaction coefficients are determined accurately. These full scale interaction coefficients are difficult to obtain and a technique of matching the simulation to trials data can be employed.

It is important to consider the environmental loading on vessel's manoeuvring performance. When performing a turning manoeuvre in wind, the vessel should head into the wind as the turn requires less sea room. In modelling current loading on the simulation, it is recommended to use the corrected current velocity in conjunction with the current loading coefficients. The automatic pilot model should account for course angle or global positioning in the earth fixed coordinate system as opposed to the heading angle.

The DnV calculation method is not considered to be applicable for the calculation of wind loads on jack up legs. In the case of a square leg geometry for an increasing angle of wind incidence, the wind forces decrease to a minimum value at 45 degrees. The method also cannot strictly be used for non cylindrical cornerpost designs because of the rules use of an equivalent diameter.

The MMEC method is based on extensive model tests at near full scale Reynolds numbers. These results are therefore believed to be accurate and credible to base comparison studies on. The MMEC method is dependent on accurate cornerpost drag coefficients. If new cornerpost designs are to be considered then model experiments

should be undertaken at near full scale Reynolds numbers to determine their windward and leeward cornerpost drag coefficients.

The prediction of the drag coefficients by the BSI method when compared with the MMEC method shows very good similarities for the square leg geometries considered.

The triangular leg geometries considered seem to behave less favourably. There is some debate on the location of the minimum drag with orientation in the DnV, BSI and ESDU prediction methods. The MMEC method does not include an orientation factor for the triangular leg geometries.

The skeg was included in the simulation model of Chapter Two by adding the skeg derivatives to the hull derivatives. The method of Jacobs Ref. 5.2, was employed to determine the skeg derivatives in conjunction with wing theory to obtain the resistance of the skeg. The simulation was matched to trials data for the 'Mighty Servant II' and the predicted advance, transfer, and tactical diameter were in general within 5% of the trials for the port and starboard turns.

The simulation model developed in Chapter Five could be used in the assessment of the manoeuvring performance of a heavy lift vessel undertaking the dry transportation of a jack up rig. It may also be possible for the model to be used as a design tool to give a greater insight into the manoeuvring performance for future heavy lift vessel designs. This may include limits on the longitudinal positioning of cargo and maximum leg lengths. The sizing of control surfaces could also be determined.

The manoeuvring model has design limits however. These limits include a maximum allowable wind heel angle chosen as 5 degrees. Additionally there are limits imposed from the non linear empirical manoeuvring derivatives. If the simulated drift angle is beyond an angle of approximately 25 degrees or the non dimensional angular velocity is in excess of 1.1 then doubts about the tow trajectory will begin to arise. These inaccuracies occur when simulating a turning manoeuvre of approximately 20 degrees in moderate to high wind

velocities. The automatic pilot simulations are generally unaffected by these environmental loading conditions.

In the simulations the longitudinal position of the jack up rig relative to the LCG of the tow system is important to the manoeuvring performance of the tow system. Additionally the exposed leg length and wind velocity are equally important. The leg lengths may be varied to counter any loss of manoeuvrability if restrictions are imposed due to trimming or by deck dimensions.

The accuracy of the simulation model could further be improved if wind tunnel experiments were undertaken to determine the wind loading coefficients for a heavy lift vessel design and for a jack up with top side structures. The leg wind loading model described can be added to the jack up wind coefficients to obtain an overall wind load. The manoeuvring model could also be extended to include roll motion. This would require further model experiments to determine the roll manoeuvring derivatives for a heavy lift vessel. Such an investment may not give a sufficient return as the wind yaw moments appear have greater influence on the simulations than the wind heeling moments.

The experiments for the jack up model using the two bar system did not produce the consistency of data that one had initially anticipated. The analysis of the resistance produced no definite conclusions. The linear derivatives for the zero leg position show the best results. When the leg was lowered and the spud can exposed, the yaw derivatives produced a larger scatter. It is therefore recommended that additional experiments are undertaken, repeating some of the previous cases as a cross check of the results and to examine the effects of an exposed lattice leg. The two bar experimental set up described was originally designed for conventional ship models. The experimental set up should be redesigned for the shorter jack up model with a single bar replacing the existing two bar system. This will reduce the number of readings required and hence the probability of experimental error. It

is also recommended that experiments are carried out to obtain the jack up rotary derivatives so that towing simulation studies of the type presented in Chapter Seven can be conducted with the effects of wind loading. The rotary derivatives can be obtained using standard PMM or rotating arm experiments. The unconstrained towing method proposed by Burcher Ref. 1.14, could also be attempted.

The theoretical predictions for directional stability were presented in the form of the Routh Hurwitz stability and the extended R2 stability figures. Both representations can be employed equally well but R2 provides a clearer understanding of the regions of directional stability.

In linear towing theory the tow point location on the towed vessel is the most sensitive parameter to the system directional stability followed by the tow rope length. The greatest degree of directional stability for a given tow rope length will occur at a tow point location just ahead of N_β/Y_β. It cannot be concluded that any increase in tow rope length will increase the tow directional stability as there is a dependency upon the tow system configuration.

Towing in shallow water or adding skegs will have a positive effect on the degree of directional stability. These factors affect the derivatives and increase the region of stability.

An increase in tow stability for an increase in tow velocity depends upon the a disproportionate increase in the towed vessel residual resistance coefficient. This will increase the tension of the tow rope and hence the stability region.

In the simulations it is important to consider the design of the tow system. If consideration is not given to the size of the tow vessel bollard pull or rudder dimensions then the results of the simulations will be unrealistic.

In the towing simulation model, it was found that the action of a head wind will increase the tow rope tension and as a result this will

increase the tow directional stability. A following wind may destablise the tow. Beam winds should be avoided. It is imperative to consider wind loading in towing operations. The location of the superstructure of the towed vessel has a significant impact on the sea room required. The results from simulations predict greater transverse displacements in beam winds for a superstructure located aft. This may have to be given serious consideration when towing jack ups and other sea going vessels.

The bridle towing simulations predict an increase in the directional stability of a tow when compared to the single line towing simulations. Additionally, it is predicted from the simulations that the bridle angle has the most significant effect on the directional stability followed by the longitudinal attachment of the bridle to the towed vessel.

The rigid and elastic tow simulation models give very similar predictions for the conditions simulated for head and following wind. There are differences however in the predictions when beam winds are considered. These differences stem from the tow rope assumptions and computer modelling. The elastic simulation model is considered more realistic than the rigid simulation model.

8.2 Recommendations for Towing Operations.

In the towing studies of the single tow point theoretical analysis and simulations, the conclusions and discussions of Chapter Seven can be used to give recommendations for towing operations.

In general the tow point location on tow vessel should be as close to the tow vessel LCG.

In undertaking a single tug tow, the system configuration should be analysed first for directional stability. This initial study can easily be conducted using the single tow line theoretical approach detailed Chapter Seven and Appendix G. The computations required for such a task can easily be conducted on a personal computer. The theoretical approach offers a quick solution although a straight course

must be assumed for the tow vessel motions. It is important to remember the sensitivity of the tow directional stability to the tow point location and tow rope length for a single point tow. When using the Kijima deep water empirical equations for the manoeuvring derivatives the applicability must be considered.

If the tow becomes unstable due to wind, it is sensible to set a course to head into the wind. A following wind may destablise a marginally stable tow configuration. Beam winds should always be avoided as the sea room required is greatly increased and this may lead to collisions in busy sea lanes. The location of the towed vessel superstructure has a significant effect on the towed vessel motions.

If towing a directionally unstable vessel such as a barge without skegs, it is sensible to use a bridle. The simulations predict a higher degree of control of the towed vessel motions for increased bridle angles, figure 7.1c.

If towing with an elastic tow rope an estimate of the tow rope diameter can be determined from the power relationships shown in figures 7.2. It will be necessary however to account for abrasion and loading. If employing a bridle then the bridle rope diameters should be considered separately from the diameter of the elastic tow rope as it is more economical to replace a broken bridle rope than a tow rope. An estimate of the maximum bridle rope diameter can be obtained from equation 7.32.

8.3 Future Work.

It is strongly recommended that further work is conducted in the future on the application of manoeuvring and towing simulation to jack up transportation. This work should concentrate on experimental programs and the development of advanced simulation programs. These experiments should include the following.

An experimental program to determine the resistance and the linear drift and rotary manoeuvring derivatives for various standard

jack up geometries such as the Santa Fe or Marathon Le Tourneau designs. The non linear derivatives are not considered essential as the drift angles under tow are small.

These experiments could be extended to study the effects of skegs and spud can submergence on the jack up directional stability.

Experimental studies should be conducted to verify the conclusions derived from the bridle simulation program. This can be undertaken with a conventional vessel.

Wind loading coefficients for the heavy lift vessel with forward superstructure should be obtained in addition to the wind loading coefficients for a jack up with top side structures. The jack up legs can be neglected as they can be added separately in the manner adopted in the simulation program.

It is common for vessels to have their superstructures located aft. In the simulations it was apparent that the conventional manner of towing these vessels from their bow lead to increased transverse displacements in moderate beam winds. It is recommended that further simulation work is conducted to study the effects of location of superstructure and determine if there is a relationship with transverse displacement of the towed vessel in wind. If the relationship were to be established then there would obviously be implications in towing of jack up rigs.

It may also be interesting to obtain the resistance and manoeuvring derivatives for a vessel towed by its stern with its superstructure in a forward position. It is acknowledged that the dynamic stability of a vessel will reduce in this condition due to the rudder location. The resistance will however increase but the overall effect on the directional stability when towed in wind is unknown. This may become important when towing tankers in strong winds.

The present towing simulation models can readily be extended to include two or multi tug towing with catenary tow rope solutions with current and wave loading. It will also be possible to simulate

towing of other bodies if the appropriate manoeuvring derivatives and wind loading coefficients are determined. The complexity of these simulation models will however result in excessive computations and this will increase the simulation c.p.u. time. The extension of the simulation model also increases the probability of errors if used by someone unfamiliar with the simulation model.

Appendix A.

A1 Formulation of Vessel Trajectory in the Time Domain.

In order to determine the trajectory of a vessel in the time domain we must first find expressions to calculate the position of the vessel as it travels within the earth fixed coordinate system.

From figure 2.5 we define the course angle or angular position of the velocity vector from earth fixed reference axis as,

$$\phi=\theta-\beta \qquad \text{A 1}$$

θ Angular position of the ship x axis from the earth fixed X axis,

β Drift angle.

The angular velocity of the vessel is written as,

$$\dot{\theta} = \frac{U}{L}r' \qquad \text{A 2}$$

$$\theta = \int \dot{\theta} dt = \frac{1}{L}\int Ur'dt \qquad \text{A 3}$$

The position of the center of gravity of the vessel, in the global coordinate system (X,Y) at a time t is derived as,

$$X = \int_0^t dx = \int_0^t U_X dt \qquad \text{A 4}$$

where,

$$U_X = U\cos\phi$$

$$= \int_0^t U\cos\phi\, dt \qquad \text{A 5}$$

and similarly for the position in the global Y coordinate system

$$Y = \int_0^t dy = \int_0^t U_Y dt \qquad \text{A 6}$$

$$U_Y = U \sin\phi$$

$$= \int_0^t U \sin\phi \, dt \qquad \text{A 7}$$

In the case for a turning circle we can determine the the advance and transfer at the heading angle of 90 degrees and the tactical diameter at 180 degrees.

From the above formulations we see that in order for us to determine the trajectory of the vessel in time we must calculate at each time step the quantities of

Ship Velocity

Drift Angle

Heading Angle obtained from the Angular Velocity.

The change in the above quantities with time is defined simply by Euler integration,

$$U_{N+1} = U_N + \dot{U}_N \, \Delta t$$
$$\beta_{N+1} = \beta_N + \dot{\beta}_N \, \Delta t$$
$$r'_{N+1} = r'_N + \dot{r}'_N \, \Delta t$$

We however employ a more complex integration method using the Runge Kutta Merson NAG Routine Ref. 2.17, as opposed to the simple Euler representation above. The above method is known as an 'initial

value problem' and therefore at time t=0 we must set the initial values of velocity, drift angle, heading angle, angular velocity.

Once this is done we must then determine the time derivatives of the initial velocity, drift angle, and angular velocity. We now examine the previously derived non dimensionalised equations of motion to obtain these quantities.

$$X' = \frac{L}{\overline{U}} M'_X \left\{ \frac{\dot{\overline{U}}}{\overline{U}} \cos\beta - \sin\beta\, \dot{\beta} \right\} + M'_Y r' \sin\beta \qquad 2.8.a$$

$$Y' = -\frac{L}{\overline{U}} M'_Y \left\{ \frac{\dot{\overline{U}}}{\overline{U}} \sin\beta + \cos\beta\, \dot{\beta} \right\} + M'_X r' \cos\beta \qquad 2.8.b$$

$$N' = I'_Z \frac{L}{\overline{U}} \left\{ \frac{\dot{\overline{U}} r'}{\overline{U}} + \dot{r}' \right\} \qquad 2.8.c$$

A2 Drift Angular Velocity.

We will first determine the drift angular velocity. In order to simplify the formulation for the time step integration and reduce the computations, we initially assume in the case of drift angular velocity that the ships' accelerations/decelerations are small and therefore are neglected even on application of the rudder. We can then rewrite the equations of motion 2.8 for the X and Y forces as,

$$X' = -M'_X \frac{L}{\overline{U}} \sin\beta\, \dot{\beta} + M'_Y r' \sin\beta$$

$$Y' = -M'_Y \frac{L}{\overline{U}} \cos\beta\, \dot{\beta} + M'_X r' \cos\beta$$

and rearranging we can obtain the drift angular velocity,

$$\sin^2\beta\, \dot{\beta} = \left\{ M'_Y r' \sin\beta - X' \right\} \left\{ \frac{\overline{U} \sin\beta}{M'_X L} \right\}$$

$$\cos^2\beta\,\dot{\beta} = \{M'_X r'\cos\beta - Y'\}\left\{\frac{\overline{U}\cos\beta}{M'_Y L}\right\}$$

$$\ddot{\beta} = \frac{\overline{U}}{L}\left\{\frac{\sin\beta}{M'_X}\{M'_Y r'\sin\beta - X'\} + \frac{\cos\beta}{M'_Y}\{M'_X r'\cos\beta - Y'\}\right\} \qquad \text{A 8}$$

A3 Acceleration.

We now investigate the velocity derivative. To determine the acceleration /deceleration (which we previously said was negligible for the case of drift velocity), we look again at the equation of motion 2.8a for X. If we rearrange for Acceleration as,

$$\frac{\dot{\overline{U}}}{\overline{U}}\cos\beta = \frac{\overline{U}}{M'_X L}\{X' - M'_Y r'\sin\beta\} + \sin\beta\dot{\beta}$$

and place in the equation the drift angular velocity equation A8, and rearrange we obtain,

$$\frac{\dot{\overline{U}}}{\overline{U}}\cos\beta = \frac{\overline{U}}{M'_X L}\{X' - M'_Y r'\sin\beta\} + \sin\beta\frac{\overline{U}}{L}\left\{\frac{\sin\beta}{M'_X}\{M'_Y r'\sin\beta - X'\} + \frac{\cos\beta}{M'_Y}\{M'_X r'\cos\beta - Y'\}\right\}$$

$$\dot{\overline{U}} = \frac{\overline{U}^2}{L\cos\beta}\left\{\frac{M'_Y r'\sin\beta}{M'_X}(\sin^2\beta - 1) + \frac{X'}{M'_X}(1 - \sin^2\beta) + \frac{M'_X r'\cos^2\beta\sin\beta}{M'_Y} - \frac{Y'\cos\beta\sin\beta}{M'_Y}\right\}$$

$$\dot{\overline{U}} = \frac{\overline{U}^2}{L}\left\{-\frac{M'_Y r'\sin\beta}{M'_X}\cos\beta + \frac{X'}{M'_X}\cos\beta + \frac{M'_X r'\cos\beta\sin\beta}{M'_Y} - \frac{Y'\sin\beta}{M'_Y}\right\}$$

$$\dot{\overline{U}} = \frac{\overline{U}^2}{L}\left\{\frac{X'}{M'_X}\cos\beta - \frac{Y'\sin\beta}{M'_Y} + r'\cos\beta\sin\beta\left(\frac{M'_X}{M'_Y} - \frac{M'_Y}{M'_X}\right)\right\} \qquad \text{A 9}$$

A4 Angular Acceleration.

The angular acceleration is derived from the equation of motion

for yaw 2.8c. First we arrange for angular acceleration and place the equation for acceleration, equation A9, derived previously we finally obtain,

$$N' = I'_Z \frac{L}{\overline{U}} \left\{ \frac{\dot{\overline{U}} r'}{\overline{U}} + \dot{r}' \right\} \qquad 2.8.c$$

$$\dot{r}' = \frac{N'\overline{U}}{I'_Z L} - \frac{\dot{\overline{U}} r'}{\overline{U}}$$

$$\dot{r}' = \frac{N'\overline{U}}{I'_Z L} - \frac{\overline{U} r'}{L} \left\{ \frac{X'}{M'_X} \cos\beta - \frac{Y' \sin\beta}{M'_Y} + r' \cos\beta \sin\beta \left(\frac{M'_X}{M'_Y} - \frac{M'_Y}{M'_X} \right) \right\} \qquad A\ 10$$

Appendix B.

B1 Trim Deep Water Derivatives.

The deep water manoeuvring derivatives for trim by stern condition are obtained by applying the following corrections to the deep water derivatives given in Chapter Two. The trim τ is defined as,

$\tau = d_A - d_F$

d_F draft forward

d_A draft aft

The mean draft is defined as,

$$d_m = \frac{d_A + d_F}{2}$$

The trimmed derivatives are obtained by multiplying the even keel deep water derivatives as follows,

$$Y'_\beta(\tau) = Y'_\beta(0)\left\{1+\left(25\frac{C_B B}{L}-2.25\right)\frac{\tau}{d_m}\right\},$$

$$Y'_r(\tau)-(m'+m'_x) = (Y'_r(0)-(m'+m'_x))\left\{1+(571\left\{d\frac{(1-C_B)}{B}\right\}^2-81d\frac{(1-C_B)}{B}+2.1)\frac{\tau}{d_m}\right\}$$

$$Y'_{\beta\beta}(\tau) = Y'_{\beta\beta}(0)\left\{1-\left(35.7\frac{C_B B}{L}-2.5\right)\frac{\tau}{d_m}\right\},$$

$$Y'_{rr}(\tau) = Y'_{rr}(0)\left\{1+\left(45\frac{C_B B}{L}-8.1\right)\frac{\tau}{d_m}\right\},$$

$$Y'_{\beta rr}(\tau) = Y'_{\beta rr}(0)\left\{1+\left(40d\frac{(1-C_B)}{B}-2\right)\frac{\tau}{d_m}\right\},$$

$$Y'_{\beta\beta r}(\tau) = Y'_{\beta\beta r}(0)\left\{1+\left(110d\frac{(1-C_B)}{B}-9.7\right)\frac{\tau}{d_m}\right\},$$

$$N'_\beta(\tau) = N'_\beta(0)\left\{1-\frac{\tau}{d_m}\right\}$$

$$N'_r(\tau) = N'_r(0)\left\{1+\left(34\frac{C_B B}{L}-3.4\right)\frac{\tau}{d_m}\right\}$$

$$N'_{\beta\beta}(\tau) = N'_{\beta\beta}(0)\left\{1+\left(58d\frac{(1-C_B)}{B}-5\right)\frac{\tau}{d_m}\right\},$$

$$N'_{rr}(\tau) = N'_{rr}(0)\left\{1-\left(30\frac{C_BB}{L}-2.6\right)\frac{\tau}{d_m}\right\},$$

$$N'_{\beta rr}(\tau) = N'_{\beta rr}(0)\left\{1+\left(48\left(\frac{C_BB}{L}\right)^2-16\frac{C_BB}{L}+1.3\right)\times10^2\frac{\tau}{d_m}\right\},$$

$$N'_{\beta\beta r}(\tau) = N'_{\beta\beta r}(0)\left\{1+\left(3\frac{C_BB}{L}-1\right)\frac{\tau}{d_m}\right\}$$

B2 Shallow Water Derivatives.

The hydrodynamic forces acting on a vessel hull will increase with decreasing water depth. The shallow water derivatives are determined by multiplying the deep water derivatives for the fully loaded condition only, by the correction factor.

$$D_{shw} = f(h)\times D_{deep}$$

D_{deep} Deep water derivative

D_{shw} Shallow water derivative

f(h) Correction factor

The correction factors are assumed as follows,

For Y'_β, $Y'_{\beta\beta}$, $Y'_{\beta rr}$, N'_β, N'_r

$$f(h) = \frac{1}{(1-h)^n}-h$$

$$h = \frac{d_m}{H}$$

$$n = 0.4\frac{C_BB}{d_m}$$

d_m Mean draft

H Water depth

for the remaining derivatives,the following factors are assumed,

$$f(h) = 1 + a_1 h + a_2 h^2 + a_3 h^3$$

$$a_1 = -5.5\left(\frac{C_B B}{d_m}\right)^2 + 26\frac{C_B B}{d_m} - 31.5$$

$$a_2 = 37\left(\frac{C_B B}{d_m}\right)^2 - 185\frac{C_B B}{d_m} + 230$$

$$a_3 = -38\left(\frac{C_B B}{d_m}\right)^2 + 197\frac{C_B B}{d_m} - 250$$

The wake fraction ratio, ε is assumed independent of water depth. The wake fraction coefficient at the propeller location in shallow water is estimated by correcting the coefficient for deep water as shown below,

$$\frac{(1-\omega_{PO})_{Shw}}{(1-\omega_{PO})_{Deep}} = \cos(C_{wpo}\, d_m / H)$$

C_{wpo} is a constant for each type vessel.

Appendix C.

The normal rudder force equation 2.25 can be viewed as a combination of the rudder characteristics in open water, the effective inflow velocity and the effective inflow angle at the rudder. This appendix will describe the back ground to the open water rudder force and the formulation of effective inflow angle at the rudder. A fuller description of these may be found in Refs. 2.6 and 2.7. The inflow velocity at the rudder will not be described as the formulations presented in Refs. 2.6 and 2.7 are redundant and references which detail the present form of the inflow velocity described in the rudder forces equations are unavailable. Additionally the appendix will show the formulation of interactions of the rudder to the hull, equations 2.24.

C1 Rudder Normal Force in Open Water.

The non dimensionalised rudder normal force is expressed as,

$$F'_N = 0.5\rho A_R U_R^2 f\,(\Lambda,\delta)/0.5\rho LDU^2 \qquad C1$$

The open water characteristics can be estimated by a theoretical calculation and the empirical method such as Fujii's formula for rectangular rudders Ref. 2.18. This relationship is seen in figure C.1.

$$f\,(\Lambda,\delta) = \frac{6.13+\Lambda}{\Lambda+2.25}\sin\delta \qquad C2$$

Λ Rudder Aspect Ratio

C2 Effective Rudder Inflow Angle.

The effective angle of inflow to the rudder α_R, plays an important role in the rudder force,

$$\alpha_R = \delta - \alpha_0 \qquad C3$$

In figure B.2 the apparent angle of inflow, relative to the ship centerline at the rudder position can be written as,

$$\alpha_0 = \gamma\beta'_R \qquad C4$$

$$\beta'_R = \beta - 2x'_R r' \qquad C5$$

The definition of γ is illustrated in figure C2. It is an empirical coefficient and is obtained by experiment. The value of 2 used in equation C 5 is described in reference 2.6.

C3 Rudder and Hull Interaction.

The rudder deflection at the ship stern gives rise to the rudder force. It also induces another form of lateral force acting on the hull as an interaction effect by the rudder. This phenomena may be accounted for by way of a disturbed circulation approach, however simplified notations may serve for practical purpose of describing these added quantities Refs. 2.6, 2.7. With reference to the figure 2.4 the total sway force on the hull due to the rudder deflection and hull interaction can be shown as,

$$Y_R = Y_{RO} + \Delta Y_{RO} = Y_{RO} + a_H Y_{RO}$$

$$= (1 + a_H) Y_{RO} \qquad C6$$

and similarly the moment is,

$$N_R = -x_R Y_{RO} - a_H x_H Y_{RO}$$

$$= -x_R \left(1 + \frac{x_H}{x_R} a_H\right) Y_{RO}. \qquad C7$$

If we approximate $x_H \approx x_R \approx 0.5L$ and rewrite the above as

$$Y_R = (1 + a_H)\, Y_{RO} \qquad C8$$

$$N_R = -0.5L\,(1 + a_H)\, Y_{RO} \qquad C9$$

The non dimensionalised form of this is rewritten as,

$$Y'_R = (1 + a_H)\, Y'_{RO}$$

$$N'_R = -0.5\,(1 + a_H)\, Y'_{RO}$$

x'_R Distance from cog to center of lateral force. (Non dimensionalised)

a_H Ratio of additional lateral force.

x'_H Distance from cog to center of additional lateral force. (Non dim.)

The values of a_H.and x'_R may be estimated from figures 2.4.

Rudder Normal Force.

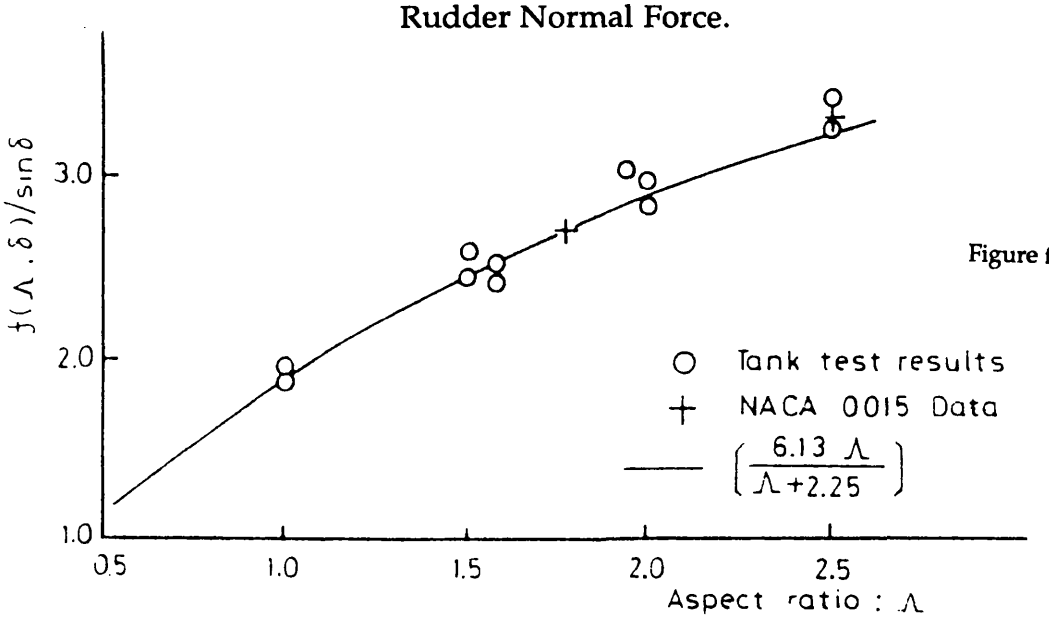

Figure from Ref. 2.18

Figure C 1

Apparent Rudder Inflow Angle.

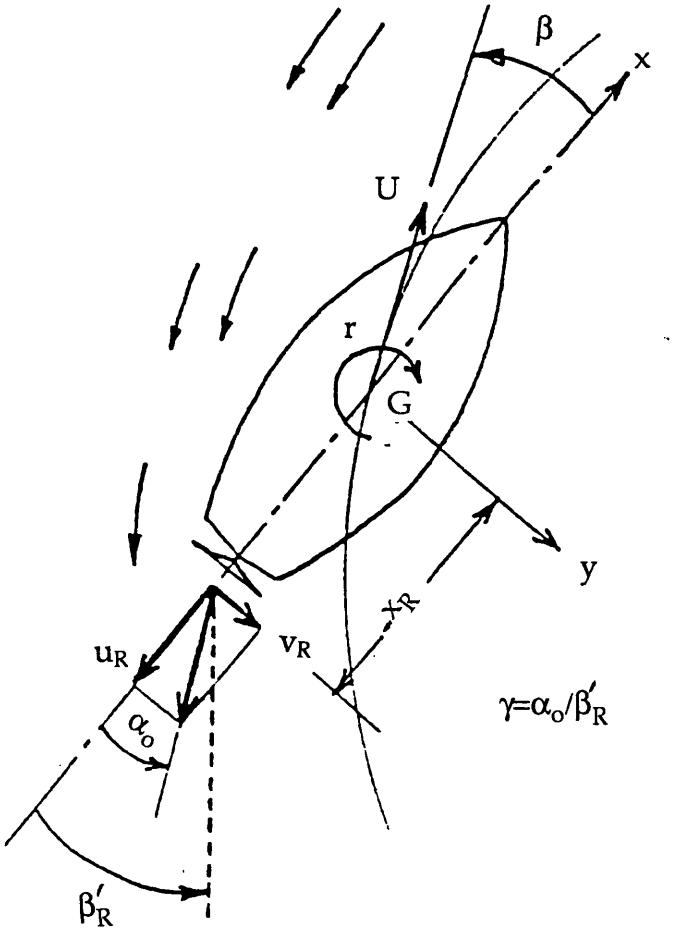

Figure C 2

Appendix D.

DNV Calculation Method.

The wind forces and pressure on members above the sea surface may normally be considered as steady loads. The wind forces are to be calculated for each of the different directions of environmental loads that are considered. The calculations are carried out by dividing the wind exposed structure into its individual parts. The equations are given below with reference to figure 4.6.

The wind force F_W acting on one bay is defined by

$$F_W = \frac{1}{2}\rho C_D D v^2 \cos^2\beta$$

D	Cross sectional dimension perpendicular to the wind direction
v	Design wind velocity
β	Angle between the wind direction and the cross sectional plane of the member
C_D	Drag (shape) coefficient
ρ	Mass density of air ($1.225 kg/m^3$)

For the calculation of the wind force acting acting on the exposed part of a lattice leg the parameters C_D and D may be replaced by C_{DE} and D_E

The equivalent diameter D_E is defined as,

$$D_E = \sqrt{\frac{4V_B}{\pi s}}$$

$V_B = \sum A_i l_i$ total volume of one bay

A_i	Cross sectional area of member i
l_i	Length of member i
s	Length of one bay

The equivalent drag coefficient is given by,

$$C_{DE} = \sum C_{DEi}$$

$$C_{DEi} = \left[\sin^2\beta + \cos^2\beta \sin^2\alpha\right]^{3/2} C_{Di} \frac{D_i l_i}{D_E s}$$

C_{Di} Drag coefficient of member i

D_E Equivalent diameter

D_i Diameter of member i

α Angle which determines the flow direction.

The expression for C_{DEi} can be simplified for vertical and horizontal members.

Vertical members.

$$C_{DEi} = C_{Di} \frac{D_i}{D_E}$$

Horizontal members.

$$C_{DEi} = \sin^3\alpha \, C_{Di} \frac{D_i l_i}{D_E s}$$

Appendix E.

BSI Calculation Method.

Method for calculation of total wind resistance on symmetrical towers without ancillaries.

The total wind resistance should be determined in the direction of the wind and in the crosswind direction in accordance with the following.

The total wind resistance $\sum R_W$, in the direction of the wind over a panel height of the structural components of a lattice tower of square of equilateral triangular cross section, having equal areas for each face, may be taken as that of the bare tower, R_T, given by,

$$R_T = K_\theta C_N A_S$$

C_N is the overall drag (pressure) coefficient

A_S is the total area projected normal to a face of the structural components within one panel height of the tower at the level concerned

K_θ Wind incidence factor

θ Angle of incidence of wind normal to the windward face

A_F Total projected area of the flat sided section members

ϕ Ratio of the total projected area within the panel height of the structural components in the windward face.

$$\phi = \frac{A_S}{hb}$$

Circular section members should be assumed to be in a sub critical regime when the effective Reynolds number R_e<4 E10-4 and may be assumed to be in a supercritical regime for higher values of Reynolds. The value of R_e is given by,

$$R_e = \frac{1.5\bar{V}_Z D}{\upsilon}$$

$\bar{V}_Z$ Wind speed relevant to the height z from the ground to the center of the member

D Member diameter (m)

υ Kinematic viscosity of air=1.46 E10-5m^2/s

$$C_N = C_{Nf}\frac{A_f}{A_F} + C_{Nc}\frac{A_c}{A_F} + C_{Nc'}\frac{A_{c'}}{A_F}$$

C_{Nf} Drag coefficient of flat sided members

C_{Nc} Drag coefficient of subcritical circular section members

$C_{Nc'}$ Drag coefficient of supercritical circular section members

A_f Area of flat sided members

A_c Area of subcritical circular section members

$A_{c'}$ Area of supercritical circular section members

The wind incidence factor is given by

$$K_\theta = 1.0 + K_1 K_2 \sin^2 2\theta \text{ for square towers}$$

$$K_\theta = \frac{A_c + A_{c'}}{A_F} + \frac{A_f}{A_F}(1.0 - 0.1\sin^2 1.5\,\theta) \text{ for triangular towers}$$

$$K_1 = \frac{0.8(A_c + A_{c'})}{A_F} + \frac{0.55A_f}{A_F}$$

$K_2 = 0.2$ for $0 \le \phi \le 0.2$ and $0.8 \le \phi \le 1.0$

$= \phi$ for $0.2 < \phi < 0.5$

$= 1 - \phi$ for $0.5 < \phi < 0.8$

The drag coefficients for towers composed of flat sided members C_{Nf}, subcritical circular section members, C_{Nc}, and supercritical circular section members, $C_{Nc'}$, are given by,

$$C_{Nf} = 1.76\, C_1 \left[1 - C_2\phi + \phi^2\right]$$

$$C_{Nc} = C_1 \left[1 - C_2\phi\right] + \left[C_1 + 0.875\right] \phi^2$$

$$C_{Nc'} = 1.9 - \sqrt{\left[1 - \phi\right]\left[2.8 - 1.14\, C_1 + \phi\right]}$$

C_1 is equal to

2.25 for square towers

1.9 for triangular towers

C_2 is equal to

1.5 for square towers

1.4 for triangular towers

Appendix F.

MMEC Calculation Method.

The MMEC method is a simple building block approach which includes factors for shielding and orientation and which agrees well with model test results.

Square Leg Geometries.

$$C_D = K_\beta\left[\sum_w A_i C_{Di} + \eta\sum_l A_j C_{Dj}\right] / LW$$

$$K_\beta = 1.1 + 0.5728\phi\,(\sin 2\beta)^{0.9}$$

$$\eta = 1.1 - C_{Dwc}\phi$$

$$\phi = \sum_w A_i / LW$$

K_β	Orientation factor
ϕ	Solidity ratio
η	Shielding factor
C_{Dwc}	Drag coefficient of windward (w) corner post
C_{Dlc}	Drag coefficient of leeward (l) corner post
C_{Di}	Component of drag coefficient of windward face
C_{Dj}	Component of drag coefficient of leeward face
A_i	Component of projected areas of windward face
A_j	Component of projected areas of leeward face
β	Yaw angle

Triangular Leg Geometries.

$$C_D = K_{\beta\Delta}\left[\sum_w A_i C_{Di} + \eta_\Delta\sum_l A_j C_{Dj}\right] / LW$$

$$K_{\beta\Delta} = 1.0$$

$$\eta_\Delta = 0.8(1.1 - C_{Dwc}\phi)$$

All symbols have same definitions as in the case of the square leg geometry.

Appendix G.

Calculation of Wind Heel Moments using ABS Classification Rules.

The wind loads and wind heeling arm acting on the jack up (excluding legs) and heavy lift vessel are determined with ABS rules for Mobile Offshore Drilling Units.

Wind Load.

The wind load is calculated for the system using the following equation.

$$F_W = \frac{\rho_A A C_S C_H U_W^2}{2}$$

The wind velocity is taken as the absolute value. No relative motion from drifting is considered.

C_H Height Coefficient See Appendix Table G 1.

C_S Shape Coefficient See Appendix Table G 2.

A Projected Area of Exposed Surfaces

ρ_A mass density of air

Wind Overturning Moment.

The wind overturning moment of the system is calculated using,

$$M_{Wt} = F_{W_{Total}} H_t$$

$F_{W_{Total}}$ Total transverse wind load on the system

H_t Vertical distance from the centre of effort to the centre of lateral resistance at half the draft

Wind Lever.

The total wind lever is calculated by dividing the wind overturning moment by the displacement of the system.

Appendix G.

Height Coefficient

Height (meters)	Coefficient	Height (meters)	Coefficient
0-15.3	1	91.5-106.0	1.48
15.3-30.5	1.1	106.0-122.0	1.52
30.5-46.0	1.2	122.0-137.0	1.56
46.0-61.0	1.3	137.0-152.5	1.6
61.0-76.0	1.37	152.5-167.5	1.63
76.0-91.5	1.43	167.5-183.0	1.67

Table G1

Shape Coefficient

Cylindrical (all sizes)	0.5
Hull (surface types)	1
Deck house	1
Isolated structural shapes (cranes, beams)	1.5
Under deck areas (smooth surfaces)	1
Under deck areas (exposed beams and girders)	1.3
Rig derrick (each face)	1.25

Table G2

Appendix H.

Linear Theoretical Prediction for Directional Stability.

The equations of motion for the towed vessel can be written with reference to figure 7.1a as,

$$m_X\dot{u} - m_Y vr = X_H + T\cos(\varepsilon_0 - \theta_1) \qquad \text{H 1a}$$

$$m_Y\dot{v} + m_X ur = Y_\beta\beta + Y_r r + T\sin(\varepsilon_0 - \theta_1) \qquad \text{H 1b}$$

$$I_Z\dot{r} = N_\beta\beta + N_r r + Tx_P\sin(\varepsilon_0 - \theta_1) \qquad \text{H 1c}$$

where,

$$m_X = m(1+k_X)$$

$$m_Y = m(1+k_Y)$$

$$I_Z = (0.24L)^2 m(1+k_Z)$$

are the virtual mass coefficients or Lambs coefficients of accession to inertia. There are no acceleration derivatives included in this stability analysis but the added mass terms take account of this (Ref. 7.1 discussion). I_z is an empirical approximation commonly used in Japanese simulation literature. x_p is the distance of the towpoint forward of the centre of gravity of the towed vessel. The forces due to the derivatives are dimensionalised in the following manner as given in Chapter Two. The non dimensionalised linear derivatives were obtained from the Kijima empirical equations.

$$Y_\beta = Y'_\beta\frac{\rho LDU^2}{2}$$

$$Y_r = Y'_r \frac{\rho L^2 DU}{2}$$

$$N_\beta = N'_\beta \frac{\rho L^2 DU^2}{2}$$

$$N_r = N'_r \frac{\rho L^3 DU}{2}$$

We can obtain an additional equation for the towline from an equality of towpoint velocity from Strandhagen, Ref. 7.1

$$(x_P r + v)\cos\theta_1 + u\sin\theta_1 = -l\dot{\varepsilon}_0 \cos\varepsilon_0 \qquad \text{H 2}$$

We can neglect the surge equation H 1a, by assuming the surge acceleration is small and products of small quantities are negligible. If we now write the sway velocity and acceleration as,

$$v = -u\sin\beta \qquad \text{H 3a}$$

$$\dot{v} = -\dot{u}\sin\beta - u\dot{\beta}\cos\beta \qquad \text{H 3b}$$

and assume for small angles,

$$\sin\beta \approx \beta, \cos\beta \approx 1$$

Remembering the surge acceleration is small, then we rewrite equations H 3 as,

$$v = -u\beta \qquad \text{H 4a}$$

$$\dot{v} = -u\dot{\beta} \qquad \text{H 4b}$$

Placing equations H 4 into equations H 1b,c and H 2 we obtain,

$$-m_Y u\dot{\beta} + m_X ur = Y_\beta \beta + Y_r r + T(\varepsilon_0 - \theta_1) \qquad \text{H 5a}$$

$$I_Z \dot{r} = N_\beta \beta + N_r r + Tx_P(\varepsilon_0 - \theta_1) \qquad \text{H 5b}$$

$$x_P r - u\beta + u\theta_1 = -l\dot{\varepsilon}_0 \qquad \text{H 5c}$$

The equations above are linear, homogenious differential equations. The general solution is obtained when we represent the towed vessel drift and heading angle and the towrope angle of the towed vessel as,

$$\beta = k_1 e^{\sigma t},\ \theta_1 = k_2 e^{\sigma t},\ \varepsilon_0 = k_3 e^{\sigma t}$$

k_1, k_2, k_3 are constants which depend on the initial conditions. Placing the above in equation H 5 and rearranging,

$$(Y_\beta + m_Y u\sigma)k_1 + ((Y_r - m_X u)\sigma - T)k_2 + Tk_3 = 0 \qquad \text{H 6a}$$

$$-N_\beta k_1 + (I_Z\sigma^2 - N_r\sigma + Tx_P)k_2 - Tx_P k_3 = 0 \qquad \text{H 6b}$$

$$-uk_1 + (x_P\sigma + u)k_2 + l\sigma k_3 = 0 \qquad \text{H 6c}$$

The above will be satisfied if the determinant is equal to zero and this can be represented in matrix form as,

$$\begin{bmatrix} Y_\beta + m_Y u\sigma & (Y_r - m_X u)\sigma - T & T \\ -N_\beta & I_Z\sigma^2 - N_r\sigma + Tx_P & -Tx_P \\ -u & x_P\sigma + u & l\sigma \end{bmatrix} \begin{bmatrix} k_1 \\ k_2 \\ k_3 \end{bmatrix} = \begin{bmatrix} 0 \\ 0 \\ 0 \end{bmatrix}$$

This is then expanded.

$$= (Y_\beta + m_Y u\sigma)\begin{bmatrix} I_Z\sigma^2 - N_r\sigma + Tx_P & -Tx_P \\ x_P\sigma + u & l\sigma \end{bmatrix}$$

$$+N_\beta\begin{bmatrix} (Y_r - m_X u)\sigma - T & T \\ x_P\sigma + u & l\sigma \end{bmatrix}$$

$$-u\begin{bmatrix} (Y_r - m_X u)\sigma - T & T \\ I_Z\sigma^2 - N_r\sigma + Tx_P & -Tx_P \end{bmatrix}$$

$$= (Y_\beta + m_Y u\sigma)\left[lI_Z\sigma^3 - N_r l\sigma^2 + lTx_P\sigma + Tx_P^2\sigma + Tx_P u\right]$$

$$+N_\beta\left[l\sigma^2 Y_r - lm_X u\sigma^2 - Tl\sigma - Tx_P\sigma - Tu\right]$$

$$-u\left[-Tx_P Y_r\sigma + Tx_P m_X u\sigma + T^2 x_P - TI_Z\sigma^2 + TN_r\sigma - T^2 x_P\right]$$

$$= lI_Z m_Y u\sigma^4$$

$$+Y_\beta lI_Z\sigma^3 - N_r lm_Y u\sigma^3$$

$$-Y_\beta N_r l\sigma^2 + lTx_P m_Y u\sigma^2 + Tx_P^2 m_Y u\sigma^2 + N_\beta l\sigma^2 Y_r - N_\beta lm_X u\sigma^2 + TI_Z u\sigma^2$$

$$+Y_\beta lTx_P\sigma + Y_\beta Tx_P^2\sigma - TN_r u\sigma + Tx_P m_Y u^2\sigma + Tx_P Y_r u\sigma - Tx_P m_X u^2\sigma - N_\beta Tl\sigma - N_\beta Tx_P\sigma$$

$$-N_\beta Tu + Y_\beta Tx_P u + T^2 x_P u - T^2 x_P u$$

The determinant may be arranged as,

$$\sigma^4 + A\sigma^3 + B\sigma^2 + C\sigma + D = 0$$

where,

$$A = \frac{Y_\beta}{m_Y u} - \frac{N_r}{I} \qquad \text{H 7a}$$

$$B = \frac{N_\beta (Y_r - m_X u) - Y_\beta N_r}{I_Z m_Y u} + \frac{T}{I_Z l}\left(\frac{I_Z}{m_Y} + x_P^2 + x_P l\right) \qquad \text{H 7b}$$

$$C = \frac{T}{I_Z m_Y}\left[-\frac{1}{u}(N_\beta - x_P Y_\beta) + \frac{x_P}{l}(Y_r - m_X u + m_Y u) + \frac{x_P}{ul}(x_P Y_\beta - N_\beta) - \frac{N_r}{l}\right]$$

H 7c

$$D = \frac{T}{I_Z m_Y l}(x_P Y_\beta - N_\beta) \qquad \text{H 7d}$$

The form of equations H 7 can be compared to those given by Abkowitz, Ref. 2.1. If we neglect the automatic control and the narrow channel effects of these equations given in Ref. 2.8 and replace the acceleration derivatives with the coefficients of inertia and the sway and yaw derivatives are replaced by the drift derivatives as,

$$Y = Y_v v = Y_\beta \beta$$

then using the relationship of equation H 4 ,

$$Y_v = -\frac{Y_\beta}{u}, \; N_v = -\frac{N_\beta}{u}$$

we then obtain the same equations as the directional stability criteria given by equations H 7 and 7.2 in the main text.

Appendix I.

Towed Vessel Velocity with the Rigid Tow Rope Assumption.

The velocity of the towed vessel used in the rigid tow rope model is determined from Ref. 7.9. The position of the towed vessel relative to the tow vessel.

$$X_1 = X_0 - a_0\cos\theta_0 - l_T\cos(\theta_1+\varepsilon_1) - f_1\cos\theta_1 \qquad \text{I 1a}$$

$$Y_1 = Y_0 - a_0\sin\theta_0 - l_T\sin(\theta_1+\varepsilon_1) - f_1\sin\theta_1 \qquad \text{I 1b}$$

we differentiate the above equations with respect to time,

$$\dot{X}_1 = \dot{X}_0 + a_0\dot{\theta}_0\sin\theta_0 + l_T(\dot{\theta}_1+\dot{\varepsilon}_1)\sin(\theta_1+\varepsilon_1) + f_1\dot{\theta}_1\sin\theta_1 \qquad \text{I 2a}$$

$$\dot{Y}_1 = \dot{Y}_0 - a_0\dot{\theta}_0\cos\theta_0 - l_T(\dot{\theta}_1+\dot{\varepsilon}_1)\cos(\theta_1+\varepsilon_1) - f_1\dot{\theta}_1\cos\theta_1 \qquad \text{I 2b}$$

Using the relations below and placing them in equations I 2

$$\dot{X}_i = \overline{U}_i\cos(\theta_i-\beta_i) \qquad \text{I 3a}$$

$$\dot{Y}_i = \overline{U}_i\sin(\theta_i-\beta_i) \qquad \text{I 3b}$$

we obtain,

$$\overline{U}_1\cos(\theta_1-\beta_1) = \overline{U}_0\cos(\theta_0-\beta_0) + a_0\dot{\theta}_0\sin\theta_0 + l_T(\dot{\theta}_1+\dot{\varepsilon}_1)\sin(\theta_1+\varepsilon_1) + f_1\dot{\theta}_1\sin\theta_1$$

$$\overline{U}_1\sin(\theta_1-\beta_1) = \overline{U}_0\sin(\theta_0-\beta_0) - a_0\dot{\theta}_0\cos\theta_0 - l_T(\dot{\theta}_1+\dot{\varepsilon}_1)\cos(\theta_1+\varepsilon_1) - f_1\dot{\theta}_1\cos\theta_1$$

We now premultiply the above equations by $\cos(\theta_1+\varepsilon_1)$ and $\sin(\theta_1+\varepsilon_1)$ respectively,

$$\overline{U}_1\cos(\theta_1+\varepsilon_1)\cos(\theta_1-\beta_1)=\overline{U}_0\cos(\theta_1+\varepsilon_1)\cos(\theta_0-\beta_0)+a_0\dot{\theta}_0\cos(\theta_1+\varepsilon_1)\sin\theta_0$$
$$+l_T(\dot{\theta}_1+\dot{\varepsilon}_1)\cos(\theta_1+\varepsilon_1)\sin(\theta_1+\varepsilon_1)+f_1\dot{\theta}_1\cos(\theta_1+\varepsilon_1)\sin\theta_1$$

I 4a

$$\overline{U}_1\sin(\theta_1+\varepsilon_1)\sin(\theta_1-\beta_1)=\overline{U}_0\sin(\theta_1+\varepsilon_1)\sin(\theta_0-\beta_0)-a_0\dot{\theta}_0\sin(\theta_1+\varepsilon_1)\cos\theta_0$$
$$-l_T(\dot{\theta}_1+\dot{\varepsilon}_1)\sin(\theta_1+\varepsilon_1)\cos(\theta_1+\varepsilon_1)-f_1\dot{\theta}_1\sin(\theta_1+\varepsilon_1)\cos\theta_1$$

I 4b

Adding the above then results in the following relationship.

$$\overline{U}_1\cos(\theta_1+\varepsilon_1-\theta_1+\beta_1)=\overline{U}_0\cos(\theta_1+\varepsilon_1-\theta_0+\beta_0)$$
$$-a_0\dot{\theta}_0\sin(\theta_1+\varepsilon_1-\theta_0)-f_1\dot{\theta}_1\sin(\theta_1+\varepsilon_1-\theta_1)$$

I 5

Rearranging then gives,

$$\overline{U}_1\cos(\varepsilon_1+\beta_1)=\overline{U}_0\cos(\theta_1+\varepsilon_1-\theta_0+\beta_0)-a_0\dot{\theta}_0\sin(\theta_1+\varepsilon_1-\theta_0)-f_1\dot{\theta}_1\sin\varepsilon_1$$

Finally placing $\dot{\theta}_i=\frac{r_i'U_i}{L_i}$ in the above gives,

$$\overline{U}_1\cos(\varepsilon_1+\beta_1)=\overline{U}_0\cos(\theta_1+\varepsilon_1-\theta_0+\beta_0)-a_0\frac{r_0'U_0}{L_0}\sin(\theta_1+\varepsilon_1-\theta_0)-f_1\frac{r_1'U_1}{L_1}\sin\varepsilon_1$$

$$\overline{U}_1\left(\cos(\varepsilon_1+\beta_1)+f_1\frac{r_1'}{L_1}\sin\varepsilon_1\right)=\overline{U}_0\cos(\theta_1+\varepsilon_1-\theta_0+\beta_0)-a_0\frac{r_0'U_0}{L_0}\sin(\theta_1+\varepsilon_1-\theta_0)$$

$$\overline{U}_1=\frac{\overline{U}_0\cos(\theta_1+\varepsilon_1-\theta_0+\beta_0)-a_0\frac{r_0'U_0}{L_0}\sin(\theta_1+\varepsilon_1-\theta_0)}{\cos(\varepsilon_1+\beta_1)+f_1\frac{r_1'}{L_1}\sin\varepsilon_1}$$

I 6

Appendix J.

Rigid Towrope Angular Velocity.

The angular velocity of the towrope is determined from a knowledge of the positions of the tow and towed vessels in the global coordinate system as shown in Ref. 7.9. The position of the towed vessel is determined from figure 7.1b as,

$$X_1 = X_0 - a_0\cos\theta_0 - l_T\cos(\theta_1+\varepsilon_1) - f_1\cos\theta_1 \qquad \text{J 1a}$$

$$Y_1 = Y_0 - a_0\sin\theta_0 - l_T\sin(\theta_1+\varepsilon_1) - f_1\sin\theta_1 \qquad \text{J 1b}$$

In order to obtain the towrope angular velocity we must differentiate the above equations with respect to time,

$$\dot{X}_1 = \dot{X}_0 + a_0\dot{\theta}_0\sin\theta_0 + l_T(\dot{\theta}_1+\dot{\varepsilon}_1)\sin(\theta_1+\varepsilon_1) + f_1\dot{\theta}_1\sin\theta_1 \qquad \text{J 2a}$$

$$\dot{Y}_1 = \dot{Y}_0 - a_0\dot{\theta}_0\cos\theta_0 - l_T(\dot{\theta}_1+\dot{\varepsilon}_1)\cos(\theta_1+\varepsilon_1) - f_1\dot{\theta}_1\cos\theta_1 \qquad \text{J 2b}$$

Using the relations below and placing in equations I 2

$$\dot{X}_i = \overline{U}_i\cos(\theta_i-\beta_i) \qquad \text{J 3a}$$

$$\dot{Y}_i = \overline{U}_i\sin(\theta_i-\beta_i) \qquad \text{J 3b}$$

we obtain,

$$\overline{U}_1\cos(\theta_1-\beta_1) = \overline{U}_0\cos(\theta_0-\beta_0) + a_0\dot{\theta}_0\sin\theta_0 + l_T(\dot{\theta}_1+\dot{\varepsilon}_1)\sin(\theta_1+\varepsilon_1) + f_1\dot{\theta}_1\sin\theta_1$$

$$\overline{U}_1\sin(\theta_1-\beta_1) = \overline{U}_0\sin(\theta_0-\beta_0) - a_0\dot{\theta}_0\cos\theta_0 - l_T(\dot{\theta}_1+\dot{\varepsilon}_1)\cos(\theta_1+\varepsilon_1) - f_1\dot{\theta}_1\cos\theta_1$$

Premultiplying the above by $\sin(\theta_1+\varepsilon_1)$ and $\cos(\theta_1+\varepsilon_1)$ respectively we then have,

$$\overline{U}_1 \sin(\theta_1 + \varepsilon_1)\cos(\theta_1 - \beta_1) =$$
$$\sin(\theta_1 + \varepsilon_1)(\overline{U}_0 \cos(\theta_0 - \beta_0) + a_0\dot{\theta}_0 \sin\theta_0 + l_T(\dot{\theta}_1 + \dot{\varepsilon}_1)\sin(\theta_1 + \varepsilon_1) + f_1\dot{\theta}_1 \sin\theta_1)$$

J 4a

$$\overline{U}_1 \cos(\theta_1 + \varepsilon_1)\sin(\theta_1 - \beta_1) =$$
$$\cos(\theta_1 + \varepsilon_1)(\overline{U}_0 \sin(\theta_0 - \beta_0) - a_0\dot{\theta}_0 \cos\theta_0 - l_T(\dot{\theta}_1 + \dot{\varepsilon}_1)\cos(\theta_1 + \varepsilon_1) - f_1\dot{\theta}_1 \cos\theta_1)$$

J 4b

Subtracting the components of the left hand side of the equations,

$$\sin(\theta_1 + \varepsilon_1)\cos(\theta_1 - \beta_1) - \cos(\theta_1 + \varepsilon_1)\sin(\theta_1 - \beta_1) = \sin(\varepsilon_1 + \beta_1) \qquad \text{J 5}$$

The first component on the right hand side of the equation is,

$$\overline{U}_0 \sin(\theta_1 + \varepsilon_1)\cos(\theta_0 - \beta_0) - \overline{U}_0 \cos(\theta_1 + \varepsilon_1)\sin(\theta_0 - \beta_0)$$
$$= \overline{U}_0 \sin(\theta_1 + \varepsilon_1 - \theta_0 + \beta_0) \qquad \text{J 6}$$

the remaining components are similarly defined,

$$a_0\dot{\theta}_0 \sin(\theta_1 + \varepsilon_1)\sin\theta_0 + a_0\dot{\theta}_0 \cos(\theta_1 + \varepsilon_1)\cos\theta_0$$
$$= a_0\dot{\theta}_0 \cos(\theta_1 + \varepsilon_1 - \theta_0) \qquad \text{J 7}$$

$$l_T(\dot{\theta}_1 + \dot{\varepsilon}_1)\sin^2(\theta_1 + \varepsilon_1) + l_T(\dot{\theta}_1 + \dot{\varepsilon}_1)\cos^2(\theta_1 + \varepsilon_1)$$
$$= l_T(\dot{\theta}_1 + \dot{\varepsilon}_1) \qquad \text{J 8}$$

$$f_1\dot{\theta}_1 \sin(\theta_1 + \varepsilon_1)\sin\theta_1 + f_1\dot{\theta}_1 \cos(\theta_1 + \varepsilon_1)\cos\theta_1$$
$$= f_1\dot{\theta}_1 \cos(\theta_1 + \varepsilon_1 - \theta_1) \qquad \text{J 9}$$

The components J 5-J 9 are then brought together and after rearranging we obtain,

$$\overline{U}_1 \sin(\varepsilon_1 + \beta_1) = \overline{U}_0 \sin(\theta_1 + \varepsilon_1 - \theta_0 + \beta_0) + a_0\dot{\theta}_0 \cos(\theta_1 + \varepsilon_1 - \theta_0) + l_T(\dot{\theta}_1 + \dot{\varepsilon}_1) + f_1\dot{\theta}_1 \cos\varepsilon_1$$

$$\dot{\varepsilon}_1 = \frac{1}{l_T}\left\{\overline{U}_1 \sin(\varepsilon_1 + \beta_1) - \overline{U}_0 \sin(\theta_1 + \varepsilon_1 - \theta_0 + \beta_0) - a_0\dot{\theta}_0 \cos(\theta_1 + \varepsilon_1 - \theta_0) - f_1\dot{\theta}_1 \cos\varepsilon_1\right\} - \dot{\theta}_1$$

J 10

If we place the expression for the angular velocity of the vessels

$$\dot{\theta}_i = \frac{r_i'\overline{U}_i}{L_i}$$

in the above equation for the towrope angular velocity J 10 we obtain,

$$\dot{\varepsilon}_1 = \frac{1}{l_T}\left\{\begin{array}{l} \overline{U}_1\left[\sin(\varepsilon_1 + \beta_1) - f_1\frac{r_1'}{L_1}\cos\varepsilon_1 - \frac{r_1' l_T}{L_1}\right] \\ -\overline{U}_0\left[\sin(\theta_1 + \varepsilon_1 - \theta_0 + \beta_0) - a_0\frac{r_0'}{L_0}\cos(\theta_1 + \varepsilon_1 - \theta_0)\right] \end{array}\right\} \qquad \text{J 11}$$

This equation is then used in the NAG routine to determine the towrope angle with respect to the towed vessel.

References.

Chapter One.

1.1 Mobile Offshore Structures. Boswell, L.F., D'Mello, C., Edwards. Proceedings of International Conference on Mobile Offshore Structures. University College, London. 15 -18 September 1987. ISBN 1-85166-277-4.

1.2 Marine Structures Volume 2, Nos 3-5, 1989. Special Issue on The Jack Up Drilling Platform.

1.3 Recent Developments in Jack Up Platforms. Edited by Boswell, L.F., D'Mello, C. Blackwell Scientific Publications 1992. ISBN 0-632-03281-2.

1.4 Proceedings of Fourth International Conference on the Jack Up Platform. September 1993. Bentham Press. ISBN 1- 874612-11-0

1.5 Sharples, B.P.M., Bennett, W.T., Trickey, J.C. 'Risk Analysis of Jack Up Rigs.' (in Ref. 1.2)

1.6 Denton, A.A., 'The Loss of a Jack Up Under Tow.' (in Ref. 1.2)

1.7 Mars. P., Normann, M.H., Walker, H., 'Safe Towage of Jack Up Installations.' Recent Developments in Jack Up Platforms. (in Ref 1.3).

1.8 Standing, R.G., Rowe, S.J. 'Stability and Seakeeping Review for Jack Ups in Transit.' (in Ref. 1.4).

1.9 Jack R.L., Noble-Smith, D.R., Huntington, J., 'Risk Reduction in Towing Offshore Structures.' Journal of Petroleum Technology. pp. 22-26. January 1980.

1.10 Cao, Z-H., Chen, X-L., 'Model Experiments on the Capsizing of a Jack Up Drilling Platform.' 2nd International Conference on Stability of Ships and Ocean Vehicles. Tokyo, October 1982.

1.11 Fernandes, A.C., 'Analysis of a Jack Up Platform by Model Tests.' Proceedings of the 5th International Symposium on Offshore Engineering. Rio de Janeiro, Brazil. 1985.

1.12 Fernandes, A.C. et. al. 'Dynamic Behaviour off a Jack Up Platform in Waves.' Proceedings of the 21st American Towing Tank Conference. Washington D.C. 1986.

1.13 Williams, O.S., 'Modelling Comparisons for Motion Response Characteristics of a Jack Up Platform in Head Seas.' University of Glasgow, Department of Naval Architecture and Ocean Engineering. Report No. 92-27. 1992.

1.14 Burcher, R.K., Zhang, H., 'Determination of Control Characteristics of Ship Models from Towing Tests.' Department of Mechanical Engineering, University College London. May 1994

1.15 Varyani, K.S. Turning Circle Manoeuvring Simulation Program dated March 1983. Department of Naval Architecture. Kyushu University. Japan.

Chapter Two.

2.1 Abkowitz, M.A., 'Stability and Motion Control of Ocean Vehicles.' MIT Press 1969

2.2 Barr, R.A., 'A Review and Comparison of Ship Manoeuvring Simulation Methods.' Transactions of SNAME 1993.

2.3 Kijima, K., Tanaka, S., Furukawa, Y., Hori, T., 'On a Prediction Method of Ship Manoeuvring Characteristics.' International Conference on Marine Simulation and Ship Manoeuvrability.' St Johns, Newfoundland, Canada. 1993.

2.4 Kijima, K., Tanaka, S., Matsunaga, M., Hori ,T., 'Manoeuvring Characteristics of a Ship in Deep and Shallow Water as a Function of Loading Condition.' Manoeuvring and Control of Marine Craft. Proceedings of the Second International Conference. Southampton, England. July 1992.

2.5 Kijima, K., Yasuaki, N., Yasuharu, T., Masaki, M., 'Prediction Method of Ship Manoeuvrability in Deep and Shallow Waters.' Proceedings of Marsim and ICSM 90. Tokyo, Japan. June 4-7th 1990.

2.6 Kose, K., 'On a New Mathematical Model of Manoeuvring Motions of Ships.' International Shipbuilding Progress. Vol. 29, No. 336, 1982.

2.7 Ogawa, A., Kasai, H., 'On the Mathematical Model of Manoeuvring Motion of Ships.' International Shipbuilding Progress. 1978

2.8 Davidson, K.S.M., Schiff, L.I., 'Turning and Course Keeping Qualities.' Transactions SNAME. 1946, pp. 152.

2.9 Kijima, K., Katsuno, T., Nakiri, Y., Furukawa, Y., 'On the Manoeuvring Performance of a Ship with the Parameter of Loading Condition.' Journal of the Society of Naval Architects of Japan, Vol. 168.

2.10 Principles of Naval Architecture. Second Revision SNAME. May 1988.

2.11 Crane, C.L. 'Manoeuvring Trials of a 278,000 DWT tanker in Shallow and Deep Waters.' SNAME Transactions Vol. 87. 1979. pp. 251-283.

2.12 Pourzanjani, M., 'Formulation of the Force Mathematical Model of a Ship Manoeuvring.' International Shipbuilding Progress. Vol. 37, No. 409. 1990.

2.13 Harvald, S.A., 'Resistance and Propulsion of Ships.' Printed Wiley Interscience. pp. 118-126. 1983. ISBN 0 471 06353-3.

2.14 Hirano, M., 'A Practical Calculation Method of Ship Manoeuvring Motion at the Initial Design Stage.' Journal of Society of Naval Architects of Japan. Volume 147, June 1980.

2.15 Inoue, S., Hirano, M., Kijima. K., 'Hydrodynamic Derivatives on Ship Manoeuvring.' International Shipbuilding Progress. Vol. 28, No. 321, 1981.

2.16 Numerical Algorithms Group, (NAG). Mark 14, Volume 2, Routine D02BBF.

2.17 Denny, S.B., Hubble, E.N., 'Prediction of Craft Turning Characteristics.' Marine Technology, Vol. 28, January 1991, pp. 1-13.

2.18 Fujii, J., Tsuda, T., 'Experimental Researches on Rudder Performance (2) and (3).' Journal of the Society of Naval Architects of Japan. Volume 110 and 111. December 1961/ June 1962. (in Japanese)

2.19 Kijima, K., Murakami, M., Katsuno, T., Nakiri, Y., 'A Study on the Ship Manoeuvring Characteristics in Shallow Water.' Transactions of the West Japan Society of Naval Architects. No. 69. March 1985.

2.20 Hirano, M., Takashina, J., Moriya, S., Nakamura, Y., 'An Experimental Study on the Manoeuvring Hydrodynamic Forces in Shallow Water.' Transactions of the West Japan Society of Naval Architects. No. 69. March 1985.

Chapter Three.

3.1 'Prediction of Wind and Current Loads on VLCC's.' Oil Companies International Marine Forum.

3.2 Isherwood, R.M., 'Wind Resistance of Merchant Ships.' Transactions RINA 1972, pp. 327-338.

3.3 Dand, I.W., 'Drifting Disabled Ships and Offshore Installations.' Proceedings of Marine and Offshore Safety Conference. Sept. 7-9, 1983. University of Glasgow.

3.4 van Berlekom, W.B., et al, 'Large Tankers-Wind Coefficients and Speed Loss Due to Wind and Sea.' RINA Spring Meetings 1974, pp. 41-58.

3.5 Inoue, S., Ishibashi, Y., 'The Influence of the Wind on Ship Manoeuvrability.' ITTC Conference 1975. Vol. 2, pp. 581-590.

3.6 Eda, H., 'Low Speed Controllability of Ships In Wind.' Journal of Ship Research, September 1968, pp. 181-200.

3.7 Martin, L.L., 'Ship Manoeuvring and Control in Wind.' Transactions

SNAME Vol.88, 1980, pp. 257-281.

3.8 Eda, H., 'Directional Stability and Control of Ships in Restricted Channels.' Transactions of SNAME, Volume 79, 1971.

3.9 Eda, H., 'Dynamic Behaviour of Tankers During Two-Way Traffic in Channels.' Marine Technology, July 1973.

Chapter Four.

4.1 Pharr Smith, N., Lorenz, D.B., Wendenburg, C.A., Laird. J.S., 'A Study of Drag Coefficients for Truss Legs on Self Elevating Mobile Offshore Drilling Units.' Transactions SNAME. Vol. 91, 1983, pp. 257-273.

4.2 Pharr Smith, N., Wendenburg, C.A., 'A Study of Jack Up Leg Drag Coefficients.' Journal of Marine Structures. Volume 2, Nos. 3-5, 1989, pp. 365-383.

4.3 Miller, B.L., 'The Hydrodynamic Drag of Roughened Circular Cylinders.' Transactions RINA. 1976, pp. 55-70.

4.4 Cook, N.J., 'The Designers Guide to Wind Loading of Building Structures.' Part 2, Static Structures. Published by Butterworths. ISBN 0-408-00871-7.

4.5 Cermak, J.E., 'Wind Engineering.' Proceedings of the Fifth International Conference, Fort Collins, Colorado, USA. July 1979. Volume 1. Pergamon Press. ISBN 0-08-024745-8.

4.6 'Lattice Towers and Masts. Code of Practice for Loading.' British Standards Institution, BSI 8100 Part 1 and 2 , 1986.

4.7 'Lattice Structures. Mean Fluid Forces on Tower-Like Space Frames' Engineering Science Data Units. Item Number 81028.

4.8 Det Norske Veritas Classification Notes for Self Elevating Units May 1984. Note No. 31.5

4.9 Georgiev, T., Ivanov, L., 'Comparative Strength Analysis of Two Variants of Leg Structures for a Self-Elevating Platform for the Black Sea.' Bulletin Technique Du Bureau Veritas, October 1983.

4.10 'Fluid Loading on Offshore Structures Volume 1.' Department of Energy. Offshore Technology Report. OTH 90 322. ISBN 0 11 413324 7.

Chapter Five.

5.1 Transport Manual of the Jack Up Rig 'Ron Tappmeyer' on the 'Mighty Servant 1' Contract 4549. May 27th 1993. Wijsmuller Transport.

5.2 Jacobs, W. R., 'Estimation of Stability Derivatives and Indices of Various Ship Forms, and Comparison with Experimental Results.' Journal of Ship Research, September 1966.

5.3 Principles of Naval Architecture. Volume III. Section 14.

5.4 Whitlock, T.G., Elementary Applied Aerodynamics. Clarendon Press 1931.

5.5 Harrington, R.L., 'Rudder Torque Prediction.' Transactions SNAME.Vol. 89. 1981.

5.6 American Bureau of Shipping. Classification Rules for Mobile Offshore Drilling Units. 1991

5.7 Van Hoorn, F., '(Un)Known Aspects of Dry Transportation.' The Jack Up drilling Platform. Design and Operation. Edit. Boswell, L. F. 1986

5.8 Van Hoorn, F., 'Assessment of the Damage Stability of a Heavy Lift Ship Transporting a MODU.' (In Ref. 1.1)

Chapter Seven.

7.1 Strandhagen, A.G., Schoenherr, K.E., Kobayashi, F.M., 'The Dynamic Stability on Course of Towed Ships.' Transactions of SNAME, Volume 88, 1950.

7.2 Takekawa, M., Nagamatsu, S., Motora, S., 'Course Stability of a Large Towed Barge.' Journal of the Society of Naval Architects of Japan. Volume 137. June 1975 (in Japanese).

7.3 Bernitsas, M.M., Papoulias, F.A., 'Rational Method for Upgrading Towed Vessel Safety.' Department of Naval Architecture and Marine Engineering. University of Michigan. Report No.DOT/OST/P-34/86/046. May 1986.

7.4. Bernitsas, M.M., Kekridis, N.S., 'Simulation and Stability of Ship Towing.' International Shipbuilding Progress. 1985. Vol. 32. No. 369.

7.5 Principles of Naval Architecture. Volume II Section 5.6 pp. 42. SNAME 1988.

7.6 Article on the escort tug 'Thorax'. Ship and Boat International

July/August 1993.

7.7 'Modern Supply Ship Design.' Ship and Boat International, March 1993

7.8 Kijima, K., Maekawa, K., Tanaka, K., 'The Directional Stability of Tow and Towed Vessels in Shallow Water.' West Japan Society of Naval Architects. 1992. (in Japanese).

7.9 Lim, S.T., 'Manoeuvring of Tug Towed Systems' Ph.D. Thesis, Department of Naval Architecture and Marine Engineering, Kyushu University 1976.

7.10 PNA, Volume III, Section 17.4, pp. 371. SNAME 1988.

7.11 McKenna, H.A., Wong, R.K., 'Synthetic Fibre Rope, Properties and Calculations Relating to Mooring Systems.' ASME, OED, Vol. 7, December 1979.

7.12 Charters, S., Thomas, G., Latorre, R., 'Analysis of Towed Vessel Course Stability in Shallow Water.' Transaction of The Royal Institution of Naval Architects 1985.

7.13 Latorre, R., 'Scale Effects in Towed Barge Course Stability Tests.' Ocean Engineering. Vol. 15. No. 4. pp. 305-317. 1988.

7.14 Petitfaux, C., Latorre, R., 'Investigation of Towed Vessel Trajectory in Shallow Water.' International Shipbuilding Progress. September 1994. Vol. 41 No. 427 pp. 267-288.

7.15 Fujino, M., ' Experimental Studies on Ship Manoeuvrability in Restricted Waters.' International Shipbuilding Progress. Vol. 15, No. 168, 1968.

7.16 Latorre, R., 'Improvement of Barge Towing, Translations of Selected Japanese and Russian Technical Articles.' Department of Naval Architecture and Marine Engineering. University of Michigan. Report No. 226. May 1980.

7.17 Tanaka, M., 'Experimental Study on the Course Stability of a Towed Barge.' Transactions of the West Japan Society of Naval Architects. No. 56. August 1978. (in Japanese).

7.18 Latorre, R., Ashcroft, F., 'Recent Developments in Barge Design, Towing and Pushing.' Marine Technology. Volume 18, No. 1, January 1981.

7.19 Bernitsas, M.M., Chung, J.S., 'Non Linear Stability and Simulation of Tow Line Ship Towing and Mooring.' Applied Ocean Research. Vol. 12, No. 2, 1990.

7.20 Kijima, K., Murakami, M., Katsuno, T., Nakiri, Y., ' A Study on the Ship Manoeuvring Characteristics in Shallow Water.' Transactions of the West Japan Society of Naval Architects, No. 69, pp 111-122, 1985. (in Japanese)